Dear Reader!
The publication of this document does not pursue for itself any commercial benefit. But such documents promote the most rapid professional and spiritual growth of readers and are advertising of paper editions of such documents.
You can download (copy) this file for educational purposes only. **PLEASE NOTE** that **ANY COMMERCIAL USE** of this file **IS STRICTLY FORBIDDEN**
You should delete it immediately after your reading is completed. Under international legislation you are responsible for prorer use of this file. All copywrite reserved by owner.

HANDBOOK OF INDUSTRIAL MEMBRANE TECHNOLOGY

Edited by

Mark C. Porter

Consultant
Pleasanton, California

Reprint Edition

np NOYES PUBLICATIONS
Westwood, New Jersey, U.S.A.

Copyright © 1990 by Noyes Publications
No part of this book may be reproduced or utilized in any form or by any means, electronic or mechanical, including photocopying, recording or by any information storage and retrieval system, without permission in writing from the Publisher.
Library of Congress Catalog Card Number: 88-17876
ISBN 0-8155-1205-8
Printed in the United States

Published in the United States of America by
Noyes Publications
Fairview Avenue, Westwood, New Jersey 07675

10 9 8 7 6 5 4

Library of Congress Cataloging-in-Publication Data

Handbook of industrial membrane technology

Bibliography: p.
Includes index.
1. Membranes (Technology)--Handbooks, manuals, etc.
I. Porter, Mark C.
TP159.M4H36 1988 660.2'842 88-17876
ISBN 0-8155-1205-8

Contributors

Richard W. Baker
Membrane Technology and Research, Inc.
Menlo Park, CA

Ingo Blume
Membrane Technology and Research, Inc.
Menlo Park, CA

John E. Cadotte
FilmTec Corporation
Minneapolis, MN

Gerardo Catapano
University of Naples
Naples, Italy

Thomas A. Davis
Graver Water
Union, NJ

Enrico Drioli
University of Naples
Naples, Italy

A. Keith Fritzsche
Ramicon, Inc.
Woburn, MA

Gabriele Iorio
University of Naples
Naples, Italy

James E. Kurz
Permea, Inc.
St. Louis, MO

Robert J. Petersen
FilmTec Corporation
Minneapolis, MN

Mark C. Porter
Consultant
Pleasanton, CA

Robert Rautenbach
Rhein Westfalen Technische Hochschule Aachen
Aachen, West Germany

Heiner Strathmann
Fraunhofer-Institut fur Grenzflachen- und Bioverfahrenstechnik
Stuttgart, West Germany

Richard G. Sudak
Separation Processes, Inc.
Solana Beach, CA

NOTICE

To the best of the Publisher's knowledge the information contained in this book is accurate; however, the Publisher assumes no responsibility nor liability for errors or any consequences arising from the use of the information contained herein. Mention of trade names or commercial products does not constitute endorsement or recommendation for use by the Publisher.

Final determination of the suitability of any information, procedure, or product for use contemplated by any user, and the manner of that use, is the sole responsibility of the user. The book is intended for informational purposes only. Expert advice should be obtained at all times when implementation is being considered.

Preface

This handbook emphasizes the use of synthetic membranes for separations involving industrial or municipal process streams. Little will be said concerning the use of membranes in medical applications as in artificial kidneys or for controlled drug release.

Most of the membrane processes are pressure driven. The notable exception to this is electrodialysis (ED) by which ions are separated under the influence of an electric field. In addition, the chapter on coupled transport covers processes which are driven under the influence of a concentration gradient.

Pressure driven processes include microfiltration (MF), ultrafiltration (UF), reverse osmosis (RO), pervaporation (PV), and gas separations (GS). With the exception of pervaporation, which is just beginning to emerge as an industrial process, each of the above will be covered in a separate chapter.

The pressure driven liquid filtration processes (MF, UF, and RO) may be distinguished by the size of the particle or molecule the membrane is capable of retaining or passing. This roughly relates to the pore-size of the membrane. Figure P.1 shows the pore sizes of MF, UF and RO membranes. Obviously, all particles or molecules larger than the rated pore size will be retained.

The smallest particle which can be seen with the naked eye, under the best of lighting conditions, is about forty (40) microns in diameter. A typical human hair has a diameter of eighty (80) microns. This means that membranes are filtering particles out of solution which are invisible to the naked eye. Even the most open MF membrane is capable of retaining yeast (3 to 12 microns) and tighter MF membranes can retain the smallest bacteria *(Pseudomonas diminuta,* 0.2 microns) (see Figure P.2).

The dividing line between MF and UF membranes at 0.1 microns (1000 Å) is somewhat arbitrary. The most open UF membranes (almost always anisotropic) have a molecular weight cut-off of approximately one million (10^6) daltons which corresponds to about 0.08 microns. There is some overlap in pore size because there are MF membranes (usually isotropic) available with pore sizes down to 0.02 microns. However, these MF membranes are used only for analytical applications and have no commercial importance for large scale processing.

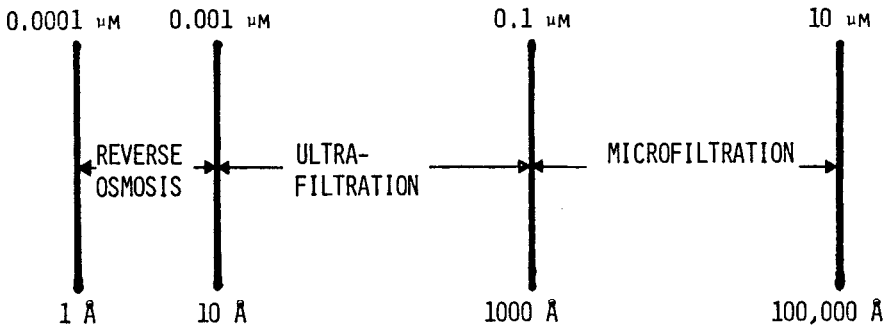


Figure P.1: Pore sizes of RO, UF, and MF membranes.

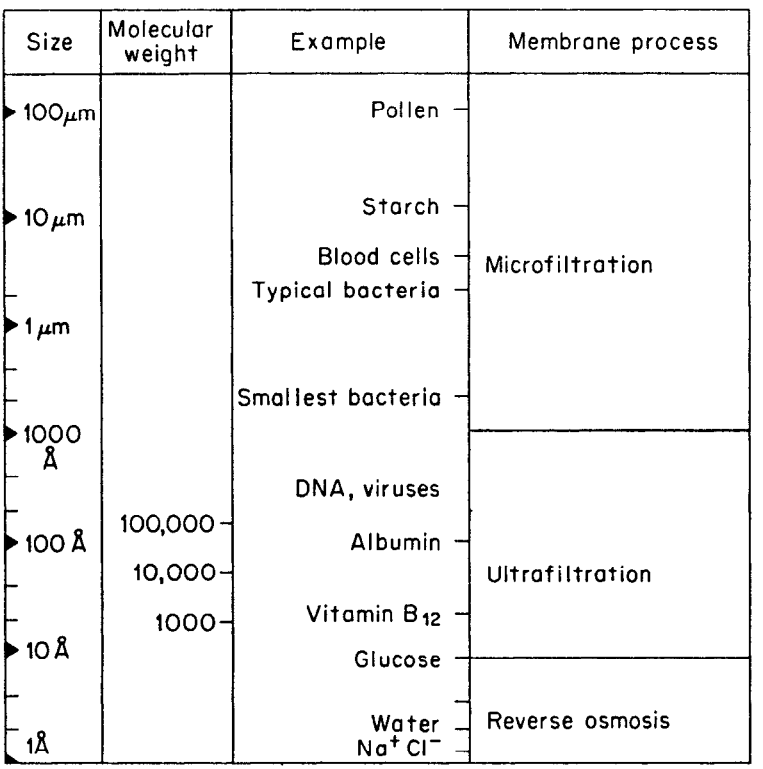


Figure P.2: Typical species retained by MF, UF and RO membranes.

Again, the dividing line between UF and RO membranes at 0.001 microns (10 Å) is semantic. It is academic to even think of pores in RO membranes since we are approaching the intermolecular spacing between the polymer chains in the membrane. Usually, we think of the tighest UF membranes as capable of retaining simple sugars and passing salts whereas RO membranes would retain both.

Another distinguishing feature between UF and RO is that RO is usually a high pressure process–operating between 200 and 1,200 psi (13 to 80 bar). This is because the osmotic pressure of salt solutions can be quite high. Since MF and UF membranes freely pass salt, there is no significant osmotic pressure to overcome and they usually operate below 100 psi (7 bar).

The phenomenon of osmosis is schematically shown in Figure P.3. When a salt solution is separated from pure water by a semipermeable membrane, which allows no passage of salt, water diffuses through the membrane from the higher chemical potential (pure water side) to the lower chemical potential (salt solution side)–resulting in an increase in pressure on the salt solution side. The increase above atmospheric pressure is called the "osmotic pressure." Obviously, to extract pure water from sea water, we must exceed the osmotic pressure as in Figure P.4. Hence, the name "reverse-osmosis."

Figure P.5 shows the osmotic pressure for several salts as a function of their concentration. Sea water containing 3.5% NaCl will have an osmotic pressure close to 400 psi (25 bar). In practice, pressures of 1,000 psi are used in the reverse osmosis of sea water.

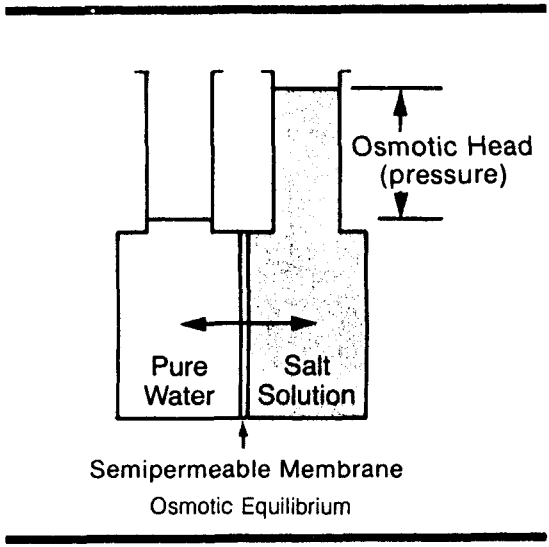


Figure P.3: Osmosis.

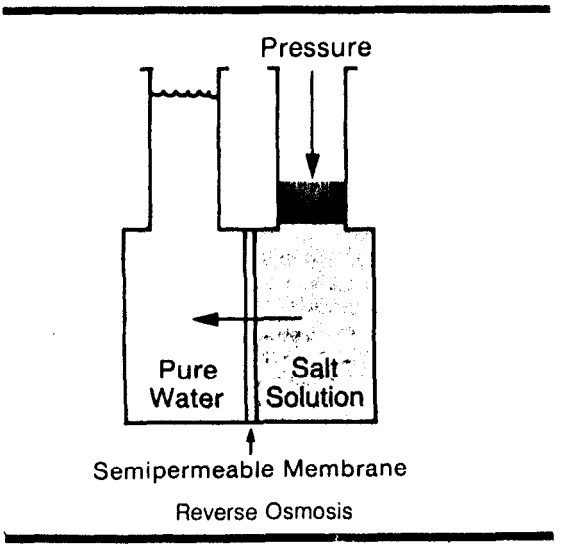


Figure P.4: Reverse osmosis.

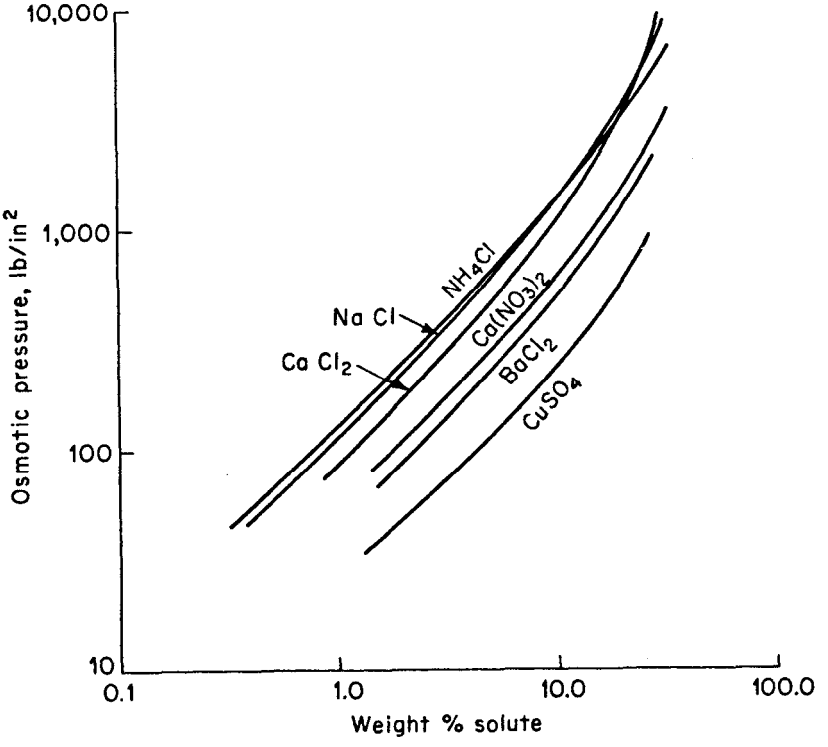


Figure P.5: Variation of osmotic pressure with salt concentration.

It has been estimated that the current worldwide membrane/equipment market is 1.6 billion dollars annually (including hemodialysis). New applications in the emerging biotechnology field along with expanded use in waste treatment promise rapid growth in the closing years of this century. It is hoped that this volume will make a significant contribution to understanding the potential and limitations of membrane technology.

Pleasanton, California
October 1989

M.C. Porter
Editor

Contents

1. **SYNTHETIC MEMBRANES AND THEIR PREPARATION** 1
Heiner Strathmann
Introduction 1
Definition of a Membrane 2
Fluxes and Driving Forces in Membrane Separation Processes 2
Discussion of Technical Relevant Synthetic Membranes Methods of Their Preparation 4
Neutral Microporous Membranes 4
Symmetric Microporous Sintered Membranes 4
Stretched Membranes 6
Capillary Pore Membranes 7
Symmetric Microporous Phase Inversion Membranes 9
Symmetric Microporous Phase Inversion Membranes from Inorganic Materials 11
Asymmetric Microporous Membranes 12
Preparation Procedures of Asymmetric Membranes 13
The Formation Mechanism of Microporous Symmetric or Asymmetric Membranes 13
The Phase Separation Process and Its Relation to the Formation Mechanism of Microporous Membranes 14
Phenomenological Description of Phase Separation 15
Mathematical Description of Phase Separation 18
General Observations Concerning Structures and Properties of Phase Inversion Membranes 20
Rationalization of the Various Membrane Preparation Procedures 29
Homogeneous Membranes 37
Homogeneous Polymer Membranes 37
Homogeneous Metal and Glass Membranes 37
Liquid Membranes 38

Ion-Exchange Membranes 39
Composite Membranes 45
Preparation Procedures of Composite Membranes 45
Industrial Scale Membrane Production 49
Membrane Modules and Their Fabrication 50
Membrane Manufacturing Equipment 53
Future Developments 56
References 56

2. MICROFILTRATION 61
Mark C. Porter
Introduction 61
Membrane Structure and Fabrication 62
Tortuous-Pore Membranes 64
Phase-Inversion Process 64
Stretching Process 64
Thermal-Phase-Inversion Process 65
Capillary-Pore Membranes 66
Pore Size Determination 70
Challenge Tests 70
Bubble-Point Test 71
Mercury Intrusion Test 77
Other Methods 77
Flow Permeability Test 77
Smoke DOP Test 78
BET Adsorption Data 78
Retention Characteristics 78
Bacteria Retention and Bubble Point 78
Retention of Deformable Particles 82
Retention by Adsorption 82
Retention by "Charged" Membranes 83
Aerosol Retention 86
Direct Interception 88
Inertial Impaction 88
Diffusional Deposition 88
Membrane Plugging and Throughput 90
Membrane Dirt-Loading Capacity 90
Prefilters 90
Effect of Filtration Rate on Throughput 95
Backwashing 99
Cross-Flow Filtration 99
Membrane Configuration 106
Plate and Frame Units 106
Pleated Cartridges 106
Tubular/Hollow-Fiber Modules 113
Applications 114
Through-Flow Filtration Applications 114
Sterilization and Particle Removal (Pharmaceuticals) 114

Sterilization and Particle Removal (Beverages) 117
Particle Removal (Semiconductor Process Fluids) 119
Particle Removal (Nuclear Power Industry) 124
Cross-Flow Filtration Applications 124
Removal of Heavy Metals 124
Industrial Laundry Wastewater 125
Plasmapheresis 126
Cell Harvesting/Washing 128
Continuous Cell Culture 131
Prefiltration for UF 131
Membrane Distillation 132
Summary and Forecast 134
References 134

3. ULTRAFILTRATION 136
Mark C. Porter
Introduction 136
Membrane Structure and Fabrication 138
Procedure for Casting Flat-Sheet Membranes 140
Procedure for Casting Tubes 144
Casting Variables for Tubes and Sheets 144
Procedure for Spinning Hollow Fibers 149
Spinning Variables for Hollow Fibers 152
Preparation of Inorganic Membranes 153
Dynamic Membranes 153
Ceramic Membranes 154
Pore Size Determination 155
Molecular Weight Cut-off and Pore Size 155
Retention of Spherical and Linear Molecules 157
Maximum Pore Size and Effective Pore Size 158
Retention Characteristics 159
Adsorption Losses 159
"Charged" Membranes 161
Effect of Pressure 161
Fractionation of Solutes 164
Membrane Flux with Concentration Polarization 166
Gel-Polarization 167
Effect of Pressure 167
Effect of Concentration 171
Effect of pH 173
Evaluation of the Mass-Transfer Coefficient 174
Laminar Flow 174
Turbulent Flow 176
Theoretical Prediction of Flux 179
Macromolecular Solutions 179
Colloidal Suspensions 180
Tubular Pinch Effect 186
Augmented Cross-Flow Effects 192

Centrifugal Force 192
Electric Field 192
Effect of Temperature 195
Membrane Fouling; Flux Decay and Restoration 198
Effect of Cross-Flow Velocity 199
Effect of Pressure 200
Effect of Membrane Surface Treatments 200
Membrane Configuration 202
Tubes 202
Hollow Fibers 205
Plate and Frame Units 208
Spiral Wound Modules 212
UF Plant Design 214
Mode of Operation 214
Optimum Recirculation Rate 216
Applications 217
Ultrapure Water 218
Semiconductor Industry 218
Pharmaceutical Industry 221
Electrocoat Paint 222
Oil-Water Separations 224
Reclamation of Waste Lubricating Oil 226
Decontamination of Crude Oil 227
PVA Recovery 227
Dyestuff Recovery and Purification 229
Latex Concentration /Recovery 229
Removal of Heavy Metals 230
Pulp and Paper Waste Treatment 230
Dairy Applications 232
Cheese Whey Protein Recovery 232
Milk Concentration 236
Food and Beverage Applications (Non-Dairy) 237
Soy Whey 237
Egg White 237
Gelatin 238
Fruit Juice 238
Wine 240
Beer 240
Corn Starch 241
Pharmaceutical and Biotechnology Applications 241
Cell Harvesting 242
Enzyme Concentration and Purification 242
Blood Plasma Processing 242
Diafiltration 243
Virus Concentration 247
Enzyme Reactors 247
Membrane Fermentors 252
Waste Treatment 254

Summary . . . 255
References . . . 256

4. REVERSE OSMOSIS . . . 260
Richard G. Sudak
Introduction . . . 260
Basic Process Considerations . . . 263
Reverse Osmosis Membranes . . . 270
Membrane Packaging . . . 274
Plate and Frame . . . 274
Spiral Wound . . . 274
Tubular . . . 277
Hollow Fine Fiber . . . 279
Dynamic Membranes . . . 281
Plant Design . . . 281
Pretreatment Section . . . 283
Reverse Osmosis Section . . . 286
Posttreatment Section . . . 290
Industrial Reverse Osmosis at a Refinery . . . 290
Reverse Osmosis and Ion Exchange . . . 296
Reverse Osmosis and Pollution Control . . . 298
Reverse Osmosis and Seawater Desalination . . . 299
General Applications of Reverse Osmosis . . . 302
Costs of Reverse Osmosis . . . 303
Future Projections . . . 305
References . . . 305

5. THIN FILM COMPOSITE REVERSE OSMOSIS MEMBRANES . . . 307
Robert J. Petersen and John E. Cadotte
Cellulose Acetate Membranes . . . 309
Microporous Polysulfone Supports for Composite Membranes . . . 311
NS-100 Composite Membrane . . . 314
PA-300 and RC-100 Membranes . . . 316
Other Interfacial Membranes Based on Polymeric Amines . . . 318
Interfacial Polymerization with Monomeric Amines:
NS-300 Membrane . . . 320
NF-40 Composite Membrane . . . 323
NTR-7250 Composite Membrane . . . 324
FT-30 Composite Membrane . . . 327
NF-50 Composite Membrane . . . 332
Mechanism of Interfacial Membrane Formation . . . 332
Sulfonated Polymer Composites: NS-200 Membrane . . . 333
PEC-1000 Membrane . . . 335
Sulfonated Polysulfone Membranes . . . 338
Plasma Polymerization in Composite Membrane Fabrication . . . 340
Solrox 0200 Membrane . . . 340
Miscellaneous Composite Reverse Osmosis Membranes . . . 342
Advantages of the Composite Membrane Approach . . . 343
References . . . 344

6. PROCESS DESIGN AND OPTIMIZATION 349
Robert Rautenbach
Introduction–Mass Transport at the Membrane Surface 349
The Local Mass Transport 349
Influence of the Asymmetric Structure of Membranes 351
Change of Conditions Along the Membrane 353
Module Concepts and Design 354
The Hollow Fiber Module 354
Cascades 360
Definitions 361
Cascades Without Reflux 364
Reflux Cascades 364
Constant Reflux 364
Constant Cut Rate, Variable Reflux 364
The "Equilibrium Curve" 367
Complete Mixing of Feed and/or Permeate 367
Membrane Column 368
Processes 374
Seawater Desalination by RO 374
Total Desalination of Brackish Water 376
Automotive Industry–Combination of UF, Cross Flow Filtration and Evaporation for Recycling of Detergents and Process Water 382
Galvanic Industry–Treatment of Effluents 384
Gas Permeation 387
Pervaporation 390
References 399

7. ENZYME MEMBRANE REACTORS AND MEMBRANE FERMENTORS 401
Enrico Drioli, Gabriele Iorio and Gerardo Catapano
Introduction 401
List of Symbols 404
Enzyme Membrane Reactors (EMR) 409
Dynamic Enzyme Gel Layer Reactors 426
Membrane Segregated Enzyme Reactors 439
Reactors with Enzymes Segregated in the Lumen of Hollow Fibers 440
Reactors with Enzymes within the Pores of Asymmetric Membranes 445
Tube and Shell Membrane Reactors with the Biocatalyst on the Shell Side 451
Perspectives 455
Membrane Bound Enzymes in Continuous-Flow Systems 456
Self-Cleaning Enzymatic Ultrafiltration Membranes 465
Membrane Fermentors 466
Cell Recycle Fermentors 468
Membrane Segregated Fermentors 473

Complex Fermentation Systems 475
References 476

8. ELECTRODIALYSIS 482
Thomas A. Davis
Introduction 482
Ion-Exchange Membranes 483
Membrane Types 484
Heterogeneous 485
Homogeneous 486
Membrane Properties 486
Water Transport 487
ED Stacks 487
Design Considerations 487
Staging of ED Stacks 490
Applications of ED 490
Bipolar Membranes 494
Electrodes and Stack Power 496
Electrode Reactions and Materials 496
Electrode Isolation 498
Power Supplies 500
Concentration Polarization 502
Membrane Fouling 507
Cost of ED 509
References 509

9. COUPLED TRANSPORT MEMBRANES 511
Richard Baker and Ingo Blume
Introduction 511
History and Background 512
Counter Transport and Co-Transport 515
Theory 517
Characteristics of Coupled Transport Membranes 520
Concentration Effects 521
Feed and Product Metal Ion Concentration Effects 523
pH and Metal Ion Effects 525
Complexing Agent Effects 526
Interfacial Reaction Rate Effects 531
Concentration Polarization Effects 532
Coupled Transport Complexing Agents 537
Membrane System Applications and Design 541
Applications 541
Copper Recovery 541
Cobalt and Nickel Recovery 542
Uranium Recovery 543
Electroplating Rinse Waters 543
Copper Etchant Baths 545
Phenol and Ammonia Recovery 547

Supported Liquid Membranes Process Design 547
Emulsion Liquid Membranes Process Design 552
The Future 555
References 555

10. THE SEPARATION OF GASES BY MEMBRANES 559
A. Keith Fritzsche and James E. Kurz
Introduction 559
A Short History 559
Theory of Gas Transport in Membranes 561
Porous Membranes 561
Non-Porous Membranes 563
Rubbery Polymers 564
Glassy Polymers 565
Engineering Aspects 570
Preparation of Membranes for Gas Separation 574
Permea's (Monsanto) Composite Membrane 574
Dry Cellulose Acetate Membranes 578
Composite Polyimide Membranes 579
Polyolefin Membranes for Air Separation 581
Other Membranes 581
Membrane Testing and Evaluation 582
Future 582
Applications of Gas Separating Membranes 582
Hydrogen Recovery 583
Carbon Dioxide Separation 588
Oxygen/Nitrogen Separation 589
Dehydration 590
Other Separations 590
References 591

INDEX 594

1

Synthetic Membranes and Their Preparation

Heiner Strathmann

INTRODUCTION

In recent years, membranes and membrane separation techniques have grown from a simple laboratory tool to an industrial process with considerable technical and commercial impact.[1] Today, membranes are used on a large scale to produce potable water from the sea by reverse osmosis, to clean industrial effluents and recover valuable constituents by electrodialysis, to fractionate macromolecular solutions in the food and drug industry by ultrafiltration,[2] to remove urea and other toxins from the blood stream by dialysis in an artificial kidney, and to release drugs such as scopolamin, nitroglycerin, etc. at a predetermined rate in medical treatment.[3] Although membrane processes may be very different in their mode of operation, in the structures used as separating barriers, and in the driving forces used for the transport of the different chemical components, they have several features in common which make them attractive as a separation tool. In many cases, membrane processes are faster, more efficient and more economical than conventional separation techniques. With membranes, the separation is usually performed at ambient temperature, thus allowing temperature-sensitive solutions to be treated without the constituents being damaged or chemically altered. This is important in the food and drug industry and in biotechnology where temperature-sensitive products have to be processed.[4] Membranes can also be "tailor-made" so that their properties can be adjusted to a specific separation task.

Membrane science and technology is interdisciplinary, involving polymer chemists to develop new membrane structures; physical chemists and mathematicians to describe the transport properties of different membranes using mathematical models to predict their separation characteristics; and chemical engineers to design separation processes for large scale industrial utilization. The most important element in a membrane process, however, is the membrane itself. To

gain an understanding of the significance of the various structures used in different separation processes a brief discussion of the basic properties and functions of membranes, and the driving forces and fluxes involved is essential.

Definition of a Membrane

A precise and complete definition of a membrane which covers all its aspects is rather difficult, even when the discussion is limited to synthetic structures as in this outline. In the most general sense, a synthetic membrane is a barrier which separates two phases and restricts the transport of various chemical species in a rather specific manner.[5] A membrane can be homogeneous or heterogeneous, symmetric or asymmetric in structure; it may be solid or liquid; it may be neutral, may carry positive or negative charges, or may be bipolar. Its thickness may vary between less than 100 nm to more than a centimeter. The electrical resistance may vary from several megohms to a fraction of an ohm. Mass transport through a membrane may be caused by convection or by diffusion of individual molecules, induced by an electric field, or a concentration, pressure or temperature gradient.

The term "membrane", therefore, includes a great variety of materials and structures, and a membrane can often be better described in terms of what it does rather than what it is. Some materials, though not meant to be membranes, show typical membrane properties, and in fact are membranes, e.g., protective coatings, or packaging materials. All materials functioning as membranes have one characteristic property in common: they restrict the passage of various chemical species in a very specific manner.

Fluxes and Driving Forces in Membrane Separation Processes

Separations in membrane processes are the result of differences in the transport rates of chemical species through the membrane interphase. The transport rate is determined by the driving force or forces acting on the individual components and their mobility and concentration within the interphase. The mobility is primarily determined by the solute's molecular size and the physical structure of the interphase material, while the concentration of the solute in the interphase is determined by chemical compatibility of the solute and the interphase material, the solute's size, and the membrane structure. The mobility and concentration of the solute within the interphase determine how large a flux is produced by a given driving force.

In membrane separation processes, there are three basic forms of mass transport. The simplest form is the so-called "passive transport". Here, the membrane acts as a physical barrier through which all components are transported under the driving force of a gradient in their electrochemical potential. Gradients in the electrochemical potential of a component in the membrane interphase may be caused by differences in the hydrostatic pressure, the concentration, the temperature, or the electrical potential between the two phases separated by the membrane. The second form of mass transport through the membrane interphase is the so-called "facilitated" transport. Here, the driving force for the transport of the various components is again the gradient in their electrochemical potential across the membrane. The different components, however, are coupled to a specific carrier in the membrane phase. Facilitated transport,

therefore, is a special form of the passive transport. Completely different, however, is the third form of mass transport through membranes. It is generally referred to as "active" transport. Here, various components may be transported against the gradient of their electrochemical potential. The driving force for the transport is provided by a chemical reaction within the membrane phase. Active transport is coupled with a carrier in the membrane interphase and is found mainly in the membranes of living cells.[6] It has, to date, no significance in synthetic membranes.

The transport of mass in a membrane is a nonequilibrium process and is conventionally described by phenomenological equations such as Fick's law which relates the fluxes of matter to the corresponding driving forces, i.e., a concentration gradient. The constant of proportionality is the diffusion coefficient. Driving forces in some membrane processes may be interdependent, giving rise to new effects. Thus, a concentration gradient across a membrane may result in not only a flux of matter, but, under certain conditions, also in the buildup of a hydrostatic pressure difference; this phenomenon is called osmosis. Similarly, a gradient in hydrostatic pressure may lead to a concentration gradient as well as a volume flow through the membrane; this phenomenon is called reverse osmosis. Frequently, fluxes of individual components are coupled, i.e., the flow of one component causes a flow of another.[7] One example of the coupling of fluxes is the transport of bound water with an ion which is driven across a membrane by an electrical potential gradient.

For membrane separation processes, only driving forces which induce a significant flux of matter are of practical importance. These driving forces are hydrostatic pressure, concentration, and electrical potential differences. These driving forces can also lead to the separation of chemical species.

(a) A hydrostatic pressure difference between two phases separated by a membrane leads to a separation of chemical species when the hydrodynamic permeability of the membrane is different for different components.

(b) A concentration difference between two phases separated by a membrane leads to a separation of various chemical species when the diffusivity and the concentration of the various chemical species in the membrane are different for different components.

(c) A difference in the electrical potential between two phases separated by a membrane leads to a separation of various chemical species when the differently charged particles show different mobilities and concentrations in the membrane.

The permeabilities of different components in a membrane depend on the mechanism by which the components are transported. For example, in homogeneous polymer membranes, the various chemical species are transported under a concentration or pressure gradient by diffusion. The permeability of these membranes is determined by the diffusivities and concentrations of the various components in the membrane matrix and the transport rates are, in general, relatively slow. In porous membrane structures, however, mass is transported under the driving force of a hydrostatic pressure difference via viscous flow and, in gen-

eral, permeabilities are significantly higher than in diffusion-controlled membrane transport. In electrically charged membranes, usually referred to as ion-exchange membranes, ions carrying the same charge as the membrane material are more or less excluded from the membrane phase and, therefore, unable to penetrate the membrane.[8] The type of membrane and driving force required for a certain mass separation will depend on the specific properties of the chemical species in the mixture.

For a given driving force, the flux through a unit membrane area is always inversely proportional to the thickness of the selective barrier. For economic reasons, membranes should in general be as thin as possible.

DISCUSSION OF TECHNICAL RELEVANT SYNTHETIC MEMBRANES AND METHODS OF THEIR PREPARATION

Although synthetic membranes show a large variety in their physical structure and chemical nature, they can conveniently be classified in five basic groups: (1) microporous media, (2) homogeneous solid films, (3) asymmetric structures, (4) electrically charged barriers and (5) liquid films with selective carriers. This classification, however, is rather arbitrary and there are many structures which would fit more than one of the abovementioned classes, e.g., a membrane may be microporous, asymmetric in structure, and carry electrical charges. Any other classification of synthetic membranes, e.g., according to their application or methods of preparation, would serve the same purpose of phenomenologically categorizing the various types of synthetic membranes.

Neutral Microporous Membranes

The neutral, microporous films represent a very simple form of a membrane which closely resembles the conventional fiber filter as far as the mode of separation and the mass transport are concerned. These membranes consist of a solid matrix with defined holes or pores which have diameters ranging from less than 2 nm to more than 20 μm. Separation of the various chemical components is achieved strictly by a sieving mechanism with the pore diameters and the particle sizes being the determining parameters. Microporous membranes can be made from various materials, such as ceramics, graphite, metal or metal oxides, and various polymers. Their structure may be symmetric, i.e., the pore diameters do not vary over the membrane cross section, or they can be asymmetrically structured, i.e., the pore diameters increase from one side of the membrane to the other by a factor of 10 to 1,000. The properties and areas of application of various microporous filters are summarized in Table 1.1.

Symmetric Microporous Sintered Membranes. Sintered membranes are the simplest in their function and in the way they are prepared. The structure of a typical sintered membrane is shown in the scanning electron micrograph of Figure 1.1. This photograph shows a microporous membrane made out of polytetrafluoroethylene by pressing a fine powder into a film or plate of 100 to 500 μm thickness and then sintering the film at a temperature which is just below the melting point of the polymer. This process yields a microporous structure of relatively low porosity, in the range of 10 to 40%, and a rather irregular pore structure with a very wide pore size distribution.

Table 1.1: Microporous Membranes, Their Preparation and Application

Membrane type	Membrane material	Pore size	Manufacturing process	Application
Microporous membrane	Ceramic, metal or polymer powder	0.1 - 20 μm	pressing and sintering of powder	Microfiltration
	Homogeneous polymer sheets (PE, PTFE)	0.5 - 10 μm	stretching of extruded polymer sheets	Microfiltration, burn dressings, artificial blood vessels
	Homogeneous polymer sheets (PC)	0.02 - 10 μm	track-etching	Microfiltration
	Polymer solution (CN, CA)	0.01 - 5 μm 2 nm - 5 μm	phase inversion	Microfiltration, ultrafiltration, sterilization

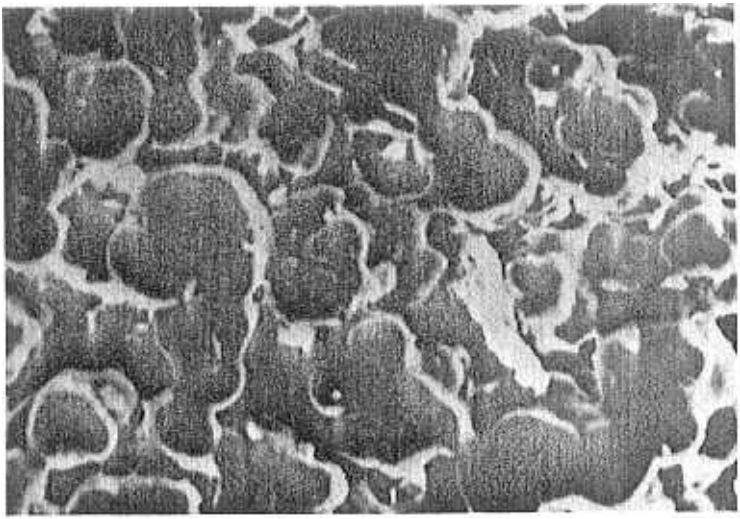


Figure 1.1: SEM of a microporous sintered membrane prepared from a PTFE-powder.

Sintered membranes are made on a fairly large scale from ceramic materials, glass, graphite and metal powders such as stainless steel and tungsten.[9] The particle size of the powder is the main parameter determining the pore sizes of the final membrane, which can be made in the form of discs, candles, or fine-bore tubes. Sintered membranes are used for the filtration of colloidal solutions and suspensions. This type of membrane is also marginally suitable for gas separation. It is widely used today for the separation of radioactive isotopes, especially uranium.

Stretched Membranes. Another relatively simple procedure for preparing microporous membranes is the stretching of a homogeneous polymer film of partial crystallinity. This technique is mainly employed with films of polyethylene or polytetrafluoroethylene which have been extruded from a polymer powder and then stretched perpendicular to the direction of extrusion.[10,11] This leads to a partial fracture of the film and relatively uniform pores with diameters of 1 to 20 μm. A typical stretched membrane prepared from tetrafluoroethylene is shown in the scanning electron micrograph of Figure 1.2.

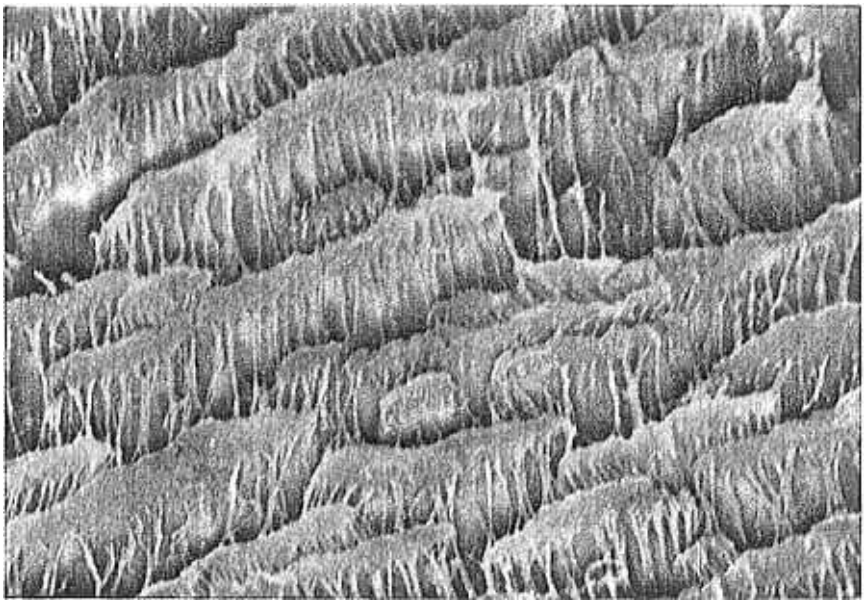


Figure 1.2: SEM of a microporous membrane prepared by stretching an extruded PTFE-film perpendicular to the direction of extrusion.

These membranes, which have a very high porosity, up to 90%, and a fairly regular pore size are now widely used for microfiltration of acid and caustic solutions, organic solvents, and hot gases. They have to a large extent replaced the sintered materials used earlier in this application. Stretched membranes can be produced as flat sheets as well as tubes and capillaries. The stretched membrane made out of polytetrafluoroethylene is frequently used as a water repellent textile for clothing, such as parkas, tents, sleeping bags, etc. This membrane type has, because of its very high porosity, a high permeability for gases and vapors, but, because of the hydrophobic nature of the basic polymer, is up to a certain hydrostatic pressure completely impermeable to aqueous solutions. Thus, the membrane is repellent to rain water but permits the water vapor from the body to permeate. More recently, this membrane has also been used for a novel process, generally referred to as membrane distillation, i.e., to remove ethanol from

fermentation broths or wine and beer to produce low alcohol products[12] and for desalination of seawater. These membranes are also used for desalination of saline solutions and in medical applications such as burn dressings and artificial blood vessels.

Capillary Pore Membranes. Microporous membranes with very uniform, nearly perfectly round cylindrical pores are obtained by a process generally referred to as track-etching.[13] The membranes are made in a two step process. During the first step, a homogeneous 10 to 15 μm thick polymer film is exposed to collimated, charged particles in a nuclear reactor. As particles pass through the film, they leave sensitized tracks where the chemical bonds in the polymer backbone are broken. In the second step, the irradiated film is placed in an etching bath. In this bath, the damaged material along the tracks is preferentially etched forming uniform cylindrical pores. The entire process is schematically shown in Figure 1.3. The pore density of a track-etched membrane is determined by the residence time in the irradiator, while the pore diameter is controlled by the residence time in the etching bath. The minimum pore diameter of these membranes is approximately 0.01 μm. The maximum pore size that can be achieved in track-etched membranes is determined by the etching procedure. The polymer will not only be dissolved along the sensitized track left by the penetrating particle but also on both surfaces of the film. Thus, with exposure time in the etching medium the pore sizes increase and the thickness of the film is correspondingly reduced. The scanning electron micrograph in Figure 1.4 shows a typical track-etched polycarbonate membrane. Capillary pore membranes are prepared today mainly from polycarbonate and polyester films. The advantage of these polymers is that they are commercially available in very uniform films of 10 to 15 μm thickness which is the maximum penetration depth of collimated particles obtained from a nuclear reactor which have an energy about 0.8 to 1 MeV. Particles with higher energy, up to 10 MeV, may be obtained in an accelerator. They are used today to irradiate thicker polymer films, up to 50 μm thickness, or inorganic materials such as mica.[14] However, these membranes are not yet available on a commercial basis.

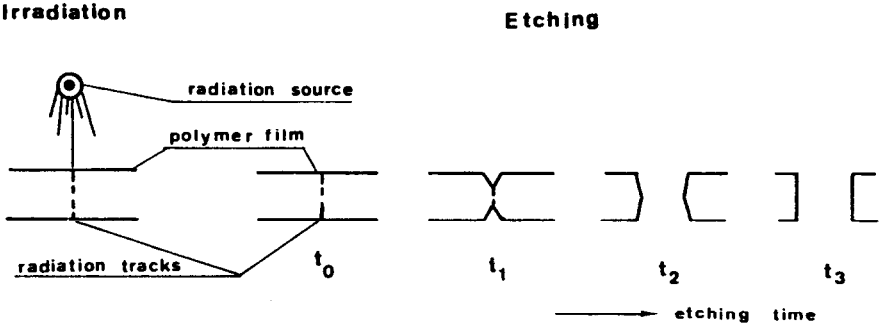


Figure 1.3: Schematic diagram illustrating the preparation of capillary pore membranes by a track-etching process.

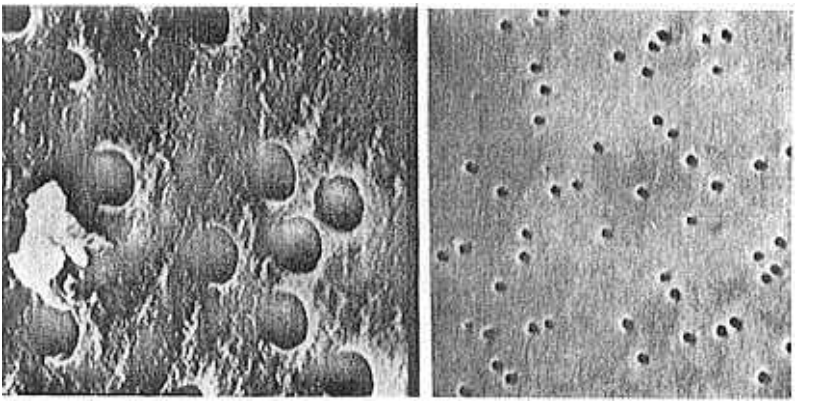


Figure 1.4: SEM of the surface of a capillary pore polycarbonate membrane.

Because of their narrow pore size distribution and low tendency to plug, capillary pore membranes made from polycarbonate and polyester have found application on a large scale in analytical chemistry and microbiological laboratories, and in medical diagnostic procedures.[15] On an industrial scale, capillary pore membranes are used for the production of ultrapure water for the electronic industry. Here, they show certain advantages over other membrane products because of their short "rinse down" time and good long-term flux stability. Because of their surface filter characteristics, particles retained by the membranes can be further monitored by optical or scanning electron microscopy. Figure 1.5 shows a scanning electron micrograph of asbestos fibers accumulated on a capillary pore membrane in an air pollution control application. The membranes are also used in standard clinical tests for red blood cell deformability studies.

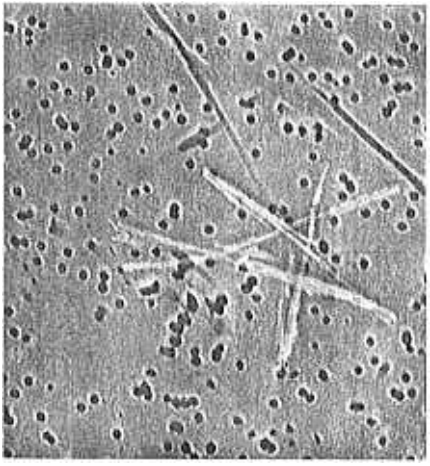


Figure 1.5: SEM of asbestos filter accumulated on the surface of a capillary pore membrane.

Human red blood cells have a diameter of approximately 6 to 8 μm. The human body, however, contains capillaries approximately 3 μm in diameter. To pass through these vessels the blood cells have to deform correspondingly. Healthy cells will do this readily but malignant cells will not. By filtering blood through a 3 μm capillary pore membrane certain blood deficiencies can be monitored.[16]

Symmetric Microporous Phase Inversion Membranes. The most important commercially available, symmetric, microporous membranes are prepared by the so-called phase inversion process.[17] In this process, a polymer is dissolved in an appropriate solvent and spread as a 20 to 200 μm thick film. A precipitant such as water is added to this liquid film from the vapor phase, causing separation of the homogeneous polymer solution into a solid polymer and a liquid solvent phase. The precipitated polymer forms a porous structure containing a network of more or less uniform pores. A microporous cellulosic membrane made by phase inversion is shown in the scanning electron micrograph of Figure 1.6. This type of membrane can be made from almost any polymer which is soluble in an appropriate solvent and can be precipitated in a nonsolvent.[18] By varying the polymer, the polymer concentration, the precipitation medium, and the precipitation temperature, microporous phase inversion membranes can be made with a very large variety of pore sizes (from less than 0.1 to more than 20 μm) with varying chemical, thermal, and mechanical properties. These membranes were originally prepared from cellulosic polymers by precipitation at room temperature in an atmosphere of approximately 100% relative humidity.[19] Lately, symmetric microporous membranes are also prepared from Nylon 66, Nomex, polysulfone, and polyvinylidene difluoride by precipitation of a cast polymer solution in aqueous liquid.[20]

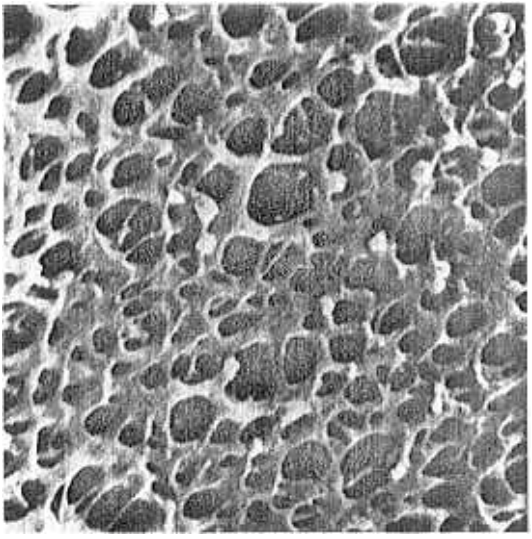


Figure 1.6: SEM of the surface of a microporous cellulose nitrate membrane prepared by precipitation from a homogeneous polymer solution by water vapor precipitation.

Polypropylene or polyethylene can also be used for the preparation of microporous membranes. However, since these polymers are not readily dissolved at room temperature, the preparation technique must be slightly varied. Polypropylene, e.g., is dissolved in an appropriate amine at elevated temperatures. A solution of 20 to 30% polymer is spread at elevated temperature into a film. The precipitation of the polymer, however, is not induced by the addition of a nonsolvent but merely by cooling the solution to a point where a two phase system forms. The resulting open foam structure is shown in Figure 1.7. The pore size depends on polymer concentration, solvent system, solution temperature, and cooling rate. This membrane preparation technique is usually referred to as thermal gelation.[21] It can be applied to metal alloys and glasses as well as polymer solutions.[9]

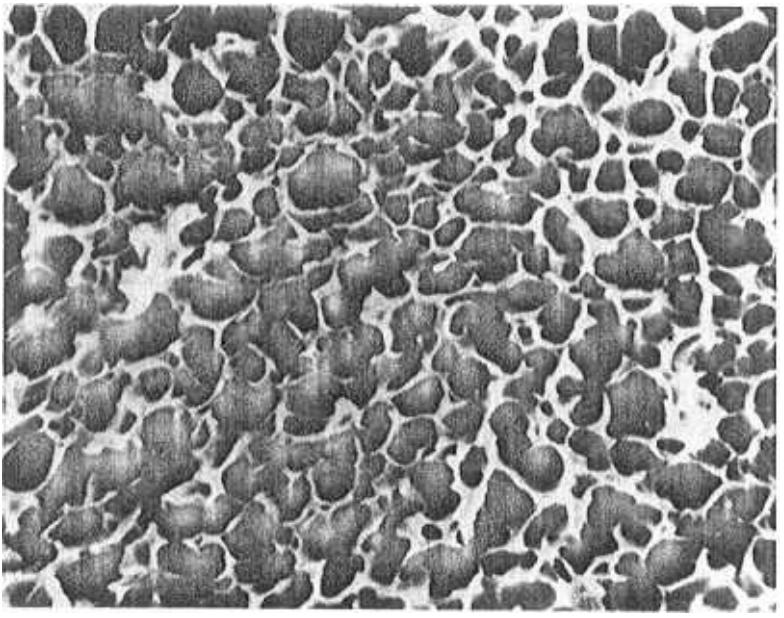


Figure 1.7: SEM of the surface of a microporous polypropylene membrane precipitated by thermal gelation from a hot homogeneous polymer solution.

The symmetric, microporous polymer membranes made by phase inversion are widely used for separations on a laboratory and industrial scale.[22] Typical applications range from the clarification of turbid solutions to the removal of bacteria or enzymes, the detection of pathological components, and the detoxification of blood in an artificial kidney. The separation mechanism is that of a typical depth filter which traps the particles somewhere within the structure. In addition to the simple "sieving" effect, microporous phase inversion membranes often show a high tendency of adsorption because of their extremely large internal surface. They are, therefore, particularly well suited when a complete re-

moval of components, such as viruses or bacteria is desired. They are suited for immobilization of enzymes or even microorganisms to be used in modern biotechnology. They are also widely used for culturing of microorganisms in water quality control tests.[23] In this test, the water is filtered through a membrane which retains all microorganisms. The membrane is then placed on a nutrient pad in an incubator for 24 to 48 hours. During this time, the microorganisms grow into easily visible colonies. Grid marked membranes assist in counting the colony density, which is an indication of water quality. The process is shown in the schematic diagram and the photograph of Figure 1.8.

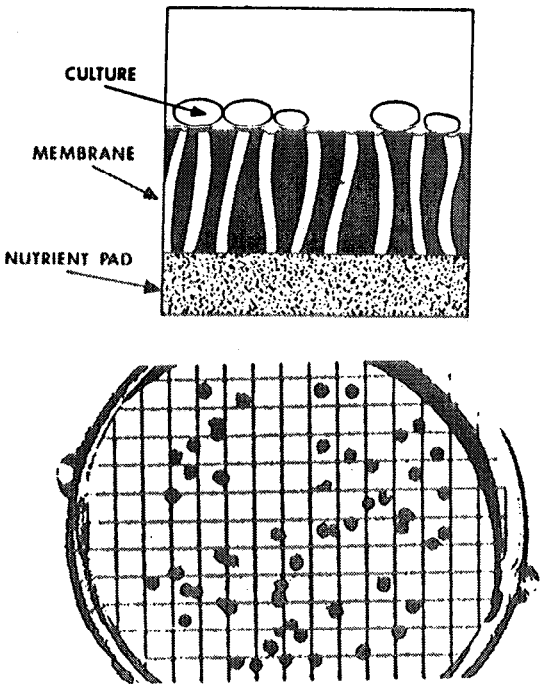


Figure 1.8: SEM of cultured microorganisms in water quality control tests and schematic diagram of the process.

Symmetric Microporous Phase Inversion Membranes from Inorganic Materials. Microporous membranes can also be prepared by phase inversion from glass or metal alloys. The preparation procedure is relatively simple: two different types of glass are homogeneously mixed; then, one glass type is removed by acid or base leaching.[24] Thus, a microporous structure is obtained with well defined pore sizes in the range of a few angstroms to several nanometers. Porous glass membranes can be made in various configurations, such as flat sheet, tubes, and hollow fibers, which are of particular importance because of their high surface area. Microporous metal membranes can be prepared from metal alloys such as Ni-Al-Cr by subsequent leaching of one component. These membranes have found their main application in gas separation processes. While

the microporous metal membranes are mainly used for gas separation tasks, microporous glass membranes have been used mainly for separation of liquid mixtures including desalination of sea and brackish waters, ultrafiltration of wastewater, and in artificial kidneys for detoxification of blood streams.[25]

Asymmetric Microporous Membranes

The most important membrane used today in separation processes is composed of a rather sophisticated asymmetric structure. In this membrane, the two basic properties required of any membrane, i.e., high mass transport rates for certain components and good mechanical strength, are physically separated. An asymmetric membrane consists of a very thin (0.1 to 1 μm) selective skin layer on a highly porous (100 to 200 μm) thick substructure, as indicated in the schematic drawing of Figure 1.9, which shows the cross section of (a) a symmetric and (b) an asymmetric membrane. The very thin skin represents the actual membrane. Its separation characteristics are determined by the nature of the polymer and the pore size while the mass transport rate is determined by the membrane thickness, since the mass transport rate is inversely proportional to the thickness of the actual barrier layer. The porous sublayer serves only as a support for the thin and fragile skin and has little effect on separation characteristics or the mass transfer rate of the membrane. Asymmetric membranes are used primarily in pressure driven membrane processes, such as reverse osmosis, ultrafiltration, or gas separation, since here the unique properties in terms of high mass transfer rates and good mechanical stability can be best utilized.[26]

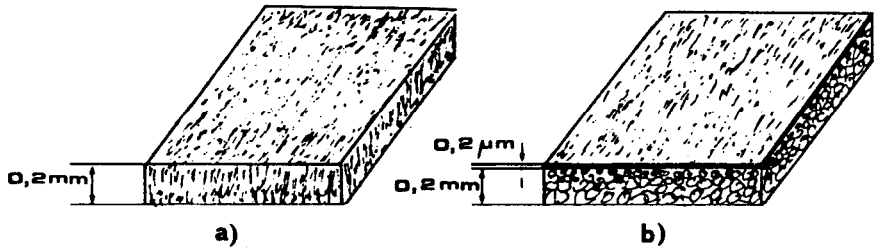


Figure 1.9: Schematic drawing of the cross section of a (a) symmetric and (b) asymmetric membrane.

In addition to high filtration rates, asymmetric membranes are most fouling resistant. Conventional symmetric structures act as depth filters and retain particles within their internal structure. These trapped particles plug the membrane and the flux declines during use. Asymmetric membranes are surface filters and retain all rejected materials at the surface where they can be removed by shear forces applied by the feed solution moving parallel to the membrane surface. The difference in the filtration behavior between a symmetric and an asymmetric membrane is shown schematically in Figure 1.10. Two techniques are used to prepare asymmetric membranes: one utilizes the phase inversion process and the other leads to a composite structure by depositing an extremely thin polymer film on a microporous substructure.

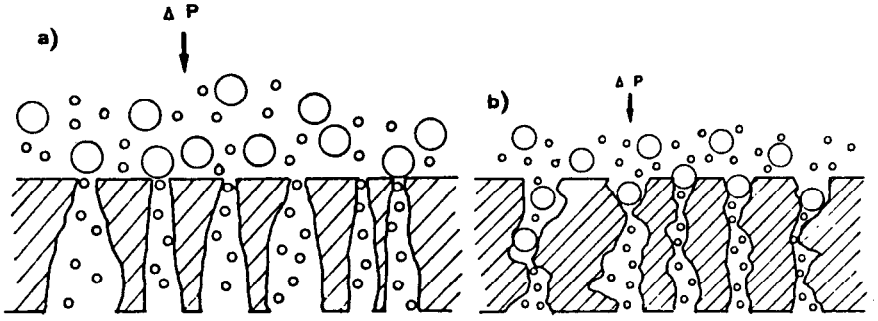


Figure 1.10: Schematic diagram of the filtration characteristics of a (a) symmetric and (b) asymmetric membrane.

Preparation Procedures of Asymmetric Membranes. The development of the first asymmetric phase inversion membranes was a major breakthrough in the development of ultrafiltration and reverse osmosis. These membranes were made from cellulose acetate and yielded fluxes 10 to 100 times higher than symmetric structures with comparable separation characteristics. Asymmetric phase inversion membranes can be prepared from cellulose acetate and many other polymers by the following general preparation procedure:[27]

(1) A polymer is dissolved in an appropriate solvent to form a solution containing 10 to 30 weight % polymer.

(2) The solution is cast into a film of typically 100 to 500 μm thickness.

(3) The film is quenched in a nonsolvent typically water or an aqueous solution.

During the quenching process the homogeneous polymer solution separates into two phases: a polymer-rich solid phase, which forms the membrane structure, and a solvent-rich liquid phase, which forms the liquid-filled membrane pores. Generally, the pores at the film surface, where precipitation occurs first and most rapidly, are much smaller than those in the interior or the bottom side of the film, which leads to the asymmetric membrane structure. There are different variations to this general preparation procedure described in the literature; e.g., Loeb and Sourirajan used an evaporation step to increase the polymer concentration in the surface of the cast polymer solution and an annealing step during which the precipitated polymer film is exposed for a certain time period to hot water of 70° to 80°C.[28]

The Formation Mechanism of Microporous Symmetric or Asymmetric Membranes. The original recipes and subsequent modifications for preparing asymmetric membranes are deeply rooted in empiricism. Detailed descriptions of membrane preparation techniques are given in the literature.[29,30] Only after extensive use of the scanning electron microscope, which provided the necessary structural information, was it possible to rationalize the various parameters for membrane preparation processes. At first, the asymmetric structure was obtained mainly in membranes made from cellulose acetate. But later it became ap-

parent that the process of making skin-type asymmetric membranes by precipitating a polymer solution is just a special case of a general procedure, which Kesting[27] refers to as phase inversion. During a phase inversion process, a one-phase polymer solution is converted into a two-phase system consisting of a solid (polymer-rich) phase which forms the membrane structure and a liquid (polymer-poor) phase which forms the pores in the final membrane.

Phase inversion membranes can be prepared from any polymer mixture which forms, under certain conditions of temperature and composition, a homogeneous solution and separates at a different temperature or composition into two phases. A further condition, however, is that both phases are continuous. If the liquid phase is discontinuous, a closed-cell foam structure will be obtained and if the solid phase is discontinuous, a polymer powder will be obtained instead of a rigid structure.

The actual phase separation can be induced by several means. One technique described in the literature is based on the controlled evaporation of a volatile solvent from a three-component mixture of solvent/precipitant/polymer, causing precipitation as the system becomes enriched in precipitant. This technique was used by Zsigmondy[31] and more recently by Kesting[32] for the preparation of ultrafiltration and reverse osmosis membranes. Alternatively, precipitation of a simple two-component polymer-solvent casting solution can be brought about by imbibing precipitant from the vapor phase. This technique was the basis of the original microporous membranes and is still used commercially today by several companies. Yet, another technique is to bring about precipitation by cooling a casting solution which forms a homogeneous solution only at elevated temperature, e.g., polypropylene dissolved in N,N-bis-(2-hydroxyethyl)tallow amine. This process is called thermal gelation. Thermal gelation is not only applicable to polymers which, because of their poor solubility, would otherwise be inaccessible to the phase inversion membrane preparation techniques; it can also be used for making microporous membranes from glass mixtures and metal alloys in combination with a leaching procedure, as indicated earlier.

The Phase Separation Process and Its Relation to the Formation Mechanism of Microporous Membranes

Detailed recipes given in the literature for the preparation of microporous structures from polymers, metals or glasses seem superficially very different. But in all cases, the basic membrane formation mechanism is governed by similar thermodynamic and kinetic parameters, such as the chemical potentials and diffusivities of the individual components and the Gibb's free energy of mixing of the entire system.[33] Identification and description of the phase separation process is the key to understanding the membrane formation mechanism—a necessity for optimizing membrane properties and structures. The techniques used to induce the phase separation in a homogeneous solution for the preparation of microporous membranes can be related to three basic procedures:

(1) Thermogelation of a homogeneous solution of two or more components;

(2) Evaporation of a volatile solvent from a homogeneous solution of two or more components;

(3) Addition of a nonsolvent or nonsolvent mixture to a homogeneous solution.

All three procedures may result in symmetric microporous structures or in asymmetric structures with a more or less dense skin at one or both surfaces suitable for reverse osmosis, ultrafiltration or microfiltration. The only thermodynamic presumption for all three preparation procedures is that the free energy of mixing of the polymer system under certain conditions of temperature and composition is negative; that is, the system must have a miscibility gap over a defined concentration and temperature range.[34]

Phenomenological Description of Phase Separation. Phase separation due to thermal gelation, evaporation of solvent and addition of nonsolvent can be illustrated with the aid of the phase diagram of a polymer solution.

Thermogelation of a Two-Component Polymer Mixture. The simplest procedure for obtaining a microporous system is by thermogelation of a two component mixture, which at sufficiently high temperature forms a homogeneous solution for all compositions, but at a lower temperature shows a miscibility gap over a wide range of compositions. This behavior is illustrated schematically in Figure 1.11, which shows a phase diagram of a two component mixture of a polymer and a solvent as a function of temperature.

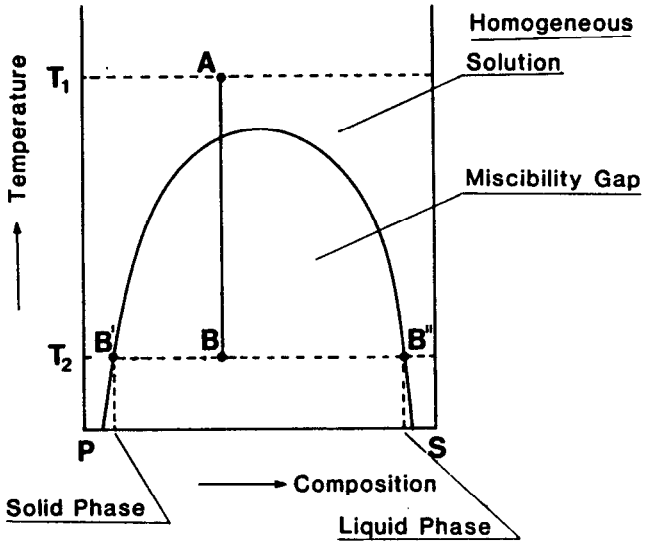


Figure 1.11: Schematic diagram showing the formation of a microporous system by thermal gelation of a two-component mixture exhibiting a miscibility gap at certain conditions of temperature and composition.

The points P and S represent the pure components, polymer and solvent respectively, and points on the line P–S describe mixtures of these two components. If a homogeneous mixture of the composition X_p at a temperature T_1,

as indicated by the point A in Figure 1.11, is cooled to the temperature T_2, as indicated by point B, it will separate into two different phases, the composition of which are indicated by the points B' and B''. The point B' represents the polymer-rich solid phase and the point B'' the solvent-rich, polymer-poor liquid phase. The lines B'-B and B''-B represent the ratio of the amounts of the two phases in the mixture; that is, the overall porosity of the obtained microporous system.

Evaporation of a Volatile Solvent from a Three-Component Polymer Solution. This process utilizes a three-component mixture: a polymer, a volatile solvent and a third component, which by itself is a nonsolvent for the polymer. This three-component mixture is completely miscible over a certain composition range but exhibits a miscibility gap over another composition range, as indicated in Figure 1.12, which represents an isothermal phase diagram of the three components. The corners of the triangle represent the pure components. Boundary lines between any two corners represent mixtures of two components, and any point within the triangle represents a mixture of all three components. Within a certain compositionally defined range of thermodynamic states, all three components are completely miscible, whereas in a different range-the miscibility gap-the system separates into two distinct phases. If the volatile solvent is completely evaporated from a homogeneous mixture of 10% polymer, 60% solvent and 30% nonsolvent, as indicated by point A in Figure 1.12, the composition of the mixture will change from that represented by point A to that represented by point B. At point B, the system consists of only two components: polymer and nonsolvent. Since this point is situated within the miscibility gap, the system is separated into two phases: a polymer-rich phase, indicated by point B' forming the rigid structure, and the phase B'' forming the liquid filled pores of the membrane.

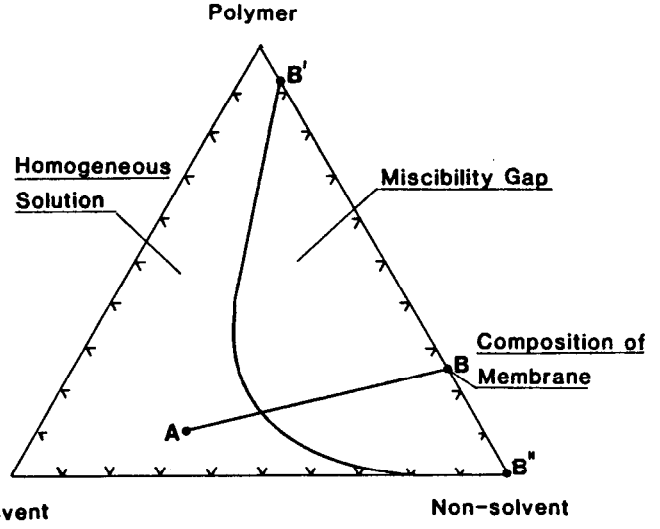


Figure 1.12: Schematic diagram showing the formation of a microporous system by evaporation of a solvent from a three-component mixture exhibiting a miscibility gap at certain conditions of temperature and composition.

Addition of a Nonsolvent to a Homogeneous Polymer Solution. This technique can again be rationalized with the aid of a three-component isothermal phase diagram shown schematically in Figure 1.13. This phase diagram of the three-component mixture exhibits a miscibility gap over a wide range of compositions. If a nonsolvent is added to a homogeneous solution consisting of polymer and solvent, the composition of which is indicated by the point A on the solvent-polymer line, and, if the solvent is removed from the mixture at about the same rate as the nonsolvent enters, the composition of the mixture will change following the line A–B. At point C, the composition of the system will reach the miscibility gap and two separate phases will begin to form: a polymer-rich phase represented by the upper boundary of the miscibility gap and a polymer-poor phase represented by the lower boundary of the miscibility gap. At a certain composition of the three-component mixtures, the polymer concentration in the polymer-rich phase will be high enough to be considered as solid. This composition is represented by point D in Figure 1.13. At this point, the membrane structure is more or less determined. Further exchange of solvent and nonsolvent will lead to the final composition of the membrane, the porosity of which is determined by point B. Point B represents a mixture of the solid polymer-rich phase and the liquid solvent-rich phase as represented by points B' and B" respectively.

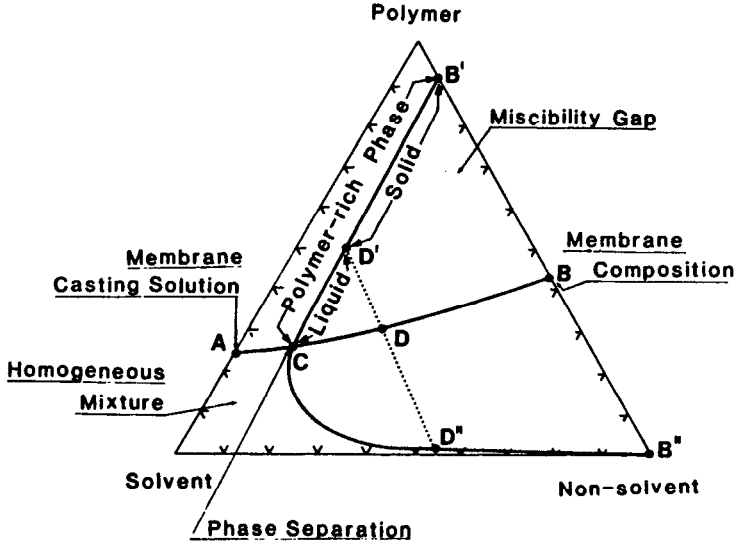


Figure 1.13: Schematic diagram showing the formation of a microporous system by addition of a nonsolvent to a homogeneous polymer solution in a three-component mixture exhibiting a miscibility gap at certain conditions of temperature and composition.

The description of the formation of microporous systems by means of the phase diagrams, as illustrated in Figure 1.11 to 1.13, is based on the assumption of thermodynamic equilibrium. It predicts under what conditions of tem-

perature and composition a system will separate into two phases and the ratio of the two phases in the heterogeneous mixture, i.e., the overall porosity. However, no information is provided about the pore sizes, which are determined by the spatial distribution of the two phases. Equilibrium thermodynamics is not able to offer any explanation about structural variations within the membrane cross section, that is, whether the membrane has a symmetric or asymmetric structure or a dense skin at the surface. These parameters are determined by kinetic effects, which depend on system properties, such as the diffusivities of the various components in the mixture, the viscosity of the solution and the chemical potential gradients which act as driving forces for diffusion of the various components in the mixture. Because these parameters change continuously during the phase separation, which constitutes the actual membrane formation process, no transient states of equilibrium will be achieved. Especially in polymer systems, frozen states will often be obtained that are far from equilibrium and that can be stable for long time periods. The chemical potential and diffusivities of the various components in the system, and their dependencies on composition, temperature, viscosity, etc., are difficult to determine by independent experiments and, therefore, are not readily available. This makes a quantitative description of the membrane formation mechanism nearly impossible. A qualitative description, however, which allows rationalization of the membrane formation and correlation of the various preparation parameters with membrane structures and properties, is possible.[35–39]

Mathematical Description of Phase Separation. The thermodynamic state of a system of two or more components with limited miscibility can be described in terms of the free energy of mixing.[40] At constant pressure and temperature, three different states can be distinguished:

(1) A stable state where all components are miscible in a single phase. In this state, the free energy of mixing is positive

$$\Delta\bar{G} > 0 \qquad (P,T = \text{const}) \tag{1}$$

(2) An unstable state where the homogeneous solution separates spontaneously into two phases which are then in equilibrium. In this state, which is located within the miscibility gap, the free energy of mixing is negative

$$\Delta\bar{G} < 0 \tag{2}$$

(3) An equilibrium state given by the phase boundary composition. In this state, the free energy of mixing is zero

$$\Delta\bar{G} = 0 \tag{3}$$

The free energy of mixing of a system describes the thermodynamic state of the system and thus provides information about the system stability. If a system is unstable and separates in two coexisting phases, transport of individual components has to take place. The transport processes are determined by thermodynamic parameters, which are expressed by driving forces, and by kinetic parameters, which are determined by diffusivities, i.e., the diffusion coefficient. Fick's law relates the diffusion coefficient to concentration gradients. However, the actual driving forces for any mass transport are gradients in the chemical po-

tential of the individual components. The diffusion coefficients of individual components can be related to their chemical potential driving force by:[41]

$$D_i = B_i \left(\frac{\delta \mu_i}{\delta X_i}\right)_{P,T} \tag{4}$$

Here, D_i is the diffusion coefficient of component i, μ_i is its chemical potential and X_i its mol fraction. B_i is a mobility term, which is always positive.

The stable, unstable and equilibrium states of the system are not only characterized by positive, negative or disappearing values of the free energy of mixing but, since the diffusion coefficient is directly related to the chemical potential of the individual components, which again is a function of the Gibb's free energy, the state of a system is also characterized by:

(1) Stable state

$$\left(\frac{\delta^2 \bar{G}}{\delta X^2}\right)_{T,P} > 0 \; ; \; \left(\frac{\delta \mu}{\delta X}\right)_{T,P} > 0 \quad \text{and} \quad D_i = \frac{B_i R T}{X_i}\left(1 + \frac{\delta \ln f_i^S}{\delta \ln X_i}\right) > 0 \tag{5}$$

(2) Unstable state

$$\left(\frac{\delta^2 \bar{G}}{\delta X^2}\right)_{T,P} < 0 \; ; \; \left(\frac{\delta \mu}{\delta X}\right)_{T,P} < 0 \quad \text{and} \quad D_i = \frac{B_i R T}{X_i}\left(1 + \frac{\delta \ln f_i^S}{\delta \ln X_i}\right) < 0 \tag{6}$$

(3) Equilibrium state

$$\left(\frac{\delta^2 \bar{G}}{\delta X^2}\right)_{T,P} = 0 \; ; \; \left(\frac{\delta \mu}{\delta X}\right)_{T,P} = 0 \quad \text{and} \quad D_i = \frac{B_i R T}{X_i}\left(1 + \frac{\delta \ln f_i^S}{\delta \ln X_i}\right) = 0 \tag{7}$$

Here f_i^S is an activity coefficient referring to the pure phase, R is the gas constant and T is the absolute temperature, B_i is a mobility term and X_i the molfraction of the component i.

Equations (4) to (7) indicate that in the case of spontaneous demixing the diffusion coefficient will become negative, i.e., the individual components will diffuse against their concentration gradients. Since:

$$\mu_i = \mu_i^o + R T \ln X_i + R T \ln f_i^S \tag{8}$$

$$\left(\frac{\delta \mu_i}{\delta X_i}\right)_{P,T} = \frac{\delta R T \ln X_i}{\delta X_i} + \frac{\delta R T \ln f_i^S}{\delta X_i} \tag{9}$$

$$\left(\frac{\delta \mu_i}{\delta X_i}\right)_{P,T} = \frac{R T}{X_i}\left(1 + \frac{\delta \ln f_i^S}{\delta \ln X_i}\right) \tag{10}$$

$$\left(\frac{\delta \bar{G}}{\delta X_i}\right)_{P,T} = \mu_i \; ; \; \left(\frac{\delta^2 \bar{G}}{\delta X_i 2}\right)_{P\,T} = \left(\frac{\delta \mu_i}{\delta X_i}\right)_{P,T} \tag{11}$$

The chemical potentials of the individual components and their dependence on concentration of other species in a mixture and the mobility term B and its dependence on viscosity determine the phase separation process.

Many aspects of the formation of symmetric or asymmetric membranes can be rationalized by applying the basic thermodynamic and kinetic relations of phase separation. There are, however, other parameters-such as surface tension, polymer relaxation, sol and gel structures-which are not directly related to the thermodynamics of phase separation but which will have a strong effect on membrane structures and properties. A mathematical treatment of the formation of porous structures is difficult. But many aspects of membrane structures and the effect of various preparation parameters can be qualitatively interpreted.

General Observations Concerning Structures and Properties of Phase Inversion Membranes. Before going into any detailed discussion of the formation mechanism of microporous membranes, several general observations concerning the membrane structure, preparation procedures, and mass transport properties are described.

Typical Membrane Structures. Using scanning electron microscope techniques, the four different structures shown in Figures 1.14 (a) to (d) can be observed for phase inversion membranes. Photograph (a) shows a cross section of a microfiltration membrane prepared from a cellulose nitrate solution by precipitation in a humidity controlled environment. The membrane shows a "sponge"-like structure with no skin on the bottom or top surface. Photograph (b) shows a cross section of a typical ultrafiltration membrane prepared from a polyamide solution and precipitated in water by immersing the polymer solution into a water bath. The membrane shows a "finger"-type structure with a dense skin at the surface and large pores penetrating the entire membrane cross section. The pores increase in diameter from the top to the bottom side. Photograph (c) shows the cross section of a typical reverse osmosis membrane prepared from a polyamide solution and precipitated in water by immersing the polymer solution into a water bath. The membrane shows a sponge-type structure with a dense skin at the surface and a porous structure underneath with increasing pore diameter from the top to the bottom side of the membrane. The only differences in the preparation procedures of the membranes shown in photographs (b) and (c) are the polymer concentration and the precipitation temperature. Photograph (d) shows the cross section of a reverse osmosis membrane prepared from a polyamide solution and precipitated in a water-solvent mixture. The membrane shows a sponge-type structure with a dense skin at the surface and a porous structure underneath with a relatively uniform pore size distribution over the entire cross section. Membranes with this type of structure can usually be dried without changing their mass transport properties. Looking at the fine structure of a membrane very often two types of structures may be obtained as indicated in Figure 1.15 which shows scanning electron micrographs of the structures of two phase inversion membranes. Figure 1.15 (a) shows a sponge-type structure consisting of spherical cells. This structure is often obtained from casting solutions with relatively high polymer content. Figure 1.15 (b) shows a structure, which in the literature is called "nodular". It consists of small polymer beads randomly fused together. The structure is often obtained from casting solutions with low poly-

mer concentrations. Very often in asymmetric membranes the structure may change from nodular to "cellular" type over the membrane cross section, as shown in Figure 1.16.

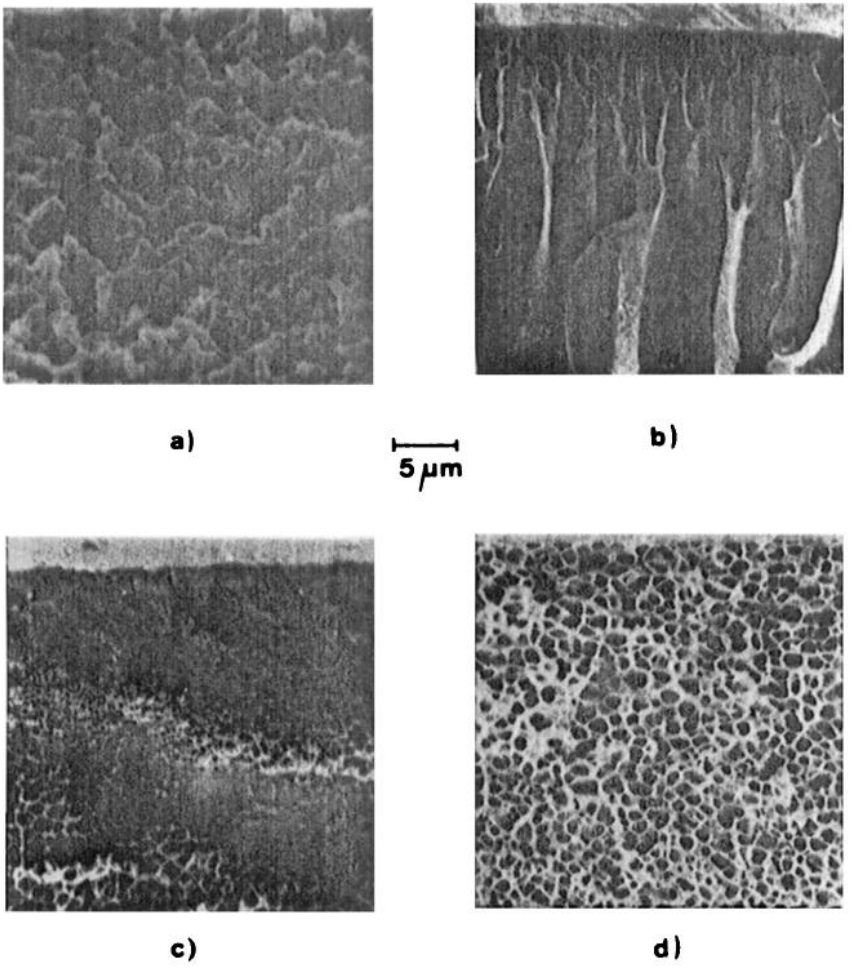
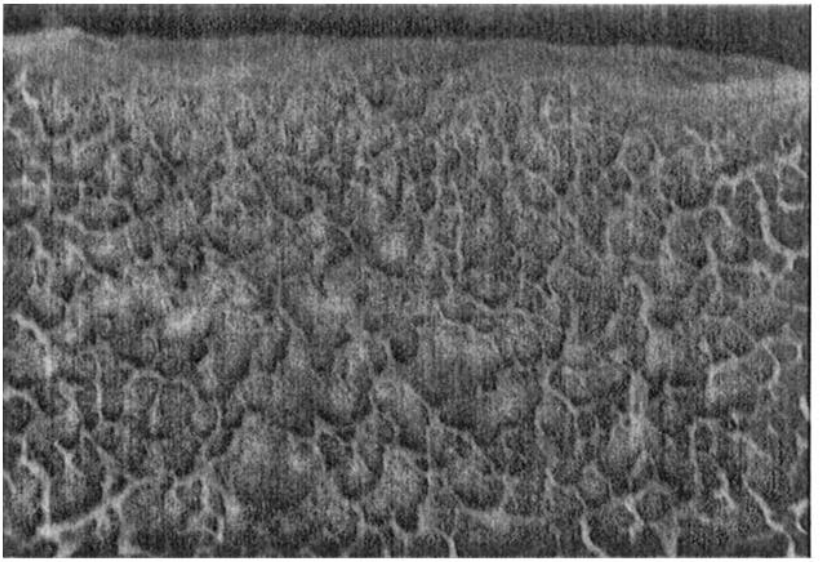
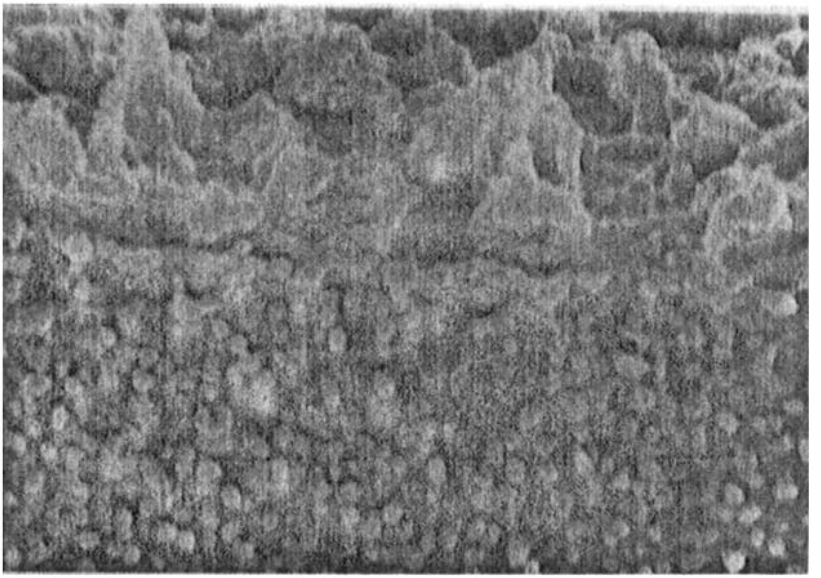


Figure 1.14: Scanning electron micrograph of membrane cross sections with typical structures: (a) symmetric microporous membrane without a "skin"; (b) asymmetric membrane with a "finger"-type structure and a dense skin at the surface; (c) asymmetric membrane with a "sponge"-type structure, a dense skin, and pore sizes increasing from the surface to the bottom side; (d) symmetric membrane with a sponge structure, a dense skin and a uniform pore size distribution in the substructure.



a



b

Figure 1.15: Scanning electron micrographs of the fine structure of two phase inversion membranes: (a) sponge-type structure consisting of spherical cells; (b) nodular structure consisting of small polymer beads fused together to form a randomly porous structure.

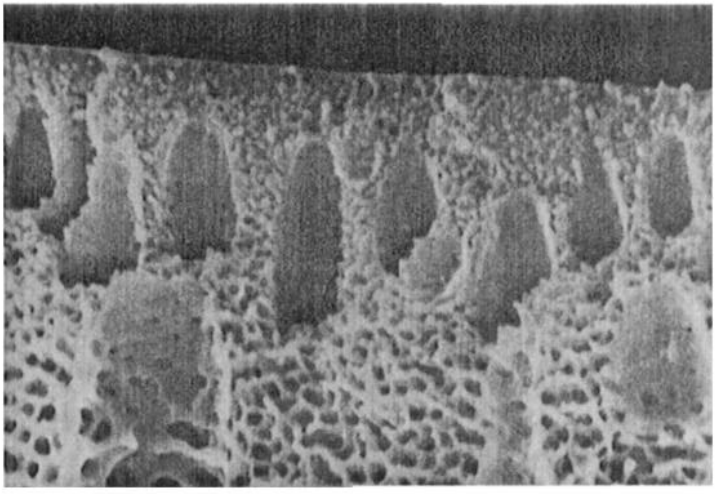


Figure 1.16: Scanning electron micrograph of a membrane showing a nodular structure at the surface which converts into a cellular structure towards the bottom side of the membrane.

The Effect of the Polymer and Polymer Concentration on Membrane Structures and Properties. The scanning electron micrograph of Figures 1.17 (a) to (c) show the cross sections of three membranes with nearly identical structures and ultrafiltration properties (listed in Table 1.2) prepared from three different polymers (cellulose acetate, polyamide and polysulfone) by precipitation in a water bath. The scanning electron micrographs of Figures 1.18 (a) to (c) show the cross sections of membranes made from one polymer-solvent system (polyamide in DMAC) with different polymer concentrations. These membranes show completely different structures and filtration properties which are listed in Table 1.3. The scanning electron micrographs of Figures 1.17 and 1.18 and the data listed in Tables 1.2 and 1.3 indicate that the same type of membrane can be prepared from various polymers and that from one polymer-solvent system, various types of membranes can be made.

The polymer concentration is a very significant parameter for tailoring a membrane in terms of its structure and separation properties. This is demonstrated in Figure 1.19 where the scanning electron micrographs of membranes are shown which are prepared from casting solutions of different polyamide concentrations in NMP. With increasing polymer concentration, the structure changes from a typical finger structure (5% polyamide in the casting solution) to a typical sponge structure (22% polyamide in the casting solution).

The flux and retention properties, the membrane porosity and the rate of precipitation change in a corresponding pattern, as shown in Table 1.4. With increasing polymer concentration, the permeability decreases and the retention increases. The overall porosity also decreases and the gelation time increases with increasing polymer concentration.

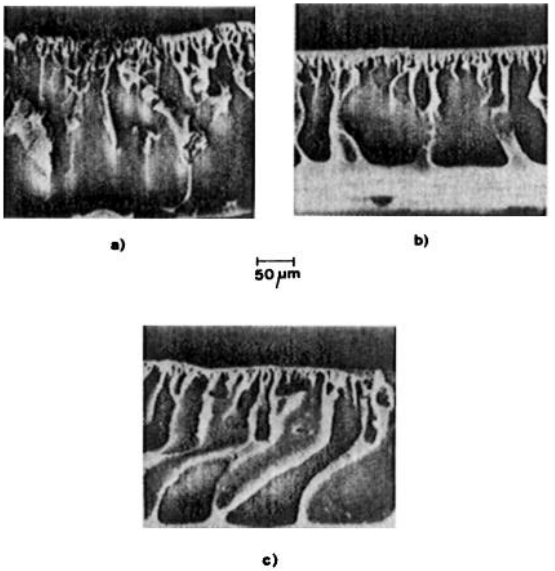


Figure 1.17: Scanning electron micrographs of membrane cross sections prepared from three different polymer-solvent systems by precipitation in water: (a) 12% cellulose acetate in DMAc; (b) 12% polyamide in DMSO; (c) 12% polysulfone in DMF.

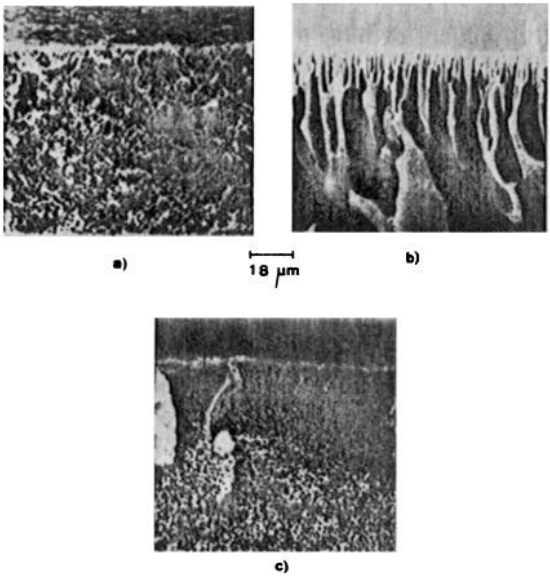


Figure 1.18: Scanning electron micrographs of membrane cross sections prepared from different polyamide solution concentrations and by different precipitation procedures: (a) 10% polyamide in DMAc precipitated by water vapor; (b) 10% polyamide in DMAc precipitated in a water bath; (c) 22% polyamide in DMAc precipitated in a water bath.

Table 1.2: Filtration Properties and Porosities of Membranes Prepared From Different Polymer-Solvent Systems by Precipitation in Water

Polymer	Filtration rate* (cm/s)	Rejection+ (%)		Membrane porosity (%)
		γ-globulin	bov.albumin	
Cellulose acetate in DMAc	3.5×10^{-3}	99	98	80
Polyamide in DMSO	2.1×10^{-3}	97	72	82
Polysulfone in DMF	1.9×10^{-3}	96	80	83

* The filtration rates were determined with DI-water at 2 bar and room temperature

\+ The rejections were determined at 2 bar and room temperature with solution of 1 % γ-globulin and bov. albumin

Table 1.3: Filtration Properties and Porosities of Membranes Prepared From Polyamide-DMAc-Water Systems

Polymer-concentration	Precipitant	Porosity (%)	Filtration rate* (cm/s)	Rejection+	Structure
10 % polyamide in DMAc	water vapor	89	2×10^{-1} at 2 bar	0 % for Dextran 100	symmetric "sponge"-type
10 % polyamide in DMAc	water	79	1.8×10^{-3} at 2 bar	88 % for bov.albumin	asymmetric "finger"-type
22 % polyamide in DMAc	water	71	8×10^{-5} at 100 bar	99 % for $MgSO_4$	asymmetric "sponge"-type

* The filtration properties were determined with deionized water and solutions of 1 % solids at room temperature

\+ The molecular weight of Dextran 100 was approximately 2 million Dalton

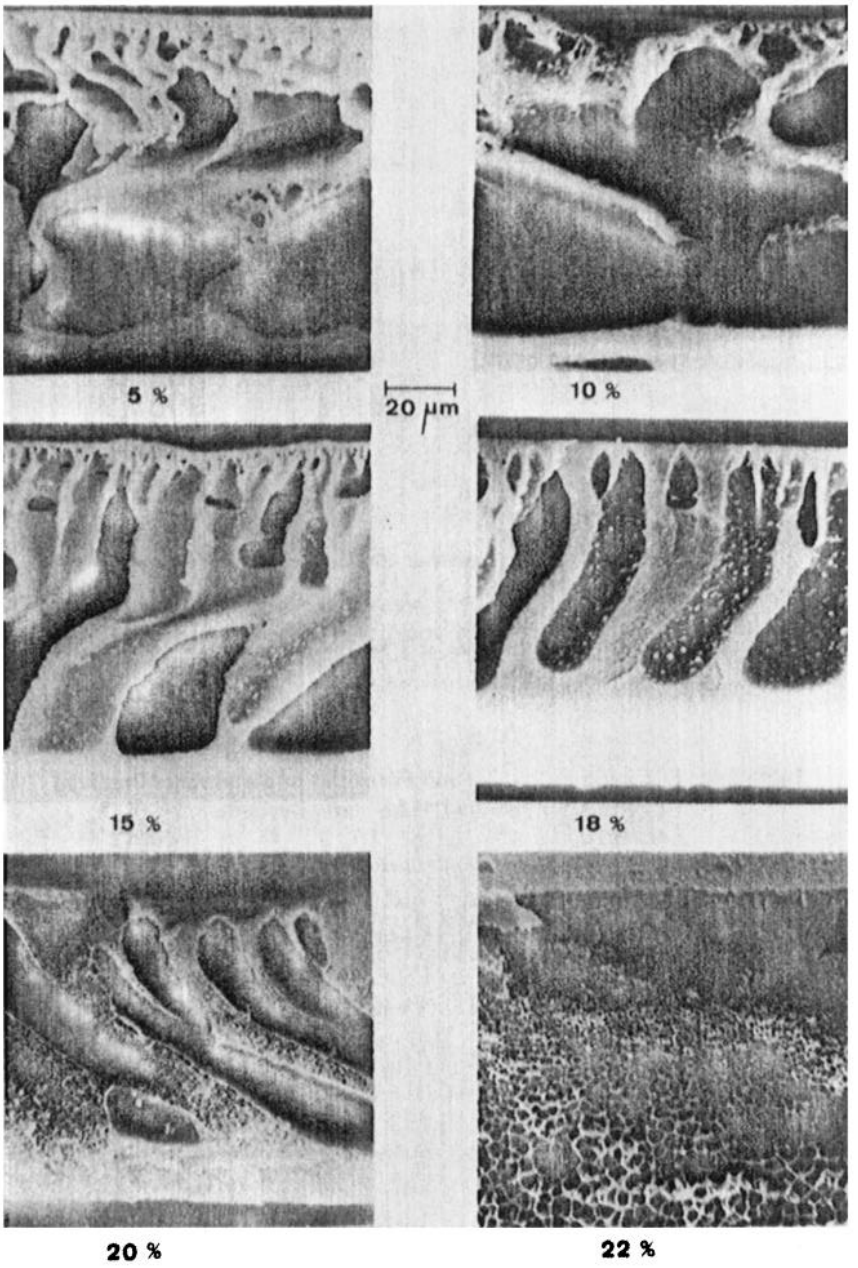


Figure 1.19: Scanning electron micrographs of membrane cross sections prepared from various polyamide concentrations in NMP by precipitation in water at room temperature.

Table 1.4: Rate of Precipitation and Filtration Properties of Membranes Prepared From Polyamide-NMP Solutions of Various Concentrations by Precipitation in Water at Room Temperature

Polymer concentration (%)	Rejection+ $MgSO_4$	Cyto-chrome C	bov. albumin	Filtration rate (cm/s x 10^4)	Porosity (vol.%)	Gelation time++ (s)
5 x	0	0	10	56	91	32
10 x	0	43	84	32	85	40
15 x	8	92	100	9	81	52
18 xx	75	100	100	18	79	83
20 xx	90	100	100	4	77	142
22 xx	98	100	100	1.6	76	212

\+ the rejection was determined with solutions of 1 % solids

++ for entire membrane

x applied pressure 5 bar

xx applied pressure 100 bar

Rate of Precipitation and Membrane Structure. Certain membrane structures can be correlated with the rate of precipitation. Very high precipitation rates (short gelation times) always lead to a "finger" structure, while slow precipitation rates (long gelation times) lead to asymmetric membranes with a "sponge" structure, and very slow precipitation rates very often lead to symmetric membranes with no defined skin at the surface, a structure with a very uniform pore size distribution over the entire cross section of the membrane. If a sponge-type structure is obtained, the pore diameters are inversely proportional to the rate of precipitation. Higher precipitation rates lead to finer pore structures, and lower precipitation rates lead to coarser structures. The rate of precipitation and its relation to the membrane structure can be easily observed with an optical microscope or by other means.[42]

The Effect of the Polymer-Solvent-Precipitant System on Membrane Structure and Properties. The effect of the polymer on membrane structure and properties is closely related to the solvent used in the casting solution and the precipitant. The solvent and the precipitant used in membrane preparation determine both the activity coefficient of the polymer in the solvent-precipitant mixture and the concentration of the polymer at the point of precipitation and solidification. The polymer-solvent-precipitant interaction can be approximately correlated in terms of the disparity of the solubility parameter of polymer and solvent.

(1) The smaller the solubility parameter disparity of solvent and polymer, the better the compatibility of solvent and polymer, and the slower the precipitation of the polymer. Thus, the tendency for a change from a sponge to a finger

structure membrane increases with decreasing compatibility of solvent and polymer. (2) The higher this disparity, the less compatible are polymer and precipitant, and the faster will be the precipitation. The tendency to change from a sponge to a finger structure will thus increase with decreasing compatibility of polymer and precipitant.

This is demonstrated in the scanning electron micrograph of Figure 1.20 which shows the cross section of membranes prepared from a solution of 15% polyamide in DMAc precipitated in water-glycerin mixtures of different compositions. Since the compatibility of the polymer with glycerin is slightly better than that with the water, i.e., the disparity in the solubility parameter of polymer-water is larger than of polymer-glycerin, the tendency of the membrane structure to go from a finger to a sponge structure will increase with increasing glycerin content in the precipitation bath. Additives to the casting solution or the precipitation bath have a similar effect.[36]

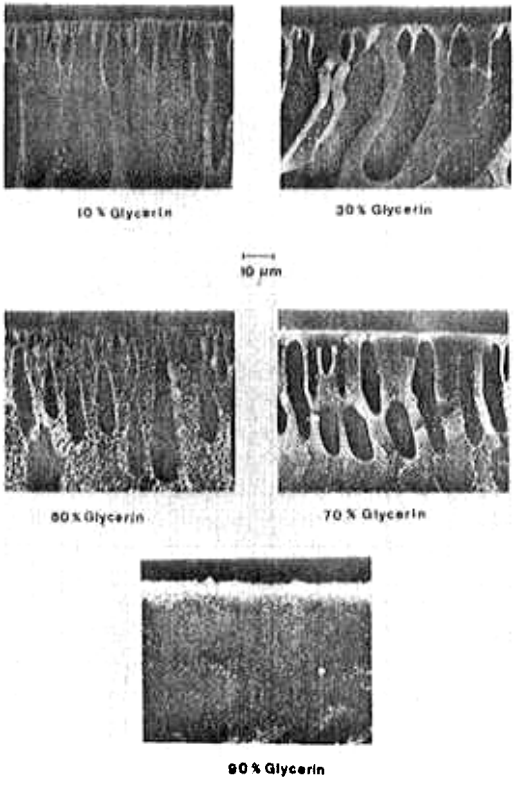


Figure 1.20: Scanning electron micrographs of membrane cross sections prepared from 15% polyamide in DMAc precipitated in water-glycerin mixture at room temperature.

Rationalization of the Various Membrane Preparation Procedures. To discuss the formation of membrane structures it is useful to describe the concentration profiles of the casting solution components in the precipitating casting solution. The schematic diagram of Figure 1.21 shows the concentration profiles of polymer, solvent and precipitant at some intermediate time during the precipitation of a polymer film cast on a glass plate.

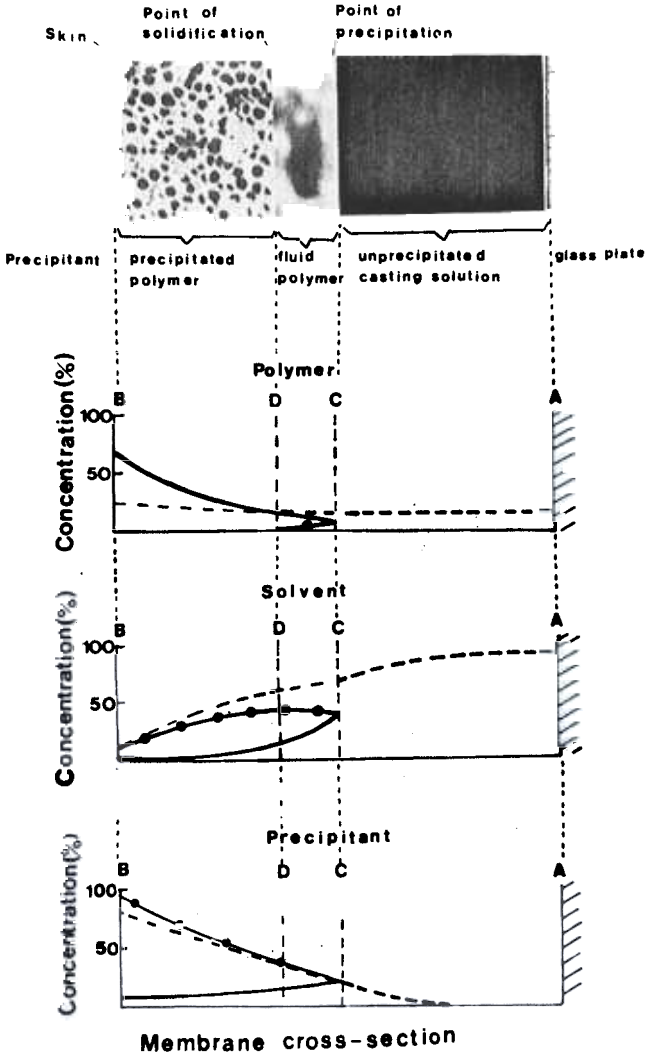


Figure 1.21: Schematic diagram showing the concentration profiles of polymer, solvent and precipitant through a precipitating membrane: --- total concentration; —— concentration in the polymer-rich phase; - ● - concentration in the polymer-poor phase; A Casting solution composition; B Membrane composition; C Point of precipitation; D Point of solidification.

During precipitation, the casting solution can be divided into three layers. Traveling from the glass plate towards the precipitation bath these layers are:

(1) The casting solution layer: This layer is closest to the glass plate, and has a composition similar to the original casting solution A. Little solvent has diffused out of and little precipitant has diffused into the layer.

(2) The fluid polymer layer: This layer lies between the point of precipitation and the point of solidification. In this layer, the casting solution divides into a polymer-rich and a polymer-poor phase. At the point of first phase separation, the polymer-rich phase still contains a high solvent concentration and a low precipitant concentration and is still liquid. The polymer nearest the precipitation bath has been precipitated longer, has lost solvent and has gained precipitant; its viscosity is therefore higher. Thus, the viscosity of the precipitated polymer climbs from the point of first separation until it becomes almost solid at the point of gelation. During this time, bulk movement of the precipitated polymer takes place to form the matrix of the final membrane.

(3) The solid polymer layer: In this layer, the solid, polymer-rich phase undergoes continuous desolvation. Shrinkage, or syneresis, of the solid polymer accompanying this composition change produces stresses in the polymer. Because the polymer is solid, these stresses cannot be as easily relieved by bulk movement of polymer as in the fluid polymer layer. Instead, the polymer structure either slowly undergoes creep to relieve the stress, or, if the stress builds up too rapidly to be dissipated by creep, the polymer matrix breaks at weak spots.

Formation of Symmetric and Asymmetric Membrane Structures. Two different techniques have been employed for the precipitation of membranes from a polymer casting solution. In the first method, the precipitant is introduced from the vapor phase. In this case, the precipitation is slow, and a more or less homogeneous structure is obtained without a dense skin on the top or bottom side of the polymer film. This structure can be understood when the concentration profiles of the polymer, the precipitant, and the solvent during the precipitation process are considered. The significant feature of the vapor-phase precipitation process is the slow diffusion of precipitant from the vapor phase adjacent to the film surface into the polymer solution. Because this process is so slow, the concentration profiles in the cast film are flat. The concentration profiles of the precipitant in the polymer film are shown schematically in Figure 1.22 for various times. Because of the flat concentration profiles of the precipitant over the cross section of the casting solution, the membrane precipitates rather slowly and in the same way over the entire film cross section. Therefore, a randomly distributed polymer structure is obtained during precipitation, as indicated in the scanning electron micrograph of Figure 1.6.

In the second membrane precipitation procedure, the precipitant is added to the casting solution by immersing the cast polymer film in a bath of the precipi-

tation fluid. In this case, the precipitation is rapid, and an asymmetric membrane structure is obtained. This structure and formation can again be understood by considering the concentration profiles of the polymer, the solvent and the precipitant during the precipitation process. These profiles over the cross section of the cast polymer film are shown schematically in Figure 1.23. The most important features in immersion precipitation are the steep concentration and activity gradients of all components found in the polymer solution close to the polymer-precipitation medium interface.

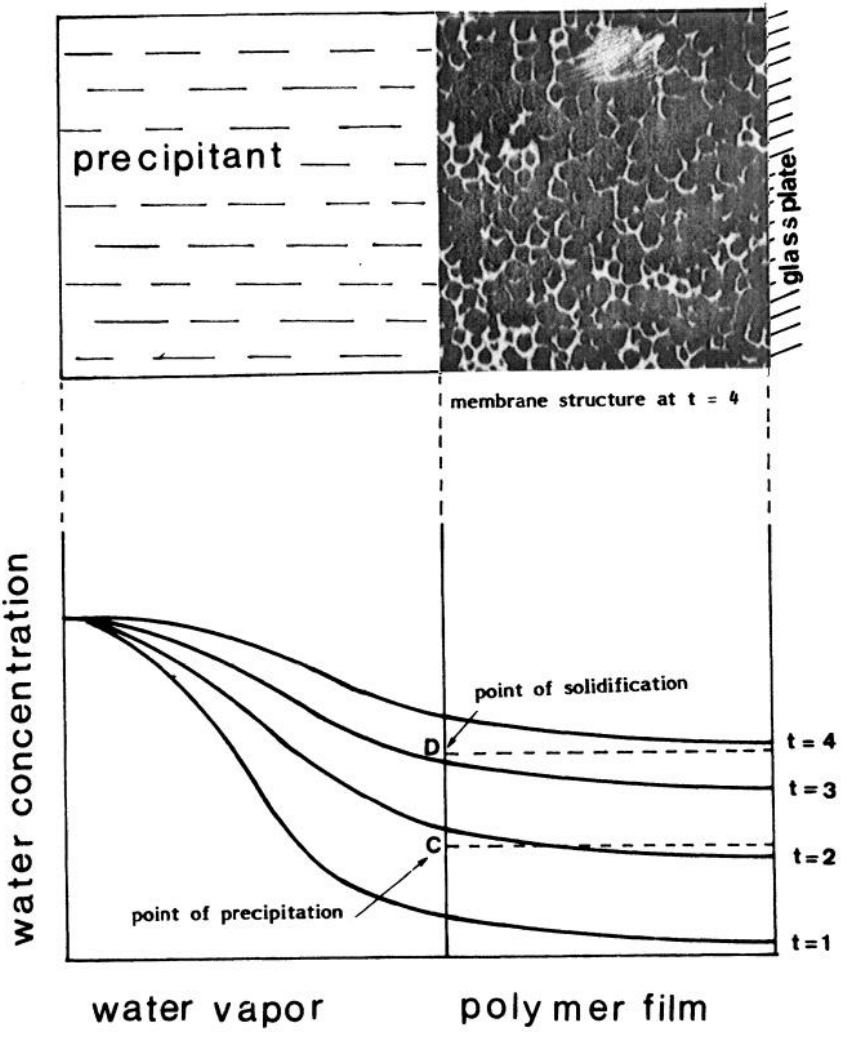


Figure 1.22: Schematic diagram showing the concentration profiles of the precipitant in the casting solution at various times during the formation of a symmetric structure membrane.

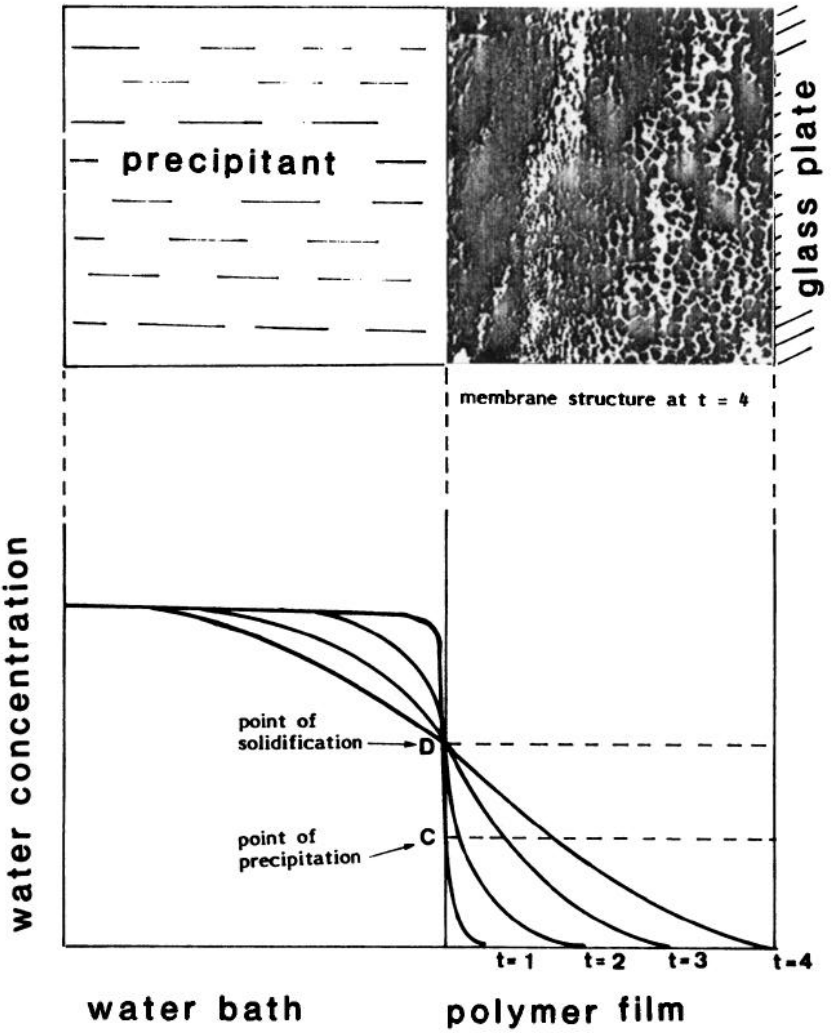


Figure 1.23: Schematic diagram showing concentration profiles of the precipitant in the casting solution of various times during the formation of an asymmetric skin-type membrane.

When the cast polymer film is immersed into the precipitation bath, solvent leaves and precipitant enters the film. At the film surface, the concentration of the precipitant soon reaches a value resulting in phase separation. In the interior, however, the precipitant concentration is still far below the limiting concentration for phase separation. Phase separation therefore occurs initially at the surface of the film, where, due to the very steep gradient of the chemical potential of the polymer, there is a net movement of the polymer perpendicu-

lar to the surface. This leads to an increase of the polymer concentration in the surface layer. It is the concentrated surface layer which forms the skin of the membrane. This skin also serves to hinder further transport of precipitant into and solvent out of the casting solution. The skin thus becomes the rate-limiting barrier for precipitant transport into the casting solution, and the concentration profiles in the casting solution interior become less steep. Thus, once the precipitated skin is formed, the same situation in the sublayer is obtained as in a membrane precipitated from the vapor phase, and a structure with uniform randomly distributed pores is formed.

Skin Type Membranes With "Sponge"- and "Finger"-Like Structures. In skin-type membranes, the two characteristic structures shown in Figure 1.14 are obtained. One is a sponge-like structure and the other is a finger-like substructure underneath the skin.

The formation of the sponge-structured membranes can also be rationalized by the precipitation process described above. With finger-structured membranes, the formation process is more complex and cannot entirely be described by the thermodynamic and kinetic arguments of phase separation processes.[43]

Other phenomena, such as syneresis, shrinkage, and stress relaxation in the precipitated polymer, also play an important role. The formation of finger-structured membranes is conveniently divided into two steps: the initiation and the propagation of fingers. The formation of the skin is identical with that of the sponge-structured membranes. However, as a result of syneresis, shrinkage stress in the solid polymer skin cannot be relieved by creep relaxation of the polymer and the homogeneous layer ruptures. The points at which the skin has been fractured form the initiation points for the growth of the fingers. Once a finger has been initiated, shrinkage of the polymer causes it to propagate by draining the freshly precipitated polymer at the bottom of the finger to the side of the finger. This is schematically shown in Figure 1.24 which shows the growth of a finger at various times. Within a finger, the exchange of solvent and precipitant is much faster than through the unfractured skin, and the precipitation front moves much faster within a finger than in the casting solution bypassed between fingers. This solution is protected from immediate exposure to the precipitant by a layer of precipitated polymer. Precipitation therefore occurs much slower and a sponge-like structure is formed between the fingers.

Uniform and Graded Pore Structure of Skin-Type Membranes. In sponge-structured, skin-type membranes, it is assumed that the diffusion of the precipitant through the skin is the rate-limiting step, leading to a more or less flat concentration profile of the precipitant in the casting solution just beneath the skin. Depending on the resistance of the skin to the flux of precipitant, the concentration profile may vary from a completely flat one (virtually no concentration gradient over the cross section of the cast polymer film) to a concentration profile showing an initially steep gradient at the beginning of precipitation which decreases as precipitation proceeds through the polymer film. A uniform pore structure is obtained when the concentration profiles are flat and the time that the system needs to move from the point of precipitation to the point of solidification is about the same over the entire film cross section. A graded pore distribution is obtained when the time between precipitation and solidification of the polymer increases with increasing distance from the skin.

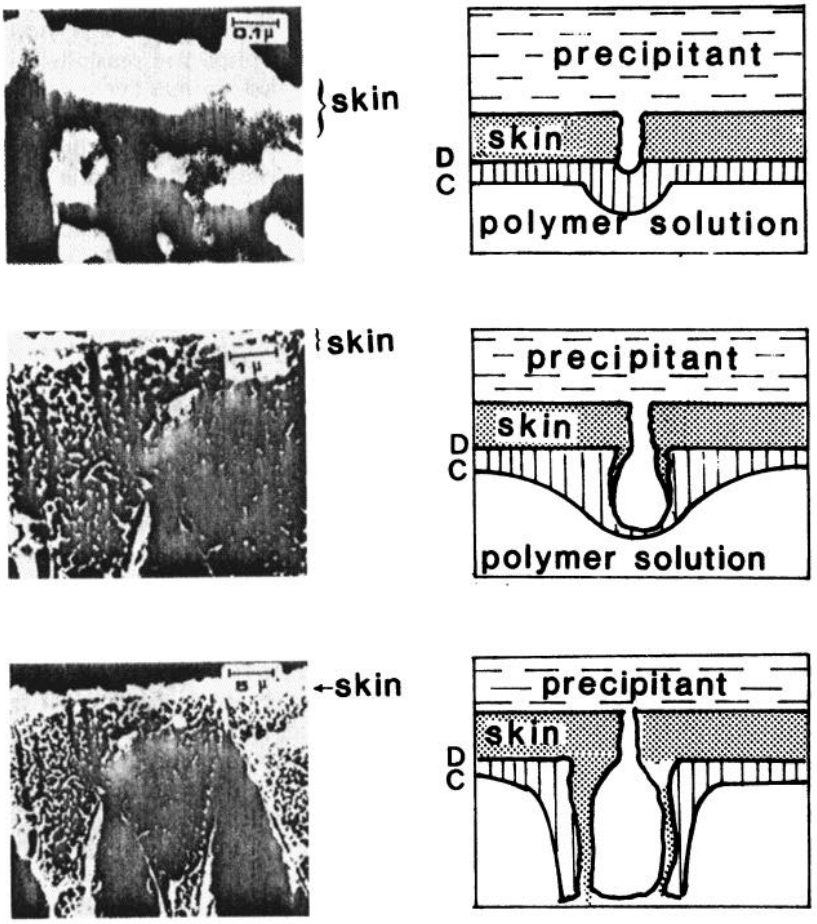


Figure 1.24: Schematic diagram of finger formation at various times during precipitation.

Cellular and Nodular Membrane Fine Structure. Several authors have commented on the two different structures shown in Figure 1.15. It is generally assumed that a fine structure is already predetermined in the casting solution prior to the actual phase separation.[44,45] A cellular structure will be obtained when in the beginning state of the phase separation, i.e., before the solidification of the polymer-rich phase, the continuous phase is formed by the polymer-rich phase. A nodular structure is obtained when the precipitant-rich phase is continuous, completely surrounding droplets of the polymer-rich phase.

The Effect of the Solvent-Precipitant System on Membrane Structure and Properties. The precipitant and the solvent used in membrane preparation determine both the activity coefficient of the polymer in the solvent-precipitant mixture and the concentration of polymer at the point of precipitation and solidification.

The effect of additives to the casting solution or to the precipitant on the membrane structure can be explained by changes of the activity coefficients of the polymer, the solvent or the precipitant and with that the rate of precipitation. The effect of additives such as salts, organic solvents, or other "pore-formers" to the casting solution or precipitation bath is described in detail in the literature.[36,47]

The Effect of the Polymer Concentration in the Casting Solution on the Membrane Structure. A low polymer concentration in the casting solution tends to induce precipitation in a finger-type structure, while high polymer concentrations tend to induce precipitation of sponge-structured membranes. The effect of polymer concentration on membrane structures can be explained by the initiation and propagation of fingers. Higher polymer concentration in the casting solution produces a higher polymer concentration at the point of precipitation, which will thus tend to increase the strength of the surface of polymer film first precipitated, and tend to prevent initiation of fingers. Increasing the viscosity of the casting solution has the same effect.

The Effect of Pre- and Post-Precipitation Procedures on Membrane Structures and Properties. In the original recipes for making phase inversion membranes, the evaporation step prior to the precipitation of the film was considered as being essential for the formation of the asymmetric membrane.[46] Meanwhile, it has become apparent that skin-type asymmetric membranes can be prepared without an evaporation step. The effect of the evaporation results in an increase of the polymer concentration at the surface of the cast film, due to a loss of solvent. This does not necessarily lead to denser membranes. This is shown in Figure 1.25, where the salt rejection of cellulose acetate membranes prepared from a casting solution containing 25% cellulose-acetate, 45% acetone, and 30% formamide, which was exposed to air at room temperature prior to precipitation in water at 0°C and annealing at 75°C for 2 minutes is shown as a function of the evaporation time. The filtration tests were carried out at a hydrostatic pressure of 100 bar with a 1% NaCl solution. At short evaporation times (<1 minute), there is no change in rejection, at longer evaporation times (>2 minutes), there is a drastic loss in rejection. This is due to a significant change in the casting solution composition at the membrane surface because of differences in the boiling temperatures of acetone (kp = 60°C) and formamide (kp = 120°C). During the air exposure time, acetone will preferentially be evaporated because it is the more volatile solvent, while the formamide concentration will increase in the film surface. Thus, the original acetone-formamide ratio of the solvent system will be changed. In an independent set of experiments, it was shown, however, that cellulose acetate membranes made from casting solutions with formamide concentrations exceeding 35% did not reject NaCl.[35]

As indicated earlier, membranes made from a casting solution containing 25% cellulose acetate, 45% acetone and 30% formamide do not show any NaCl-rejection unless they are annealed hot water. Thus, for this type of membrane the annealing is an essential postprecipitation membrane treatment step. The effect of the annealing procedure on membrane flux and sale rejection is demonstrated in Figure 1.26 where the flux and salt rejections of membranes precipitated in ice water from a casting solution of 25% cellulose acetate, 45% acetone and 30% formamide are shown as a function of the annealing temperature. The annealing time was kept constant at 2 minutes and the membranes were tested at 100 bars with a 1% NaCl-solution.

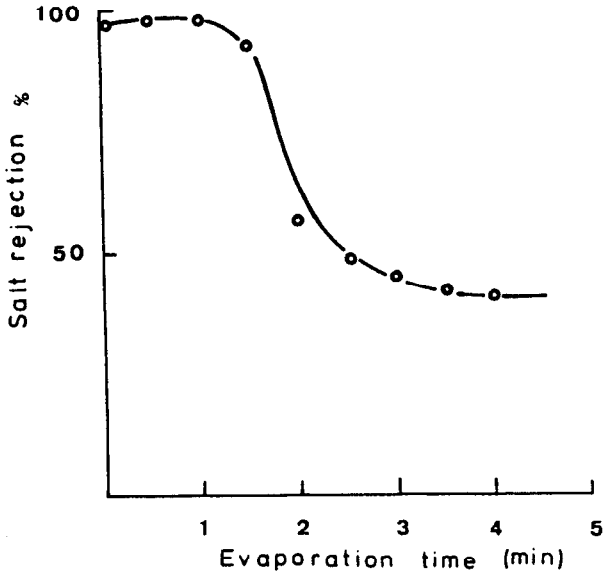


Figure 1.25: Rejection of a cellulose acetate membrane prepared from a casting solution containing 25% cellulose acetate, 45% acetone and 30% formamide by precipitation in a water bath at 0°C as a function of the evaporation time prior to the precipitation. (Test condition: 1% NaCl-solution, 100 bar hydrostatic pressure).

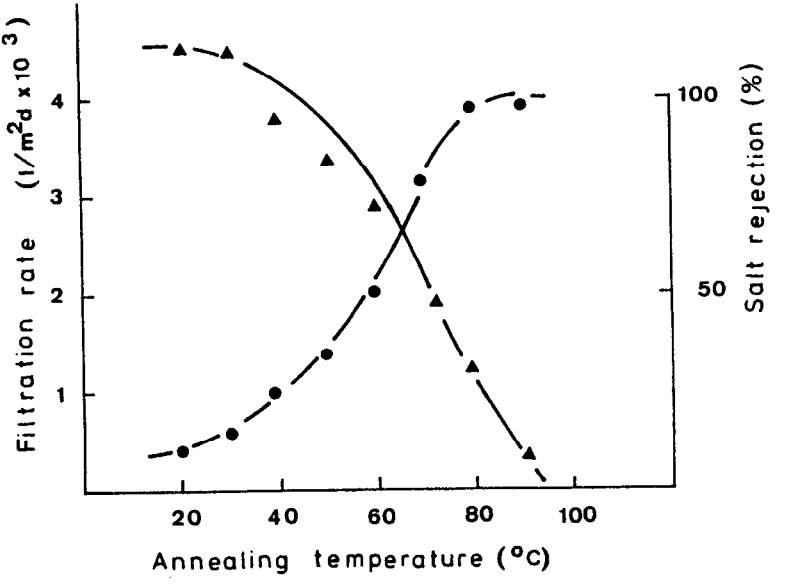


Figure 1.26: Transmembrane flux and salt rejection of a membrane prepared from a solution of 25% cellulose acetate, 45% acetone and 30% formamide by precipitation in water as a function of the past precipitation annealing temperature. (Test conditions: 1% NaCl-solution, 100 bar hydrostatic pressure).

Homogeneous Membranes

A homogeneous membrane is merely a dense film through which a mixture of chemical species is transported under the driving force of a pressure, concentration, or electrical potential gradient. The separation of various components in a solution is directly related to their transport rates within the membrane phase, which is determined mainly by their diffusivity and concentration in the membrane matrix.[48–52] An important property of homogeneous membranes is that chemical species of similar size, and hence similar diffusivities, may be separated when their concentration, that is their solubility in the film, differs signigicantly. The membrane phase itself may be solid or liquid. The mass transport in homogeneous membranes occurs strictly by diffusion; thus permeabilities are rather low. Homogeneous membranes should, therefore, be as thin as possible.

Homogeneous Polymer Membranes. Although there are a number of homogeneous membranes made from inorganic materials, such as glass or certain metals,[53,54] the technically more important structures are of polymeric origin. Modern polymer chemistry is highly proficient in tailoring polymers to specific aims in terms of mechanical or thermal stability and chemical compatibility. In general, mass transfer will be greater in amorphous polymers than in highly crystalline or cross-linked polymers.[55] Thus, crystallization and orientation are to be avoided as much as possible when high permeabilities and transmembrane fluxes are desired. However, physical properties and, in particular, the mechanical strength of the polymer as well as its selectivity may then be adversely affected, and the final product will represent a compromise between necessary strength, selectivity and mass-transfer rates.[56] The principle aim is to create as thin a barrier as possible, consistent with the required strength and absence of pinholes and defects. The two basic membrane configurations are flat sheets and hollow fibers.[57,58] Flat sheets can be prepared by casting from solution, by extruding from a polymer melt or by blow and press molding. Hollow fibers are generally made by extrusion with central gas injection.[59] Because of their high selectivity for different chemical components homogeneous membranes are used in various applications, which in general involve the separation of different low molecular weight components with identical or nearly identical molecular dimensions. The most important applications of homogeneous polymer membranes are in gas separation, pervaporation, and reverse osmosis. For the separation of gases silicon rubber, because of its relatively high permeability, is the more widely used basic material.[60,61] For reverse osmosis, cellulose esters and various polyamides serve as the barrier polymer for the membrane preparation.[62,63]

Most technically utilized homogeneous polymer membranes consist of a composite structure where a very thin homogeneous selective polymer film is supported by a thicker microporous structure providing the mechanical strength.

Homogeneous Metal and Glass Membranes. There is only one type of homogeneous metal membrane of technical importance. This is the palladium, or palladium-alloy membrane used for the separation and purification of hydrogen. The permeability of hydrogen in palladium, palladium alloys and several other metals such as platinum, silver, iron, nickel, etc. is several orders of magnitude higher than of any other gases.[64] The permeability of hydrogen in palladium alloy membranes is highly temperature dependent. The separation is, therefore, carried out at elevated temperature (~400°C).[64] The membranes generally consist of 10 to 50 μm thick metal foils. Because of their high selectivity, these

membranes are used for production of high purity hydrogen (>99.99% H_2). Although the process seems technically feasible, there are only very few commercial plants in operation.[65] The same is true for the use of homogeneous silica glass membranes, the only other homogeneous inorganic material which shows any promise to be used as selective barrier especially for the separation of helium. Like metal membranes, glass membranes are operated at elevated temperature. Until today, however, no commercial industrial size plants are in operation. Homogeneous glass membranes also have a high selectivity for H^+-ions, thus they are used as the selective barrier in pH-electrodes. Their preparation is described in some detail in the literature and shall not further be discussed in this chapter.

Liquid Membranes. Liquid membranes have gained increasing significance in recent years in combination with the so-called facilitated transport which utilizes selective "carriers" transporting certain components such as metal-ions selectively and at a relatively high rate across the liquid membrane interphase.[66,67] It is relatively easy to form a thin fluid film. It is difficult, however, to maintain and control this film and its properties during a mass separation process. In order to avoid a break-up of the film, some type of reinforcement is necessary to support such a weak membrane structure. Two different techniques are used today for the preparation of liquid membranes. In the first case, the selective liquid barrier material is stabilized as a thin film by a surfactant in an emulsion-type mixture.[68,69] In the second technique for making liquid membranes, a microporous polymer structure is filled with the liquid membrane phase.[70,71] In this configuration, the microporous structure provides the mechanical strength and the liquid-filled pores the selective separation barrier. Both types of membranes are used today on a pilot-plant stage for the selective removal of heavy metal-ions or certain organic solvents from industrial waste streams. They have also been used rather effectively for the separation of oxygen and nitrogen.[72]

Supported Liquid Membranes. The preparation of supported liquid membranes is extremely simple, when certain requirements concerning the selective barrier and the microporous support material are fulfilled. The liquid membrane material should have a low viscosity and low vapor pressure, i.e., high boiling point and, when used in aqueous solutions, a low water solubility. Otherwise, the useful lifetime of the membrane is rather limited. The microporous substructure should have a high porosity, a pore size small enough to support the liquid membrane phase sufficiently under hydrostatic pressure and the polymer of the substructure should be hydrophobic in nature for most liquid membranes used in contact with aqueous feed solutions. In practice, liquid membranes are prepared by soaking a hydrophobic microporous membrane, such as a Goretex (Gore Corp.) or Cellgard (Celanese Corp.) type stretched polytetrafluorethylene or polyethylene membrane, in the hydrophobic liquid which may consist of a selective carrier such as certain oximes or tertiary or quaternary amines dissolved in kerosene. The disadvantage of supported membranes is their thickness which is determined by the thickness of the microporous support structure, which is in the range of 10 to 50 μm, and therefore about 100 times the thickness of the selective barrier of an asymmetric polymer membrane. Thus, the fluxes of supported liquid membranes can be low even when their permeabilities are high.[73]

Unsupported Liquid Membranes. Very thin unsupported liquid membranes may be obtained, when the selective membrane material is stabilized by an appro-

priate surfactant in an aqueous emulsion. The preparation procedure is indicated in Figure 1.27. A hydrophobic membrane phase is transformed into an emulsion by stirring with an aqueous phase. Ideally, droplets form in this process, in which the aqueous phase is surrounded by a relatively thin hydrophobic membrane forming phase which is surrounded by a second aqueous phase. The mass exchange occurs between the inner and outer aqueous phases through the liquid membrane interphase. In reality, the hydrophobic membrane phase and the surrounding aqueous phases are more fractionated and the diffusion pathways become longer as a result. With another aqueous solution, the component to be eliminated is supplied to the original emulsion and passes through the membrane into the internal solution.

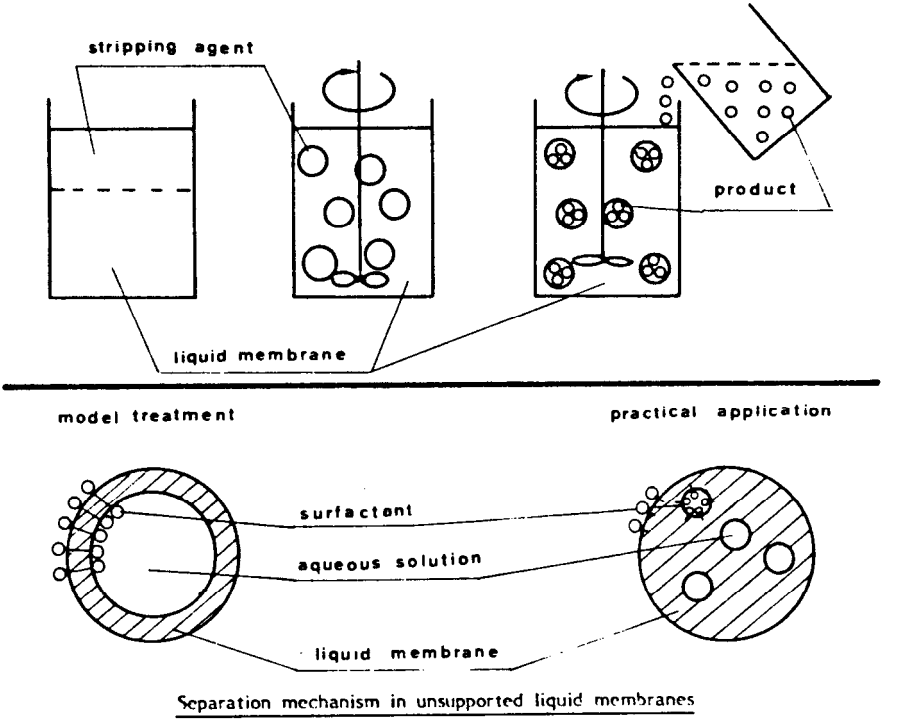


Figure 1.27: Schematic diagram showing the formation of an emulsified liquid membrane.

Ion-Exchange Membranes. Ion-exchange membranes consist of highly swollen gels carrying fixed positive or negative charges. The properties and preparation procedures of ion exchange membranes are closely related to those of ion-exchange resins.[74] As with resins, there are many possible types with different polymer matrixes and different functional groups to confer ion-exchange properties on the product. Although there are a number of inorganic ion-exchange materials, most of them based on zeolites and bentonites, these materials are rather unimportant in ion-exchange membranes and will not be discussed further.

There are two different types of ion-exchange membranes: (1) cation-exchange membranes which contain negatively charged groups fixed to the polymer matrix, and (2) anion-exchange membranes which contain positively charged groups fixed to the polymer matrix. In a cation-exchange membrane, the fixed anions are in electrical equilibrium with mobile cations in the interstices of the polymer, as indicated in Figure 1.28. This figure shows schematically the matrix of a cation-exchange membrane with fixed anions and mobile cations, which are referred to as counter-ions. In contrast, the mobile anions, called co-ions, are more or less completely excluded from the polymer matrix because of their electrical charge which is identical to that of the fixed ions. Due to the exclusion of the co-ions, a cation-exchange membrane permits transfer of cations only. Anion-exchange membranes carry positive charges fixed on the polymer matrix. Therefore, they exclude all cations and are permeable to anions only. The most required properties from ion-exchange membranes are:

- High permselectivity–an ion-exchange membrane should be highly permeable for counter-ions, but should be impermeable to co-ions.
- Low electrical resistance–the permeability of an ion-exchange membrane for the counter-ions under the driving force of an electrical potential gradient should be as high as possible.
- Good mechanical and form stability–the membrane should be mechanically strong and should have a low degree of swelling or shrinking in transition from dilute to concentrated ionic solutions.
- High chemical stability–the membranes should be stable over a pH-range from 1 to 14 and in the presence of oxidizing agents.

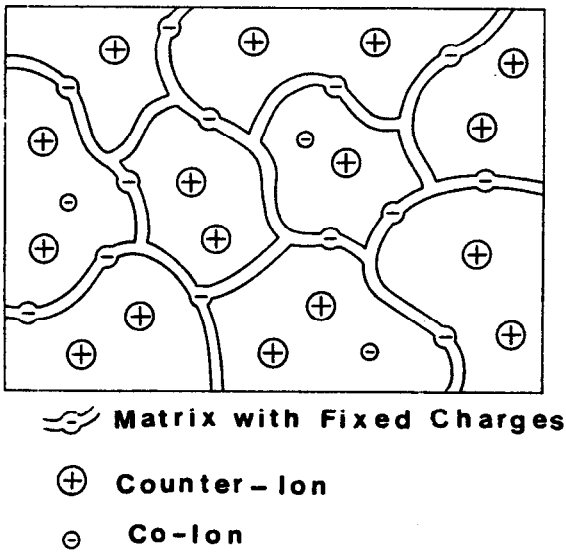


Figure 1.28: Schematic diagram of the structure of a cation-exchange membrane showing the polymer matrix with the negative fixed charges, the positive counter-ions, and the negative co-ions.

It is often difficult to optimize the properties of ion-exchange membranes because the parameters determining the different properties often act contrary. For instance, a high degree of crosslinking improves the mechanical strength of the membrane but also increases its electrical resistance. A high concentration of fixed ionic charges in the membrane matrix leads to a low electric resistance but, in general, causes a high degree of swelling combined with poor mechanical stability. The properties of ion-exchange membranes are determined by two parameters, i.e., the basic polymer matrix and the type and concentration of the fixed ionic moiety. The basic polymer matrix determines to a large extent the mechanical, chemical and thermal stability of the membrane. Very often the matrix of an ion-exchange membrane consists of hydrophobic polymers such as polystyrene, polyethylene or polysulfone.[75] Although these basic polymers are insoluble in water and show a low degree of swelling, they may become water soluble by the introduction of the ionic moieties. Therefore, the polymer matrix of ion-exchange membranes is very often crosslinked. The degree of crosslinking then determines to a large extent the degree of swelling, and the chemical and thermal stability, but also has a large effect on the electric resistance and the permselectivity of the membrane.[76,77]

The type and the concentration of the fixed ionic charges determine the permselectivity and the electrical resistance of the membrane, but they also have a significant effect on the mechanical properties of the membrane. The degree of swelling, especially, is affected by the fixed charge concentration. The following moieties are used as fixed charges in cation-exchange membranes:[78–84]

$$-SO_3^- \ , \ -COO^- \ , \ -PO_3^{2-} \ , \ -AsO_3^{2-}$$

In anion-exchange membranes, fixed charges may be:[80,81]

$$-NH_3^+ \ , \ \geq NH_2^+ \ , \ \equiv N^+ \ , \ \geq S^+ .$$

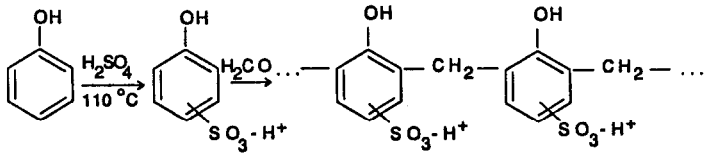
These differently charged groups have a significant effect on the ion-exchange behavior of the membrane. The sulfonic acid groups, e.g., $-SO_3^-$ is completely dissociated over nearly the entire pH-range, while the carboxylic acid group $-COO^-$ is virtually undissociated in the pH-range <7. The quaternary ammonium group again is completely dissociated over the entire pH-range, while the primary ammonium group is only weakly dissociated. Accordingly, ion-exchange membranes are referred to as being weak or strong acid or basic in character.[82] Most commercial ion-exchange membranes can be divided, according to their structure and preparation procedure, into two major categories, i.e., homogeneous and heterogeneous membranes. In general, heterogeneous ion-exchange membranes have several disadvantages, the most important of which are relatively high electrical resistance and poor mechanical strength when highly swollen in dilute salt solutions.

Homogeneous ion-exchange membranes have significantly better properties in this respect, since the fixed ion charges are distributed homogeneously over the entire matrix.

Preparation Procedure of Homogeneous Ion-Exchange Membranes. The methods of making homogeneous ion-exchange membranes can be summarized by three different basic procedures:

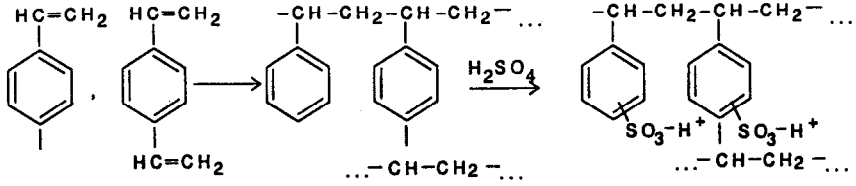
(1) Polymerization or polycondensation of monomers, of which at least one must contain a moiety that either is or can be made anionic or cationic.

The first membranes made by this procedure were prepared from phenol by polycondensation with formaldehyde according to the following reaction scheme:[82]

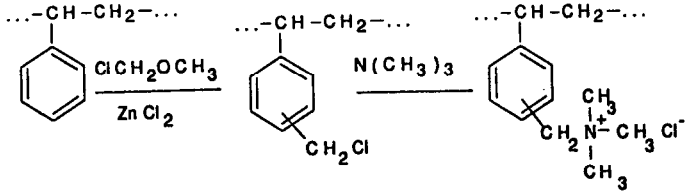


Phenol is treated with concentrated H_2SO_4 at elevated temperatures leading to phenolsulfonic acid in paraform, a brown crystalline material. The phenolsulfonic acid and a solution of formaldehyde in water is treated at elevated temperatures for several hours. The solution is cast into a film. Excess monomers are removed by washing the film in water.

A very common method of preparing a cation- or anion-exchange membrane is the polymerization of styrene and divinylbenzene and subsequent sulfonation or amination. The cation-exchange membrane is obtained by the following reaction scheme:[83]



The anion-exchange group is introduced into the polymer by chloromethylation and amination with trimethylamine according to the following reaction scheme:



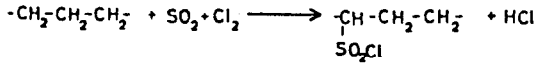
There are numerous literature references to the preparation of ion-exchange membranes by polymerization.

(2) Introduction of anionic or cationic moieties into a preformed film by techniques such as imbibing styrene into polymer films, polymerizing the imbibed monomer, and then sulfonating the styrene.

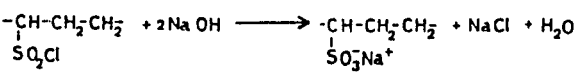
Starting with a film makes the membrane preparation rather easy. The starting material may be a film from a hydrophilic polymer, such as cellophane or polyvinyl alcohol, or a film from a hydrophobic polymer, such as polyethylene

or polystyrene. Ion-exchange membranes made by sulfochlorination and amination of polyethylene sheets have low electrical resistance combined with high permselectivity and excellent mechanical strength. The reaction scheme for preparation of ion-exchange membranes by sulfochlorination and amination of polyethylene sheets is given below.[84]

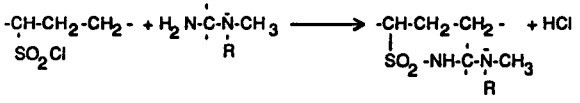
Sulfochlorination



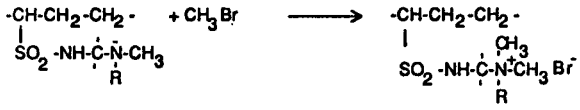
Hydrolysis



Amination

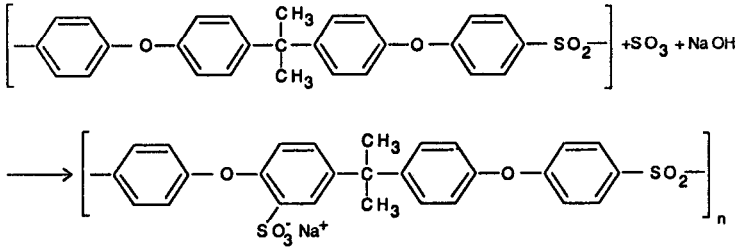


Quaternization **Anion-exchange membrane**



(3) Introduction of anionic or cationic moieties into a polymer chain such as polysulfone, followed by dissolving the polymer and casting it into a film.

Membranes made by any of the above methods may be cast around screens or other reinforcing materials to improve their strength and dimensional stability. The reaction scheme for the sulfonation of polysulfone is as follows:[85]



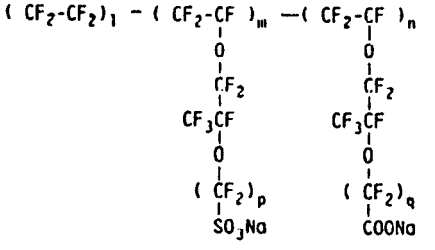
The sulfonated polysulfone can be cast into a film on a screen and precipitated after most of the solvent has been evaporated, leading to a reinforced membrane

with excellent chemical and mechanical stability and good electrochemical properties.

Heterogeneous Membranes. These membranes consist of fine colloidal ion-exchange particles embedded in an inert binder such as polyethylene, phenolic resins or polyvinyl chloride.[86] Such a membrane can be prepared simply by calendering ion-exchange particles into an inert plastic film. Another procedure is dry molding of inert film-forming polymers and ion-exchange particles and then milling the mold stock. Also, ion-exchange particles can be dispersed in a solution containing a film-forming binder, and the solvent evaporated to give an ion-exchange membrane. Similarly, ion-exchange particles can be dispersed in a partially polymerized binder polymer, and the polymerization subsequently completed. Heterogeneous membranes with usefully low electrical resistances contain more than 65% by weight of the crosslinked ion-exchange particles. Since these ion-exchange particles swell when immersed in water, it has been difficult to achieve adequate mechanical strength combined with low electrical resistance. Most heterogeneous membranes that possess adequate mechanical strength generally show poor electrochemical properties. On the other hand, a membrane that contains ion-exchange particles large enough to show an adequate electrochemical performance exhibits poor mechanical strength.

Special Property Membranes. In the literature, there are numerous methods reported for the preparation of ion-exchange membranes with special properties,[87–89] for instance, for use as battery separators, ion-selective electrodes, or in the chlor-alkali process. Especially membranes recently developed for the chlor-alkali industry are of commercial significance. These membranes are based on polytetrafluoroethylene and carry sulfone groups in the bulk of the membrane phase and carboxyl-groups on the surface as the charged moiety. They combine good chemical stability with high selectivity and low electric resistance.

The structure of a membrane produced by Asahi Chemical is shown in the following diagram:[90]



Significant effort has also been concentrated on the development of anion-exchange membranes with low fouling tendencies. In a conventional electrodialysis plant, the limiting current density through the anion-exchange membrane is lower than in the cation-exchange membrane, largely due to the risk of precipitation of inorganic or organic negatively charged materials. As a consequence, its electrical resistance may rise during operation. To overcome this problem, different companies produce special anionic membranes, which are characterized by the fact that they can be used at a higher current density. In

general, the permselectivity of these membranes is lower than of regular membranes.

Composite Membranes

In processes such as reverse osmosis, gas separation and pervaporation, the actual mass separation is achieved by a solution-diffusion mechanism in a homogeneous polymer layer. Since the diffusion process in a homogeneous polymer matrix is relatively slow, these membranes should be as thin as possible, as indicated before. Therefore, an asymmetric membrane structure is mandatory for these processes. Unfortunately, many polymers with satisfactory selectivities and permeabilities for the various components in gas mixtures or liquid solutions are not well suited for the preparation of asymmetric membranes by the phase inversion process described before. This has led to the development of the so-called composite membranes. A composite membrane is shown schematically in Figure 1.29. It is composed of a 20 to 100 nm thin dense polymer barrier layer formed over an approximately 100 μm thick microporous film. Composite membranes differ from asymmetric reverse osmosis membranes by the mode of preparation which consists of two steps: (1) casting of the microporous support, and (2) deposition of the barrier layer on the surface of this microporous support layer. This preparation mode leads to significant advantages of the composite membrane compared to the integral asymmetric membrane. In an integral asymmetric membrane, the selective barrier layer and the microporous support always consist of the same polymer. In a composite membrane, different polymers may be—and in general are—used for the microporous support and the selective barrier layer. This means polymers which show the desired selectivity for a certain separation problem, but have poor mechanical strength or poor film-forming properties, and which are therefore not suited for preparation into integral asymmetric membranes, may well be utilized as the selective barrier in composite membranes. This, of course, expands the variety of available materials for the preparation of semipermeable membranes.

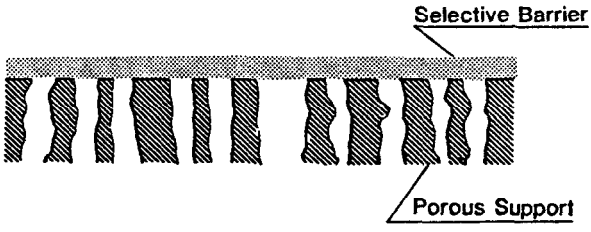


Figure 1.29: Schematic diagram of an asymmetric composite membrane showing the microporous support structure and the selective skin layer.

Preparation Procedures of Composite Membranes. In making composite membranes, two completely different tasks have to be solved. One is the preparation of a suitable microporous support and the second task is the preparation of the actual barrier layer and laminating it to the surface of the support film. The performance of a composite membrane is not only determined by the proper-

ties of the selective barrier layer, but it is also significantly effected by properties of the microporous support film.

Preparation and Deposition of the Selective Barrier Layer on the Microporous Support. The techniques used for the preparation of composite structures may be grouped into four general types:[91-95]

(1) Casting of the barrier layer separately, e.g., *on the surface of a water bath* followed by lamination to the microporous support film.

(2) Dip-coating of the microporous support film in a polymer, a reactive monomer or prepolymer solution followed by drying or curing with heat or radiation.

(3) Gas-phase deposition of the barrier layer of the microporous support film from a glow discharge plasma.

(4) Interfacial polymerization of reactive monomers on the surface of the microporous support film.

Casting an ultrathin film of cellulose acetate on a water surface and transferring the film on a microporous support was one of the earliest techniques used for preparing composite reverse osmosis membranes for water desalination. The actual selective barrier was prepared by dissolving 2–10 percent cellulose diacetate in a solvent exhibiting slight water solubility such as cyclohexanone. Casting an ultrathin film from a dilute acetone solution on a glass plate and releasing the film from the plate after the evaporation of the acetone by immersion in water was another method of preparing ultrathin selective barriers. Although both preparation techniques lead to barrier layers of less than 100 nm with correspondingly high flux rates, they are not well suited for large scale industrial production.[96]

Dip coating a microporous support membrane in polymer or prepolymer solution was also first developed for the preparation of reverse osmosis membranes. Here, a microporous membrane prepared from mixed cellulose esters was first coated by a protective layer of polyacrylic acid to prevent the solvent of the casting solution of the barrier layer, which consisted, e.g., of cellulose triacetate in chloroform, from dissolving the support membrane. This technique was later improved by using a microporous sublayer, which had better overall mechanical and thermal stability and which was insoluble in the solvent of the barrier layer, such as an "open" polysulfone ultrafiltration membrane. Today, dip coating is applied mainly for the preparation of composite membranes to be used in gas separation and pervaporation.[97] Particularly, polymers such as polydimethylsiloxane, which are available as still soluble prepolymers that can easily be crosslinked by a heat treatment procedure thus becoming insoluble in most solvents, are suited for the preparation of this type of composite membrane. If the pore dimension in the support membrane is selected properly, the prepolymer is unable to penetrate the support and a rather thin uniform barrier layer of 0.05 to 1 μm thickness can easily be prepared. A typical composite membrane prepared by dip coating an asymmetric polysulfone ultrafiltration membrane into a 1 wt % solution of polydimethylsiloxane followed by thermal crosslinking is shown in the scanning electron micrograph of Figure 1.30.

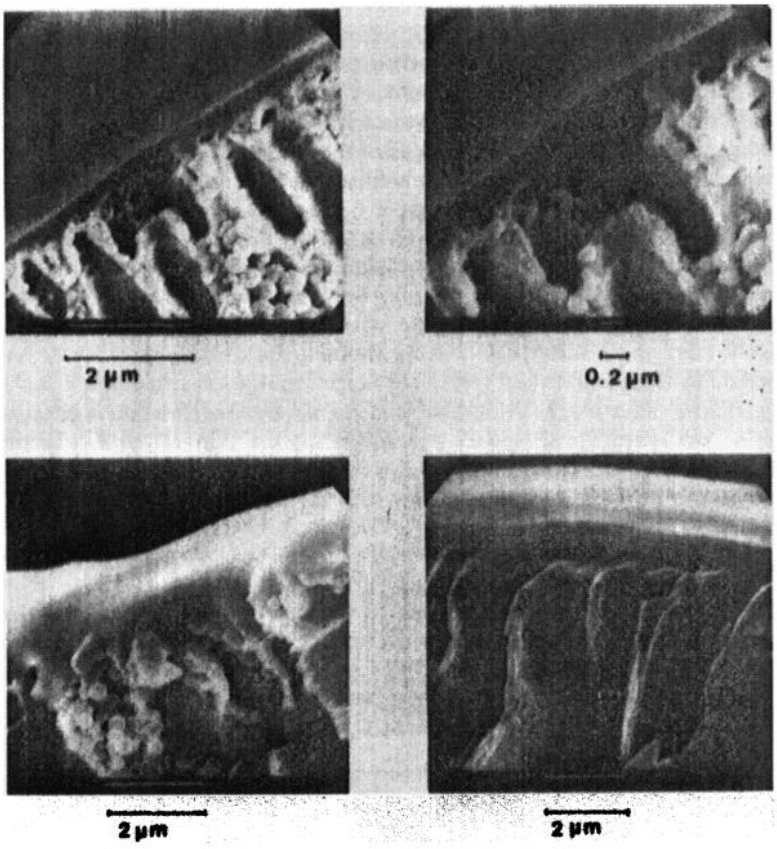


Figure 1.30: Scanning electron micrograph showing a composite membrane with polydimethylsiloxane as the selective layer deposited on a polysulfone support membrane.

Gas phase deposition of the barrier layer on a dry microporous support membrane by plasma polymerization was also successfully used for the preparation of reverse osmosis membranes. Many organic compounds having adequate vapor pressure can be used to form a barrier layer on a microporous support. The plasma reactions are rather heterogeneous not only involving polymerization but depolymerization and modification of functional groups. Although reverse osmosis membranes with excellent desalination properties showing salt rejection in excess of 99%, and fluxes of 1.5 $m^3m^{-2}d^{-1}$ when tested with seawater have been prepared on a laboratory scale,[98] large scale industrial production utilizing plasma polymerization for the preparation of composite membranes seems to be difficult.

Today, by far the most important technique for preparing composite membranes is the interfacial polymerization of reactive monomers on the surface of a

microporous support film. The first membrane produced on a large scale with excellent reverse osmosis desalination properties was developed in the early seventies in the North Star Research Institute under the code name NS 100.[99] The preparation procedure of this membrane, which exhibited water fluxes of about 1 $m^3m^{-2}d^{-1}$ and salt rejections in excess of 99% when tested with seawater at 60 bar pressure, was rather simple. A polysulfone support membrane was soaked in an aqueous solution of 0.5 to 1% polyethyleneimine, which was reacted interfacially at the membrane surface with a 0.2 to 1% solution of toluene diisocyanate in hexane. A heat curing step at 110°C leads to further crosslinking of the polyethyleneimine. The preparation is shown schematically in Figure 1.31. The process seems to involve two types of reactions. In a first step, the polyethyleneimine reacts rapidly at the interphase with the toluene diisocyanate to form a polyamide surface skin while amine groups below this surface remain unreacted. In the second heat treatment step, internal crosslinking of the polyethyleneimine takes place. Thus, the final membrane has three distinct layers of increasing porosity: (1) the dense polyamide surface skin which acts as the actual selective barrier, (2) a thin crosslinked polyethyleneimine layer which extends into the pore of the support film, and (3) the actual polysulfone support membrane.

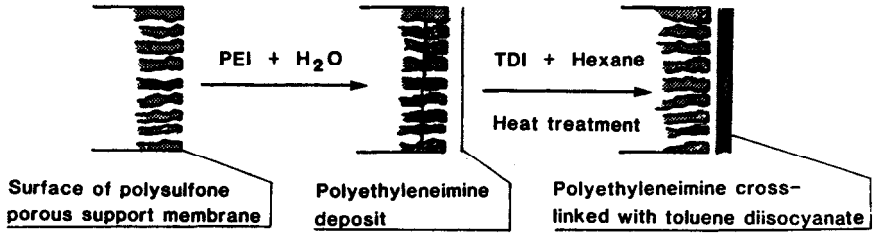


Figure 1.31: Schematic diagram showing the formation of a composite membrane by interfacial polymerization of polyethyleneimine with toluene diisocyanate.

Although the NS-100 membrane showed significantly higher salt rejection capability and higher fluxes than most integral asymmetric reverse osmosis membranes, further improvements were achieved by using aromatic diamines and triacyl chloride reactants. One of these membranes, the FT-30, produced by Film Tec Corporation from monomeric diamine reactants such as m-phenylenediamine interfacially polymerized with trimesoyl chloride shows not only excellent desalination properties but also highly improved stability towards oxidizing agents.[100]

Preparation of the Microporous Support of Composite Membranes. Although the selectivity of a composite membrane is determined nearly exclusively by the actual barrier layer, its overall performance is strongly affected by the microporous substructure. The mechanical stability of the membrane as well as its flux rate is to a large extent determined by the pore size and the overall porosity of the substructure as can easily be demonstrated by the schematic diagram of Figure 1.32. This diagram shows an idealized homogeneous barrier layer with a

thickness of 0.1 μm on a microporous support, with the average pore diameter being 0.2 μm and a porosity of 50%. The actual diffusion pathway of the component through the barrier layer is always longer than the thickness of the layer. The average path length, λ_M, can, to a first approximation, be expressed as a function of the membrane overall porosity, ϵ, the thickness of the barrier layer, λ_o, and the radius of the pores, r, in the support structure, by the following relation:

$$\lambda_M = \varepsilon \lambda_0 + (1-\varepsilon)\frac{1}{2}\left[\sqrt{r^2\left(\frac{1-\varepsilon}{\varepsilon}\right)\cdot \lambda_0} + \lambda_0\right] \qquad (12)$$

This relation which can be obtained by simple geometric considerations indicates that the effective diffusional path length is always longer than the thickness of the barrier layer and that it is strongly affected by the overall porosity of the substructure. For practical purposes, the porosity of the support should be as high as possible. Unfortunately, many ultrafiltration membranes have a rather low surface porosity of 2–4%. While at relatively high surface porosities, i.e., in excess of 50%, the effective diffusional length is approximately identical with the thickness of the barrier layer it will increase according to equation (12) by about an order of magnitude, when the porosity is less than 1% assuming the barrier layer thickness is approximately the same as the pore radius. Accordingly, the flux will decrease by the same magnitude. The geometrical consideration expressed in equation (12) indicates that the surface porosity of the support layer will significantly effect the membrane flux, and it should always be as high as possible when optimal flux rates shall be achieved with thin film composite membranes. For mechanical strength, the pore diameter should not be significantly larger than the film thickness.

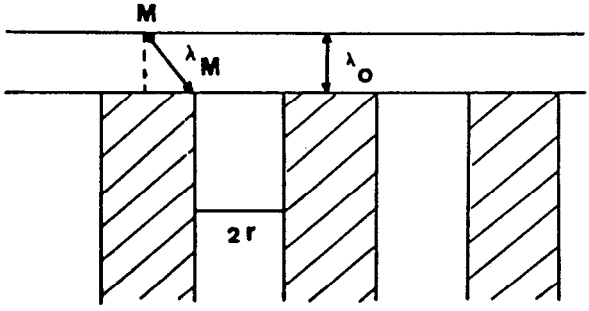


Figure 1.32: Schematic diagram showing a homogeneous barrier film on a microporous substructure. The actual average diffusional pathlength λ_M of a component through a film of the thickness λ_o is expressed as a function of the overall porosity and the pore radius.

Industrial Scale Membrane Production

For any membrane to be useful in an industrial process it has to be produced on a large scale and installed into an appropriate device which should be com-

pact, reliable, and inexpensive. For technical use membranes are, therefore, integrated into so-called modules. Besides economic considerations, chemical engineering aspects are of prime importance for the design of membrane modules. Since the various membrane separation processes differ significantly in their operational concept and their applications, the membrane modules used for the various processes are equally different.

Membrane Modules and Their Fabrication. A large number of different module systems are described in the literature. However, only six basic types are used today on a large industrial scale. These modules are shown schematically in Figure 1.33 (a)–(f). The pleated cartridge filter module, which is shown in (a) is used mainly in dead-end microfiltration. It consists of a pleated membrane cartridge installed in a pressurized housing. The feed solution enters the filter from the housing side and the product is collected in a center tube which is sealed against the housing by an O-ring.

Cartridge type filters are operated at relatively low hydrostatic pressures. Their useful life is limited due to plugging of the membrane pores by retained solutes. The actual cartridge is made by pleating a membrane sheet and potting the ends by an appropriate resin or hot-melt-glue as indicated in Figure 1.33 (a).

Another module type used on an industrial scale for various membrane separation processes including ultrafiltration, reverse osmosis, and gas separation is the plate-and-frame module. Its design has its origins in the conventional filter press concept. The membranes, porous membrane support plates, and spacers forming the feed flow channel are clamped together and stacked between two endplates as indicated in the schematic diagram of Figure 1.33 (b). There are various types of plate-and-frame modules on the market which offer, however, only slight variations in their basic configuration.[101]

A variation of the basic plate-and-frame concept is the spiral-wound module, which is widely used today in reverse osmosis, ultrafiltration, and gas separation. Its basic design is illustrated in Figure 1.33 (c). The feed flow channel spacer, the membrane, and the porous membrane support are rolled up and inserted into an outer tubular pressure shell. The filtrate is collected in a tube in the center of the roll.

While the previously described three membrane modules required flat sheet membrane material for their preparation, special membrane configurations are needed for the preparation of the tubular, capillary, and hollow fiber modules. The tubular membrane module consists of membrane tubes placed into porous stainless steel or fiber glass reinforced plastic pipes. The pressurized feed solution flows down the tube bore and the permeate is collected on the outer side of the porous support pipe, as indicated in Figure 1.33 (d). The diameters of tubular membranes are typically between 1–2.5 cm. In some modules, the membranes are cast directly on the porous pipes and in others they are prepared separately as tubes and then installed into the support pipes.

The capillary membrane module, which is shown schematically in Figure 1.33 (e), consists of a large number of membrane capillaries with an inner diameter of 0.2 to 3 mm arranged in parallel as a bundle in a shell tube. The feed solution is passed down the center of the membrane capillary and the filtrate, which permeates the capillary wall, is collected in the shell tube. The capillary membrane module requires as basic material membranes in a self-supporting capillary configuration, which, when asymmetrically structured, carry the selective

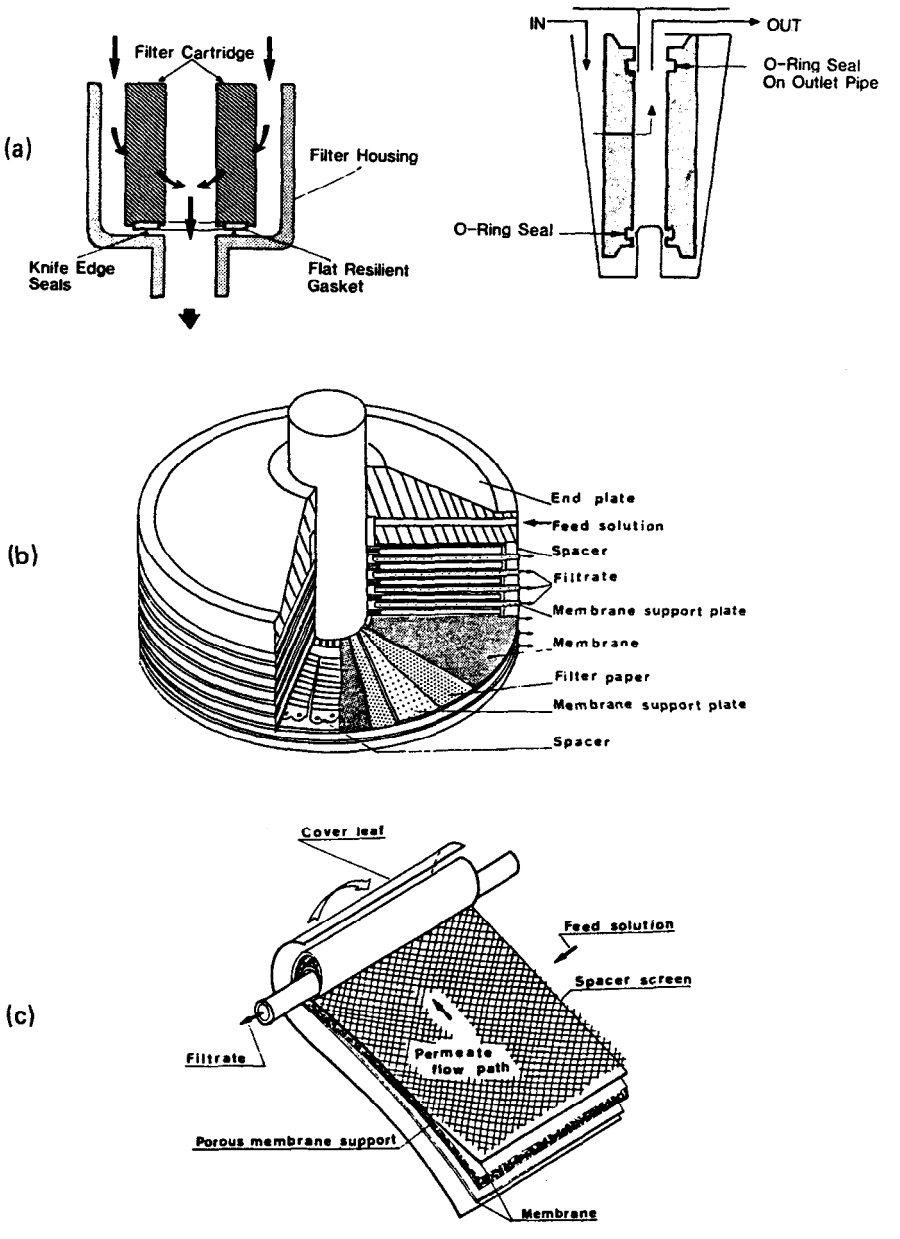
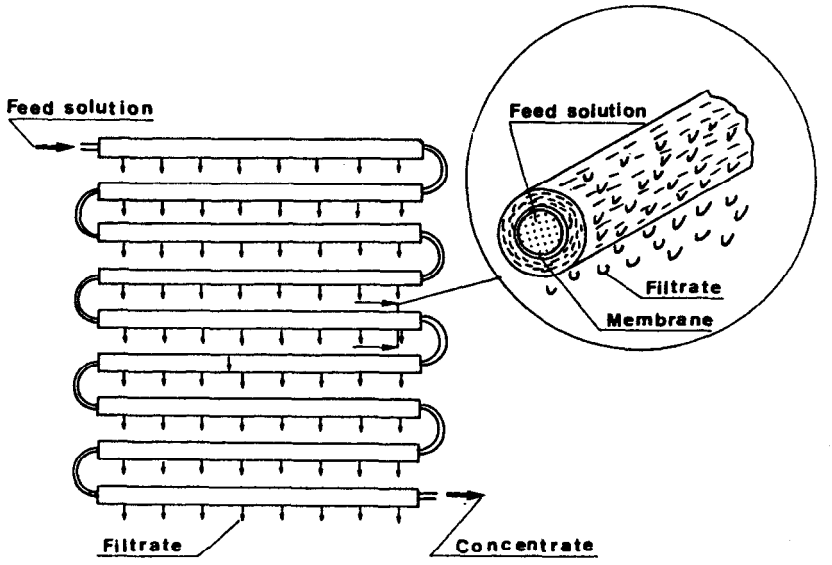
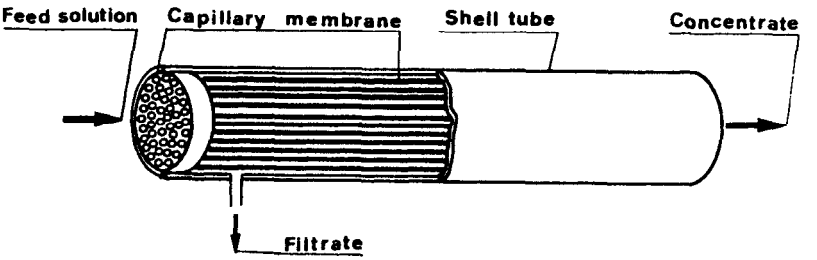


Figure 1.33: Schematic diagram showing membrane modules presently used in industrial separation processes: (a) pleated membrane filter cartridge; (b) plate-and-frame membrane module; (c) spiral wound membrane module; (d) tubular membrane module; (e) capillary membrane module; (f) hollow fiber membrane module.

(d)



(e)



(f)

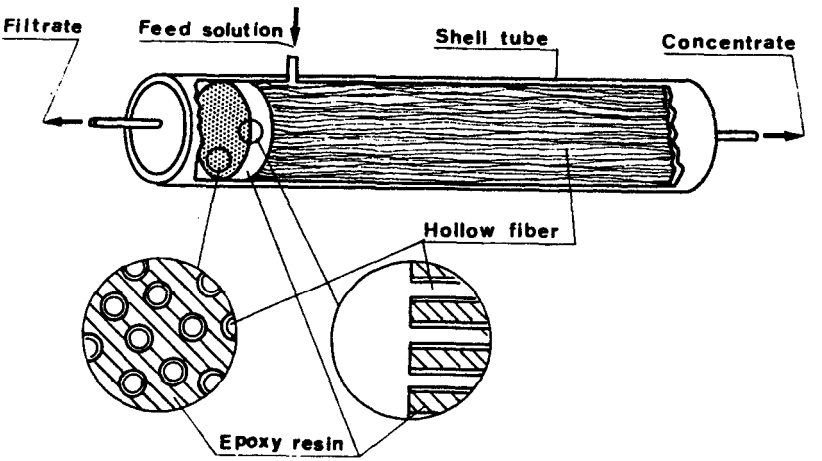


Figure 1.33: (continued)

barrier on the inner side of the capillary as indicated in the scanning electron micrograph of Figure 1.34, which shows a typical capillary ultrafiltration membrane prepared in a wet-spinning process.

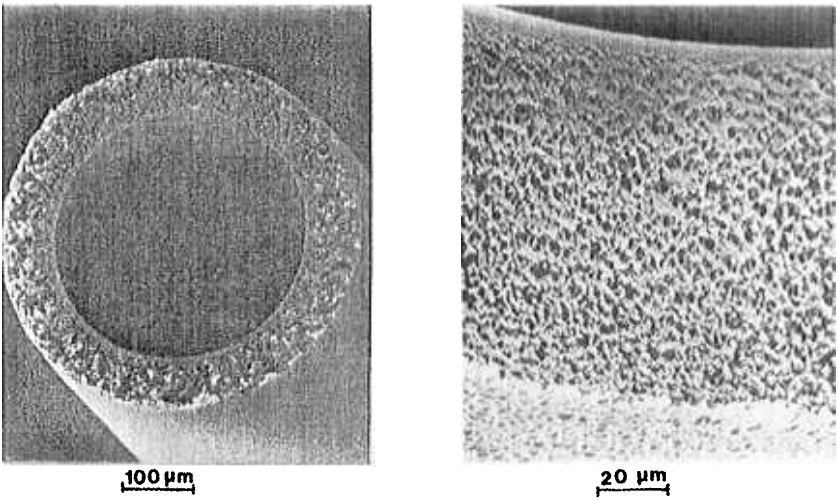


Figure 1.34: SEM of a capillary membrane.

The same basic spinning process is used for the preparation of hollow fiber membranes, which have an outer diameter of 50 to 100 µm. In hollow fiber membranes, the selective layer is on the outside of the fibers, which are installed as a bundle of several thousand fibers in a half loop with the free ends potted with an epoxy resin in a pressure tube as indicated in Figure 1.33 (f). The feed solution is introduced around the outside of the hollow fibers. The filtrate passes through the fiber walls and flows up the bore to the open end of the fibers at the epoxy head.

Membrane Manufacturing Equipment

Based on the different modules used in technical scale membrane separation processes, there are four basic membrane configurations produced today on a large scale. These are flat sheet, tubular, capillary, and hollow fiber membranes.

Flat sheet membranes are generally manufactured on a casting machine, which is shown schematically in Figure 1.35. A polymer solution is cast by a casting knife on a polyester or polyethylene support paper, which is continuously supplied from a roll. The cast polymer film is fed to the precipitation bath, where the actual membrane is formed. After a certain residence time in a rinse bath, where residue solvent is removed, the membrane is collected as a flat sheet on the take up roll. The membranes, which are obtained as up to 2 m wide continuous sheets, are then further processed into the desired module configuration.

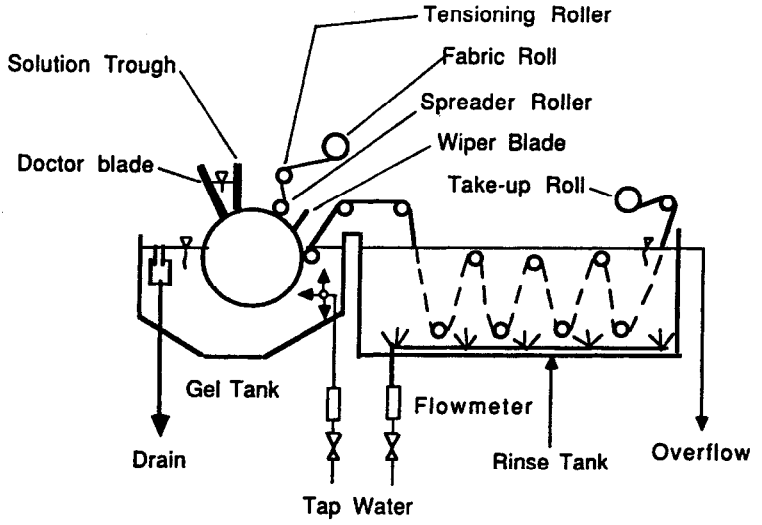


Figure 1.35: Schematic diagram indicating the function of a casting machine used for the preparation of supported flat sheet membranes.

Capillary and hollow fiber membranes are manufactured generally by a wet-spinning process using a spinneret with a double bore nozzle as indicated in Figure 1.36 (a), which shows a schematic diagram of a spinneret for the production of asymmetric hollow fiber or capillary membranes. The casting solution is always fed in the outer bore of the nozzle. If an asymmetric capillary membrane with the skin on the inside shall be produced, the precipitant is directed through the central bore, thus, the precipitation progresses from the inside to the outside and a capillary with the selective layer on the inside is formed immediately at the outlet of the spinneret. The capillaries, therefore, have about the dimensions of the spinning nozzle.

If an asymmetric hollow fiber with the skin on the outside is to be produced, the precipitant in the inner bore is replaced by an inert gas and the fiber is spun into the precipitation bath. Between the precipitation bath and the spinneret there is an air gap as indicated in Figure 1.36 (b) where the fiber may be drawn to obtain the desired dimensions before precipitation. Hollow fibers have, therefore, often significantly smaller diameters than the nozzle.

Tubular membranes are prepared either by an ultrasonic welding process from flat sheet membranes or by direct casting on a porous support tube using a conical casting device pulled through the porous tube. Since the outer diameter of the casting cone is slightly smaller than the inner diameter of the tube, a thin polymer solution film is formed on the inside of the tube, which is then converted into a membrane by immersing the entire tube into a precipitation bath.

There are many variations of the basic membrane preparation techniques described in this chapter. But most of them have only limited technical significance and shall not be discussed further.

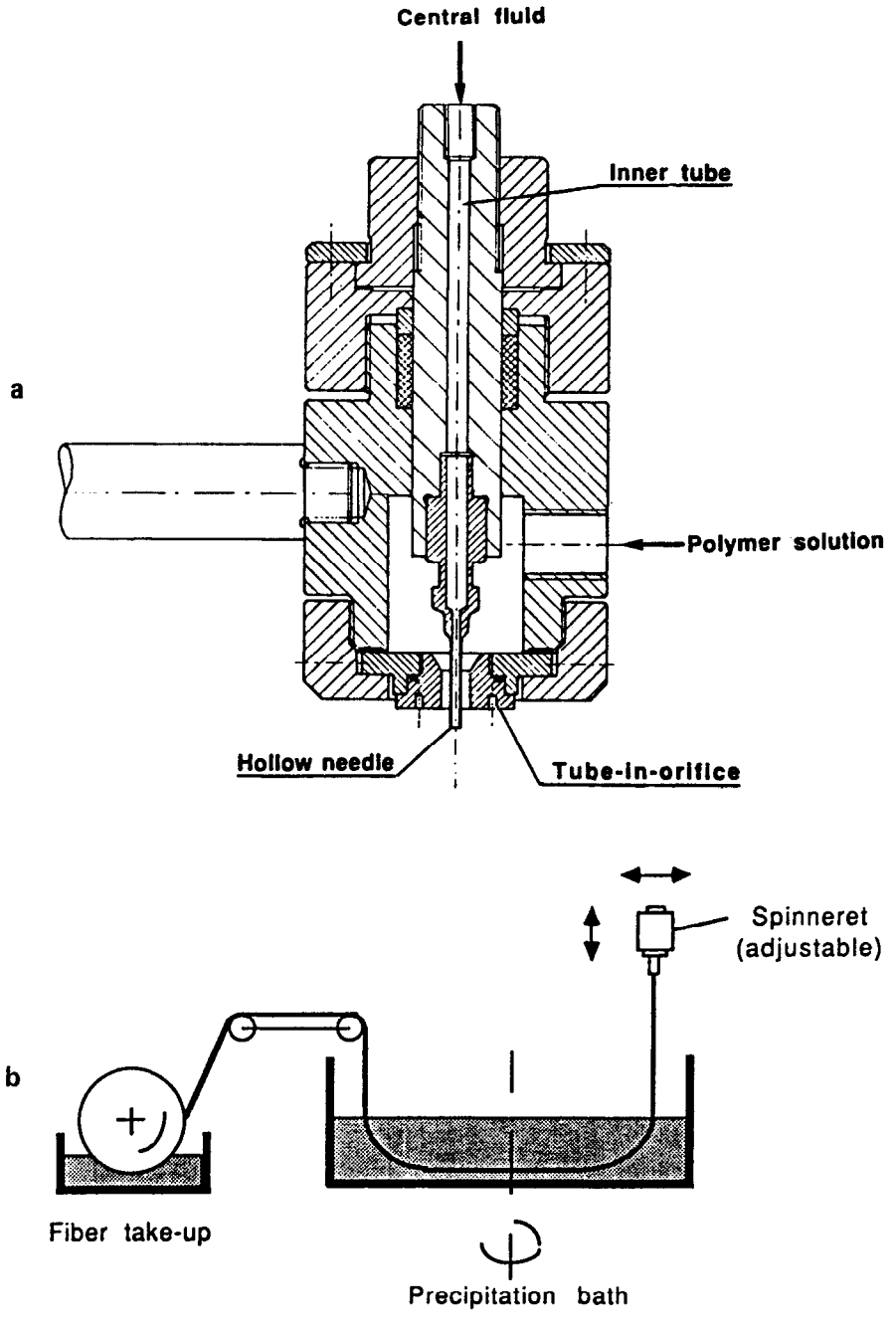


Figure 1.36: Manufacturing device for capillary and hollow fiber membranes: (a) spinneret; (b) hollow fiber uptake unit.

FUTURE DEVELOPMENTS

For many separation processes, such as sea and brackish water desalination by electrodialysis and reverse osmosis or the production of ultrapure water by microfiltration, membranes with quite satisfactory properties are commercially available today. But, even for comparatively mature processes such as microfiltration and reverse osmosis, "better" membranes are desirable. In microfiltration, research is concentrated on membranes having an asymmetric structure with high surface porosities in excess of 70% and average pore sizes at the surface between 0.01 and 0.1 μm. These membranes are made from polymers, such as Nylon 6.6 which show good solvent resistance and low adsorption for "fouling" materials. In reverse osmosis water desalination work is concentrated mainly on the development of membranes with improved stability against oxidizing agents such as chlorine or hypochlorite with higher fluxes and better flux stability. With the emerging use of microfiltration, ultrafiltration, reverse osmosis, and electrodialysis in biotechnology and the chemical process industry, completely new requirements are put on the membranes to be used in these applications.

The main effort as far as synthetic membranes are concerned is concentrated on the development of completely new membranes for processes such as pervaporation, gas separation, membrane distillation, or as ion transferring separators in batteries, fuel cells or electrochemical production processes. Liquid membranes with selective carriers used today for the separation and concentration of heavy metal ions or certain organic compounds are being developed further to be used in gas separation.

A very important area of today's ongoing research is the development of functional synthetic membranes which mimic the function of the biological membrane.[102] Biocatalytic membranes, energy and information transducing membranes have already been produced on a laboratory scale[103] and are used today as biosensors for monitoring devices. Although a significant number of functional synthetic membranes have been developed, they are all far behind the actual biological membranes. But basic research in membrane technology combined with progress in molecular engineering should help to improve the properties of functional synthetic membranes and thereby increase their use far beyond today's level.

REFERENCES

1. Lonsdale, H.K., *J. Memb. Sci.*, 10 (1982) 81-181.
2. Porter, M.C., Membrane filtration, in: P.A. Schweitzer (Ed.), *Handbook of Separation Techniques for Chemical Engineers*, McGraw-Hill, New York (1979), pp. 2-3 to 2-103.
3. Baker, R. (Ed.), *Controlled Release of Bioactive Materials*, Academic Press, New York (1980).
4. Strathmann, H., *Trends in Biotechnology*, 3 (1985) 112-118.
5. Strathmann, H., *Trennung von molekularen Mischungen mit Hilfe synthetischer Membranen*, Steinkopff Verlag, Darmstadt (1979).
6. Katchalsky, A. and Curran, P.T., *Nonequilibrium Thermodynamics in Biophysics*, Harvard University Press, Cambridge, Mass. (1967).

7. Kedem, O. and Katchalsky, A., *Trans. Faraday Soc.*, 59 (1963) 1918.
8. Helfferich, F., *Ion-Exchange*, McGraw-Hill, London (1962).
9. Hwang, S.-T. and Kammermeyer, K., *Membranes in Separations*, John Wiley & Sons, New York (1975).
10. Druin, M.L., Loft, J.T. and Plovan, S.G., U.S. Pat. 3,801,404 (1974).
11. Gore, R.W., U.S. Pat. 3,962,153 (1976).
12. Schneider, K. and van Gassel, T.J., *Chem. Ing. Tech.*, 7 (1985) 514–521.
13. Fleischer, R.L., Price, P.B. and Walker, R.M., *Sci. Amer.*, 220 (1969) 30.
14. Riedel, C. and Spohr, R., *J. Membr. Sci.*, 7 (1980) 225–234.
15. Porter, M.C., *Am. Lab.*, November 1974.
16. Reid, H.L., Barnes, A.J., Lock, P.J. and Dormandy, J.A., *J. Clin. Path.*, Vol. 29, No. 9 (September 1976).
17. Kesting, R.E., *Synthetic Polymeric Membranes*, McGraw-Hill, New York (1971).
18. Strathmann, H., Production of microporous media by phase inversion processes, in: *Material Science of Synthetic Membranes*, D.R. Lloyd (Ed.), pp. 165–195, ACS Symposium Series 269, American Chemical Society, Washington D.C. (1985).
19. Zsigmondy, R., U.S. Pat. 1,421,341 (1922).
20. Pall, D.B., U.S. Pat. 4,340,479 (1982).
21. Hiatt, W.C., Vitzthum, G.H., Wagener, K.B., Gerlach, K. and Josefiak, C., Microporous membranes via upper critical temperature phase separation, in: *Material Science of Synthetic Membranes*, D.R. Lloyd (Ed.) pp. 229–244, ACS Symposium Series 269, American Chemical Society, Washington D.C. (1985).
22. MacLean, D.W., *J. New England Water Works Assoc.*, 72 (1958) 272.
23. Cotton, R.A. and Fifield, C.W., Standardization of membrane filters for microbiological applications, in: B.J. Dutka (Ed.), *Membrane Filtration: Applications, Techniques, and Problems*, Marcel Dekker, New York (1981), pp. 19–39.
24. Hood, H.P. and Nordberg, M.E., U.S. Pat. 2,106,744 (1938).
25. Schnabel, R., Proceed. 5th Intern. Symp., Fresh water from the sea, Vol. 4 (1976) 409–413.
26. Michaels, A.S., *Pure Appl. Chem.*, 46 (1976) 193–204.
27. Kesting, R.E., Phase inversion membranes, in *Material Science of Synethetic Membranes*, D.R. Lloyd (Ed.), pp. 131–164, ACS Symposium Series 269, American Chemical Society, Washington D.C. (1955).
28. Loeb, S. and Sourirajan, S., U.S. Patent 3,133,132 (1964).
29. U. Merten (Ed.), *Desalination by Reverse Osmosis*, MIT Press, Cambridge, Mass. (1966).
30. Manjikian, S., *Ind. Eng. Chem. Prod. Res. Dev.*, 6 (1967) 23.
31. Zsigmondy, R. and Carius, C., *Chem. Ber.*, 60 B (1927) 1074.
32. Kesting, R.E., *J. Appl. Polym. Sci.*, 17 (1973) 1771.
33. Strathmann, H. and Kock, K., *Desalination*, 21 (1977) 241.
34. Wijmans, J.G., Baaij, J.P.B. and Smolders, C.A., *J. Membr. Sci.*, 14 (1983) 263–274.
35. Strathmann, H., Scheible, P. and Baker, R.W., *J. Appl. Polym. Sci.*, 15 (1971) 811–828.
36. Strathmann, H., Kock, K., Amar, P. and Baker, R.W., *Desalination*, 16 (1975) 179–302).

37. Broens, L., Altena, F.W. and Smolders, C.A., *Desalination*, 32 (1980) 33.
38. Frommer, M.A., Feiner, I., Kedem, O. and Block, R., *Desalination*, 7 (1970) 393.
39. Altena, F.W. and Smolders, C.A., *Macromolecules*, 15 (1982) 1491.
40. Haase, R., *Thermodynamik der Mischphasen*, Springer Verlag, Berlin (1956).
41. Jost, W., *Diffusion in Solids, Liquids and Gases*, Academic Press, New York, N.Y. (1970).
42. Frommer, M.A., Matz, R. and Rosenthal, U., *Ind. Eng. Chem. Prod. Res. Dev.*, 10 (1971) 193.
43. Ray, R.J., Krantz, W.B. and Sani, R.L., *J. Membr. Sci.*, 23 (1985) 155–182.
44. Kamide, K. and Manabe, S., Role of microphase separation phenomena in the formation of porous polymeric membranes, in: *Material Science of Synthetic Membranes*, D.R. Lloyd (Ed.), pp. 197–228, ACS Symposium Series 269, American Chemical Society, Washington D.C. (1985).
45. Wijmans, J.G., *Synthetic membranes*, Ph.D. Thesis, Twente University, Enschede, Holland (1984).
46. Sourirajan, S. and Kunst, B., Cellulose acetate and other cellulose ester membranes, in: *Reverse Osmosis and Synthetic Membranes*, S. Sourirajan (Ed.), National Research Council Canada, Ottawa, Canada (1977).
47. Kesting, R.E., *Synthetic Polymeric Membranes, A Structural Perspective*, Wiley-Interscience, New York, N.Y. (1985).
48. Lonsdale, H.K., Merten, U. and Riley, R.L., *J. Appl. Polym. Sci.*, 9 (1965) 1341–1362.
49. Stannett, V., Szwarc, M., Ghargava, R.L., Meyer, J.A., Myers, A.W. and Rogers, C.E., Permeability of Plastic Films and Coated Paper to Gases and Vapors, Tappi Monograph Series, No. 23, Technical Association of the Pulp and Paper Industry, New York (1962).
50. Brubaker, D.W. and Kammermeyer, K., *Ind. Engr. Chem.*, 44 (1952) 1465–1474.
51. Stern, S.A. and Walawender, W.P., Jr., *Sep. Sci.*, (1969) 129–159.
52. Stannett, V.T., Koros, W.J., Paul, D.R., Lonsdale, H.K. and Baker, R.W., *Adv. Polymer Sci.*, 32 (1979) 99–151.
53. Buck, R.P., Thompsen, J.C. and Melroy, O.R., A compilation of ion-selective membrane electrode literature, in: *Ion-Selective Electrodes in Analytical Chemistry*, H. Freiser (Ed.), Plenum Publishing Co., New York (1978).
54. Kammermeyer, K., *Chem. Ing. Tech.*, 48 (1976) 672–675.
55. Crank, J. and Park, G.S. (Eds.), *Diffusion in Polymers*, Academic Press, New York (1968).
56. Stern, S.A., The separation of gases by selective permeation, in: *Membrane Separation Processes*, P. Meares (Ed.), Elsevier, Amsterdam (1976).
57. Ward, W.J. III, Browall, W.R. and Salemme, R.M., *J. Memb. Sci.*, 1 (1976) 99–108.
58. Richter, J.W. and Hoehn, H.H., U.S. Pat. 3,567,632, March 2, 1971.
59. McLain, E.A. and Mahon, H.I., U.S. Pat. 3,423,491, January 21, 1969.
60. Browall, W.R., Kimura, S.G. and Ward W.J., III, Ultrathin membranes for oxygen enrichment, paper presented at the Interamerican Congress of Chemical Engineers, Caracas, Venezuela, July 13–16, 1975.
61. Product bulletin, *OECO Membrane Type Oxygen Enricher*, Oxygen Enrichment Co., Schenectady, New York (December 1980).

62. Lonsdale, H.K., *Desalination*, 13 (1973) 317–332.
63. Lloyd, D.R., Meluch, T.B., Selection and evaluation of membrane materials for liquid separation, in: *Material Science of Synthetic Membranes*, D.R. Lloyd (Ed.), pp. 47–79, ACS Symposium Series 269, American Chemical Society, Washington, D.C. (1985).
64. Hunter, J.B., U.S. Pat. 2,773,561 (1956).
65. Hunter, J.B., *Platinum Metals Rev.*, 4 (1960) 130.
66. Ward, W.J., III, *AIChE J.*, 16 (1970) 405–410.
67. Cussler, E.L., *AIChE J.*, 17 (1971) 1300–1303.
68. Li, N.N., U.S. Pat. 3,410,794 (1968).
69. Li, N.N., *AIChE J.*, 17 (1971) 459.
70. Babcock, W.C., Baker, R.W., LaChapelle, E.D. and Smith, K.L., *J. Membr. Sci.*, 7 (1980) 71–87.
71. Largman, T. and Sifniades, S., *Hydrometallurgy*, 3 (1978) 153–162.
72. Baker, R.W., Roman, J.C., Smith, K.L. and Lonsdale, H.K., *Industrial Heating* (July 1982).
73. Babcock, W.C., Baker, R.W., LaChapell, E.D. and Smith, K.L., *J. Memb. Sci.*, 7 (1980) 80–100.
74. Kunin, R., *Ion-Exchange Resins*, Wiley, New York (1958).
75. Bergsma, F. and Kruissink, C.A., *Fortschr. Hochpolym.-Forsch.*, 2 (1961) 307–362.
76. Meares, P., Trends in ion-exchange membrane science and technology, in: *Ion-Exchange Membranes*, D.S. Flett (Ed.), E. Horwood Ltd., Chichester, England (1983).
77. Spiegler, K.S. and Laird, A.D.K. (Eds.), *Principles of Desalination*, 2nd edition, Academic Press, New York (1980).
78. Juda, W. and McRae, W.A., U.S. Patent 2,636,851 (April 28, 1953).
79. Ogami, K. and Kanda, C., Jap. Pat. 1897 (1958).
80. Atsugi, Ichikawa, T.M. and Yamada, M., Jap. Pat. 2293 (1958).
81. Onogram, K. and Mizutani, Y., Jap. Pat. 91 (1959).
82. Evers, W.L., U.S. Pat. 2,518,420 (1948).
83. Bodamer, G.W., U.S. Pat. 2,597,438 (1952).
84. deKörösy, F. and Schorr, Y., U.S. Pat. 891,562 (1963).
85. Zschocke, P. and Quellmalz, D., *J. Membr. Sci.*, 22 (1985) 325–332.
86. Bodamer, G.W., U.S. Pat. 2,681,320 (1954).
87. Grot, W.G., *Chem. Ing.-Tech.*, 47 (1975) 617.
88. Grot, W.G., U.S. Pat. 3,784,399 (1974).
89. Sata, T., Motani, K. and Ohaski, Y., Perfluorinated exchange membrane "Neosepta-F" and its properties, in: *Ion Exchange Membranes*, D.S. Flett (Ed.), E. Horwood Ltd., Chichester (1983).
90. Seko, M., Yomiyama, A. and Ogawa, S., Chlor-alkali electrolysis using perfluorocarboxylic acid membranes, in: *Ion-Exchange Membranes*, D.S. Flett (Ed.), E. Horwood Ltd., Chichester (1983).
91. Riley, R.L., Lonsdale, H.K., Lyons, C.R. and Merten, U., *J. Appl. Polym. Sci.*, 11 (1967) 2143–2158.
92. Riley, R.L., Fox, R.L., Lyons, C.R., Milstead, C.E., Seroy, M.W. and Tagami, M., *Desalination*, 19 (1976) 113–126.
93. Cadotte, J.E., King, R.S., Majerle, R.J. and Petersen, R. J., *J. Macromol. Sci. Chem.*, A15 (1981) 727–755.

94. Yasuda, H. and Marsh, H.C., *J. Appl. Polym. Sci.*, 20 (1976) 543.
95. Cadotte, J.E., U.S. Pat. 4,039,440 (1977).
96. Cadotte, J.E., Evolution of composite reverse osmosis membranes, in: *Material Science of Synthetic Membranes*, D.R. Lloyd (Ed.), pp. 273-294, ACS Symposium Series 269, American Chemical Society, Washington DC (1985).
97. Henis, J.M.S. and Tripodi, M.K., *Sep. Sci. Tech.*, 15 (1980) 1059-1068.
98. Yasuda, H. and Lamaze, C.E., *J. Appl. Polym. Sci.*, 17 (1973).
99. Rozelle, L.T., Cadotte, J.E., Cobian, K.E. and Kopp, C.V., Nonpolysaccharide membranes for reverse osmosis: NS-100 Membranes, in: *Reverse Osmosis and Synthetic Membranes*, S. Sourirajan (Ed.), pp. 249-261, National Research Council Canada, Ottawa, Canada (1977).
100. Cadotte, J.E., King, R.S., Majerle, R.J. and Petersen, R.J., *J. Macromol. Sci. Chem.*, A15 (1981) 727-755.
101. Madsen, R.F., *Hyperfiltration and Ultrafiltration in Plate-and-Frame Systems,* Elsevier Publishing Company, Amsterdam (1977).
102. Bader, H., Dorn, K., Hupfer, B., Ringsdorf, H., in *Advances in Polymer Science: Polymer Membranes,* M. Gordon (Ed.), Springer Verlag, Berlin (1985).
103. Shimidzu, T., Yoshikawa, M., *J. Membr. Sci.*, 13 (1983) 1-3.

2

Microfiltration

Mark C. Porter

INTRODUCTION

The beginnings of microfiltration (MF) can be traced back into the 19th century with the synthesis of nitrocellulose in 1845 by Schoenbein. Fick then used ether-alcohol solutions of the same (collodion) to form the first nitrocellulose membranes in 1855. Even today, the most common polymers used in MF membranes are mixed esters of cellulose-including cellulose nitrate.

At the turn of the century (1906), Bechhold produced graded pore sizes in collodion membranes and measured the pore size with the "bubble-point" method (to be described later).

In the first quarter of the twentieth century, researchers like Bigelow, Gemberling, Schoep, Brown, Zsigmondy, and Bachmann made significant advances in the methodology of casting and regulating pore size. It is astonishing that the art of controlling pore size and microstructure was developed to such a high degree of sophistication before understanding the mechanism of membrane formation.

With the help of Professor Dr. Zsigmondy, who was Director of the Institute of Colloid Chemistry of the University of Goettingen, Sartorius-Werke Aktiengesellschaft developed a commercial process for making cellulose nitrate membranes. The membrane was known as the "Zsigmondy Membranfilter." Commercial production began in 1927, but sales were largely confined to the laboratory market.

The first important application of these membranes emerged during World War II. Gertrude Mueller and others of the Hygiene Institute of the University of Hamburg developed the membrane for filtering and culturing bacteria. German water supplies were often devastated or contaminated by bombing raids. A more efficient method for detecting coliform or pathogenic bacteria was needed. Conventional culturing techniques in liquid or gel-like nutrient media could take up

to 96 hours. Mueller discovered that the entire bacterial flora in one liter of water could be deposited on a 47 mm diameter membrane within approximately 15 minutes. The membrane could then be placed on top of a nutrient pad allowing the nutrients to diffuse up through the pores of the membrane to the bacteria on the surface of the membrane filter. Each bacterium collected would grow into a colony of thousands overnight. In less that 24 hours of incubation (37°C), the colony would be readily visible and countable by the naked eye.

After the war (1947), the U.S. Joint Intelligence Objectives Agency sent Dr. Alexander Goetz to Germany to obtain information on membrane filter production methods. Goetz visited Membranfiltergesellschaft (Sartorius), and based on his findings, was awarded a contract by the U.S. Chemical Corps. to further develop the membrane. By 1950, Goetz had improved production methods to make membranes with higher flow rates and more uniform pore sizes. He also imprinted grid-lines on his filters to facilitate counting of bacterial colonies.

Based on Goetz's developments, the Lovell Chemical Company in Watertown, Massachusetts was awarded further contracts in 1952 to commercialize production. In 1954, the Lovell Chemical Company sold its membrane manufacturing facility to the newly organized Millipore Corporation. Other companies in both the United States and England then began to exploit the German technology base to manufacture membrane filters.

Eventually, membranes made of materials other than cellulose nitrate began to appear:

1962	Gelman Instrument Co.	Cellulose tri-acetate
1963	Sartorius Co.	Regenerated cellulose
1963	Millipore, Gelman, Sartorius, S&S	Polyvinyl chloride and polyamide
1963	General Electric	Polycarbonate
1964	Selas Flotronics	Silver membrane
1970	Celanese Co.	Polypropylene
1970	Gore Corp.	Polytetrafluoroethylene
1975	Membrane/Enka	Polypropylene
1979	Gelman	Polysulfone
1980	Millipore	Polyvinylidene fluoride
1981	Nuclepore	Polyester
1984	Norton Co., Ceraver	Alumina

MEMBRANE STRUCTURE AND FABRICATION

All current MF membranes may be classified as either "tortuous-pore" or "capillary-pore" membranes (see Figure 2.1). The "capillary-pore" structure is distinguished by its straight-through cylindrical capillaries, whereas the "tortuous-pore" structure resembles a sponge with a network of interconnecting tortuous pores.

The "tortuous-pore" membranes are the most common and include typical cellulosic membranes and virtually all other polymers. The "capillary-pore" membranes are currently manufactured commercially only by Nuclepore Corp. and Poretics Corp. They are available as polycarbonate or polyester membranes.

A unique feature of the "capillary-pore" membranes is that the pore size

can be measured directly with a scanning electron microscope. This is not possible with a "tortuous-pore" membrane since the pore openings do not correspond to the limiting pore size within the depth of the membrane. This is demonstrated in Figure 2.1 where both membranes (of the same pore size rating) are viewed at the same magnification. The "tortuous pore" membrane appears to have some very large pore openings on the surface.

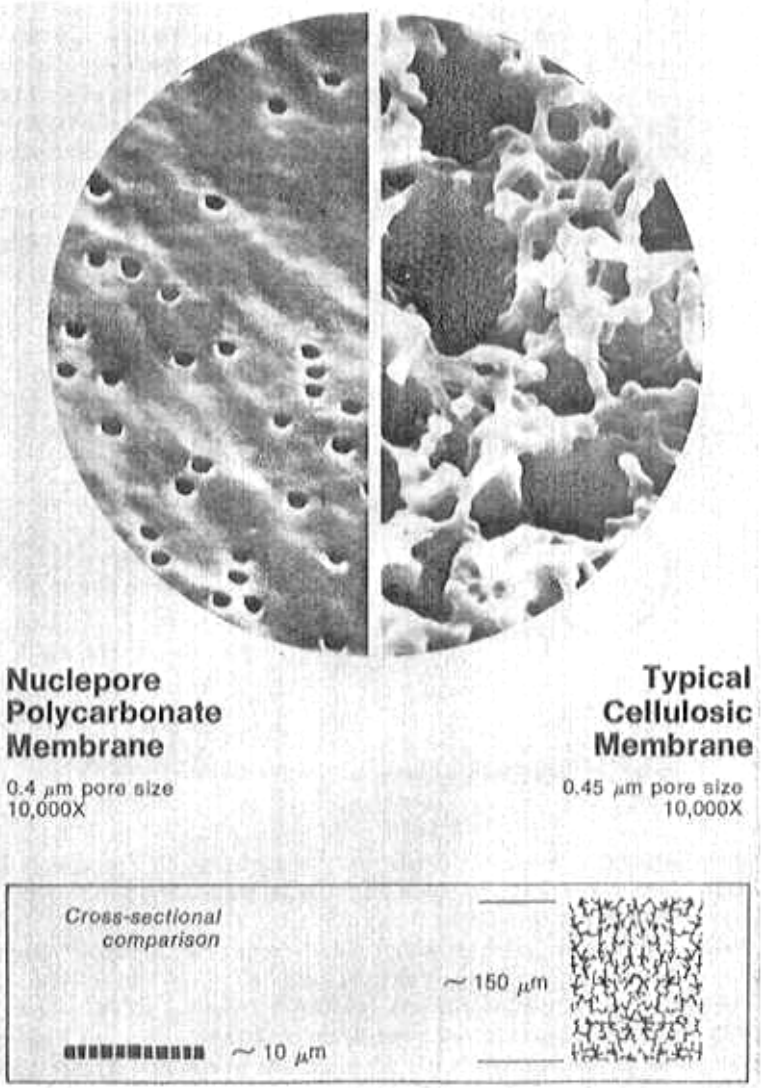


Figure 2.1: Capillary-pore and tortuous-pore membranes.

A look at the open area of the two membranes in Figure 2.1 indicates that the "tortuous-pore" membranes are more porous-having a porosity over 75%. The "capillary-pore" membranes generally have porosities less than 5%. However, the fact that the latter are 1/15 the thickness of the "tortuous pore" membranes means that the flow rates are often comparable.

Tortuous-Pore Membranes

Phase-Inversion Process. Most tortuous-pore membranes are made by a casting process known as "phase inversion." Figure 2.2 is a simplified schematic of a casting machine which makes cellulose ester membranes. Typically, a casting solution made up of the polymer and a multicomponent solvent system is metered onto a stainless steel belt or web. The belt passes through a series of environmental chambers usually containing water vapor at elevated temperatures. The more volatile solvents evaporate and the water vapor precipitates the polymer around the less volatile solvent which becomes the "pore-former." Subsequently, (not shown in Figure 2.2), after the membrane is formed, the residual solvents are washed out of the pores, surfactants are added, and the membrane is dried.

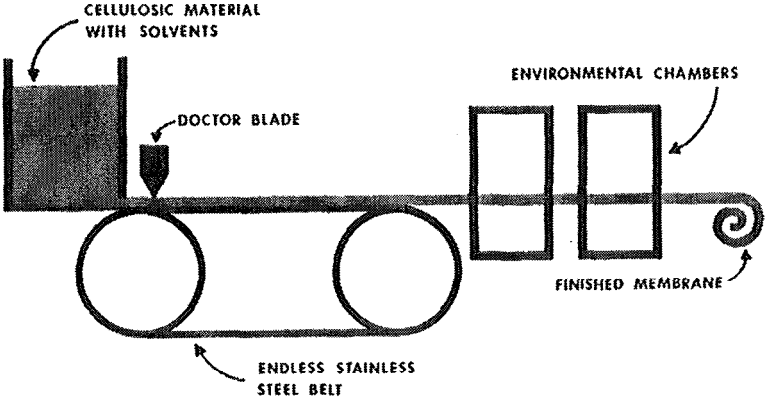


Figure 2.2: Schematic of casting machine for MF membranes.

There are also a few cases where the "phase-inversion" process is accomplished by passing the belt through a liquid water bath to precipitate the polymer as is done with polyvinylidene fluoride.[1]

Stretching Process. Polytetrafluoroethylene (PTFE) or other chemically-resistant polymers cannot always be dissolved in an organic solvent. Robert Gore developed a stretching process for making porous PTFE membranes.[2] Gore's process uses a paste-forming extrusion technique where the extrudate is stretched at a rate exceeding 2000% per second at an elevated temperature. The final length of the stretched product is over 50 times the original length. Figure 2.3 shows the nodes and interconnected fibrils of the porous membrane produced-Goretex™.

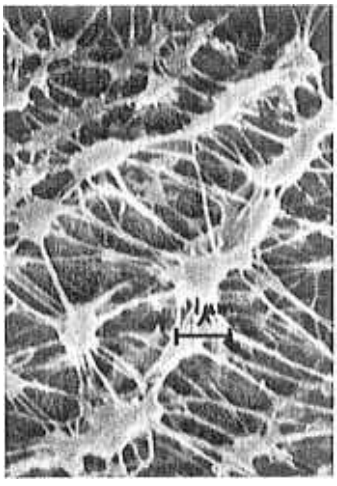


Figure 2.3: Photomicrograph of **PTFE** membrane (GoreTex™).

A similar approach has been used by Celanese Corp. to make Celegard™, an expanded polypropylene membrane (see Figure 2.4). The stretching creates elongated pores measuring 0.02 by 0.20 μ or 0.04 by 0.40 μ. The low flow rates of this membrane limit applications primarily to battery separators and airvents.

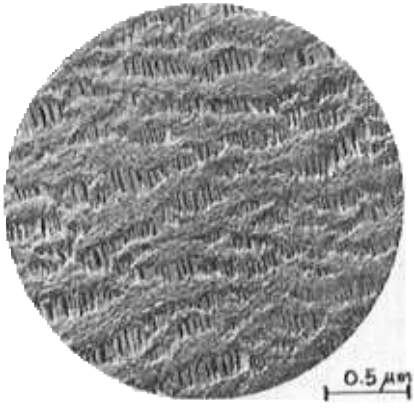


Figure 2.4: Photomicrograph of polypropylene membrane (Celgard™).

Thermal-Phase-Inversion Process. Still another approach to forming porous membranes out of polymers not soluble at room temperature is to elevate the temperature until they dissolve in a selected solvent. The resulting solution is then cooled in a controlled way until the polymer precipitates around the solvent which serves as the "pore-former" at room temperature. The process is called "thermal-phase-inversion."

Tracor Hydronautics and Enka (Membrana) have used this process to make polypropylene MF membranes. It has been speculated that the solvents used were kerosene or various amines. Enka produces both tubes (5.5 mm I.D./8.6 mm O.D.) and capillaries (1.8 mm I.D./2.6 mm O.D.) in pore sizes of 0.2 and 0.4 μ (see Figure 2.5).

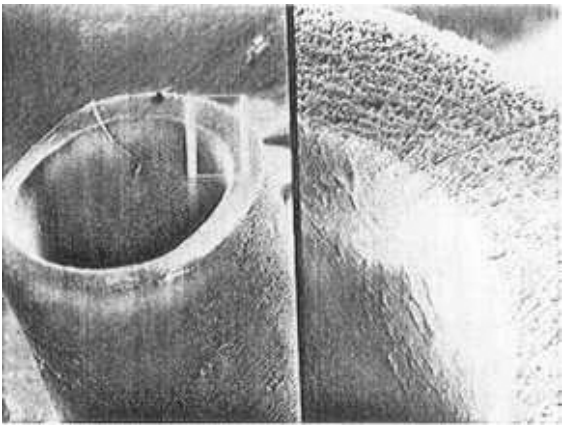


Figure 2.5: Photomicrograph of polypropylene capillary membrane (made by ENKA'S thermal-phase-inversion process).

Capillary-Pore Membranes

Many techniques have been proposed for making capillary-pore membranes including laser beams, electroforming, photochemical etching, and ionotropy to orient anisotropic gel particles to form ionotropic-gel membranes.[3]

Glass capillary arrays are now commercially available for laboratory use. They are formed by assembling a large number of parallel glass capillary tubes, heating to fuse and draw down to individual capillary diameters of 0.5 μ. The bundle is then sliced to form thin discs with a regular capillary array.

Further, a new alumina capillary-pore membrane has just been introduced by Anotec Separations Ltd. The capillary-pore structure appears to result from controlled growth of alumina crystals.

To date, none of these methods has produced submicron capillary-pore membranes at a reasonable cost in the large areas suitable for industrial applications except the "track-etch" membrane produced by Nuclepore Corp.

The "track-etch" process was first patented by Price and Walker.[4] It consists of a two-step process (see Figure 2.6) involving a nuclear reactor and an etch bath. In the first step, a fairly thin film (less than 20 μ) of polycarbonate or polyester is passed between two fission plates of U^{235}. Thermal neutrons in the reactor result in massive charged fission fragments bombarding the film. These particles leave "damage tracks" in the film where polymer chains have been ruptured and ionized (see Figure 2.7). Theoretically, any dielectric material subjected to this treatment will be left with "damage tracks" which will be more vulnerable to chemical attack than the bulk of the material.

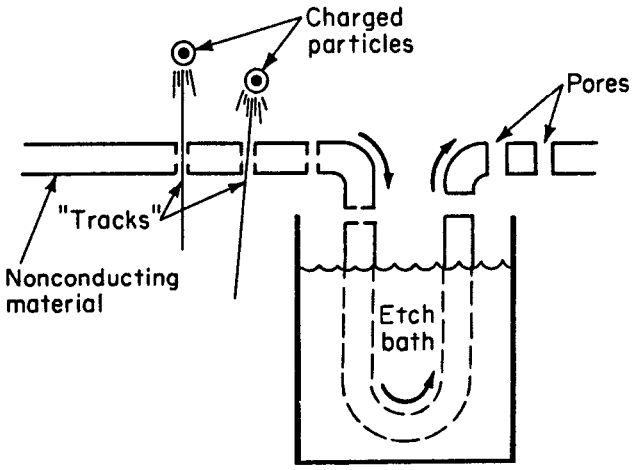


Figure 2.6: Track-etch process for capillary-pore membranes.

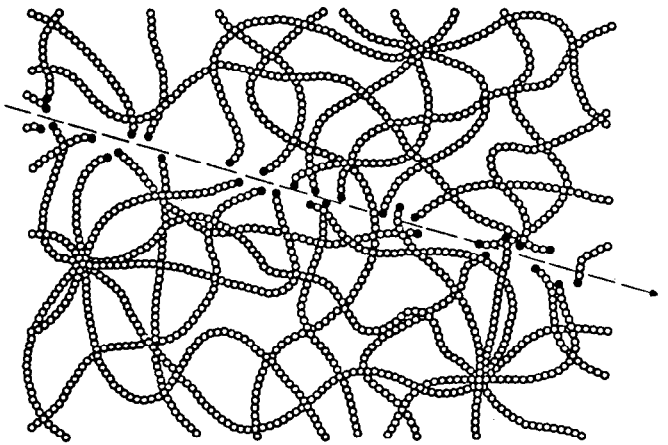


Figure 2.7: Damage-track in an organic polymer.

In the case of polycarbonate or polyester films, the "damage tracks" are susceptible to attack by caustic (NaOH) solutions in the second step. The caustic will immediately "strike-through" the track and then begin to etch radially out from the track. The longer the residence time in the etch tank, the higher the temperature and caustic concentration, the larger the pore size. Once "strike-through" has been accomplished, the etch rate is the same in the pores as on the surface of the film. Thus, when etching a 10 μ pore, approximately 10 μ of surface will be removed from the film. Since films thicker than 15 to 20 μ will not allow penetration of the fission particles, there is an upper limit to pore size of about 12 μ. For example, in Table 2.1, the starting thickness is 18 μ when etching a 12 μ pore. The final membrane thickness, after removal of 12 μ of surface, is only 6 μ.

Table 2.1: Capillary-Pore Membrane Specifications

Pore Size (μm)	Pore Density (pores/cm^2)	Nominal Wt. (mg/cm^2)	Nominal Thickness (μm)	Typical Flow Rates	
				Water (ml/min/cm^2)	Nitrogen (l/min/cm^2)
12.0	1×10^5	1.0	6	1400	110
10.0	1×10^5	1.0	8	1200	75
8.0	1×10^5	1.0	10	1100	55
5.0	4×10^5	1.0	10	1000	50
3.0	2×10^6	1.0	10	1000	50
2.0	2×10^6	1.0	10	450	25
1.0	2×10^7	1.0	10	300	20
0.8	3×10^7	1.0	10	300	20
0.6	3×10^7	1.0	10	200	15
0.4	1×10^8	1.0	10	70	10
0.2	3×10^8	1.0	10	15	4.0
0.1	3×10^8	0.5	5	8.0	2.0
0.08	6×10^8	0.5	5	2.0	1.0
0.05	6×10^8	0.5	5	0.2	0.5
0.03	Experimental material--firm specifications not yet established				
0.015	Experimental material--firm specifications not yet established				

The density of pores (number of pores/cm^2) is determined by the residence time and/or power in the nuclear reactor. Higher pore densities result in higher flow rates. However, for each pore size, there is an upper limit of pore density above which the membrane becomes intolerably weak. In general, porosities above 10% result in low strength membranes. In an attempt to maximize flow rate and still maintain good strength, the pore density is increased for the smaller pore sizes in Table 2.1. However, pore densities above 6×10^8 pores/cm^2 require longer residence times in the reactor which tend to scorch the film with the longer exposure to radiation. Therefore, at pore sizes of 0.1 μ and below, the membrane thickness is reduced by 50% to 5 μ to increase the flow rate by a factor of 2.

Since the irradiation step is a random bombardment process, there is a small probability that two tracks will be adjacent to each other forming doublet pores, triplets, etc. (see Figure 2.8). Obviously, two or three pores which run through the entire thickness of the membrane, adjacent and parallel to each other, can have a marked effect on the retention characteristics of microorganisms. The probability of this occurrence is further reduced by collimating the fission fragments so that they bombard the membrane at angles between 0° to 29° with an average angle of attack of 10° (see Figure 2.9). This is of little help when the pore size is large as in Figure 2.10. Here, two 5 μ pores diverge, but not enough to form two distinct pores over a thickness of only 10 μ. However, at a 0.2 μ pore size, which retains the smallest bacteria, the L/D ratio for the pore is much higher 10/0.2 = 50.

Even so, when one considers the number of pores in one cm^2 (3×10^8), the statistical probability of pore overlap on both faces of the membrane is very high.[5,6] Further, in a 10-inch pleated cartridge, there are 20 square feet of membrane containing 6×10^{12} pores. There is an overwhelming probability that many doublets, triplets, quadruplets, etc. are present. Apart from damage to the membrane during manufacturing, this is the underlying reason why Nuclepore will never be able to make a "bubble-pointable" cartridge out of this membrane.

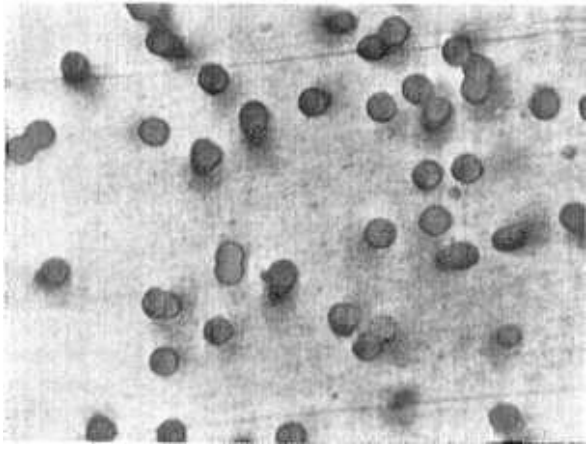


Figure 2.8: Doublet and triplet pores in capillary-pore membrane.

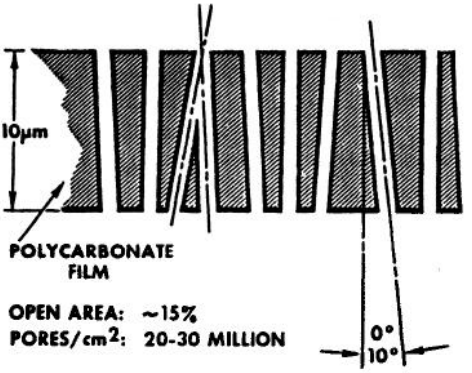


Figure 2.9: Angle of pores in capillary-pore membrane.

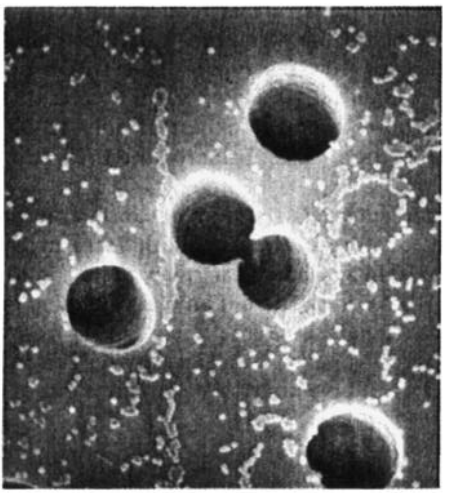


Figure 2.10: Doublet pore in 5.0 micron capillary-pore membrane.

PORE SIZE DETERMINATION

Challenge Tests

It is easy to measure the pore size of capillary-pore membranes with a scanning electron microscope, but tortuous pore membranes are more difficult.

Since the first applications of MF membranes were in the filtration and culturing of microorganisms, membranes were characterized by their ability to retain specific organisms 100%. As shown in Figure 2.11, *Pseudomonas diminuta* was thought to have a minimum diameter of 0.22 μ, and this became the pore size rating for those membranes which retained Pseudomonas completely. Likewise, *Serratia marcescens* was thought to have a diameter of 0.45 μ, etc. In fact, a significant variation in size has been documented: up to 30% in diameter and 67% in length.

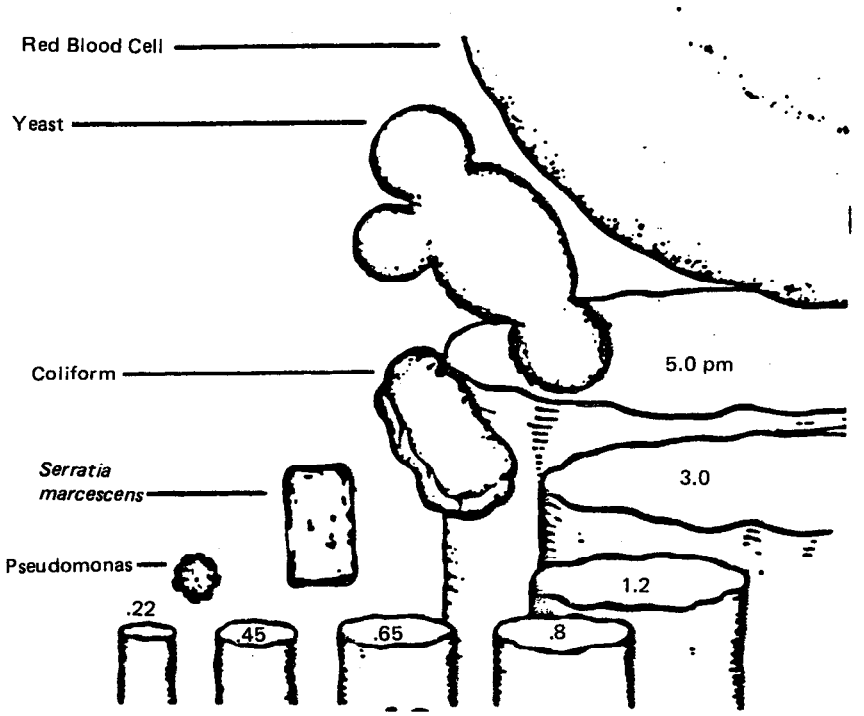


Figure 2.11: Challenge organisms for various pore sizes.

Every manufacturer still challenges tests measuring the "Beta ratio" (the number of organisms challenging the membrane ÷ number of organisms passing through). Normally, a membrane is considered good if challenged with enough bacteria to plug the pores (typically 10^8-10^9 organisms per cm^2 of filter area) and none pass. However, some manufacturers are more conservative than others-starving bacteria before the test to challenge the membrane with the smallest viabile organism possible.

Other particles may also be used to test the membrane. Monodisperse latex spheres (produced by Dow Chemical) in concentrations of 10^6-10^9 particles per ml are sometimes used. Normally, a second membrane is used downstream of the test membrane to collect particles which pass. The number of spheres collected are counted with the use of a scanning electron microscope. This is much more tedious and less accurate than the bacteria challenge test where bacteria collected on the second membrane may be grown into colonies visible to the naked eye. Alternatively, automatic particle counters are used before and after the membrane, but the method is not as sensitive and is limited to particles over 0.5 μ in size.

Bubble-Point Test

An easier test which is also nondestructive is the "bubble-point" test. The maximum pore size may be determined by measuring the gas pressure required

to overcome the capillary forces holding a wetting liquid within the pores (see Figure 2.12).

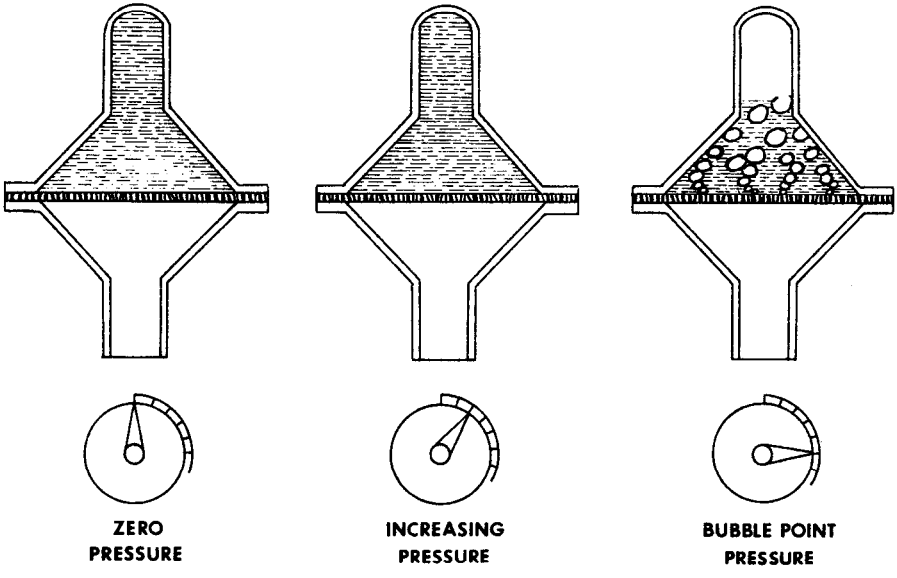


Figure 2.12: Procedure used in determining bubble-point.

The bubble point equation is essentially the capillary rise equation:

(1) $$P = \frac{4\gamma \cos \theta}{d}$$

where P = bubble point pressure

d = pore diameter

γ = surface tension of the liquid filling the pores

θ = liquid-solid contact angle ($\theta = 0^\circ$ for perfectly wetting fluids; $\theta > 90^\circ$ for nonwetting fluids).

For water, with a surface tension of 72 dynes/cm, and a contact angle of 0°, equation (1) reduces to:

(2) $$P = \frac{42}{d}$$

where P is in psi and d is in microns.

For isopropanol, which wets almost all polymers, the equation becomes (with the same units):

(3) $$P = \frac{12}{d}$$

First, the membrane is completely wetted with liquid and then a gas pressure is applied to one side. As the gas pressure is gradually raised (see Figure 2.12), there will be no gas flow through the pores until capillary forces are overcome releasing liquid from the pore. Obviously, from equation (1), the first gas bubble will emerge from the largest pore–where the capillary forces are lowest. The pressure at which this occurs is called the "bubble-point" pressure. The maximum pore size may then be calculated.[7]

If the gas pressure is raised further, more pores will begin to bubble until the liquid is displaced from the smallest pore and the gas-flow through the membrane equals that through a dry membrane. A pore size distribution may be calculated from these data. Indeed, an ASTM test method[8] outlines the procedure:

(1) Measure the dry air flow and plot versus pressure (see Figure 2.13).

(2) Wet the membrane and raise the air pressure until the first air-bubble appears; this is the "bubble point" and may be used to calculate the *maximum pore size*.

(3) Continue to raise the air pressure and measure airflow through the wet membrane as a function of pressure.

(4) Continue to raise the pressure until the airflow through the wet membrane equals that through the dry membrane at the same pressure. At this point, all liquid has been expelled from the membrane and the pressure may be used to calculate the *minimum pore size*.

(5) To calculate the *mean-pore size*, ASTM method R316 constructs a line equal to one-half of the dry air flow through the membrane. The pressure at which the wet airflow intersects this line is the point at which the liquid has been expelled from one-half of the pores and may be used to calculate the *mean pore size*.

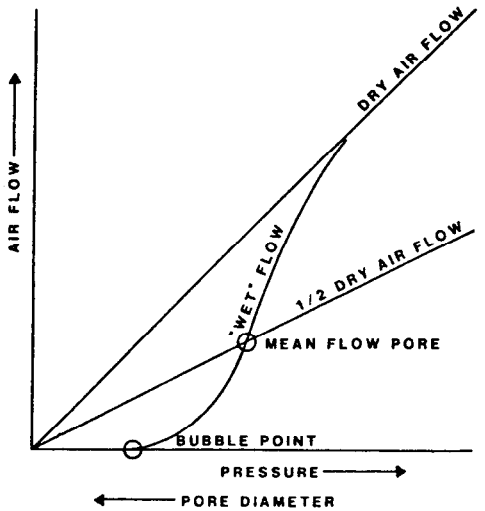


Figure 2.13: Procedure used in determining maximum, mean, and minimum pore size.

There is one complication in the bubble-point test referred to as "diffusional-flow." A small amount of gas-flow can result even through a pore is filled with liquid. The gas dissolves in the liquid in the pores at high pressure, diffuses across the liquid-filled pore in solution, and comes out of solution on the low-pressure side of the membrane. In practice, "diffusional-flow" is not even detected when small membrane areas are involved. Even for large areas, it is easily distinguished from the much larger gas-flow at the bubble point.

It is helpful to estimate the amount of flow expected due to diffusion:

$$J = \frac{N\pi d^2}{4}(DH)\frac{\Delta P}{\ell} \tag{4}$$

where J = gas flow rate per unit area of membrane

N = number of pores per unit area

d = pore diameter

D = diffusivity of the gas in the liquid
($D = 1.64 \times 10^{-5}$ cm^2/sec for N_2 in water at 20°C)

H = the solubility of the gas in the liquid
($H = 6.9 \times 10^{-7}$ gm mols/atm/cm^3 for N_2 in water at 20°C)

ΔP = the pressure differential across the membrane

ℓ = the tortuous path length through the pore and across the membrane

Figure 2.14 is a convenient chart to use in estimating "diffusional-flow." The chart was originally constructed for use with capillary pore membranes with a thickness of 10 μ. However, since the parameter $N\pi d^2/\ell$ in equation (4) is approximately the same for capillary and tortuous pore membranes, the chart may be used for both. Table 2.1 should be used to identify the density corresponding to the pore size in question. For example, a 0.2 μ pore size has a density of 3×10^8 pores/cm^2. Therefore, both capillary and tortuous pore membranes would be expected to show a diffusional-flow of about 0.1 ml/min/ft^2/psi. For a 10 square foot pleated cartridge tested at 30 psi, the diffusional flow rate should only be 30 ml/min. (This can be readily measured with a liquid-filled inverted graduate or burette-see Figure 2.15).

The estimates obtained from Figure 2.14 will be slightly low for tortuous pore membranes at pressures near the bubble point. This is because the pore opening is generally larger than the pore neck (see Figure 2.16). At higher pressures, the liquid will flow from the pore entry region until it reaches the smaller neck where it will stop unless the pressure exceeds the bubble point. Thus, the diffusion path through liquid in the pore is reduced, resulting in higher diffusional-flow rates by equation (4). In practice, this increase is mitigated by the fact that the membrane support also offers additional resistance to diffusion.

As previously noted, $N\pi d^2/\ell$ is the key parameter in equation (4).

Membranes of equal porosity and thickness will show the same "diffusional-flow." This is why the so-called "forward-flow" test advocated by some manufacturers is so misleading. They claim they can correlate bacteria retention with the diffusional-flow measured. Yet, most pore sizes of tortuous-pore membranes have approximately the same porosity and thickness. Equation (4) makes it clear

that a "forward-flow" test cannot distinguish between a 1.2 μ membrane which passes *Pseudomonas diminuta* quantitatively, and a 0.22 μ membrane which will retain it quantitatively–if the membranes have the same porosity.

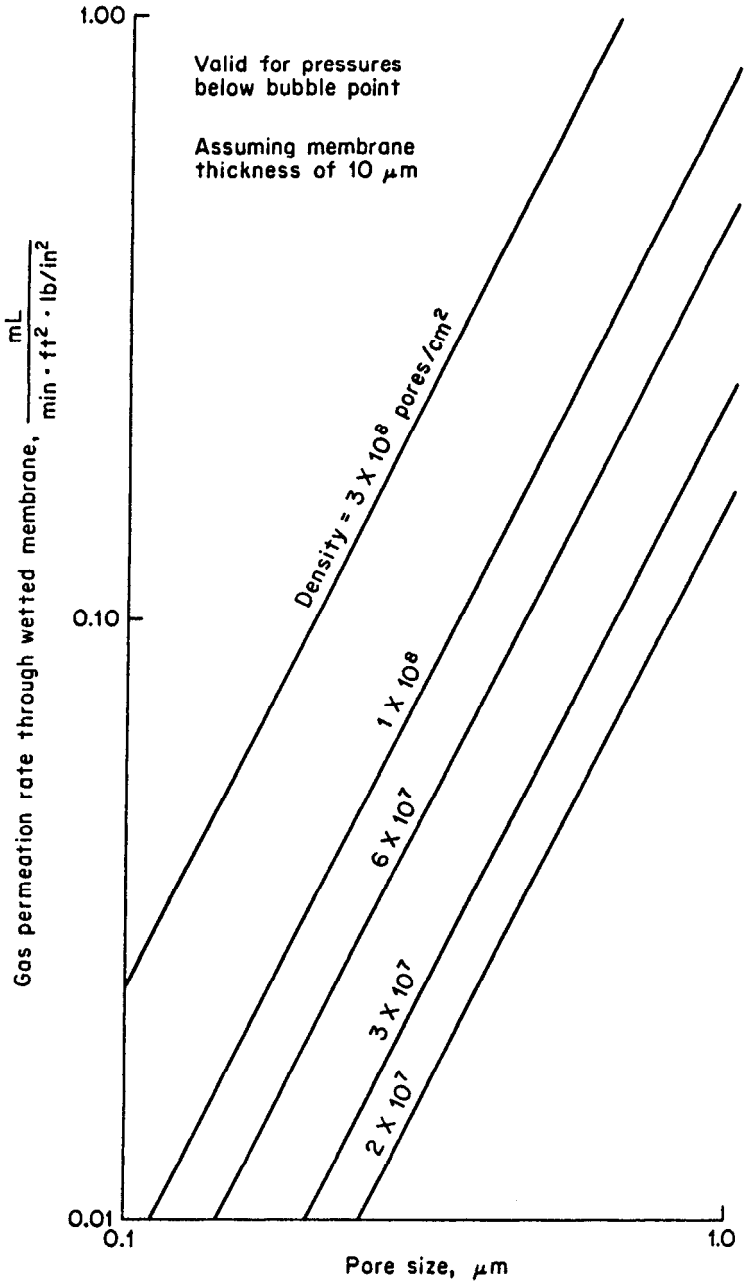


Figure 2.14: Diffusional-flow for various pore sizes and pore densities.

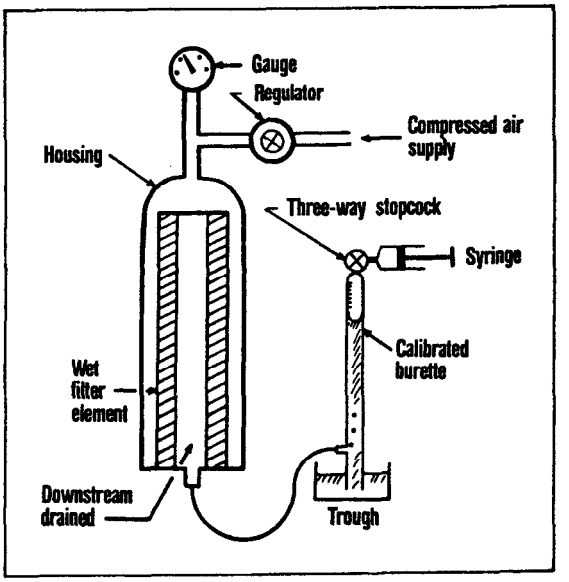


Figure 2.15: Method for measuring diffusional-flow rate.

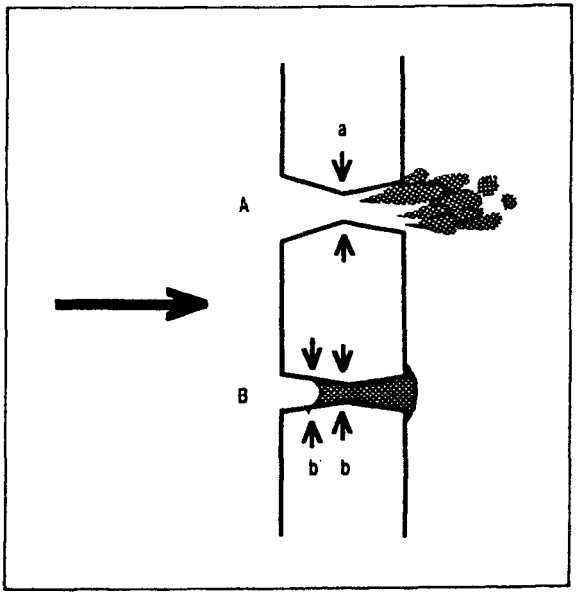


Figure 2.16: Bubble-point in membranes with pore openings larger than the internal pore size.

Mercury Intrusion Test

Mercury is a non-wetting fluid for most materials. Because the contact angle (θ) is 180°, cos = -1, and pressure is required to force mercury into the pores–see equation (1). We speak of mercury "intrusion pressures"; these are quite high due to the high surface tension of mercury (476 dynes/cm). Thus, for a given pore size, the pressure required to force mercury into the pores is almost seven times greater than the pressure required to expel water from the pores.

The technique places as much membrane area as possible into a chamber which is evacuated. Mercury is then admitted into the chamber as the pressure is slowly elevated. The incremental volume of mercury added for each increase in pressure is measured precisely.

The greatest ambiguity is that the volume of mercury penetrating dead-ended "pits" is registered along with that penetrating "pores." Further, the high pressures required may collapse some pores. Nevertheless, mercury porosimetry can be helpful in confirming the pore-size distribution obtained by other methods such as bubble-point.

Other Methods

A number of other techniques have been used to determine pore size, but they are not accurate enough to be used as standard characterization tools.

Flow Permeability Test. A rough estimate of an equivalent mean pore size may be made by measuring the porosity (ϵ) and permeability (J) of the membrane. Assuming laminar flow, the Hagen Poiseuille relationship may be modified for a porous membrane:

$$J = \frac{N\pi d^4 \Delta P}{128\mu \ell} \tag{5}$$

where J = volumetric liquid flow rate per unit area of membrane

N = number of pores per unit area

d = pore diameter

ΔP = the pressure differential across the membrane

μ = viscosity of the liquid

ℓ = the length of the pore

The porosity (ϵ) of the membrane is the same as the void volume of the membrane and may be determined by measuring the difference between the wet and dry weights of the membrane. Since

$$\epsilon = \frac{N\pi d^2}{4} \tag{6}$$

$$J = \frac{\epsilon d^2 \Delta P}{32\mu\ell} \tag{7}$$

or

$$d = \sqrt{\frac{32J\mu\ell}{\epsilon\Delta P}} \quad (8)$$

All the variables on the right side of equation (8) are experimentally measurable except for ℓ, the length of the pore. Obviously, ℓ is related to the thickness of the membrane by a "tortuosity factor." The problem is that we cannot measure the "tortuosity factor" with any degree of certainty.

Even the case of "capillary-pore" membranes where ℓ is only slightly larger than the thickness of the membrane, inertial losses, especially "front-and-back-face" losses, may be significant.

Smoke DOP Test. The classic method[9] for determining the filtration efficiency of various air filters is to challenge the filter with a liquid aerosol of dioctyl phthalate (DOP). Typically, the aerosol particles are 0.3 μ in diameter.

Although the method has been used to characterize MF membranes for the filtration of gases, the retention of a liquid aerosol does not correlate well with the retention of particles suspended in a liquid.

BET Adsorption Data. A wealth of information about the size and shape of pores may be obtained from adsorption isotherms where the mols of nitrogen adsorbed on the membrane are measured as a function of pressure. However, the use of this techniques is not widespread due to the tedious regimen required in gas adsorption measurements. Further, the hysteresis effects make conclusions about pore-structure ambiguous.

RETENTION CHARACTERISTICS

Bacteria Retention and Bubble Point

In 1974-1976, Wallhausser wrote several controversial papers,[10,11] showing that MF membranes may pass microbes at high challenge levels (see Table 2.2). Previously, membrane manufacturers had insisted that their membranes were "absolute" and many were skeptical of Wallhauser's data.

Shortly thereafter, other data began to appear in the literature confirming Wallhausser's findings. Eventually the manufacturers collected their own data which showed that no membrane is truly "absolute," for example, Table 2.3[12] shows that filtration time as well as challenge level is a factor.

Some researchers used the term "grow-through" to explain the results. The idea was that bacteria trapped in the neck of the pore subdivide during growth so that the new organisms emerge through the neck to the other side. However, calculation of the maximum pore-size from the bubble-point shows that there are some pores larger than challenging organism. For example, the theoretical water bubble-point of a membrane with a membrane with a maximum pore size of 0.2 μ is calculated from equation (2) to be 200 psi. Most 0.20 μ cellulose ester membranes (water wet) have bubble-points between 45 and 60 psi, which is only one-fourth of the theoretical value.

Table 2.2: Wallhausser's Data on Bacterial Break-through[11]

Pore size 0.2 μm (flow-rate: 100 ml water in 22 sec) and 0.45 μm (flow-rate: 100 ml water in 13 sec).

Initial bacterial concentration*)	10^3/ml		10^4/ml		10^5/ml	
Filtrate	No. of bacteria after filtration					
	0.2 μm	0.45 μm	0.2 μm	0.45 μm	0.2 μm	0.45 μm
100 ml	0	0	0	1	1	> 1000
200 ml	0	0	2	4	4	∞
1000 ml	0	0	9	25	17	∞ (> 10^4)
Filtration time for 1000 ml	6'52"	2'27"	2 h 12'	2'30"	3 h 15'	8'

*) Pseudomonas diminuta ATCC 19 146.

Table 2.3: Bacterial Penetration with Time[12]

Filter No.*	Rating	Time, hr	Bacteria Recovered
PA 5-248B	0.2 μm	24	0/L
		48	0/L
		168	62/L
		312	750/L
PA 5-248D	0.2 μm	72	0/L
		119	0/L
		170	16/L
		265	20/L
		314	19/L
CET-1	0.22 μm	24	19 total
CED-1	0.22 μm	41	19 total
		162	260 total
		216	1000 total
CET-2	0.22 μm	24	1 total
CET-3	0.22 μm	24	0
PA 538	0.2 μm	24	11 total
		48	1000 total
PA 562	0.2 μm	89	0
PA 595	0.2 μm	90	0

* PA = nylon 66. CE = Cellulose ester.

Note: All tests run to plugging (40^+ psid). Input levels ranged from 10^4 to 10^5 bacteria/liter.

The manufacturers early recognized the discrepancy between theoretical and experimental bubble points. They introduced an experimental constant into equation (1) called a "shape-factor" which supposedly took into account the fact that tortuous pores are not cylindrical in shape. However, a shape factor of 0.25 cannot be justified from the capillary rise equations, as any good textbook on surface chemistry will attest. Indeed, for noncircular pores, equation (1) is adjusted to:

$$P = \frac{p\gamma \cos \phi}{A} \tag{9}$$

where p is the perimeter of the pore and A is its area. Thus, for pores of equal areas, the one with an irregular shape will yield a higher bubble point than a circular pore!

Still, other researchers explained the discrepancy between theoretical and experimental bubble-points with surface tension depression. It is true that most manufacturers treat their membranes with wetting agents. It is conceivable that these surfactants can dissolve in the test fluid and lower the surface tension.

However, the discrepancy between theoretical and experimental values exists for all test fluids. For example, it is impossible to postulate a depression in the surface tension of isopropyl alcohol from 22 to 5 dynes/cm.

It is apparent that the bubble point is telling us that a 0.2 μ pore size membrane has at least one pore up to 0.8 μ in diameter. This is confirmed by mercury porosimetry data (see Figure 2.17).

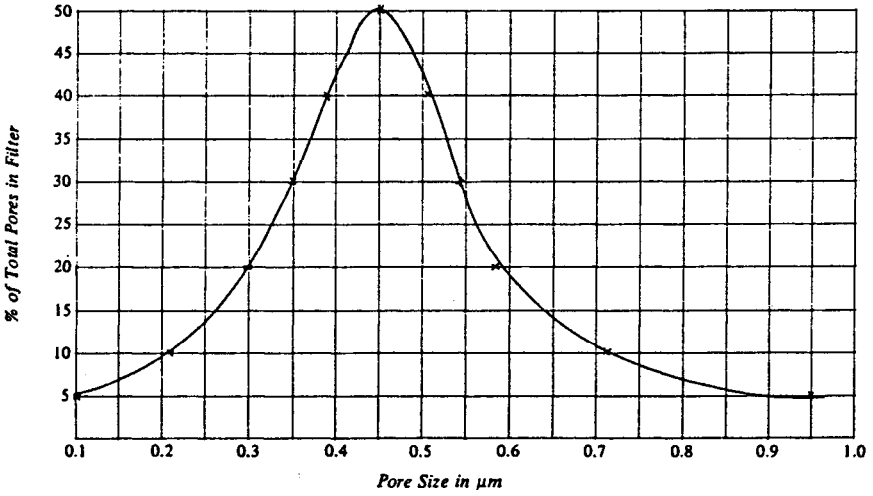


Figure 2.17: Distribution of pore sizes in 0.45 micron membrane (by mercury porosimetry).

To verify the theoretical equation for bubble point, a series of 0.2 μ capillary pore membranes were made with extremely low pore densities. The lowest densities virtually eliminated all doublets and triplets and yielded bubble points equal to the theoretical value. Though the low density rendered the membrane useless for applications requiring a reasonable flow rate, it nevertheless demonstrated that a membrane can be made where a direct measurement of the pores (with S.E.M.) agreed with that calculated from the bubble-point.

From the above, it is clear that given enough time and bacteria, some will find a leak-path through the MF membrane.

There is, however, a long history of successful membrane usage in the sterilization of fluids by filtration. Indeed, for all practical intents and purposes, the membrane has been "absolutely retentive." There are few applications which subject the membrane to the challenge levels used by the manufacturers in their quality control (typically, 10^8-10^9 organisms per cm^2 of filter area). Such a challenge provides more than one organism per square micron of filter area and often clogs the membrane.

It is true that in ultrapure water loops, where the membrane is in service for many months, the accumulation of bacteria on the membrane can reach these levels. This explains why there can be more organisms in the filtrate than can be detected in the feed stream.

Retention of Deformable Particles

Some researchers have argued that, under pressure, bacteria will pass through pores of smaller diameter due to deformation. Most microbiologists are doubtful that *Pseudomonas diminuta* will deform to this degree. Nevertheless, it is recognized that larger microorganisms can deform.

For example, Figure 2.18[13] demonstrates the transmission of normal deformable red cells through various capillary-pore membranes. After hardening the red cells, they will not pass anything below a 9 μ pore size.

The author has seen data on the passage of yeast particles through pore sizes under 3 μ which has suggested passage by deformation.

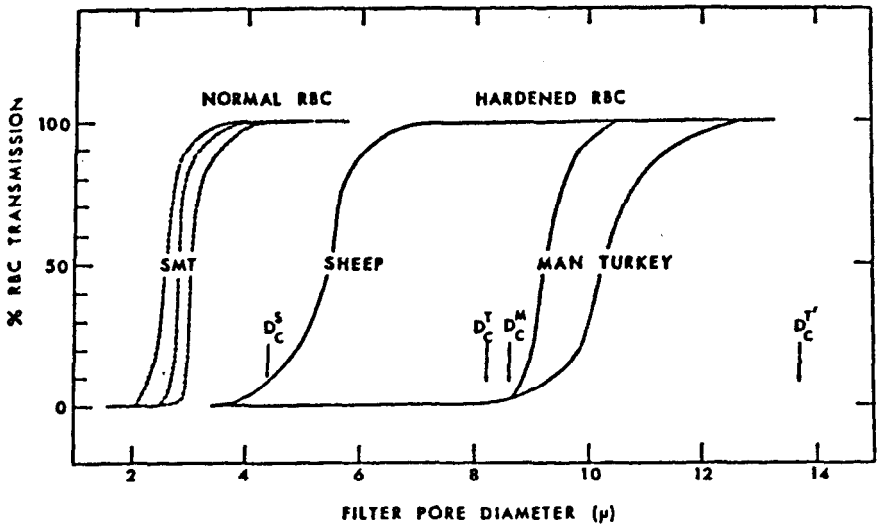


Figure 2.18: *Transmission of red blood cells through capillary-pore membranes.*[13]

Retention by Adsorption

Lukaszewicz et al[14] has postulated an "adsorptive" mechanism to explain the excellent retention of bacteria by membranes with some pores larger than the microorganism. He contends that the adsorptive sequestrations of the membrane are more important than the geometric restraints of sieving.

Davis et al[15] investigated the retention of 0.05 and 0.005 μ Au colloids by "capillary-pore" and "tortuous-pore" membranes. Table 2.4 shows clearly that the "tortuous-pore membranes" retain particles much smaller than the rated pore size. Indeed, a 5 μ pore size will retain 60% of the 0.05 μ colloidal particles and 18% of the 0.0005 μ colloid. On the other hand, "capillary-pore" membranes retain less than 1% of either. "Tortuous-pore" membranes have 25 to 50 times more internal surface area for adsorption than "capillary-pore" membranes, and the tortuous path also results in a greater likelihood of small particles contacting the pore-wall.

Table 2.4: Retention of Au-Colloids on Capillary-Pore and Tortuous-Pore Membranes

Colloid Size (μm)	0.05	0.005
0.1μm Nuclepore	1.2	0.2
0.1μm Cellulosic	92.0	8.2
0.4μm Nuclepore	1.3	0.2
0.45μm Cellulosic	46.9	12.7
1.0μm Nuclepore	0.7	0.3
1.2μm Cellulosic	46.5	6.7
3.0μm Nuclepore	0.4	0.2
5.0μm Cellulosic	59.3	17.9

These results suggest that a "tortuous-pore" configuration is best for "clean-up" applications where the removal of all particles from the process stream is desired. On the other hand, the "capillary-pore" configuration is best for fractionation of particles. For example, capillary-pore membranes have been used in fractionating silver colloids to improve resoltuion on photographic films.

For dilute process streams, product may be lost via adsorption on the membrane. The "recovery" of this product may be improved by pretreating the membrane such that most of the adsorption sites are occupied. For example, in the data of Hahn et al[16] (Table 2.5), polio virus adsorption on cellulosic "tortuous-pore" membranes was significantly higher than that on polycarbonate "capillary-pore" membranes. (i.e., The virus recovery is low due to adsorption.) The recovery was improved from 5 to 76% by pretreating the membrane with a beef extract solution.

Table 2.5: Recovery of Poliovirus in Retentate or Filtrate after Filtration on Various Filters

Filter	Size (μm)	Suspending medium*					
		BSS	Water	BSA (1%)	BE (0.003%)	BE (0.03%)	BE (0.3%)
Silver	.2	30	60	60	75	98	86
Silver	.45	79	79	78			
Cellulose	.22	<5	<5	<5	7	67	76
Cellulose	.45	<5	<5	3			
Polycarbonate	.5	73	80	70	80		

* BSS, Hanks balanced salt solution; BSA, bovine albumin in distilled water; BE, beef extract in BSS.

Retention by "Charged" Membranes

In certain aqueous streams, the retention of charged species may be enhanced without sacrificing the filtration rate by using charge modified membranes. Since most particles are negatively charged, these membranes are usually positively charged. Normally a crosslinking epoxy resin with cationic functional groups (e.g., quarternary ammonium groups) is used to impart the charge. The combination of electrokinetic adsorption with mechanical sieving is claimed to result in significant improvements in retention.

The most significant claim is for the removal of "pyrogens" (endotoxins). Table 2.6 [17] compares the pyrogen removal efficiency for a positively charged nylon 0.2 μ pore size membrane, Zetapor™, and a conventional cellulosic 0.22 μ membrane. Normally, a 10,000 molecular weight cut-off UF membrane is required to remove pyrogens. (These membranes have an equivalent pore-size of 30 Å or 0.003 μ). As expected, the conventional MF membrane shows no retention whatsoever, but the positively charged membrane shows better than 97% retention.

Table 2.6: Pyrogen Removal by "Charged" Membranes

Filter Area 3.9 cm²	Endotoxin Concentration Before Filtration pg/ml	Endotoxin Concentration in Filtrate pg/ml			
		50ml	100ml	150ml	200ml
Zetapor .2 μm	2000	100	<50	<50	<50
Cellulose Acetate .22 μm	2000	2000	2000	2000	2000

Procedure: *E. coli* purified endotoxin was added to 0.9% NaCl solution at pH 6.7 and passed through filters contained in a 25mm filter holder.

It is also claimed that positively charged 1.2 μ pore size MF membranes will retain *Pseudomonas diminuta*. Data from Pall Corp.[18] on their 1.2 μ N_{66} Posidyne™ membrane show better than 99.99% retention of Pseudomonas. Their conventional 1.2 μ ULTIPOR N_{66}™ membrane (without the charge) retained less than 50% of the Pseudomonas. In both cases, challenges between 2×10^{10} and 7×10^{12} bacteria per square foot of filter area were used. This means that comparable removal of Pseudomonas can be achieved with more than 10 times the flow rate of a 0.2 μ pore-size membrane.

Further, if all of the particles retained are considerably smaller than the rated pore size (say less than 25%) and no larger particles are present, the membrane does not clog even with the processing of very high volumes. The small particles do not "bridge" and cause only a slight change in the pore diameter.

The difficulty is that, with use, the filtration efficiency of these positively-charged membranes begins to drop. As the membrane adsorbs more and more negatively-charged particles the adsorption sites (cationic functional groups) are used up. Just as a saturated ion-exchange resin is incapable of further retention of ions, the membrane begins to pass negatively charged particles. Figure 2.19[19] shows the decline in retention for 0.2 μ latex particles.

Similarly, high flow rates (pressure drops) through the membrane may strip the negative particles away from the membrane (see Figure 2.20).[19] The hydraulic shear forces have overcome the electrostatic attraction.

For critical applications, one cannot afford to guess when the adsorption capacity is used up. However, in some cases, a positively charged membrane of larger pore size than the final membrane may be used as a prefilter, decreasing the load on the "absolute" filter and extending its life. For example, it is reported that a 3 μ positively charged prefilter can extend the life of a 0.2 μ final membrane filter by a factor of 2- to 6-fold.[18]

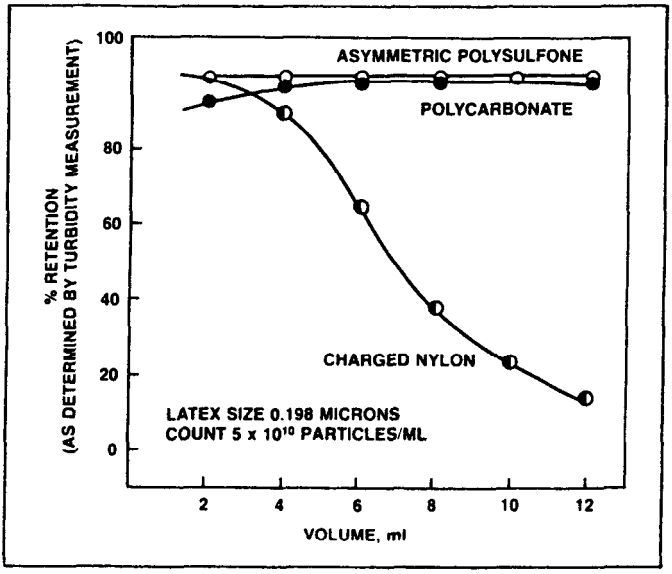


Figure 2.19: Retention of 0.2 micron latex particles by "charged" and uncharged membranes as a function of volume filtered.

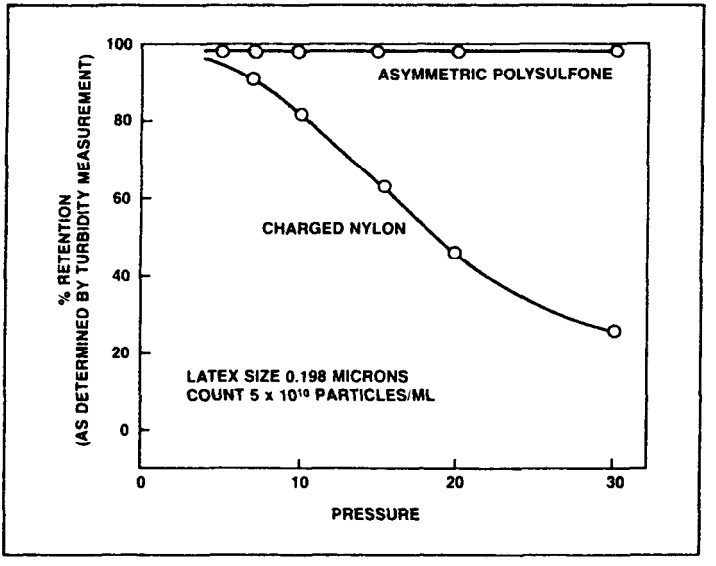


Figure 2.20: Retention of 0.2 micron latex particles by "charged" and uncharged membranes as a function of filtration pressure.

Alternatively, two positively charged membranes may be used in series. The adsorption capacity of the upstream filter will be exhausted first. When the effluent from this filter begins to show passage, it is replaced by the downstream filter. A new filter is then placed in the downstream position.

Negatively charged membranes are also available. The *fractionation capability* of "tortuous-pore membrane" is enhanced considerably by using filters with a zeta potential of the *same* sign as the particles (usually negative). It should be noted that untreated nylon membranes have a negative zeta potential at pH values above 6.5 (see Figure 2.21).[18]

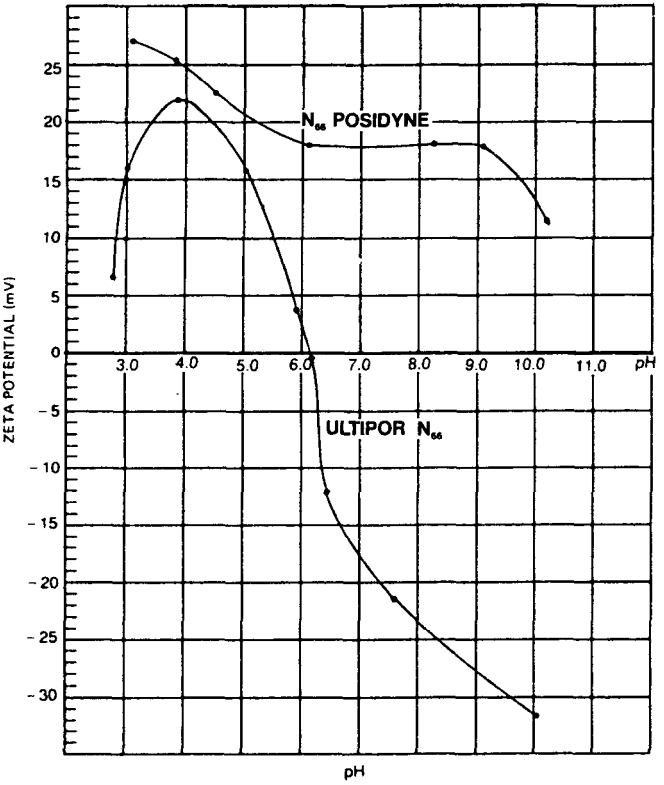
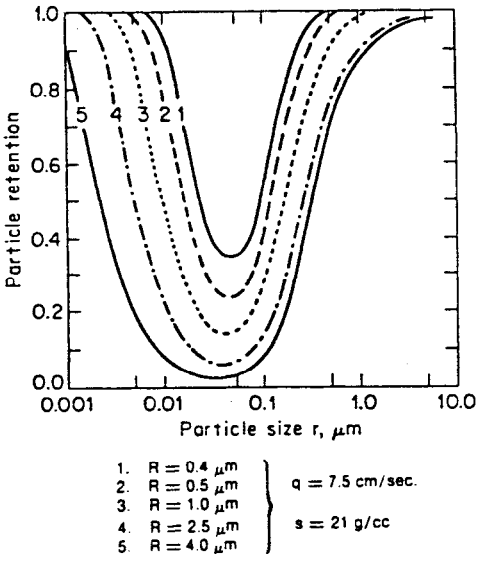


Figure 2.21: Zeta potential of positively charged and uncharged nylon membranes.

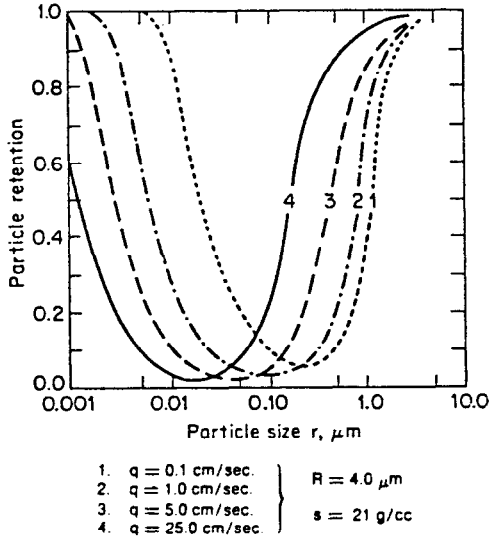
Aerosol Retention

The filtration of particles in a gas stream can be quite different from the filtration of the same particles in a liquid stream. The three mechanisms of aerosol particle retention may be illustrated from the data of Spurny et al[20] in Figures 2.22 and 2.23. The U-shaped curves are characteristic of the efficiency of aerosol particle collection as a function of particle size. However, "capillary-pore" membranes have a deeper minimum in the curves than do "tortuous-pore membranes."



R = Pore Radius; r = Particle Radius; q = Face Velocity of Gas;
S = Particle Density; E = Particle Collection Efficiency.

Figure 2.22: Aerosol retention on a capillary-pore membrane as a function of particle size and pore size.



R = Pore Radius; r = Particle Radius; q = Face Velocity of Gas;
S = Particle Density; E = Particle Collection Efficiency.

Figure 2.23: Aerosol retention on a capillary-pore membrane as a function of particle size and gas velocity.

Direct Interception. This mechanism is common to both liquid and gas filtration. The particle is simply too large to pass through a pore. Both Figure 2.22 and 2.23 show that 100% of all particles larger than the pore radii (R) are captured.

Inertial Impaction. Particles smaller than the rated pore size can still be captured by "inertial impaction" if they have enough mass to continue in a straight line when the flow streamlines bend to go through the pores. The result is that the particles impinge on the rim of the pore or on the pore-wall near the pore-entrance (see Figure 2.24). The smaller pore sizes increase capture by inertial impaction (see Figure 2.22) because there is less likelihood the particles will be able to follow the flow lines all the way through a narrow pore. Also, higher gas velocities impart additional momentum or inertia to the particles, thereby increasing the number of particles captured (see Figure 2.23).

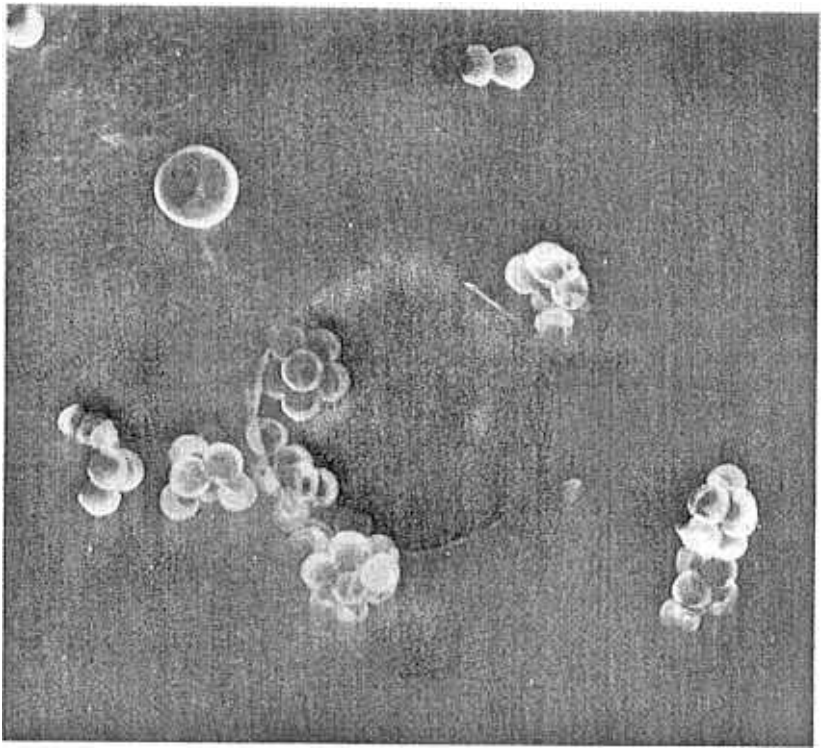


Figure 2.24: Latex particles captured on a capillary-pore membrane by inertial impaction.

Diffusional Deposition. Very small particles will not be captured by interception or by inertial impaction since their mass is too small. However, these

smaller particles have greater Brownian motion and greater diffusivities. In gases, the diffusivity is large enough to result in deposition on the pore-wall (see Figure 2.25). In this case, smaller pore sizes increase the probability of particle impact with the pore wall because of the shorter path length (see Figure 2.22). Lower gas velocities favor particle deposition because of a longer residence time in the pore (see Figure 2.23). For dry gases, electrostatic forces can also boost the capture of these small particles.

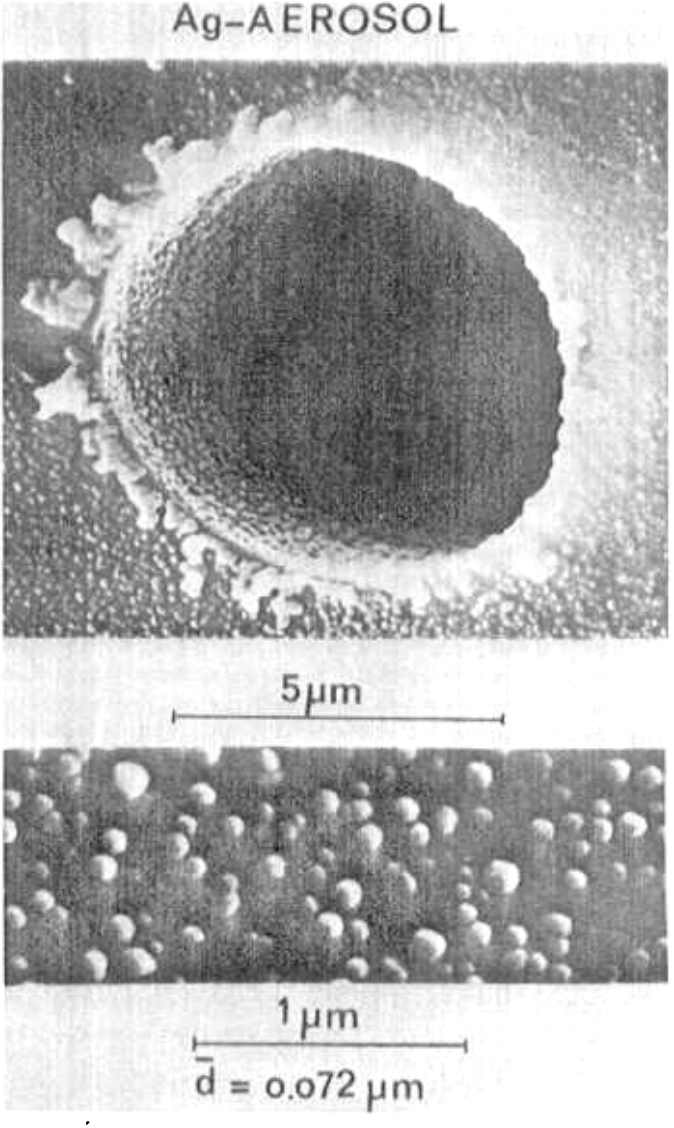


Figure 2.25: Silver (Ag) particles captured by a capillary-pore membrane by diffusional deposition.

"U-shaped retention curves" are seldom seen in liquid filtration. The particle diffusivities in the higher viscosity fluid are much smaller. As a result, the retention efficiency does not increase with smaller particle sizes.

For "tortuous-pore membranes" the minimum in the curves of Figures 2.22 and 2.23 is much less pronounced. This is because the tortuous path results in more and smaller particles captured by inertial impaction. Further, the longer path length through the pore results in more and larger particles captured by diffusional deposition.

Thus, if the objective is to capture as many particles as possible on the membrane, "tortuous-pore" membranes are preferred.

On the other hand, for some specialized analytical applications where fractionation of the aerosol particles is the objective, "capillary-pore" membranes are preferred. For example, it has been found that an 8 μ "capillary-pore" membrane will collet air-pollution particles that are normally deposited in the upper respiratory tract (nasopharynx.)[21] Air sampling stations have used this membrane in the first stage; particles passing are collected on a tortuous-pore membrane in a second stage to simulate what is deposited in the lungs.

MEMBRANE PLUGGING AND THROUGHPUT

Once membranes with the appropriate retention characteristics have been identified, their cost and "throughput" (volume processed before plugging) will often dictate the membrane of choice. Further, those process schemes and operating variables which maximize filter life and throughput need to be considered to improve the economics of filtration.

Membrane Dirt-Loading Capacity

It should be obvious from the section on "Retention by Adsorption" that "tortuous-pore membranes", with 25 to 50 times more internal surface area for adsorption than "capillary-pore" membranes should have higher "throughputs". That this is the case is shown in the throughput curves of Figure 2.26. The data were run at constant flow rate and show the increase in pressure drop across 47 mm filters (ΔP) with increasing volumes of fluid passing the filter. "Tortuous-pore" cellulose ester (CE) and polytetrafluoroethylene (PTFE) membranes showed the highest throughputs. "Capillary-pore" polycarbonate (PC) membranes plugged most rapidly. One must use more area of the "capillary-pore" membranes to equal the same dirt-loading capacity of a "tortuous-pore" membrane.

Prefilters

The use of positively-charged open-pore membranes as prefilters for a final "absolute" membrane has already been mentioned. In general, a prefilter serves to take the load off the final filter. The best prefilters will have a high internal surface area (high dirt-loading capacity).

It is well known that fibrous depth filters provide enormous dirt loading capacity compared with membrane filters. Using this kind of filter media as a prefilter for the final membrane filter often provides an ideal combination (see Fig-

ure 2.27). Most of the contaminants are removed by the prefilter but the final membrane serves as the ultimate barrier trapping all particles leaking through the prefilter-including fibers which "sluff-off" the fibrous media due to "media-migration".

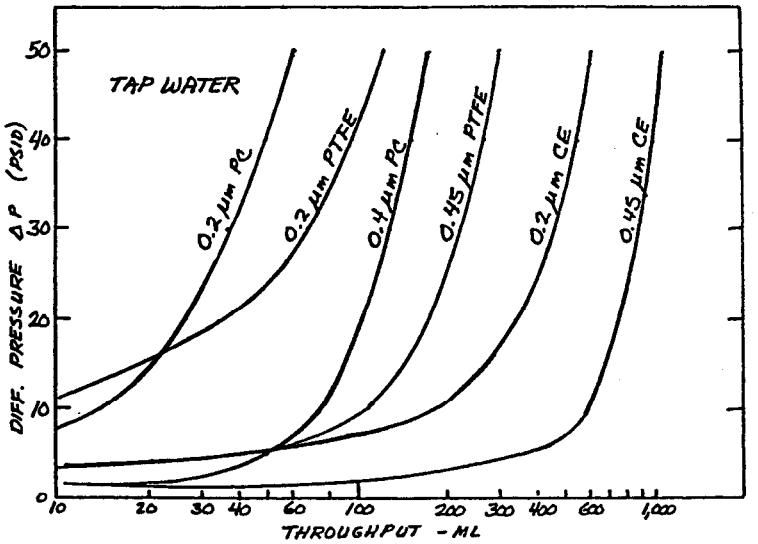


Figure 2.26: Tap-water through-put for polycarbonate (PC) capillary-pore membranes and cellulose ester (CE), polytetrafluoroethylene (PTFE) totruous-pore membranes.

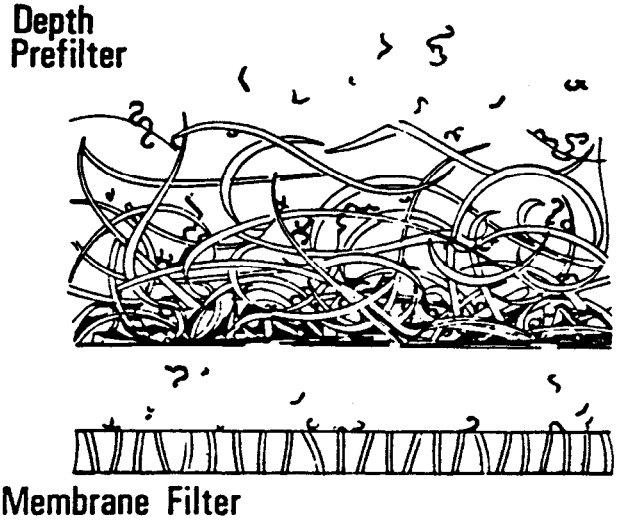


Figure 2.27: Depth prefilter over final membrane filter.

The smaller the fiber diameter used in the prefilter, the greater the surface area for adsorption of particles and the better the retention of small particles. In the sixties, asbestos fibers were recognized as the best prefilter media. The individual fibrils were smaller than 0.01 μ and they had a positive zeta potential. However, when it was suspected that asbestos fibers presented a health hazard, fine diameter glass and synthetic polymer fibers were substituted. Unfortunately, neither media equals the performance of asbestos. Glass fibers are available in the finest diameters, but some users are fearful they may represent a similar health hazard. The trend has been to use polypropylene or polyester fiber prefilters. Melt blown or spun-bonded fibers are available in diameters near 1 μ. Multilayers of these media with appropriate calendering have resulted in surprisingly efficient prefilters.

The selection of the optimum prefilter/membrane combination is best done experimentally on the user's process stream. The manufacturers give some guidance as to which prefilters should be used for a given membrane pore-size, but unfortunately, there is no standard rating system for prefilters.

The experimental procedure used by the author places various prefilters on top of the selected membrane in 47 mm holders which are run in parallel on the process stream to be filtered. Usually, the test is carried out at constant flow rate and the rise in pressure drop is recorded versus the volume processed until the membrane plugs. The combinations providing the highest throughput are then evaluated with respect to cost of the media.

The search for the optimum prefilter media is often facilitated by testing the membrane and prefilter separately after the combination has reached the limiting pressure drop. If the final membrane is plugged but the prefilter shows a low pressure drop (see Figure 2.28), the prefilter is too coarse and a more retentive prefilter should be selected to protect the final filter.

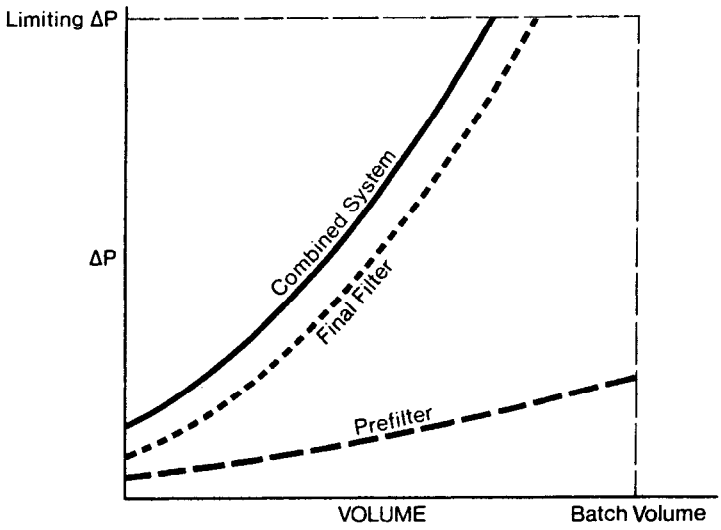


Figure 2.28: Inadequate prefilter (too coarse) for final membrane filter.

On the other hand, if the prefilter shows a high pressure drop and the membrane a low pressure drop (Figure 2.29), the prefilter is doing a great job protect-

ing the final filter, but additional dirt-loading capacity is required. This may be accomplished by adding additional prefilter area. In some cases, a more open prefilter can be used before the tighter prefilter. If the final membrane has a large pore-size, it is also possible that the prefilter may be too tight.

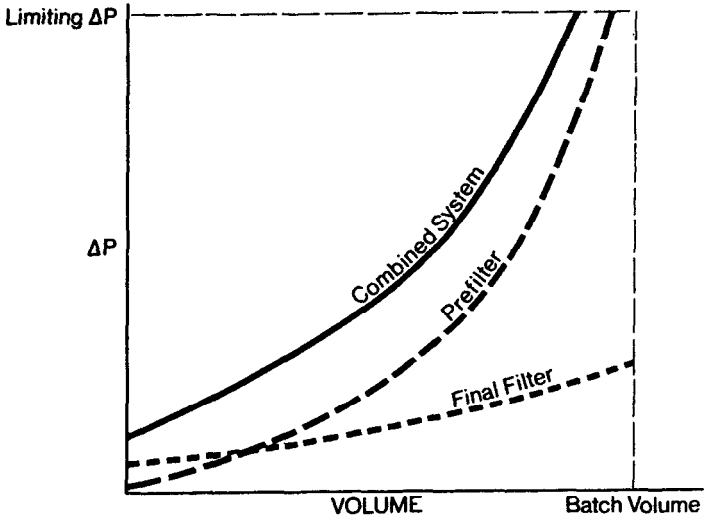


Figure 2.29: Inadequate prefilter area for final membrane filter.

The optimum match between prefilter and membrane will usually show both prefilter and membrane plugged so that neither one has carried the complete load by itself (see Figure 2.30).

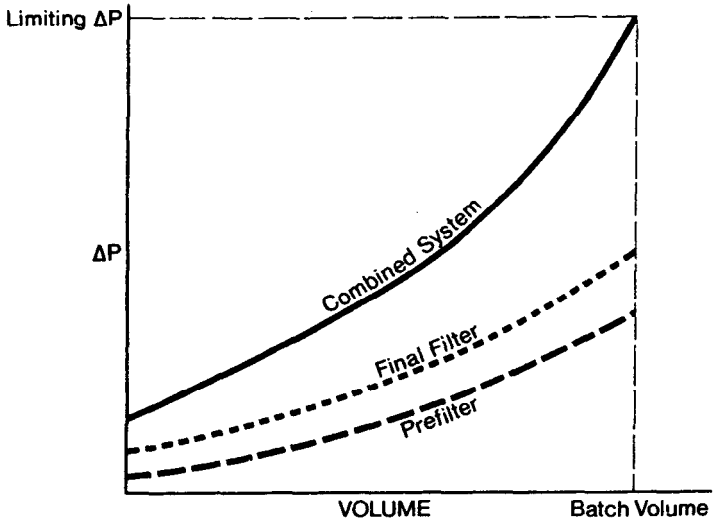


Figure 2.30: Optimized prefilter/membrane combination.

A series of graded prefilters can provide the highest throughput. In Figure 2.31, tests were run on serum at constant pressure showing the volume processed at various times. The declining slope of the curves reflects the declining flow rate with time. More open membranes were used as prefilters for the final 0.45 μ pore-size membrane. P100 is a glass-fiber prefilter normally matched with a 1 μ pore-size final membrane. Obviously, the increases in throughput achieved by additional media must be weighed against media costs.

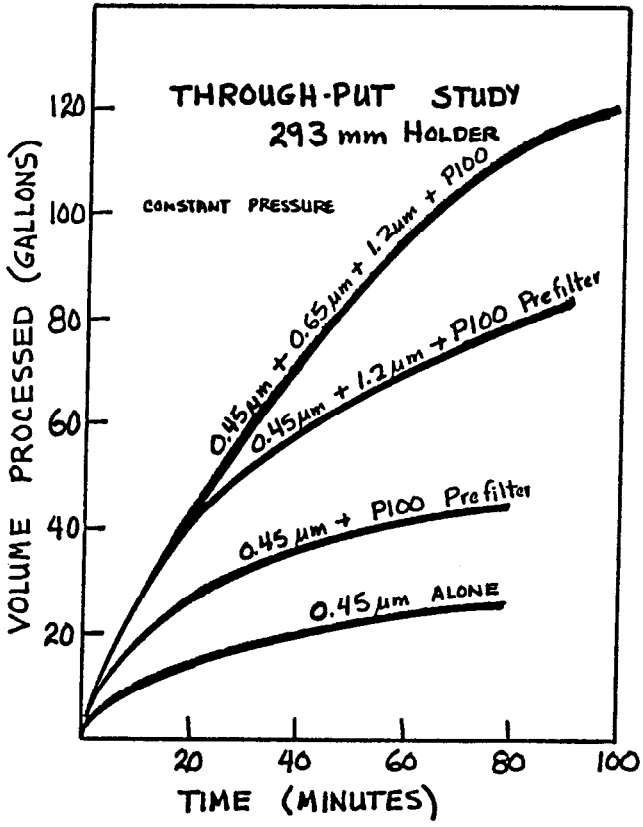


Figure 2.31: Serum through-put as a function of various combinations of prefilters.

Some MF membranes have a variation in pore size from upper to lower face (see Figure 2.32). We call this "anisotropy". At least one manufacturer intentionally makes an anistropic MF membrane. The idea is to provide a built-in prefilter with the more open pore-size upstream of the finer pore-size. Indeed, an improvement in throughput is achieved, but usually at the expense of retention. When using discs of anisotropic membranes, orientation can have a dramatic effect on throughput. One manufacturer puts a note in every box of membrane: "Use this side upstream".

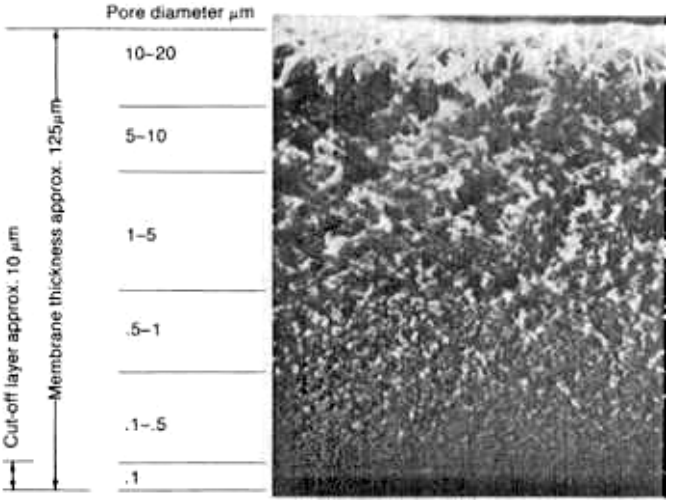


Figure 2.32: Cross-section photomicrograph-anisotropic tortuous-pore membrane.

Effect of Filtration Rate on Throughput

Irregardless of the type of filtration media, it is universally true that lower filtration rates result in higher throughputs. It should be obvious that two identical filters run at two different flow rates will show different pressure drops across the filter. At half the filtration rate, the pressure drop will be one-half as well. For the same volume processed, and the same degree of pore-plugging, the filter run at 50% of the flow rate of the other will show 50% of the pressure-drop as well. If the limiting pressure drop is 30 psi (as in Figure 2.33), the filter run at 50% of the flow rate will process a larger volume before its pressure drop reaches the limit.

For any type of pressure filtration, the filtration rate per unit area or flux (J) will be proportional to the pressure drop (ΔP) across the membrane or filter (i.e., the driving force) divided by the resistance to flow. The resistance term consists of two parts: the resistance of the cake which accumulates on the upstream surface of the membrane (R_c) and the resistance contributed by the membrane itself (R_m).

In conventional filtration of particulates:

$$J = \frac{\Delta P}{R_m + R_c} \tag{10}$$

The resistance of the membrane, (R_m) is easily determined by the resistance to flow observed with ultrapure water and should be a constant for a given membrane operating with a specified fluid and temperature.

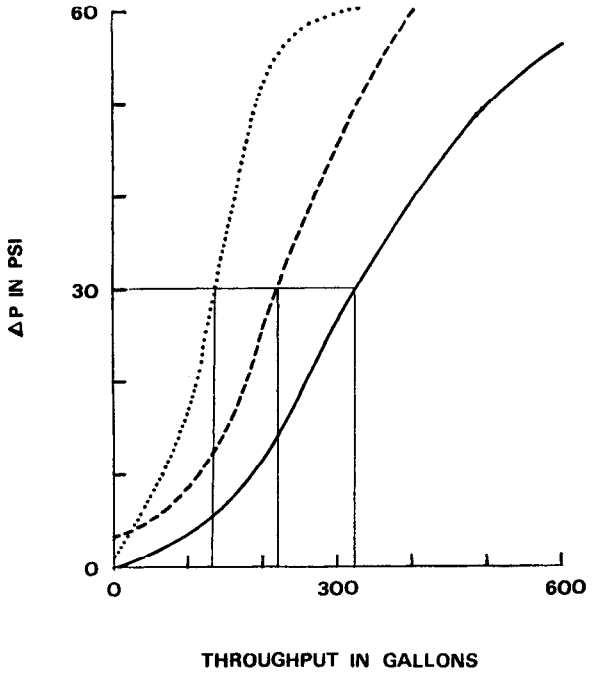


Figure 2.33: Through-put curve run at three different filtration rates.

The resistance of the cake of accumulated particulates, R_c, is more complicated; it is a variable which increases as filtration proceeds resulting in a progressively lower filtration rate at constant pressure. This is due to the continually increasing thickness of the cake and its compaction under the pressurized conditions of filtration. If R_m is defined as above, R_c must also include the effect of pore plugging within the membrane.

In the conventional filtration of particulates:

$$R_C = \frac{\alpha' w' V_t (\Delta P)^s \mu}{A} \tag{11}$$

where α' = constant dependent on properties of the cake

w' = is the weight of dry particulates per unit volume of filtrate

V_t = volume of filtrate delivered or "throughput"

ΔP = pressure drop

s = compressibility exponent of the cake. (s is zero for a perfectly noncompressible cake and unity for a perfectly compressible cake; normal values range between 0.1 to 0.8 for commercial slurries.)

μ = viscosity of the filtrate

A = area of the filtering surface

Combining equations (10) and (11)

$$(12) \qquad J = \frac{\Delta P}{\frac{\alpha' w' V_t (\Delta P)^s \mu}{A} + R_m}$$

Thus, the flux declines as the throughput increases.

Inverting equation (12)

$$(13) \qquad \frac{1}{J} = \frac{\alpha' w' V_t (\Delta P)^{s-1} \mu}{A} + \frac{R_m}{\Delta P}$$

If one assumes that the limiting resistance to flow is that due to accumulated particulates on the membrane or within the pores, equation (12) becomes:

$$(14) \qquad J = \frac{A \Delta P^{1-s}}{\alpha' w' V_t \mu}$$

It is interesting to note that for a "perfectly compressible" cake, the flux becomes independent of pressure. Higher pressures simply increase the resistance to flow of the cake enough to offset increases in the flow rate due to the higher driving force (ΔP).

Rearranging equation (14) gives us the dependence of throughput on other variables.

$$(15) \qquad \frac{V_t}{A} = \frac{\Delta P^{1-s}}{\alpha' w' J \mu}$$

Equation (15) shows that as a first approximation, the throughput (total volume processed) per square foot of membrane area will be inversely proportional to the flow intensity or flux (in gal/min/ft^2). Figure 2.34 shows that equation (15) is a good approximation in at least one case. In other cases (see Figure 2.35), the throughput seems to increase more sharply for a decrease in flow intensity. This may be due to an inertial impaction phenomena, which equation (15) does not take into account. Particles smaller than the rated pore size may be captured on the membrane at high velocities, whereas at low velocities, they may follow the flow streamlines more eqsily and pass through the membrane without capture.

The variation of throughput with filtration rate has far-reaching implications on the most economical way to run conventional membrane filtration processes. For example, if a fixed volumetric flow rate (gal/min) must be filtered, the total volume (in gallons) which may be processed before plugging (run to a set ΔP) is

proportional to the square of the membrane area. [J in equation (15) has units of gal/min/ft^2]. Thus, increasing the fixed capital investment (in housings, etc.) by two times (to increase the membrane area by a factor of 2) will increase the volume processed (to membrane exhaustion) by a factor of four. Consequently, replacement costs of membranes will be reduced by a factor of 2.

Incidentally, this also explains how "capillary-pore" membrane cartridges can equal the throughput of "tortuous-pore" cartridges. Two to three times the area of the "tortuous-pore" membranes can be pleated into a similar cartridge because the capillary-pore membranes are so much thinner.

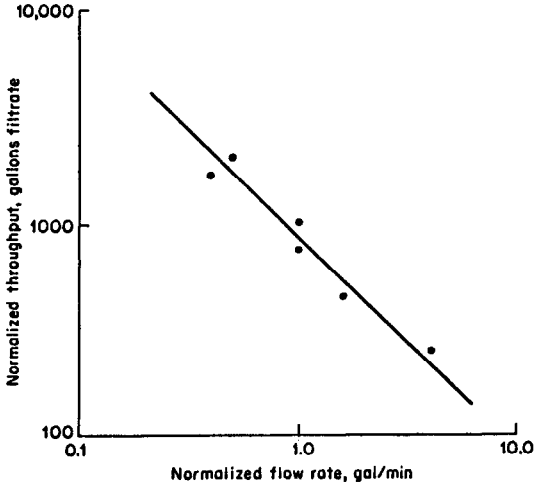


Figure 2.34: Tap-water through-put inversely proportional to filtration rate.

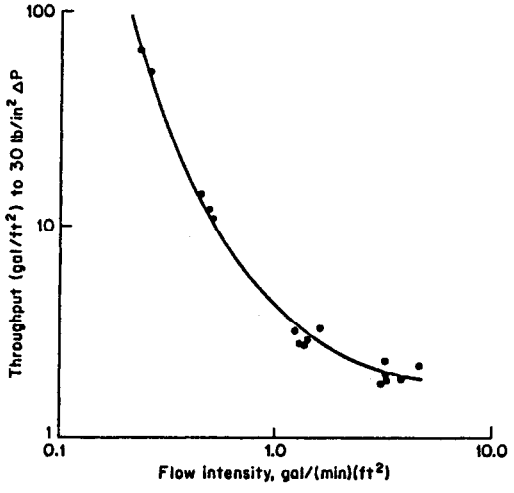


Figure 2.35: Dramatic decrease in through-put with increasing flow intensity.

Backwashing

The life of conventional filter media can often be extended by "backwashing". This technique has also been applied with moderate success to MF membranes.

In plate and frame systems (see Figure 2.36), the filtrate itself is often used as the backwash fluid. Sometimes, larger membrane housings are used to serve as an accumulation reservoir for the filtrate. A backwash fluid outlet is provided up-stream of the membrane to purge "backwash debris" from the system. Of course, the membrane must be supported on both sides.

As might be suspected, "capillary-pore" membranes appear to be more ammenable to backwashing than "tortuous-pore" membranes. However, some process streams deposit particulates on the membrane that cannot be backwashed from either type. Figure 2.37 shows a relatively successful backwash experiment on "capillary-pore" membranes used to filter beer.

Though not recommended by the manufacturers, pleated cartridges of both "tortuous-pore" and "capillary-pore" membranes are now backwashed in several wineries. Current pleated cartridge design gives the membrane good support in the forward-flow direction but poor support in the reverse direction. Nevertheless, several users have extended the life of their cartridges significantly using low-pressure backwashing.

Cross-Flow Filtration

Ultrafiltration and reverse osmosis have always used a fluid management technique known as "cross-flow filtration" to sweep away deposited particles from the membrane surface. "Cross-flow filtration" (CFF) is compared with "through-flow filtration" (TFF) (sometimes called "dead-ended filtration") in Figure 2.38.

Currently, most MF systems operate with the more conventional "through-flow filtration"–one stream in and one stream out. The particles accumulate on the membrane and are disposed of with the membrane.

In "cross-flow filtration", with one stream in and two streams out, the objective is to extend the life of the membrane indefinitely. Generally, pumping energy must be supplied to recirculate the cross-flow stream at velocities 10 to 100 times higher than the permeation rate (see Figure 2.39). Particles removed from the process stream are not all deposited on the filter; most are circulated as a retentate stream with ever-increasing concentration. A bleed stream (reject stream) may be removed to keep the concentration constant. In some applications, like cell harvesting, the product is the concentrated retentate stream. In other applications, where the product is the filtrate, the disposal of the retentate stream becomes a problem. Indeed, in some applications, having the particles collected on the filter facilitates disposal and favors the more conventional TFF.

Figure 2.40 shows the cross-flow concentration of yeast with a "capillary-pore" membrane. Since the yeast particles are considerably larger than the 0.2 μ pore size, internal pore fouling was nil. The sweeping action of the cross-flow stream tangential to the membrane surface maintained a stable flux at constant concentration. The ability to concentrate yeast from 0.1 to 10% with a stable flux would be impossible with TFF.

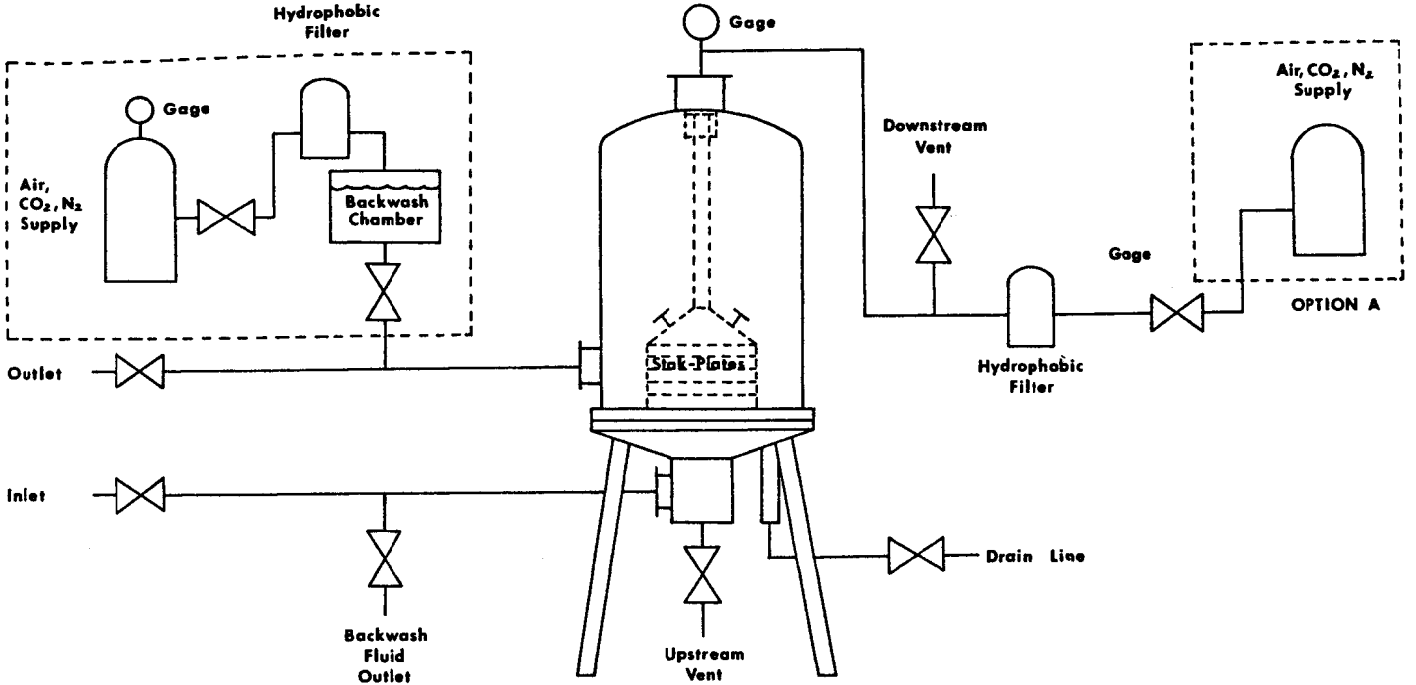


Figure 2.36: Schematic of plate and frame system with back-wash capability.

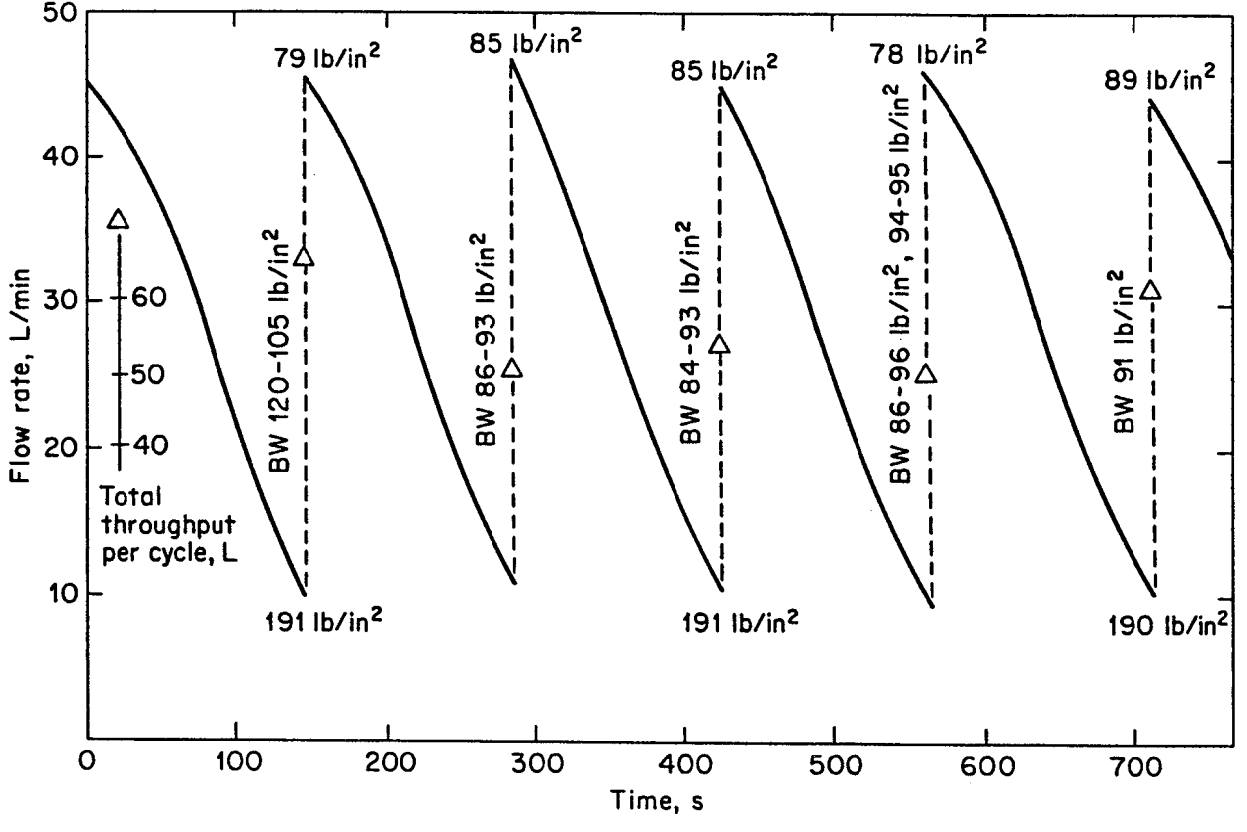


Figure 2.37: Recovery of filtration rate on beer with periodic back-wash of capillary-pore membranes.

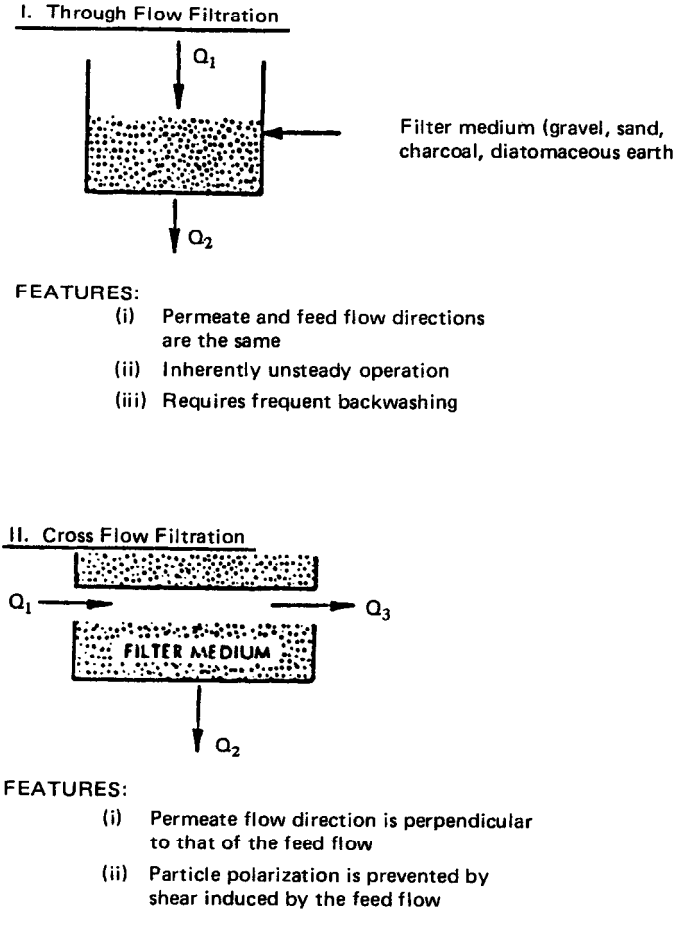


Figure 2.38: Through-flow filtration (TFF) and cross-flow filtration (CFF).

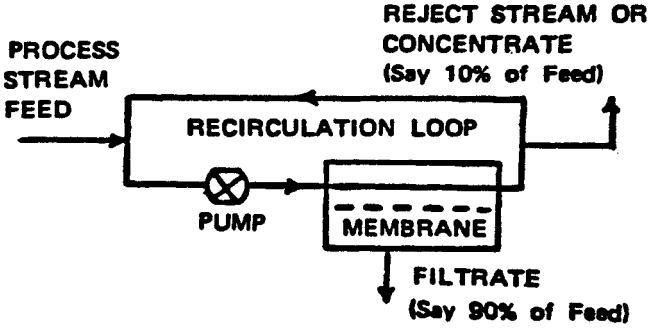


Figure 2.39: Schematic of recirculation loop for cross-flow filtration (CFF).

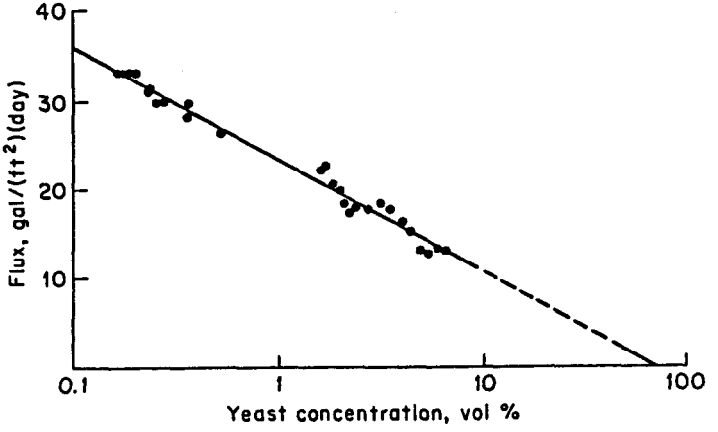


Figure 2.40: Cross-flow concentration of yeast with a capillary-pore membrane.

For suspensions of particles with sizes nearer to the pore size, some internal pore fouling will occur but at a greatly reduced rate. Figure 2.41[22] shows cross-flow filtration of a single cell protein suspension on a "tortuous-pore" membrane. The flux declines rapidly at first, as boundary layer conditions are established, and then levels off with a diminishing rate of flux decay.

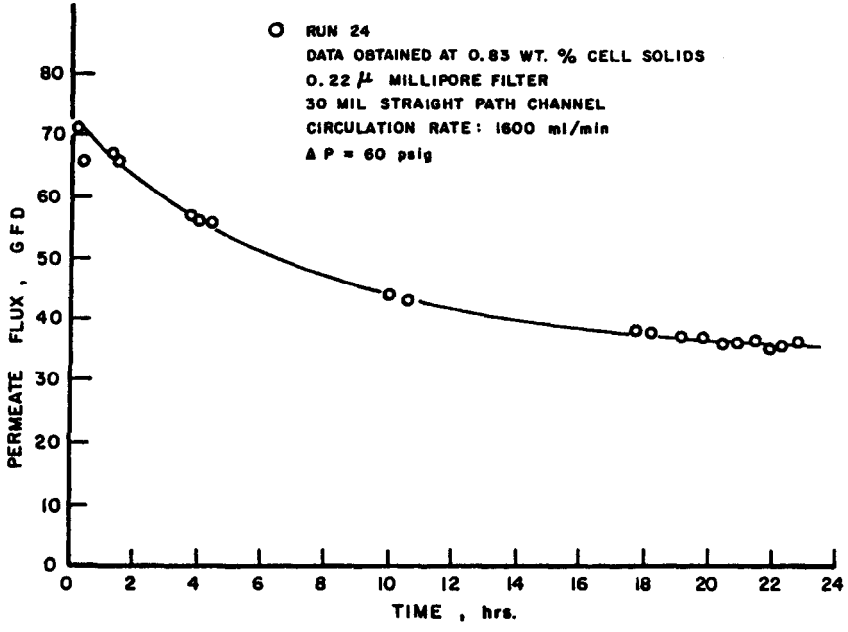


Figure 2.41: Cross-flow filtration of single cell protein suspension (0.83 wt %) with 0.22 micron tortuous-pore membrane.

Referring to equation (13), we can examine what happens to the cake resistance (R_c) in cross-flow filtration by plotting the reciprocal of the flux (1/J) versus the throughput volume (V_t). In through-flow filtration at constant pressure, we would expect to see a straight line with a slope proportional to the concentration of particles in the feed stream. In cross-flow filtration, we obtain results like those of Figure 2.42. The intercept with the ordinate ($V_t = 0$) is equal to $R_m/\Delta P$, the resistance of the membrane divided by the pressure drop. As the filtrate volume begins to accumulate, the data shows a growing cake resistance. The break in the line is due to the sweeping action of the flow tangential to the membrane surface. There is a finite thickness of cake that is never removed, and there is a growing resistance due to internal pore fouling, albeit at a slower rate.

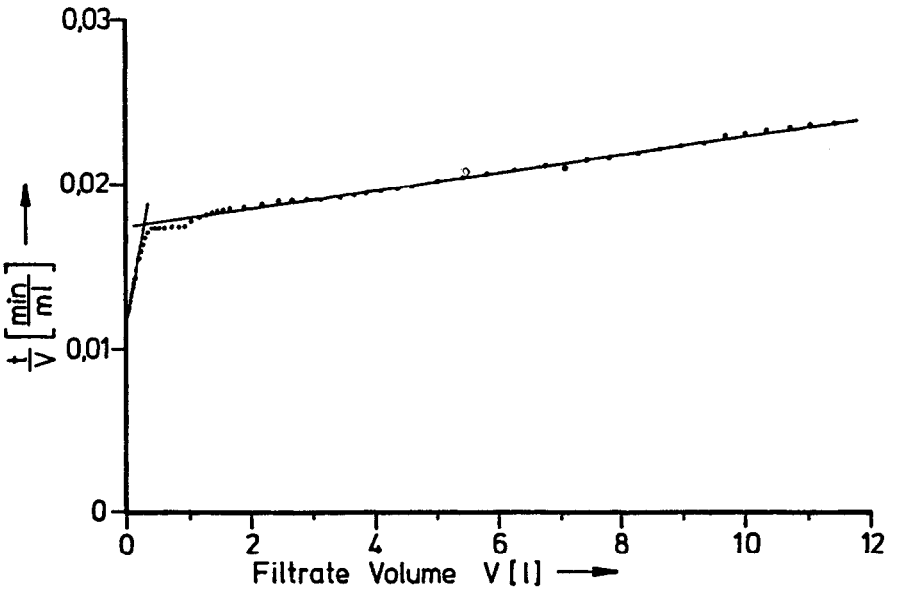


Figure 2.42: Increase in cake resistance (reciprocal of flux) as a function of through-put for cross-flow filtration (CFF).

The flux decay due to internal pore fouling can often be relieved with back-flushing or chemical cleaning as in Figure 2.43, but the ultimate solution is to develop MF membranes which have a high degree of anisotropy. For example, UF membranes are so anisotropic that internal pore fouling is virtually eliminated. The skin of the membrane, with exceedingly small pores, faces the feed stream. Since the smallest passage-way is at the pore entrance, any species gaining admittance passes completely through the membrane with no opportunity to block internal pores. The only bottleneck is at the pore entrance which leads into an ever expanding chamber. Unfortunately, there are no MF membranes currently on the market which have this degree of asymmetry (compare the cross section SEM photos of Figure 2.32 with those in Chapter 3).

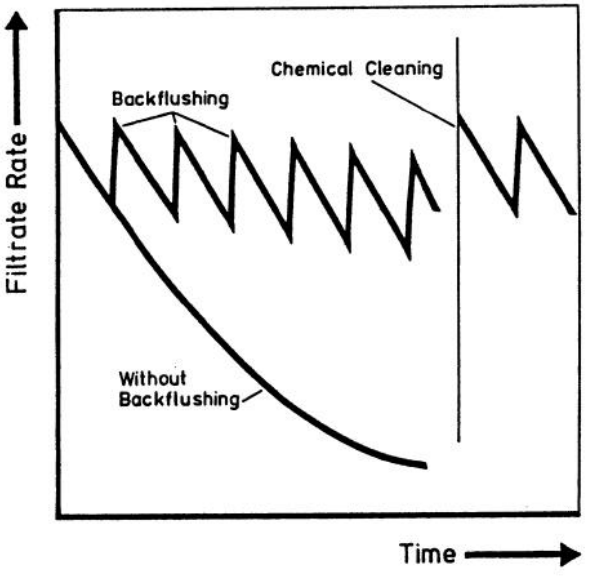


Figure 2.43: Restoration of CFF flux by backflushing and chemical cleaning.

Some inorganic membranes (alumina) have been recently introduced which are anisotropic (see Figure 2.44) but the skin is too thick. In other words, the pore entrance resembles a long narrow passage more than an orifice. Plugging can occur by particles bridging across the passage. However, some improvement in flux decay has been reported for these membranes operating with cross-flow on certain process streams.

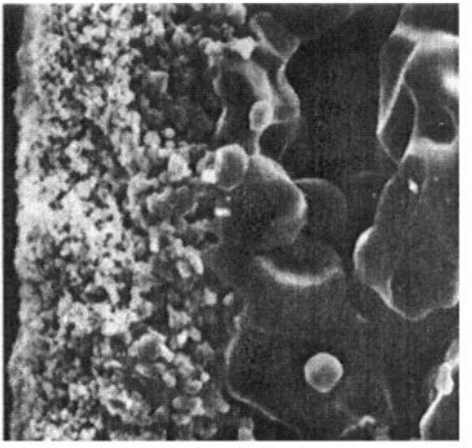


Figure 2.44: Cross-section photomicrograph of anisotropic ceramic MF membrane.

The development of a truly anisotropic MF membrane will be a major breakthrough for cross-flow microfiltration.

MEMBRANE CONFIGURATION

The configuration of the membrane will obviously affect cost, ease of replacement, and efficiency of filtration. There are currently three primary configurations for MF membranes in industrial use:

(1) plate and frame units

(2) pleated cartridges

(3) tubular/hollow-fiber modules

Plate and Frame Units

Figure 2.45 shows the internals of a stacked-plate membrane filter housing accommodating up to sixty 293 mm membranes with a maximum filtration area of 33 square feet (3.0 m^2).

Only "tortuous-pore" membrane discs may be used in such a stack. The reason is that the polycarbonate or polyester "capillary-pore" membranes currently available are very thin (typically 10 μ thick) and easily pick up an electrostatic charge. It is almost impossible to load 293 mm discs of these membranes onto the plates. They cling to hands and wrinkles cannot be totally eliminated. It is possible to buy (in Japan) a heat sealed "sandwich" with polyester screens on both sides of the "capillary-pore" membrane (see Figure 2.46) which facilitates handling. The "sandwich" is sealed around the periphery to prevent lateral leakage.

After loading such a stack of membranes, it is imperative that the unit be "bubble-pointed" to establish the integrity of the stack. It is very easy to damage a membrane in the process of loading. Even a pin-hole will show a bubble-point of less than one psi. Further, every plate has gasket and "o-ring" seals which may be out of place. A small piece of dirt or grit in an "o-ring" groove can also create a leak which will show up as a very low bubble-point.

Plate and frame units are also used for cross-flow filtration. Some units take sheet stock MF membranes while others work best with a preassembled membrane cassette-a sandwich of two outer layers of membrane sealed to an inner filtrate collection screen (see Figure 2.47). A cross-flow spacer is placed between the filter packets and stacked in a plate and frame arrangement (see Figure 2.48). In some systems, the cross-flow spacer is a screen, but the "flow-channel" spacer shown in Figure 2.47 is less prone to fouling.

Pleated Cartridges

Stacked plate units were the first successful configuration for large scale MF, in spite of three distinct problems:

(1) Membrane damage during loading

(2) "O-ring" gasket seal problems

(3) High labor and downtime for membrane replacement.

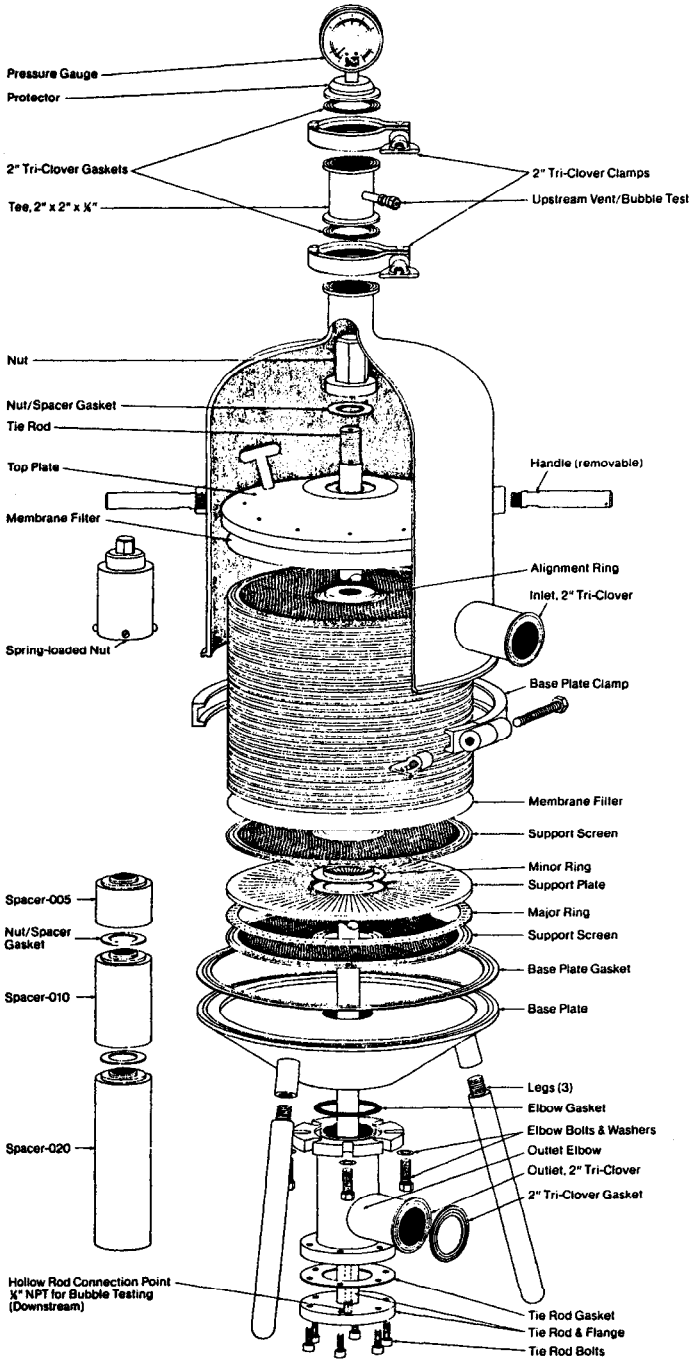


Figure 2.45: Internal components of plate and frame (stacked-plate) membrane filter holder.

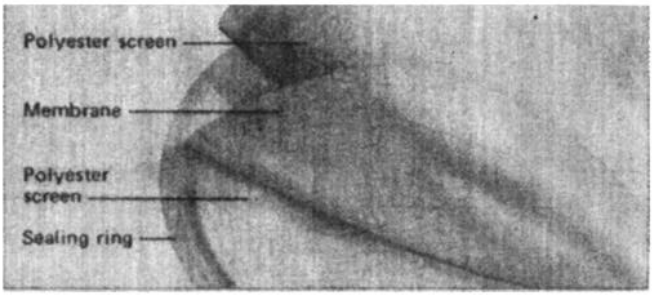


Figure 2.46: Capillary-pore membrane cassette (sandwiched between two support screens).

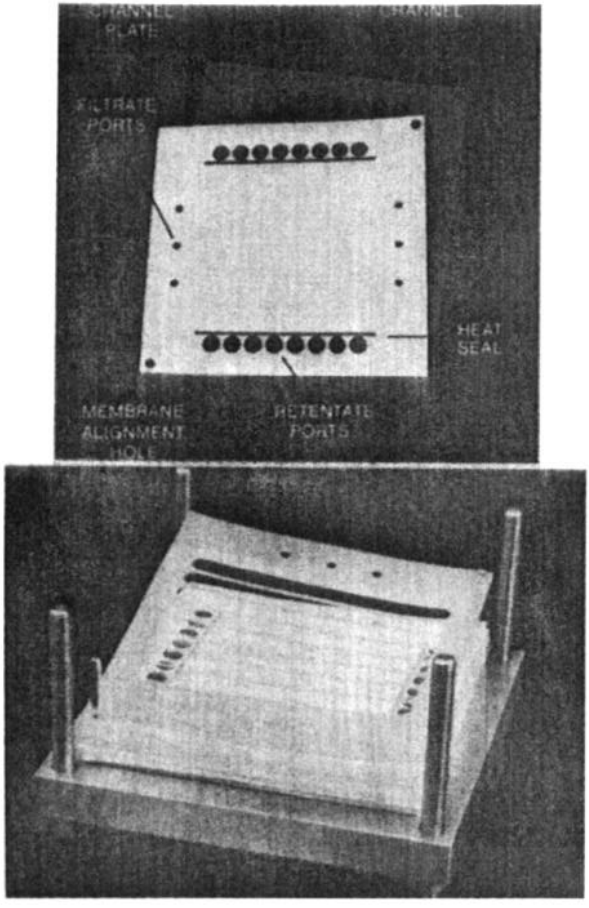
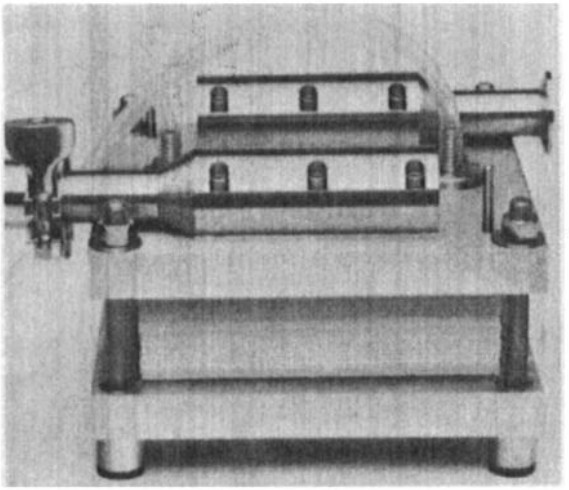


Figure 2.47: Cross-flow membrane cassette (two layers of membrane enclosing inner collection screen) and flow-channel spacer.



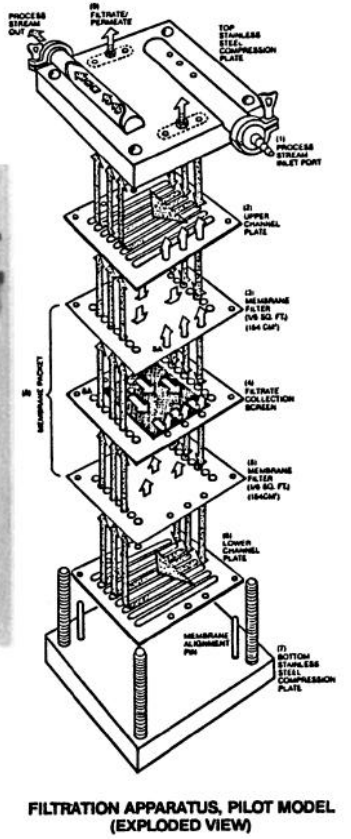


Figure 2.48: Plate and frame cross-flow filtration unit.

It was early recognized that, if the replaceable element contained more membrane area (preferably in a protective package), the installation time could be greatly reduced. Unfortunately, the early "tortuous-pore" membranes could not be pleated without loss of integrity. Therefore, the first cartridges were a closed-end 2 inch diameter tube almost 2 feet long with one square foot of membrane wrapped around the outside and sealed longitudinally. This permitted the fabrication of a "bubble-pointable" tube. Unfortunately, the 22 inch tube contained only twice the area of a single 293 mm disc.

For noncritical applications, pleated cartridges were fabricated showing less than full bubble point. For example, Figure 2.49 is a cartridge designed for filtration for deionized water. It contains five square feet of pleated 0.5 μ membrane prefilter and 0.2 μ membrane. Because the pleated membranes could not be "bubble-pointed", a final core wrap of 0.8 μ membrane was incorporated to give the cartridge a bubble-point of around 10–12 psi. The tighter 0.2 μ pore-size membrane could not be used for the core-wrap because of the high pressure differential it generated across the core wrap (only 0.2 square feet in filtration area).

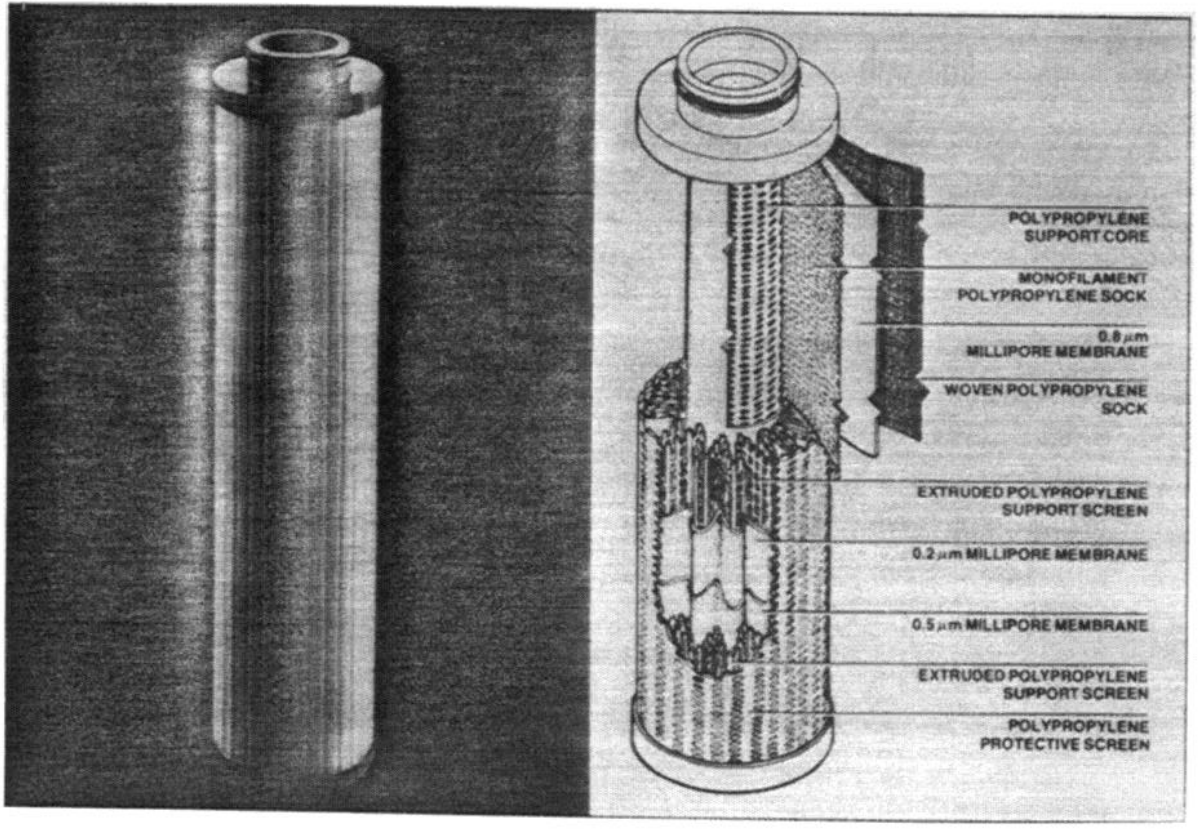


Figure 2.49: Typical pleated cartridge cut-away.

In the last decade, some manufacturers have been able to produce "bubble-pointable" (45–50 psi) pleated cartridges. These include "tortuous-pore" nylon and polyvinylidene fluoride membranes. The 0.2 μ cartridges show quantitative retention of *Pseudomonas diminuta* at challenge levels of 10^{10} to 10^{13} organisms.

For reasons enumerated earlier, "capillary-pore" membranes, though pleatable, will not yield satisfactory bubble-points and begin to pass *Pseudomonas diminuta* at challenge levels above 10^3-10^5 organisms even though the membrane area is 2 to 3 times greater.

Most pleated cartridges are sealed inside housings with "o-rings". There are external and internal "o-rings" designs, both of which are vastly superior to the old gasket seals which can easily unseat under pressure.

Some pleated cartridges are encapsulated in a disposable plastic housing so that, apart from external hose connections, there are no seals to worry about.

Pleated cartridges are considerably more expensive than the equivalent membrane area in 293 mm discs (2 to 4 times as much). Some users insist that the lower replacement labor does not off-set the additional expense. However, the trend is definitely towards pleated cartridges for through-flow filtration. The movement to pleated cartridges has been accelerated with the discovery that some exhausted cartridges can be reused after backwashing.

Modified pleated cartridges have also been used in a cross-flow operating mode.[23] In the simplest modification, a sleeve is placed around the cartridge and the housing modified to withdraw the retentate stream from the bottom of the housing (see Figure 2.50). The cross-flow stream is forced into the pleats where it moves tangential to the membrane. Even with this simple modification, dramatic increases in throughput were observed in the dewatering of yeast (Figure 2.51) and activated carbon (Figure 2.52). The increase in throughput was found to be a strong function of the cross-flow velocity–as would be expected. The data of Figure 2.51 and 2.52 were run at a recirculation/permeate ratio of 16.

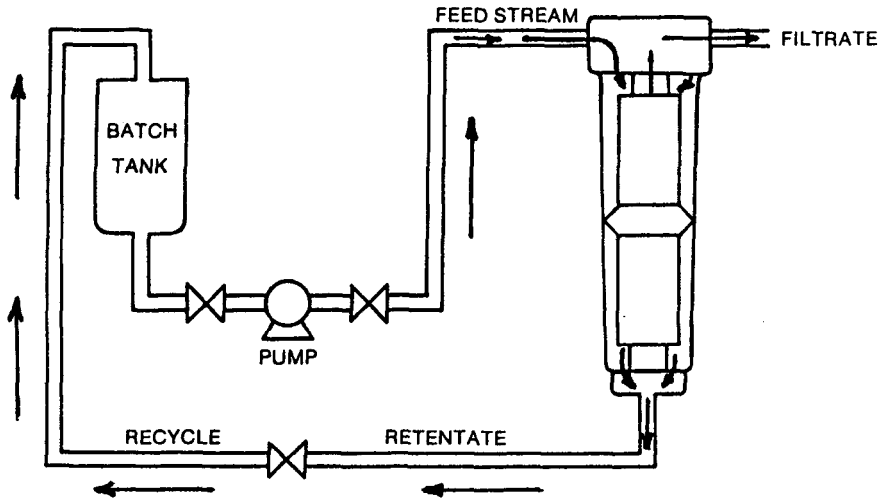


Figure 2.50: Modified pleated cartridge and housing for cross-flow filtration (CFF).

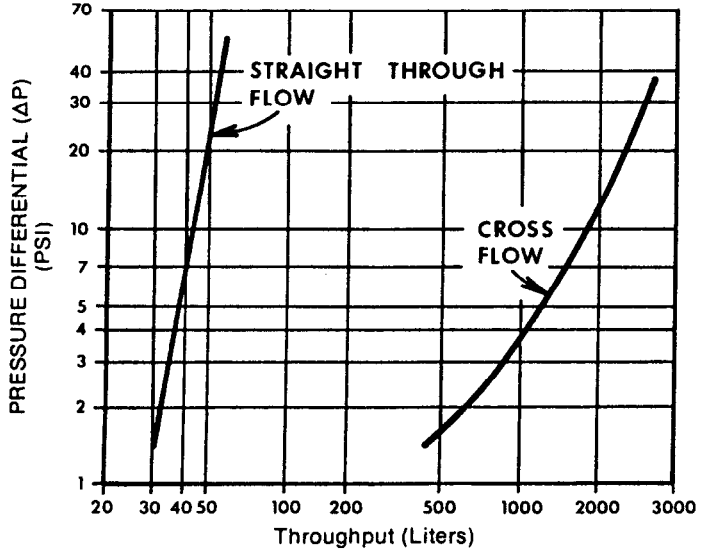


Figure 2.51: Increase in through-put for cross-flow filtration of 0.5% yeast with modified 0.2 micron capillary-pore membrane pleated cartridge.

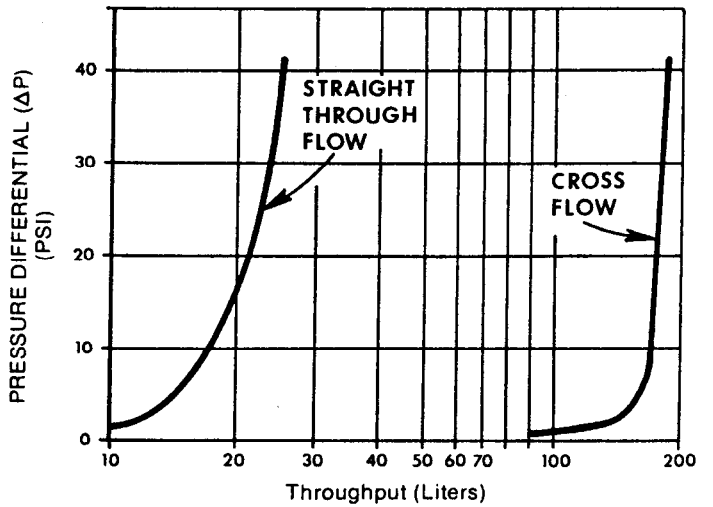


Figure 2.52: Increase in through-put for cross-flow filtration of 0.25% activated carbon with modified 0.2 micron capillary-pore membrane pleated cartridge.

More recently, a line of cross-flow pleated cartridges has been introduced with a controlled spacing for the cross-flow path between the pleats (see Figure 2.53).[24] This alleviates the most serious problem with the simple modifications described in the preceding paragraph where bunching of pleats creates a non-uniform distribution of cross-flow channels.

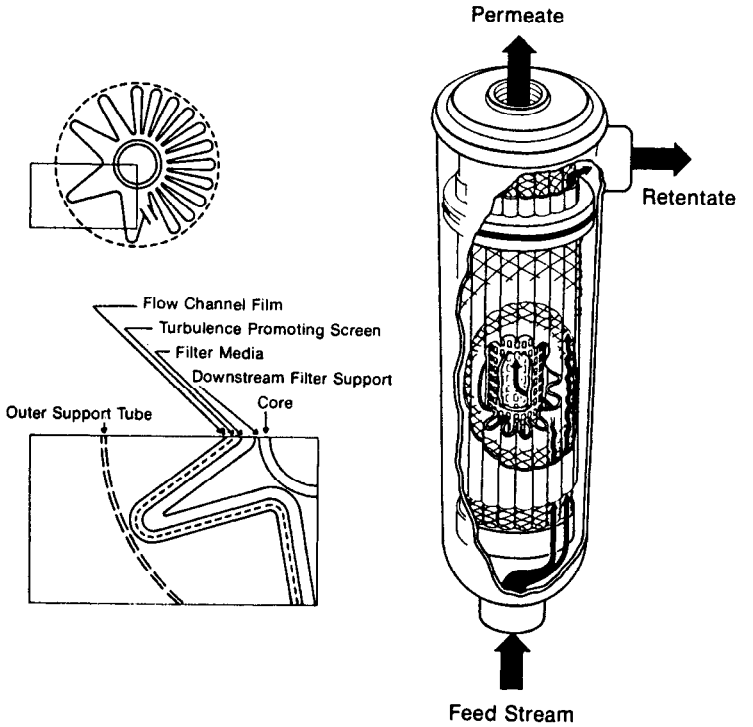


Figure 2.53: Improved cross-flow pleated cartridge with controlled flow-channel spacing (Acroflux™).

Tubular/Hollow-Fiber Modules

Various "tortuous-pore" membranes are also available in tubular and hollow-fiber modules:

MEMBRANE	PORE-SIZE (Microns)	TUBES (I.D. in mm)	HOLLOW-FIBERS (I.D. in mm)
Alumina	0.2-5.0	3-15	———
Cellulose Ester	0.2	———	0.37-0.61
Polypropylene	0.2	5.5	0.6-1.8
Polysulfone	0.1-0.4	———	0.5-1.0
Polyvinyl alcohol	0.4	———	0.4
Polyvinylidene difluoride	0.08	25.4	———

The polyvinylidene difluoride (PVDF) membrane is anisotropic and might better be called an open UF membrane. In addition, the alumina membrane is somewhat asymmetric (see Figure 2.44). None of the other membranes are anisotropic.

All of the tubes and hollow-fibers are self-supporting except for the PVDF membrane which is cast on the inside of a porous polypropylene tube. In most cases, they are potted on the ends to separate the process stream from the permeate (see Figure 2.54). This bundle of tubes or capillaries becomes the replaceable module.

APPLICATIONS

Many of the applications for MF derive from the excellent retention these membranes have for microorganisms. Indeed, the retention for bacteria or other organisms is often superior to what may be obtained from tighter UF and RO membranes. We may divide large-scale MF applications according to whether they utilize through-flow filtration (TFF) or cross-flow filtration (CFF). The former are more common.

Through-Flow Filtration Applications

Sterilization and Particle Removal (Pharmaceuticals). A great many of the drugs and solutions produced by the pharmaceutical industry or made up in the hospital pharmacy have to be both sterile and relatively free of particulate matter–especially if the product is to be injected into the bloodstream. For drugs and other products that will not withstand heat, sterilizing filtration is the only alternative. Tissue culture media, parenteral solutions, vaccines, human plasma fractions, antibiotics, diagnostic injectables are all sterilized by membrane filters.

Even if MF has been applied by the manufacturer, the solution may need to be filtered again by the pharmacist due to contamination during mixing or reconstitution. A single microorganism can grow into thousands overnight. Serious and sometimes fatal infections can result.

There is a growing clinical evidence that particulate matter in IV solutions can also be a serious health hazard. Direct blockage of blood vessels can occur. For example, the partial occlusion of retinal arteries can result in blind spots. Clot formation and emboli result because of the tendency of red cells to adhere to particles. Granulomas have resulted from inflammatory reactions where a particle is embedded in tissue.

The U.S. Food and Drug Administration (FDA) has specified that:

> Prior to filling, large volume parenteral drug products shall be filtered through systems having a final mean porosity of no more than 0.45 μ. Process specifications shall indicate the maximum time during which a filtration system may be used. Such time lengths shall preclude microbial build-up to levels that may affect the biological quality of the large volume parenteral, and in no case shall it exceed 8 hours.[25]

Achieving low particulate levels in the final drug or parenteral solution usually requires filtration of the constituent water. The *United States Pharmacopoea* defines specifications and methods for production of water for injection. Ultrapure water systems in the pharmaceutical industry use reverse osmosis, ion exchange, and MF just as in the electronics industry (see below). Both industries seek to produce sterile/particle free water. However, in the pharmaceutical in-

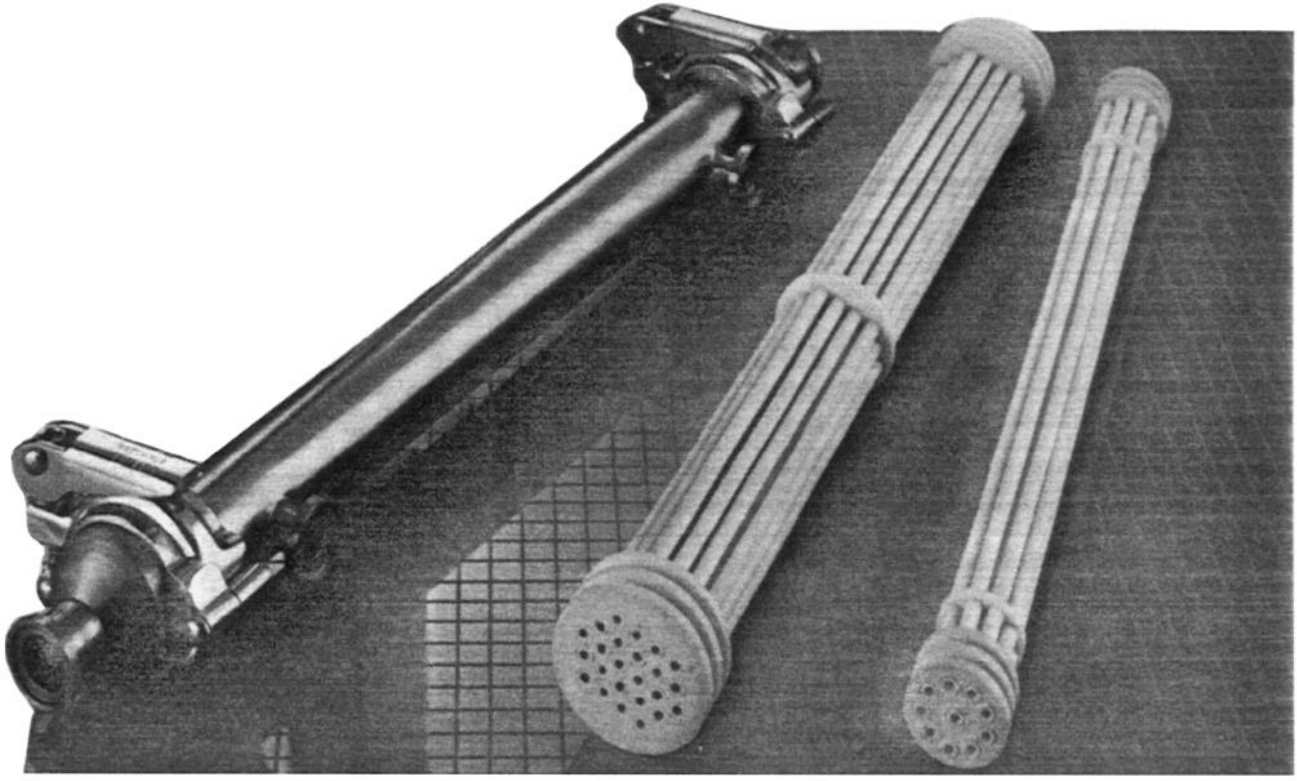


Figure 2.54: Ceramic MF tubular module.

dustry, most water produced must also be pyrogen free. This requires charge modified MF membranes, or UF/RO.

MF is also used to remove microorganisms and particulates from air and other gases used in the pharmaceutical industry. Some specific applications include: vent filters; filtration of compressed air used in sterilizers, filtration of air or nitrogen used for solution transfers or at filing lines, and filtration of air or nitrogen used in fermentors.

Again, the need for "vent-filters" has been recognized by the FDA:

> All stills and tanks holding liquid requiring microbial control shall have air vents with nonfiber-releasing sterilizable filters capable of preventing microbial contamination of the contents. Such filters shall be designed and installed so that they do not become wet. Filters shall be sterilized and installed aseptically. Tanks requiring air vents with filters include those holding water for manufacturing or final rinsing, water for cooling the drug product after sterilization, liquid components, and in-process solutions.[25]

It is clear enough why microbe retentive filters must be used as air-vents on fermentation vessels. The reason for the FDA requirement on storage or holding tanks is that the movement of liquids into and out of these vessels entails the flow of air or nitrogen to maintain a pressure balance; thus the vent provides an entryway for airborne contamination.

For gas filtration, the membrane should be treated to make it hydrophobic if not already inherently so. Membranes made from polytetrafluoroethylene or polypropylene are already nonwetting, and wettable polymers are treated by the manufacturer to render them hydrophobic. If the gas filter is hydrophilic, water condensing on the filter or entrained by the gas will wet the pores and be retained by capillary action unless the differential pressure across the filter exceeds the "bubble-point" pressure. In this case, the filter is "blinded" by water and the flow is restricted considerably.

In the case of air-vents, even if the filter has been sized adequately to handle the passage of air commensurate with liquid filing and withdrawal rates, the use of hydrophilic filters has caused the implosion or collapse of more than one storage tank. A hydrophobic filter passes air preferentially; indeed, a water intrusion pressure is required to force water into the pores.

Of course, the opposite phenomenon occurs with hydrophilic liquid filters where air bubbles are present in the liquid process stream; it is called "air-binding". Often a hydrophobic vent-filter will be used in conjunction with the main hydrophilic membrane filter to allow escape of accumulated air without permitting liquid leakage.

Naturally, any filter used to sterilize liquids or gases must be sterile itself when installed. Again, quoting the FDA:

> Solution filters shall be sterilized and installed aseptically. The integrity of solution filters shall be verified by an appropriate test, both prior to any large volume parenteral solution filtering operation, and at the conclusion of such operation before the filters are discarded. If the filter assembly fails the test at the conclusion of the filtering operation, all materials filtered through it during that filtering operation shall be rejected. Rejected materials may be refiltered using filters whose integrity has been verified.[25]

Therefore, membrane filters which can be autoclaved or steam sterilized are

in demand for these applications. If the membrane or cartridge cannot be autoclaved, other chemical sterilizing agents may be used (e.g., formaldehyde).

Sterilization and Particle Removal (Beverages). MF has been used extensively in the filtration of wine and beer. It is also currently used in the clarification of cider and other juices.

The objectives for beverage filtration are to obtain a biologically stable product with good clarity and no deposits.

Since wine and beer are fermentation products, shelf life will be limited unless all yeast are removed. Unless beer is kept very cold, a few surviving pediococci, lactobacilli, or wild yeasts may grow and produce off-flavors in the beer. Though the juices are not fermentation products, they nevertheless provide the perfect media for bacteria growth. In all cases, it is important to produce a sealed sterile product.

There are three routes to biological stability:

Heat stabilization

Injection of chemical preservatives

Sterile filtration

Heat pasteurization is an effective means of biological stabilization, but flavor is affected. The bouquet of a good wine is highly susceptible to heat. The vintner goes to great lengths to protect his wine from oxidation, and heat accelerates it. In addition, elevated temperatures can result in precipitation of proteins to form haze.

Pasteurization is still the most common practice in breweries in spite of some deterioration in flavor. A number of years ago, the brewing industry forecast a tremendous increase in demand for "draft-beer", and membrane filtration was substituted for pasteurization. However, the "draft beer craze" never materialized and many breweries reverted back to pasteurization.

Chemical stabilization has been accomplished by the addition of sorbates, benzoates, ascorbic acid, sulfur dioxide, or diethyl pyrocarbonate (DEPC). This method has not been universally accepted because of the public's general aversion to chemical preservatives and undesirable side affects. For example, DEPC is very toxic until it breaks down into ethyl alcohol, carbon dioxide, and ethyl pyrocarbonate.

The trend is toward the third approach of *sterile filtration*. Almost all wineries use it, though many breweries still prefer flash or "in-the-bottle pasteurization". MF not only removes organisms but improves the clarity of the product.

Juice producers are also beginning to explore membrane filtration. One large cranberry juice maker claims ceramic MF tubes pay for themselves in a year because of reduced labor, maintenance costs and waste. It is hoped that membrane filtration will also eliminate the need for heating the juice which changes its flavor. With the long-term trend of higher energy costs, it is expected that MF will eventually replace all pasteurization.

MF has also made its debut in the Japanese soft drink industry for the filtration of liquid sugar. Figure 2.55 is a flow schematic for two parallel plate and frame backwash systems to remove yeast from the liquid sugar. The parallel lines permit backwashing without interruption of the process flow stream.

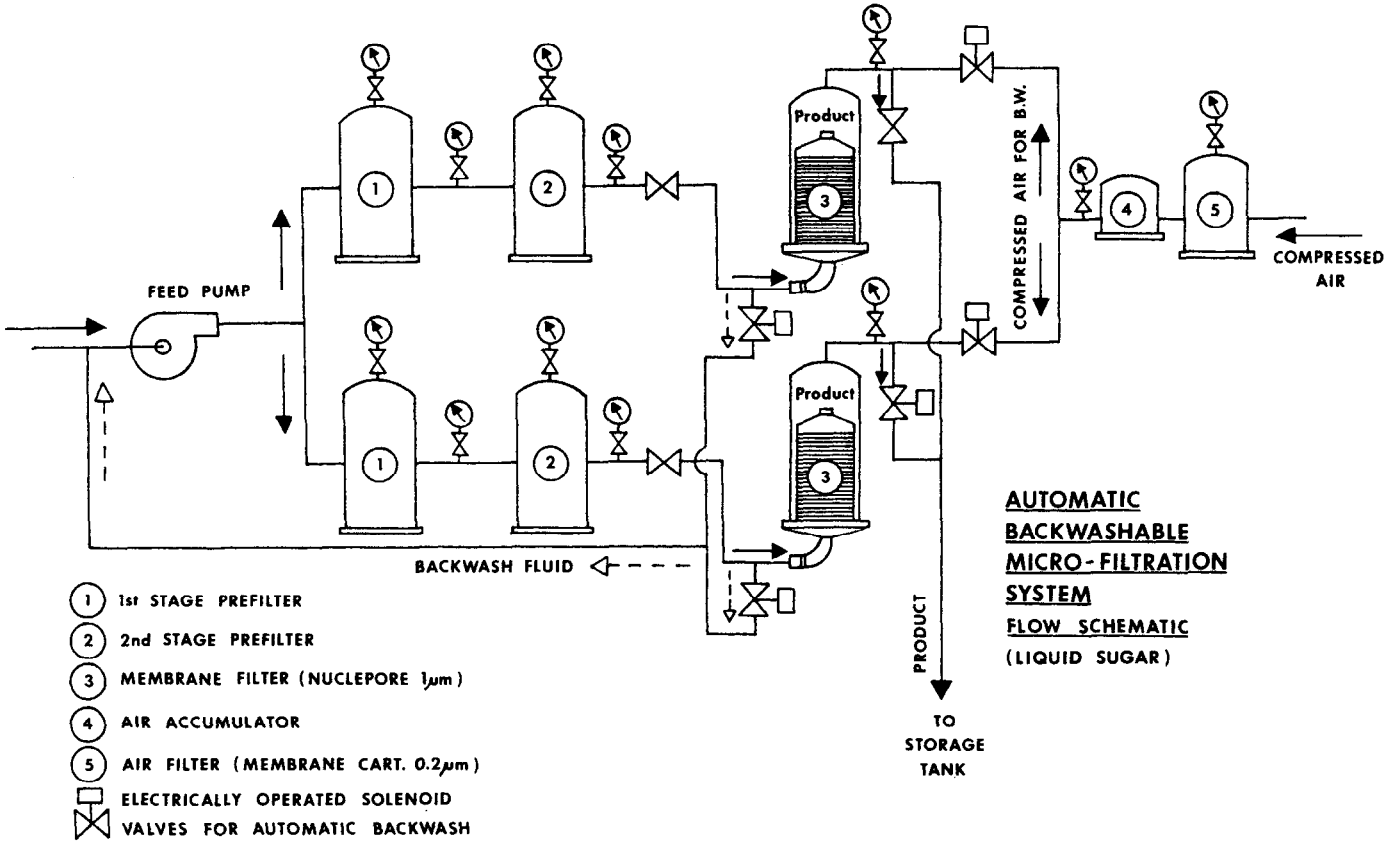


Figure 2.55: Flow schematic of back-wash system for MF of liquid-sugar.

Bottlers of carbonated soft-drinks are also experimenting with MF to remove bacteria and particles. Greater consistency in taste and longer-lasting carbonation are cited as benefits. The latter is due to the removal of particulates which act as "nucleation sites" to cause premature carbonation loss.

Particle Removal (Semiconductor Process Fluids). The fluids that come in contact with photo masks and wafers during integrated circuit (IC) production are often contaminated with particles which, if not eliminated, can cause defects and reduce production yields.

The early solid-state devices were not as sophisticated as devices produced today. A single transistor consisted of a relatively large crystal of germanium or silicon 0.25 inch square and 0.125 inch thick to which conductors were attached. The manufacturing processes were relatively insensitive to outside impurities.

The development of the transistor in the early fifties and the first IC's in 1959 made possible miniaturization on a scale never dreamed possible. Today, it is not uncommon to have over a million components per circuit on a single wafer. Conductor widths and spacing can be less than a micron. Thus, submicron particles can mask critical areas during etching and other key manufacturing steps. This results in pinholing, shorts, undercutting, internal arcing, poor adhesion of photoresist coalings, and other unwanted changes in current carrying properties. According to the commonly employed "Rule of Ten", advanced VLSI (very large scale integrated) microcircuits with one micron geometries are sensitive to particulate contamination greater than 0.1 μ.

Deionized (DI) Water. DI water is crucial in the microelectronics manufacturing process; nearly every operation in IC manufacturing ends with a DI water rinse. Wafer-rinsing operations following wet-chemistry cleaning, stripping and etching processes all require ultrahigh-purity process water as does process chemical-bath make up. If the water is not of sufficient quality, decreased wafer yields or subsequent device failure may result. Table 2.7[26] summarizes typical requirements for process water used in the manufacturing of high-density microelectronic devices. Obviously, these specifications are a trade-off between desired purity and practical purity and some water supplies will require more treatment than others to achieve these specifications.

The heart of any ultrapure water system is ion exchange (IX). It was clearly recognized that the presence of mobile ions such as sodium would produce leaky junctions and threshold voltage shifts in the final device. No other process, including reverse osmosis (RO), is as effective as IX in removing ions to produce high resistivity water (18MΩcm). For a typical feedwater with 200 ppm TDS (total dissolved solids), a single pass through an RO membrane can reduce the TDS to 2-20 ppm, and a double pass to 0.02-2 ppm. As shown in Table 2.8, the resistivity of the permeate from a double pass RO system is still insufficient (0.1 to 10 MΩcm). Thus, all ultrapure water systems utilize IX usually in the form of separate cation and anion resin beds followed by mixed bed polishing columns.

Later, it was discovered that 18 MΩcm water could still contain submicron particles and organics which introduce defects into the IC. Indeed, IX seems to aggravate the problem. The accumulation of organic debris on the resins provides an almost ideal growth environment for bacteria which multiply at an exponential rate. They quickly foul the resins and overrun the distribution system. Further, because of the constant agitation and tumbling of the resin beads under forced-flow conditions, there is constant mechanical breakdown of the resins

themselves with the generation of resin fines and other particulates. Thus, there is a need for MF to remove all bacteria and other submicron particles after demineralization.

Table 2.7: Typical Requirements for Process Water Used in Microelectronics Device Fabrication[26]

Parameter	Level
Resistivity (at 25°C)	18 MΩ-cm (90% of the time) 17 MΩ-cm, minimum
SiO_2 (total), maximum	75×10^{-3} mg/L (ppm)
Particle count, maximum	two particles larger than 1 μm per milliliter
Living organisms, maximum	one colony per 100 ml
Total organic carbon, maximum	200×10^{-3} mg/L (ppm)
Total solids, maximum	10×10^{-3} mg/L (ppm)
Sodium, maximum	2×10^{-3} mg/L (ppm)
Chloride, maximum	10×10^{-3} mg/L (ppm)

Table 2.8: Resistivity of DI Water as a Function of T.D.S.

Water Purity	Resistance at 25°C (MΩ-cm)	Approximate Equivalent of Extraneous Electrolytes (ppm)
Pure	0.1 or more	2 to 5
Very Pure	1.0 or more	0.2 to 0.5
Ultrapure	10 or more	0.01 to 0.02
Theoretical	18.3	0.00

A typical ultrapure water system is shown in Figure 2.56. As stated before, the heart of the system is the IX demineralizers. All other components of the system are present to make the IX more efficient or to alleviate problems created by the IX columns–such as particle generation.

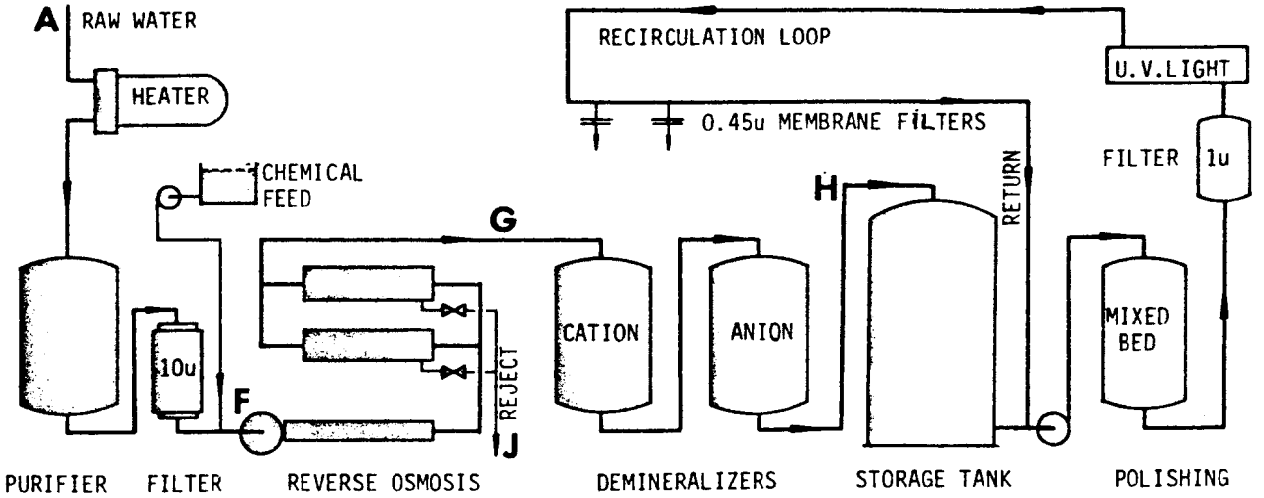


Figure 2.56: Flow schematic of typical ultrapure water system.

RO with its attendant pretreatment (to prevent membrane fouling and hydrolysis) precedes IX to reduce the ionic load on these columns. Although IX regeneration costs are directly proportional to the TDS, RO operating costs are nearly independent of TDS in the normal range of operation. As shown in Figure 2.57, the combination of RO + IX is often more cost effective at TDS values below 300 ppm. Indeed some economic analysis show cross-over values as low as 100 ppm.

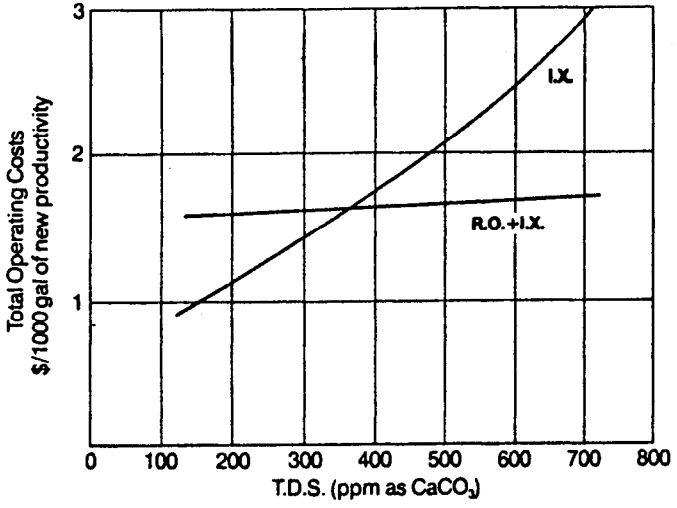


Figure 2.57: Total operating costs as a function of T.D.S. for ion exchange (I.X.) with and without reverse osmosis (RO).

In any event, most ultrapure water systems utilize RO to help prevent fouling of the IX columns (resulting in decreased exchange capacity). The foulants that most often plague cation resins are hydrous oxides of iron, manganese, copper, aluminum and magnesium, calcium sulfate, oil, grease, and suspended matter. Anion resin fouling is generally caused by colloidal silica and high-molecular-weight organic acids. RO can effectively remove many of these foulants inhibiting bacteria growth, and upgrading general system performance.

Since acid addition is normally used to prevent scaling in the RO unit and to prevent hydrolysis of cellulose acetate RO membranes, the reaction of the acid with bicarbonate in the feedwater produces carbon dioxide which can further deplete the ion exchange capacity. Forced-draft degasification removes the CO_2.

After passage through the cation and anion exchange columns (primary deionization), the water is typically placed in a storage tank which acts as a buffer during periods of peak usage. Since high resistivity water is very corrosive and will leach ions from tanks and piping, one of the fastest ways to degrade this water is to allow it to stand still for any length of time. Therefore, a continuously recirculating loop (see Figure 2.58) with a polishing mixed-bed deionizer is utilized by upgrade and maintain high quality 18 MΩcm water. Ultraviolet steriliza-

tion is used to kill up to 99.9% of the bacteria to keep the total population in the system within bounds. This reduces the load on the 0.2 micron MF cartridges.

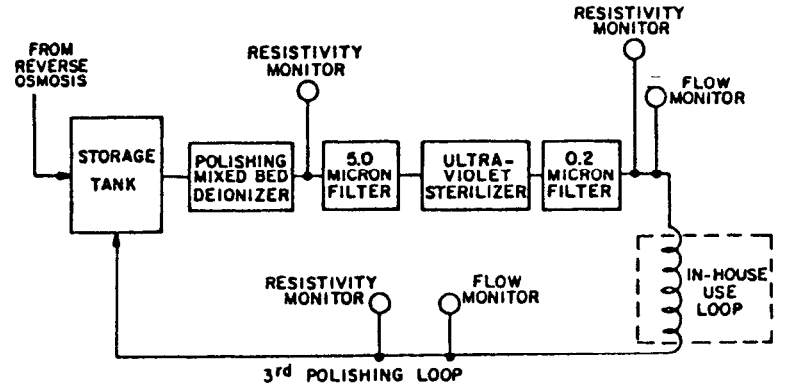


Figure 2.58: Flow schematic of recirculating polishing loop for D.I. water.

MF is used to remove bacteria and other particulates both in the recirculating loop and also at the point-of-use. Even though piping in the recirculating and distribution system is made of unpigmented polyvinylidene difluoride (PVDF), which does not leach like polyvinyl chloride (PVC) piping, particles can still build up on pipe walls and sluff off in time. UF has also been used in the recirculating loop as well as at the point-of-use. When it is utilized only in the recirculating loop, MF cartridges are still used for insurance at the point-of-use.

Selection of the optimum MF cartridge for this application must take into account conductivity rinse-down and particle sloughing as well as retention and throughput.

When first installed on a 18 MΩcm water line, all pleated cartridges degrade the water to a much lower resistivity. Even though the cartridges are prerinsed in ultrapure water by the manufacturer, after drying, initial exposure to ultrapure water results in further leaching of ions from the various components in the cartridge. Depending on the type of cartridge, the time for conductivity rinse-down or resistivity recovery of the filtrate can vary from as little as 2 minutes to as much as 60 minutes. The water filtered by MF is expensive; a fair amount has already been invested in pretreatment by RO, IX, etc. Therefore, the rinse-down time can have a significant economic impact on water treatment costs as well as plant down-time, particularly if cartridges must be replaced frequently.

In addition, particle sloughing can be a problem with some cartridges. Figure 2.49 shows the support screen which is downstream of the membrane. Even though rinsed in ultrapure water for long times, most support screens continue to slough submicron particles even after many gallons of throughput. Thus, the MF membrane may do an excellent job of removing particles while the support screen is continually generating other plastic particles in the filtrate.

Chemicals. Wet etchants and cleaners, photoresist developers, dielectric polymers, dopants and cleaning solvents are all a potential source of impurities

which may reduce semiconductor device yields. For example, the need for controlling contamination in photoresist and related photolithographic chemicals (e.g., adhesion promoters such as HMDS) is particularly critical in high density devices. Even though the photochemical manufacturers usually filter their products to 0.2 μ before packaging, degradation of the resists can take place due to autopolymerization-generating "gel slugs". In addition, insoluble particles generated from the photoresist pump at the point-of-use can recontaminate the material as it is being dispensed on the wafer. MF membranes or cartridges at the point-of-use ensure high production yields.

PTFE membranes or cartridges are ideally suited to aggressive chemical environments. Since these membranes are hydrophobic, they will not wet spontaneously with fluids having a surface tension greater than 32 dynes/cm. This includes aqueous solutions and even some organic solvents like ethylene glycol (44 dynes/cm). In these cases, the membrane must first be wetted with a miscible organic solvent such as isopropyl alcohol (27 dynes/cm). The aqueous solution may then be used to displace the wetting fluid and the pores will remain water wet. If there are air bubbles or entrained gases in the liquid, the membrane may need to be rewetted periodically.

Gases. Inert gases are used to dry silicon wafers. Even high purity gases can contain more than 1,000 particles per cubic foot. In addition, particles can be generated from moving parts in compressors, valves, and piping. Point-of-use membrane filtration and central process gas filtration are recommended to minimize the particle levels in the entire system.

Particle Removal (Nuclear Power Industry). There is a build up of corrosion products in the primary coolant loop of boiling water reactors (BWR's) which must be removed. These radioactive materials, primarily iron oxides (hematite, magnetite, etc.) with small amount of copper, nickel, aluminum and zinc, are referred to as "crud". Previously, precoat filters have been used to remove the crud. However, the precoat material including the RAD wastes represents a sizeable volume of material which must be stored and treated for final disposal. For this reason, nuclear power plants have looked at MF and UF for removal of the crud. Both through-flow and cross-flow systems have been investigated. One advantage of through-flow MF is that the RAD wastes are deposited on the filter which may be disposed of more conveniently. However, the replacement of cartridge filters is a major undertaking because of the radioactivity hazard. Therefore, high throughputs are important.

Several plate and frame MF units have been installed in Japanese nuclear power plants. The units operate with automatic periodic backwash using accumulated filtrate. Typically, the units backwash every 3 hours at a back pressure twice that of the final forward pressure. The backwashed crud is removed from the system as concentrated RAD wastes. In this sense, these back-wash systems are not dissimilar to cross-flow units using MF or UF-membranes. In either case, a reject stream containing concentrated crud must be disposed of.

Cross-Flow Filtration Applications

Removal of Heavy Metals. Federal, state and local regulations place strict limits on the quantities of heavy metals which may be released to the environment. The controlled metals include: Ag, As, Cd, Cr, Cu, Pb, Hg, Ni, Sb and Zn. U.S. electroplaters, metal finishers, and printed-circuit-board manufacturers are under mounting pressure to clean up their waste waters.

MF may be used to remove these heavy metals provided pretreatment chemicals are added to precipitate the metals to particles of filterable size. The chemical pretreatment step is crucial since it will affect the performance of the membrane and the resultant sludge volume as well as the contaminant removal efficiency. Reduction/oxidation, absorption/oxidation, and/or catalytic reactions are utilized along with pH adjustment to provide the optimum precipitation. Although conventional methods of waste water treatment may use a similar pretreatment chemistry, the final solid/liquid separation by gravity settling is usually not as effective as membrane filtration.

Typically, the cross-flow membrane modules (usually tubular) concentrate the slurry to 2–10% solids. Further concentration to 20% solids is accomplished by gravity settling, and if need be, a filter press can produce a dry (30 to 50% solids) cake for disposal. To enhance settling, polymers or electrolytes are introduced to flocculate and/or coagulate the colloidal suspended solids. The polymers and/or electrolytes neutralize the electrostatic surface charges which repel particles of like charge preventing coagulation.

Figure 2.59[27] is a typical flow sheet for treating spent process water from printed circuit board manufacturing. Usually, MF membranes are preferred over UF because of the higher flux. However, the MF membranes are more prone to flux decay as discussed earlier. Therefore, periodic cleaning or backflush is necessary to maintain the flux at a high level. Note the cleaning tank in Figure 2.59.

If the metals are of high value, the metal precipitate may be redissolved in concentrated acid to recover the metals in solution.[28,29]

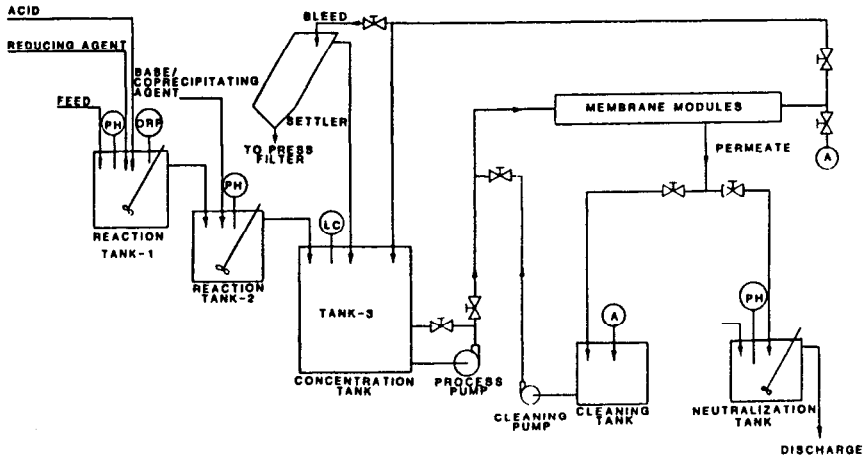


Figure 2.59: Flow schematic of wastewater CFF to remove precipitated heavy metals by MF.

Industrial Laundry Wastewater. The laundry industry is a major generator of wastewater. In the United States, industrial laundries alone account for over 10 billion gallons (38 million M^3) of wastewater annually. Wastewater from all laundry sources accounts for approximately 10% of municipal sewer discharges. In addition to high suspended solids and BOD loading, the levels of oil and grease, heavy metals and other organics exceed municipal discharge standards.

Until recently, the standard method for treatment of these wastes consisted of lime coagulation and flocculation with clarification by dissolved air flotation. Subsequently, the underflow is polished with sand or diatomaceous earth filtration. Finally, the sludge is dewatered by vacuum filtration. The effluent quality is variable and does not always meet discharge standards.

Pilot studies in 1982 have led to the installation of cross-flow MF in some industrial laundries. Both chemical conditioning and the addition of adsorbing and/or absorbing agents are necessary to render the contaminants filterable. The permeate may be recycled into the plant. Table 2.9[27] shows the nature of the raw wastewater and the effluent from the membrane system.

Table 2.9: Cross-Flow MF of Industrial Laundry Water

Assays	Raw Wastewater (mg/L)	Recycling Criteria (mg/L)	Memtek Effluent (mg/L)
BOD	1,300	30	<30
COD	5,000	100	<100
O&G	1,100	10	<10
Suspended Solids	1,000	none	none
Pb	4.5	0.1	<0.1
Zn	3.0	0.1	<0.1
Cu	1.7	0.1	<0.1
Cr	0.9	0.1	<0.1
Ni	0.3	0.1	<0.1
Fe	40	0.1	<0.1
Chloroform	3.3	0.1	<0.1
Benzene	2.5	0.1	ND*
Perchlor-ethylene	9.1	0.1	ND
Toluene	5.2	0.1	ND
pH		6–9	6–9

* Nondetectable.

Plasmapheresis. The separation of plasma from whole blood by continuous membrane filtration represents an improvement over conventional centrifugation techniques in terms of efficiency, safety and cost. In the past, plasmapheresis was carried out with blood donors by collecting their whole blood in plastic bags which were then centrifuged to separate the red cells from the plasma. The supernatant plasma was then decanted and the red cells returned to the donor-enabling plasma to be drawn from the same person as frequently as three times per week. Most of this plasma is then processed to yield purified components such as albumin or anti-hemophilic factor (Factor VIII).

Continuous flow plasmapheresis is a superior alternative. Whole blood is continuously withdrawn from the donor and red cells are returned while plasma is continuously removed. There are two major advantages:

(1) There is less chance of a mixup, since the donor's red cells are not removed in bags for remote processing prior to reinfusion.

(2) The time required for collection can be reduced considerably.

Continuous flow centrifuges are now available with disposable rotating bowls. However, these devices are expensive and quite complex, requiring the attendance of skilled personnel during operation. Cross-flow filtration (CFF) is potentially a less expensive and simpler separation tool for continuous plasmapheresis. Large scale plasmapheresis of animal blood is also facilitated by CFF.

The early attempts at membrane filtration of blood were disappointing. Stirred-cells were used to reduce the accumulation of blood cells on the membrane, but the stirring hemolyzed the red cells and the flux was low even at high stirring rates.

In the late sixties, Blatt and co-workers at Amicon developed a thin-channel cross-flow device for plasmapheresis.[30] In this device, red cells and plasma could be readily separated with a 0.6 μ MF membrane at an acceptable flux. As shown in Figure 2.60, the flux increases with the cross flow velocity. However, there is a limiting velocity above which the degree of hemolysis is unacceptable. We discovered that pore sizes above 0.8 μ occasionally leaked nonhemolyzed red cells while pore sizes below 0.2 μ retained some of the higher molecular weight plasma proteins (notably albumin and I_gG). Therefore, pore sizes between 0.4 and 0.6 μ were selected with 0.6 μ preferred because of higher plasma fluxes.

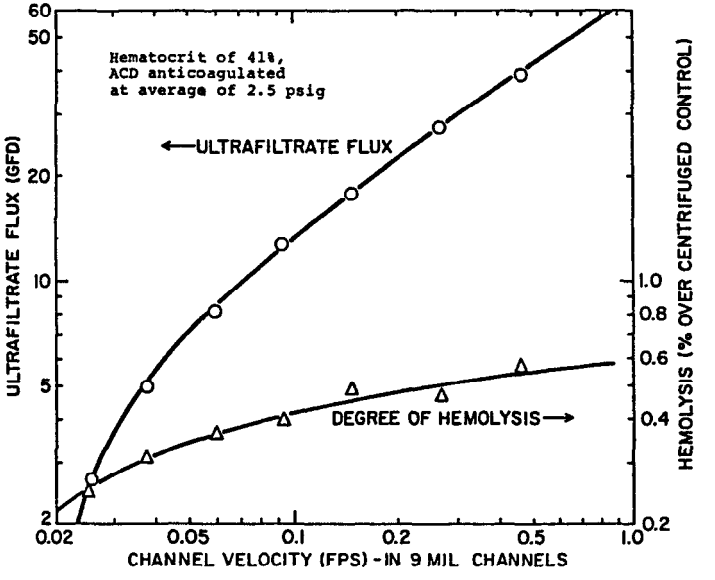


Figure 2.60: Plasmapheresis membrane flux and hemolysis as a function of cross-flow velocity.

Later, work at Amicon for the Red Cross[31] determined that for each cross-flow velocity (fluid shear rate) there is a critical transmembrane pressure above which significant hemolysis occurs. Apparently, the compaction of red cells on the membrane at higher pressures results in lysis of the cells. (For a more complete description of polarization effects on the membrane, see chapter 3 on Ultrafiltration.) Membranes having smaller pore sizes could be operated at higher transmembrane pressures before hemolysis was observed–suggesting that the red cells are lysed through distortion into the pores. In addition, it was discovered[32] that significant flux decay occurred not only with whole blood but with cell-free plasma. Since individual protein molecules should pass through 0.4 and 0.6 μ pores, plugging by lipoproteins or protein aggregates is suggested.

Plasmapheresis is currently used not only in the collection of plasma by blood banks but also therapeutically. Plasma exchange therapy (PET), removes harmful components in a patient's plasma by returning his cellular components with either replacement or purified plasma. In most instances, the offending substance is an antibody whose activity is directed against the patient's own tissues, or the product of an antigen-antibody reaction, which accumulates to produce so-called "immune-complex disease". The most striking success of this modern form of "blood-letting" has been in the treatment of autoimmune diseases such as Good pasture's syndrome and myasthenia gravis. Clinical improvement has also been reported with patients suffering from disseminated breast cancer, hepatic coma, and a host of other diseases and immunological/metabolic disorders. The technique has also been used to detoxify patients from drug overdoses or poisons.

Sometimes it is preferable to purify the patient's own plasma rather than to replace it. This is accomplished by treating the plasma filtrate with sorbents or further filtration. This avoids damage to the cellular components. In the metabolic disease states, the abnormal solutes are generally of low molecular weight and/or protein bound. Anion exchange resins have been used to remove bilirubin and bile acids. Charcoal sorbents have been used to remove aromatic amino acids, free fatty acids, and bile acids. In other disease states, the offending substance may also be precipitated out of the serum at reduced temperatures (4°C). For example, rheumatoid arthritis has been treated successfully by cooling the plasma to precipitate and filter out these so-called "cryoprecipitates" before returning the plasma to the patient.

Though most of the applications for plasmapheresis are medically related, some of the larger pharmaceutical houses are beginning to process pooled animal blood in a similar way but on a larger scale. The cellular components and the plasma are then processed separately to obtain the desired final products.

Cell Harvesting/Washing. In recent years, the use or microorganism-based fermentations for the production of chemical products has greatly expanded. Interferon, insulin, novel antibiotics, cytotoxic antitumor agents, numerous enzymes, fine chemicals, and even fuels have been produced in carefully controlled fermentations. A key step in the fermentation cycle is the separation of the cells or cellular debris from the liquid phase of the fermentation broth–commonly called "cell harvesting".

The products of the fermentation may be either extracellular or intracellular. In the case of extracellular products, the product must be isolated from the cells and other soluble components of the broth/growth medium. With intracellu-

lar products, the cells must first be concentrated and then ruptured (lysed) to free the products. Subsequently, the cell debris must be separated from the soluble products.

Traditionally, the cellular biomass is separated by centrifugation. Ammonium sulfate is then added to the supernatant to precipitate the protein product from the media. This is followed by further centrifugation and dialysis to remove the residual ammonium sulfate from the protein product. Cross-flow filtration (CFF) can replace all of these steps with a significant improvement in recovery and yield. Indeed, CFF appears to offer many advantages over conventional separation processes like centrifugation, vacuum filtration and precipitation/dialysis for this application.

Continuous flow or batch centrifugation separates the cells according to their density difference, but the resultant supernatants are often turbid, even when processed at slow rates with relatively high *g*-forces. Up to 25% of the cells are lost in the supernatant. CFF can usually recover more than 99% of the cells from the broth even when the cell density is the same as that of the broth; clear supernatants (filtrates) are obtained. The generation of potentially harmful aerosols in centrifugation (when harvesting pathogenic organisms) is virtually eliminated with CFF due to operation in a closed system with vented tanks. Batch sizes are unlimited with CFF whereas the rotor or bowl capacity of a centrifuge limits the volume which can be processed at one time. Further, CFF offers the versatility of cell washing in a single continual process known as "diafiltration" (see chapter 3 on Ultrafiltration); new buffer or solvent may be added as filtrate is removed. Cell washing with centrifugation requires repetitive steps of pelleting and resuspension.

Likewise, CFF is not plagued with losses by adsorption on rotary drum vacuum filters (up to 15%) or by phase changes in precipitation. Further, the addition and removal of precipitants is not necessary with CFF, thereby avoiding potential contamination of the product.

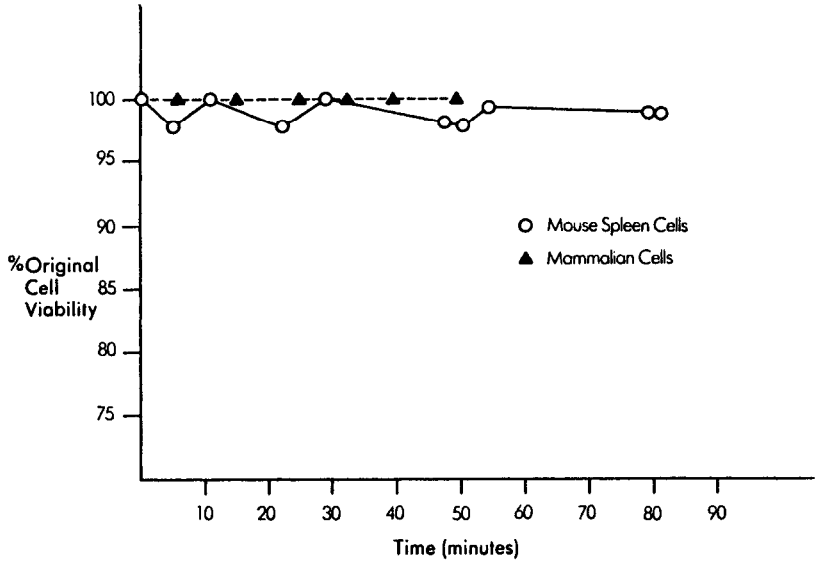
There is some concern that the fluid shear forces present in CFF could damage fragile cells. However, viable cell recovery has in general been higher than with centrifugation. Figure 2.61 shows data on cell viability as a function of time while recirculating through an open-channel plate and frame CFF system.[33] Mammalian cells, like those used in these experiments, are particularly fragile and shear sensitive. Viable cell recovery was over 95% for both mouse spleen and mammalian cells after concentrating 6 fold from an initial concentration of 10^6 cells/ml.

Of the various CFF modules available, plate and frame devices which utilize screen spacers between membranes are prone to accumulation of cells on the cross-members of the screen resulting in flow blockage. "Flow-channel spacers" like those shown in Figure 2.47 are less prone to fouling.

Hollow fiber membrane modules have minimum hold-up volumes and can operate without blockage of the fibers if the I.d. of the fiber is substantially larger than the maximum cell aggregate. Until recently, hollow fiber modules were only available with UF membranes. The advent of polysulfone MF hollow fibers makes possible cleaning with acid and base and even autoclaving at 121° in some instances. Since MF membranes are prone to internal pore fouling, membrane cleanability with flux recovery is particularly important.

In some cases, cell harvesting can be accomplished more efficiently with

asymmetric UF membranes which are not as susceptible to internal pore fouling as the symmetrical structure of MF membranes. However, when the *products* of the fermentation are retained along with the *cells* by the UF membrane, MF is the only choice.



Initial cell density: 0.5-1.5x10⁶ cells/ml; flux: 80-100 liters/m²/hr; concentration: 6-fold; viable cell recovery: 95-100%.

Figure 2.61: Harvested cell viability during CFF in open-channel plate and frame system.

Figure 2.62 shows flux data for the recovery of hemoglobin from the stroma (lysed red cells) using a 0.2 μ pore size MF membrane. Here, the intracellular product is hemoglobin having a molecular weight of 64,000. Theoretically, a 1,000,000 molecular weight cut-off (MWCO) UF membrane (pore size of 0.08 μ) should be able to make this separation. However, in this case, pores below 0.1 μ showed an unacceptable retention for hemoglobin presumably because of trace amounts of gamma globulins (>160,000 daltons) from the plasma which form a retentive dynamic membrane on the surface of the UF membrane (see chapter 3-Ultrafiltration-on the formation of gel layers). However, if the red cells are washed free of all plasma proteins (using cross-flow MF) before lysing, UF may be used for the final separation of stroma from hemoglobin. Indeed, even a 300,000 MWCO UF membrane was able to pass the hemoglobin with no significant retention.

Figure 2.40, presented earlier, is an example of concentration of whole yeast cells. Though the concentration of cells at the end of the run was only 10%, the data imply that cells may be concentrated up to the close packed sphere density of 75 volume percent. Indeed, yeast, and *E. coli* concentrations of 60% and 37% respectively have been harvested.

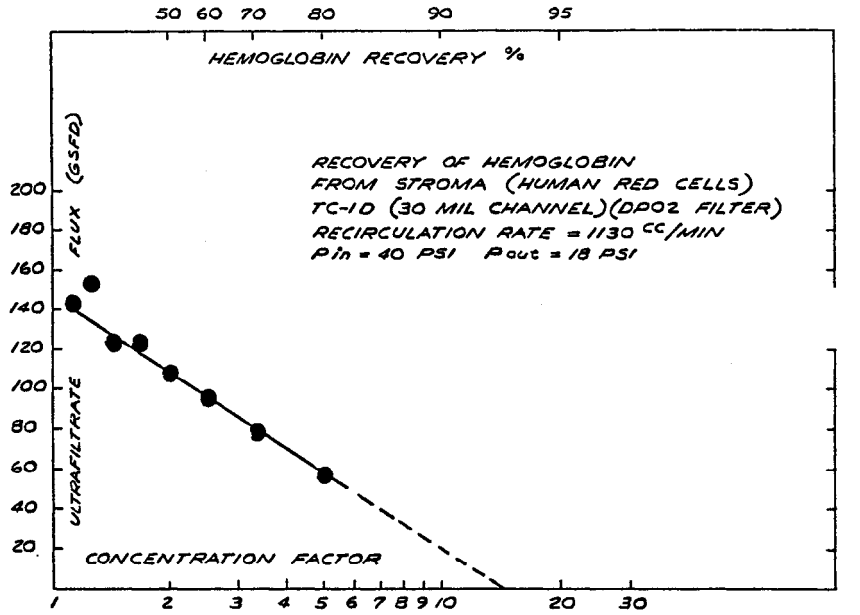


Figure 2.62: Recovery of hemoglobin from stroma using 0.2 micron MF in cross-flow.

The ability to concentrate yeast to high levels with CFF makes possible the recovery of beer from tank sediment (the so-called "geläger"), which is about 6 to 12% dry solids. In some countries, the tax on beer lost in this sediment is not refunded, so there is considerable economic incentive for recovery. Conventional processes, including yeast-presses, precoated vacuum filters and centrifuges, are not able to recover beer of good quality from this residue. Tubular MF is recommended for this application since UF membranes retain some of the proteins and other flavor components in the beer along with the yeast.

Continuous Cell Culture. The continuous separation of cells from the products of fermentation by membranes opens up the possibility of a "continuous membrane fermentor" (see Figure 2.63). This concept has been explored both for MF and UF membranes and will be discussed more thoroughly in chapter 3 on Ultrafiltration. Suffice it to say that the continuous removal of growth-inhibiting metabolites from a cell culture along with the products of the fermentation can lead to significant increases in cell densities and product yield. In some cases, the products of the fermentation may be larger than the pores of a UF membrane necessitating the use of cross-flow MF.

Prefiltration for UF. In most cases, MF is too expensive for use as a prefilter. However, there are some feed streams which severely foul UF membranes and where prefiltration with cross-flow MF is cost effective. For example, in the UF of milk or cheese whey; fat, casein fines, coagulated protein, and microorganisms all cause severe membrane fouling. In the concentration of milk, the use of tubular MF as a prefilter increased the UF flux by 100% on the average. CFF is required because TFF (through-flow filtration) would plug the MF membrane immediately.

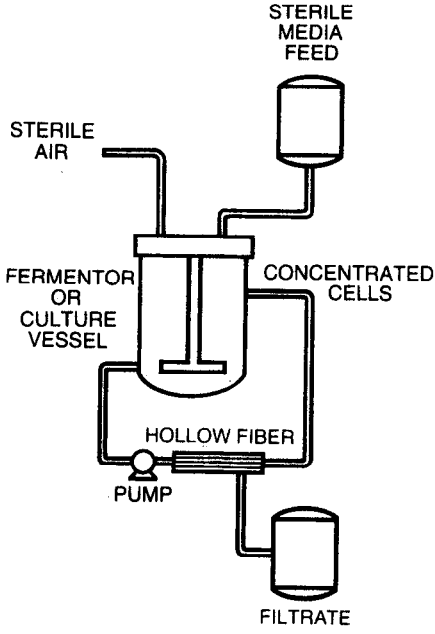


Figure 2.63: Flow schematic of continuous membrane fermentor.

Membrane Distillation. In evaporating solutions, heat consumption is reduced by using an increased number of effects or stages, each of which must normally be at a different pressure from the others. However, if evaporation-condensation is reduced to the essentials only, as in "flash" evaporation, the only requirement is solution, vapor, and condensate separated and at suitable temperatures.

These requirements can be met by a porous hydrophobic membrane which excludes liquid from the pores but not vapors. For example, seawater may be separated from its distillate by a PTFE (polytetrafluorethylene) or a PP (polypropylene) MF membrane. If a temperature difference is maintained across the membrane, with the vapor pressure of the seawater higher than that of the distillate, evaporation will occur at the seawater side of the membrane and vapors will flow through the pores to the cooler surface, where they will condense (see Figure 2.64).[34] The difference in vapor pressures provides the pressure driving force.

The process is, in effect, a multieffect evaporation process with liquid flowing from pore to pore (or "stage to stage") but with the following advantages. The liquids involved can be at any convenient pressure higher than the vapor pressure and less than the membrane water intrusion pressure. Since there is complete separation between the seawater and the distillate, there is no entrainment and high purity distillate is produced. Scaling will be unlikely against a nonwettable surface. The warm seawater is fed countercurrent to the distillate through a membrane module designed to permit only small temperature differences across the membrane (see Figure 2.65).[34] By using a heat exchanger be-

tween the distillate and the seawater, part of the evaporation heat can be recovered. This recovered heat can be 80% or more if low temperature differences are maintained and lower fluxes are acceptable.

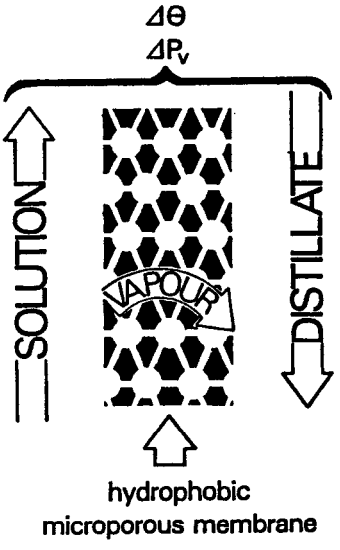


Figure 2.64: Trans membrane distillation with hydrophobic MF membrane.

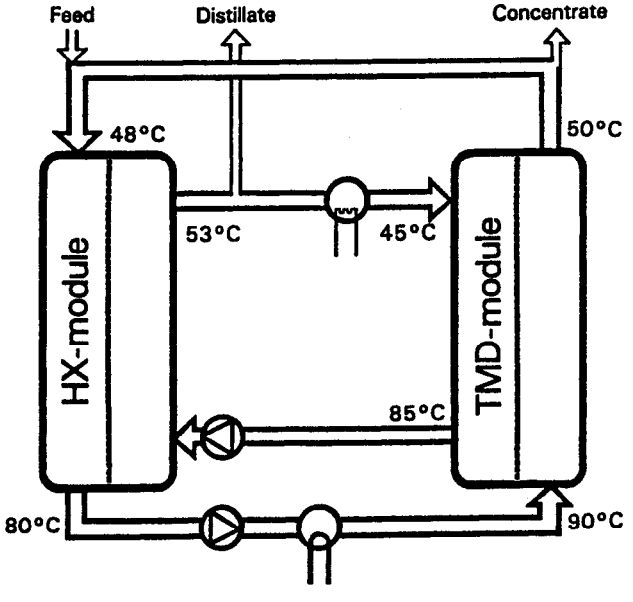


Figure 2.65: Flow schematic of trans membrane distillation (TMD) with heat exchanger (HX) for recovery of heat of evaporation.

Hollow fibers and spiral wound modules have been constructed for this application. A module 18 inches in diameter and 5 feet long can produce up to 1,500 GPD. Plants now exist in the Florida Keys, the Bahamas, and the Cayman Islands ranging in size from 10,000 to 60,000 GPD. They have the highest capacity per unit volume for evaporation plants now in existence. It is claimed that these plants are more cost effective than multiple-effect evaporators, but in the author's view, it is doubtful they can compete with reverse osmosis.

SUMMARY AND FORECAST

Cross-flow microfiltration (CFMF) is expected to grow rapidly during the next decade and beyond. The emerging biotechnology market promises new and unusual applications for CFMF. Recovery of dispersed catalyst particles by CFMF is now under investigation by the chemical process industry. In addition, facilitated/active transport can be carried out through liquid membranes retained in the pores of an MF membrane by capillarity (see chapter 9-Coupled Transport Membranes). These "supported liquid membranes" are currently being investigated for gas and metal ion separations.

MF as a whole is expected to grow at an average annual increase of over 10% during the next decade to a total market of over 1.5 billion dollars.

REFERENCES

1. Grandine, J.D., U.S. Patent 4,203,848 (May 20, 1980).
2. Gore, R.W., U.S. Patent 3,962,153 (June 8, 1976).
3. Kesting, R.E., *Synthetic Polymeric Membranes*, McGraw-Hill, NY, 1971 pp. 104-112.
4. Price, P.B. and Walker, R.M., U.S. Patent 3,303,085 (Feb. 7, 1967).
5. Jaech, J.L., Vol. 9, No. 2, May 1967, pp. 319-324.
6. Porter, M.C., "Pore Coincidence through the Film", Nuclepore internal memo 7/28/76.
7. ASTM, *Maximum Pore Diameter and Permeability of Rigid Porous Filters for Laboratory Use*, ANSI/ASTM E 128-61 (Reapproved 1976) Replaced E 128-57T.
8. ASTM, *Pore Size Characteristics of Membrane Filters for Use with Aerospace Fluids*, ANSI/ASTM F316-70 (Reapproved 1976) Replaced D 2499-69.
9. ASTM, *Evaluation of Air Assay Media by the Monodisperse DOP Smoke Test*, ASTM D 2986-71.
10. Wallhausser, K.H., *Pharm. Ind.*, Vol. 36, No. 12, 1974, pp. 931-942; Vol. 37, No. 1, 1975, pp. 10-17.
11. Wallhausser, K.H., *Pharm. Ind.*, Vol. 38, No. 2A, 1976, pp. 107-112.
12. Howard, G., Jr. and Duberstein, R., *J. of Parenteral Drug Assoc.*, Vol. 34, No. 2, March-April, 1980, pp. 95-102.
13. Chien, S., Usami, S., Dellenback, R.J. and Bryant, C.A., *Biorheology*, Vol. 8, 1971, pp. 35-57.

14. Lukaszewicz, R.C., Tanny, G.B. and Meltzer, T.H., *Pharm. Tech.*, Nov. 1978, pp. 77-83.
15. Davis, M.A., Jones, A.G. and Trindade, H., *J. Nucl. Med.*, Vol. 15, No. 11, Nov. 1974, pp. 923-928.
16. Hahn, R.G., Hatlen, J.B. and Kenny, G.E., *Appl. Microbiology*, Vol. 19, No. 2, Feb. 1970, pp. 317-320.
17. Cuno Microfiltration Products, *Zetapor Membrane* product literature 9-15-83.
18. Pall Corp., *The Pall N_{66} Posidyne Membrane Filter Guide* product literature 1982.
19. Tolliver, D.L. and Schroeder, H.G., *Microcontamination*, June/July 1983.
20. Spurny, K.R., Lodge, J.P., Jr., Frank, E.R. and Sheesley, D.C., *Environ. Sci. Technol.*, Vol. 3, No. 5, May 1969, pp. 453-464.
21. Cahill, T.A., Ashbaugh, L.L., Barone, J.B., Eldred, R.A., Feeney, P.J., Flocchini, R.J., Goodort, Shadoan, D.J. and Wolfe, G.W., *APCA Journal*, Vol. 27, No. 7, July 1977, pp. 675-678.
22. Henry, J.D., Jr., *Recent Developments in Separation Science*, Vol. 2, ed. N. N. Li, CRC Press, 1972, pp. 205-225.
23. Porter, M.C. and Olson, P., U.S. Patent 4,178,248, Dec. 11, 1979.
24. Gelman Sciences, *Acroflux Cartridges*, product literature, July 1980.
25. Federal Register, Section 212.68, 212.72 and 212.116 Filtration, June 1, 1976.
26. Couture, S.D. and Capaccio, R.S., *Microcontamination*, April/May 1984, p. 45 ff.
27. Tran, Tam V., *Chem. Eng. Process.*, March 1985, pp. 29 ff.
28. Porter, M.C., Schratter, P. and Rigopulos, P.N., *Ind. Water Eng.*, 8, June/July 1971, pp. 18-24.
29. Christensen, E.R. and Delwiche, J.T., *Water Res.*, Vol. 16, 1982, pp. 729-737.
30. Blatt, W.F., Agranat, W.A. and Rigopulus, P.N., U.S. Patent 3,705,100, Dec. 5, 1982.
31. Lysaght, M.J., Colton, C.K., Castino, F. and Friedman, L.T., "The Use of Microporous Membranes to Separate Plasma from Whole Blood", 4th Annual Meeting of European Society for Artificial Organs, London, England, Nov. 28-30, 1977.
32. Lysaght, M.J., Colton, C.K., Friedman, L.I. and Castino, F., "Investigation of Factors Controlling the Rate of Plasma Filtration with Microporous Membranes", A. I. Ch. E. 83rd Nat. Meeting, Houston, Texas, March 20-24, 1977.
33. Millipore Corp., *Get the Most Out of Cell Processing*, product literature No. SD 203, Sept. 1985.
34. Enka/Membrana, *Trans Membrane Distillation*, product literature, 1984.

3

Ultrafiltration

Mark C. Porter

INTRODUCTION

The beginnings of ultrafiltration (UF) are coincident with that of reverse osmosis (RO) around 1960. Despite the fact that the term "ultrafiltration" first appeared in the colloid literature toward the end of the last century and Bechhold, in 1906 produced collodion membranes with pore sizes below 0.01 micron, these membranes were little more than laboratory curiosities. The hydraulic permeability was low and the pores were easily plugged.

The breakthrough, which resulted in an anisotropic RO membrane in 1959, paved the way for the first anisotropic UF membrane in 1963. Though UF membranes are porous and RO membranes are not, the evolutionary development of both occurred in parallel. Before 1960, membranes showing the retention properties of RO and of UF were available, but both had impractical filtration rates (flux).

In the years immediately following the end of World War II, the United States Government became concerned about shortages in water before the end of the century. The U.S. Department of the Interior set up the Office of Saline Water (OSW) and committed substantial financial resources to the development of various separation processes for water desalination. A significant portion of these funds was dedicated to the development of membranes for desalination-with funded programs continuing for over two decades (1950-1973). The result was one of the most promising large-scale processes for inexpensive desalination of seawater and brackish water-reverse osmosis (RO). It is no coincidence that the United States is a world leader, not only in RO, but also in those technologies that are direct spin-offs-namely UF and gas separations.

The first work in RO toward water-desalting was undertaken by Prof. Charles E. Reid[1] at the University of Florida in the mid-1950's. He discovered that cellulose acetate (CA) is semipermeable to seawater electrolytes.[2] The diffi-

culty was that the water fluxes were too low to be interesting. Reid and coworkers attempted to cast thinner films, but found that below 6 μ in thickness, the films had defects which passed salt and were too fragile to handle.

Similtaneously, and unbeknownst to Reid, Sourirajan at the University of California, Los Angeles (UCLA) obtained the same results-94% salt rejection-but with water fluxes even lower than those reported by Reid.

Sourirajan's partner, Sidney Loeb, began to experiment with laboratory UF membranes (not fully asymmetric) made by Schleicher and Schuell of cellulose acetate (CA). Loeb heated the membranes under water (annealing) to temperatures between 80° to 90°C, thereby increasing the salt rejection from 0 to 92%, but the water flux decreased to unacceptable levels.

Loeb uncovered the work of a French investigator, Dobry[3] in a literature search. Her work provided the clue which Loeb was looking for. Dobry dissolved acetylated CA in an aqueous solution of magnesium perchlorate, $Mg(ClO_4)_2$. This casting dope was spread as a thin film on a glass plate which was then plunged under water. The CA precipitated around the $Mg(ClO_4)_2$ leaving a porous film of CA. Eventually the $Mg(ClO_4)_2$ diffused out of the pores into the water bath. Loeb repeated Dobry's recipe, but the membranes were too porous and had no rejection for salt. He attempted to increase the ratio of CA to $Mg(ClO_4)_2$ but the casting solution viscosity was too high. The solution to the problem, suggested by Lloyd Graham, a UCLA graduate student, was to partially replace the aqueous $Mg(ClO_4)_2$ solution with acetone, a solvent for CA.

Loeb's standard casting solution contained CA, acetone, water, and $Mg(ClO_4)_2$ in the weight percentages of 22.2, 66.7, 10.0 and 1.1.[4] When immersed in ice water, a high flux membrane was obtained albeit with low salt rejection (typically 5% or less). Loeb then annealed these membranes to 80°C to yield a salt rejection of 99%. The significant breakthrough was that the annealed membrane water-flux was 200 times greater than Sourirajan's CA films and 5 times greater than the annealed S & S membrane.

The reason for this breakthrough resided in the asymmetric structure of the membrane. When the product of the water flux and the total membrane thickness was calculated, the value was 666 times greater than Sourirajan's CA films. The most obvious explanation was that the *effective* membrane thickness was much less than the *total* membrane thickness. Loeb postulated the existence of a dense skin less than 1 μ in thickness supported by a relatively porous substrate. Thus, the substrate provided mechanical strength and the thin skin minimized the resistance to hydraulic permeability through the membrane. For the first time in history, it became possible to remove salt from water (95 to 98%) at pressures of 50 to 75 atmospheres with flux values of 10 to 15 gallons of product water per day per square foot of membrane area (GSFD).

In the early 1960's, the techniques utilized in the fabrication of asymmetric RO membranes were discovered to be applicable to the production of high-flux UF membranes with pores in the range of 10 to 1000 Å (see Figure P.1 in the Preface). Suddenly, UF on an industrial scale became practical. Macromolecular separation could be carried out at modest pressures (less than 6 atm.) with astonishingly high filtration rates.

Prof. Alan S. Michaels, of the Massachusetts Institute of Technology and the founder of Amicon Corporation, cast UF membranes from polyelectrolyte complex hydrogels in 1963. A joint development program between Amicon and

Dorr-Oliver began to search for other polymers suitable for casting asymmetric UF membranes. By 1965, the first laboratory-scale UF membranes and cells appeared on the market. The ten-year period between 1965 and 1975 was a period of intense development where chemically and thermally resistant membranes were made from polymers like polysulfone (PS) and even polyvinylidene difluoride (PVDF) in molecular weight cut-offs (MWCO) from 500 to 1,000,000. Hollow fibers were also developed during this decade and a whole host of module configurations. Tubes, plate and frame units, and spiral-wound modules became available.

MEMBRANE STRUCTURE AND FABRICATION

Figure 3.1 is a cross section of a typical asymmetric (anisotropic) UF membrane. The prominent feature of these membranes is the thin skin on the surface–usually 0.1 to 1 μ in thickness. This thin skin permits high hydraulic permeability while the more open/porous substructure (typically 125 μ in thickness) provides good mechanical support. In addition, the pore configuration virtually eliminates internal pore-fouling. Since the minimum pore size is at the membrane surface, once a solute molecule gains entrance into the pore, it easily passes through to the other side of the membrane. The solute molecule sees an ever-widening pore channel with no restrictions or bottlenecks leading to entrapment.

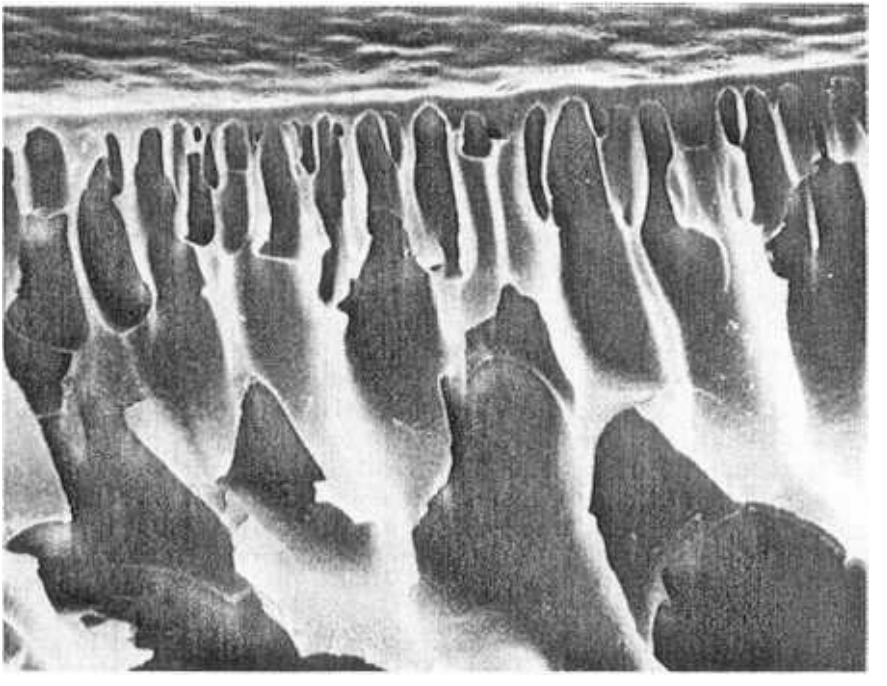


Figure 3.1: Cross-section photomicrograph of asymmetric UF membrane.

Additional strength is sometimes provided by casting the membrane on a spun-bonded polyethylene or polypropylene backing (see Figure 3.2).

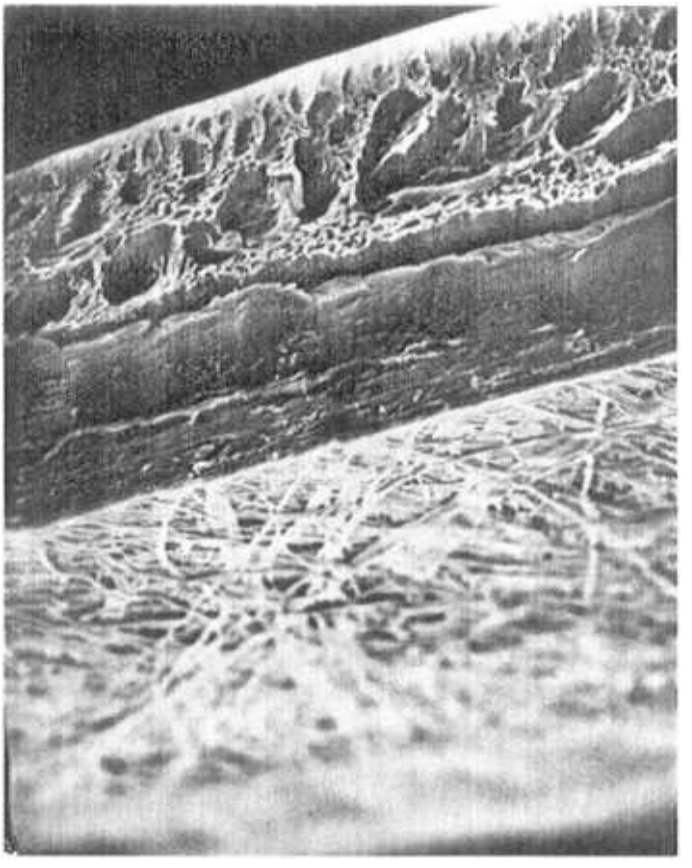


Figure 3.2: Cross-section of UF membrane cast on spun-bonded polyethylene backing.

As mentioned earlier, the procedure used by Loeb and Sourirajan to make RO membranes from CA produces a very tight UF membrane (only 5% NaCl rejection) prior to annealing. In fact, the line of demarcation between UF and RO usually refers to the tightest UF membranes as those able to pass salts but retain the simple sugars. Cellulose acetate and polyelectrolytes were among the first synthetic polymers to be used for UF membranes. Today, UF membranes are made from a wide variety of chemically and thermally stable synthetic polymers including polyvinyl chloride (PVC), polyacrylonitrile (PAN), polycarbonate (PC), aliphatic, and aromatic polyamides (PA), polyimides (PI), polysulfone (PS), polyarylsulfone (PAS), and polyvinylidene difluoride (PVDF). In addition, there are inorganic UF membranes made from zirconium and aluminum oxides.

With the exception of the inorganic membranes, all of the above are solution cast or spun from a polymer solution. For the more chemically resistant polymers like PS, PAS and PVDF, solvents like dimethylformamide (DMF), dimethylsulfoxide (DMSO), or dimethylacetamide (DMAc) are required.

Procedure for Casting Flat-Sheet Membranes

In general, the procedure for casting anisotropic UF membranes can be thought of as a six-step process:

(1) *Preparation* of the casting solution [dissolving the polymer in an appropriate solvent(s) with or without various additives].

(2) *Metering* the casting solution onto a casting belt, a rotating drum, or a reinforcing web/fabric.

(3) *Immersing* the freshly cast film into a nonsolvent liquid bath (normally water) until all of the polymer has precipitated/solidified and most of the solvent has left the film.

(4) *Leaching* remaining solvent out of the film.

(5) *Applying* surfactants, wetting agents, or plasticizers (for drying) as needed.

(6) *Drying* (optional) at appropriate temperature/humidity.

Step number 3 in the above sequence is responsible for the formation of an anisotropic membrane. In Chapter 1, Strathmann describes the difference between a vapor-phase precipitation process (Figure 1.22) as used in MF membrane formation and the liquid-phase precipitation process (Figure 1.23) used in UF membrane formation. In the former case, the rate limiting step is the slow diffusion of precipitant (e.g., water vapor) from the vapor phase to the polymer solution. Since this is a relatively slow process, precipitation of polymer is also slow resulting in fairly large pores in the membrane. In the latter case, described here, bringing liquid water in contact with the polymer solution results in catastrophic precipitation under supersaturated conditions.

In an earlier paper,[5] Strathmann uses the analogy of crystallization from supersaturated solutions. With increasing supersaturation, the rate of precipitation is higher, the critical nucleus size decreases and the individual crystals are smaller (more finely dispersed). Likewise here, at the outer surface of the casting solution, in contact with liquid water, the degree of supersaturation is extremely high and the density of nuclei is high resulting in a finely dispersed structure which corresponds to the final membrane skin. Once the skin is formed, it becomes a barrier to further diffusion of water into the bulk of the casting solution. Thus, the degree of supersaturation is significantly lowered and the precipitate becomes increasingly coarse. Consequently, the pore size increases as we move from the skin into the substructure (see Figure 3.3).

Figure 3.4[6] is a schematic of a "drum casting machine" which carries out steps 2-4 in the above procedure. For small batches, the casting solution can be made up the night before the run and put on a roll mill in sealed glass jars which are heated by infra-red lamps. The solution must then stand until all air bubbles are eliminated. If there is appreciable solvent-loss with time, the solution trough shown in Figure 3.4 should be closed.

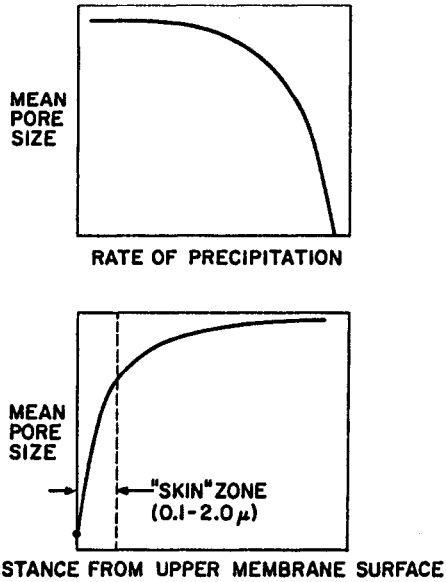


Figure 3.3: Scale of heterogeneity in cast membranes-variation in pore size with rate of precipitation and distance into membrane.

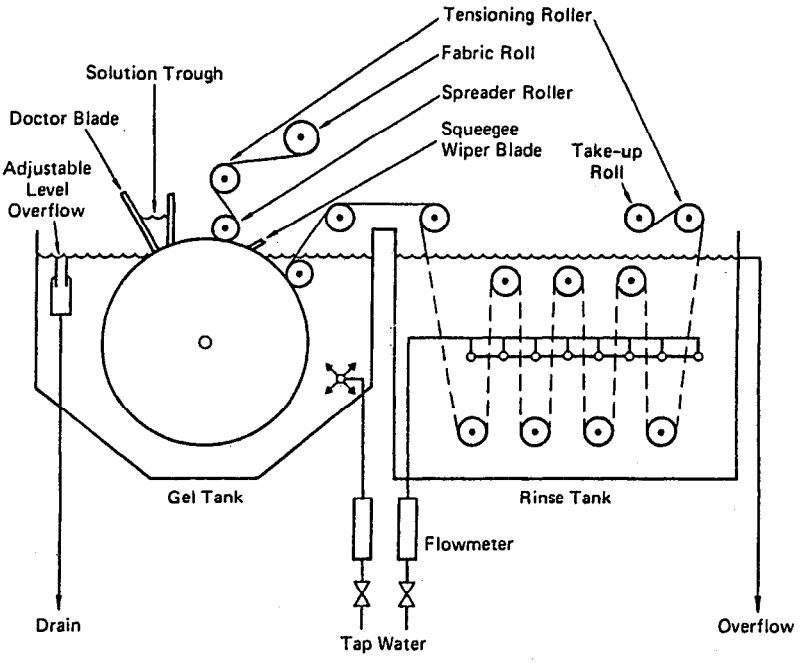


Figure 3.4: Schematic of drum casting machine.

The doctor blade on the solution trough is adjusted so as to meter a coating thickness on the drum or fabric between 100 and 500 μ in thickness. If the viscosity of the casting solution is such that it rapidly penetrates into the fabric, a greater thickness is required. Considerable attention must be given to obtaining the proper match between a reinforcing fabric and the viscosity of the casting solution. If there is too little penetration into the fabric, the bond between the membrane and the backing will be weak, resulting in membrane delamination. On the other hand, too much penetration will result in a considerable resistance to flow in the backing material, which is often thicker than the membrane itself.

It will be noted that the cast film is immersed in the nonsolvent (water) of the gel tank immediately and no roller touches the surface of the film until it is completely gelled. Indeed, the speed of the casting process is determined by the gelation time of the membrane and the physical dimensions of the gel tank. Because the gelation time for casting UF membranes with a liquid precipitant is much less than that for MF membranes with a gaseous precipitant, UF casting machines have a much higher rate of output. A 60 foot long casting machine with environmental chambers for casting MF membranes may run as slowly as one foot per minute. A 10 foot long casting machine with gel tank for casting UF membranes may run as fast as ten feet per minute–an order of magnitude faster than the MF caster. Therefore, contrary to popular myth, UF membranes are often less expensive to make than MF membranes. This cost difference is accentuated by the fact that an MF caster must often run for an hour before any product comes off the machine. The feedback for adjustments to the process is greatly delayed resulting in considerable waste material before conditions in the environmental chambers are set. With a UF caster, product is produced almost immediately and feedback is rapid. Further, the process is much simpler than that required to make MF membranes.

It is advisable to use DI water in the gel tank. The author has successfully cast many large batches of UF membranes using tap water in the quench bath. However, this often results in membrane product which is discolored (iron oxide) and variable with the seasons as the tap water quality changes. DI water with an 18MΩ resistivity is the best standard. However, it must be borne in mind that high resistivity water will result in faster leach rates of solvent from the gelling casting solution which may affect the pore size of the final membrane.

When producing membranes for use in the pharmaceutical industry, the use of depyrogenated water is required. Otherwise, pyrogens will be incorporated in the cast membrane and some will leach out in the filtrate with use. Depyrogenization may be accomplished by filtering water from the ion exchange columns with a 10,000 MWCO UF membrane.

Water in the gel bath must be replaced periodically or better yet, continuously to minimize the buildup of solvents or other contaminants in the quench bath. If bacteria slime or turbid water is noted, the tank should be drained and cleaned.

Though Figure 3.4 shows the rinse tank adjacent to the gel tank with continuous rinsing of the cast/precipitated product, in practice it is a separate operation. This is necessary because of the long residence times required in the rinse tank to remove final traces of solvents from the membrane. A separate tank may also be used to apply wetting agents or plasticizers.

Plasticizers are necessary for some membranes, if they are to be dried, to

prevent collapse of the pores during drying. Figure 3.5 shows the capillary stress in the small pores of a UF membrane during drying.

$$\Delta P = \frac{2\gamma}{r} \quad (1)$$

where ΔP = the pressure difference across the curved interface between the liquid and gas.

γ = the surface tension of the liquid in the pores ($\gamma = 72$ dynes/cm for water).

r = radius of curvature of the interface (equal to the radius of the pore for perfectly wetting or perfectly nonwetting pores).

The pores of UF and RO membranes are small enough that the capillary stresses at the air-water interface can exceed the yield strength of "soft" polymers. Hydrophobic polymers like PVDF can be dried without irreversible damage to the pores, but must be rewetted to initiate flow. "Hard" polymers with the larger pore sizes can also be dried without ill-effect. The "soft" polymers can be dried if the surface tension of the liquid filling the pores is reduced. This may be accomplished by replacing the water with a low boiling organic like alcohol or acetone which has a low surface tension and can be evaporated without creating large capillary stresses. Alternatively, a 15% solution of glycerin or polyethylene glycol in water or isopropanol can be used to saturate the pores prior to drying. This not only reduces the surface tension, but the glycol remains behind after drying-serving as a plasticizer and wetting agent in the dry membrane. This latter method is used by most manufacturers who ship "dry" membranes.

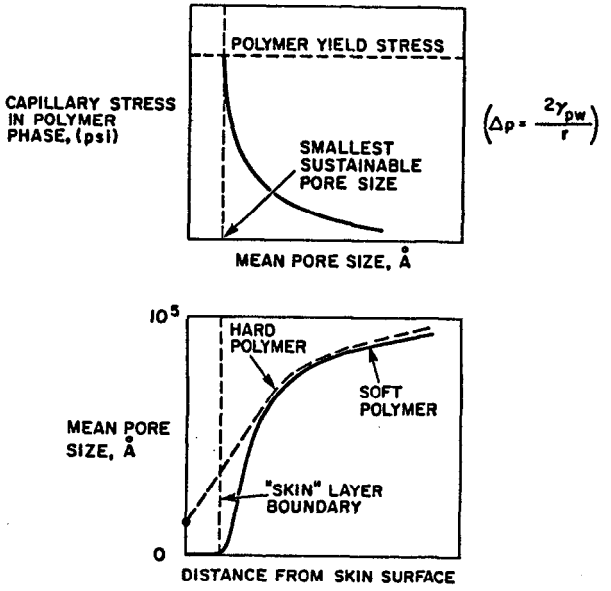


Figure 3.5: Capillary consolidation stress in a UF membrane.

Procedure for Casting Tubes

The same six steps in the procedure for casting sheet stock can be applied to the casting of membrane on the inside of a porous tube.

Figure 3.6[7] is a schematic of a tube casting operation. In this case, the tube is lowered over a casting bob which meters the casting solution uniformly on the inside wall of the tube. As the tube is lowered further, it is immersed in a water bath which precipitates the membrane. All other steps are similar to those taken with sheet stock membranes.

The challenge is to find an inexpensive porous tube which has sufficient strength to withstand 100 psi pressure internally for long periods of time. Porous polyethylene, polypropylene, and fiberglass-reinforced epoxy support tubes have been utilized.

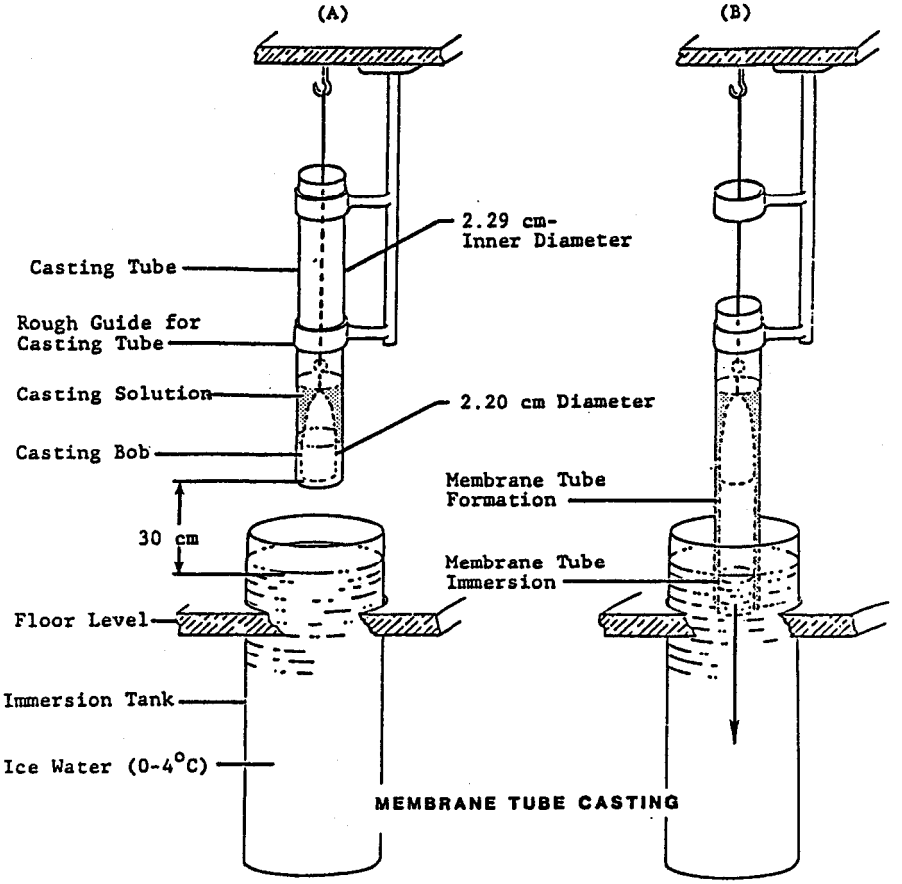


Figure 3.6: Schematic of tube casting operation.

Casting Variables for Tubes and Sheets

In Chapter 1, Dr. Strathmann used a ternary phase diagram (Figure 1.13) to describe what happens when a nonsolvent like water is added to a homogeneous

solution of polymer. This is a very useful tool in understanding how we can alter the casting variables to form membranes of varying pore size and permeability. The tool is limited because it does not provide direct information about pore sizes; nor does it distinguish between the dense skin and the porous sublayer. However, if we assume that a membrane having a larger porosity overall will have a higher porosity in the skin as well as in the substructure, and that the higher porosity is associated with higher permeability and larger pores, the model can be very instructive.[5]

The overall porosity of an anisotropic membrane is determined by the polymer content of the casting solution and by the relative rates at which nonsolvent enters and nonsolvent leaves the casting solution (i.e., the precipitation path in the phase diagram).

Figure 3.7[5] is a ternary phase diagram for a casting dope made of CA and acetone; it shows several different paths of precipitation for porous UF membranes and dense RO membranes. Path AE produces an open UF membrane because water enters the film faster than the solvent leaves, and CA precipitates around a larger volume of solvent which acts as the "pore-former". Path AD leads to a tight RO membrane because solvent leaves the film faster than water enters. When CA precipitates, there is less volume of solvent present resulting in a lower porosity and smaller pores.

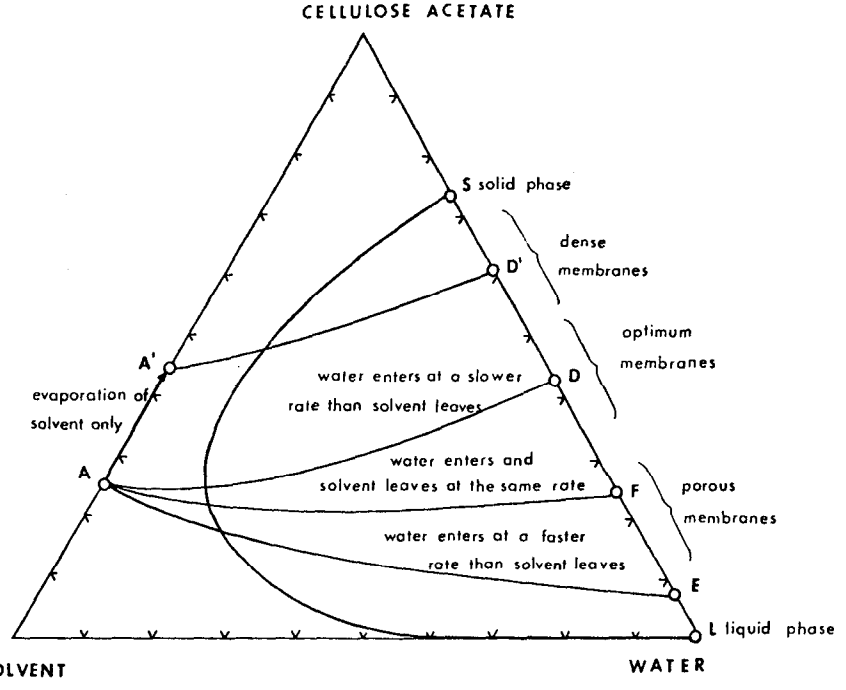


Figure 3.7: Ternary phase diagram for formation of UF membranes from cellulose acetate.

Obviously, the simplest way to adjust the overall porosity is to adjust the polymer content of the casting solution unless the resultant viscosity is out of

bounds. If the solids are increased by direct addition to the casting solution or by an evaporation step (moving from point A to A' on Figure 3.7), a lower porosity and tighter membrane will result.

Various methods have been used to adjust the rate of water entry and solvent removal. They include the use of additives in the casting dope or in the precipitant (water) and temperature adjustments to both.

From a thermodynamic standpoint, any additive in the *casting dope* would be expected to increase the rate of water entry and decrease the rate of solvent removal-resulting in more open membranes. This is because additives in the casting dope would be expected to reduce the chemical potential of other species in the casting dope. Reducing the chemical potential of water in the dope will increase the chemical potential driving force for water entry. Likewise, reducing the chemical potential of solvent in the casting dope will decrease the chemical potential driving force for solvent removal.

Additives in the *water bath* can have the opposite effect, decreasing the rate of water entry into the cast film because of the decreased chemical potential of water. This produces tighter membranes with lower porosity. One may also reduce the chemical potential driving force for water entry by reducing the temperature of the water bath. Loeb used ice water (see Figure 3.6) in the formation of RO membranes.

On the other hand, if the additive in the water bath is the same solvent used in the casting solution, the rate of solvent removal from the cast film is also slowed along with the rate of water entry. The result can be a reasonably homogeneous pore structure with fairly large pores. For example, this technique has been used to form MF membranes from polyvinylidene difluoride (PVDF).[8] The casting solution is 16 to 19% PVDF in acetone at a temperature of 50°C. The gelation bath is a blend of 70 to 80% acetone in water. The result is an MF membrane with relatively large pores (over 0.1 μ). If the acetone concentration in the water bath is reduced below 50%, a skin begins to form and an asymmetric UF membrane is produced.

Figure 3.8[5] shows the effect of additives in the *casting solution* (formamide, $ZnCl_2$, $Mg(ClO_4)_2$ on the porosity of CA membranes. Formamide is a standard additive for CA-acetone casting solutions; it is well known that an increase in formamide concentration will increase membrane permeability and decrease salt rejection.

Water was one of the earliest additives incorporated into cellulose acetate casting solutions resulting in more open membranes. Again, this is readily explained by the ternary phase diagram shown in Figure 3.9[5] The maximum water content, without incipient precipitation of polymer, is only slightly above 15%. At this level, only a small amount of water need diffuse in before gelation occurs. Since very little acetone has diffused out of the casting solution, polymer begins to precipitate around a large volume of solvent resulting in a very porous membrane.

In addition to polymer content additives, and temperature, the nature of the solvent can have a marked influence on the transport properties of the resulting membrane. Eirich et al[9] discovered that regardless of the nature of the polymer, the highest porosity membranes were made from casting solutions utilizing solvents with high solubility parameters. Eirich investigated cellulose acetate, polystyrene, polyvinyl chloride, polyvinylidene difluoride, polycarbonate, polymethyl methacrylate, polyacrylonitrile, and polyacrylonitrile/polyvinyl

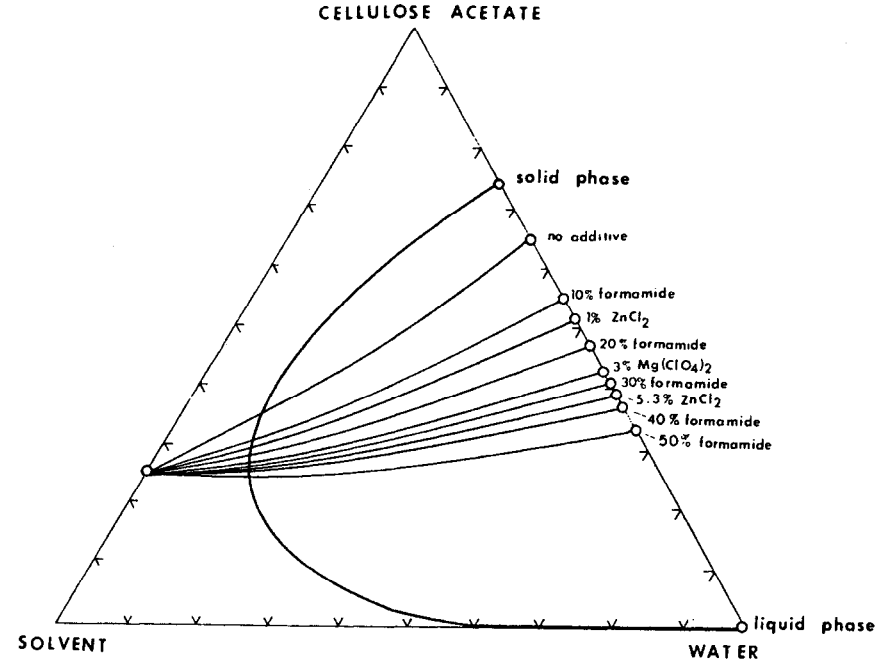


Figure 3.8: Effect of additives on formation of UF membranes portrayed on ternary phase diagram.

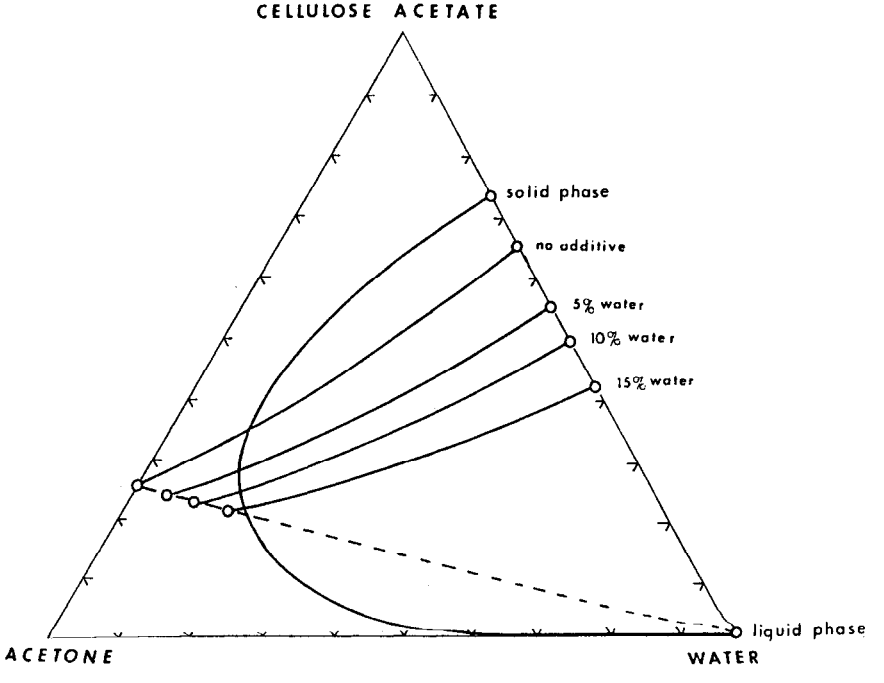


Figure 3.9: Effect of water in casting dope on formation of UF membranes.

chloride copolymer with a whole host of solvents. The data for cellulose acetate are plotted in Figure 3.10[9] Though some of the polymers investigated were not soluble in all of the solvents shown in Figure 3.10, the trend was the same–the water content (porosity) increased with higher solubility parameters of the solvent. Tetrahydrofuran always resulted in very dense membranes while dimethyl sulfoxide yielded very porous membranes. Of 41 polymer-solvent systems investigated, only 7 cases were out of line. Of the 7 exceptions, 5 were dimethylformamide casting solutions which gave membranes of lower porosity than the correlation would predict.

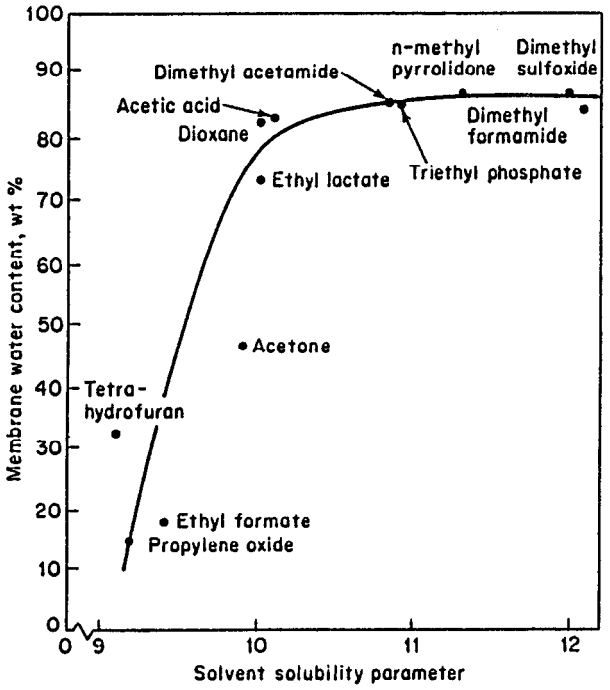


Figure 3.10: CA membrane porosity (water content) as a function of the solvent used in the casting dope.

Since water (the precipitant) has a solubility parameter (23.4) higher than any of the solvents investigated, it would appear experimentally that the disparity between the solubility parameters of the solvent and the precipitant is a key factor in understanding these results.

The solubility parameter for solvents is calculated as the square root of the cohesive energy density (the energy of vaporization divided by the molar volume). It is a measure of all cohesive forces tending to hold the molecules of the solvent together, whether they be dispersion (London) forces, hydrogen bonding or dipolar interactions. In general, two solvents with similar solubility parameters are more compatible and have a greater affinity for each other. Likewise, since a polymer's solubility parameter cannot be calculated because of its nonvolatility,

it is normally determined experimentally by arranging a list of solvents for the polymer in order of increasing solubility parameter; the solubility parameter for the polymer is taken to be that at the midpoint of the soluble range.

The simplest explanation for the data of Eirich (though not suggested by Eirich or his co-workers) seems to be related to the greater compatibility of water with solvents having higher solubility parameters. When the polymer begins to precipitate, the residual solvent may tend to exclude water if there is too great a disparity between the solubility parameter. The result is a dense, low porosity membrane. On the other hand, smaller differences in the solubility parameter would tend to favor inclusion of water resulting in a membrane with higher porosity.

Procedure for Spinning Hollow Fibers

Figure 3.11 is a photomicrograph of a typical asymmetric hollow fiber with the skin on the inside wall. Hollow fibers for UF have the skin on the inside whereas hollow fibers for RO are smaller and have the skin on the outside. This is because of the high pressure required in RO; commercially available fibers cannot withstand internal pressures up to 400 psi and above. Thus, for RO, the feed stream is pressurized on the outside of the fiber, and the permeate flows from the lumen of the fiber (see Figure 3.12). Actually, considerable research effort has been spent in developing composite hollow fibers for RO which can withstand internal pressures up to 900 psi because, as we shall see, flowing the feed stream down the lumen of the fiber greatly reduces concentration polarization effects.

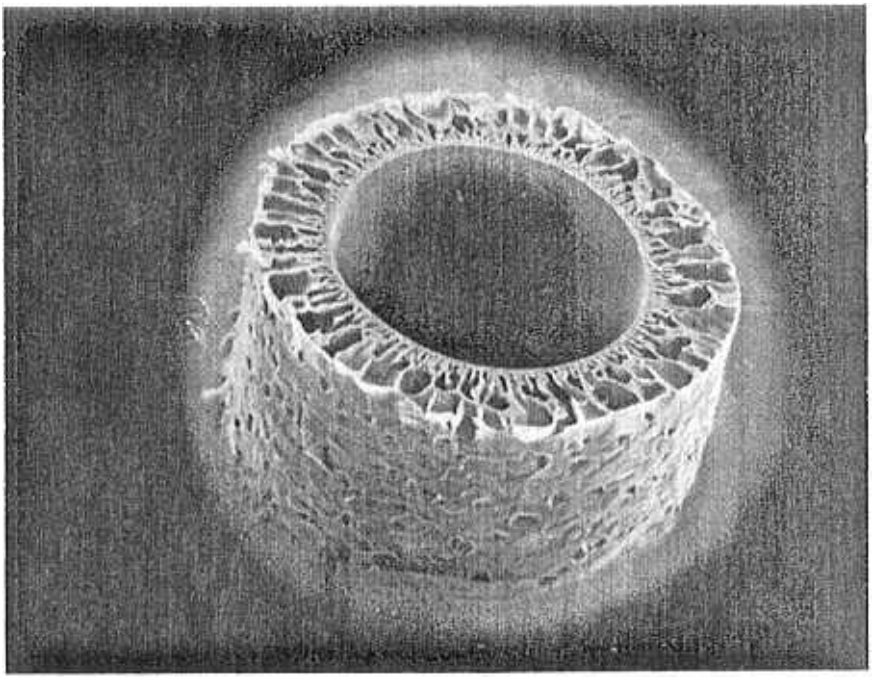


Figure 3.11: Photomicrograph of asymmetric UF hollow fiber.

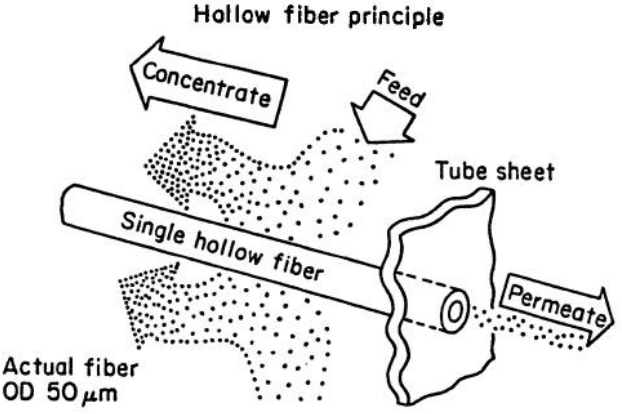


Figure 3.12: Feed stream on outside of RO hollow fiber.

The lower pressures required in UF make possible better fluid management with pressurized feed on the inside of the fiber (see Figure 3.13). Since most UF hollow fibers have burst pressures ranging between 60 and 100 psi, inlet operating pressures are limited to an inlet pressure of 30 psi. Naturally, with feed in the bore of the fiber, the inside diameter must be larger to prevent plugging. Figure 3.14 shows UF fibers made by Romicon with inside fiber diameters up to 1 mm (1,000 μ). This is 25 times larger than the inside diameter of a DuPont RO hollow fiber (42 μ I.D.). Actually, the trend is to go with even larger diameters (1.5 and 2.0 mm I.D.) to improve fouling resistance.

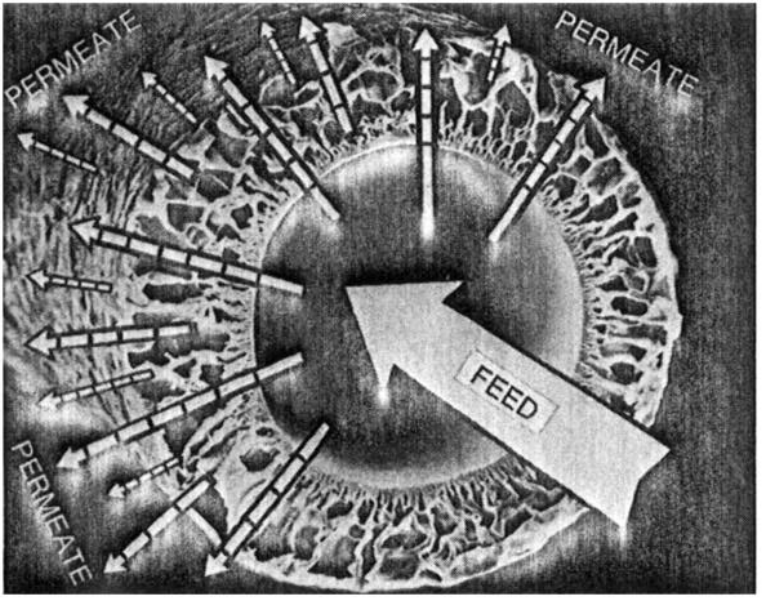


Figure 3.13: Feed stream on inside of UF hollow fiber.

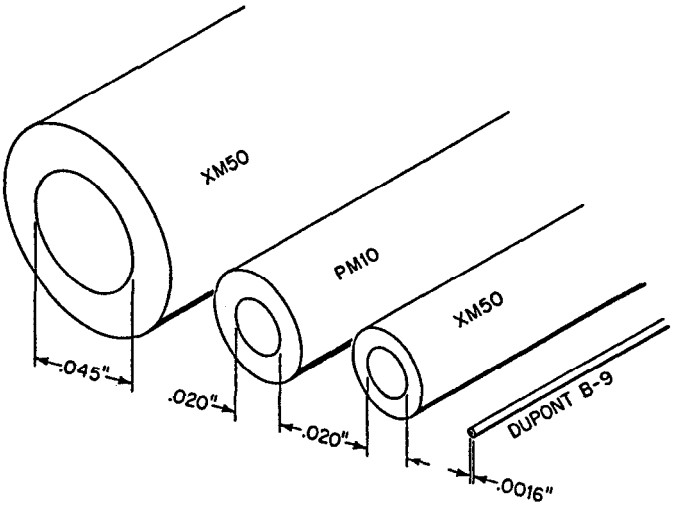


Figure 3.14: Dimensions of various hollow fibers supplied by Romicon (UF) and by DuPont (RO).

The spinning of asymmetric hollow fibers with the skin on the inside closely resembles the procedure used in casting flat-sheet membranes. Figure 3.15[10] is a schematic diagram of a spinneret used to spin these fibers. The degassed and filtered polymer solution is forced under pressure into a coaxial tube spinneret. The liquid is extruded through an annular orifice and the hollow fiber (still liquid) is stabilized and precipitated by an internal coagulating fluid (usually water) which flows out the center tube.

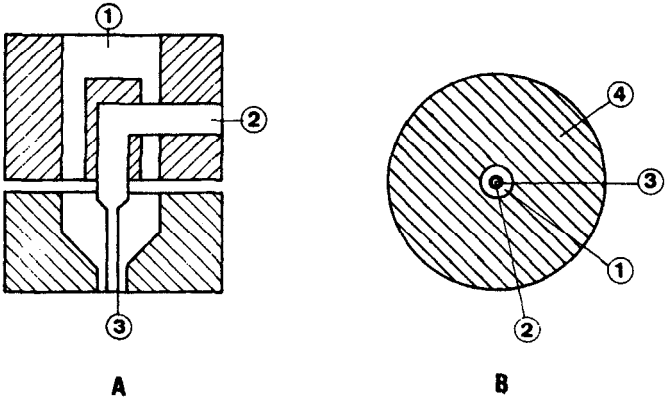


Figure 3.15: Schematic of tube-in-orifice spinneret.

The spinneret is usually positioned some distance above a water bath, so that the outside of the emerging fiber is in contact with air before being collected in the water bath. If the fiber hits the water bath before being fully gelled, a secondary skin will form on the outside of the fiber (see Figure 3.16).

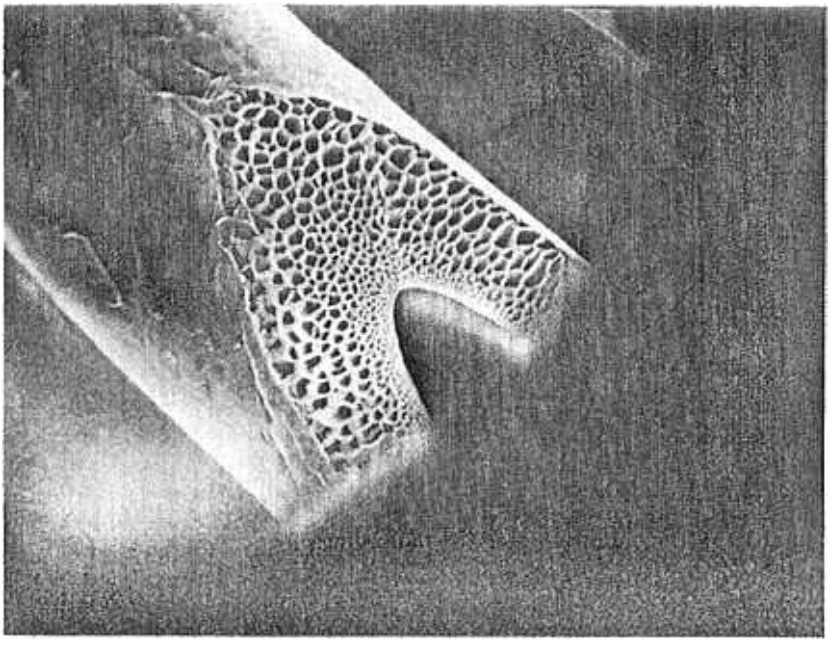


Figure 3.16: Photomicrograph showing secondary skin on outside of UF hollow fiber.

This is disadvantageous when potting the hollow fibers in a header. The potting material (usually epoxy) will not penetrate into the wall of the fiber resulting in a poor bond and a possible leak path for the feed stream through the cross section of the fiber wall and out into the permeate, by-passing the internal skin.

The spinning procedure accomplishes each of the six steps used in casting flat sheets or tubes. The spinneret design (the diameter of the center tube and the width of the annular space between the inner tube and the extrusion orifice) will determine the dimensions of the final fiber. Collection of the gelled fiber in a water bath permits leaching of remaining solvent from the fiber. During long runs, this water bath is continuously replenished with fresh water. If need be, the fibers may be collected and immersed in other baths to add plasticizers, etc. to prepare for drying before potting.

Spinning Variables for Hollow Fibers

All of the variables discussed in conjunction with casting sheet and tubes apply to hollow fibers as well. Higher polymer content in the casting dope, additives in the coagulating fluid, and reduced temperature of the coagulant will result in tighter, more retentive hollow fibers. On the other hand, additives in the casting dope and solvents with high solubility parameters favor more open fibers with a higher permeability.

In addition to the above, there are other variables unique to the spinning process which offer additional handles for controlling fiber permeability and retentivity.

(1) The velocity of the spinning solution through the annular orifice of the spinneret.

(2) The velocity of the coagulating fluid through the inner tube.

(3) The distance between the spinneret and the collecting bath (the "air-gap").

In general, an increase in the spinning solution velocity and the "air-gap" will result in tighter fibers with lower permeability and increased retentivity. An increase in the coagulating fluid velocity will have the opposite effect, leading to more open fibers of higher permeability and reduced retentivity.

The effect of increased spinning solution velocity in producing tighter fibers is explained by the shear forces in the annular orifice. It is known that polymer molecules under shear flow tend to align themselves in the direction of flow. Since the internal wall of the fiber precipitates immediately upon contact with the coagulant after emerging from the spinneret, this alignment of polymer chains will be frozen in place in the solid skin. As a consequence, the pores in the skin (which control retention and permeability) will be elongated. If the kinetics of gelation remain unchanged, rectangular pores of the same area as circular pores will show retention for smaller molecules and a lower permeability. Indeed, if the width of the rectangular pore is equal to the radius of the circular pore of the same area, the permeability through the rectangular pores will be only 2/3 of that through the circular pores.

Likewise, an increase in the "air-gap" (distance between the spinneret and the collecting bath), will further extend the polymer chains as they pass through the spinneret because of the added weight of the fiber below. Any tendency towards relaxation of the polymer chains after emerging from the spinneret and before gelation will be alleviated by this weight tending to stretch the fiber. Thus, an increase in the "air-gap" will only increase the degree of orientation resulting in tighter fibers. However, very small "air-gaps" can result in the formation of a secondary skin on the outer surface of the fiber which may tend to decrease the hydraulic permeability as well-though the retentivity of the fiber (determined by the internal skin) would be more open.

The alignment of polymer chains in shear flow through the spinneret may explain why hollow fibers generally have lower permeabilities than flat-sheet membranes with the same retention rating.

On the other hand, an increase in the velocity of the coagulating fluid through the inner tube tends to counteract the elongation of pores in the skin; the increased pressure in the fiber lumen tends to expand its diameter and thereby enlarge the width of the elongated pores. The result is a more open fiber with increased permeability and decreased solute rejection.

Preparation of Inorganic Membranes

Dynamic Membranes. In the late sixties, workers[11] at the Oak Ridge National Laboratory discovered that cross-flow filtration of dilute colloids through a microporous tube made the support tube retentive for macromolecules and even salts (in some cases). While numerous colloidal materials and organic polyelectrolytes were tested, the most successful system was based on hydrous zirconium oxide. This inorganic dynamic membrane could have flux values as high as 1,000 GSFD (gallons per square foot per day) at 950 psi with a NaCl rejec-

tion of 50% at dilute salt concentrations (0.05 M). Further, the rejection could be improved by applying a thin layer of polyacrylic acid, (PAA) at high pH on top of the Zr(IV) oxide dynamic membrane. Rejections of 90% for 0.05 M NaCl were obtained.[12]

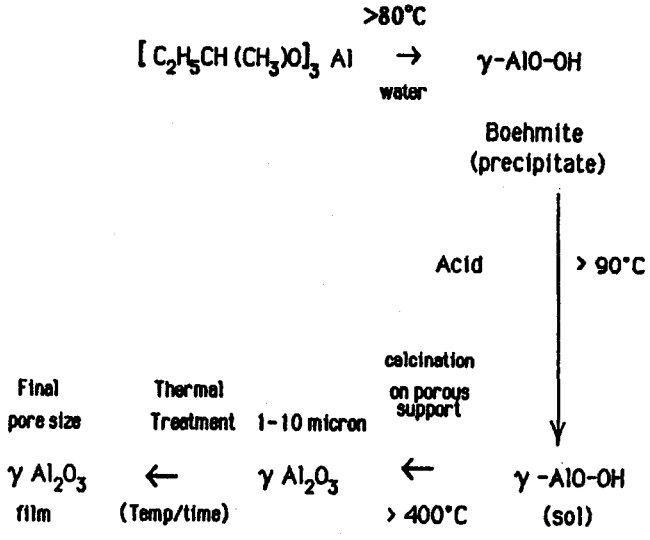
One company (Carre Inc., Seneca, SC) has exploited this technology by selling plants utilizing porous stainless steel tubes and the know-how to apply the hydrous Zr(IV) oxide dynamic membrane. When the membrane becomes fouled, it is stripped off with acid and a new membrane applied using cross-flow of the Zr(IV) oxide slurry feed.

Union Carbide went one step further–sintering the hydrous Zr(IV) oxide dynamic membrane in place on a porous carbon tube at elevated temperatures. This resulted in a high-temperature (300°F) inorganic membrane which is resistant to a pH of 1–14. Further, the membrane may be cleaned with organic solvents that would dissolve conventional polymer membranes. This technology was subsequently licensed to SFEC (Société de Fabrication d'Eléments Catalytiques) in Bolléne, France and to Gaston County Filtration Systems in Stanley, NC.

Ceramic Membranes. Alumina membranes for UF have been introduced by Ceraver (Tarbes, France) (membrane division recently purchased by Alcoa). The Norton Co. (Worcester, MA) is reportedly about to introduce an alumina UF membrane in addition to its current MF membrane.

The difficulty with existing ceramic UF membranes is resistance to high pH. The alpha form of Al_2O_3 is used to make MF membranes (0.2 μ pore size and above) and is resistant to a pH of 1–14. To make the finer pores (down to 40 Å) in a UF membrane, the existing technology uses the gamma form of Al_2O_3 which will not withstand high pH.

The methods used to make these membranes are diverse and highly proprietary. However, one method for preparing gamma-alumina membrane films on porous supports (which can be made from alpha-alumina) has been reported by Dutch researchers.[13] They use a sol/gel technique with Boehmite (γ–AlO–OH) as the precursor because it can be easily dispersed with acids.



The pore size of the membrane is determined by the type of acid and its concentration during dispersion (typically 0.03 to 0.15 mol acid per mol of AlO–OH) along with the final thermal treatment, both of which affect the crystallite size of the gamma-alumina. The porous support is dipped into the sol and capillary action pulls the sol into the pores increasing the concentration of Boehmite at the entrance of the pores to form a gel. The calcination of this gel film (above 400°C) yields the final film of gamma-alumina.

PORE SIZE DETERMINATION

As shown in Figure P.2 (in the Preface), UF membrane pore sizes range from 10 to 1000 Å (0.001 to 0.1 μ). It is difficult to measure the pores directly by any of the techniques used for MF membranes. The anisotropic structure and the wide distribution of pore sizes make this almost impossible.

Instead, we are accustomed to think of the molecular weight of the macromolecules which are retained by or pass through the membrane. Unfortunately, existing UF membranes do not have a "sharp cut-off" because of the wide distribution of pores in the skin of the membrane (see Figure 3.17). Most UF membranes have "diffuse cut-off" characteristics.

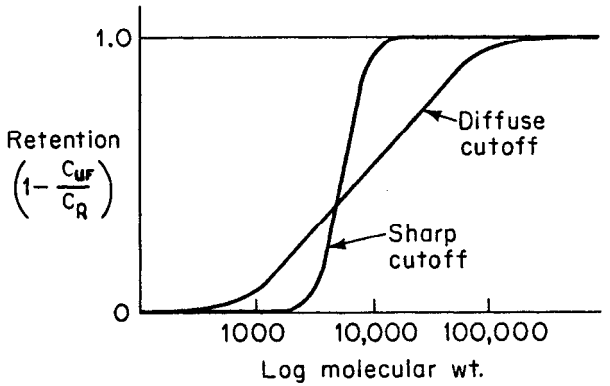


Figure 3.17: Sharp vs diffuse cut-off membranes.

Molecular Weight Cut-Off and Pore Size

What we mean by the molecular weight cut-off of a "diffuse cut-off" membrane must be clearly defined. The convention established by AMICON and adopted by most UF membrane manufacturers is based on the retention of globular proteins (spherical macromolecules). The retention R (in percent) may be defined as follows:

$$R = 100\left(1 - \frac{C_{uf}}{C_R}\right) \tag{2}$$

where C_{uf} = concentration of the solute in the ultrafiltrate

C_R = concentration of the solute in the retentate

The convention states that *the molecular weight cut-off of the membrane is equal to the molecular weight of globular proteins which are 90% retained by the membrane.*

Figure 3.18 shows how this is determined. The retention values of a series of globular proteins (spherical molecules) are measured on the same membrane. The molecular weight at which the retention curve crosses a retentivity of 90% is the "molecular weight cut-off" of the membrane. This means that larger molecules are said to be retained by the membrane and smaller molecules are said to pass.

Normally UF membranes are designated by prefix letters which refer to the membrane type followed by one or more digits which refer to the molecular weight cut-off in thousands of daltons. For example, in Figure 3.18, UM, PM and XM refer to three different polymers; PM-10 indicates the membrane has a 10,000 molecular weight cut-off (MWCO). The approximate molecular diameter (Å) at the top of Figure 3.18 is taken from radius of gyration data reported in the literature. This may be used to estimate the effective pore size (see Figure 3.19).

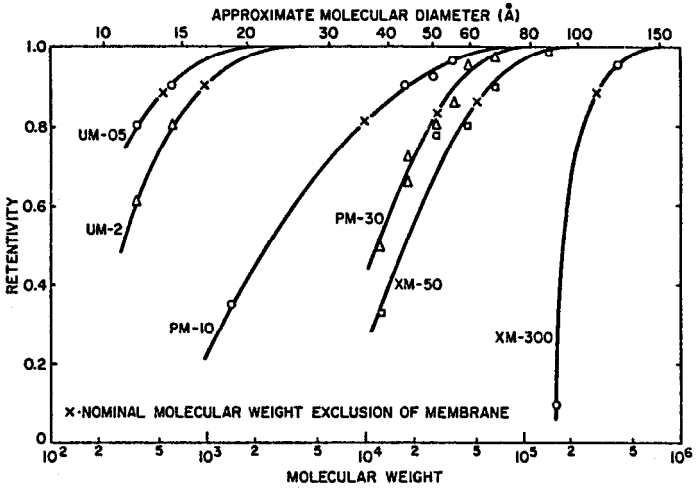


Figure 3.18: Retentivity of a series of globular proteins on various UF membranes.

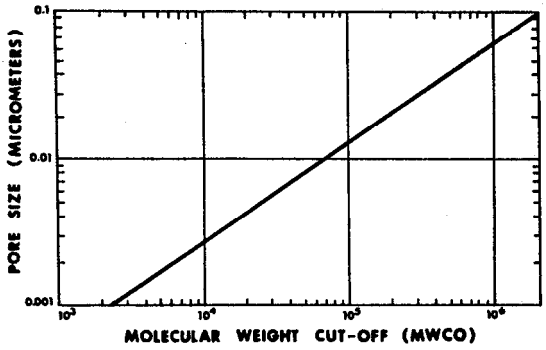


Figure 3.19: Pore size variation with MWCO.

Retention of Spherical and Linear Molecules

Two different molecules of the same molecular weight can have different configurations such that their molecular diameter is different. For example, a linear polymer may snake through the pores while a spherical polymer of the same molecular weight, but of greater diameter, is retained (see Figure 3.20).

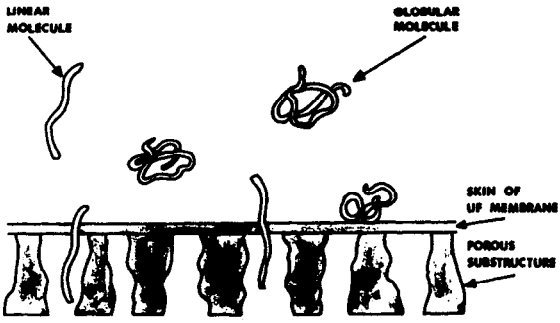


Figure 3.20: Retention of spherical and linear molecules.

Table 3.1[14] shows the effect of size and shape of the molecule on its retentivity by various MWCO membranes. Each membrane retains those molecules positioned above the line but passes those below the line. Since characterization of a membrane's MWCO is based on globular proteins, the retention of these molecules is as expected. However, the retention of branched polysaccharides and linear flexible proteins is lower than might be expected. For example, Dextran 250 with a molecular weight of 236,000 passes through a 50,000 MWCO membrane. Apparently, the fluid shear in the vicinity of the pores is high enough to uncoil free draining chains. This is illustrated in Figure 3.21 which shows the difference in the retentivity of a 1,000,000 MWCO membrane for a series of globular proteins and a comparable series of polysaccharides.

Table 3.1: Effect of Size and Shape of Molecules on UF Retentivity

	Solute Class		
Membrane*	Globular Proteins	Branched Polysaccharides	Linear, Flexible Polymers
Diaflo XM50	γ-Globulin (160,000)** Albumin (69,000)		
Diaflo PM30	Pepsin (35,000)	Dextran 250 (236,000)	
	Cytochrome C (13,000)		Polyacrylic acid (pH 10; 50,000)
	Insulin (5,700)		
		Dextran 110 (100,000)	Polyacrylic acid (pH 7; 50,000)
Diaflo PM10			
	Bacitracin (1,400)		
		Dextran 40 (40,000) Dextran 10 (10,000)	Polyethylene glycol (20,000)
Diaflo UM10			

* Molecules above a horizontal membrane line are completely retained by the membrane; below the line partial retention or complete clearance is observed.

** Number in parentheses denote molecular weights.

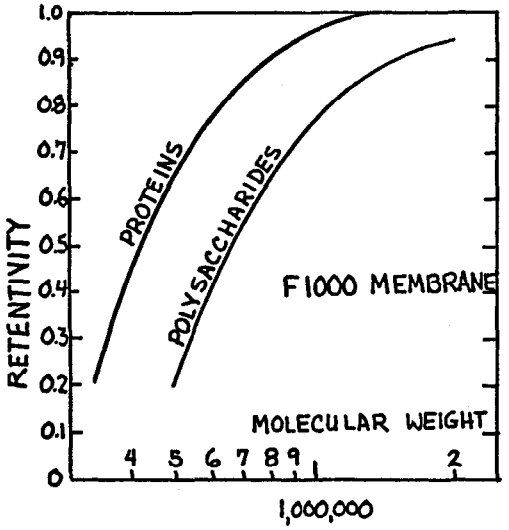


Figure 3.21: Retentivity of proteins and polysaccharides on a 1,000,000 MWCO membrane.

It is also known that the pH and ionic strength of solutions of polyelectrolytes can have a marked influence on their retentivities. The more a polyelectrolyte is charged in solution, and the lower the ionic strength of the medium, the larger the effective size of the polyelectrolyte for a given molecular weight.

Maximum Pore Size and Effective Pore Size

Since the effective pore size is estimated from the molecular diameter of globular proteins which are retained 90% by the membrane, it is obvious that larger pores do exist. The measurement of a membrane's bubble point (see the section on the bubble point test in Chapter 2) permits calculation of the maximum pore size in the skin of the membrane.

Figure 3.22 shows the bubble point measured with isopropanol (IPA) on polyvinylidene difluoride UF membranes with MWCO's between 10,000 and 1,000,000. A 300,000 MWCO membrane (F300) should have an estimated effective pore size of 0.02 μ; yet the bubble point indicates a maximum pore size in the skin over 0.4 μ. This is one reason why UF membranes can be less retentive for bacteria than MF membranes. However, Figure 3.22 also indicates that a 10,000 MWCO membrane can have a (I.P.A.) bubble point of 100 psi. Equation 3 of Chapter 2 may be used to calculate a maximum pore diameter of 0.12 μ which should be retentive for all bacteria. Indeed, small laboratory discs of these membranes can be subjected to high challenge levels of bacteria with absolute retention (zero passage). However, industrial scale UF modules often employ 10 to 100 square feet of membrane area; it is difficult to manufacture a pinhole-free module with this much area. Broken fibers, bubbles in glue-line seals, and other defects provide leak paths for bacteria.

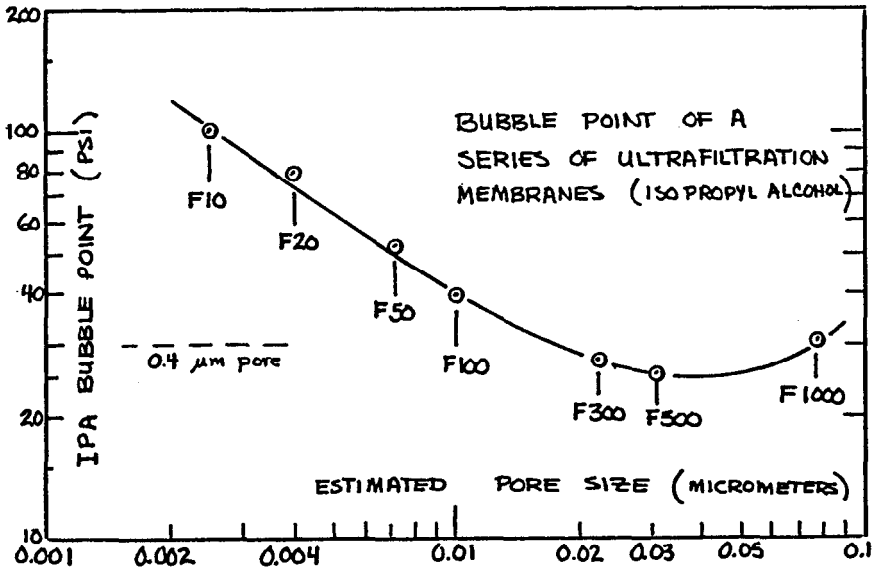


Figure 3.22: IPA bubble point of a series of UF membranes.

RETENTION CHARACTERISTICS

The polymer from which a UF membrane is made does not generally affect the retention characteristics of the membrane. However, the nature of the polymer can affect adsorption of species onto the membrane surface. For example, when processing small volumes of dilute solutions, strong adsorption of the solute can diminish its concentration in both the retentate and in the filtrate, and this can affect the apparent retention calculated from Equation 2.

Adsorption Losses

The retention of membranes are often measured in stirred cells. A mass balance on the cell; integrated over time from an initial retentate volume (V_o) and initial concentration (C_o) to a final retentate volume (V_f) and final retentate concentration (C_f) yields the following expression for the retention (R):

$$R = 100 \frac{\ln(C_f / C_o)}{\ln(V_o / V_f)} \tag{3}$$

Equation 3 is used to calculate retention solely on the basis of changes in the retentate volume and concentration. Obviously, if adsorption losses are appreciable, the retention calculated from Equation 3 will be *too low* since C_f will be lower than it would be without adsorption. For this reason, the retention should also be calculated with reference to the solute concentration in the ultrafiltrate (permeate).

A simple cumulative mass balance on the cell leads to another expression for

retention (R) based on the final (average) ultra filtrate concentration (C_{uf}), the initial concentration of the retentate (C_o) and charges in the retentate volume from V_o to V_f:

$$R = \frac{\ln\left[\frac{V_o}{V_f} - \frac{C_{uf}}{C_o}\left(\frac{V_o}{V_f} - 1\right)\right]}{\ln\left(\frac{V_o}{V_f}\right)} \quad (4)$$

Again, if there are significant adsorption losses, the retention calculated from Equation 4 will be *too high* since C_{uf} will be lower than it would be without adsorption.

If the initial and final retentate concentration (C_o and C_f) are measured along with the final ultrafiltrate concentration (C_{uf}), the retentivities calculated from Equations 3 and 4 may be compared.

If there is an appreciable difference, adsorption losses can be significant. The magnitude of the loss may be calculated from the amount of solute in the retentate (C_fV_f) and in the filtrate ($C_{uf}[V_o-V_f]$) compared with that charged to the cell (C_oV_o).

If a small volume of a dilute solution is placed in contact with a large membrane area, the adsorption from solution can be appreciable. This technique may be used to measure the relative adsorption of various membranes as in Table 3.2. Fifty ml of a dilute solution (150 micrograms/ml) of cytochrome "C" were concentrated to 10 ml in a 50 ml stirred cell (membrane area of 13.4 cm^2) to compare the various membranes listed in Table 3.2.

Table 3.2: Adsorption Losses of Cytochrome C on Various UF Membranes

Membrane Types		Adsorption loss(%)	Retention for CytochromeC(%)
Nuclepore C-10	Regenerated Cellulose Acetate	0.8	97
Amicon YM-10	Regenerated Cellulose Acetate	2.3	97
Amicon UM-10	Polyelectrolyte Complex	4.3	26
Millipore PTGC (10^4)	Polysulfone	11.3	>99
Nuclepore A-10	Polyamide	12.4	85
Nuclepore F-10	Polyvinylidenedifluoride	22.5	>99
Amicon PM-10	Polyarylsulfone	24.6	53

In general, hydrophilic polymers tend to have a lower adsorption than the hydrophobic polymers.

"Charged" Membranes

Polyelectrolyte complex UF membranes can be made with a net charge to obtain moderate rejection of salts or amino acids (75 to 90%) at relatively high flux and low pressure.[15,16] For example, the Millipore PSAL membranes contain fixed sulfonic acid groups which have a negative charge capacity of 800 millimols/liter.

Charged UF membranes reject low concentrations of salts primarily by the Donnan exclusion mechanism. Because the fixed charged groups on the membrane skin reject ionic solutes via repulsion of coions, the rejection would be expected to depend on solute type and coion charge. Obviously, divalent and trivalent ions are rejected better than monovalent ions. Highly hydrated ions are rejected better than poorly hydrated ions.

Effect of Pressure

Figure 3.23[17] presents rejection data for three different dextrans on the same UF membrane as a function of pressure. Figure 3.24[18] shows the effect of pressure on the rejection of 0.1 M NaCl by a cellulose acetate RO membrane. It is obvious that the mechanism for solute transport through the membrane is different for UF and RO.

In the case of RO (Figure 3.24), the increase in salt rejection with increasing pressure suggests a "solution-diffusion" model as opposed to a "pore-flow" model for transport of solvent and solute across the membrane. It is known that although the water flux through RO membranes increases with pressure, the salt flux is almost invariant with pressure. The net result is that a higher water flux dilutes the salt concentration in the filtrate resulting in a higher calculated rejection by Equation 2. If "pore-flow" were in effect, leakage of salt through large pores would also be expected to increase with pressure. This suggests that the RO membrane acts as a nonporous diffusion barrier.

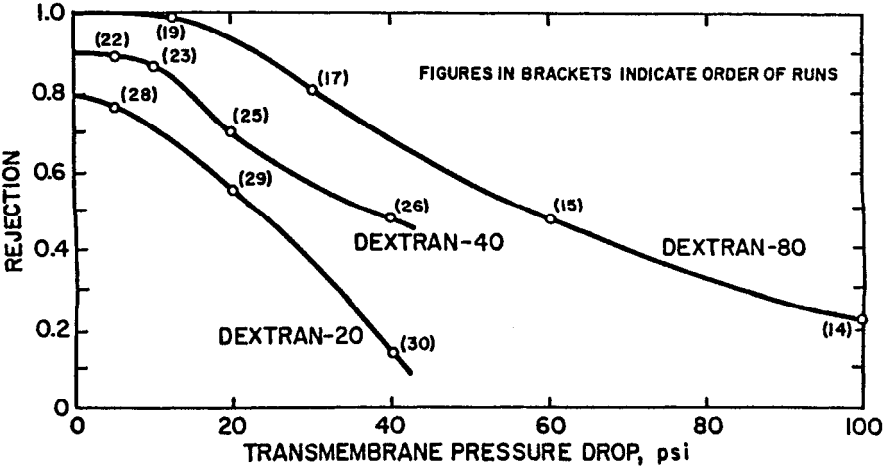


Figure 3.23: Effect of pressure on UF rejection of dextrans.

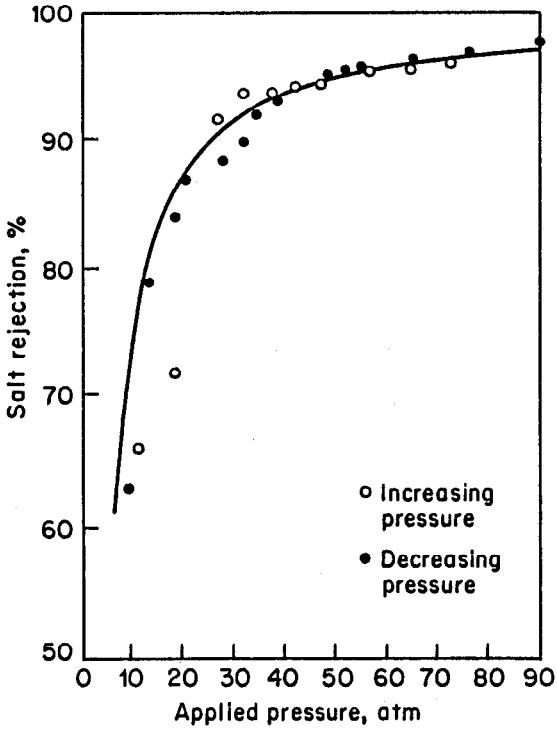


Figure 3.24: Effect of pressure on RO rejection of 0.1 M NaCl.

In a "solution-diffusion" process, the rate of transport of water and salt is proportional to the chemical potential gradient of each species across the membrane. The chemical potential of each is affected by pressure and concentration. For water, there is little difference in concentration across the membrane, the dominant effect is the difference in pressure. For salt, the ratio of upstream to downstream salt concentration is very large and this dominates over the effect of the pressure difference. The water flux is higher than the salt flux because the solubility of water in the membrane and its diffusivity through the membrane is higher than that of salt.

The "solution-diffusion" model explains why molecules larger than salt sometimes pass through an RO membrane more readily. For example, cellulose acetate membranes which show a 95% rejection for NaCl (MW 58) and a 99% rejection for dextrose (MW 180), show a negative -34% rejection for 2,4-dichlorophenol (MW 163). This means the dichlorophenol passes through the membrane more readily than water. This is hard to explain with a "pore-flow" sieving mechanism.

In a "pore-flow process", the solute flux (J_s) should be proportional to the water flux (J_w) which carries solute to the membrane and through the larger pores.

(5) $$J_s = \sigma J_w C_s$$

where C_s = concentration of solute at the upstream surface of the membrane

σ = the fraction of the total liquid flowing through pores large enough to pass solute molecules

The retention for solute may be expressed as:

(6) $$R = 1 - \frac{J_s}{J_w}$$

or

(7) $$R = 1 - \sigma C_s$$

Thus, in a "pore-flow" model, R would *not be expected to increase* with pressure since the solute and solvent flux are "coupled". As the pressure is increased, both fluxes increase.

However, the phenomenon of "concentration polarization" may cause the rejection to *decrease* with increasing pressure as in Figure 3.23. The reason is that the concentration of solute at the surface of the membrane (C_s) has increased over that in the bulk stream (C_b). As the pressure is increased, the solvent flux is increased and the convective transport of solute ($J_w C$) to the membrane is increased (see Figure 3.25). If the solute is retained by the membrane, it accumulates at the surface of the membrane until the back diffusive mass transport, $D_s(dc/dx)$, is equal to the forward convective transport. Even if a steady state is maintained, there must be a concentration gradient (dc/dx) to remove solute from the membrane. Thus, C_s will increase with pressure resulting in a decrease in solute retention by Equation 7 and as shown in Figure 3.23. The pores large enough to pass solute, at higher pressures, pass more solvent, carrying a higher concentration of solute (C_s).

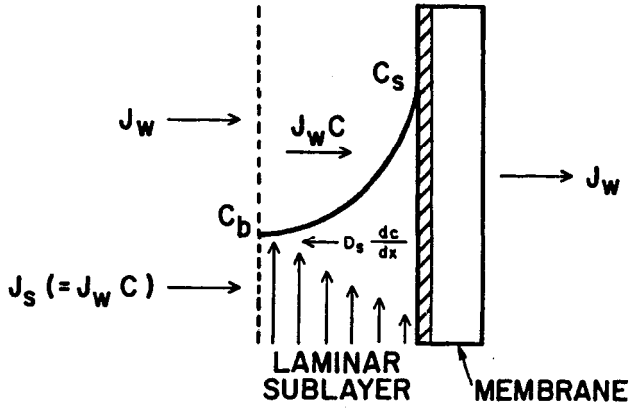


Figure 3.25: Concentration polarization in UF.

Further increases in pressure will increase the solute concentration at the surface of the membrane (C_s) to a limiting concentration. Proteins begin to form a semisolid gel on the membrane surface with a gel concentration (C_g) between 20 and 50 wt %. Colloidal suspensions form a densely packed layer of close-packed spheres usually between 70 and 80 volume %. Under these conditions (see Figure 3.26), the membrane is said to be "gel-polarized", and further increases in pressure will not increase C_s. Therefore, once the membrane is "gel-polarized", the retention should be independent of pressure (see Equation 7). In Figure 3.23, the rejection of Dextran-80 is beginning to level out at the higher pressures as the membrane becomes gel-polarized.

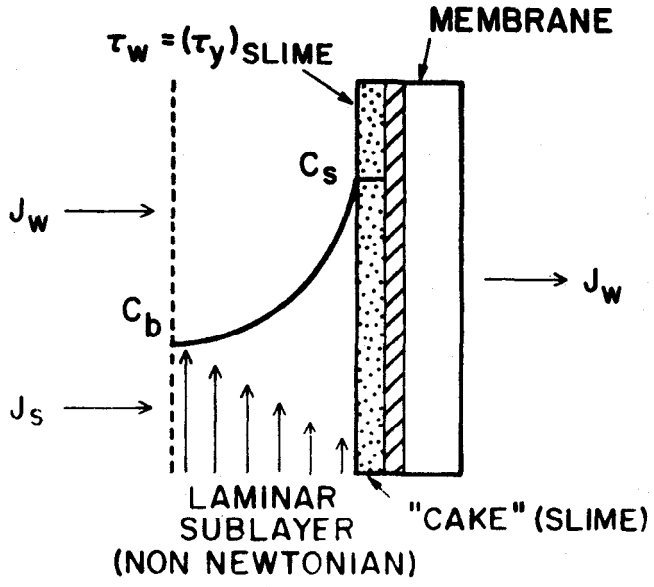


Figure 3.26: Gel formation due to concentration polarization.

Fractionation of Solutes

The retention of a single solute is determined solely by the properties of the membrane (pore size distribution, charge, and adsorption characteristics) and by the operating conditions (e.g., pressure, pH and ionic strength of the solution). The retention of individual solutes from a mixture is more complicated. Fractionation may or may not be possible.

Consider a 100,000 MWCO membrane which has a retention for gamma globulin (160,000 daltons) of 95% and a retention for albumin (67,000 daltons) of less than 15%. The retention for albumin in the presence of gamma globulin is shown in Figure 3.27. Because the gamma globulin is retained by the membrane, it forms a gel-layer which is retentive for albumin. Without this "dynamic secondary membrane", the albumin would pass the primary membrane. Indeed, at low concentrations of gamma globulin, the rejection of albumin approaches the single solute rejection by the membrane.

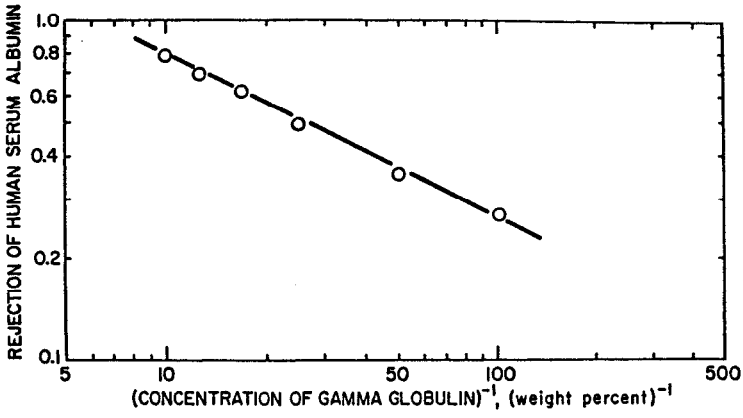


Figure 3.27: Retention of albumin in the presence of gamma globulin.

The pharmaceutical industry would prefer to make the gamma globulin/albumin separation with a UF membrane rather than Cohn fractionation (sequential precipitation with ethanol). But to do so, they would have to dilute the mixture way down to accomplish the separation. The processing of the large diluted volumes followed by concentration of the two fractions would make the membrane process more cumbersome and expensive than Cohn fractionation.

Separations involving globular proteins appear to be the most difficult. Figure 3.28 shows how three different solutes which are retained by a 30,000 MWCO membrane influence the retention of a 0.2% solution of cytochrome C (12,400 daltons) which by itself passes through the membrane with 0% retention.

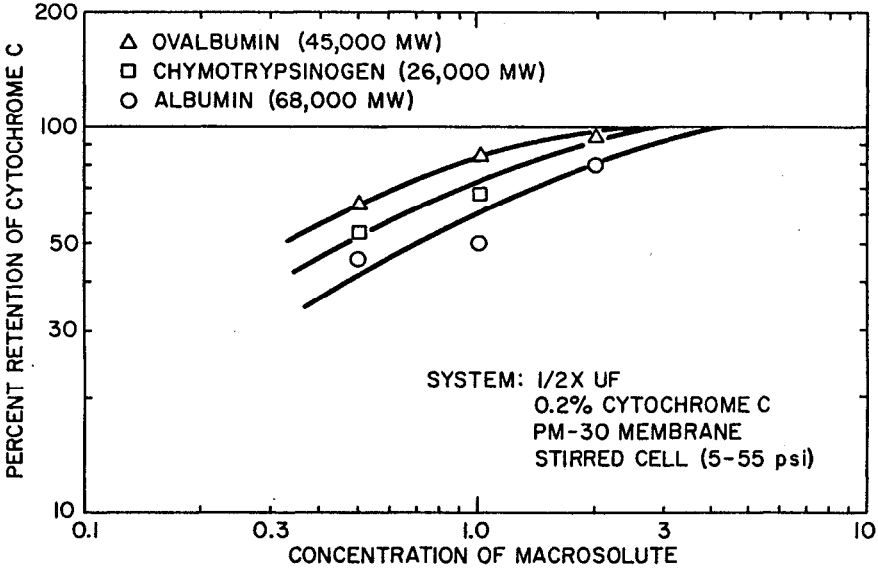


Figure 3.28: Retention of cytochrome C in the presence of larger species.

On the other hand, polymers like hydroxyethyl starch, polyethylene glycol, and polyvinyl pyrrolidone (see Figure 3.29)[19] can be fractionated more readily.

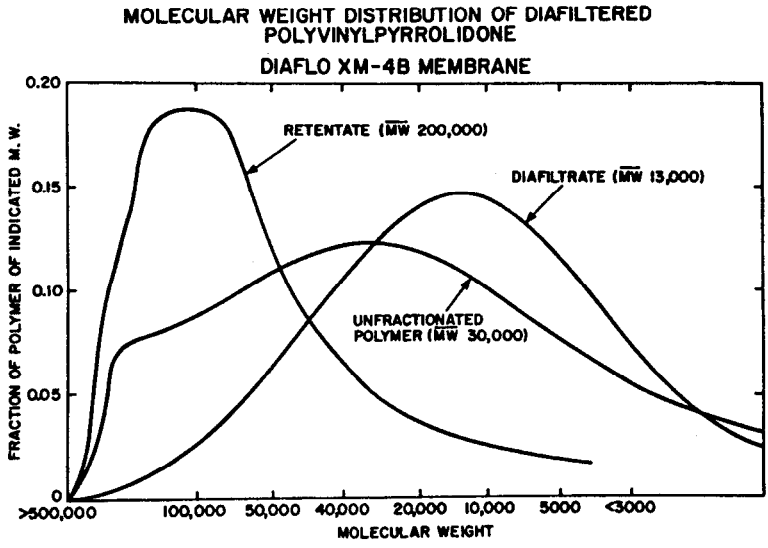


Figure 3.29: Fractionation of PVP.

MEMBRANE FLUX WITH CONCENTRATION POLARIZATION

The effect of "concentration polarization" on retention was discussed in the previous section. In this section, it will be seen that concentration polarization can severely limit the flux. The control of polarization by proper fluid management techniques is essential to the economic feasibility of the process.

Without the development of an anisotropic UF membrane, UF would not be a commercial process today. The thin skin minimizes the resistance to flow, and the asymmetry of the pores virtually eliminates internal pore fouling. However, the hydraulic permeability of these membranes also increases the convective transport of solutes to the membrane surface. Consequently, the polarization modulus (defined as the ratio of the solute concentration at the membrane surface, C_s, to that in the bulk process stream, C_b) is higher than that experienced with lower permeability RO membranes.

This accumulation of solute at the membrane interface (see Figure 3.25 can severely limit the flux. In the case of RO, the salts retained have a significant osmotic pressure (π) and the effective pressure gradient is reduced by the osmotic pressure difference across the membrane ($\Delta\pi$), thereby reducing the flux. Some researchers have used this "osmotic pressure model" in an attempt to explain the effect of concentration polarization on UF membrane flux.[20-22] Even though the macromolecules and colloidal suspensions retained by UF membranes are quite large and have negligible osmotic pressures, it is argued that the high solute

concentrations at the membrane surface can result in an osmotic pressure difference across the membrane which should be taken into account. At present, the "gel-polarization model" appears to do a better job predicting the UF flux for a wider range of process streams than the "osmotic-pressure model". Therefore, the following treatment will neglect the osmotic pressure.

Gel-Polarization

If the transmembrane pressure drop (Δp) and the solute concentration in the bulk process stream (C_b) are high enough, the concentration at the membrane surface (C_s) can rise to the point of incipient gel precipitation forming a dynamic "secondary membrane" on top of the primary structure (see Figure 3.26). This "secondary membrane" can offer the major resistance to flow. In a stagnant "dead-ended" system, the gel layer will grow in thickness until the pressure activated convective transport of solute with solvent towards the membrane surface just equals the concentration gradient activated diffusive transport away from the surface. Thus, the flux in stagnant "dead-ended" systems is often so small as to be virtually nonexistent unless the bulk stream concentration is extremely low. Furthermore, by the very nature of the process, increased pressures will not help since the gel layer only grows thicker to offer more resistance to the increased driving force.

(8) $$Jw = \frac{\Delta P}{R_c + R_m}$$

where J_w = water flux (volume/time/membrane area)

ΔP = transmembrane pressure drop

R_m = hydraulic resistance of the membrane

R_c = hydraulic resistance of the deposited cake

Since R_m is a constant which can be calculated from the *pure* water flux, R_c can be calculated from the experimental flux. Figure 3.30 is a plot of the cake resistance (R_c) as a function of stirrer speed (in a stirred cell), protein concentration, and pressure. As the stirrer speed increases, the boundary layer thickness decreases (see Figure 3.25), thereby increasing the concentration gradient (dc/dx) for removal of the cake. Lower protein concentrations in the bulk (C_b) also increase the concentration gradient; the gel concentration at the membrane surface is fixed (C_g).

Effect of Pressure. One of the curious aspects of data like those in Figure 3.30 is that flux does not increase monotonically with pressure. Indeed, when flux is plotted versus pressure, as in Figure 3.31, the flux often becomes independent of pressure in the steady state.

When the pressure is increased, the flux does increase initially. The increase results in a higher rate of convective transport of solute to surface of the membrane. If the system is not "gel-polarized", the solute concentration at the surface (C_s) increases resulting in an increase in the concentration driven back diffusive transport away from the membrane. In fact, C_s will increase until the back-diffusive transport of solute just equals the forward convective transport.

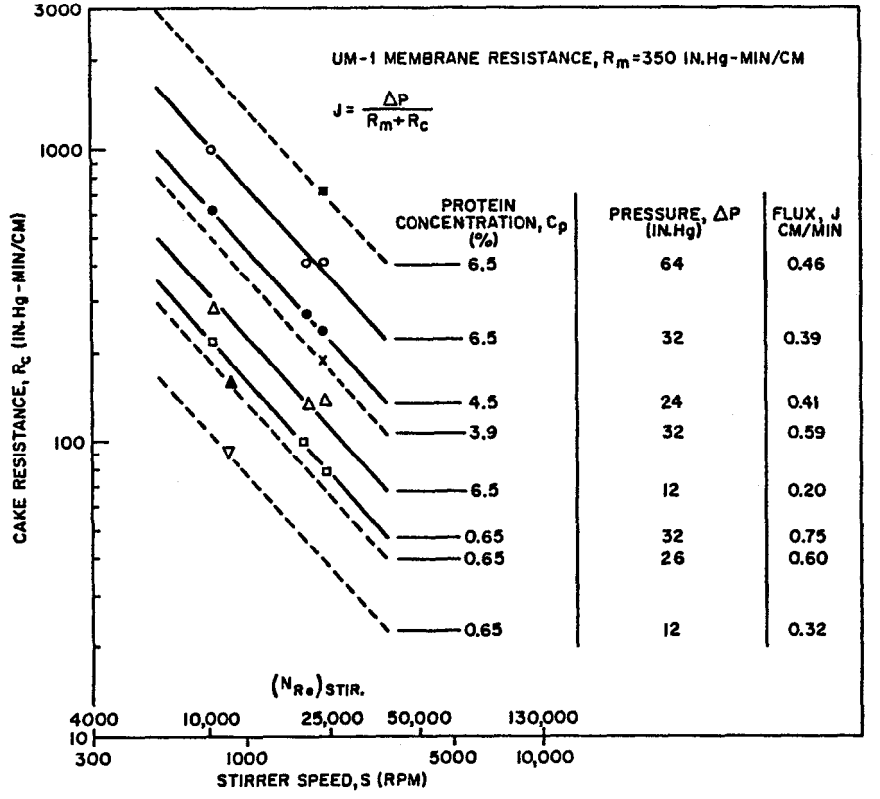


Figure 3.30: Gel (cake) resistance as a function of stirrer speed, protein concentration and pressure.

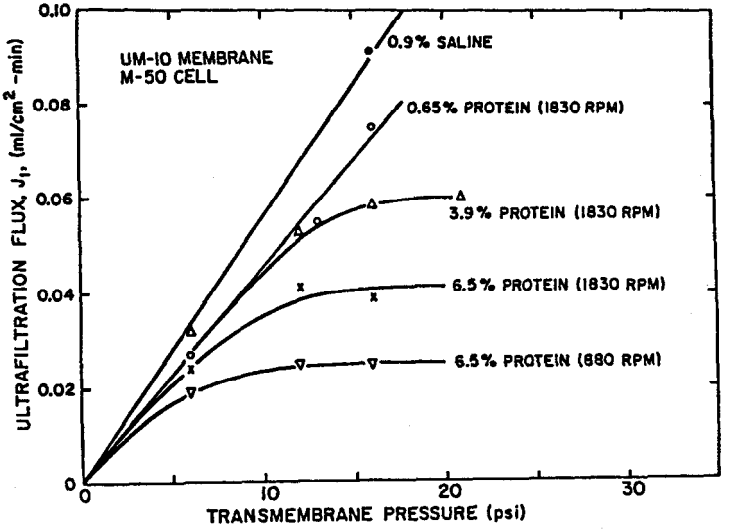


Figure 3.31: Effect of pressure on flux (flux becomes independent of pressure).

Eventually the concentration at the membrane surface will be high enough for a gel to form ($C_s = C_g$). Further increases in pressure will again temporarily increase the convective transport (J_c) to the membrane surface. However, since the surface concentration is at a maximum, the back diffusive transport will be fixed (assuming no changes in the fluid dynamics in the boundary layer), and solute will accumulate on the membrane. The gel layer will thicken or compact just compensating for the increased driving force (ΔP) by an equal increase in the resistance of the cake (R_c). The net result is that the flux will decrease to its original value in the steady state. Therefore, in the "gel-polarized regime", flux is independent of pressure and is solely determined by the back-diffusive transport.

In the steady state, the convective transport to the membrane must equal the back-diffusive transport away from the membrane.

$$JC = -D\frac{dc}{dx} \tag{9}$$

where J = solvent flux through the membrane

C = concentration of membrane retained solutes or colloids

D = solute diffusivity

x = distance from the membrane surface

In the gel-polarized regime, the boundary conditions are fixed:

C = C_b at large distances away from the membrane

C = C_g at the membrane surface.

Integrating Equation 9 assuming that the diffusivity (D) is constant

$$J = K \ln\left(\frac{C_g}{C_b}\right) \tag{10}$$

where K is the mass transfer coefficient:

$$K = \frac{D}{\delta} \tag{11}$$

and δ is the boundary layer thickness.

It is recognized that the diffusivity (D) is really a function of the concentration profile near the membrane surface. If one accepts an exponential mode of the diffusivity:

$$D = D_0 \exp(-\alpha C) \tag{12}$$

where D_o = diffusivity at infinite dilution

α = constant

If one integrates Equation 9 taking into account Equation 12, the final equation is considerably more cumbersome than Equation 10 without much gain

in accuracy.[23] Suffice it to say that the calculation of flux from Equation 10 will overestimate the flux slightly because the diffusivity in the boundary layer is lower than that at infinite dilution (D_o).

Equation 10 shows that the flux is independent of pressure in the gel polarized regime. Figure 3.31 shows that below some "threshold pressure" (P_t), flux still increases with pressure. Lower solute concentrations (C_b) have higher threshold pressures (P_t). Low solute concentrations favor a high back-diffusive transport of solute, and a much higher flux is required to transport enough solute to the membrane (JC) to begin to form a gel. This also means that the asymptotic flux in the gel-polarized region of Figure 3.31 is higher for lower protein concentrations; the concentration gradient (C_g-C_b) driving back-diffusive transport is higher.

Likewise, at the same concentration, higher stirrer speeds result in a higher asymptotic flux, because the boundary layer thickness (δ) has been reduced-increasing the mass transport coefficient (K) (see Equations 10 and 11). This also means that the threshold pressure (P_t) will be higher for higher stirrer speeds. The higher removal rate of solute from the membrane requires higher pressures and flux to carry enough solute to the membrane to form a gel.

Once the gel-layer is formed, it is often the limiting resistance to flow. Figure 3.32 shows two membranes with widely different membrane resistances (R_m). The pure water flux differs by a factor of 3.75; yet in the presence of protein (retained by both), the water flux differs by a factor of only 1.11, for pressures over the threshold pressure of 20 psi. It will be noted that the higher hydraulic permeability of PM 30 membrane results in a much lower threshold pressure (7 psi).

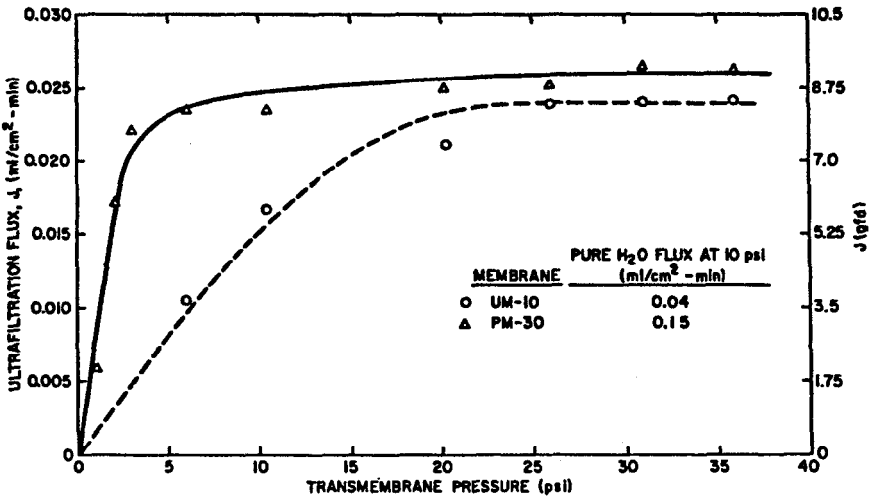


Figure 3.32: Limiting resistance of gel layer (vs membrane resistance).

Of course, Equation 10 applies to all forms of fluid management-cross-flow as well as stirred cells. For large scale systems, cross-flow techniques are preferred-where the feed stream flows tangential to the membrane surface (see

Figure 3.33). There is a pressure drop down the channel or tube which means that the first part of the channel may be gel-polarized; while the exit region may not be. (Usually, a restrictor is placed on the exit retentate stream to keep the exit pressure high so as to maximize flux throughout the channel length.) For laminar flow, the entrance region of the channel may not be gel-polarized either, because the boundary layer is not well developed at this point.

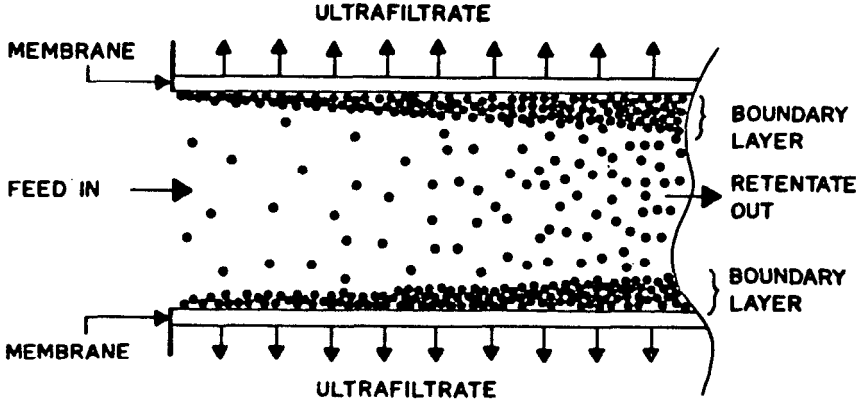


Figure 3.33: Cross-flow UF system.

Effect of Concentration. If Equation 10 applies, it should be possible to plot the solvent flux versus the logarithm of the concentration (C_b) and get a straight line with a negative slope equal to the mass transfer coefficient (K):

$$J = K \ln (C_g) - K \ln (C_b) \tag{13}$$

The form of Equation 13 has been demonstrated for a large number of macromolecular solutions and colloidal suspensions. The data of Figure 3.34 show the semilogarithmic variation of flux with concentration for two proteins and two colloidal suspensions. According to Equation 13, the intercept with the abscissa should occur when $C_b = C_g$. This provides a way of experimentally determining the gel concentration. The values obtained from Figure 3.34 are entirely reasonable. Many protein solutions reach their solubility limit between 25 and 35%. Likewise, for colloidal suspensions, the equivalent of a gel layer should be a layer of close packed spheres having a packing density between 60 and 75%.

The negative slope of each of the straight lines in Figure 3.34 is equal to the mass transfer coefficient which is a strong function of the stirrer speed or the tangential velocity across the membrane. Figure 3.35 shows increasing slopes with increasing recirculation rate (the volumetric flow rate of retentate recirculated back as feed to the channel, which is proportional to the tangential velocity across the membrane). All lines converge at zero flux where the concentration equals the gel concentration (C_g = 28%). Experimentally, it is difficult to carry out a concentration at constant cross-flow velocity (recirculation rate); the viscosity increases with concentration requiring constant adjustment of the pump. Some data in the literature show flux vs. log concentration *curves*. Often the reason for the curvature is the inconstancy of the recirculation rate; as the

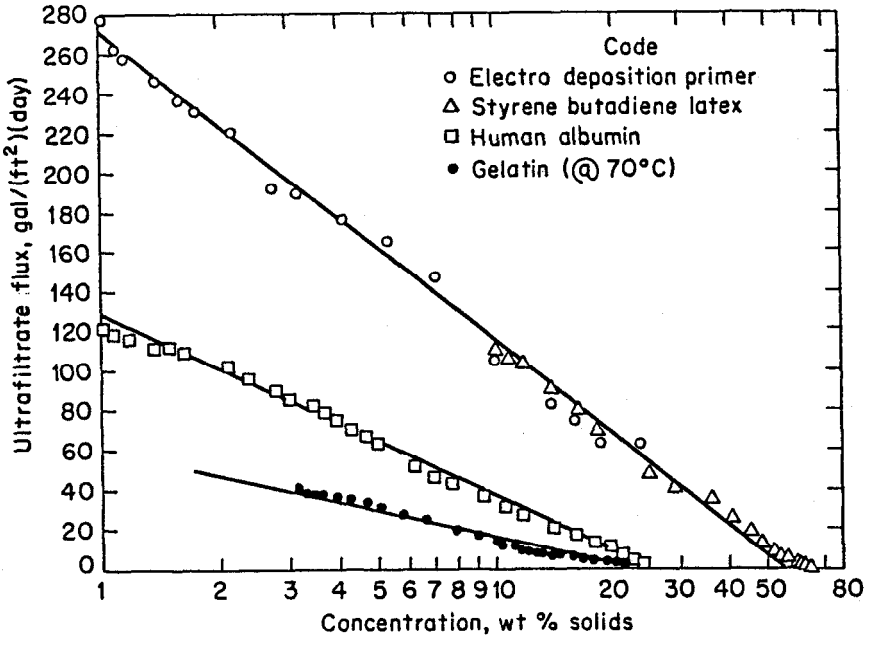


Figure 3.34: Semilogarithmic variation of flux with solute concentration.

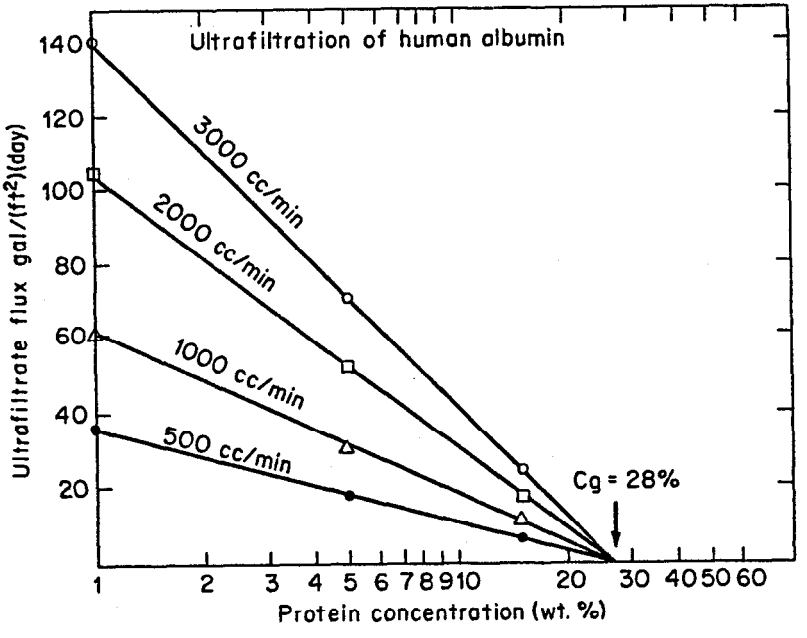


Figure 3.35: Effect of recirculation rate (cross-flow velocity) on flux variation with concentration.

process stream is concentrated, the recirculation rate decreases, and the flux drops to lower operating lines (see Figure 3.35). When the data are extrapolated to zero flux, the inconstancy of recirculation rate can lead to inaccurate estimates of the gel concentration (C_g).

In addition, if the data are not gel-polarized, Equation 13 will not plot as a straight line on semilog paper. The concentration at the surface of the membrane (C_s) is less than C_g and not constant. Therefore, at low pressures or low concentrations, some curvature is expected. In Figure 3.36, protein concentrations below 1% at high recirculation rates are not fully gel-polarized; the back-diffusive mass transport removes protein from the membrane surface at a high rate. Low recirculation rates (<2.5 GPM) have lower back-diffusive transport and are gel-polarized. All data on Figure 3.36 could be gel-polarized if the average transmembrane pressure were raised sufficiently. However, at extremely low solute concentrations, there is a ceiling on solvent flux due to the limiting hydraulic resistance of the membrane; eventually, the flux will reach an asymptotic value equal to the pure solvent flux of the membrane.

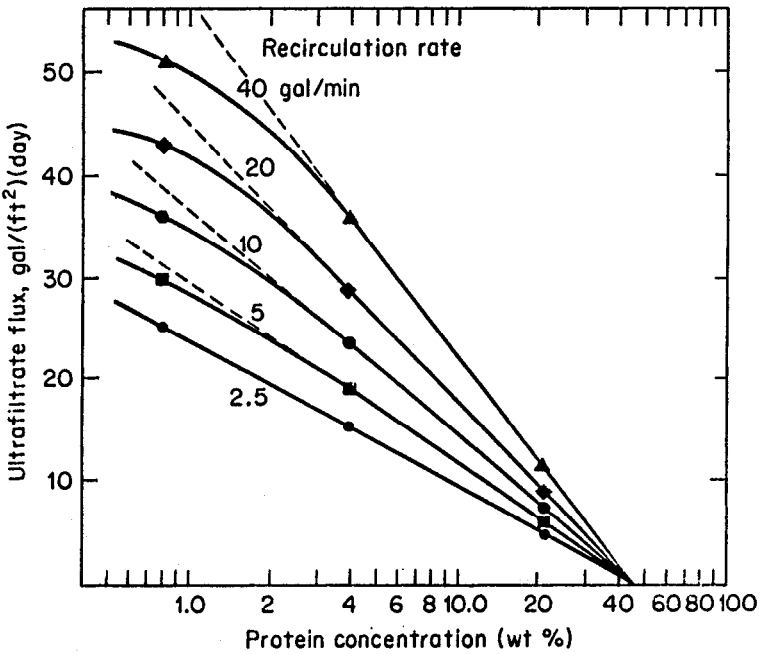


Figure 3.36: Variation from semi-log dependence in non gel-polarized regime.

Effect of pH. Comparing Figures 3.35 and 3.36, both showing flux data on human albumin solutions, it will be seen that the gel concentration is 28% in one case and 45% in the other. This reflects the difference in solubility of proteins for different conditions such as pH.

Since the isoelectric point of most proteins is between a pH of 4 and 5, it would be expected that operation in this pH range would result in the lowest gel concentration. Further, since changes in pH are not expected to change the

mass transfer coefficient (K), the operating lines in Figures 3.35 and 3.36 do not change in slope but are simply shifted to the left or right depending on the gel concentration (C_g). Thus, for a given concentration, there can be dramatic change in flux with pH.

Figure 3.37 shows the variation in the UF flux from cheese whey with pH. Notice the minimum at the isoelectric point.

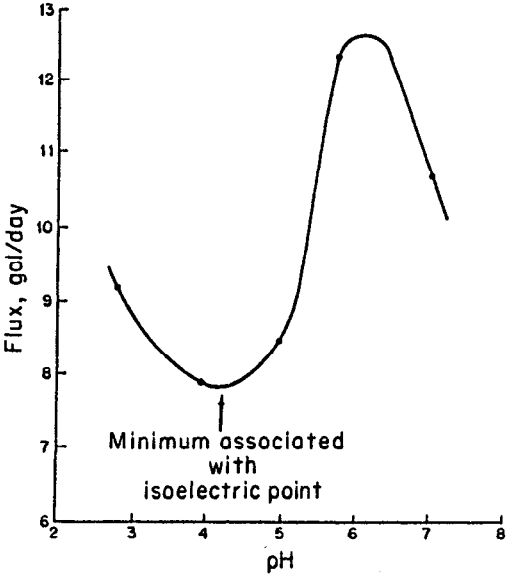


Figure 3.37: Effect of pH on flux (Cheshire cheese whey).

Evaluation of the Mass-Transfer Coefficient

It is clear from Equation 10 that the UF flux is determined largely by the mass-transfer coefficient (K). With proteins and other polyelectrolytes, we can modify the gel concentration (C_g) by altering the pH and/or ionic strength of the medium. However, for most process streams, that option is not permissable. Therefore, the optimization of flux is largely effected through the parameters that effect the mass transfer coefficient.

The mass transfer-heat transfer analogies well known in the chemical engineering literature make possible an evaluation of the mass transfer coefficient (K) and provide insight into how membrane geometry and fluid-flow conditions can be specified to optimize flux.[24]

Laminar Flow. The Graetz or Lévêque solutions[25,26] for convective heat transfer in laminar flow channels, suitably modified for mass transfer, may be used to evaluate the mass transfer coefficient where the laminar parabolic velocity profile is assumed to be established at the channel entrance but where the concentration profile is under development down the full length of the channel. For all thin-channel lengths of practical interest, this solution is valid. Lévêque's solution[26] gives:

(14) $$\mathrm{Sh} = 1.62\left(\mathrm{Re}\,\mathrm{Sc}\,\frac{d_h}{L}\right)^{0.33}$$

$$\text{for } 100 < \mathrm{Re}\,\mathrm{Sc}\,\frac{d_h}{L} < 5000$$

where Sh = Sherwood Number = Kd_h/D
Re = Reynold's Number = Ud_h/ν
Sc = Schmidt Number = ν/D
d_h = equivalent hydraulic diameter
L = channel length
U = average velocity of fluid
ν = kinematic viscosity = μ/ρ
μ = viscosity of fluid
ρ = density of fluid

or

(15) $$K = 1.62\left(\frac{UD^2}{d_hL}\right)^{0.33}$$

for flat rectangular channels, where $d_h = 2b$; (b = channel height).

(16) $$K = 0.816\left(\frac{6\,UD^2}{bL}\right)^{0.33}$$

or

(17) $$K = 0.816\left(\frac{6\,QD^2}{b^2wL}\right)^{0.33}$$

where Q = the volumetric flow rate
w = the channel width

More generally,

(18) $$K = 0.816\left(\frac{\dot{\gamma}}{L}D^2\right)^{0.33}$$

where $\dot{\gamma}$ = the fluid shear rate at the membrane surface
= 6U/b for rectangular slits
= 8U/d for circular tubes

A review of Equations 14-18 shows that the flux (or mass transfer coeffi-

cient) may be increased by increasing the channel velocity (U or Q) or by decreasing the channel height (b). In more general terms, any fluid management technique which increases the fluid shear rate ($\dot{\gamma}$) at the membrane surface will increase the flux.

Indeed, Equation 18 shows that in laminar flow, for a fixed bulk stream concentration (C_b), the flux should vary directly as the cube root of the wall shear rate per unit channel length. This has been confirmed for a large number of solutions ultrafiltered in a variety of channel geometries (see Figure 3.38).

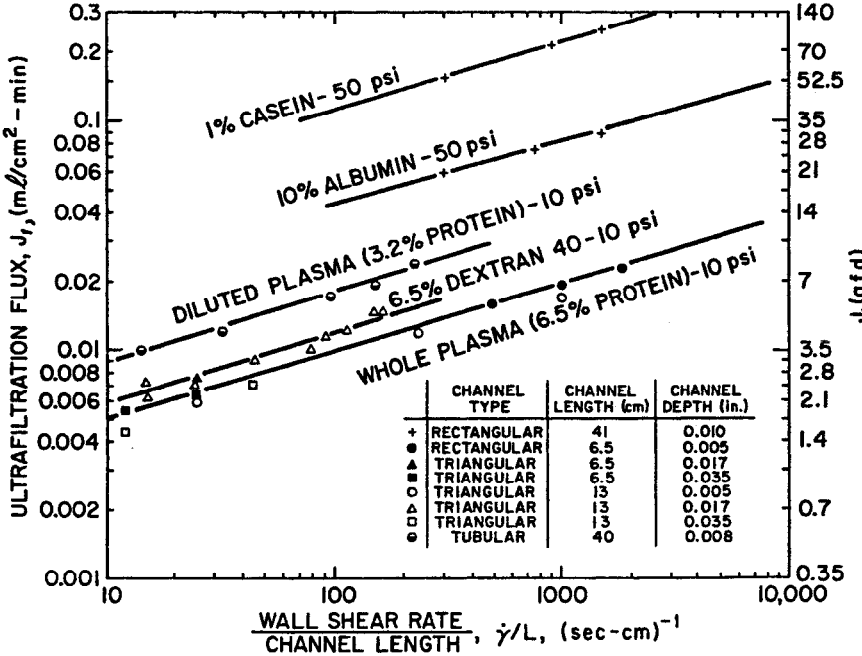


Figure 3.38: Experimental confirmation of 0.33 power dependence of flux on wall shear rate/channel length (in laminar flow).

In laminar flow, the channel length (L) is important because the boundary layer develops as fluid moves down the channel. Longer channels have a thicker boundary layer (at the end) which reduces the back diffusive transport. Consequently, the average flux is lower. This would argue for shorter channel lengths. In practice, this is not cost effective since a significant portion of the cost of manufacturing a module is associated with potting or connecting the channels/tubes to a common "header". Short channel lengths mean a high cost per unit of membrane area.

Turbulent Flow. Perhaps the best known heat-transfer correlation for fully developed turbulent flow is that owing to Dittus and Boelter.[27] The mass transfer analogy based on the Dittus-Boelter correlation is:

(19) $$Sh = 0.23\ Re^{0.8}\ Sc^{0.33}$$

(20) $$K = 0.023 \left(\frac{U^{0.8} D^{0.67}}{d_h^{0.2} \upsilon^{0.47}} \right)$$

It can be argued that any turbulent flow correlation should not be applied for Re <10,000. However, in current thin-channel ultrafiltration devices, the entrance geometry is such that fully developed turbulent flow occurs at much lower Reynold's numbers. Measurements of fluid velocity versus pressure drop show a definite transition from laminar to fully developed turbulent flow at Re = 2000.

For flat rectangular channels where $d_h = 2b$, Equation 20 becomes:

(21) $$K = 0.02 \left(\frac{U^{0.8} D^{0.67}}{b^{0.2} \upsilon^{0.47}} \right)$$

or

(22) $$K = 0.02 \left(\frac{Q^{0.8} D^{0.67}}{b\, w^{0.8} \upsilon^{0.47}} \right)$$

As in laminar flow, the flux (or mass transfer coefficient) may be increased by increasing the channel flow rate (Q) and by decreasing the channel height (b). The effect is, however, much more dramatic in turbulent flow-the flux varying with flow rate to the 0.8 power and inversely with channel height. Furthermore, the flux is independent of channel length since both the velocity and concentration profiles are established rapidly in the entrance region of the channel. Again as in laminar flow, most of the ultrafiltration data taken on solutions in turbulent flow are in good agreement with theory, i.e., with the Dittus-Beelter correlation. For example, the turbulent flow data of Figure 3.39 show a 0.75 power dependence of flux on recirculation rate (Q) in good agreement with the predicted 0.8 power. (The 10-mil channel data were taken in laminar flow, whereas the 30-mil channel data were taken in turbulent flow.)

The laminar flow data of Figure 3.39 have a higher slope (0.52 than predicted by theory (0.33)-probably because of "secondary flow effects". The data were taken in a spiral flow thin channel device. Whenever fluid passes through a curved tube or channel, centrifugal forces tend to throw fluid outward from the center of the channel. It then recirculates inward along the walls of the channel (see Figure 3.40). It is well known that coiled tube heat exchangers possesses superior heat transfer characteristics because of secondary flow effects.

At small curvatures, the Dean number (De) governs the transport processes in coiled tubes and channels:

(23) $$De = Re \sqrt{\frac{a}{R}}$$

where a and R are tube and coil radii respectively. Dravid et al[28] has shown experimentally that the heat-transfer coefficient in a coiled tube varies as $De^{0.55}$ in

the fully developed region of the boundary layer. By analogy, the mass-transfer coefficient for laminar flow in a spiral channel should vary as $Re^{0.55}$ rather than as $Re^{0.33}$. This is precisely what occurs in the data of Figure 3.39.

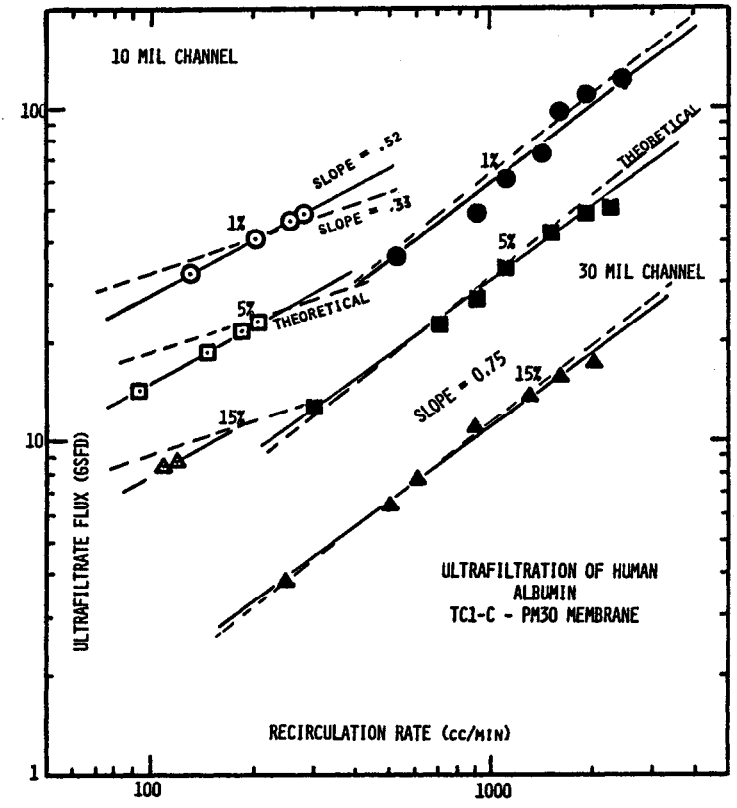


Figure 3.39: Experimental confirmation of 0.8 power dependence of flux on recirculation rate (in turbulent flow).

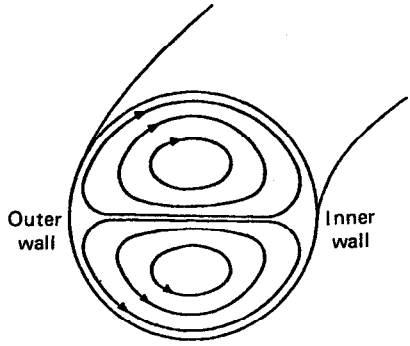


Figure 3.40: Secondary flow patterns in helically coiled tube.

Theoretical Prediction of Flux

The success of the Lévêque and Dittus-Boelter relationships in indicating the variation (power dependence) of ultrafiltrate flux with channel geometry and fluid velocity for macromolecular solutions is gratifying. The more crucial test of the theory, of considerable interest to the design engineer, is whether these relationships can be used to calculate *quantitatively* the ultrafiltrate flux knowing the channel geometry, fluid velocities and solute characteristics.

Macromolecular Solutions. Figure 3.39 shows that agreement between theoretical and experimental values is good in at least some cases (i.e., spiral flow channel plates). Equation 17 for laminar flow and Equation 22 for turbulent flow were used to calculate the mass-transfer coefficient (K). The diffusivity of albumin ($D = 6 \times 10^{-7}$ cm^2/sec) was obtained from a handbook.[29] The gel concentration (C_g) was determined experimentally from data like those in Figure 3.35. Although the slope in laminar flow was 0.52 compared with the theoretical slope of 0.33, the experimental values were still well within 25% of the theoretical values. Agreement in the turbulent regime is more striking. The accuracy of the Lévêque and Dittus-Boelter relationships has also been verified in linear thin-channel tubular equipment ultrafiltering protein solutions. Figure 3.41 presents laminar flow data from 15-mil channel tubes compared with theoretical values using a diffusivity of 6×10^{-7}cm^2/sec and a gel concentration of 45% as determined from Figure 3.36. Again, experimental and theoretical values agree within 25% although the theoretical values are consistently lower.

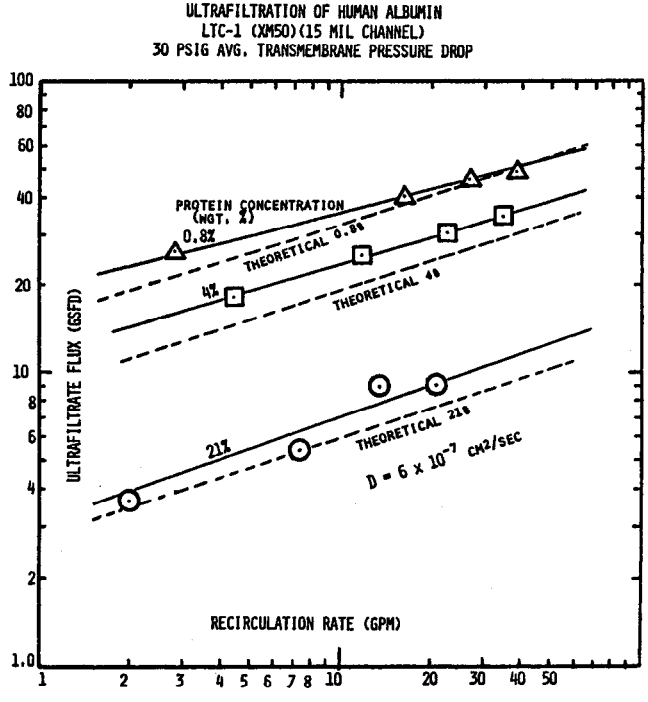


Figure 3.41: Theoretical vs experimental values of flux with recirculation rate (in laminar flow).

The ability of the Lévêque solution to adequately describe the variation in flux with diffusivity of the retained solute is illustrated in Figure 3.42. Here, albumin data were compared with whole serum data. The larger globulins in whole serum have a lower diffusivity $D = 4 \times 10^{-7}$ cm^2/sec[29] and a lower solubility limit (C_g). The theoretical curves are 15 to 20% below the experimental data in both cases. Thus, the dependence of flux on diffusivity to the 0.67 power is confirmed.

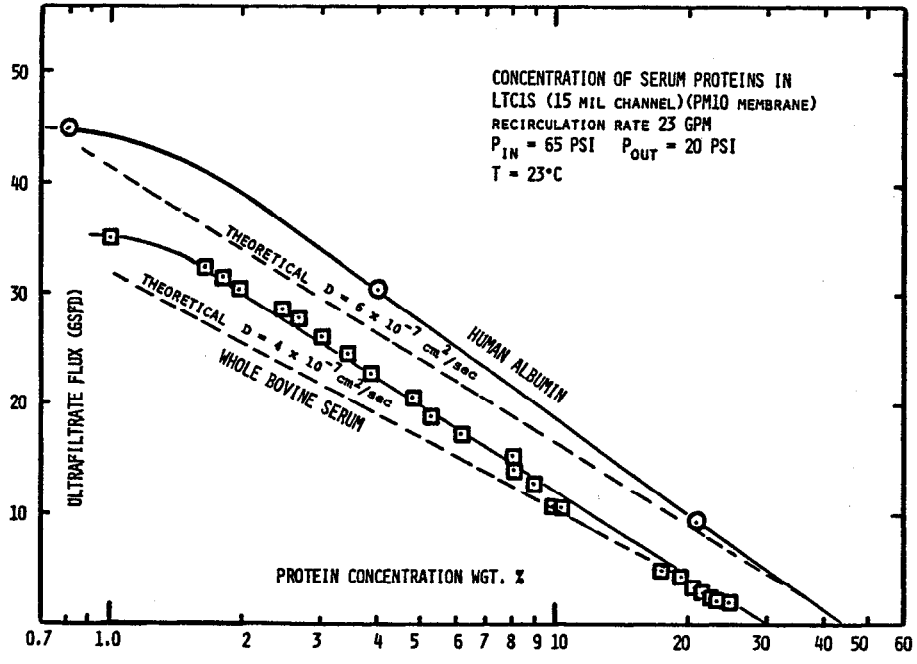


Figure 3.42: Variation in flux with diffusivity of retained solute.

Other macromolecules in solution seem to fit the gel-model as well as protein solutions. For example, data from the literature[30] on the ultrafiltration of polyethylene glycol (Carbowax 20 M) solutions in one inch diameter tubular membranes operating in turbulent flow are plotted along with theoretical flux values, in Figure 3.43. The theoretical values were calculated using a diffusivity of 5×10^{-7} cm^2/sec[31] and a gel concentration of 7.5%.[30] The agreement between theoretical and experimental values is within 14 to 27% at the higher and lower Reynold's numbers, respectively.

Colloidal Suspensions. The agreement between theoretical and experimental ultrafiltration rates for *macromolecular solutions* can be said to be within 15 to 30%. For colloidal suspensions, experimental flux values are often one to two orders of magnitude higher than those indicated by the Lévêque and Dittus-Boelter relationships.

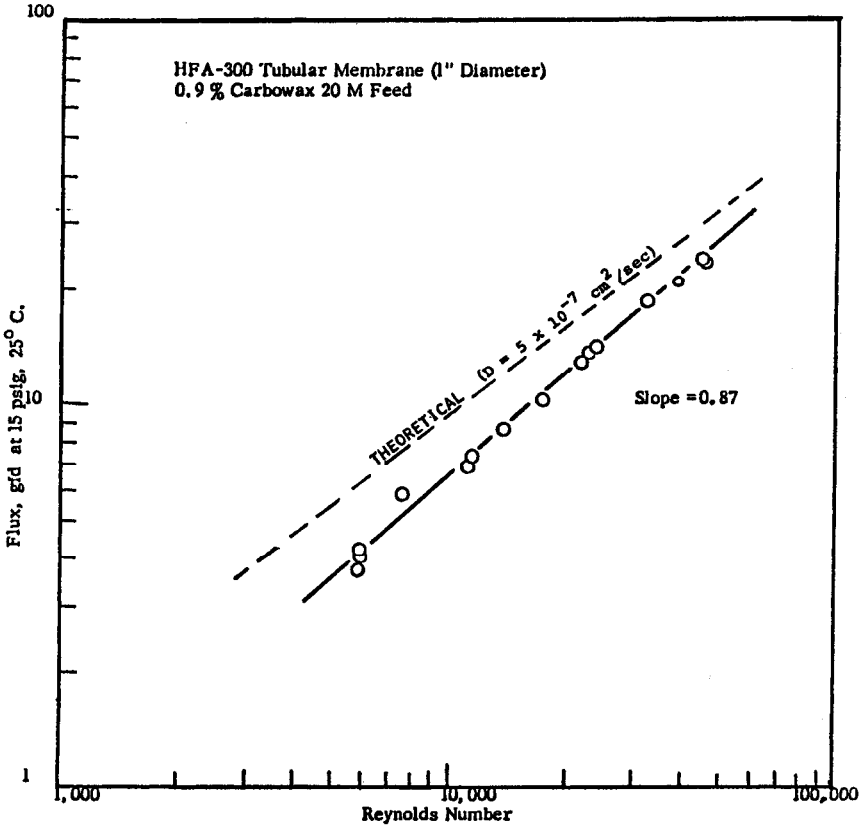


Figure 3.43: Theoretical vs experimental values of flux for 0.9% polyethylene glycol solution.

Equations 17 and 22, for laminar and turbulent flow respectively, both indicate that the mass transfer coefficient should vary with the diffusivity of the retained solute to the 0.67 power. That this is the case for macromolecules in solution was shown in Figure 3.42.

The Stokes-Einstein relation for diffusivity is:

$$D = \frac{kT}{6\pi\mu r_p} \qquad (24)$$

where k = Boltzman constant (i.e., the molar gas constant divided by the Avogadro number) = 1.380×10^{-16} erg deg^{-1}

T = Absolute temperature °K

μ = viscosity in poise

r_p = radius of the particle diffusing in cm

Macromolecules of higher molecular weight will have larger particle dimensions and lower diffusivities. For example, protein diffusivities of interest in this chapter are as follows:

Protein	M.W.	$D_{20°C}$ $cm^2/sec.$
Albumin	65,000	6×10^{-7}
γ globulin	170,000	4×10^{-7}
Collagen (gelatin)	345,000	0.7×10^{-7}

These proteins should exhibit decreasing flux rates in the order given, and this can be seen in Figures 3.34 and 3.42. Referring to Equation 24, one would expect that the ultrafiltration rate from whole blood, including the 8 μ red cells, should be considerably less than that from the plasma above. That such is *not* the case is illustrated in Figure 3.44.

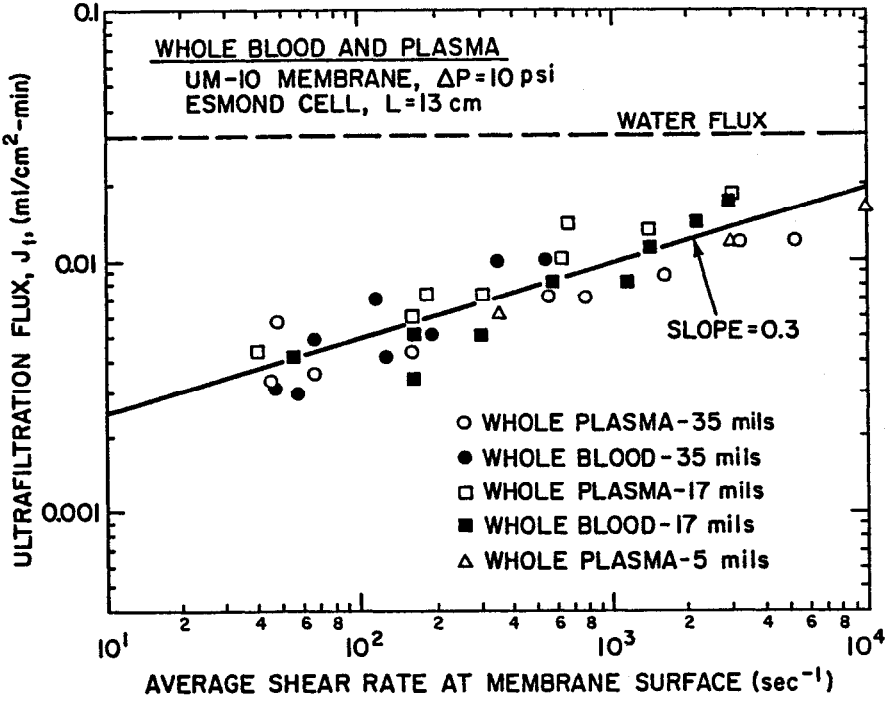


Figure 3.44: UF of whole blood and plasma.

Likewise, the polymer latex data of Figure 3.34 have a much higher slope (mass transfer coefficient) than would be expected from the latex particle diffusivity. Monodisperse polystyrene latexes have both suspension viscosities and

sedimentation coefficients in good agreement with the predicted Stokes-Einstein diffusivity. The Stokes-Einstein diffusivity was calculated to be 2.3×10^{-8} cm^2/sec for a carboxylic modified styrene-butadiene copolymer latex which had an average particle size of 0.19 μ. This is in good agreement with other values reported in the literature.

The gel concentration of this material has been determined to be 75% for numerous thin-channel runs in both tubular (see Figure 3.45) and spiral flow equipment.

Using the values cited above for the diffusivity (D) and the gel concentration (C_g), the theoretical flux is plotted for the 40 GPM recirculation rate in Figure 3.45 (thin-channel tubes) and found to be 1/38 of the experimental thin-channel tube value! Even if the calculated diffusivity were an order of magnitude larger, the theoretical flux would still be less than 1/8 of the experimental value!

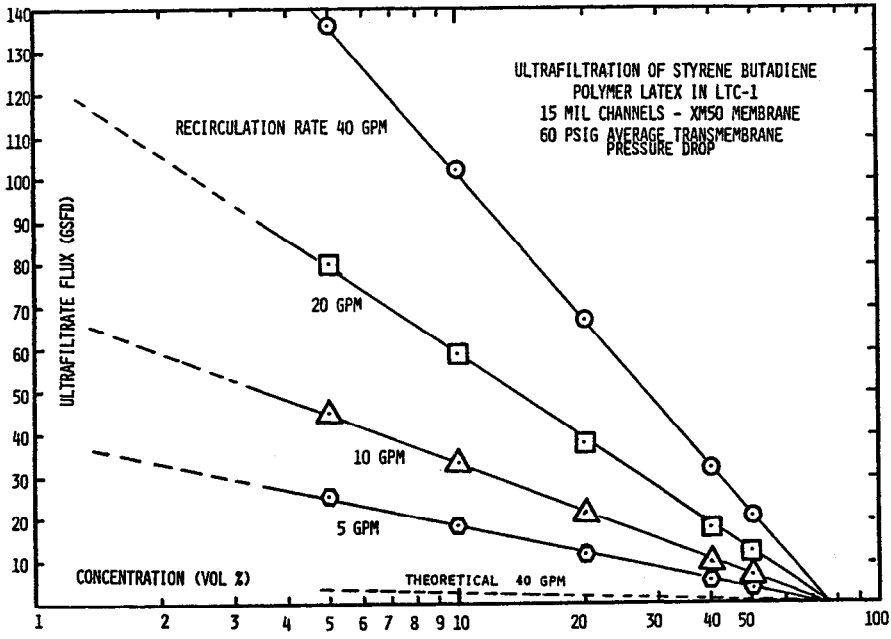


Figure 3.45: UF of styrene butadiene polymer latex showing disparity between experimental results and theoretical prediction.

Flux vs. recirculation rate data for a thin-channel tubular unit are plotted in Figure 3.46. Theoretical values are also plotted assuming laminar and turbulent flow. Most of the data on this plot (below 30 GPM) are taken at Reynold's numbers below 2000 and therefore assumed to be in laminar flow. The discrepancy between the experimental flux value and theoretical laminar flow value is a factor of 38 at 40 GPM and a factor of 15 at 5 GPM! If the assumption is made that these data were taken in turbulent flow (completely unwarranted), the slope is more nearly that indicated by theory, but the discrepancy is still a factor of 7.5 at all recirculation rates.

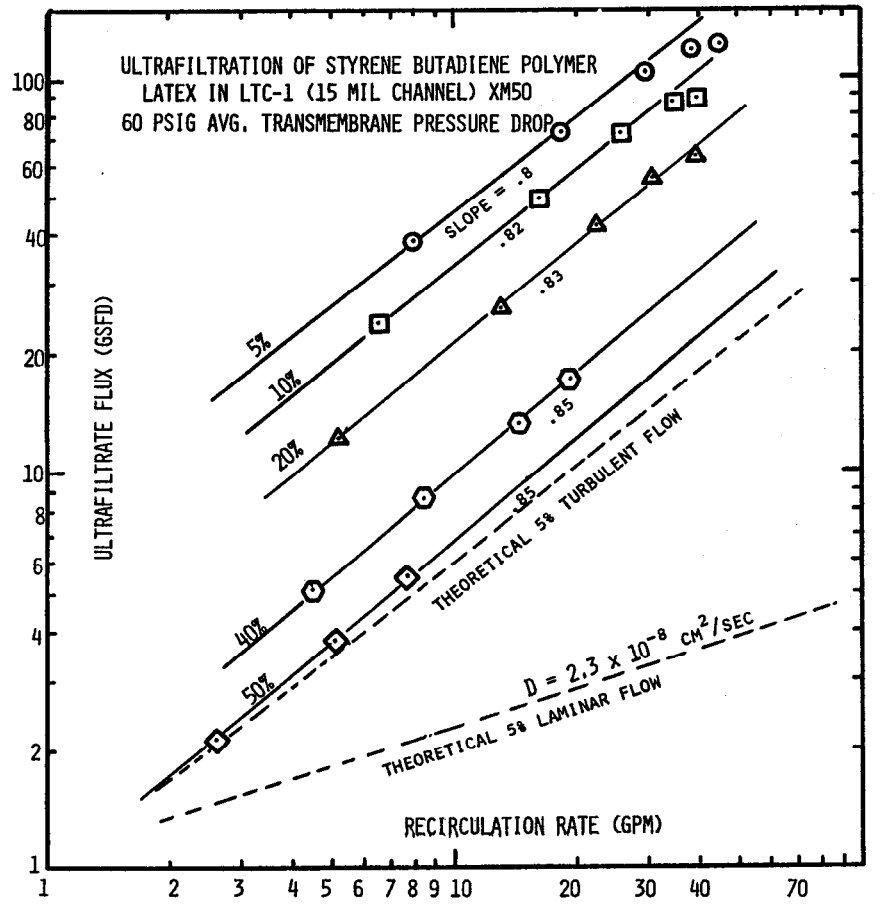


Figure 3.46: Flux vs recirculation rate in linear thin channels (styrene butadiene polymer latex).

The gross discrepancy between theoretical and experimental flux values also exists in data obtained from spiral flow thin-channel equipment (see Figure 3.47). In these data, the transition from laminar flow is clearly seen (change in slope) at Reynold's numbers only slightly below 2000. However, there is no abrupt change in flux, as calculated from theory, suggesting that the data labeled "turbulent flow" may be in a more nebulous transition region between laminar and turbulent flow. The experimental slopes tend to be higher than the theoretical slopes in both laminar and turbulent flow except for the laminar flow data at 1% concentration which follows the predicted $\frac{1}{3}$ power dependence. Again, the gross failure of the theory in estimating experimental values is evident. The experimental laminar flow values are a factor of 19–29 higher than the theoretical values whereas the experimental turbulent flow values are a factor of 8–15 higher than the theoretical values.

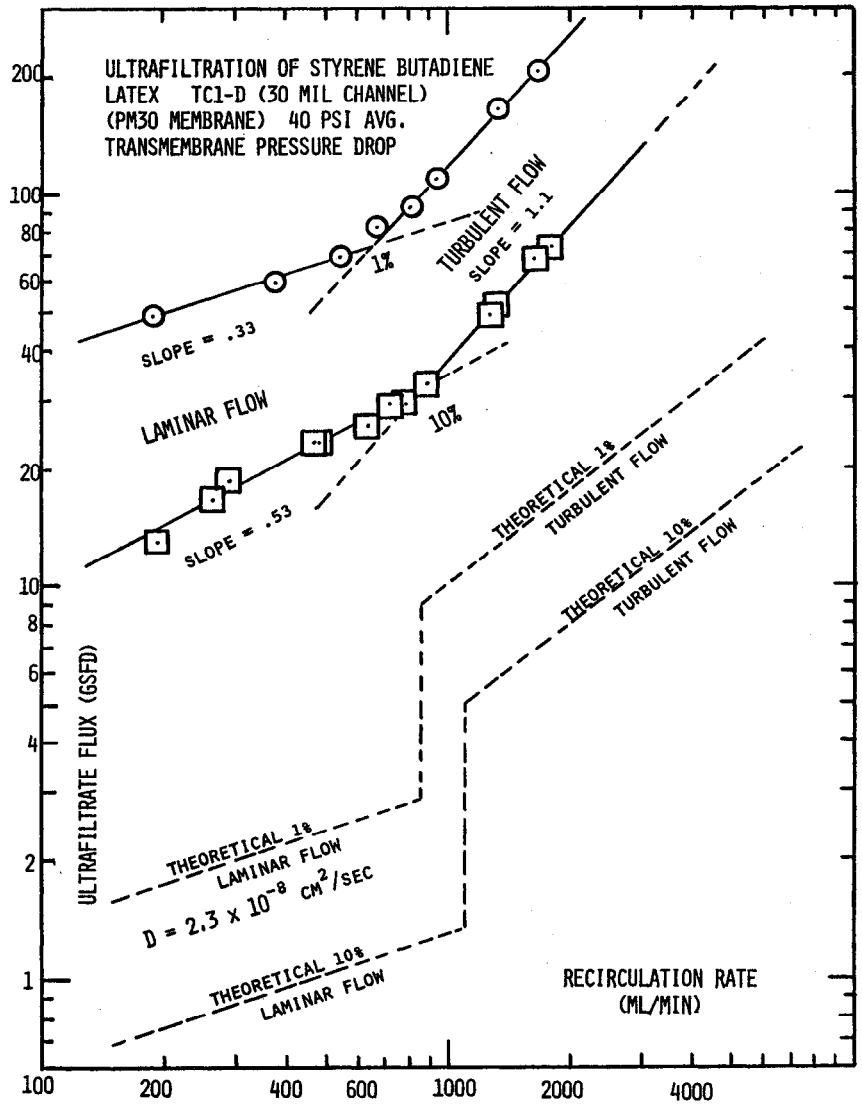


Figure 3.47: Flux vs recirculation rate in spiral thin channels (styrene butadiene polymer latex).

An evaluation of more than 40 different colloidal suspensions in our laboratories has indicated that the diffusion coefficient calculated from the ultrafiltrate flux using the Lévêque or Dittus-Boelter relationships is generally from one to three orders of magnitude higher than the theoretical Stokes-Einstein diffusivity.

It is evident from the above that minor adjustments in molecular parameters

such as diffusivity, kinematic viscosity, or gel concentration are incapable of resolving order of magnitude discrepancies.

Similar discrepancies were noted by Blatt et al[32] for colloidal suspensions such as skimmed milk, casein, polymer latexes, and clay suspensions. Actual ultrafiltration fluxes are far higher than would be predicted by the mass transfer coefficients estimated by conventional equations, with the assumption that the proper diffusion coefficients are the Stokes-Einstein diffusivities for the primary particles. Blatt concluded that either (a) the "back diffusion flux" is substantially augmented over that expected to occur by Brownian motion or (b) the transmembrane flux is not limited by the hydraulic resistance of the polarized layer. He favored the latter possibility, arguing that closely packed cakes of colloidal particles have quite high permeabilities. However, this is not a plausible hypothesis for the following reasons:

(1) If the gel layer is not the limiting resistance to flow, the membrane must be, and the flux should be proportional to the transmembrane pressure drop. Experimental data deny this-showing threshold pressure (above which flux is independent of pressure) (see Figure 3.48).

(2) If the gel layer is not the limiting resistance to flow, the layer will continue to grow until the channel is completely full of 75% solid material-resulting in a drop in recirculation rate with time. Thin channel tubes and spiral flow modules running continuously at constant latex feed concentration and pressure drop for periods approaching one year have shown no decreases in recirculation rate or accumulation of polymer latex in the channels.

These observations lead to the conclusion that the back-diffusive transport of colloidal particles away from the membrane surface into the bulk stream is substantially augmented over that predicted by the Lévêque or Dittus-Boelter relationships. It is known that colloidal particles flowing down a tube tend to migrate across the velocity gradient toward the region of maximum velocity; this is called the "tubular pinch effect".

Tubular Pinch Effect. The lateral movement of particles across the streamlines in laminar flow was first observed and recorded in 1836 by Poiseville. He noted that the region immediately adjacent to the walls of blood capillaries tends to be free of blood cells.

This phenomenon also explains why many colloidal suspensions exhibit less frictional pressure drop than would be expected from the fluid viscosity. The apparent viscosities of such suspensions vary with tube radius, length, and flow rate.[33] To account for such anomalies it has been postulated that there exists a lubricating particle-depleted ("plasmatic") layer at the wall of vessels in which there is a nonuniform shear field. For example, blood flowing through fine glass capillaries reaches an equilibrium state in which the red cell concentration in the tube is less than that in the inflowing or outflowing blood-presumably the result of axial drift of red cells and their consequent faster average transit than plasma. Palmer[34] was able to skim off a plasma rich layer at the wall through fine branches and was able to measure increases in hematocrit from near the wall to the axial region.

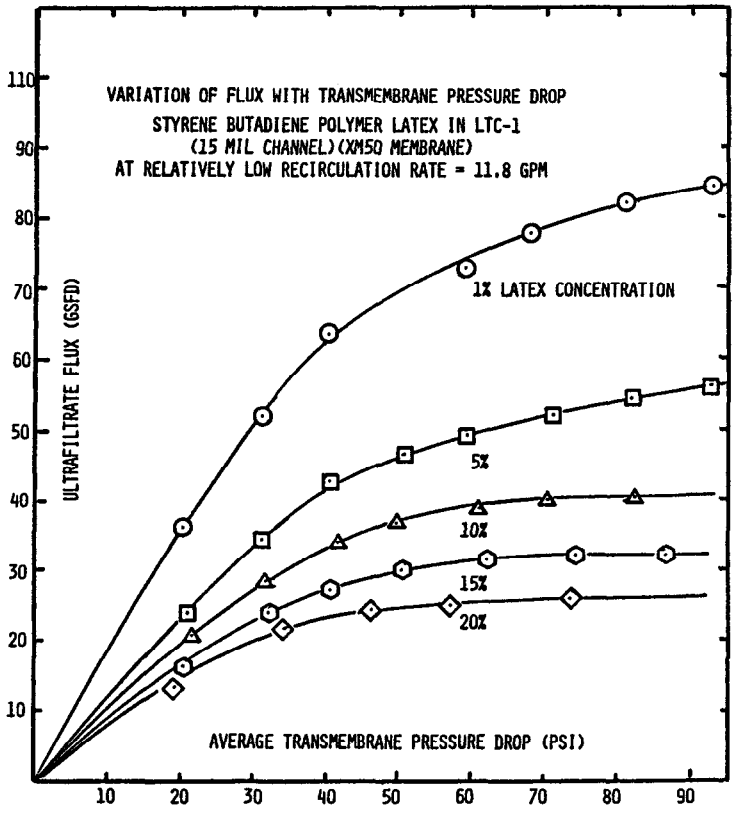
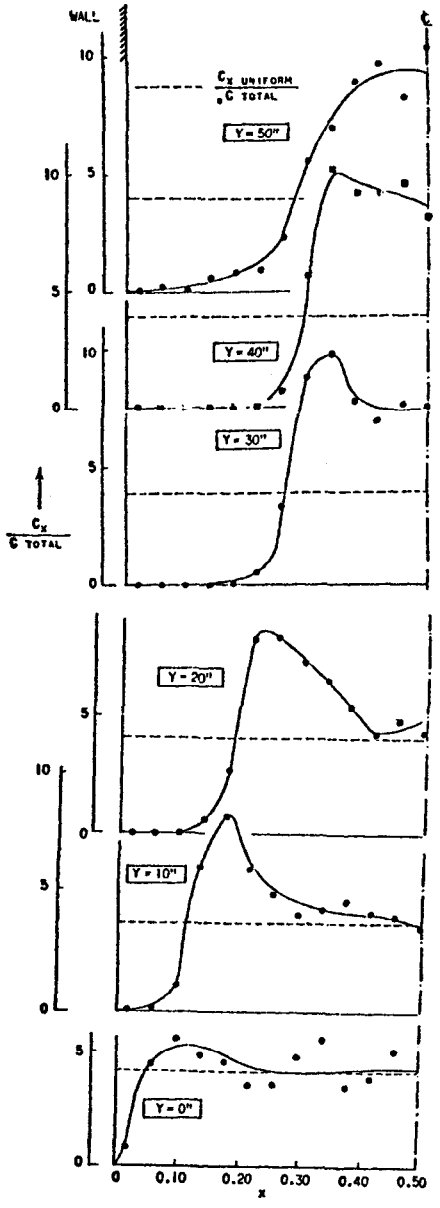


Figure 3.48: Independence of flux on pressure (styrene butadiene polymer latex).

Segré and Silberberg[35,36] *working with dilute suspensions of rigid spheres,* were the first to publish their observations of the "tubular pinch effect", where the particles migrated away both from the tube wall and the tube axis reaching equilibrium at an eccentric radial position. At this position, the spheres became regularly spaced in chains extending parallel to the tube axis. The observations of Segré and Silberberg have spawned a number of theoretical and experimental studies investigating the effect and analyzing the cause. The "tubular pinch effect" has also been observed experimentally for suspensions of rubber disks, carbon black, polystyrene spheres, PVA spheres, aluminum-coated nylon rods, elastomer filaments, aluminum particles, insoluble salts, glycerol and silicone oil in various continuous flowing media.

One of the more spectacular visual studies was made by Brandt and Bugiarello.[37] They made direct photographic observations of small Dylite spherical beads suspended at concentrations of 1.7 to 5% in a glycerin-water solution and flowing in laminar flow (Re from 400 to 1640) through long rectangular channels made of Plexiglass. The ratio of the channel width to the bead diameter was 25.6. Figure 3.49 gives the average half-channel particle distribution (obtained photographically) expressed as the ratio of the number of particles per band (C_x) to the total number of particles (C_{total}) in the entire channel width.



Particle distributions. $\bar{C}_{avg} = 5.0\%$; $Q = 20$ cm^3 sec^{-1}.

Figure 3.49: Particle migration to center line of flowing channel (tubular pinch effect). Brandt and Bugliarello (1966).

The plots show very clearly the migration of particles to the center of the channel as the distance (Y) from the inlet of the channel increases. Brandt and Bugliarello found that the process was accelerated by increases in flow rate and delayed by increases in average concentration.

Colloidal particles are large enough that any given particle, not in the center of the tube, will experience a pressure difference across its diameter due to the higher velocity on one side than on the other. Thus, the particle will experience a "lift-force" tending to move it away from the wall toward the center of the channel. This "lift-force" is not unlike the aerodynamic lift on an airfoil due to the "Bernoulli effect".

The Navier-Stokes equation has been solved By Cox and Brenner (unpublished data) who computed the lateral force required to maintain a sphere at a fixed radial position (r). They used Stoke's law for the neutrally buoyant case:

$$V = \frac{1}{2} U \, \mathrm{Re} \left(\frac{r_p}{R}\right)^3 F\left(\frac{r}{R}\right) \tag{25}$$

where V is the radial migration velocity

U is the average fluid velocity down the channel or tube

Re is the Reynold's number

r_p is the particle radius

R is the tube radius

r is the radial position of the particle in the tube

F(r/R) is a function of the radial position of the particle in the tube or channel.

Equation 25 has the same form as the *empirical equation* used by Segré and Silberberg[36] to correlate their data:

$$V = 0.17 \, U \, \mathrm{Re} \left(\frac{r_p}{R}\right)^{2.84} \frac{r}{R}\left(1 - \frac{r}{r^*}\right) \tag{26}$$

where r^* is the equilibrium radial position of the particle which was found to decrease as (r_p/R) increased.

The tubular pinch effect can explain much of the anamolous UF data for colloidal suspensions. With UF, the water flux through the porous wall will still carry particles to the wall, but the "lift" of particles away from the wall (due to the tubular pinch effect) will certainly augment the back diffusive mass transfer described by the Lévêque and Dittus-Boelter relationships.

Equations 25 and 26 both predict a radial migration velocity (V) increasing as the *square* of the cross-flow velocity (U) [The Reynolds Number (R_e) also includes U). This can explain why the dependence of UF flux on cross-flow velocity (U) can be higher than 0.33 in laminar flow and 0.75 in turbulent flow (e.g., see Figures 3.50 and 3.51).

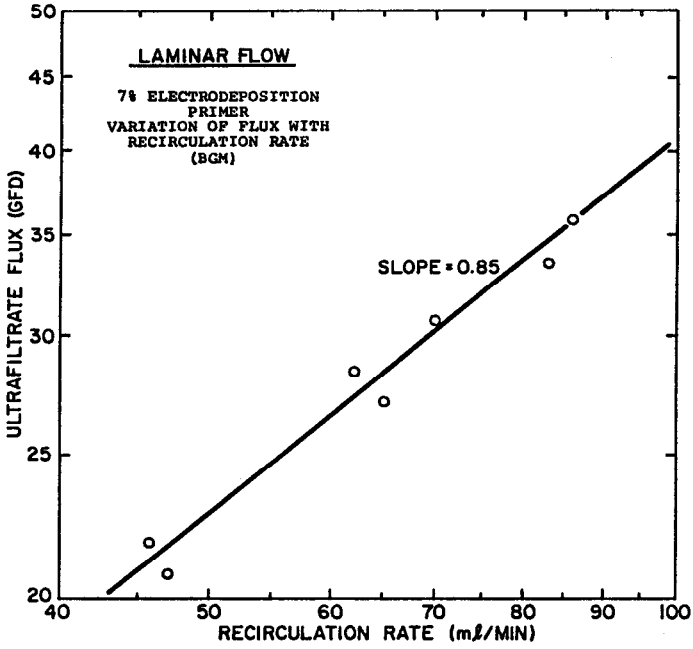


Figure 3.50: UF of electrodeposition primer (0.85 power dependence on recirculation rate in laminar flow).

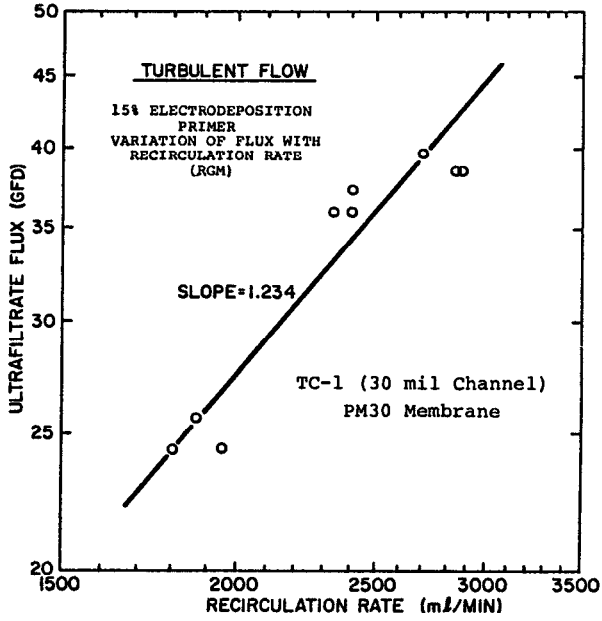


Figure 3.51: UF of electrodeposition primer (1.23 power dependence on recirculation rate in turbulent flow).

The data of Figure 3.44 show similar flux values for whole blood and plasma. Presumably, the tubular pinch effect tends to depolarize the membrane surface of red cells yielding a flux similar to that obtained with plasma alone. In some cases, the flux with the red cells present is higher than that with plasma alone. The migration of the larger red cells away from the membrane surface tends to drag the plasma proteins along.

Bixler et al[38] found that adding glass and plastic beads (ranging in size from 30 to 100 μ) to a protein solution augmented the UF flux (see Figure 3.52). He attributed this to (1) the mixing action of the particles and (2) the mechanical scouring of the membrane surface.

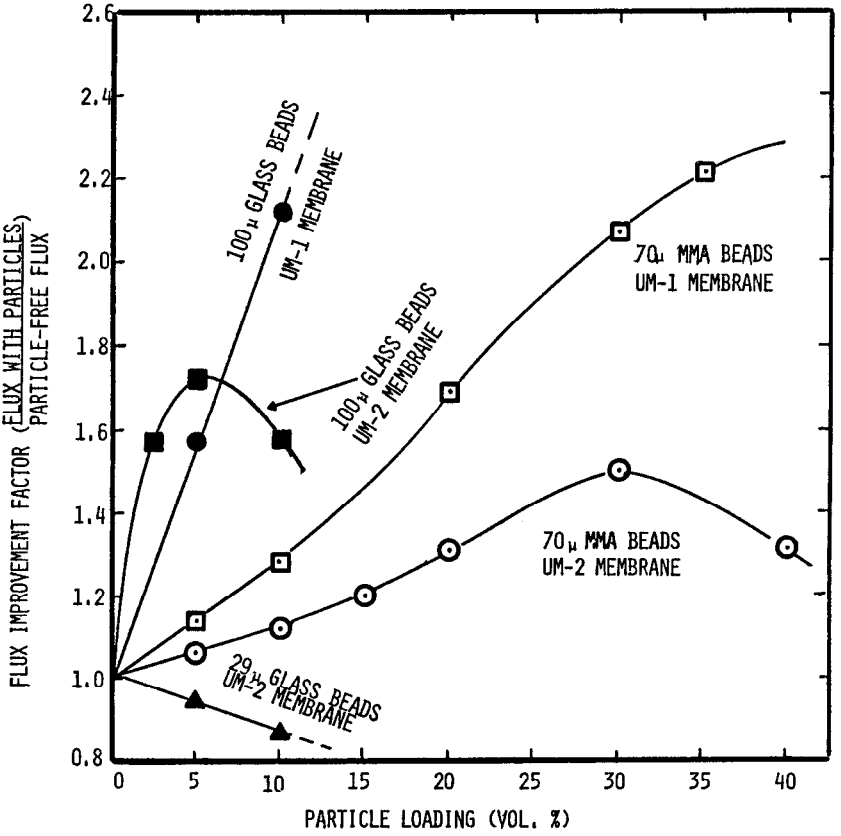


Figure 3.52: Enhancement of protein flux with particle addition.

Equations 25 and 26 also predict that the radial migration velocity (V) will increase as the tube radius (R) decreases. Thin channels are more effective in depolarizing the membrane surface via the tubular pinch effect. This may explain the larger discrepancies between experimental and theoretical flux values in 15 mil channels (see Figure 3.46) than in 30 mil channels (see Figure 3.47).

Green and Belfort[39] have combined the equations for particle migration due to the tubular pinch effect with the normal back-diffusive transport to calculate

flux values which are closer to the experimental results. A step-wise iterative procedure was used to calculate a detailed particle trajectory analysis. Unfortunately, these complex theoretical calculations still come short of accurately predicting the experimental flux from various colloidal suspensions.

Augmented Cross-Flow Effects

Other methods have been sought to augment the depolarization of the membrane by cross-flow. For particles with a higher density than water, centrifugal force has been explored. For particles bearing an electric charge, an electric field has been investigated.

Centrifugal Force. Robertson et al[40] designed an apparatus in which the centrifugal force vector was perpendicular to the membrane surface but opposite (and parallel) to the flux vector. Solutions of casein and dextran (60,400 daltons) were passed over the membrane in laminar flow. When the apparatus was spun, centrifugal field strengths from 100 to 600_G resulted in flux improvement factors of 3 to 16.

Figure 3.53 shows the increase in the mass transfer coefficient (K), as calculated from Equation 10, due to the centrifugal force. The family of curves are for different concentrations of casein.

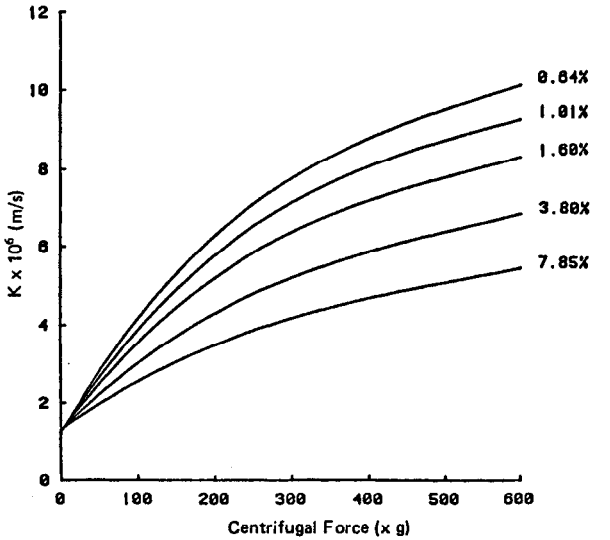


Figure 3.53: Increase in mass transfer coefficient (K) with the imposition of centrifugal force.

Electric Field. Many particles and/or macromolecules bear a charge (usually negative). Consequently, the application of an electric field can cause these species to migrate away from the membrane, thereby augmenting the mass transfer coefficient (K). Henry et al[41] has investigated cross-flow electro-filtration of kaolin clay suspensions and oil-water emulsions. Since both are negatively charged in aqueous suspensions, an electric field will always give higher filtration rates than cross-flow filtration alone (see Figures 3.54 and 3.55). The increase in UF flux depends on the electric-field strength as well as the cross-flow velocity.

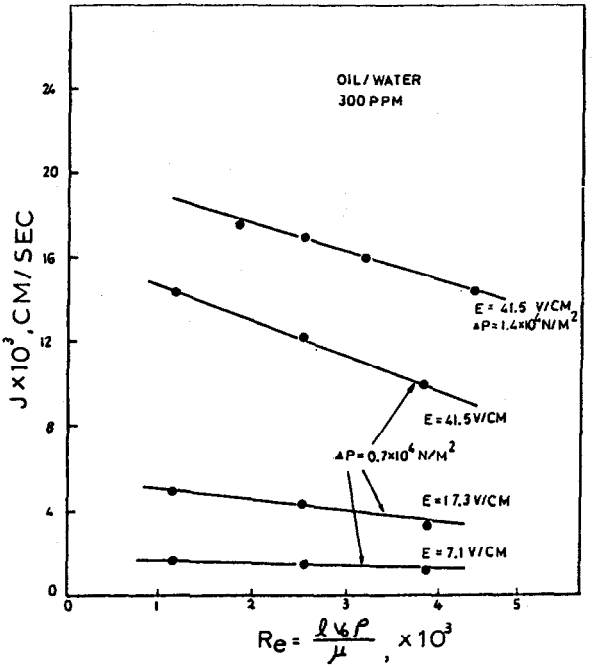


Figure 3.54: Cross-flow electro-filtration of oil/water emulsion.

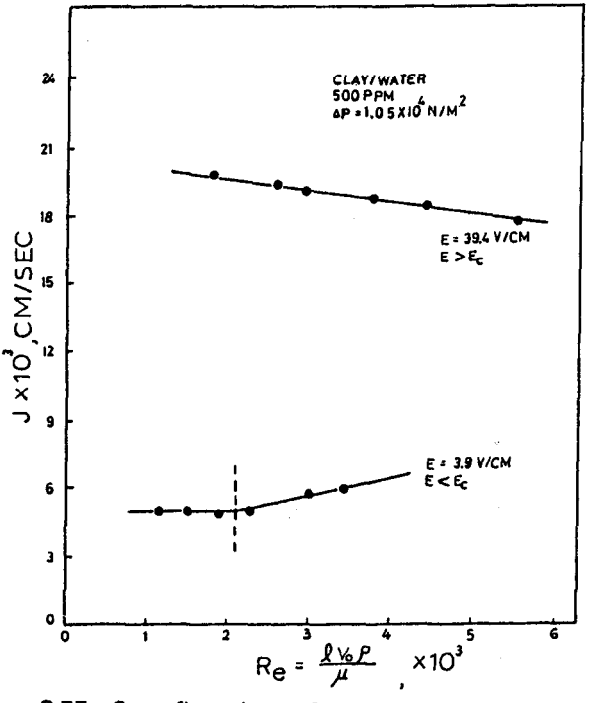


Figure 3.55: Cross-flow electro-filtration of kaolin suspension.

One of the more curious phenomena associated with cross-flow electrofiltration is that above some critical voltage (E_c), increases in the tangential velocity across the membrane may actually decrease the membrane flux as in Figures 3.54 and 3.55. This can be explained by referring to Figure 3.56.

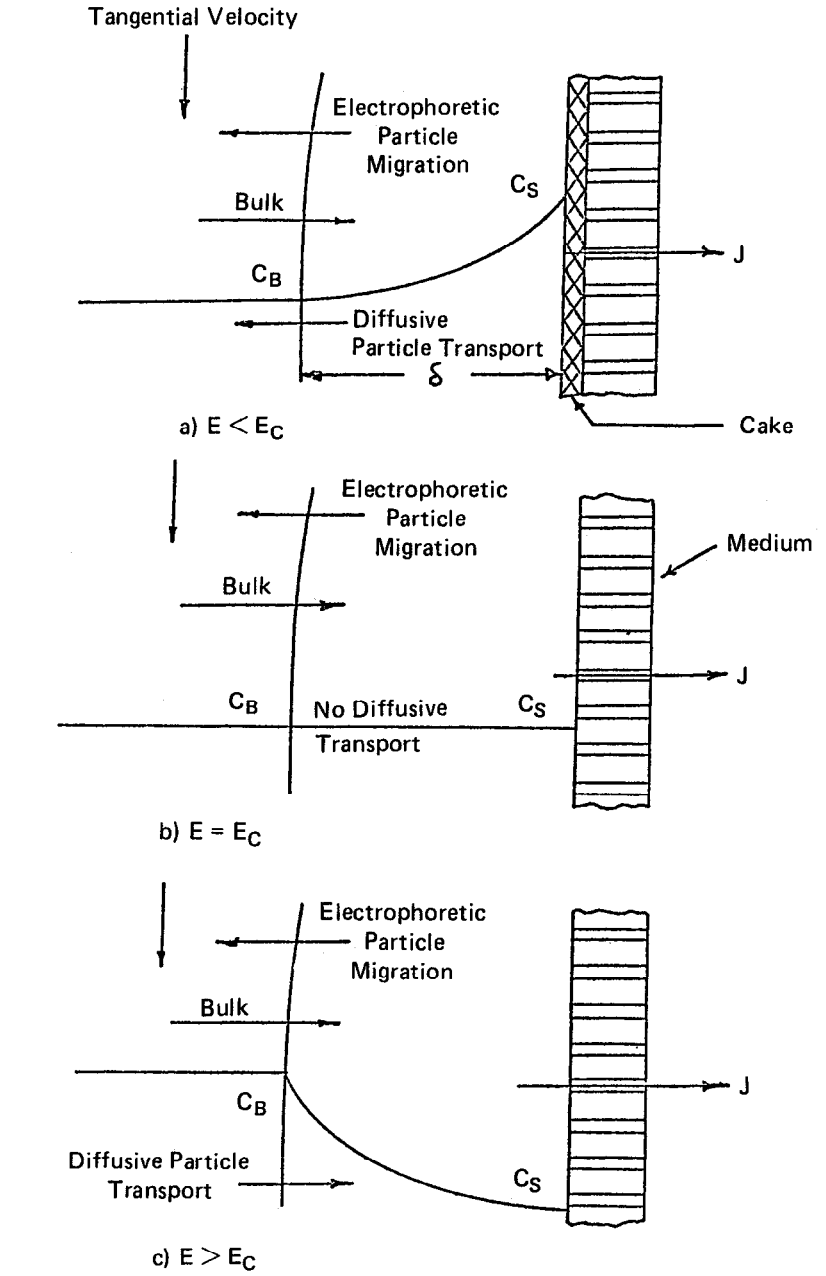


Figure 3.56: Three operating regimes for cross-flow electro filtration.

There are three operating regimes in cross-flow electrofiltration depending on whether the field strength (E) is above, below, or equal to the critical voltage (E_c). The critical voltage is defined as the voltage at which the net particle migration toward the membrane is zero, i.e., where the convective transport of particles toward the membrane is exactly equal to the electrophoretic migration of particles away from the membrane.

Regime (a) in Figure 3.56 is for E less than E_c. Concentration polarization still exists, but the flux is higher than normal because the back-diffusive transport of particles away from the membrane is augmented by the electrophoretic particle migration. In this regime, increases in the tangential velocity will diminish the boundary layer thickness resulting in a higher flux.

At the critical voltage, regime (b), there is no concentration polarization because the electrophoretic transport is equal to the convective transport. In this regime, increasing the tangential velocity is expected to have no influence on the flux because fluid shear can only improve the transport of particles down a concentration gradient. In this case, there is no concentration gradient.

When the voltage is greater than the critical voltage, regime (c), the electrophoretic migration of particles away from the membrane is greater than the convective transport to the membrane. Thus, the concentration of particles near the membrane surface is depleted due to removal by the electric field. In this case, increasing the tangential velocity *decreases* the flux, because the diminished thickness of the boundary layer increases the diffusive transport of particles down the conventration gradient toward the membrane (see Figures 3.54 and 3.55).

In Figure 3.55, the lower curve for E = 3.9 v/cm shows a transition in slope. The flux decreases with decreasing Reynolds number until a point is reached where the convective transport of particles toward the membrane is just equal to the electrophoretic migration away from the membrane (i.e., the voltage becomes critical as we decrease the cross-flow velocity). Further decreases in cross-flow velocity will not decrease the flux as there is no concentration polarization.

Though cross-flow electrofiltration has not yet been commercialized, its greatest potential appears to be in the elimination of the gel layer altogether, by the application of voltages above E_c. Solutions/suspensions which cannot be ultrafiltered economically due to severe fouling problems might be filtered with this technique if the particles and/or macromolecules bear a charge. It is even possible that this technique might make the fractionation of gamma globulin from albumin feasible. Oil-water emulsions might be separated by higher flux MF membranes. Without the electric field, the oil droplets would not be retained by the larger pore sizes in MF membranes, but above the critical voltage, breakthrough can be avoided. For example, the data of Figure 3.54 were taken using a 0.6 μ pore size membrane. (Normally, most oil droplets in emulsions are between 0.1 and 0.5 μ in diameter.)

Effect of Temperature

It has been found experimentally for a large number of membrane systems (including MF, UF and RO) and feed streams that the permeation rate is inversely proportional to the fluid viscosity. Since the viscosity of water decreases by about 2.5% for every °C rise in temperature, membrane researchers often refer to the 3% rule (that flux increases 3% per °C) as a rough rule of thumb.

Pure Water Transport. These results are not unexpected for the transport of pure water through porous membranes. Poiseuille's law predicts that flow (J) through any porous media should be described as follows:

$$J = \frac{N\pi d^4 \Delta P}{128 \mu \ell} \quad (27)$$

where N = number of pores per square foot
d = pore diameter (average)
ΔP = pressure drop
μ = fluid viscosity
ℓ = pore length (including a tortuosity factor)

The only variable in Equation 27, which is temperature dependent, is the viscosity:

$$\mu = \mu o \exp \frac{\Delta E_0}{RT} \quad (28)$$

where ΔE_0 is the activation energy (3750 cal/g-mol for water).

However, as we have seen, the membrane itself is no longer the limiting resistance to flow when "gel-polarized". The flux is given by Equation 10 instead of Equation 27. The mass-transport coefficient (K) and the gel concentration (C_g) vary with temperature.

Figure 3.57 is an illustration of how different protein solubilities at 4°C and 25°C will shift the gel-concentration. (Incidentally, the lower slope of the low-temperature data was due to a lower recirculation rate due to the increased viscosity of the process stream). Clearly, the inverse viscosity rule does not apply for all points on the graph. At 45% solids, the ratio of the flux at 25°C to that at 4°C goes to infinity.

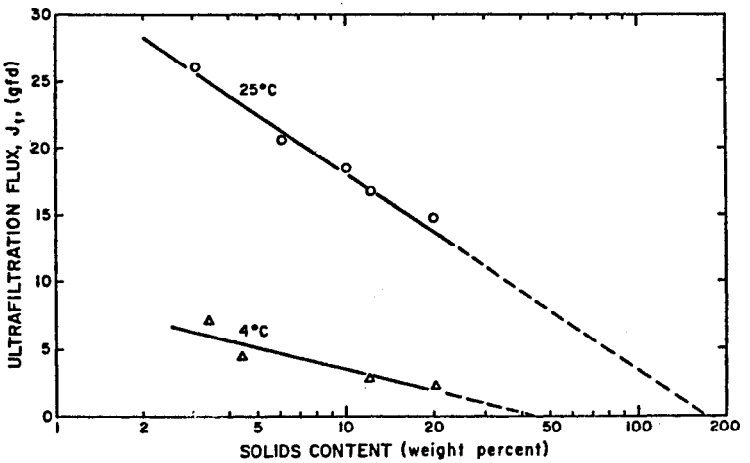


Figure 3.57: Effect of temperature on UF of a high-protein meal.

On the other hand, some proteins seem to show a gel concentration invariant with temperature (see Figure 3.58). In this case, the higher temperatures tend to denature the proteins (reducing their solubility), thereby compensating for the expected increase in solubility with temperature. Thus, the effect of temperature on gel concentration is complicated and often unique for the solute/solvent system being filtered.

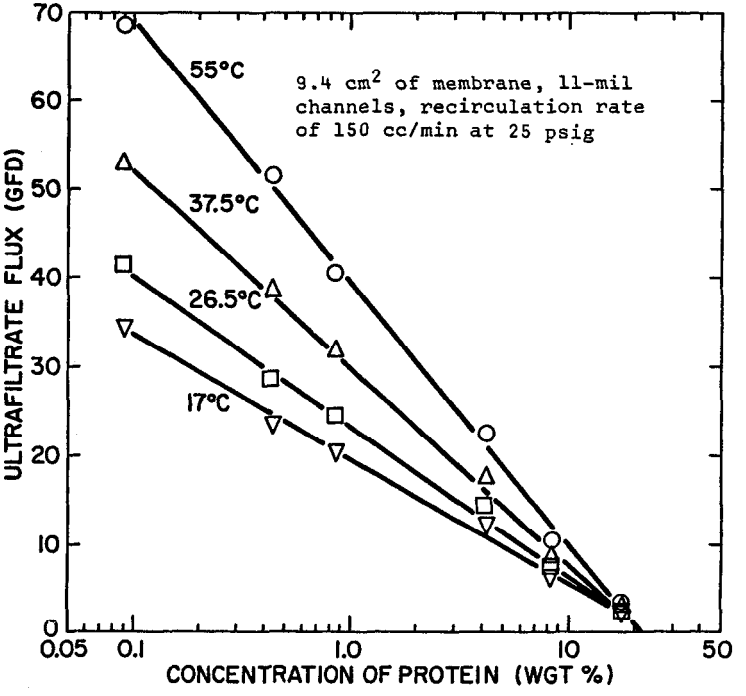


Figure 3.58: Effect of temperature on UF of bovine serum.

Differentiating Equations 16, 21, 24 and 28 yields the following expressions for the dependence of flux on temperature:

For laminar flow gel polarization

$$\frac{dJ_w}{dT} = J_w(0.66)\left[\frac{1}{T} + \frac{\Delta E_0}{RT^2}\right] \quad (29)$$

For turbulent flow gel polarization

$$\frac{dJ_w}{dT} = J_w(0.66)\left[\frac{1}{T} + \frac{1.75\,\Delta E_0}{RT^2}\right] \quad (30)$$

The derivation of Equations 28 and 29 may be found in Reference 17-Appendix E, pp. 2-97 to 2-99. It assumes that C_g is invariant with temperature. When these equations are used to calculate the percent variation of flux with temperature near room temperature, the results are usually within 25% of that predicted by the inverse viscosity rule.

MEMBRANE FOULING; FLUX DECAY AND RESTORATION

With some process streams the flux can be stable for months or even years without cleaning or membrane replacement. For most applications, however, there is a gradual flux decay with time as in Figure 3.59. This is not due to internal pore fouling (as in symmetrical MF membranes). Rather it is the result of the accumulation of materials on the membrane which no longer participate in the mass-transport to or away from the membrane. In effect, they "blind" small sections of the membrane, thereby reducing the effective area and the flux through the membrane.

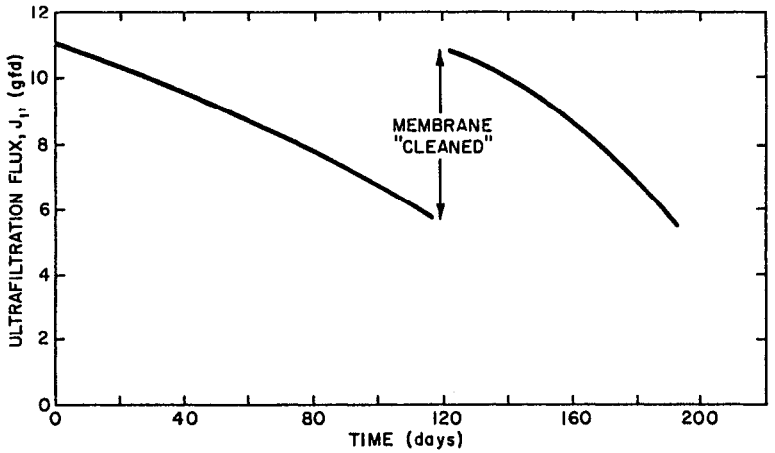


Figure 3.59: Long term flux decay and restoration by cleaning.

Often preventive measures may be taken to avoid fouling the membrane. Prefilters or screens can be used to remove large particles which block thin channels or accumulate in stagnant areas of the module. High cross-flow velocities tend to sweep deposits away. Low pressures avoid compaction of gels on the membrane. Some polymers have a higher susceptibility to fouling and chemical modification of the membrane surface can have a profound effect on the propensity to foul.

If fouling does occur, the membrane deposits can sometimes be removed by aggressive cleaning agents, such as detergents, acids, bases, or even organic solvents. The advantage of a chemically-resistant membrane is that severe cleaning agents may be used. However, even with periodic cleaning, the flux cannot always be restored to the initial value. This results in an overall long-term decay.

Effect of Cross-Flow Velocity

High cross-flow velocities tend to prevent fouling and also aid in the cleaning process. Figure 3.60 shows the flux decay on a log-log plot for low, medium and high recirculation rates (Q_L, Q_M and Q_H). Plotting the data in this way often permits a reasonably good extrapolation of the flux for much longer times-up to 2 or 3 years. The flux decay data usually plots on a straight line, and because of the cyclical nature of the log-log plot, 10 days of data often permits extrapolation to 100 or even 1,000 days.

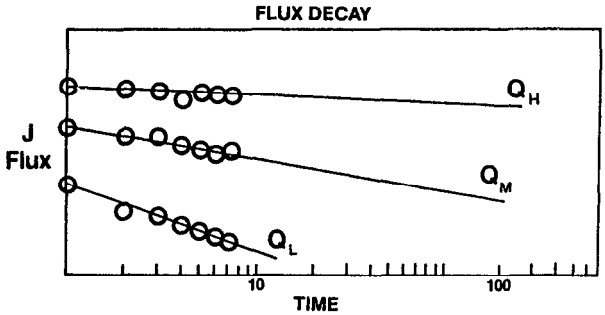
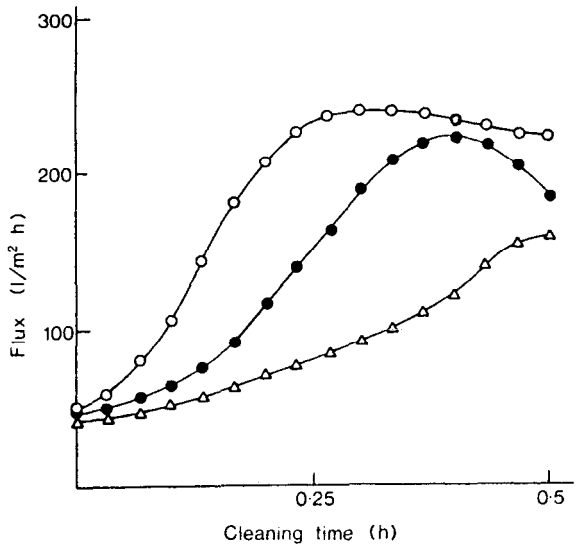


Figure 3.60: Effect of cross-flow velocity on long term flux decay.

High cross-flow velocities also facilitate cleaning. Figure 3.61[42] shows that the flux is restored more rapidly and to a higher level with high velocities.



The effect of detergent circulation rate (-○- 1.51 l/s; -●- 1.14 l/s; -△- 0.57 l/s) and time on flux during cleaning of tubular ultrafiltration membranes.

Figure 3.61: Effect of recirculation rate on detergent cleaning.

Effect of Pressure

If no fouling occurs, the maximum flux will be obtained in the gel-polarized regime above the threshold pressure (P_T). However, for solutes which form semi-gels on the membrane, pressures (P_H) higher than the threshold pressure may compact the gel layer resulting in greater fouling. Flux decay data like that of Figure 3.62 may show greater flux stability at pressures (P_L) lower than the threshold pressure. Even though the initial flux at P_L is lower (since not gel polarized), the long-term flux at this pressure may be higher.

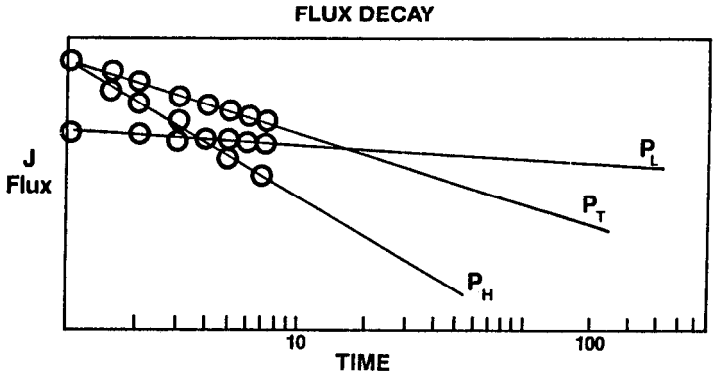


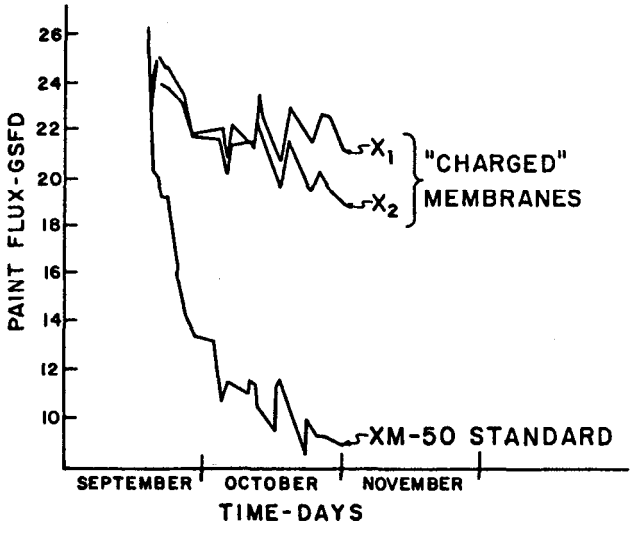
Figure 3.62: Effect of pressure on long term flux decay.

Effect of Membrane Surface Treatments

Changes in cross-flow velocity or transmembrane pressure cannot always alleviate fouling. Membranes made from hydrophilic polymers like cellulose acetate are generally less prone to fouling than the hydrophobic polymers. However, cellulose acetate is limited in its tolerance to high or low pH, organic solvents and elevated temperature. In some cases, surface modification of the more chemically-resistant polymers has rendered them less susceptible to fouling.

For example, a vinyl copolymer membrane (Romicon's XM-50) was used for years with anodic paint. The slight electronegativity of this membrane repelled the negatively charged anodic paint producing stable flux over a long period of time. When the electropaint users switched to cathodic paints, the XM-50 membrane experienced catastrophic flux decline-presumably because of the electrostatic interaction with the positively charged paint particles. Cellulose acetate membranes provided a stable flux but could not be cleaned with the solvents used in paint makeup (e.g., butyl Cellosolve). Therefore, a "charged" XM-50 membrane (designated CXM) was developed for cathodic paints. Figure 3.63 compares the performance of the "charged" membranes with the uncharged.

Various functional groups may be applied to a membrane by techniques such as chemical grafting, plasma polymerization, and sputtering. Figure 3.64 shows an increasing resistance of the protein gel-layer (R_g) (decreasing flux) with time for three samples of the same membrane, two which have been coated with carbon and a polysiloxane. In this case, the inorganic coatings tend to resist fouling producing a more stable flux.



Comparative data showing the flux versus time performance of the XM50 membrane versus that of the newly developed "charged" membranes on cathodic paint (PPG). The designation X_1 and X_2 refer to different "charge density" levels

Figure 3.63: Effect of "charged" membrane on long term flux decay with cathodic paint.

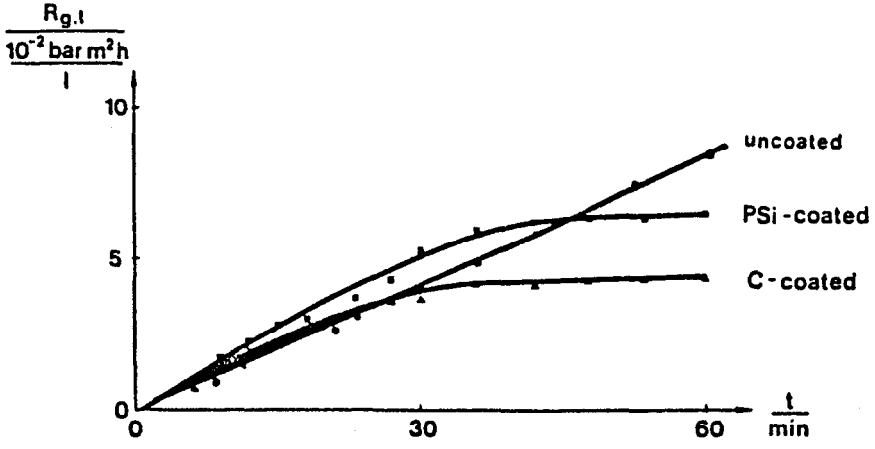
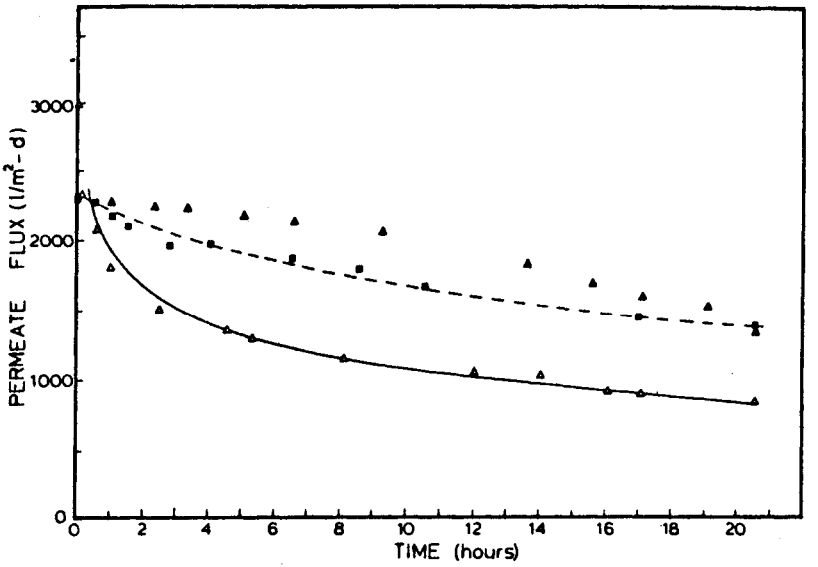


Figure 3.64: Effect of inorganic coatings on flux decay.

Howell and Velicangil[43,44] have developed a "self-cleaning" membrane by attaching food-grade proteases onto UF membranes. The enzyme protease hydrolyzed fouling proteins, thereby increasing the permeability of the gel layer.

This resulted in a 25 to 75% improvement in the permeate yield during a 22-hour run concentrating 0.5% albumin or hemoglobin. Figure 3.65 shows the effect of papain and fungal proteinase in decreasing the rate of flux decline over a 20.5-hour run concentrating BSA from 0.5 to 5.0%. The net protein loss through the membrane due to cleavange of albumin by the active enzyme was found to be only 4% of the total. The enzyme may be crosslinked and immobilized on the membrane surface with 0.125% glutaraldehyde in a phosphate buffer (pH 6.5).



Modelling flux of prototype and control/effect of different enzymes: PM-10 membrane, BSA. (▲) Control, H1; (▲) papain (Corolase S100), I1; (■) fungal proteinase P, H2; (---) model.

Figure 3.65: Effect of immobilized protease on UF of BSA (a self-cleaning membrane).

MEMBRANE CONFIGURATION

The design of the membrane package or module and the fluid management within that module will profoundly affect membrane performance. Further, the optimum design for one application may be totally unsatisfactory for other applications. For example, Equations 17 and 22 show clearly that thin channels promote higher mass transport and flux, but this must be balanced against their greater propensity to foul. In addition, high performance modules must be evaluated in terms of cost, ease of cleaning and replacement. There are currently four generic configurations for UF membranes in industrial use: tubes, hollow fibers, plate and frame units, and spiral wound modules.

Tubes

Perhaps the simplest configuration is a tube with the membrane cast on the

inside wall of the tube (see Figure 3.6). Tube diameters from 0.25 to 1 inch are less prone to foul and more easily cleaned than any other configuration.

Tubes may be effectively cleaned by introducing a number of sponge rubber balls slightly larger than the tube diameter (see Figure 3.66) into the process stream. Periodic passage of these balls can prevent severe flux decline (see Figure 3.67). Figure 3.68 is a schematic diagram of a device to dispense and recover these balls automatically at preset intervals. In this way, cleaning can be done simultaneously with processing. When severe fouling is encountered, a cleaning solution may be used in conjunction with the sponge balls.

The biggest disadvantage of tubes is their cost. The porous support tube (often fiberglass reinforced epoxy) is the dominant cost factor and the membrane area per foot of tube is low. When the membrane is spent, usually the whole tube must be replaced. PCI utilizes a "paper" insert on which the membrane is cast as the replaceable element. Others have developed epoxy bonded consolidated sand as the porous support in an attempt to reduce costs.

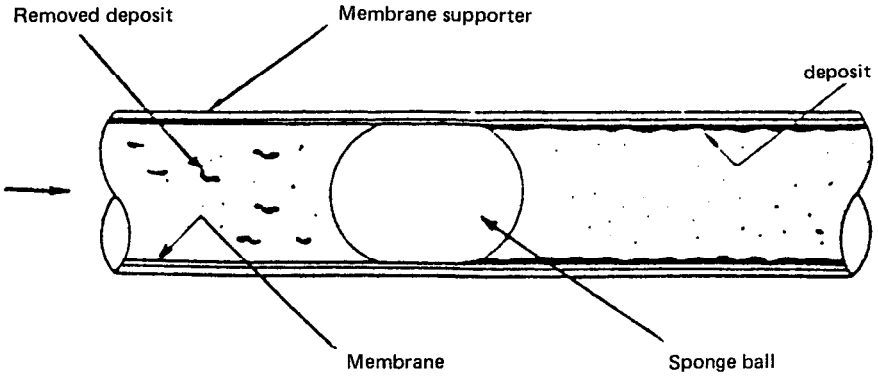


Figure 3.66: Schematic of sponge ball cleaning.

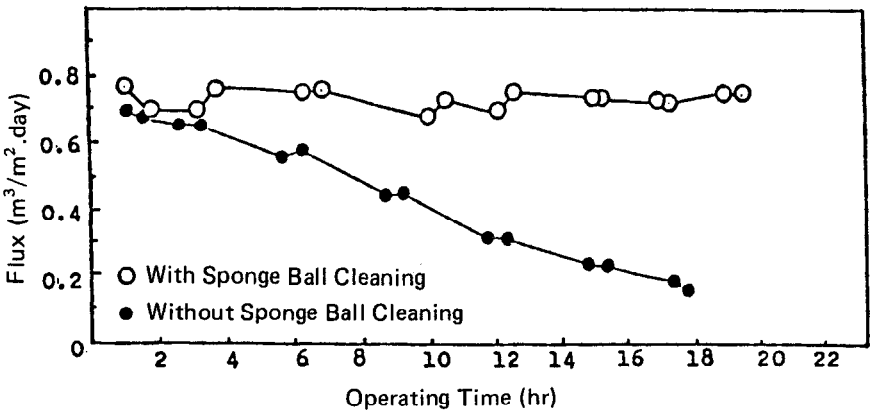


Figure 3.67: Effect of sponge ball cleaning on long term flux decay.

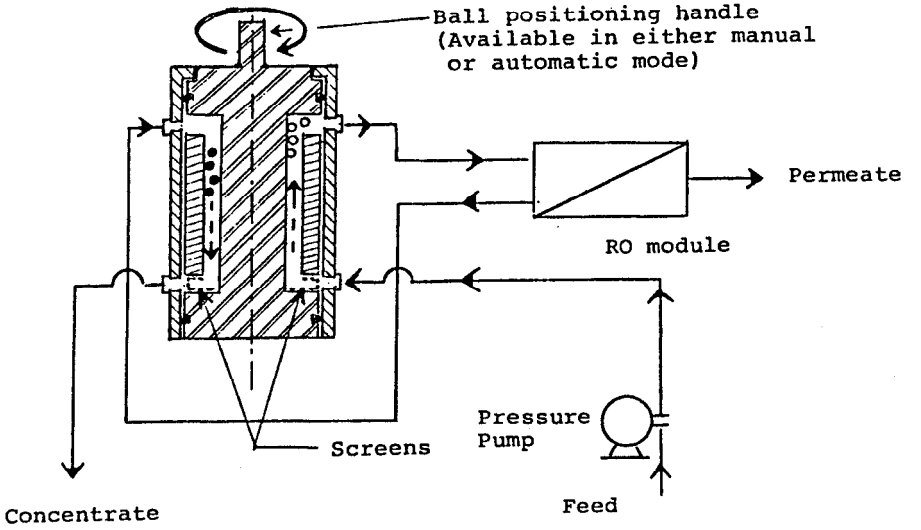


Figure 3.68: Sponge ball dispenser and collector.

The trend is toward using smaller diameter tubes or volume displacement rods to reduce the volume of fluid pumped per unit area of membrane. For example, the splined core in Figure 3.69 has sheet stock wrapped around the core and sealed longitudinally. The tube is braided on the outside for strength. This makes a fairly inexpensive tube, but the packing density (membrane area per unit volume) is still quite high and there is considerable "parasite drag" due to the splined core.

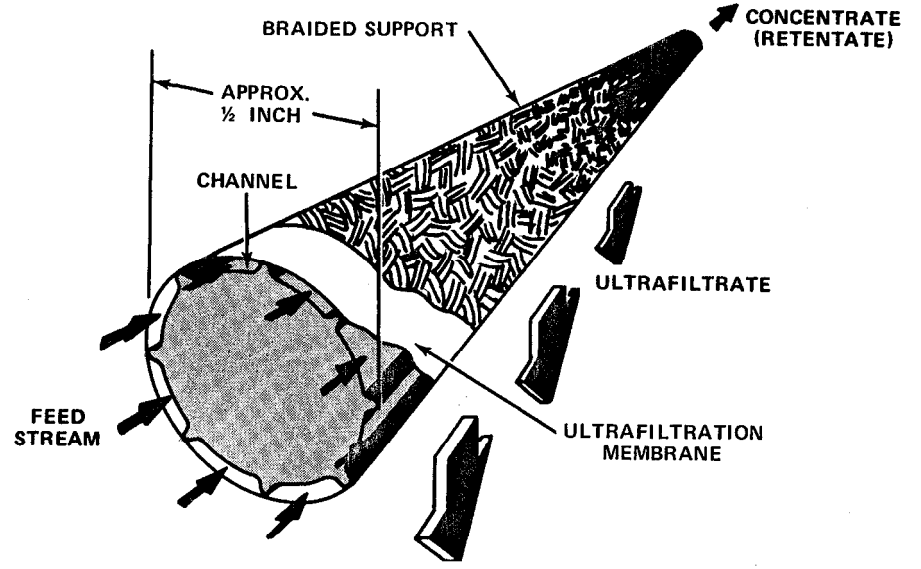


Figure 3.69: Splined core linear thin channel.

Hollow Fibers

Conceptually, hollow fibers are the ideal membrane configuration. There is no "parasite drag" and no expensive porous support tube. The fibers may be pressurized on the inside (up to 30 psig) permitting "thin-channel" fluid management of the feed stream (refer to Figure 3.13).

The biggest disadvantage is the pressure constraint which limits the cross-flow velocity down the lumen of the fiber. Shorter fiber lengths permit higher velocities at maximum inlet pressures of 30 psig. However, since most of the manufacturing costs are associated with potting the fibers at the ends of the module (see Figure 3.70), shorter modules have a higher cost per unit of membrane area. There are several methods under development for increasing the burst-strength of hollow fibers to permit higher operating pressures.

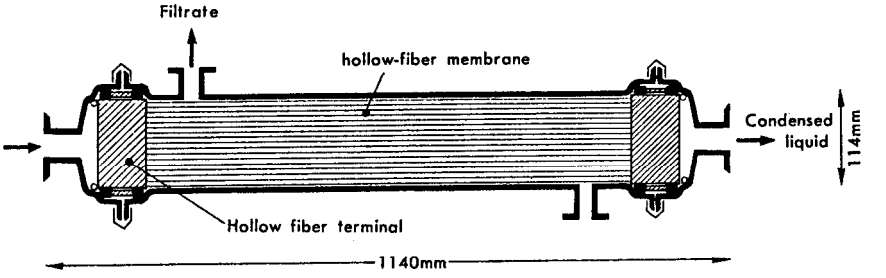


Figure 3.70: Schematic of hollow fiber module.

Potentially, hollow fibers should be the most economical membrane configuration available. Unfortunately, low manufacturing yields have kept selling prices ($/sq ft) equal to or greater than that for spiral-wound modules. Reject modules with only a few fiber leaks can be repaired using a "bubble point test" (see Chapter 2). The open-ended module is immersed in a tank of water. A gas line is used to pressurize the permeate port on the shell of the module with just a few psig. The end of the module is observed to pin-point bubbling fibers (leakers). These fibers are plugged using hot-melt, stainless steel nails with epoxy, etc. The module is then turned upside down and the test repeated to plug the leaking fibers on the other end. The same technique may be used in the field to reclaim leaking modules.

In general, the hollow fiber configuration is more susceptible to fouling and plugging than any of the other three configurations. Larger diameter fibers (up to 2.5 mm I.D.) are becoming popular to improve fouling resistance. The lower burst-pressures associated with these large diameter fibers generally limit the maximum diameter to below 2 mm I.D.

Fortunately, hollow fibers may be cleaned by back-washing which tends to compensate for their propensity to foul. Manufacturers of tubes, plate and frame units, and spiral wound modules do not recommend back-washing due to problems with membrane delamination and glue line seal rupture. Because hollow fibers are self-supporting and hold up well under the compression force of a reverse transmembrane pressure drop, they can easily withstand back-wash pressures of 15 to 20 psi. However, the back-wash fluid should be filtered to remove any particles which would tend to lodge in the porous wall of the fiber.

The permeate itself is often the ideal back-wash fluid since it has been through the membrane once. Unfortunately, permeate by itself will not always restore the flux (see Figure 3.71) and more aggressive cleaning solutions must be used. An auxiliary pump and filter must be provided to deliver the cleaning solution under pressure through the permeate port to the shell side of the module. The materials back-flushed will exit from the fiber lumen and must be discharged from the system so as not to redeposit on the walls of the fiber.

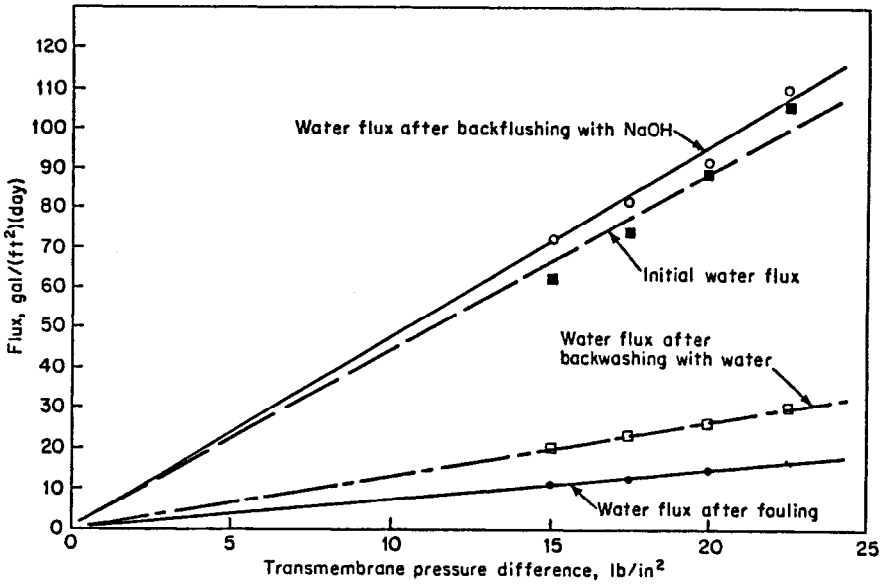


Figure 3.71: Restoration of flux in hollow fibers by back washing. Cleaning study showing the effect of back-flushing with sodium hydroxide on recovering the flux of a cartridge intentionally fouled with cultured skim milk.

Perhaps the simplest cleaning technique of all is to continue circulating the process stream through the module with the permeate port(s) closed (see Figure 3.72). The permeate will collect in the shell side casing of the module, until the pressure builds up to the average of the inlet and exit pressures inside the fibers. The inlet half of the module permeate will flow in the normal forward direction through the membrane to the shell side; but in the exit half of the module, permeate will flow in the backward direction from the shell side to the inside (lumen) of the fibers. This is called "cleaning by recycling". This gentle back-wash of the exit half of the module often recovers up to 80% of the flux decay. The reason is that hollow fibers often operate in laminar flow, and the gel layer is most fully developed in the exit half of the module. Further, the sweeping action of the process stream along the surface of the membrane effectively removes material loosened by the gentle back-wash. If the modules are installed with auxiliary piping so that the process stream flow direction may be reversed, the other half of the module may be back-washed.

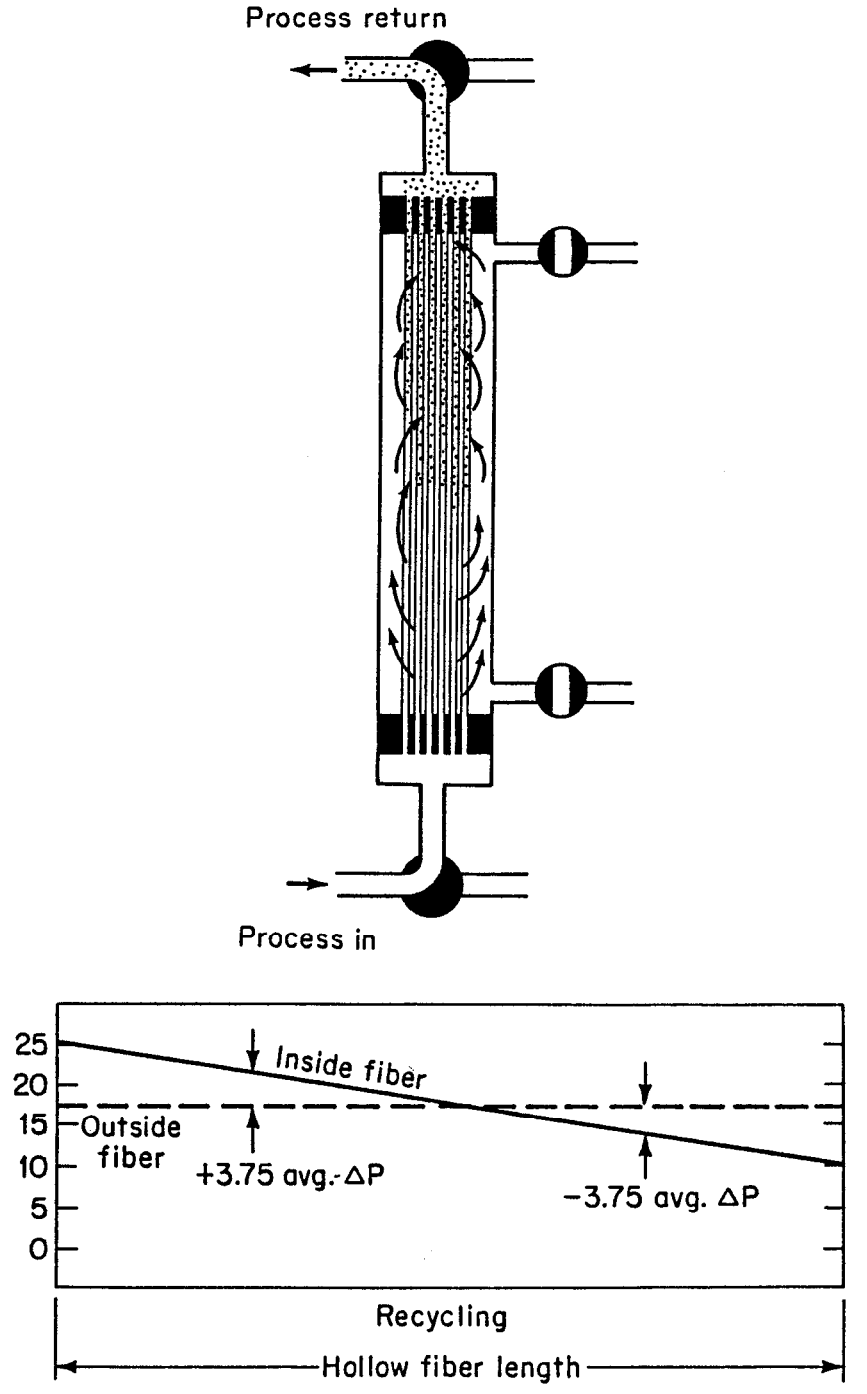


Figure 3.72: Cleaning hollow fibers by recycling (shutting permeate ports).

Plate and Frame Units

Flat sheet membranes in a plate and frame unit offer the greatest versatility of any configuration but at the highest capital cost. In many of these units, virtually any membrane may be cut to the appropriate shape and installed in the unit. The membrane replacement costs are potentially low, but the replacement labor is high. Disassembly also facilitates cleaning. There are many variations on the plate and frame theme. Representative designs are shown in Figures 3.73 to 3.77.

One of the advantages of the DDS (Figure 3.73) and Rhone-Poulenc (Figure 3.74) designs is that each support plate has a separate permeate port. If a leak develops in one membrane, it can often be located visually without disassembling the whole stack. Alternatively, the permeate tube from the leaking membrane may be pinched off since the loss of one plate out of 50 to 100 plates is not a significant percentage of the flow.

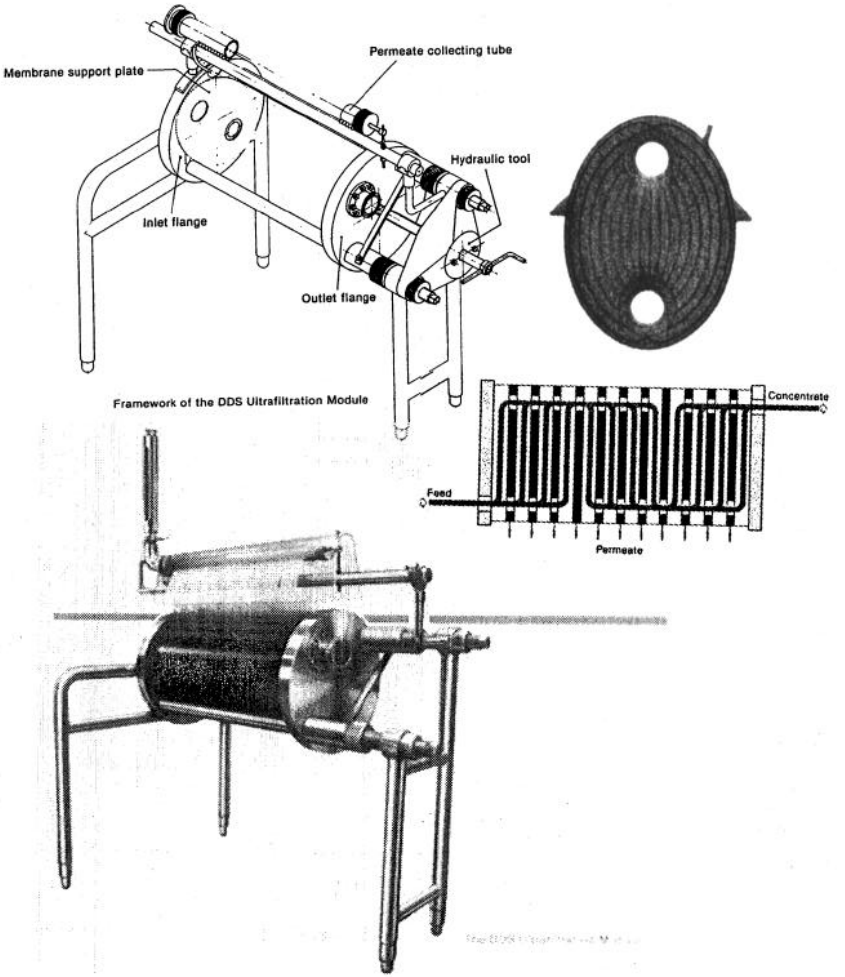


Figure 3.73: DDS plate and frame design.

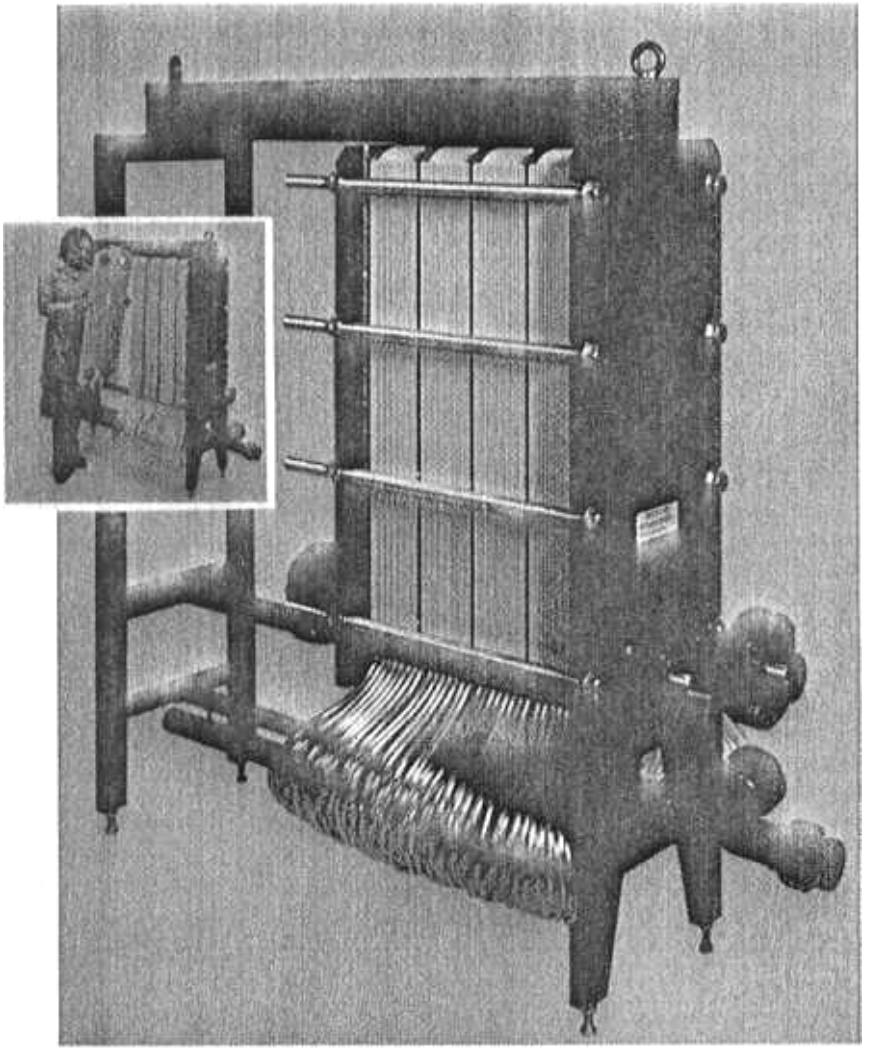


Figure 3.74: Rhone-Poulenc plate and frame design.

The Dorr Oliver design (Figures 3.75 and 3.76) heat seals the membrane to plates which drain off filtrate through a central permeate port to the outside of a pressure housing.

Millipore Corp. and New Brunswick Scientific Co. sell a "cassette" plate and frame system. The "cassette" is a membrane packet (schematically shown in Figure 3.77) comprised of two membranes enclosing a filtrate collection screen (sealed around the edges). Alternating holes on the edge of the cassette carry retentate or filtrate to the appropriate manifold. The cassettes are separated by screens or channel plates (see Figures 2.47 and 2.48 in Chapter 2). When filtering cellular or colloidal suspensions, the channel plates are preferred over the

screens which collect particles on the cross members of the screen. Flat sheet membranes with alternating gasket screens and channel plates may be used in lieu of the cassettes only if the lateral permeability through the membrane is low enough to prevent contamination of the filtrate with the retentate or leakage out the edges of the stack. The maximum number of membranes in such a stack is limited by the volume of flow which can be supplied through the manifold. Since the membranes operate in parallel, the cross-flow velocity across each membrane will diminish as the membrane area is increased.

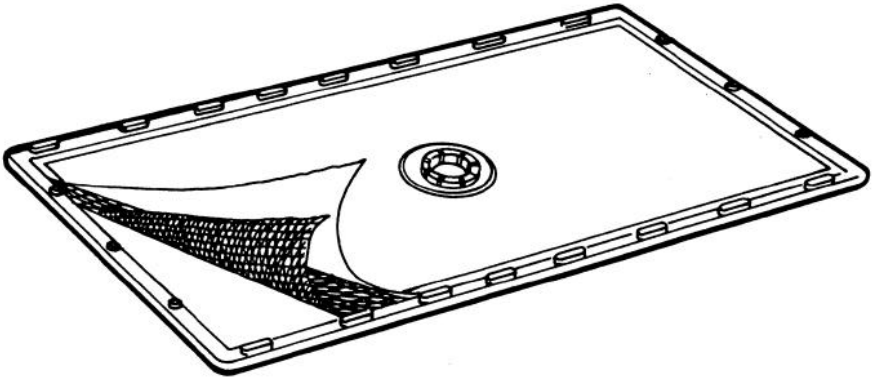


Figure 3.75: Dorr-Oliver flat-plate membrane element.

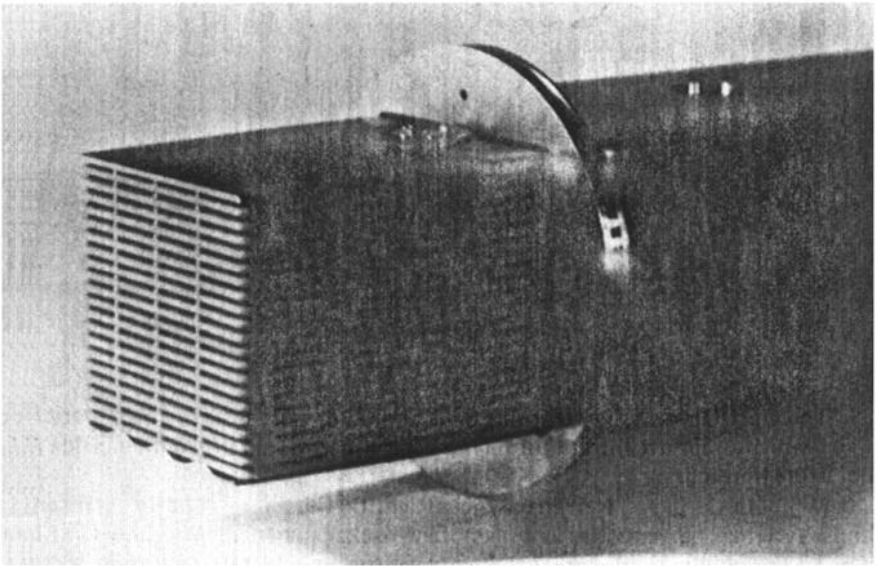
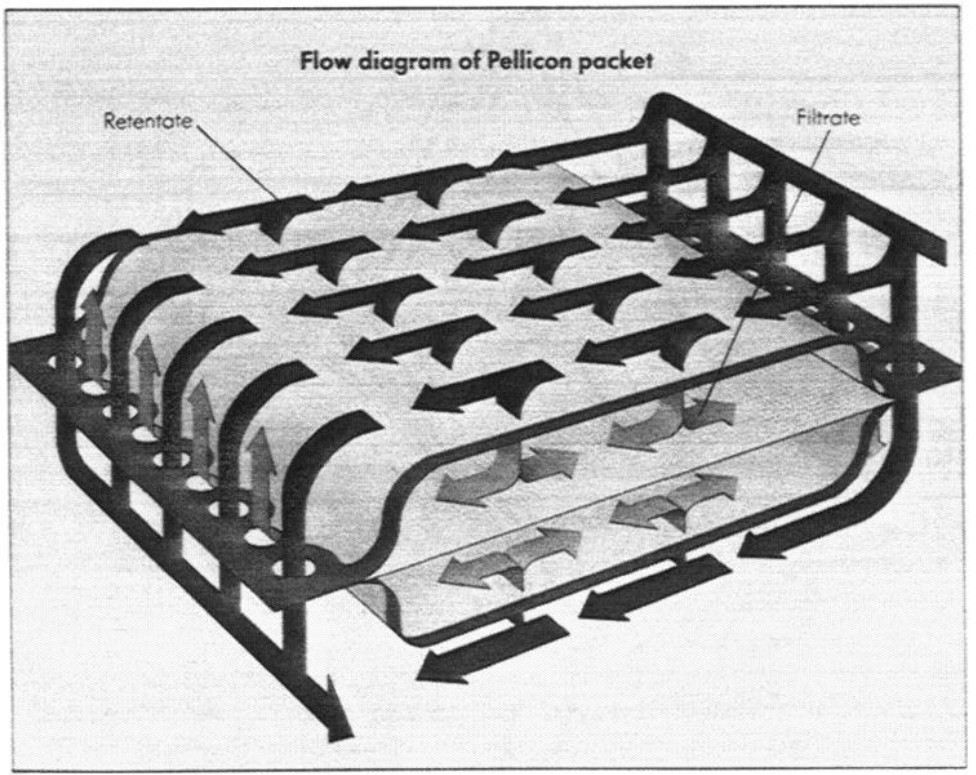
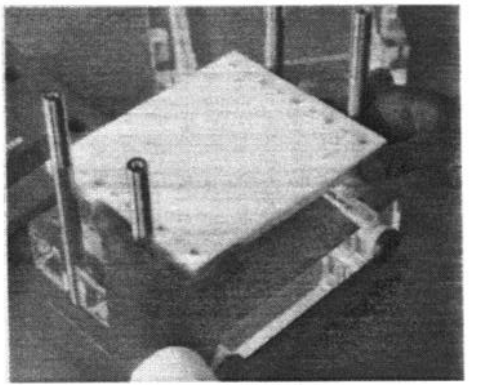


Figure 3.76: Dorr-Oliver assembled flat-plate cartridge.





Installation of the Pellicon cassette filter. To change from one procedure to another requires only a simple five-minute filter change.

Figure 3.77: Millipore cassette plate and frame design.

Spiral Wound Modules

Spiral wound modules were originally developed for RO but are capturing an ever increasing share of the UF market. They currently provide one of the least expensive UF modules available in terms of cost per unit of membrane area.

A spiral wound module is essentially the cassette of Figure 3.77 rolled up in a "jelly-roll" configuration. An envelope of two membranes enclosing a filtrate carrier is sealed around three edges and the fourth edge is connected to a perforated tube which carries the permeate (product water) (see Figure 3.78). As the module is rolled up, the membrane layers are separated by a screen or corrugated spacer where the feed solution flows parallel to the tube axis (see Figure 3.79). Again, the corrugated spacers are preferable for cellular suspension processing. The whole module is inserted in a pressure vessel; sometimes several modules are placed in one long pressure vessel. Often a chevron seal is used to seal the outer surface of the module to the inside of the pressure vessel; this insures that all of the feed stream is forced between the membrane layers. However, for sanitary applications, a screen (controlled bypass spacer) is used to permit flow in the annular region between the module and the pressure vessel; this eliminates the stagnant area and facilitates in-place cleaning and sterilization.

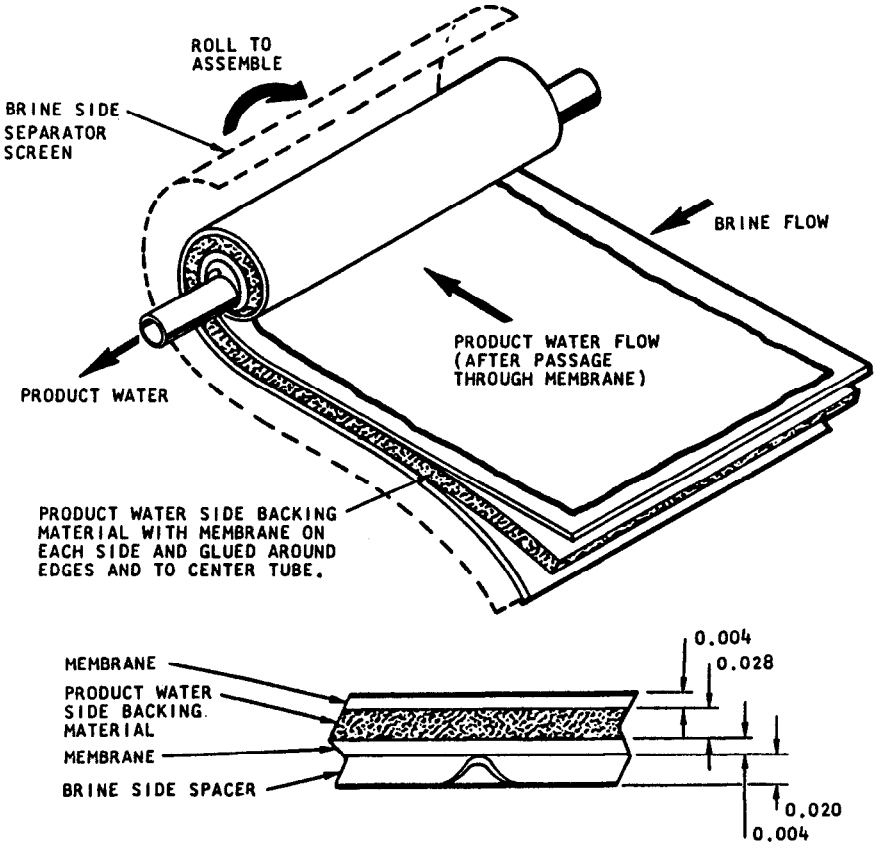


Figure 3.78: Spiral wound module unrolled.

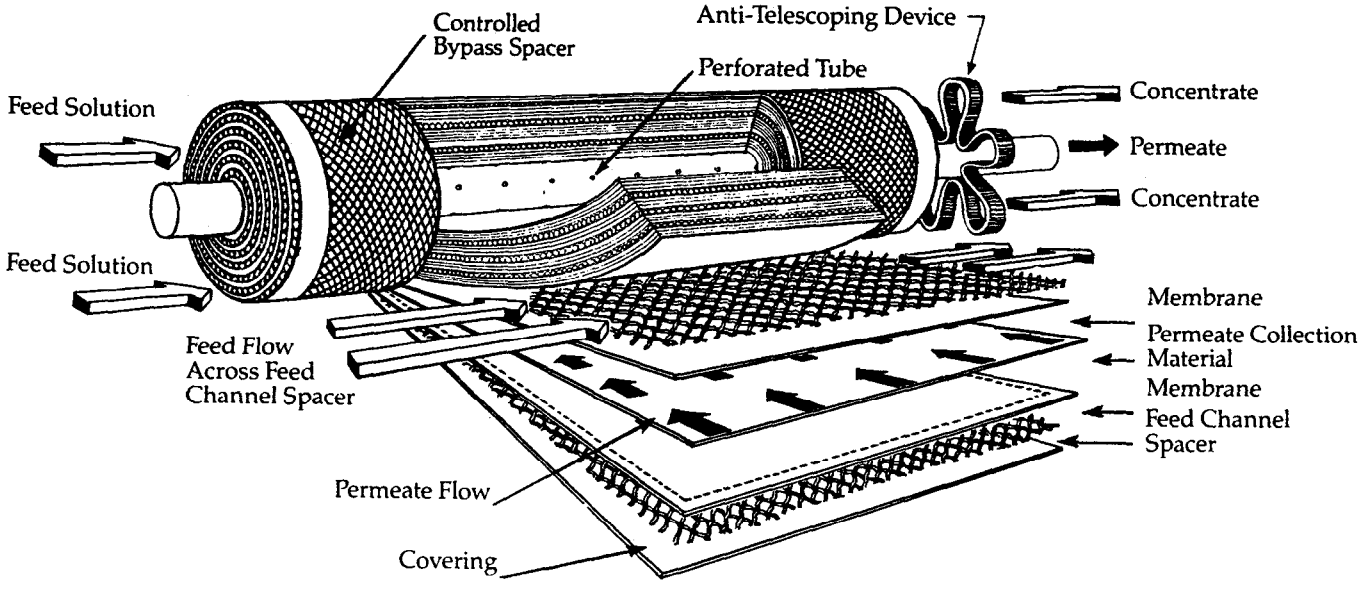


Figure 3.79: Spiral wound module showing screen spacer.

Spiral-wound modules cannot be unwrapped for cleaning lest the glue line seal rupture; and most cannot be autoclaved. They are more prone to fouling than tubes and some plate and frame units (depending on the type of feed channel spacer), but they are more resistant to fouling than hollow fibers.

Table 3.3 compares the relative advantages and disadvantages of the four basic configurations.

Table 3.3: UF Membrane Configurations

	Tubular	Hollow Fiber	Plate & Frame	Spiral Wound
Cost/Area	High	Low	High	Low
Membrane Replacement cost (not including labor)	High	Moderate	Low	Moderate/ Low
Flux (GSFD)	Good	Fair/Poor	Excellent/ Good	Good
Packing Density (Ft^2/ft^3)	Poor	Excellent	Good/Fair	Good
Hold-up Volume	High	Low	Medium	Medium
Energy Consumption	High	Low	Medium	Medium
Fouling	Excellent	Poor	Good/Fair	Good/Fair
In Place	Excellent	Good	Fair/Poor	Fair/Poor

UF PLANT DESIGN

Mode of Operation

The arrangement of the membrane modules and their mode of operation can affect the economics as much as the module design. There are basically 3 different operating modes for UF. These are shown in Figure 3.80.

Single-pass UF can only be used on relatively pure water streams (e.g., deionized water). If the retained species are low in concentration, the "recovery" of permeate can be as much as 95 to 99% of the feed. In the case of deionized water, the colloidal silica, microorganisms, and organic molecules in the concentrate can be sent to the drain as "blow-down". In the case of the hundred-fold concentration of a dilute hormone, 99% of the feed will pass through the membrane. Although the single pass operation in Figure 3.80 shows the UF modules operating in parallel, it is sometimes advantageous to operate in series to maintain a longer contact time with the membranes and to reduce the volumetric

pumping requirement. The plate and frame units can often be arranged to operate with the membranes in parallel or in series.

In most cases, the flux is too low to operate in the single-pass mode; the recovery of permeate in a single pass is a small percentage of the feed (very little concentration of retained species). Recirculation of the process stream across the membrane is necessary to obtain the desired concentration or recovery. Typically the ratio of recirculation rate to permeate flux is 10 to 100-fold. Recirculation can be accomplished with either a batch concentration or with a feed and bleed operating mode.

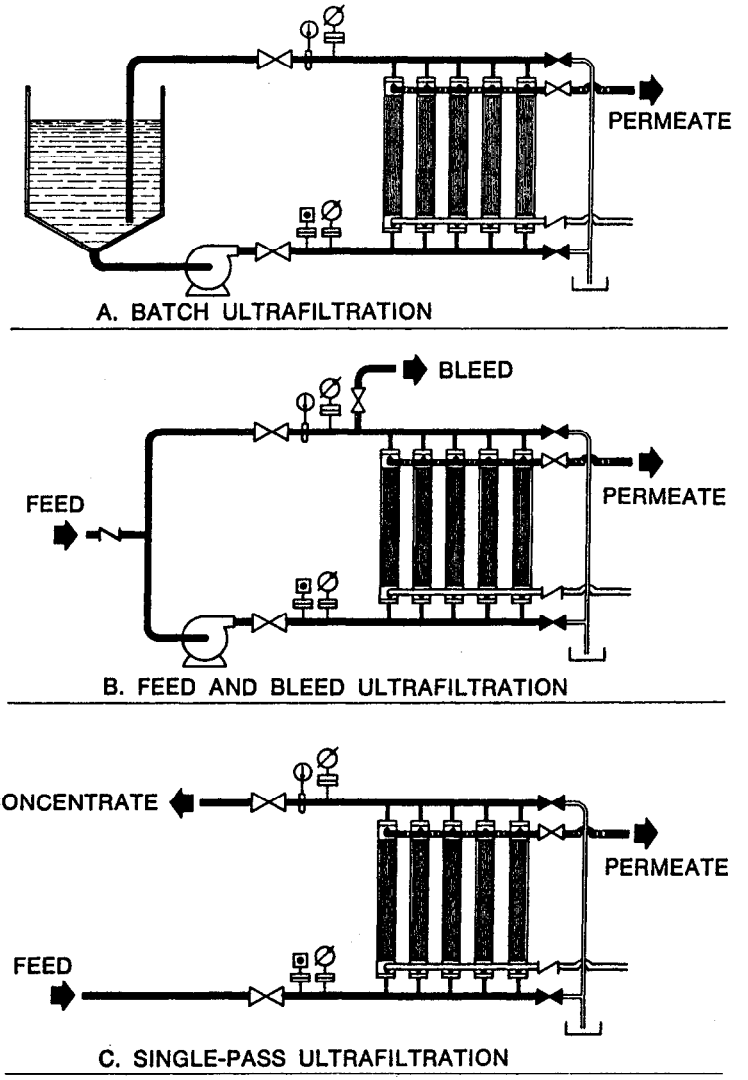


Figure 3.80: UF operating modes.

In a *batch operating mode*, the retentate is circulated back to the feed reservoir. As the permeate is removed, the volume in the reservoir goes down and the concentration of retained species goes up. Freely permeable species (e.g., salts) remain at the same concentration in the reservoir and in the permeate stream. Eventually, the volume in the reservoir becomes too small to pump and the run is over. A new batch must be charged to the reservoir to continue.

The *feed and bleed mode* permits continuous filtration; the feed stream is fed into a recirculating loop. The concentration of retained species will continue to increase with ever decreasing flux, unless a purge stream is taken from the loop.

Often a ratio controller is used to keep the feed to bleed ratio constant-equal to the volumetric concentration ratio required. This means that even with flux decay, the concentration ratio and recovery will remain constant.

It is unwise to use the feed and bleed mode to concentrate a batch of solution. Once steady state is achieved, the membrane filter at the final concentration for the duration of the run. In a batch process, a higher average flux is achieved due to the gradually increasing concentration. Thermodynamically, the feed and bleed mode is less efficient due to increase in entropy upon mixing the low concentration feed with the high concentration recirculating retentate.

The total membrane area required in a feed and bleed mode can be reduced considerably by arranging the modules in two or more feed and bleed stages. In this multistage (cascade) system, the bleed stream of the first stage becomes the feed stream of the second stage, etc. For example, the first stage might concentrate from 1 to 2%, the second stage from 2 to 4%, the third stage from 4 to 7%, and the last stage from 7 to 10%. Since flux decreases with increasing concentration, it is advantageous to operate as many stages as possible at the lower concentrations. Obviously, the additional pumps and controllers for each stage add to the capital cost and must be considered in arriving at an optimum number of stages. (See Chapter 6: Process Design and Optimization.) Though the optimum number of modules per stage will vary, equal numbers of modules for each stage often comes close to the optimum configuration.

Optimum Recirculation Rate

There is an optimum recirculation rate for each stage. Higher recirculation rates will result in greater productivity (flux), less membrane area, and longer membrane life due to greater flux stability. They also require larger pumps and increased power costs.

Figure 3.81 shows some of the major operating costs. Increasing the cross-flow rate through a module decreases the membrane replacement costs due to less area (higher flux) and longer life (greater flux stability). Indeed, all costs associated with the size of the plant will go down, but the utilities costs go up. The optimum design point will depend on the current cost of power and membranes (along with their productivity).

In a multistage feed and bleed system, the optimum cartridge flow rate can be different for the later stages operating at high concentration than those operating at low concentration. Often, the first stage is not fully gel polarized (due to the low concentration) and high cross-flow velocities are not as critical as high operating pressures (approaching the threshold pressure).

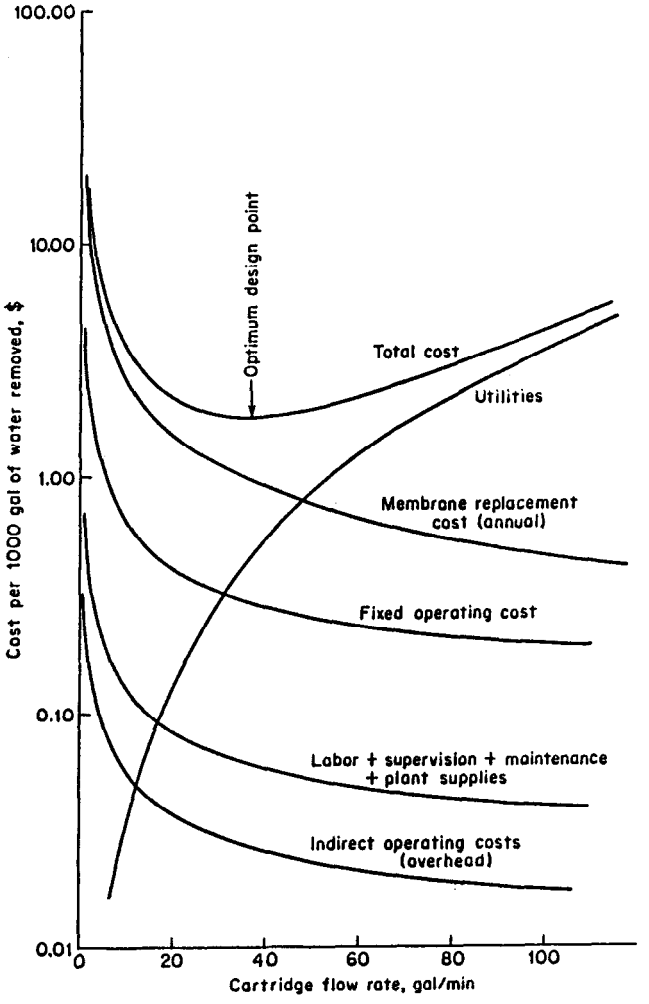


Figure 3.81: Determination of optimum recirculation rate.

APPLICATIONS

The largest current applications for UF (in terms of installed membrane area) were not envisioned in the early sixties (e.g., UF of electrocoat paint). Further, many of the projected applications have not yet materialized (e.g., fractionation of polymers and proteins).

In some applications, the product is the retentate, and the objective is to concentrate or purify the retained species (passing unwanted contaminants through the membrane).

In other applications, the product is the permeate, and the objective is to re-

move unwanted contaminants which are large enough to be retained by the membrane.

In a few applications, both retentate and filtrate are important. For example, if a valuable product or by-product is a pollutant in a waste stream, recovery and use of the product will often pay for the pollution abatement. The clean permeate may then be reused in the plant; in cases where the plant effluent is at elevated temperatures, the hot permeate may be reused in the plant saving additional energy costs. There are only a few applications where UF can be justified for pollution abatement without the recovery of a valuable by-product or energy credit. In these cases, the economic incentive is found in the avoidance of a sewer tax or shut down by the Environmental Protection Agency.

Ultrapure Water

Semiconductor Industry. In Chapter 2, the application of MF and RO in a deionized water loop was discussed. The rapid miniaturization of integrated circuits (IC_s), and the need for even greater water purity has prompted the use of UF.

Traditionally, MF has been used after the ion exchange columns (see Figures 2.56 and 2.58) to remove microorganisms, resin fines and other particles. Increasingly, UF is being used after the ion exchange units and before MF. Originally, UF was justified on the basis of savings in the MF replacement cost since reducing the load on the MF cartridges naturally extends their life. In one case, the savings in replacement cartridges and labor were expected to pay for the UF plant in less than a year.

Except for ultrapure water plants where the DI water is dirty and the MF cartridges must be changed every two weeks or less, MF operating costs are considerably less than UF. Typically, MF cartridges can last from 3 to 6 months (even without UF). Even with replacement every other week, MF operating costs are usually no more than 50¢ per 1,000 gallons. UF operating costs often run more than this when membrane replacement costs, labor, maintenance, power usage, and amortization are included.

The economic justification for UF is usually found in improved IC yields due to better quality water. An 80,000 MWCO UF membrane can remove all particles and macromolecules larger than 0.005 μ, and a 10,000 MWCO can remove particles down to 0.002 μ. This means that high molecular weight organics and colloidal particles, which pass through an MF membrane, will be retained by UF. The organics adhere to the silicon chips resulting in poor adhesion of the polymer masks used to control etching. Further, dead bacteria fragments/pyrogens (down to 10,000 MW) can adhere to wafer surfaces resulting in MOS gate failures. "Pin-holing" in angstrom thick oxides can occur due to pyrogens. Recent reports (DM Data Inc., Scottsdale, Arizona) indicate that Japanese manufacturers of silicon chips get almost twice the yield of usable chips that U.S. manufacturers get. One significant difference between U.S. and Japanese semiconductor plants is that most of the large Japanese plants are using UF. Currently, only a few U.S. plants have UF.

The effectiveness of UF in particle/colloid filtration can be measured with an MF plugging test similar to the "silt density index" (see Chapter 4, Figure 4.10). Water is fed at 30 psig through a 47 mm diameter 0.22 μ membrane filter

monitoring the flow rate with time. Figure 3.82[45] shows the improvement in the quality of the UF permeate at the Western Electric plant in Allentown, PA. It should be realized that the water is relatively clean (the UF unit is operating in the single-pass mode with 95% recovery), and that the use of a 47 mm filter accelerates the time to plugging.

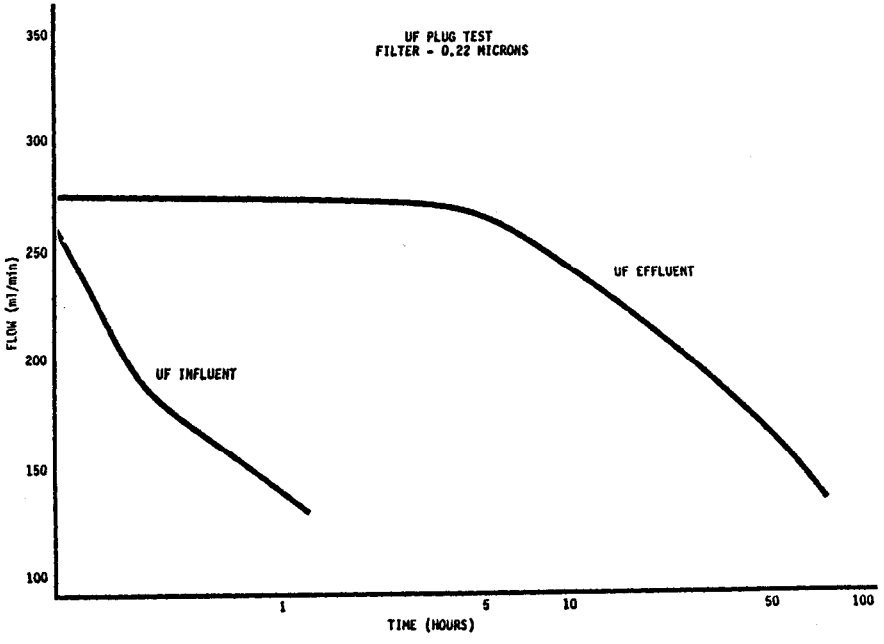


Figure 3.82: Effectiveness of UF (ultrapure water) using MF-plugging test.

The removal of organics is measured as a reduction in total organic carbon (TOC). With an 80,000 MWCO membrane, there is usually no problem in meeting the specification cited in Table 2.7 (Chapter 2) of less than 0.2 ppm TOC. In some case, a 20,000 or 10,000 MWCO membrane will be necessary to meet the more stringent Japanese specification of less than 0.05 ppm TOC.

Though the retention of microorganisms by a UF membrane is well over 99%, it is not as "absolute" as an MF membrane (see Chapter 2). For this reason, it is wise to install an MF cartridge at the point-of-use for final insurance. (Replacement should be infrequent.) The Center for Disease Control has reported[46] that spiral-wound modules produce water with consistently lower bacteria counts than hollow-fiber modules when challenged with high populations of bacteria in the feed water. With continued filtration, bacteria counts on the membrane increase exponentially. For this reason, all UF membranes must be sanitized periodically. Sodium hypochlorite is preferred, but cannot be used with polyamide membranes. It also attacks stainless steel. Table 3.4 lists common sanitizing agents.

Table 3.4: Common Sanitizing Agents *

H_2O_2	1-5% hydrogen peroxide for 30-90 minutes (preferred in electronics where sodium ion residuals must be avoided.)
Cl_2	100-500 mg chlorine gas per liter of water for 30-90 minutes.
NaOCl	5-10 ppm sodium hypochlorite for 60 minutes.
Hot H_2O	180°F for 1-2 hours
O_3	Ozone at 0.1-0.2 mg/liter for 30-90 minutes

* Check for chemical compatibility with the filters used in the system before selecting a sanitizing agent.

UF sometimes provides an unexpected bonus in reducing the conductivity of the water. Though "charged" UF membranes with a low MWCO might offer some rejection of divalent and trivalent ions, they should pass an 80,000 MWCO membrane. Figure 3.83[45] shows tremendous fluctuations in the influent conductivity. UF reduced the conductivity to a stable minimum. It is hypothesized that charged colloidal particles or large molecular weight complexes contribute to the conductivity.

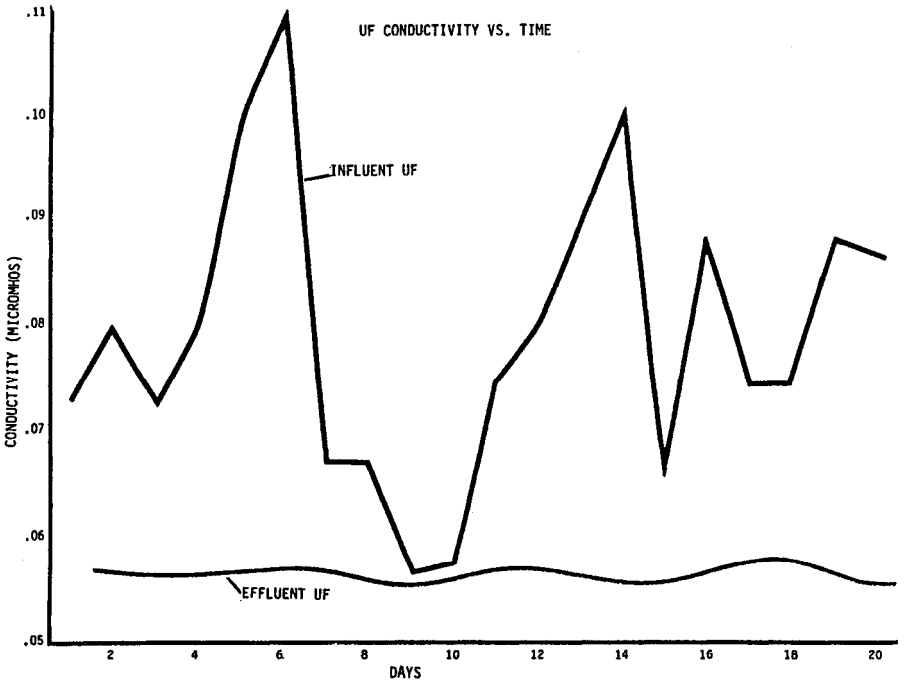


Figure 3.83: Stabilization of ultrapure water conductivity with UF.

A more recent development is the use of UF for point-of-use processing. When UF is installed in the central system, the plastic (PVC) piping to the various rinse stations collects particles and leaches organics. A small 4 gpm hollow fiber unit at the rinse station removes all particles, colloids and organics down to an average size of 0.005 μ. In some cases, these units are operated dead-ended with a periodic fast-forward flush to remove accumulated particles inside the hollow fibers.

UF has also been used in ultrapure water loops before the ion exchanger units to protect resins from fouling and as pretreatment for RO.

Pharmaceutical Industry. Water is, of course, the most common ingredient in pharmaceutical products. It is crucial that all microorganisms, pyrogens, and other particles be removed from water for injection (WFI). The smallest blood vessels in the body have a diameter slightly less than 3 μ. Thus, particles larger than 3 μ can block blood vessels resulting in partial occlusion of retina arteries (leaving blind spots), clot formation and emboli, and granulomas. Though MF membranes can remove the microorganisms and particles above 0.2 μ, they cannot effectively remove pyrogens. It has been repeatedly demonstrated that a 10,000 MWCO UF membrane can remove all pyrogens.

The word "pyrogen" means "fever-producing" and has been used to cover any substance which causes a body temperature increase on injection. In fact, the first compendial pyrogen test was published in the 1942 edition of the *United States Pharmacopeia*. It involved the measurement of the rise of body temperature in rabbits upon intravenous injection of a test product. More recently (1977), the FDA approved the Limulus amebocyte lysate (LAL) test which can be run for less than 10% of the cost of a rabbit test.

Because of their fever-producing capability, pyrogens must be barred entrance to the blood stream, particularly in persons who are ill or whose immune systems are weaker than normal. It is well known that pyrogens can produce shock and even death.[47]

Historically, pyrogens have been defined on the basis of their physiological action rather than on their chemical characteristics. However, in recent years considerable progress[47] has been made in identifying pyrogens as lipolysaccharides (LPS) primarily from Gram-negative bacteria (GNB). These materials occur in the outermost layer of the cell walls; thus, a pyrogenic response can result from the presence of dead bacteria or even cellular debris. This explains why normal autoclaving does not destroy pyrogens and filtration through 0.2 μ sterilizing membranes does not remove them. Further, since GNB grow in solutions containing minimum nutrients, even distilled water can evoke a pyrogenic response. Indeed, pyrogens can even be entrained and carried along with water droplets into the condenser during evaporation.

Because the LPS molecules contain both hydrophobic and hydrophilic regions, they form micelle-like aggregates. If the LPS is reduced to its smallest subunit, it will pass through a 1,000,000 MWCO ultrafilter but be retained by a 10,000 MWCO membrane.[47] Experiments show that the 10,000 MWCO membrane will reduce the pyrogen concentration by 2 to 5 orders of magnitude.[48] Other researchers[49] seeking to remove pyrogens from peritoneal dialysis solutions found that a 50,000 MWCO membrane was adequate and provided a higher flux.

Electrocoat Paint

The electrocoat paint market constitutes the largest single application of UF in the world. Virtually every automobile plant in the world uses electrocoat for the undercoat and virtually every installation utilizes UF. There are over 1,000 UF units in the automotive industry alone–not to mention appliance manufacturing, metal furniture, coil coating, and other metal electrocoat operations.

The electrocoat process for primer coating involves the electrophoretic deposition of charged colloidal resinous particles in aqueous dispersion onto a conductive substrate such as an automobile body. The process is universally favored because once the paint particles are deposited, they insulate the body from further deposition at that point. The impressed electric field thereby causes the migration of paint particles to uncoated areas. The result is an extremely uniform, coherent and defect free coating–even on sharp edges and in recessed areas inaccessible to other methods.

UF provides a cost effective way of solving several problems associated with electrodeposition systems. The continuous feed of paint to the tank is balanced only by the deposition of charged particles on the substrate. This results in the accumulation of several water-soluble ions in solution with consequent decreased "throwing power", lower rupture voltage, staining, thin films, and pinholing due to rupture. Further, excess drag-out paint from the paint tank must be rinsed off the metal part to prevent "orange-peel" and other coating anomalies. This dilute paint cannot be returned to the tank due to the excess water. It is, therefore, discarded to the sewer resulting in a horrendous pollution problem and tremendous losses of paint.

At first, in the early nineteen-sixties, UF was used as a kidney to remove contaminating ions. Later, PPG (a paint manufacturer), envisioned UF in a closed loop rinse system (see Figure 3.84) to solve the pollution problem as well as the contaminant build-up. In this system, a portion of the ultrafiltrate is purged to the drain to remove ionic contaminants. The majority of the permeate is used in the rinse tunnel to wash excess drag-out paint back into the tank. Thus, all excess paint is recovered alleviating a serious pollution problem and, at the same time, justifying the UF unit economically.

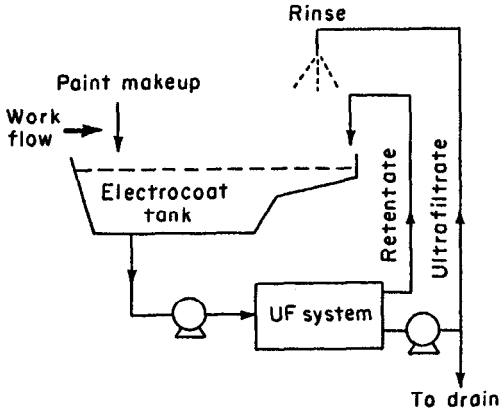


Figure 3.84: UF of electrocoat paint, single-rinse system.

The size of the UF unit may be reduced considerably by utilizing a counter-current rinse scheme (Figure 3.85). The ultrafiltrate is used only at the last rinse station. The dilute paint (0.05 to 0.2%) from this rinse is used in the first and second rinse stations, eventually returning all excess paint to the paint tank.

The paint savings alone typically pay for the UF unit is less than six months. Additional savings result from reduced deionized water use, lowered waste treatment costs, and better control of bath composition.

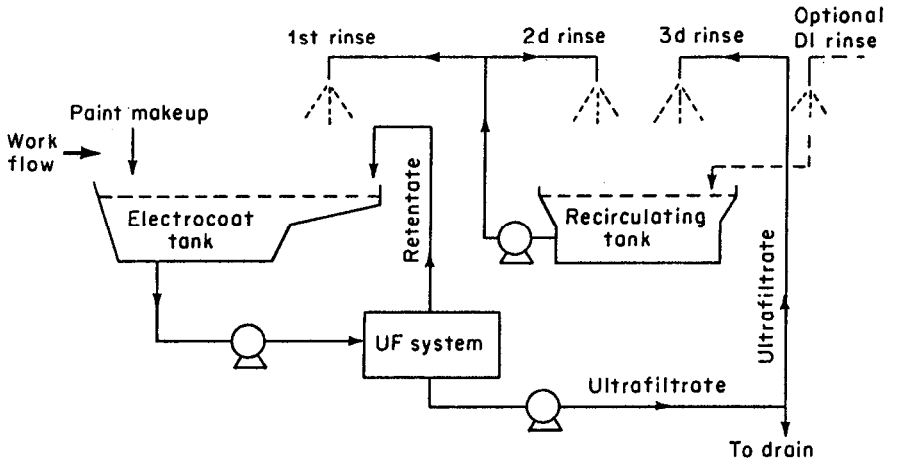


Figure 3.85: UF of electrocoat paint, multi-rinse system.

In the nineteen-sixties, most electrocoat tanks were anodic, i.e., the work piece was positively charged and served as the anode while the paint particles were negatively charged. These systems were ideal since many UF membranes tend to be slightly electronegative with good fouling resistance and excellent flux stability (Figure 3.86).[50]

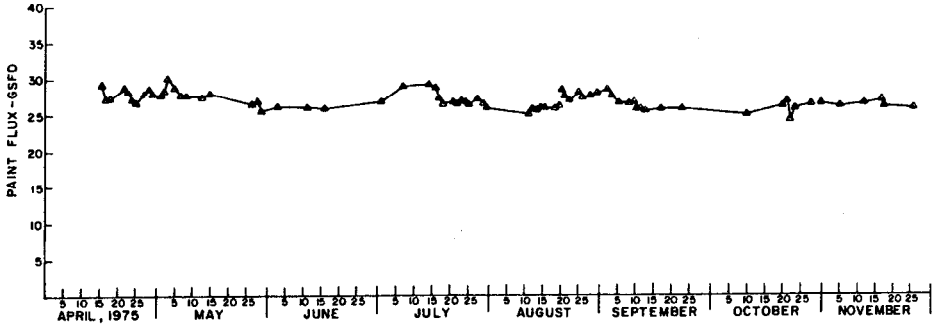


Figure 3.86: UF of electrocoat paint–stability of anodic paint flux with XM-50 membrane.

In the nineteen-seventies, a cathodic paint process was developed where the work piece was negatively charged and the paint particles positively charged. This was a superior coating process but led to severe fouling problems with some of the standard UF membranes (Figure 3.63).[50] The advantage of the cathodic process is related to the fact that there is no metal oxidation and hence no metal ions in the paint film, giving improved resistance of the finished article to corrosion. The membrane fouling problem was solved by using positively charged membranes as in Figure 3.87 or membranes with less electronegativity.

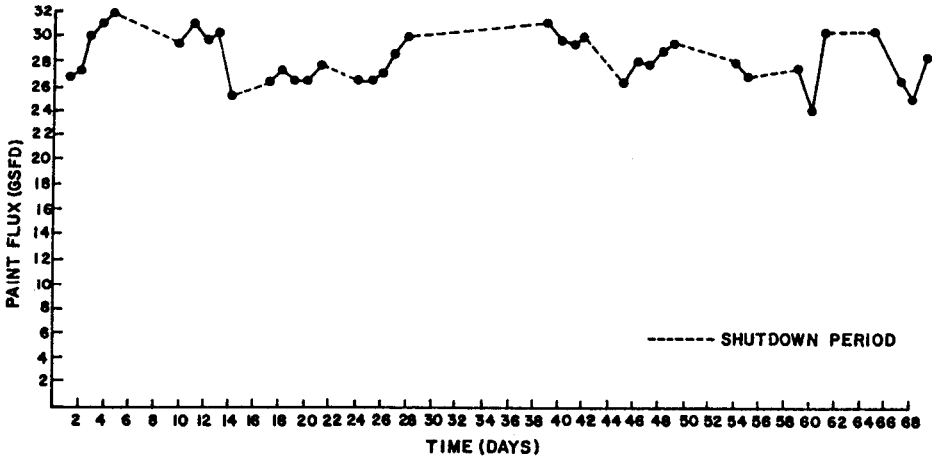


Figure 3.87: UF of electrocoat paint–stability of cathodic paint with CXM membrane (positively charged).

Oil-Water Separations

Billions of gallons of oily wastewater are generated daily. Strict environmental legislation now requires industry to clean up these wastes.

Industrial oily wastewaters can be divided into three broad categories according to the distribution of the oil phase:

(1) Free-floating oil

(2) Unstable oil-water emulsions

(3) Stable oil-water emulsions

Free oil is readily removed by mechanical gravity separation devices. Unstable oil-water emulsions can be broken mechanically or chemically. It is the stable oil-water emulsions which are most difficult and at the same time most amenable to treatment by UF. Chemical coagulation/flotation or contract hauling are usually more expensive alternatives. Further, all chemical treatment methods produce a sludge in which the dirt, floc and trapped water remain in the oil phase.

Stable oil-water emulsions are generated in many diverse industries. *Metal working* operations use water-soluble coolants, cutting and grinding oils, and lubricants for machining. *Metal cleaning* tanks and alkaline degreasing baths gener-

ate an oily wastewater. *Rolling and drawing* operations use oil lubricants and coolants. *Food processing* has waste streams with natural fats and oils from animal and plant processing–particularly vegetable oily wastes. Peel oil is another example from the citrus industry. *Textile manufacturing* will produce natural oils from wool scouring or fabric finishing oils.

Metal cleaning and wool scouring wastes are illustrative of the diversity of oily wastewater treatable by UF.

Metal cleaning operations normally precede painting or plating operations–the objective being to remove dirt and grease. UF can be very useful in this application in extending the useful life of the wash water and reducing the waste disposal problem. Figure 3.88 is a schematic of a prepaint phosphating line before and after introduction of UF. The phosphating treatment prepares the metal surface for bonding with the paint. A well run phosphate line counterflows the rinse stages into the first stage cleaner tank; fresh water is introduced into the third stage rinse which overflows into the second stage, etc. The buildup of oil and dirt in the alkaline cleaning stage is removed by UF; the hot clear, detergent-laden washer solution is then returned for reuse in the first stage reservoir. This closed-cycle counterflow system lowers the oil level in the third stage, reduces detergent costs, and decreases spray nozzle clean-out maintenance time. Further, the savings in disposal charges alone (30-fold reduction in volume) can pay for the UF system in less than two years.

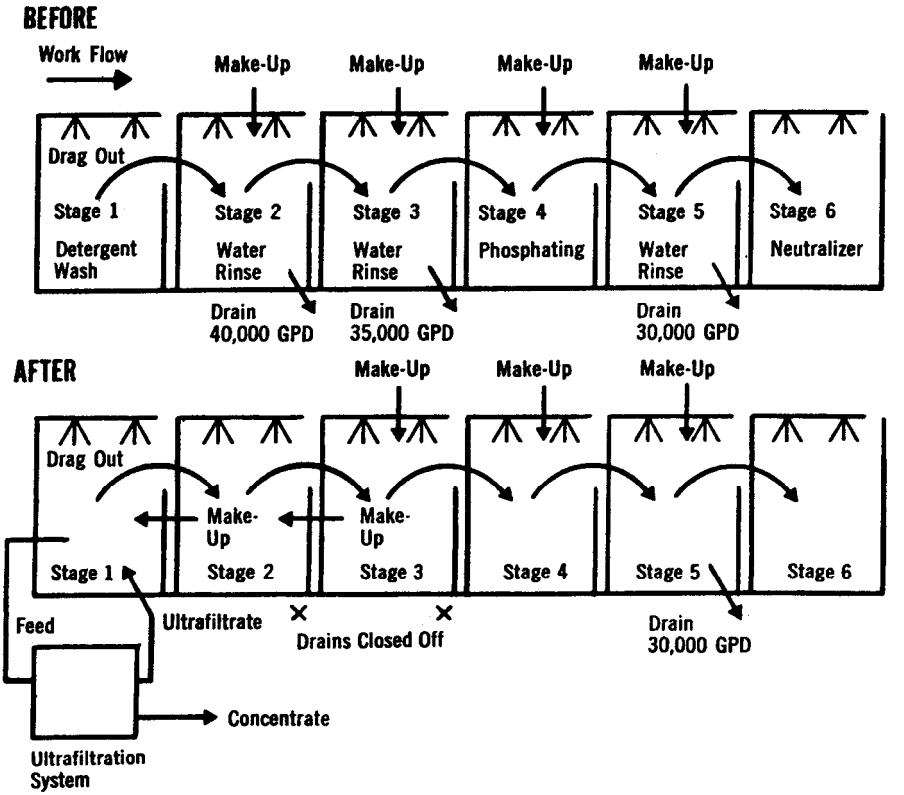


Figure 3.88: Flow schematic of prepaint phosphating line with and without UF.

In the wool scouring process, aqueous detergent solutions are used to remove contaminants from raw wool-principally wool grease and suint (sheep sweat) with smaller amounts of soil and fecal matter. During scouring, the wool grease is emulsified by the detergent solution, the suint dissolves, and the mineral particles become suspended. The waste stream is highly polluting with a COD of 80,000 ppm. UF has been effective in reducing the COD to less than 15,000 ppm as well as decreasing disposal costs.

Oily waste waters suitable for treatment by UF contain 0.1 to 10% oil in a stable emulsion. A limited amount of free oil can be processed but usually quantities above 1 to 5% are removed with a centrifuge prior to UF. The difficulty with free oil or unstable emulsions is that the oil accumulates at the membrane interface and may form a continuous layer which preferentially wets the membrane over water (the surface tension is lower). In this case, the membrane will pass oil and retain water. (See Chapter 2 on the bubble point test). The secret of successful UF is to maintain discrete and stable emulsoid particles of oil (generally over 0.1 μ in size) which are larger than the membrane pore size (0.01 μ or below). When this is the case, oil in the permeate will generally be less than 10 to 50 ppm.

In the presence of poorly stabilized oil emulsions, cellulosic membranes significantly outperform medium surface free energy membranes which, in turn, significantly outperform low surface free energy membranes. Noncellulosic membranes can become wetted with oil more easily-losing their water flux and rejection for oil. If the chemical nature of the oily wastewater requires a more chemically resistant hydrophobic membrane, it is important that a high cross-flow velocity be maintained. (Oil wetting of hydrophobic membranes begins at stagnation points.)

Oil-water emulsions behave like colloidal suspensions showing typical "gel-concentrations" of 75 to 80% (close packing of spheres) and a flux independent of pressure (in the "gel-polarized regime"). Low lubricity emulsions (with a high "synthetic" oil content) are usually characterized by high flux and low fouling rates. Oils containing large amounts of "tramp oil" with moderate to low lubricity show lower flux and require more frequent membrane cleaning. High lubricity oils (containing natural fatty materials) exhibit low flux and are prone to foul the membrane.

Cleaning is normally done with detergent solutions at elevated temperatures (60°C) and high pH for 1 to 2 hours. Usually, UF can concentrate the oil up to 40 to 60%. This can reduce the contract hauling costs by two orders of magnitude. Further, oil concentrations of over 50% can support combustion. If the oil concentrate can be burned in a boiler, any fuel credit can help offset the cost of the UF plant.

Reclamation of Waste Lubricating Oil

U.S. motorists discard about 1.25 billion gallons of oil every year by changing the oil in their automobile crankcase. Despite the fact that these are among the highest quality products refined from our best crude oils, only about 100 million gallons reach recyclers to be re-refined into clean lubricants. The rest is burned as fuel or disposed of as waste. Indeed, a conservative estimate is that over 500 million gallons of used lubricating oil are annually injected directly into the environment through landfills, burning, and other disposal methods.

The idea of recycling these lubricants has flourished when oil is scarce. Presently, the oil glut has put many re-refiners out of business. In 1935, Adolph Hitler prodded German industry to collect and recycle its dirty lubricating oil to help reduce oil imports. Since then, subsidies and legislation have made the concept a permanent fixture in Germany. It is said that even today some two-thirds of West Germany's waste crankcase oil is recycled. Eventual shortages of petroleum reserves will necessitate some form of recycling.

The standard re-refining process uses sulfuric acid to dissolve sludge. The oil phase is further cleaned by clay filtration. The process is so inefficient that one-third of the oil is lost and disposal of the acid solution is increasingly difficult.

The "water-alcohol" method utilizes isopropyl alcohol to decompose metallic soaps. The mixture is then centrifuged to yield clean oil and a watery metallic sludge. Alcohol is recovered for reuse.

UF has the potential of removing all contaminants, but the flux is very low at room temperature. Inorganic UF membranes operating at 300°C and a pressure of 7 bar (105 psi) are capable of processing the oil economically. In one plant in Europe, where the spent lubricating oil is pretreated with thermal shock and centrifugation at 180°C, the UF flux is reported stable between 1000–2000 LSMD (25–50 GSFL) over six months without cleaning.

Decontamination of Crude Oil

Nearly all metal contained in crude oil is either chemically bound with asphaltene type structures or associated with asphaltenes (1000–10,000 daltons). It is necessary to remove these metals to prevent contamination of catalysts.

The present process uses a solvent like hexane or pentane to flocculate the asphaltenes and is relatively expensive. UF can retain the metal asphaltene complexes while passing virtually all other crude oil fractions. Again, the flux is low due to high viscosity. However, an inorganic membrane operating at 330°C on a 10% asphaltene feed produced a permeate with less than 0.5% asphaltenes.

The removal of the carbon-forming asphaltenes and catalyst-fouling metals also reduces the process costs for desulfurization of fuel oil.

PVA Recovery

Polyvinyl alcohol (PVA) is used as a sizing agent to improve the strength and surface characteristics of warp yarns prior to weaving operations where they are subjected to considerable abrasion and tensile stress. The traditional warp sizing agents (starch, gelatins and gums) have been replaced by improved synthetic materials like PVA or sodium carboxymethylcellulose (CMC). PVA sales for this application now exceed 40 million pounds annually. Later in the textile manufacturing process, the sizing agent is removed from the cloth by scouring before dyeing and finishing operations. Because the synthetic sizing agents are not biodegradable, they pose a serious pollution problem.

Although chemical precipitation of these sizing agents is possible, there is a sludge disposal problem. Due to the high cost of PVA and CMC, their recovery with UF and reuse is a much more attractive solution. Figure 3.89 is a schematic of the PVA recovery system. Not only can the PVA be reused, but hot permeate (185°F) can be recycled directly to the desizing bath. The dollar value of the PVA and energy recovered will generally pay for the UF system in 10 to 18 months.

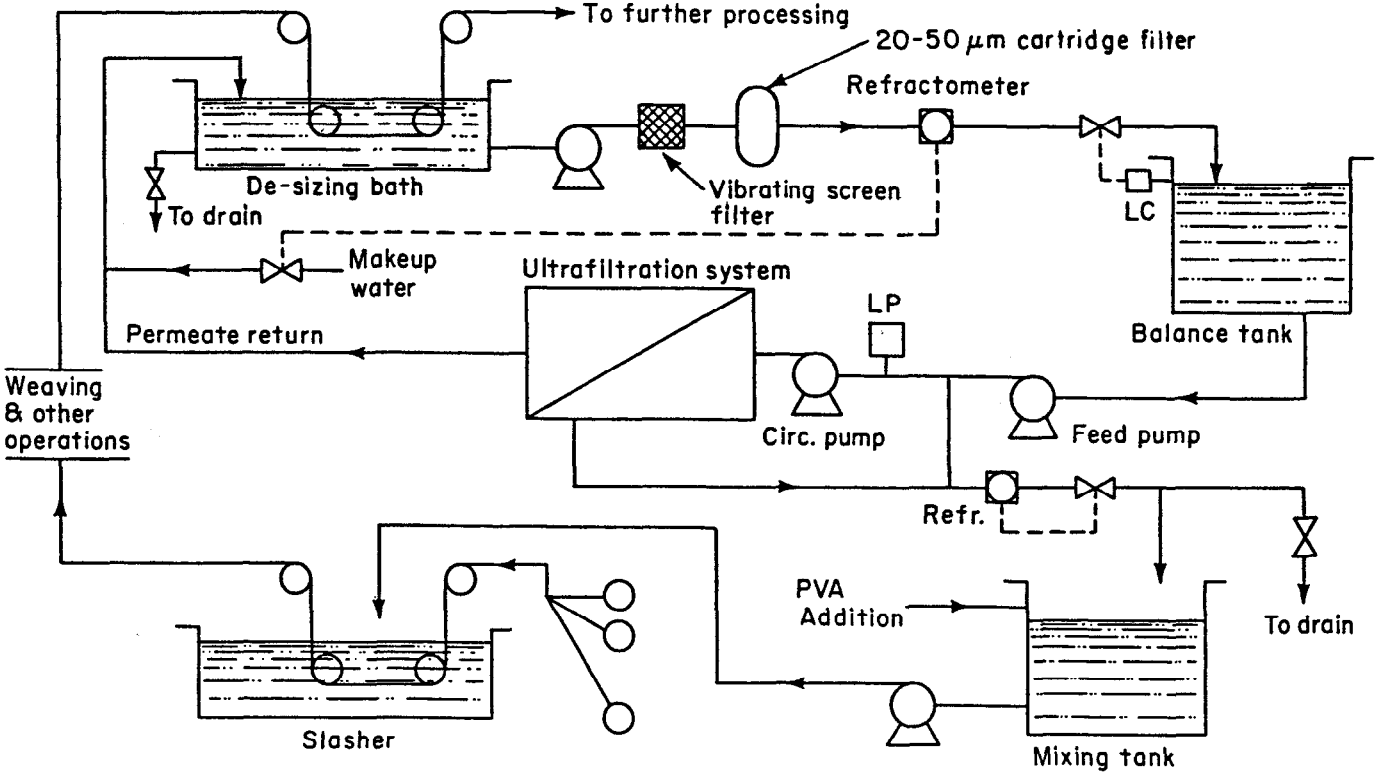


Figure 3.89: Flow schematic of PVA recovery system.

The UF membranes are protected from yarn fibers by a vibrating screen filter and 20 to 50 μ cartridge filters. This makes possible the use of spiral wound modules which have a life of 24 to 30 months. The desizer waste effluent usually contains between 0.5 and 1.5% PVA. The UF concentrates this PVA up to 10% for direct use in the slasher. This final concentration is monitored and automatically controlled by an in-line refractometer. A small amount of desizer waste is purged to drain to prevent the buildup of low MW solutes.

Dyestuff Recovery and Purification

Many dyes are too small to be retained by a UF membrane. Exceptions include polymeric dyes and indigo; the latter has a low molecular weight (262 daltons) but can be retained by a 50,000 MWCO membrane, when in the oxidized state due to its insolubility in water.

The economics of an indigo dye house can be improved dramatically with the recovery of indigo from the plant effluent. Losses through the rinse system can account for more than 10% of the mills' total indigo consumption. A membrane life of 3 years is reported.

Whether recovered by UF or RO, it has been established that recovered dyes can be reused in dyeing operations with no attendant problems and meeting all color specifications.[51]

UF has also been evaluated[52] as a method for purification of polymeric dyes made by the attachment of an azo-chromophore onto a polymeric backbone. This is particularly important when these dyes are used as food colorants. The low molecular weight species and oligomers must be removed to ensure that the product will be nonabsorbable following ingestion.

As expected, these polymeric dyes were rejected completely by the membrane. Surprisingly, Sunset Yellow (MW 452), Schaeffer's salt (MW 246) and tartrazine (MW 534) chromophores were significantly rejected by membranes with MWCO's in the range of 10,000 to 50,000. It is known that dye molecules of this type can associate in solution; but an increase in NaCl concentration, expected to increase the degree of association, decreased the rejection of the dyes. Therefore, it is more probable that the dye molecules adsorb to the membrane making an effective anionic membrane rejecting the charged dyes. At high ionic strength, the charge on the membrane is screened allowing passage. It was found by Cooper et al[52] that a sodium chloride concentration of 15 g/ℓ was necessary to achieve good transport of the small MW chromophores. Alternatively, a high pH[12] had a similar effect.

Latex Concentration/Recovery

The concentration of latex emulsions was one of the early applications suggested for UF. Unfortunately, not all latexes are amenable to processing with UF. Many latexes are unstable under the high shear induced by pumps or even in the thin channels of UF modules. However, the use of diaphragm pumps and careful control of hydrodynamic shear within the module helps prevent coagulation.

UF has been used in place of evaporation to concentrate in-process latex streams from 30% to as high as 65% with reduced energy consumption. Polyvinyl chloride is the most prominent latex in this application.

UF has also been used to clean up polymerization kettle wash waters before disposal. The dilute latex can be concentrated from 0.5 to 25%, thus reducing the volume to be hauled away to $^1/_{50}$ of the original volume. In some cases, the waste latex is recycled for reformulation. Where there is a significant sewer tax, UF is an economical alternative even without recovery of the latex. The dilution of latex during polymerization kettle rinse-down may deplete the surfactant on the polymer particles or introduce multivalent ions, resulting in decreased latex stability. Adjustment of pH or addition of surfactant can prevent coagulation of the latex on the membrane.

If the feed is preconditioned properly, the UF flux is often quite stable. One thousand hours of continuous operation between cleanings is common. When flux decay does occur, detergent washing is usually sufficient to restore flux. In some cases, polymer solvents may be required. Proper selection of a solvent resistant membrane and/or solvents which will dissolve the latex but not affect the membrane is crucial. For PVC latex, the solvents of choice are methyl isobutyl ketone (MIBK) and methyl ethyl ketone (MEK). Styrene butadiene rubber will swell in MIBK, MEK or toluene. Polyvinyl acetate will dissolve in the low MW alcohols such as propyl alcohol. Generally, the membranes are first washed with water, then detergent, followed by another water flush. The system is then drained of all water since it will affect polymer solubility in MEK. Finally, a solvent rinse is employed. If the module is tubular, sponge balls will enhance cleaning.

Removal of Heavy Metals

UF can remove metal values from metal plating wastes provided the metals are first precipitated to form a colloidal suspension. The process is described in Chapter 2 in the section on cross-flow applications. Even though MF membranes provide a higher flux, they are more prone to flux decay than UF due to internal pore fouling. The long term UF flux may be higher than that from MF.

Pulp and Paper Waste Treatment

Although UF cannot recover the low MW sugars in waste from the pulp and paper industry, it can remove lignin compounds and most of the color bodies.

Pulp is made by separating wood into individual fibers. This is done mechanically or chemically. Only 50% of the material in the tree is used as pulp. The remainder is often discarded as waste in the spent pulping liquor.

In the mechanical process, logs are pressed against a rotating grindstone; the resulting fibers are mixed with water and screen filtered. This mechanical pulp contains lignin, gums and mineral salts in addition to the wood fiber.

In the chemical pulp process, wood chips are digested with a chemical "cooking liquor" under high pressure and temperature. There are three major cooking processes. The sulfate or kraft process is the most prominent; about 75% of the wood pulp produced in the U.S. is made by the kraft process. It uses a solution of NaOH and Na_2S, called "white liquor," to remove the lignin that binds the cellulose fibers together in the wood. The loose fibers are then separated from the spent cooking solution–called "black liquor". The soda process uses caustic (NaOH) and the sulfite process uses sulfurous acid (H_2SO_3). If the pulp is to be used in high-grade white paper, it is bleached with chlorine.

Much of the BOD contribution is pulping wastes comes from low MW carbohydrates. RO can often reduce the BOD by 70 to 90% whereas UF effects only a 45 to 55% reduction in BOD.[53] However, UF can remove 85 to 98% of the color bodies.

UF is finding some utility in recovering lignin compounds-used in the production of vanillin, adhesives, detergents, and dispersants. Separating the sugars and lignin compounds solves the problem of sugar contamination in the feed stream to a vanillin plant. Unfortunately, a clean fractionation between the two is not possible even with UF since some of the sugars are bound in lignin-carbohydrate complexes.

Table 3.5[54] shows the retention of sodium base spent sulfite liquor by a series of UF membranes. The multistage UF was carried out in succession from the largest to the smallest pore size-i.e., the permeate from the first stage became the feed for the second stage. Although 90% of the sugar passed through membranes between 100,000 and 20,000 MWCO, the retention increases for 10,000 and 500 MWCO membranes up to 36%. It has been estimated that about 1/6 of the sugars are bound in complexes with molecular weights above 10,000 and an additional 10% in complexes above 500 daltons. In other words, ¼ of all the monosaccharides present in spent sulfite liquor are bound. On the other hand, 100,000 MWCO membranes retained over 50% of the lignosulfonates. It appears (from Table 3.5)[54] that about 70% of the lignosulfonate compounds have a MW over 50,000; only 7.2% had a MW less than 10,000.

Table 3.5: UF of Sodium Base Spent Sulfite Liquor-Retention of Sugars & Lignins

Ultrafilter		Nominal retention, mol.wt.	Original sugar, %		Original lignin, %	
			Passing	Retained	Passing	Retained
XM	100	100,000	92.0	8.0	45.9	54.1
XM	50	50,000	84.5	7.5	30.2	15.7
PM	30	30,000	76.1	8.4	27.6	2.6
UM	20	20,000	69.4	6.7	12.6	15.0
UM	10	10,000	50.9	18.5	7.2	5.4
UM	05	500	32.6	18.3	3.9	3.3

It has also been shown that hydrolysis of the spent sulfite liquor with 6% H_3PO_4 can improve lignin retention by raising its MW through polymerisation.[54]

The discharge of colored effluent is regulated primarily for esthetic reasons, but it may also interfere with plant and animal life cycles by blocking sunlight. Color bodies from pulp and paper mills are difficult to remove by conventional sedimentation and biological treatment; it requires massive lime treatment and is ineffective with spent sulfite liquor (less than 80% color removal). UF can usually remove over 90% of the color bodies and often achieves over 98% removal.

The rejection data of Table 3.6[55] indicate that more than 97% of the color-bearing material has an effective MW greater than 10,000. In these data, the premeate from the UM 10 membrane was fed to the UM 2 membrane and its permeate was fed to the UMO5 membrane. Thus, the UM2 membrane can remove 99% of the color, 64% of the COD and 43% of the TDS.

Table 3.6: UF of Caustic Extraction Effluent-Color Rejection

25-28°C, 47 psig

	Raw Feed	UM10 Permeate	UM2 Permeate	UM05 Permeate
pH	9.9	9.7	9.3	8.5
Color, units	3,190	90	25	20
COD, mg/liter	1,450	540	504	485
BOD, mg/liter	266	214	---	---
TDS, mg/liter	2,945	2,044	1,676	1,560
Product Recovery as percent of feed volume	--	61	88	99
Average Flux (gsfd)	--	21.4	28.4	16.2

Though membranes have been operative in the pulp and paper industry since 1970, growth has been slow. Economic justification has sometimes been marginal; fouling problems often limit membrane life to less than a year.

Dairy Applications

Cheese Whey Protein Recovery. Perhaps the best publicized application for UF is in cheese whey processing. "Cheese whey" is the supernatant liquid produced in the cheese making process after precipitation of casein from milk. There are two types of whey; "sweet" whey (minimum pH of 5.6) results when rennet-type enzymes are used to coagulate the casein to form Gouda and Cheddar cheeses; "acid" whey (maximum pH of 5.1) results from acid-induced coagulation of cottage cheese or casein. The typical composition of cheddar cheese whey and cottage cheese whey is shown in Table 3.7. Whey contains half of the milk solids; i.e., two gallons of milk (17 pounds) yield one pound of cheese and one pound of whey solids. Most of the lactose winds up in the whey along with 20% of the protein.

Table 3.7: Composition of Cheddar and Cottage Cheese Whey

Components	From Cheddar Cheese %	From Cottage Cheese %
Total solids	7.31	6.53
Lactose and lactic acid	5.2.	4.39
Protein (amino acid nitrogen)	0.87	0.86
Ash	0.53	0.61
Fat	0.71	0.67

The lactose is the prime contributor to the high BOD of the whey stream (35,000 to 55,000 ppm). The 150 billion pounds of cheese whey produced each year has become a significant pollution problem choking out aquatic life in

many streams and lakes and imposing a severe added burden on sewage treatment facilities (1,000 gallons = the waste from 1,800 people).

The valuable component of cheese whey is not the lactose but the whey proteins, primarily lactalbumin. The amino acid profile of these proteins is superior nutritionally to casein and is equal to or better than whole egg protein. The heat-denatured form of these proteins has been manufactured for many years usually by heating the cheese whey to precipitate the proteins. The product was tan colored and completely insoluble. With the advent of UF, these proteins could be recovered, concentrated and demineralized athermally. The result was a "whey protein concentrate" (WPC) with improved solubility and other functional properties (emulsification, foamability, water binding, gelation and cloud stability).

Unfortunately, UF of cheese whey does little to help the pollution problem since the lactose passes through the membrane. Initially, a two-step process involving RO, after UF, to recover lactose was envisioned (see Figure 3.90). The recovery of proteins in the first stage (UF) and lactose in the second stage (RO) is shown in Table 3.8.[56] The first stage can be justified economically with the value of the high-grade proteins.

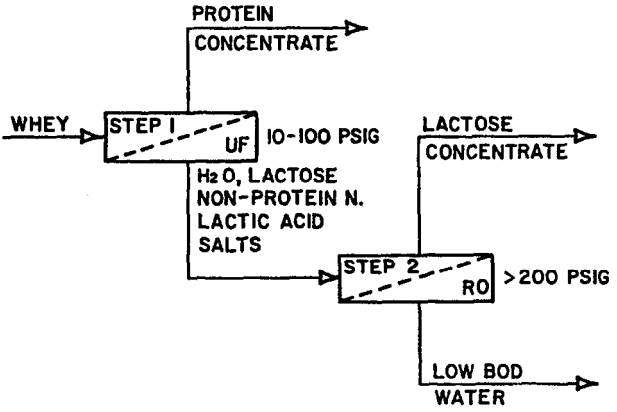


Figure 3.90: Flow schematic of two-stage (UF/RO) membrane process for whey treatment.

Table 3.8: Retention of Proteins, Lactose and COD in Cottage Cheese Whey by UF and RO

	Feed Stream	First Stage Permeate	Second Stage Permeate
Total solids	7.8	6.8	1.8
COD, ppm	65,600	54,100	800
Protein and amino acid N_2, %	0.6	0.15	0.002
Lactose, %	3.9	3.5	0.05
Lactic acid, %	0.52	0.52	0.11

Unfortunately, lactose cannot demand a price sufficient to pay for the second stage. Current world production of lactose is less than 5% of that in whey and future demand shows no significant increase.

The growth of UF for this application has been hindered by the difficulty of using the permeate profitably. This boils down to a profitable utilization of lactose. Figure 3.91 shows the principal uses currently envisioned[57] for UF permeate.

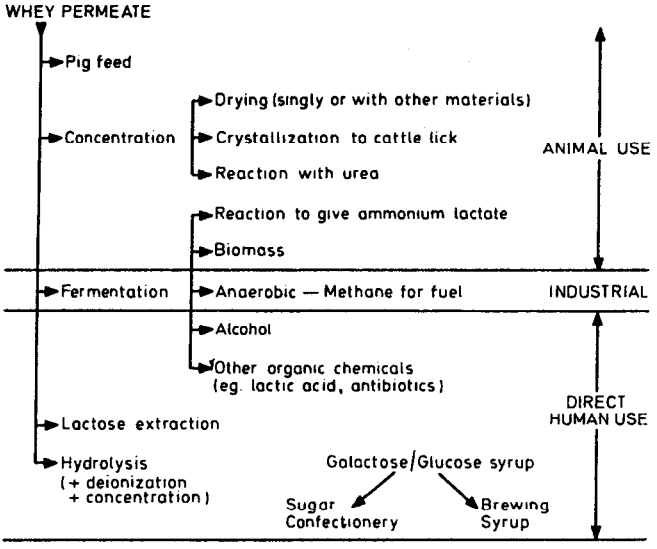


Figure 3.91: Principal uses envisioned for UF permeate.

In Switzerland, 92% of the whey is used for pig feed. Reaction with urea to form lactosyl urea permits greater quantities of non-protein nitrogen to be used in ruminant feeds.

The lactose can also be fermented under aerobic conditions to yield a biomass for animal feed with a crude protein content of about 45%. Several commercial plants in France and Austria are producing biomass in this way, but with marginal economics.

Anerobic fermentation can be used to produce methane to fuel the steam boilers in the creamery, or to produce alcohol for fuel. One ton of lactose will produce a half a ton of alcohol. In 1983, the first fully integrated commercial plant for converting whey to fuel-grade ethanol was constructed in Manteca, California. It has the capacity to process nearly 500,000 lb of whey per day producing 400,000 gal of anhydrous alcohol. In addition to ethanol, the plant was designed to produce whey protein animal feed in wet cake form and a high-protein liquid feed supplement for cattle, hogs and poultry.

Whey wine is an experimental product being test marketed. After deproteinizing with UF, the lactose is fermented for about a week by special lactose-fermenting yeast. The finished product is a pale-yellow, tart, dry wine with a subdued aroma and bouquet.

Hydrolysis of lactose to galactose/glucose enhances its solubility (from 22 to 60%) and sweetness (from 15 to 70%). In 1983, a plant utilizing immobilized lactase to hydrolyze deproteinized lactose (UF) to galactose and glucose was constructed in Winchester, KY (Nutrisearch–a joint venture between Kroger and Corning Glass). A similar plant was constructed in Cheshire, England (joint venture between Corning Glass and the Milk Marketing Board). The resulting syrup is used as a sweetener and as a growth medium for baker's yeast.

Figure 3.92 is a process schematic of the world's largest cheese plant (at time of startup in 1985) in Corona, California. The plant utilizes many of the processes described above producing 5 million lb/year of WPC (by UF) (50 to 75% protein) and 2.2 million gal/year of ethanol for gasohol. The lactose permeate from the UF unit is concentrated by RO before use as a fermentation medium to produce alcohol.

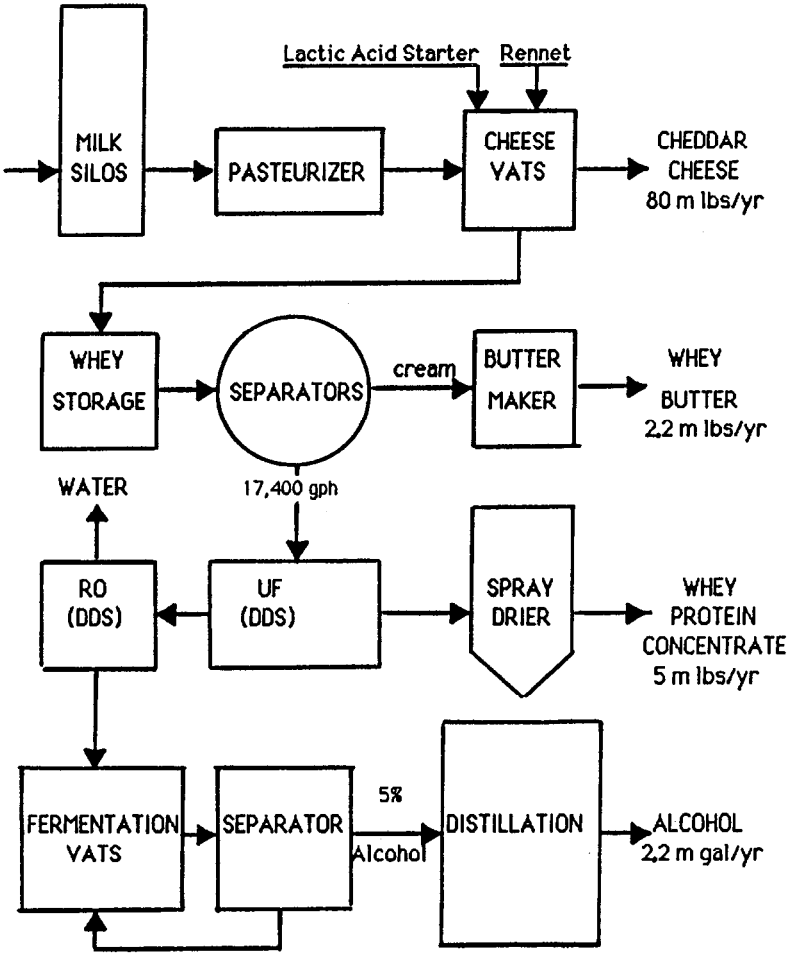


Figure 3.92: Flow schematic of world's largest cheese plant (Corona, CA).

Perhaps the greatest impediment to the use of UF is membrane fouling with a decline in flux; it is particularly severe with cheese whey. Usually a cheese plant cleans its equipment once a day for sanitary purposes with high and low pH. Early cellulose acetate membranes could not withstand the standard cleaning cycles. Today, however, polysulfone and polyvinylidene fluoride membranes may be cleaned with hot (60°C) solutions pH 1–12. In some cases, nonionic detergents (0.1%) are used to remove fat deposits and enzyme detergents are used to hydrolyze protein deposits. Complexing agents such as EDTA and SHMP are useful in removing inorganic deposits such as insoluble calcium slats. Sanitation for all but the polyamide membranes is accomplished with solutions of sodium hypochlorite (with 100 to 200 ppm available chlorine).

Various pretreatments are sometimes utilized to prevent fouling. We have already seen that pH has a marked affect on flux (see Figure 3.37) by altering the solubility of the proteins; pH adjustment can also be beneficial in preventing precipitation on the membrane.

Some of the best work on fouling and pretreatments has been done by Lee and Merson at the University of California at Davis.[58,59] They examined membrane deposits with a scanning electron microscope in an attempt to develop preventive measures against membrane fouling. Systemic prefiltration experiments were conducted[60] to study the effects of removing certain constituents from the whey. The hypothesis was that small amounts of relatively large-sized protein structures and microorganisms provide anchor points which facilitate attachment of the lactoglobulin proteins. Prefiltration designed to remove these anchor structures did indeed lead to a higher flux with greater stability. For example, passing untreated whey through Whatman #1 filter paper doubled the permeation rate of a 10,000 MWCO membrane. They also found that calcium sequestration and raising the ionic strength of the whey increased the flux.

It is expected that new surface treatments of the membrane itself will provide significant improvements in flux stability. UF should be a standard whey processing step in the future. Even today it is estimated that UF treats 10 to 15% of the total world production.

Milk Concentration. One of the most promising innovations in cheese making is to concentrate the casein and proteins in milk with UF prior to coagulation of the casein. Maubois[61] is the inventor of this process. Though the UF permeate still contains lactose, all of the proteins are incorporated in the cheese resulting in a 5 to 20% reduction in milk usage depending on the type of cheese.[62] A two-fold concentration can double the production capacity of each cheese vat and reduce rennet consumption by up to 80%. The savings in milk usage alone can often pay for the UF plant in less than one year.

At first, UF was used to make soft cheese of the Camembert type. Next, semihard cheese like mozzarella was made and more recently, hard cheeses like Cheddar. In 1981, 105,000 tons of hard cheese was made by this process. Denmark has taken the lead in the production of cheese (primarily feta) by UF; in 1981, 92,000 tons (32% of Denmark's total cheese production) was produced by UF.

Because some of the minerals are lost with UF, there are some differences between traditional cheese and that made with UF. In the U.S., this application has been hindered by concern over whether cheese made with UF meets the established standards of identity. In the Spring of 1985, the FDA said feta cheese made from UF may be acceptable in the U.S.A.

There is economic incentive to concentrate the milk on the dairy farm rather than at the cheese factory. This reduces hauling costs but requires a greater capital investment in automating a number of small UF units on many dairy farms. Pioneered in France by Maubois, the first U.S. commercial study on-the-farm was initiated at a 900 cow farm near Lodi, CA in late 1984. The UF project is supervised by R. Zall of Cornell University and is co-sponsored by the California Milk Advisory Board and Dairy Research Inc. Raw milk is heated to 163°F to stabilize micelles in the casein fraction and seal the whey proteins. The milk is then concentrated by UF to half of the original volume and is shipped to several cheese makers producing Monterey Jack, Cheddar and mozzarella. The permeate (containing lactose and soluble salts) is fed to the cows. Preliminary reports indicate significant savings due to reduced transportation and refrigeration costs plus a dollar credit for livestock feed.

If fouling of UF membranes is a problem with cheese whey, it is an even greater problem when concentrating milk. The units on the Lodi farm above are cleaned as follows:

(1) Flush with permeate for 5 minutes

(2) Circulate warm (110°F) water for 20 minutes

(3) Circulate acid for 30 minutes

(4) Circulate warm water for 20 minutes

(5) Circulate chlorinated (200 ppm) alkaline solution for 30 minutes

(6) Rinse with water for 20 minutes

A considerable improvement in UF flux (+100%) and stability can be achieved by prefiltering the milk with a 0.4 μ pore size MF membrane to remove bacteria, fat, lipoproteins and coagulated (denatured) proteins. The MF must be operated in cross-flow to prevent plugging.

There are other markets for concentrated milk besides cheese making. Condensed milk or dietary milks (without lactose or salts) can be easily prepared with UF. The solids concentration can be increased to well over 20% but with large increases in viscosity (over 30,000 cp).

Food and Beverage Applications (Non-Dairy)

Soy Whey. The pollution problem facing cheese makers is also a problem for food processors isolating protein from soybeans, cottonseed and other oilseeds. Purification of soy protein from defatted soy flake involves extraction and precipitation. The supernatant after precipitation is similar to cheese whey except that the protein concentration is only one-third to one-half of that in cheese whey. These low protein concentrations reduce the incentive to use UF; as a result, very few plants use it.

Egg White. The wide spread use of egg white in the baking and candy industries (more than 300 million pounds in the U.S. per annum) arises from its ability to form stable foams which can support relatively large quantities of sugar and/or flour. Fresh egg white contains approximately 88.5% water; it is desirable to remove some of this water to save processing, packaging, refrigeration and transportation costs. However, the proteins are sensitive to heat. Concentration by evaporation or spray drying destroys the functional properties of the

proteins by thermal denaturation. Athermal concentration by UF is ideal.

UF is more appropriate than RO for this application because glucose and inorganic salts pass through the membrane. Glucose reacts with the amino acids in the proteins (the "Maillard reaction") resulting in the development of caramel-like flavors and odors, evolution of CO_2 and the eventual separation of an air-insoluble, dark brown, humus-like material.[56]

Several alternative methods have been developed to retard this browning reaction. The most prevalent method is to reduce free glucose by a controlled bacteria or yeast fermentation to gluconic acid. The fermentation takes anywhere from 2 to 72 hours and adds considerable expense. With UF, protein concentration and glucose reduction can be accomplished simultaneously.

UF concentrates have been shown to have equivalent functional properties with fresh egg white.[56] Even dried solids obtained by spray drying the UF concentrate show improved characteristics over that using spray drying alone.[63]

Economic analysis[64] indicates that savings in transportation and drying costs result in a 40% return on the capital investment required for the UF plant.

Gelatin. Gelatin is a colloidal protein substance whose principal value depends on its coagulative, protective and adhesive powers. It swells up and absorbs 5 to 10 times its weight of water. Water containing only 1% gelatin by weight will gel when cold. There are three different types of gelatin: (1) edible, (2) photographic and (3) inedible (i.e., glue). All types are derived from hydrolysis of collagen (MW 100,000). Since the hydrolysate contains only 3 to 15% gelatin, it must be concentrated. The traditional method has been steam evaporation followed by drum dryers. Again, these elevated temperatures degrade the product with a resulting loss in gelling power. In addition, the salts in crude gelatin tend to degrade the polymer structure and are commonly removed by ion exchange.

UF can perform the required concentration at lower temperatures with simultaneous removal of salts.[65] It is of course true that even with UF elevated temperatures (above 50°C) must be used to keep gelatin liquid. It is advantageous to operate at 70°C to take advantage of the lower viscosity and higher flux.

Fruit Juice. Apple juice processors are using UF to increase juice recovery, improve clarity, reduce materials cost, and to cold sterilize for aseptic packaging.

Before the advent of UF, juice precessors hydrolyzed cloud-stabilizing polysaccharides such as pectin and starch with pectinase, coagulated with gelatin, and then clarified the cloudy cider with a diatomaceous earth filter. The materials collected on the filter provided an ideal substrate on which to grow and multiply bacteria. This resulted in high microbial counts in the juice, but high temperature pasteurization is not desirable because of its effect on flavor.

UF can remove the colloidal haze in apple juice (due to pectins, starch or protein) while all the sugars (fructose, glucose, sucrose) and flavors (sorbital, esters, organic acids) freely permeate the membrane. In the process, all bacteria are removed to produce a clear "sparkling" apple juice which has a long shelf life.

Table 3.9 is a comparison of operating costs for a 70,000 GPD plant replacing the conventional filter press with UF. The major savings are associated with the elimination of diatomaceous earth filtration and the reduction in enzyme (pectinase) requirements. Even with amortization, the operation costs with UF are only 45% of the conventional system costs. The ROI is 42% with a payback in 2.4 years.

Table 3.9: Operating Costs for Clarification of Apple Juice (Conventional Filter Press vs UF)

BASIS: 70,000 GPD (20 HR. DAY)

OPERATING COSTS / DAY ($)

	UF	CONVENTIONAL FILTER PRESS
PECTINASE	363	w Gelatin 1209
MEMB. REPLACE.(3 YRS)	190	polish filter 88
ROUGH FILTER DE		160
POLISH FILTER DE		195
LABOR	40	480
MAINTENANCE	40	60
POWER	58	88
CLEANING CHEM.	39	25
	730	2305
DEP/FINANCING	518	450
TOTAL ($18/1000 GAL)	$1248	45% of $2755

CAPITAL	350,000	PAYBACK	2.4 YRS.
INSTALLATION	20,000	ROI	42%
	$370,000	($5.29/GPD)	After Tax

It is possible to eliminate pectinase altogether, but the UF flux decreases and a larger plant is required. Figure 3.93[66] shows the effect of "depectinization" on the flux. Adding pectinase precipitates soluble pectin into colloidal particles which are more easily ultrafiltered.

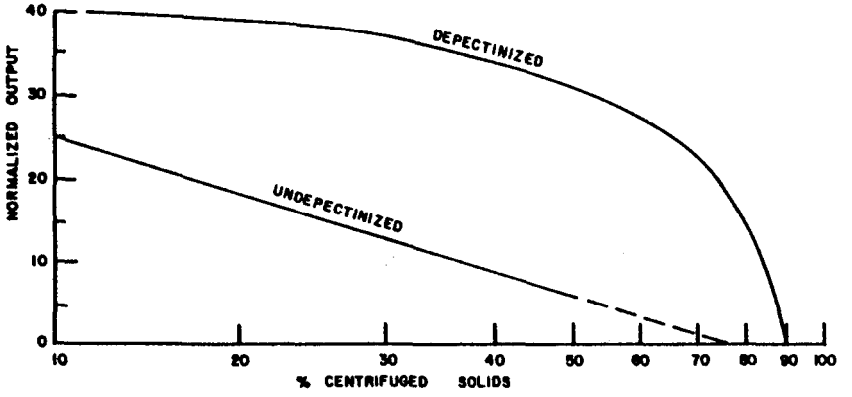


Figure 3.93: Effect of pectin on flux in UF of apple juice.

In some cases, the UF concentrate may be diafiltered (see the section on pharmaceutical applications) to recover the sugar left in the concentrate.

UF produces a superior product with a shelf life of up to 24 months with "sparkling" clarity. The UF permeate will typically read from 0.4 to 0.6 NTUs on a turbidimeter, while conventional juice after DE filtration ranges from 1.5 to 3.0 NTUs. Product yields with UF are typically 96 to 99% compared to 80 to 94% without. Cranberry juice and other juices can be clarified in the same way.

UF of raw sugar juice yields a clear, colloid-free filtrate from which sucrose can be directly crystallized in high yield and purity.[67] In some cases, the UF permeate is then concentrated by RO; this reduces fouling in the RO module and permits a higher RO flux.

Wine. MF membranes (0.45 μ and above) have been used for years to cold sterilize wine and to remove particles and haze. The recent interest in UF of wine is surprising; in the past, winemakers have been reluctant to try even a 0.2 μ pore size for fear it would affect the taste. Yet, several wines processed with UF have recently won awards as some of the best wines in their class.

The current interest in UF is primarily because of its ability to replace several processing steps with a single filtration. The haze in wine is often due to heat-unstable proteins, oxidized/polymerized phenols, gums and pectins. Bentonite and gelatin are added as fining agents to precipitate colloidal proteins so they can be removed with conventional filters. With UF, precipitation is not necessary. It can remove all colloids, tannins, carbohydrates and proteins normally removed by diatomaceous earth and EK pads after fining. In addition, UF can remove the yeast and/or bacteria normally removed by MF.

Some wineries have tried UF as a last resort when wines show recurring heat stability problems. Taste panels have been surprised to find that a UF-processed wine had cleaner nose and better body; the selection of the best MWCO has been determined by the taste panel. In one case,[68] a 10,000 MWCO membrane was chosen to filter a Sauvignon Blanc after the taste panel noticed a significant difference in body with a 1,000 MWCO membrane and the lab determined that a 100,000 MWCO membrane did not provide the heat stability desired.

Press wines are sometimes slightly brown due to higher levels of oxidized phenolics; UF can remove these color bodies along with the slight bitterness from phenols. As a rule, UF appears to accentuate acidity and the lighter fruity elements while eliminating tannic-related "off notes". UF can also be used to increase the tannin content in red wines with poor body or mouth feel (tannin is retained by the membrane).

Often, MF is kept as a final filter for insurance. UF prolongs the life of this filter indefinitely. In spite of DE and pad filtration, MF can clog within 4 to 5 hours without UF.

Beer. There are two primary applications for UF emerging within breweries: treatment of tank sediment and alcohol reduction.

A number of different kinds of filtration have been used to extract beer from tank sediment-including yeast presses and DE filtration. The beer recovered with conventional filter techniques is not of good quality. UF produces a sterile permeate of excellent clarity. Membrane life for tubular systems appears to be about 9 months.

There is an increasing demand for low-alcohol beers which have the beer taste but with fewer calories and not enough alcohol to cause drunkenness. Beer fermented to a low alcohol strength does not develop a satisfactory body, taste and flavor (too little wort). Using UF in the diafiltration mode (see the section on pharmaceutical applications), the alcohol can be reduced to any desired level from the same type of beer. In "diafiltration", as the water-alcohol mixture passes through the membrane, the permeate volume is replaced by an equal volume of pure water so as to not change the concentration of the retained components in the beer.

Corn Starch. UF can recover colloidal starch and other high molecular weight compounds that contribute to the high COD level of the waste effluent from a corn starch plant. Unfortunately, the value of the materials recovered is not high. The plant must be justified on the basis of pollution abatement.[67]

Pharmaceutical and Biotechnology Applications

The diversity of applications for UF in the pharmaceutical industry is unequaled in any other industry group. Concentration, purification, desalting, fractionation and sterilization are all practiced in one form or another. In some cases, the product is in the retentate; in others, it is in the permeate. Occasionally, both retentate and permeate contain valuable products. The fact that all of these operations are possible with UF at ambient temperatures without phase change or addition of chemicals/solvents makes it an ideal separation tool for labile drugs and biologicals. Proteins, polysaccharides, vitamins, hormones, viruses, vaccines and antibiotics are all processed with UF. Even the water to make up these pharmaceutical solutions is often sterilized and depyrogenated by UF (see the discussion on ultrapure water in an earlier section of this chapter).

One of the fastest growing markets for UF and chromatography is in biotechnology. Broadly defined, biotechnology includes any technique that uses living organisms or parts of organisms to make or modify products, to improve plants or animals, or to develop microorganisms for specific uses. In this sense, biotechnology has been practiced by man since the dawn of civilization in baking, brewing, and cheese making. Today's new biotechnology focuses on applications for agriculture and industry. To date, most applications in industry are part of the pharmaceutical industry, which is why we are considering pharmaceutical and biotechnology applications together.

"New biotechnology" focuses on the industrial use of recombinant DNA (r DNA) and cell fusion. For example, "old biotechnology" would produce wine by fermentation but "new technology" seeks to use r DNA to produce wine with a higher alcohol content. Genetic engineering can now take a gene from one organism and slip it into the genetic material of another organism. This reprograms the microbe to perform differently and creates a hybrid without the time delays and chance which occurs in cross-breeding of plants and animals by traditional means. This makes possible the synthesis of new hormones, antibiotics, insulin and interferon.

The commercial success of r DNA and cell fusion technologies is dependent on advances in "bio-process engineering". Most industrial biological syntheses are carried out on a batch scale, with a small amount of product recovered from large quantities of water, cellular components, nutrients, and wastes. It is in this

recovery and/or concentration and purification of products where membranes may be most useful.

The two most important separation techniques for biotechnology appear to be membranes and chromatography. Membrane separations are more easily scaled up and more amenable to continuous processing at less expense than chromatography. On the other hand, chromatography can separate proteins and other macromolecules with greater specificity. Ion exchange chromatography (separating on the basis of electrical charge), high performance liquid chromatography (using gel exclusion principles depending on the pore sizes of the beads), and affinity chromatography (reversibly binding some proteins with very specific ligands/antibodies) can fractionate proteins with a precision unknown in current UF technology (see the section on fractionation of solutes). However, antibodies and antigens have been immobilized on both MF and UF membranes and are sold as immuno affinity membranes for immunodiagnostic tests. These membranes have the potential of combining the specificity of affinity chromatography with the low-cost processing of UF.

Cell Harvesting. In Chapter 2, the application of cross-flow MF to cell harvesting was discussed. Where the products of the fermentation can pass through the UF membrane, it is preferred over MF for cell harvesting. The reason is that asymmetric UF membranes are less prone to fouling and internal pore plugging than are MF membranes.

Enzyme Concentration and Purification. The number of existing enzymes is estimated to be more than 10,000 of which more than 100 have been purified in crystalline form and over 600 in fairly purified form. The molecular weight of enzymes varies from 12,700 (ribonuclease) to over 1,000,000 (L-glutamate dehydrogenase, d-carboxylase). All enzymes are proteins, conjugated proteins or metalloproteins containing one or more active sites per molecule.

Enzymes are highly specific biological catalysts which have an optimum pH and temperature (usually fairly mild conditions) for maximum activity. From a chemical engineering point of view they are the ideal catalyst. Inorganic catalysts are seldom as specific (enzyme catalysts yield almost no by-products) and require high temperatures and/or extremes in pH to be effective.

Because of their protein structure, enzymes may be inactivated temporarily or permanently by heat, chemicals, or shear forces. UF systems can be designed to recover enzymes athermally with minimum shear inactivation (using diaphragm pumps).

The majority of microbial enzymes are produced in relatively small batch fermenters. After separation from the biomass with open membranes, filter presses, or centrifuges, UF is used to concentrate the enzyme and remove small peptides, oligosaccharides and salts.

Crude extracts of enzymes are also obtained from macerated tissues, germination seeds, fermented bran, or the "beer" from the submerged fermentation of selected strains of microorganisms. After extraction and prefiltration to remove suspended solids and particulates, UF is applied as above.

Blood Plasma Processing. Purified therapeutic proteins are derived from human blood plasma via cryoprecipitation followed by sequential precipitations effected through increasing ethanol concentrations at controlled temperature, pH and ion composition ("Cohn precipitation"). As discussed in the section on fractionation of solutes, UF cannot be used to fractionate the various plasma

proteins; but it is used in subsequent processing steps. Indeed, the concentration and purification of the various protein fractions was among the earliest applications for UF in the pharmaceutical industry.

When the ethanolic precipitates are separated from their supernates, they must be redissolved and concentrated. Further, ethanol and salts must be removed prior to sterilizing filtration with MF and dispensing into containers suitable for I.V. delivery. UF is preferred for protein concentration, ethanol removal and desalting; there is less denaturation and it is more efficient than gel permeation, vacuum freeze-drying, or thin-film evaporation. A major advantage of concentration by UF over conventional evaporation or lyophilization is that the salts are not concentrated by the process, but freely pass through the membrane. Thus, the ionic environment for the protein remains constant. Further, since the solvent does not undergo a phase change, no latent heat is required, and energy costs are reduced. Finally, since the product need not come into contact with an air interface, there is less denaturation.

Albumin preparations are routinely concentrated with a 10,000 to 30,000 MWCO membrane so as to contain up to 25% protein; in some cases, concentration to 40% has been reported.

Gamma-globulin is also routinely concentrated by UF. Buffer solutions are used to enhance its solubility; gamma-globulin is more prone to precipitation than albumin.

UF has also been used to concentrate antihemophilic coagulation factor VIII (AHF) with no measurable loss in activity; it is particularly susceptible to thermal and shear denaturation. All of the other plasma proteins, including antithrombin III have been concentrated as well.

Removal of alcohol salt and other low molecular weight substances can be done most efficiently with UF in the diafiltration mode.

Diafiltration. Diafiltration refers to the process by which UF can rapidly and efficiently remove salts and/or lower molecular weight species from larger macromolecules. It is commonly used for fractionation as well as desalting and is practiced both as a discontinuous and as a continuous process.

Figure 3.94 is an example of the *discontinuous process* occurring in three steps: (1) concentration, (2) dilution and (3) recovery.

In the first step, the enzyme is concentrated six-fold from 3 to 18%. (Notice that even though salt is removed in the permeate, the salt concentration remains at 3% in retentate and permeate since it is freely permeable to the membrane.) In the second step, the process stream is diluted by a factor of three to reduce the salt concentration from 3 to 1%. (As a consequence, the enzyme is now also diluted by a factor of three; from 18 to 6%). In the third step, the enzyme is reconcentrated three-fold from 6 to 18%. The net result is the enzyme has been concentrated six-fold while the salt concentration has been reduced three-fold.

Continuous diafiltration is generally more efficient and preferred. In this approach, a batch of the solution to be desalted is maintained at constant volume by adding pure water (dialysate) at the same rate permeate is removed. In this way, the proteins (or other macromolecules retained by the membrane) remain at their initial concentration while the salt concentration decreases continuously. This has been called "constant volume molecular washing" because the salts are washed out of solution. Continuous diafiltration reduces the processing time required in the discontinuous process.

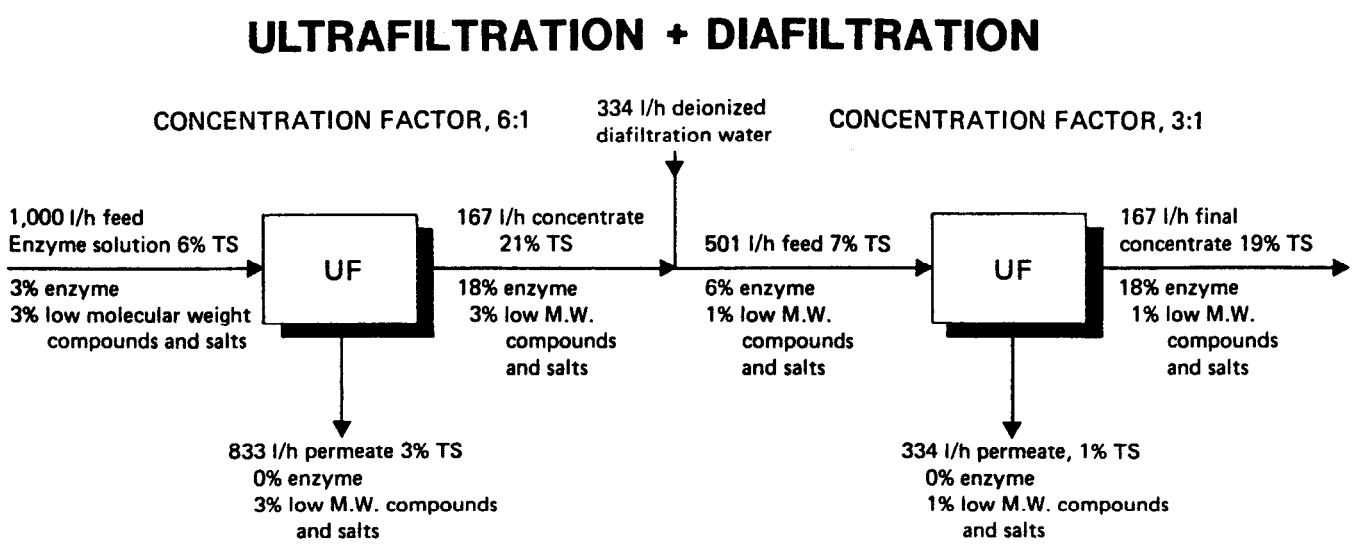


Figure 3.94: Flow schematic for discontinuous diafiltration and concentration of enzymes.

When microsolute exchange is desired, the dialysate fluid contains the microsolute intended to replace the microsolute in the starting solution. For example, diafiltration can be used to exchange one surfactant for another in a polymer latex to enhance stabilization. In the pharmaceutical industry, one buffer can be exchanged for another using diafiltration.

Fractionation of two macromolecules (with a large difference in molecular weight) can be accomplished more completely using diafiltration. The entire fractionation can be carried out at low concentrations, avoiding problems associated with higher concentrations like low flux or denaturation.

In the past, the most common method used for microsolute removal has been batch dialysis. The solution to be dialyzed was placed in seamless regenerated-cellulose tubing ("sausage bags") and suspended in the dialysate allowing salts to diffuse across the membrane. With diafiltration, the same degree of salt removal can be accomplished much more rapidly with smaller volumes of dialysate. The pressure driven convective transport of solutes across the membrane is much faster than concentration driven diffusion (particularly at low salt concentrations). In addition, with diafiltration, all solutes (salts and alcohol) are removed at the same rate independent of the size and diffusivity of the various species; this makes the process more predictable and controllable.

Assuming the microsolute to be removed is freely permeable to the membrane (R = O), a simple mass balance reveals that solute removal is exponential:

$$\ln\left(\frac{C_0}{C_f}\right) = \frac{V_t}{V_0} \tag{31}$$

where C_0 = the initial microsolute concentration in the batch

C_f = the final microsolute concentration after volume V_t of wash solution (dialysate) has passed through the batch

V_t = the volume of wash solution (dialysate) added to the batch, also equal to the volume of ultrafiltrate removed through the membrane

V_o = the initial volume of the batch.

When microsolutes are to be exchanged or "washed in", Equation 31 becomes:

$$\ln\left(\frac{C_d}{C_d - C}\right) = \frac{V_t}{V_0} \tag{32}$$

where C_d = the concentration of microsolute in the dialysate feed (constant)

C = the concentration of the microsolute washed in with volume V_t

Since continuous diafiltration involves the processing of a fixed volume (V_o), it is convenient to speak of the number of volume turnovers, V_t/V_o required to

achieve a fixed reduction in microsolute content. For example, Equation 31 predicts that a 3 volume turnover will effect a 95% reduction in microsolutes and a 5 volume turnover will wash out more than 99% of the salts. Equation 31 is plotted in Figure 3.95.

When the permeable species is partially rejected by the membrane (as in fractionation), a higher wash volume turnover will be required to achieve the same degree of clearance. Figure 3.96 may be used to predict solute clearance for a specified membrane retention (R).

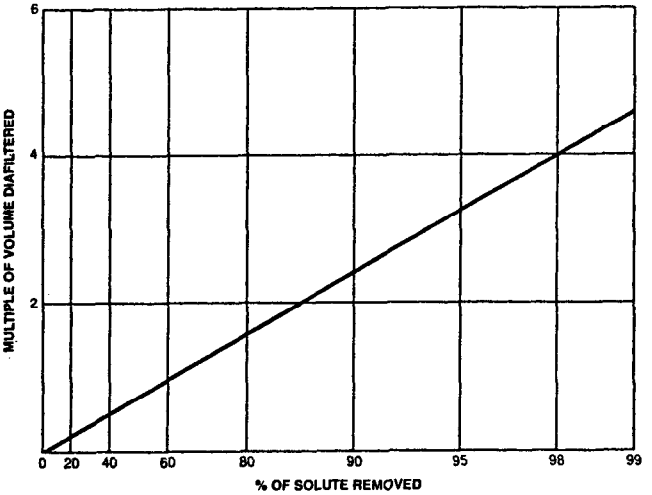


Figure 3.95: Turnover required to achieve a specified reduction in microsolutes (R = 0) by diafiltration.

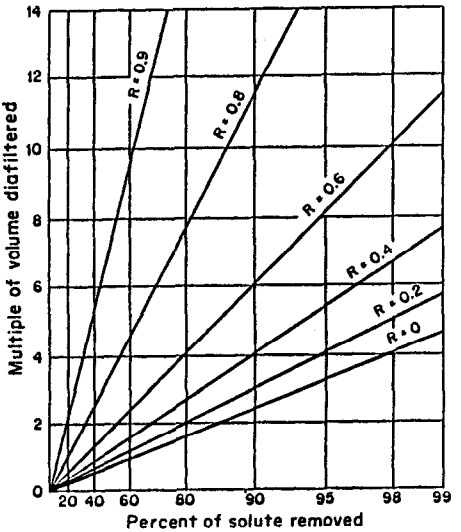


Figure 3.96: Turnover required to achieve a specified reduction in microsolutes (having various rejections) by diafiltration.

Often, the end result requires both concentration of macrosolute and reduction of microsolute concentration as in Figure 3.94. To optimize the process, we must find the macrosolute concentration at which the diafiltration processing time is minimized. If we diafilter at the starting concentration (3% in Figure 3.94), we will achieve high flux but the volume of dialysate required for the desired salt removal will be enormous. On the other hand, if we first concentrate the enzyme to its final concentration (18% in Figure 3.94), we will reduce the volume to be processed, but the flux will decrease. Ng[69] and Cooper[70] have derived the equation which specifies the optimum concentration (C*) at which the diafiltration process time is minimum.

$$C^* = \frac{C_g}{e} \tag{33}$$

where C_g is the gel concentration and e is exponential e = 2.718.

For example, if the gel concentration (C_g) of the enzyme of Figure 3.94 is 27%, the optimum concentration (C*) at which to carry out diafiltration would be 10%. Thus, the minimum processing time would start with concentration of the enzyme from 3 to 10%, diafiltration at 10% (requiring 1.1 volume turnovers to reduce the salt concentration by three-fold-see Equation 31 and Figure 3.95), followed by concentration of the enzyme from 10% to the final concentration (18%). Since diafiltration does not change the volume of the batch, the *total* concentration time would be constant regardless of whether it is carried out in one step or two steps separated by diafiltration. Because the processing time required for diafiltration is a minimum at 10%, the time required for diafiltration at 3% or 18% would be greater.

Virus Concentration. In large scale virus production, concentration of the virus or its proteins is frequently necessary to obtain workable volumes for subsequent processing. Often continuous-flow zonal centrifuges are used for this purpose but with a significant loss in biological activity. Most viruses are larger than 0.01 μ and can be safely (closed system) concentrated with a 80,000 MWCO membrane without loss of activity.

Hormones, extracts and a host of other materials can be concentrated or purified by UF.

Enzyme Reactors. We turn now to new developments, not fully commercialized, which utilize UF membranes in the processing of pharmaceuticals and biologicals. The first of these is the enzyme reactor.

Enzymes facilitate many biochemical reactions, serving as a catalyst-i.e., the enzyme itself is not consumed in the reaction. In fact, it must be separated from the products of the reaction. In the past, the enzyme was discarded and fresh enzyme was charged to the reactor with substrate. Obviously, the economics of such a reactor can be improved dramatically if the enzyme can be recovered and reused. One way of doing this is to immobilize the enzyme on a column of glass beads; substrate is fed into one end of the column and products are withdrawn from the other end. Because the enzyme is affixed to the stationary phase, it does not contaminate the product and may be used over and over again.

Enzymes may also be immobilized on membranes in the same fashion. Three types of enzyme reactors using UF membranes are introduced here. The equa-

tions which describe their operation may be found with a more thorough description in Chapter 7.

Mobile Enzyme. Figure 3.97 is a schematic of a continuous enzyme membrane reactor where the enzyme is free and mobile. It is, however, retained by a UF membrane which is permeable to the products of the reaction. (In this scheme, the enzyme must be larger in size than the products.) The advantage of this configuration is that there is no steric hindrance to the proper orientation of enzyme molecules with the substrate molecules. The disadvantage is that the enzyme is more likely to become inactivated due to the continuous pumping recirculating the enzyme through the UF unit.[71]

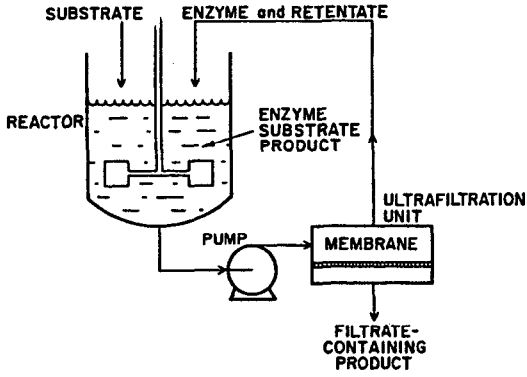


Figure 3.97: Flow schematic of a continuous enzyme membrane reactor (mobile enzyme).

Figure 3.98 shows data of Wang[72] on the continuous hydrolysis of starch to glucose by glucoamylase The difference in carbohydrate concentrations in the retentate and filtrate is small because the product glucose is freely permeable across the 10,000 MWCO membrane. Only the larger dextrins entering the cell as substrate are rejected.

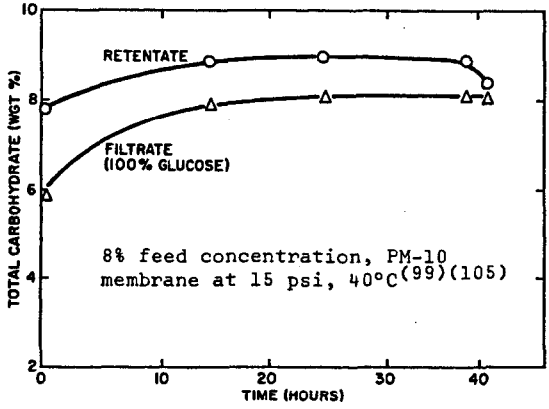


Figure 3.98: Continuous hydrolysis of starch by glucoamylase in membrane reactor.

Figure 3.99 shows Wang's data on the hydrolysis of starch by α-amylase using the same MWCO membrane. Here the difference in carbohydrate concentrations between retentate and permeate is much larger because the products of α-amylase hydrolysis are predominantly maltose and larger dextrins. Eventually the dextrins are hydrolyzed to glucose, but at a slower rate. Thus, the carbohydrate concentration in the reactor increases with time. These results suggest that the selection of membrane MWCO can control the products of the reaction.

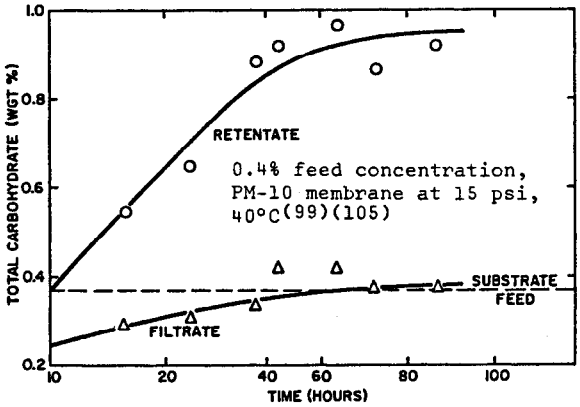


Figure 3.99: Continuous hydrolysis of starch by α-amylase in membrane reactor.

Immobilized Enzyme. Figure 3.100 is a schematic of a continuous immobilized enzyme membrane reactor. Here the enzyme is immobilized within the sponge wall of UF hollow fibers. The membrane skin, on the inner wall of the fiber, acts as a retentive barrier to enzyme transport into the lumen of the fiber. This means it is not necessary to immobilize the enzyme onto the membrane surface unless deactivation results. (If immobilization is desirable, glutaraldehyde may be used to crosslink the enzyme or cyanogen bromide may be used to covalently bond the enzyme in place.)

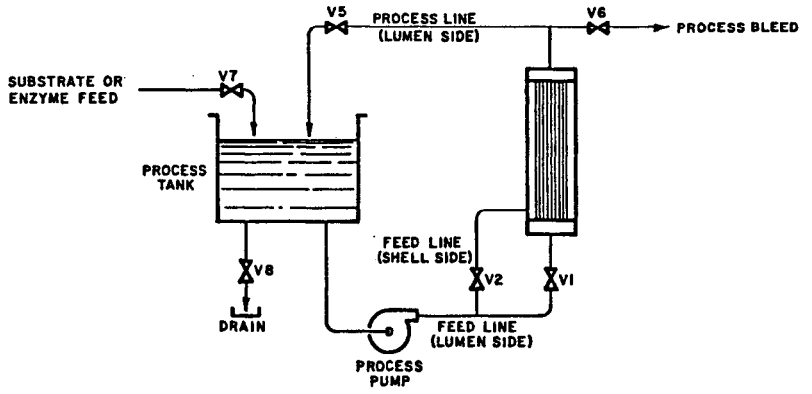


Figure 3.100: Flow schematic of continuous immobilized enzyme membrane reactor.

This reactor can be operated in two ways. When the substrate is fed to the shell side of the hollow fiber module ("back flush mode"), the substrate comes in contact with the enzyme in the fiber wall and product passes into the lumen of the fiber from which it exits the module. When the substrate is fed to the lumen of the fibers (with all permeate ports closed), it will pass from the lumen to the shell side where it contacts the enzyme and products will recycle back to the lumen ("recycle mode") (see Figure 3.72). The "recycle mode" has the advantage over the "back flush mode" in that the substrate does not have to be free of suspended matter. In the "back flush mode", particles in the substrate would plug the sponge wall.

Breslau and Kilcullen[73] have compared the "back flush mode" with the "recycle mode" on hydrolysis of lactose with lactase. Table 3.10 shows their results. Note they operated the "back flush reactor" in both recirculating and single pass modes. If there is significant product inhibition, a single pass may be required. To achieve higher conversions, the product stream may be taken through valve V 6 to subsequent stages to get 4 passes as in the table. Both modes of operation can achieve the desired conversion.

Table 3.10: Lactose Hydrolysis Via Hollow Fiber Reactors

A. Backflush Reactor

Fiber Diameter:[1]	20 mil	45 mil
Loading Density:[2]	0.9 gms lactose/ft^2	5.45 gms lactose/ft^2
Substrate:	4.5% Lactose	10.0% Lactose
Method of Operation:	Recirculating	Single Pass

Time Min.	Conversion, %	Number of Passes	Conversion, %
0	0.0	0	0.0
20	5.3	1	21.1
60	9.2	2	30.8
90	11.0	3	36.0
1440	40.9	4	40.0

B. Recycle Reactor[3]

Fiber Diameter:[1]	45 mil
Loading Density:[2]	5.45 gms lactose/ft^2
Substrate:	10.0% lactose
Method of Operation:	Recirculating

Time Min.	Conversion, %	Time Min.	Conversion, %
0	0.0	120	17.7
15	3.8	180	22.0
60	10.6		

Footnotes

1. Fibers used in this study were 20 mil diameter XM50 and 45 mil diameter XM50. These fibers have a molecular weight cutoff of 50,000. Fibers with molecular weight cutoffs of 10,000 and 5,000 are also available.
2. Wallerstein lactase (200,000 LU/gram activity)
3. The recycle reactor was operating at 25 psi inlet, 23.5 psi outlet in this study which gave an average driving force for permeate flow of less than 1 psi.

Disperse Soluble Immobilized Enzyme. As we have seen, enzymes immobilized on a membrane have increased stability. The primary disadvantage to immobilization is the restricted access of the enzyme to the substrate. Dunhill et al[74] have explored the immobilization of enzymes to mobile supports. Specifically, they have attached the enzyme to a soluble high MW polymer which tended to stabilize the enzyme while reducing steric hindrance and increasing access of enzyme to substrate. For example, chymotrypsin has been attached to a soluble dextran using 2-amino-4,6-dichloro-s-triazine as a coupling agent. This complex was retained in a reactor by a 100,000 MWCO UF membrane in a configuration similar to that shown in Figure 3.97. Table 3.11 shows the relative activities as a result of immobilization. Though less than the free enzyme, the dextran enzyme complex had more than six times the activity of the enzyme immobilized on solid DEAE-cellulose.

Table 3.11: Relative Activities of Immobilized Chymotrypsin

	Substrate	
	ATEE	Casein
Chymotrypsin	100	100
Dextran - Chymotrypsin	81	73
DEAE - Cellulose - Chymotrypsin	13	7

Enzyme stability at 40°C is demonstrated in Figure 3.101 for the complex. A reactor was operated continuously for two weeks at 20°C hydrolyzing casein with no loss in enzyme activity.

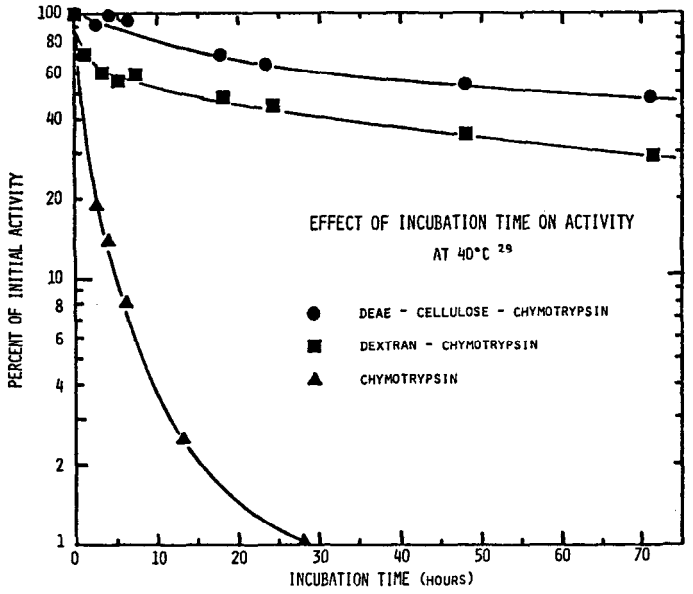


Figure 3.101: Immobilized enzyme stability (chymotrypsin).

For those reactions where the products are larger in molecular weight than the enzyme, one is forced to go to an immobilized enzyme system or to this system where the dextran-enzyme complex can be made larger than the products.

Membrane Fermentors. Many of the advantages of enzyme membrane reactors are applicable to fermentors. In some cases, a fermentor is simply an enzyme reactor using intracellular enzymes rather than extracellular enzymes. Enzymes are usually more stable within the cell wall and the living cell can regenerate itself along with the enzyme. A possible disadvantage is that the enzyme activity per unit reactor volume may be less in the cells than that of a pure enzyme preparation.

There are two primary types of membrane fermentors. These are discussed more thoroughly in Chapter 7.

Mobile Cells. Figure 3.102[75] shows one of the earliest concepts of a continuous membrane fermentor. The membrane retains the biomass while products of the fermentation are continuously withdrawn through the membrane. In addition, metabolic waste products, which inhibit cell growth, are removed continuously through the membrane, thereby improving cell growth and fermentor productivity.

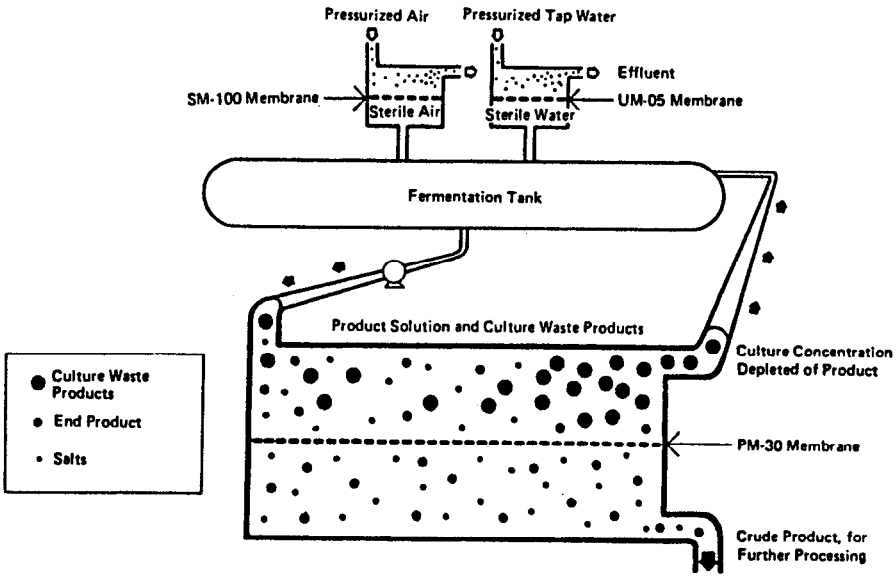


Figure 3.102: Flow schematic of continuous membrane fermentor.

The increase in cell production due to UF is shown in Figure 3.103.[76] *Clostridium histolyticum* is cultivated in batch and continuous fermentors. In the batch system, the organism approaches a stationary phase at about the twelfth hour due to toxic metabolite production. In the continuous fermentor, fresh substrate is fed continuously and the toxic products are continuously removed enabling growth to continue well past the fortieth hour. Likewise, the enzyme production from this fermentor is enhanced (see Figure

3.104).[76] In the stationary phase of the batch fermentation, enzyme activity begins to decrease due to an increasingly unfavorable environment. In the membrane fermentor, protease (the enzyme) continued to be excreted by the growing biomass for 50 hours. The ratio of enzyme excreted per unit mass of cell produced in the membrane system (70 units/mg) was almost twice that from the batch system (45 units/mg). This would indicate that under the more favorable environment in the membrane fermentor, the organism is more efficient.

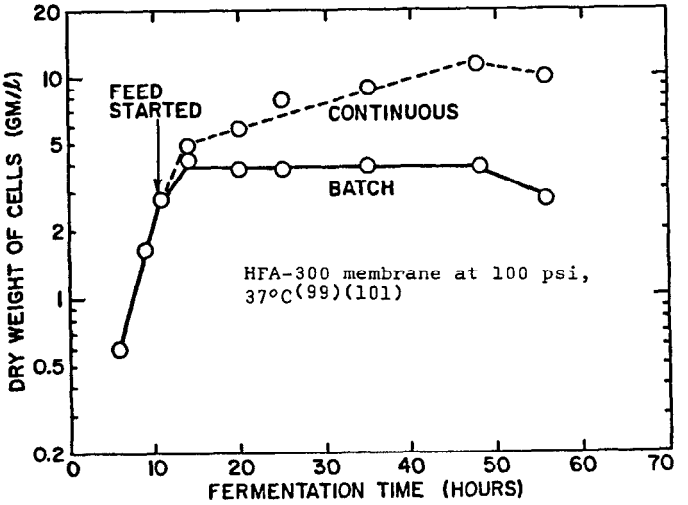


Figure 3.103: Comparison of batch and continuous fermentors in cell production.

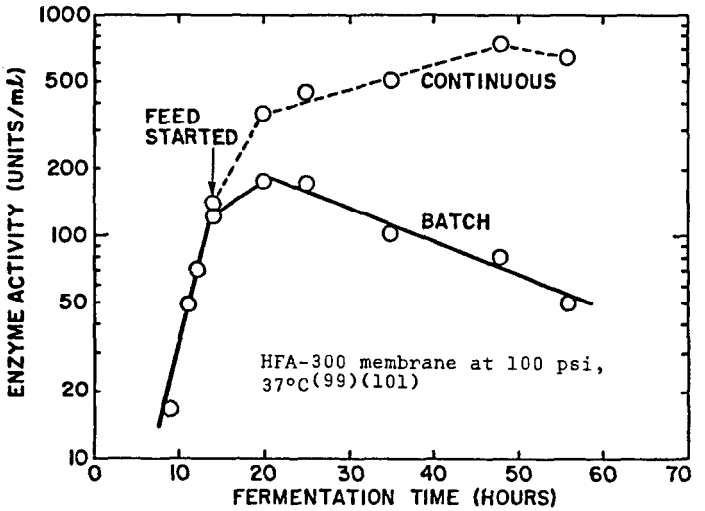


Figure 3.104: Comparison of batch and continuous fermentors in enzyme production.

Other continuous membrane fermentors show similar results. In the continuous production of ethanol from *Zymomonas mobilis*, the production rate was 120 g/hr/ℓ compared to less than 8 g/hr/ℓ for the batch system.[77]

Immobilized Cells. Cells can be immobilized in the walls of UF hollow fibers and can grow to tissue-like densities (10^6-10^7 cells /cm^2) between the fibers. This is about 10 times higher than densities achieved in roller bottles; the hollow fibers act like natural capillaries in carrying nutrients to the cells and in removing toxic wastes. Cultures can be maintained for months at a time. Products like interferon, monoclonal antibodies, antigens, viruses and hormones may be produced continuously with dramatic increases in yield. In addition, where proteins such as monoclonal antibodies are being produced, subsequent purification steps can be simplified because the product occurs in high concentrations with lower concentrations of serum components than is the case with conventional mouse ascites fluid or suspension culture procedures.

Drioli[78,79] has also been successful in casting cellulose acetate and polysulfone UF membranes with a thermophilic microorganism (*Caldariella acidophila*) in the casting solution (30 to 40%). The organism showed good resistance to organic solvents like acetone used in the casting solution. Drioli reports significant activity compared with a similar amount of free cells and no decrease in activity after 90 days. He has used this bioreactor to hydrolyze lactose to glucose and for malolactic fermentations. For more information, see Chapter 7.

Waste Treatment

Though UF can do little in removing low MW contributors to BOD and COD, Dorr-Oliver has commercialized a process which couples a UF membrane to an activated sludge reactor.[80] Referring to Figure 3.102, an activated sludge reactor replaces the fermentation tank. Comminuted raw sewage is fed continuously to this reactor and mixed liquor is continuously circulated through the UF unit. All of the effluent passes through the membrane.

The addition of UF to an activated sludge reactor has a number of advantages.[81]

(1) Since the membrane retains the biomass, clarifiers are unnecessary. This also means that the concentration of mixed-liquor suspended solids in the reactor can be increased from 3,000 to 50,000 ppm, thereby reducing the size of the reactor. It is also thought[82] that the presence of this large biomass absorbs components in the raw sewage which would normally foul the membrane-perhaps irreversibly.

(2) Since the membrane is retentive of slowly biodegradable components in the sewage, the required detention time may be reduced or the treatment efficiency at the same contact time may be increased. Essentially infinite detention time is provided for the slowly biodegradable materials making it possible to metabolize raw sewage almost completely, with no generation of excess activated sludge. Thus, sludge wastage from such a system occurs infrequently (perhaps bimonthly or quarterly) and in very small volumes. The system is "self-assimilating".

(3) By virtue of the infinite detention times for large unassimilated organics and the adsorption of small pollutants within the biomass, the BOD and COD of the effluent is considerably reduced not to mention the complete elimination of all suspended solids.

	BOD (ppm)	TSS(ppm)
Conventional Activated Sludge	<55	<60
Extended Aeration	<30	<70
Bio-membrane Process	<10	0

The diffusate BOD and TSS values for the biomembrane process indicate an overall BOD reduction of 95% or better and a 100% reduction of TSS.

In addition, coliform bacteria density determinations over a period of six months indicated that 90% of the time, the effluent contained less than 100 coliform bacteria/100 ml.

(4) The addition of powdered carbon to the biomembrane loop facilitates rapid start up and prevents fouling of the membranes with oils and greases. Carbon adsorbs soluble organic constituents and slime generating grease, preventing pollution of the final effluent (diffusate) until the biomass has developed to the point where it can digest these pollutants. Furthermore, the activated carbon acts as a catalyst to enhance the multiplication rate of the biota population in the system. Thus, start up times are reduced from days to hours. Carbon is left in the system to scour away foulants from the surface of the membrane and is regenerated biochemically.

Several bio-membrane plants utilizing this process have been put into operation by Dorr-Oliver. The oldest were installed in industrial plants in Connecticut in 1967.

In 1970, a 30,000 gpd plant (15,000 gallons in a 12-hour period) was supplied to the city of Colorado Springs for treatment of sanitary waste originating at the tourist station located on the top of Pikes Peak. The rapid start up (3 to 4 hours) is ideal for the short tourist season on the mountain. The compactness of the unit ($8' \times 8' \times 20'$) is an asset since space is a premium. The reclaimed water is not used for drinking, only for washing and flushing toilets, but analysis shows the effluent is of better quality than the Colorado Springs tap water.

SUMMARY

In its twenty-five year (plus) life, ultrafiltration has been shown to be a reliable and economical process for many applications. It has eliminated severe pollution problems while recovering valuable by-products which have sometimes paid for the plant in less than a year.

Yet to be solved are the fouling and flux decay problems encountered in the processing of milk and cheese whey. Permanent surface treatments of mem-

branes by grafting techniques promise to alleviate fouling problems in some instances.

Bioreactors utilizing UF hollow fibers appear to have tremendous potential for continuous enzyme reactors and fermentors.

As more stringent environmental controls are required and long-term energy costs rise, there is no doubt that UF will expand rapidly into many new applications.

REFERENCES

1. Reid, C.E. and Kuppers, J.R., *J. Appl. Polym. Sci.*, 2 (1959) p. 264 ff.
2. Reid, C.E. and Breton, E.J., *J. Appl. Polym. Sci.*, 2 (1959) p. 133 ff.
3. Dobry, A., *Bull. de la Societe Chim. de France*, 5 (1936) pp. 312-318.
4. Loeb, S. and Sourirajan, S., *Sea Water Demineralization by Means of a Semipermeable Membrane*, UCLA Dept. of Eng., Sea Water Research, Rept. 60-60 (July, 1960).
5. Strathmann, H., Scheible, P. and Backer, R.W., *J. Appl. Polym. Sci.*, Vol 15 (1971) pp. 811-828.
6. Epperson, B.J. and Burnette, L.J., *Development and Demonstration of a Spiral-Wound Thin-Film Composite System for the Economical Production of Oxygen-Enriched Air*, Final report, Dept. of Eng., No. CS/4029H (Nov., 1983).
7. Loeb, S., "A Composite Tubular Assembly for Reverse Osmosis Desalination", Dept. of Eng., UCLA, unpublished.
8. Grandine, J.D., II, U.S. Patent 4,203,848 (May 20, 1980).
9. Eirich, F.R., So, M.T., Strathmann, H. and Baker, R.W., *Polymer Letters*, Vol. 11 (1973) pp. 201-205.
10. Aptel, P., Abidine, N., Ivaldi, F. and Lafaille, J.P., *J. Membr. Sci.*, 22 (1985) pp. 199-215.
11. Shor, A.J., Kraus, K.A., Smith, W.T., Jr. and Johnson, J.S., Jr., *J. Phys. Chem.*, 72, No. 6 (June, 1968) pp. 2200-2206.
12. Johnson, J.S., Jr., "Polyelectrolytes in Aqueous Solutions-Filtration, Hyperfiltration and Dynamic Membranes", from *Reverse Osmosis Membrane Research*, ed. by Lonsdale, H.K. and Podall, H.E., Plenum Press, N.Y. (1972).
13. Leenaars, A.F.M., Keizer, K. and Burggraaf, A.J., *Chemtech* (Sept., 1986) pp. 560-564.
14. Porter, M.C. and Nelson, L., "Ultrafiltration in the Chemical, Food Processing, Pharmaceutical and Medical Industries" from Vol. II of *Recent Developments in Separation Science* edited by N.N. Li, CRC Press (1972) p. 233.
15. Bhattacharyya, D., Schaaf, D.P. and Grieves, R.B., *Can. Chem. Eng.*, Vol. 54 (June, 1976) pp. 185-189.
16. Bhattacharyya, D., Balco, M.G., Cheng, C. and Gentry, S.E., "Use of Negatively-Charged Ultrafiltration Membranes", from *Ultrafiltration Membranes and Applications*, ed. by A.R. Cooper, Plenum Press, N.Y. (1980) pp. 605-608.

17. Porter, M.C., "Membrane Filtration", Section 2.1 of *Handbook of Separation Techniques for Chemical Engineers*, ed. by P.A. Schweitzer, McGraw-Hill, N.Y. (1979) pp. 2-3 to 2-103.
18. Breton, E.J., Jr., *Water and Ion Flow Through Imperfect Osmotic Membranes*, Office of Saline Water R&D Progress Report, No. 16, PBI 61391 (1957).
19. Baker, R.W., *J. Appl. Polym. Sci.*, Vol. 13 (1969) pp. 369-376.
20. Wales, M., "Pressure Drop Across Polarization Layers in Ultrafiltration", Chapter 11 in *Synthetic Membranes, Vol. I, Desalination*, A.F. Turback, editor, ACS Symposium Series 153, (1981) pp. 159-170.
21. Tretlin, D.R. and Doshi, M.R., "Pressure-Independent Ultrafiltration-Is it Gel Limited or Osmotic Pressure Limited"?, Chap. 22 in *Synthetic Membranes, Vol. II, Hyper and Ultrafiltration Uses*, A.F. Turbak, editor, ACS Symposium Series 154 (1981) pp. 373-409.
22. Aptel, P. and Clifton, M., "Ultrafiltration", from *Synthetic Membranes: Science, Engineering and Applications*, edited by P.M. Bungay, H.K. Lonsdale and M.N. de Pinho, NATO ASI Series, D. Reidel (1986) pp. 249-305.
23. Brown, C.E., Tulin, M.P. and Van Dyke, P., *Hydronautics*, Laurel, Md. (May, 1970).
24. Porter, M.C., *Ind. Eng. Chem. Prod. Res. Dev.*, Vol. 11 (Sept., 1972) pp. 234-248.
25. Graetz, L., *Ann. der Physik und Chemie*, Vol. 18 (1883).
26. Lévêque, M.A., *Ann. Mines*, Vol. 13 (April, 1928) pp. 201; 305-308.
27. Dittus, F.W. and Boelter, L.M.K., Univ. Calif. Berkeley, *Publ. Eng.*, Vol. 2 (1930) p. 443.
28. Dravid, A.N., Smith, K.A., Merrill, E.W. and Brian, P.L.T., "The Effect of Secondary Fluid Motion on Laminar Flow Heat Transfer in Helically Coiled Tubes", paper presented at 68th Nat. A.I. Ch. E. meeting, Houston, Texas (1971).
29. Sober, H.A., ed.; *Handbook of Biochemistry*, Chemical Rubber Co., Cleveland, OH (1968).
30. de Filippi, R.P., Goldsmith, R.L., "Application and Theory of Membrane Processes for Biological and Other Macromolecular Solutions", from *Membrane Science and Technology*, ed. by J.E. Flinn, Plenum Press, NYC (1970) pp. 33-46.
31. Brandup, J., Immergul, E.H., *Polymer Handbook*, Interscience, NYC (1967).
32. Blatt, W.F., Dravid, A., Michaels, A.S. and Nelsen, L., "Solute Polarization and Cake Formation in Membrane Ultrafiltration: Causes Consequences, and Control Techniques," from *Membrane Science and Technology*, ed. by J.E. Flinn, Plenum Press, NYC (1970) pp. 47-97.
33. Eirich, R.R., *Rheology, Theory and Applications*, Vol. 4, Chapter 2, Academic Press, NYC (1967).
34. Palmer, A.A., *Amer. J. Phys.*, 209 (1965).
35. Segré, G. and Silberberg, A., *Nature*, 189 (1961) 209.
36. Segré, G. and Silberberg, A., *J. Fluid Mech.*, 14 (1962) 13.
37. Brandt, A. and Bugliarello, G., *Trans. Soc. Rheol.*, 10 (1) (1961) pp. 229-251.

38. Bixler, H.J. and Rappe, G.D., U.S. Patent 3,541,006 (Nov. 17, 1970).
39. Green, G. and Belfort, G., *Desalination*, 35 (1980) pp. 129-146.
40. Robertson, G.H., Olieman, J.J. and Farkas, D.F., *Concentration Polarization Reduction in a Centrifugally Driven Membrane Separator*, Western Regional Research Center Report, U.S. Dept. of Agriculture, Berkeley, CA (August, 1981).
41. Henry, J.D., Lawler, L.F. and Kuo, C.H.A., *A.I.Ch.E. J.*, 23, 6 (1977) pp. 851-859.
42. Parkin, M.F. and Marshall, K.R., *N.Z. Jl. Dairy Sci. Technol.*, 11 (1976) pp. 107-113.
43. Velicangil, O. and Howell, J.A., *Biotechnol. Bioeng.*, Vol. XIX (1977) pp. 1890-1894.
44. Howell, J.A. and Velicangil, O., *J. Appl. Polym. Sci.*, Vol. 27 (1982) pp. 21-32.
45. Kaszyski, M.J., Jones, G.D., Gagnon, S.R., "The Role of Ultrafiltration in the Production of Ultra-High Purity Water", paper presented at 41st Annual Meeting of the International Water Conference of the Engineers Society of Western Pennsylvania (1981).
46. Center for Disease Control, *Informal Quarterly Report of April-June, 1975*, U.S. Dept. of Health, Education and Welfare, Public Health Service (July, 1975) p. 8.
47. Good, C.M. and Lane, H.W., *The Biochemistry of Pyrogens*, Bul. of PDA, Vol. 31, No. 3 (May-June, 1977) pp. 116-135.
48. Abramson, D., Butler, L.D. and Chrai, S., *J. Parenteral Sci. and Tech.*, Vol. 35, No. 1 (Jan.-Feb., 1981) pp. 3-7.
49. Henderson, L.W. and Beans, E., *Kidney International*, Vol. 14 (1978) pp. 522-525.
50. Breslau, B.R., Testa, J.A., Milnes, B.A. and Medjonis, G., "Advances in Hollow Fiber Ultrafiltration Technology" in *Ultrafiltration Membranes and Applications*, ed. by A.R. Cooper, Plenum Press, NY (1980) pp. 109-127.
51. Porter, J.J. and Brandon, C.A., *Chem. Tech.* (June, 1976) pp. 402-407.
52. Cooper, A.R. and Booth, R.G., *J. Appl. Polym. Sci.*, Vol. 23 (1979) pp. 1373-1384.
53. Wiley, A.J., Dubey, G.A., Holderby, J.M. and Ammerlaan, A.C.F., *J. Water Pollut. Control Fed.*, Vol. 42, No. 8, Part 2 (Aug., 1970) pp. 279-289.
54. Bar-Sinai, Y.L. and Wayman, M., *Jour. of TAPPI*, Vol. 59, No. 3 (March, 1976) pp. 112-114.
55. Beder, H. and Gillespie, W.J., *Jour. of TAPPI*, Vol. 53, No. 5 (May, 1970) pp. 883-887.
56. Porter, M.C. and Michaels, A.S., *Chemtech.*, Vol. 1 (April, 1971) pp. 248-254.
57. Coton, S.G., *Jour. of Soc. of Dairy Tech.*, Vol. 33, No. 3 (July, 1980) pp. 89-94.
58. Lee, D.N., Miranda, M.G. and Merson, R.L., "Scanning Electron Microscope Studies of Membrane Deposits from Whey Ultrafiltration", *J. Food Tech.*, Vol. 10 (1975) pp. 139-146.
59. Lee, D.N. and Merson, R.L., *J. Dairy Sci.*, Vol. 58 (Oct., 1975) pp. 1423-1432.

60. Lee, D.N. and Merson, R.L., *J. Food Sci.*, Vol. 41 (1976) pp. 403-410.
61. Maubois, J.L., Mocquot, G. and Vassal, L.J., U.S. Patent 4,205,090 (May 27, 1980).
62. Maubois, J.L. and Mocquot, G., *J. Dairy Sci.*, Vol. 58, No. 7 (1975) pp. 1001-1007.
63. Sugihara, T.F., Meehan, J.J. and Kline, L., "Application of Instantizing Methods of Egg Solids", paper at 1962 Annual Meeting-Inst. of Food Technologists, Miami Beach, Fla.
64. Tsai, L.S., Ijichi, J. and Harris, M.W., *J. Food Prot.*, Vol. 40, No. 7 (July, 1971) pp. 449-455.
65. Porter, M.C. and Michaels, A.S., *Chem. Tech.* (July, 1971) pp. 440-445).
66. Milnes, B.A., "The Application of Ultrafiltration to Apple Juice Processing", paper presented at the Apple Juice Workshop, Cornell-NY SAES (May 3, 1984).
67. Porter, M.C. and Michaels, A.S., "Membrane Ultrafiltration-Part 4-Application in Processing Vegetal Foods and Beverages", *Chem. Tech.*, Vol. 1 (Oct., 1971) pp. 633-637.
68. Gnekow, B., "Protein Stabilization of Sauvignon Blanc by Ultrafiltration", paper at 34th Annual Meeting of the Amer. Soc. of Enology and Viticultrue (June 22, 1983).
69. Ng, P., Lundblad, J. and Mitra, G., *Sep. Sci.*, 11 (5), (1976) pp. 499-502.
70. Cooper, A.R. and Booth, R.G., *Sep. Sci. and Tech.*, 13 (8), (1978) pp. 735-744.
71. Porter, M.C., *Applications of Membranes to Enzyme Isolation and Purification*, Biotech & Bioeng. Symp. No. 3, John Wiley & Sons (1972) pp. 115-144.
72. Butterworth, T.A., Wang, D.I.C. and Sinskey, A.J., *Biotechnol. Bioeng.*, Vol. XII (1970) pp. 615-631.
73. Breslau, B.R. and Kilcullen, B.M., "Hollow Fiber Enzymatic Reactors An Engineering Approach," paper at Third Int. Conf. on Enzyme Engineering, Portland, Oregon (Aug. 3-8, 1975).
74. O'Neill, S.P., Wykes, J.R., Dunhill, P., Lilly, M.D., *Biotechnol. Bioeng.*, Vol. XIII (1971) pp. 319-322.
75. Porter, M.C. and Michaels, A.S., *Chem. Tech.* (Jan., 1972) pp. 56-61.
76. Wang, D.I.C., Sinskey, J. and Butterworth, T.A., "Enzyme Processing Using Ultrafiltration Membranes", from *Membrane Science and Technology*, ed. by J.E. Flinn, Plenum Press, NYC (1970) pp. 98-119.
77. Charley, R.C., "Optimization of Process Design for Continuous Ethanol Production by Zymomonas Mobilis ATCC 29191", submitted to *Biotech. Letters* (1982).
78. DeRosa, M., Gambacorta, A., Esposito, E., Drioli, E. and Gaeta, S., *Biochimie*, 62 (1980) pp. 517-522.
79. Drioli, E., Iorio, G., DeRosa, M., Gambacorta, A. and Nicolaus, B., *J. Membr. Sci.*, 11 (1982) pp. 365-370.
80. Budd, W.E. and Okey, R.W., U.S. Patent 3,472,765 (Oct. 14, 1969).
81. Porter, M.C., "Membrane Ultrafiltration for Pollution Abatement and Byproduct Recovery", *Water* AIChE Symposium Series, No. 129, Vol. 69 (1972) pp. 100-122.
82. Stavenger, P., *Chem. Eng. Prog.*, Vol. 67, No. 3 (March, 1971) pp. 30-36.

4

Reverse Osmosis

Richard G. Sudak

INTRODUCTION

The first large industrial application of reverse osmosis occurred in 1970 when a 100,000 gallon per day (GPD) system was placed in operation at Texas Instruments' electronics manufacturing facility in Dallas, Texas. In this application, the reverse osmosis plant was used to pretreat Dallas municipal water which was being converted to ultrapure process water by ion exchange resins. It was reported by the facility engineer that the use of reverse osmosis increased the yield in the manufacturing operation to such an extent that the resultant savings paid for the reverse osmosis plant in about two weeks. Now, virtually every electronics plant in the United States uses reverse osmosis as pretreatment in the preparation of ultrapure water.

The worldwide total reverse osmosis operating capacity by the end of 1970 was 880,000 GPD. By the end of 1976, reverse osmosis operating capacity had grown to 167,000,000 GPD[1] and, by the middle of 1980, this capacity had more than doubled to 390,500,000 GPD.[2] Reverse osmosis continued to expand and it was reported[3] that the operating capacity by the end of 1984 was 524,000,000 GPD.

Figure 4.1 shows that the rate of growth in reverse osmosis capacity was slow between 1970 and 1973. From 1974 through 1980, there was an accelerated rate of growth during which time the reverse osmosis capacity increased from 62,500,000 GPD to 412,500,000 GPD or an increase of 560% in the 7-year period. Between 1981 and 1984 (4 years), the total operating capacity increased from 412,500,000 to 524,000,000 GPD, an increase of 27%.

Reverse osmosis finds applications predominantly in the following areas:

Industrial - Used to prepare industrial process water or to process wastes.

Irrigation - Used to upgrade waters for agricultural purposes.

Military - Used for military purposes.

Municipal - Used to upgrade waters to municipal drinking water levels.

Power - Used to prepare process water in electric power stations.

Miscellaneous - Used for various purposes.

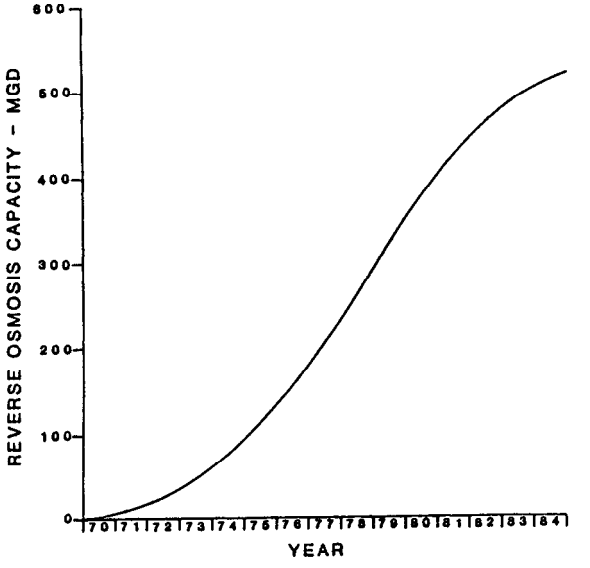


Figure 4.1: Reverse osmosis capacity vs. year.

Table 4.1[3] below shows the uses of reverse osmosis as described above.

Table 4.1: Reverse Osmosis Product Water Usage

Product Water Use	Capacity, MGD*	Percent of Total
Industrial	158	31.5
Irrigation	2	0.4
Military	13	2.6
Municipal	191	38.0
Miscellaneous	10	2.0
Power	55	11.0
Yuma Desalting Plant	73	14.5
Total	502	100.0

* MGD = One million gallons per day

Reverse osmosis finds much of its application in the production of potable water for municipal water supplies. However, the use of reverse osmosis to prepare industrial process waters and to treat industrial waste is in a close second place. Agricultural irrigation accounts for only a very small percentage of total capacity because current sources of agricultural water are much cheaper than water from reverse osmosis. The military use of the reverse osmosis process was small as of the end of 1984 but the U.S. military services have discovered reverse osmosis to be a process ideally suited to providing drinking water in the field. The process not only is suitable for converting brackish and seawaters into potable supplies but it will also remove toxic and biological agents which result from germ, chemical and nuclear warfare. Consequently, military use of reverse osmosis should increase in the future. Power plants have found reverse osmosis very useful in preparing boiler feedwater. In Yuma, Arizona, a desalting plant is being constructed by the U.S. Government to improve the quality of the Colorado River prior to its flowing into Mexico. That plant alone accounts for 14.5% of the worldwide capacity of the reverse osmosis process.

Reverse osmosis is a process that transforms an unusable water supply into a usable resource. It is capable of renovating a broad spectrum of feedwaters from municipal water supplies that need polishing for industrial purposes to seawater that is refined into a potable water supply. Table 4.2[3] shows the different types of feedwater being processed by reverse osmosis units. Seawater is considered to have a nominal total dissolved solids (TDS) content of 35,000 mg/ℓ. Wastewater is from industrial or municipal sources and the TDS is variable. Brackish water is defined for the purposes of Table 4.2 only as a water that may have a TDS from that of municipal water supplies up to 10,000 mg/ℓ.

Table 4.2: Source of Reverse Osmosis Feedwater

	Capacity, MGD	Percent of Total
Sea Water	67.9	13.0
Waste Water	26.5	5.0
Brackish Water	429.6	82.0
Total	524.0	100.0

As of the end of 1984, the desalination of brackish water accounted for 82% of capacity. This is due to the fact that early reverse osmosis membranes were incapable of single stage seawater desalination and, thus, they were limited to brackish water desalination. Within the last 10 years, significant advances have been made in both the flux and rejection capability of membranes and reverse osmosis is technically able to desalt seawater in a single stage. In the recent past, it has been an effective competitor to the distillation process in seawater desalination. In fact, reverse osmosis is now beginning to replace existing distillation capacity in the Middle East.[4]

Although reverse osmosis is a relatively new technology, there is sufficient operating capacity in a number of varied applications to warrant confidence in the process. From a technical and economic point of view the process is ca-

pable of desalting a broad range of feedwaters from municipal water supplies to seawater. It has economic viability in a large number of industrial applications.

BASIC PROCESS CONSIDERATIONS

An industrial reverse osmosis plant usually will consist of three separate sections which are shown in Figure 4.2. The first section is the pretreatment section in which the feedwater is treated to meet the requirements of reverse osmosis element manufacturers and the dictates of good engineering practice. Following pretreatment, the feedwater is introduced into the reverse osmosis section where the feedwater is pressurized and routed to the reverse osmosis elements which are in pressure vessels. The feedwater flows across the membrane surface where product water permeates through the membrane and a predetermined amount remains behind as reject. The reject is discharged to waste while the product water is routed to the posttreatment section. The third or posttreatment section treats the product water to remove carbon dioxide and adds chemicals as required for industrial use of the product water.

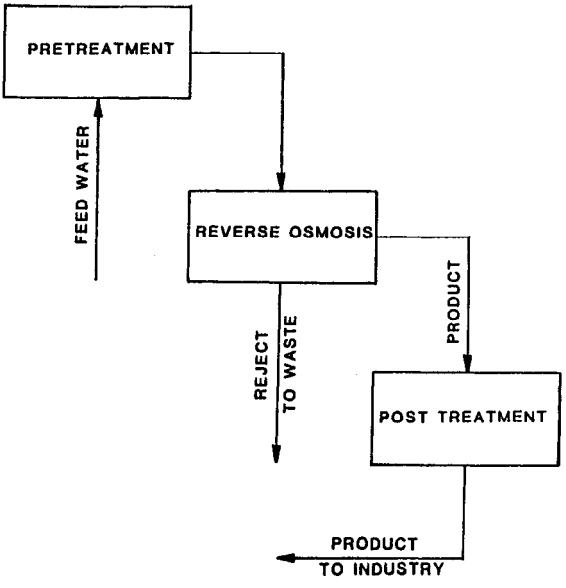


Figure 4.2: Industrial reverse osmosis.

Although operating reverse osmosis plants are commonplace, the subject of salt and water transport is still controversial. Several transport models have been proposed and these will be discussed briefly below. A more thorough presentation is made in a paper by Soltanieh and Gill.[5]

The sieve mechanism is the simplest and easiest model to understand. This model proposes that salt and water are separated due to physical size differences by a membrane with a pore size that lies between the sizes of salt and water. While most laymen prefer this concept, it is unfortunate that for solutions, such as sodium chloride in water, the sizes of the salt and water molecules are almost the same. This fact would seem to rule out the sieve mechanism model.

Another model proposed is the wetted surface mechanism or the water clustering concept of transport. It is generally recognized that reverse osmosis membrane material is wettable and that water tends to be absorbed on the membrane by hydrogen bonding. In this concept, it is theorized that the water film at the surface of the membrane obstructs the pores and prevents salt from entering the pores. The water passes through the membrane by passing from one absorbed site to the next until it reaches the other side of the membrane barrier layer. The energy requirements for solvent migration are much less than the energy requirements for salt migration and, thus, the separation of salt from water takes place.

Another concept of water and salt transport in reverse osmosis is the preferential sorption-capillary flow mechanism. In this model, the surface of a membrane is microporous and heterogeneous at all levels of solute separation. It is hypothesized that, due to the chemical nature of the membrane skin layer in contact with the aqueous solution, a preferential sorption for the water causes a sorbed water layer to be formed at the skin. This layer of purified water is then forced through the capillary pores by pressure.

The solution-diffusion model of transport assumes a nonporous, homogeneous membrane surface layer. Each component in a pressurized solution dissolves in the membrane and then diffuses through the membrane. The flow of water and salt through the membrane is uncoupled, i.e., they are independent of each other, and the water transports through the membrane at a more rapid rate than the salt.

The product water flow through the membrane is defined as follows:

$$F_w = A^*(\Delta P - \Delta \pi)$$

where F_w = water flux through the membrane

A = water transport coefficient

ΔP = pressure differential across the membrane

$\Delta \pi$ = osmotic pressure differential across the membrane

The flow of water through a reverse osmosis membrane is primarily dependent on the applied pressure differential and the osmotic pressure differential across the membrane. The osmotic pressure is directly dependent on the salt concentration of the process stream. As a rule of thumb, each 100 mg/ℓ of dissolved solids is roughly equivalent to one psi of osmotic pressure. Since the product stream usually has a very low salt content, the osmotic pressure of that stream is negligible. In addition, the product stream normally leaves the reverse osmosis pressure vessels at near atmospheric pressure so that the applied pressure differential is the feed pressure. Consequently, the term "net applied pressure" has come to mean the applied pressure minus the feed osmotic pressure.

The flow of salt or dissolved solids across the membrane is dependent on the following equation:

$$F_s = B^*\Delta C$$

where F_s = salt flux

B = salt transport coefficient

ΔC = salt concentration gradient across the membrane

The salt transport is primarily dependent upon the concentration of dissolved solids on each side of the membrane.

The solution-diffusion model seems to represent the performance of a reverse osmosis membrane. Figure 4.3 shows the salt rejection and flux of a low pressure polyamide membrane as a function of applied pressure. The membrane was operated on a 5,000 mg/ℓ aqueous solution of sodium chloride at 25°C. As can be seen, there was no product water flow until the applied pressure exceeded the osmotic pressure (50 psi). After this, the flux increased linearly as would be predicted by the above water flux equation. Rejection is poor at lower pressures and increases rapidly until it reaches an asymptote at an applied pressure of about 150 psig. This can be attributed to a near constant flow of salt with a rapidly increasing product water flow which results in a more dilute product or in increased rejection. These data tend to substantiate the assertion of the solution-diffusion model that flow is uncoupled.

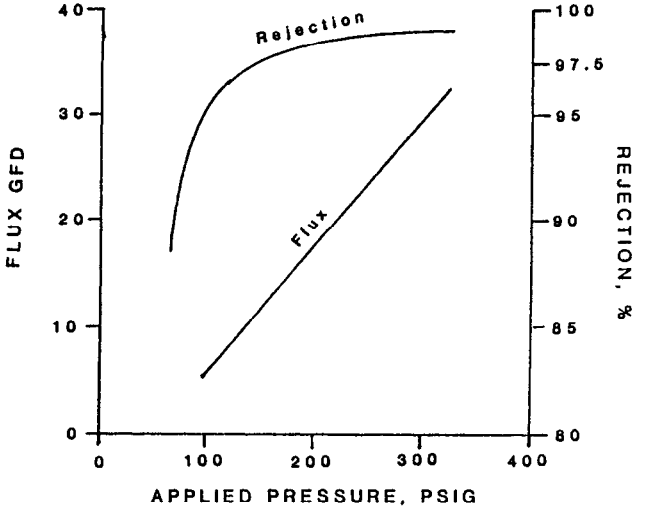


Figure 4.3: Membrane flux and rejection vs. applied pressure.

It is noted that the data shown in Figure 4.3 was derived in membrane test cells with near perfect small areas of membrane. In a practical system, there would be a number of imperfections in the membrane and the salt flow through these capillaries would contribute to the total salt flow. Therefore, a practical

salt transport model must also take into account the contribution of the membrane imperfections to salt flow.

The water transport coefficient (A) is not a constant in that it varies with temperature. The product flow as a function of temperature may be estimated[6] by using the following equation:

$$Q\,25/\,Qt = e^{x}$$

where $Q\,25$ = flow at 25°C or 77°F

Qt = flow at temperature T, °C

e = 2.71828

x = $U\,[1/(T + 273) - 1/298]$

T = Temperature in °C

U = 2723 (for cellulose acetate membranes).

Figure 4.4 graphically shows the ratio of water flux at 25°C to water flux at other temperatures.

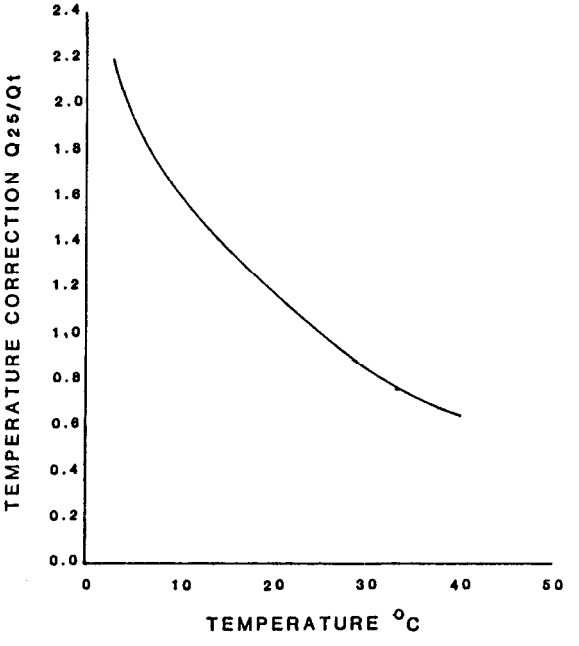


Figure 4.4: Temperature correction factor.

As a rule of thumb, the product water flow with constant net applied pressure will increase about 3% for each degree centigrade increase in feedwater temperature. Salt flux through the membrane is also directly proportional to temperature and the ratio of salt flux to water flux is essentially constant at different temperatures. This results in little or no change in rejection as a function of

temperature. For some of the newer composite membranes, the water and salt permeation coefficients also vary as a function of pH.

Reverse osmosis is a cross-flow membrane separation process which separates a feed stream into a product stream and a reject stream. The recovery of a reverse osmosis plant is defined as a percentage of feedwater that is recovered as product water. As all of the feedwater must be pretreated and pressurized, it is economically prudent to maximize the recovery in order to minimize power consumption and the size of the pretreatment equipment. Since most of the salts remain in the reject stream, the concentration of salts increases in that stream with increased recovery. For instance, at 50% recovery, the salt concentration in the reject is about double that of the feed and at 90% recovery, the salt concentration in the reject is nearly 10 times that of the feed. In cases of sparingly soluble salts, such as calcium sulfate, the solubility limits may be exceeded at a high recovery. This could result in precipitation of the salt on the membrane surface resulting in decreased flux and/or increased salt passage. In addition, an increase in recovery will increase the average salt concentration in the feed/reject stream and this produces a product water with increased salt content. Consequently, the recovery of a reverse osmosis plant is established after careful consideration of the desired product quality, the solubility limits of the feed constituents, feedwater availability and reject disposal requirements.

While the above equations are helpful in describing the reverse osmosis process, the water and salt transport coefficients seldom are used to describe membrane performance. Most manufacturers test reverse osmosis membrane with standard solutions as described below.

(1) *Brackish Water Membrane*—The flux and rejection of the membrane is determined when the membrane is tested on a feedwater of an aqueous sodium chloride solution with a concentration of 2,000 mg/ℓ at an applied pressure of 420 psig (net applied pressure = 400 psig) with a temperature of 25°C and a feed pH of from 5.0 to 6.0 for 30 minutes prior to data collection.

(2) *Seawater Membrane*—The seawater test is similar to the brackish water test except that the feedwater is an aqueous sodium chloride solution with a concentration of 35,000 mg/ℓ and the test pressure is 800 psig.

The results are reported as gallons per day per square foot of membrane area (membrane flux) and as rejection of sodium chloride. Rejection is calculated as follows:

$$R = (1 - CP/CF)\,100$$

where R = Rejection, percent

CP = Product water concentration

CF = Feedwater concentration

The sodium chloride rejection differs from that of other inorganic and organic dissolved solids, and membrane manufacturers will provide information and rejection data that are available for their specific membrane. Table 4.3

shows typical results for a composite membrane when tested on a multicomponent solution. The rejection of the divalent ions such as calcium and sulfate is much better than the rejection of the monovalent ions such as sodium and chloride. If salt passage is defined as product concentration divided by the feed concentration, or one minus rejection, then it can be seen that the salt passage for the divalent ions is about one-fifth of the salt passage for the monovalent ions.

Table 4.3: Ionic Rejections

Ion	Feed, mg/l	Product, mg/l	Rejection, %
Calcium	61	0.2	99.6
Sodium	150	3.0	98.0
Potassium	12	0.3	97.4
Bicarbonate	19	0.7	96.2
Sulfate	189	0.4	99.8
Chloride	162	2.9	98.2
Nitrate	97	3.5	96.4
TDS	693	11.0	98.4

The abovedescribed tests are conducted at a low recovery rate to minimize the effects of concentration polarization which is described below. For example, membrane tests above are conducted at less than 1% recovery and tests with spiral wound elements are conducted at recoveries from 5 to 10%.

Reverse osmosis is a cross-flow process and, as in any dynamic hydraulic process, the fluid adjacent to the membrane moves slower than the main stream. While the main stream flow may be turbulent, the layer next to the membrane surface is laminar. This thin, laminar flow film is called the boundary layer. When water permeates through the membrane, nearly all of the salt remains behind in the boundary layer next to the membrane. The salt must then diffuse across the boundary layer and back into the bulk stream. This results in a boundary layer with a salt concentration which is more concentrated than the bulk stream. The effect has been termed concentration polarization, and it is defined by the following equation:

$$\beta = CB/CM$$

where β = Concentration polarization

CM = Concentration in the main stream

CB = Concentration in the boundary layer

Concentration polarization increases the salt concentration at the membrane surface, and this results in an increased osmotic pressure at that surface. The increased osmotic pressure causes a drop in water flow as shown in the following equation:

$$Fw = A * (P - \beta\pi)$$

where Fw = the water flow
A = the water transport coefficient
P = applied pressure
β = concentration polarization
π = osmotic pressure of main stream

The increased salt concentration at the membrane surface will also increase the tendency of sparingly soluble salts to precipitate on the membrane.

The flow of salt also increases and this can be simply shown in the following equation:

$$Fs = B * (\beta C1 - C2)$$

where Fs = salt flux
B = salt transport coefficient
β = concentration polarization
C1 = main stream salt concentration
C2 = product water salt concentration

In the imperfect membrane with a small number of pores, the increased salt concentration at the membrane surface would also result in increased salt passage through the pores which would be directly proportional to concentration polarization.

The information shown in Table 4.4 below assumes a membrane operating on various feedwaters with a total dissolved solids (TDS) content of 2,000, 5,000 and 35,000 mg/ℓ. It is assumed that the membrane will deliver 20 gallons per square foot per day at a 400 psi "net applied pressure" and have a rejection of 99% when there is no concentration polarization, i.e., $\beta = 1.0$.

Table 4.4: Effects of Concentration Polarization

Feed TDS, mg/l	2,000	5,000	35,000
Flux, gfd			
$\beta = 1.0$	20.0	20.0	20.0
$\beta = 1.1$	19.9	19.8	18.3
$\beta = 1.5$	19.5	18.8	11.3
$\beta = 2.0$	19.0	17.5	2.5
Rejection, %			
$\beta = 1.0$	99.0	99.0	99.0
$\beta = 1.1$	98.9	98.9	98.8
$\beta = 1.5$	98.5	98.4	97.3
$\beta = 2.0$	97.9	97.7	84.0

The penalty of a high concentration polarization is not as severe with a low TDS feedwater as it is with a high TDS feedwater. The recommendations as to minimum flows or maximum recoveries which are specified by the reverse osmosis element manufacturer should be followed at all times, especially when the application is the desalination of high TDS waters.

Concentration polarization cannot be eliminated, but it can be minimized by decreasing boundary layer thickness. This is done by increasing the flow rate across the membrane surface or introducing turbulence promoters into the feed/reject stream. In order to achieve optimum performance, most membrane manufacturers will recommend a minimum feed rate to or from their elements and a maximum recovery in order to minimize the effects of concentration polarization.

REVERSE OSMOSIS MEMBRANES

Osmotic phenomena have been observed since the middle of the eighteenth century. The first experiments were conducted with animal membranes and it wasn't unitl 1867 that artificial membranes were employed. In the early 1950's, research workers at the University of Florida demonstrated, with thick films, that cellulose acetate possessed unique salt and water transport properties which made it potentially attractive as a reverse osmosis desalination membrane. During the 1960's, Loeb and others at the University of California at Los Angeles developed techniques to prepare cellulose acetate membranes with an economical water flux and salt rejection at moderate driving pressures. With this development, reverse osmosis became a practical possibility.

The early cellulose acetate membranes were only suitable for brackish water desalination as they were not capable of operating at the high pressures required for seawater desalination (see below). In addition, the membrane rejection was insufficient to desalt seawater in one stage. The first membranes were fabricated from cellulose diacetate which is subject to hydrolysis at either a low or high pH, biological attack and compaction at temperatures in excess of 85°F. Cellulose acetate also compacts (densifies) at pressures above 400 psig and temperatures below 85°F. Suitable feedwater pretreatment lessens the adverse effects of temperature, pH and biological organisms to the point where the membrane can be used in practical reverse osmosis plants.

A considerable amount of research has been done to develop a membrane of cellulose triacetate as this material is more stable to extremes of temperature and pH and it will better withstand chemical and biological attack. While the cellulose triacetate membranes operated quite well on a short term basis, they were prone to compact at an operating pressure of 400 psig, with the resultant loss of flux to an impractical level, in a short period of time.

It has been demonstrated that a blend of cellulose diacetate and cellulose triacetate provides an improved membrane in that:

(1) it is more stable than the cellulose diacetate membranes;

(2) it has a better flux and rejection than the cellulose diacetate; and

(3) it is more resistant to compaction than either the diacetate or triacetate.

Incidentally, all of the cellulose acetate membranes will tolerate a limited amount of residual chlorine which allows chlorine to be used for feedwater disinfection.

The cellulose acetate membranes are asymmetric and fabricated from a single polymer. The use of electron microscopy in the 1960's demonstrated that the cellulose acetate membranes consisted of a relatively thin dense layer and a thicker porous layer of the same material. The membrane thickness is usually about 100 micrometers with the dense layer accounting for about 0.2% of the thickness and the remainder being an open cell porous matrix (see Figure 4.5).

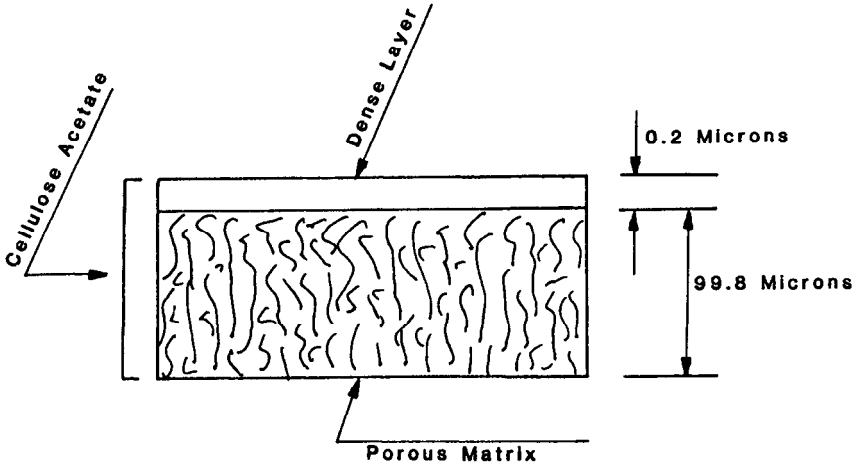


Figure 4.5: Single component asymmetric membrane.

During the 1960's, the DuPont Company screened numerous polymers to determine the suitability of materials other than cellulose acetate for use in reverse osmosis desalination. The results of this work indicated that aromatic polyamides were the "choice as the best polymer type for use in the DuPont commercial permeators".[7] The company was most successful in developing an asymmetric aromatic polyamide reverse osmosis membrane in a hollow fine fiber configuration which successfully competed with cellulose acetate in the market place.

Shortly after the concept of an asymmetric membrane was established, composite membrane research was initiated. A composite membrane is also asymmetric but it consists of two polymer layers which are the membrane barrier layer and the porous support layer (Figure 4.6). The porous support is formed separately, by conventional membrane casting techniques, from one polymer. The porous support has a thickness of between 75 and 100 micrometers and its porosity is due to numerous small perforations through the support. The membrane barrier layer is a dense thin film of another polymer that is formed or deposited in a subsequent operation on the porous support. The membrane barrier layer varies in thickness from 400 to 1,000 angstroms.

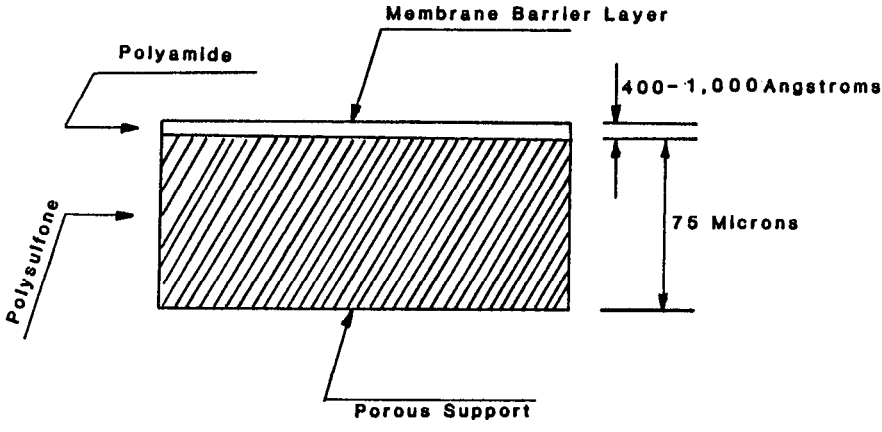


Figure 4.6: Two component composite membrane.

Several polymers have been used as porous supports. One of the earliest composite membrane systems was a porous support formed from cellulose nitrate-cellulose acetate with a membrane barrier layer of cellulose triacetate. While this membrane successfully desalted seawater, it was fragile and expensive. To a large degree, present day commercially available composite membranes use a polysulfone porous support.

Membrane barrier layers have been formed on porous supports in the following manner:[8]

(1) solution,

(2) thin film polymerization and

(3) interfacial polycondensation.

The solution coating technique was used in the preparation of the cellulose triacetate membrane discussed above. A solution of cellulose triacetate in chloroform was deposited on the porous support and the solvent was then evaporated leaving a thin film on the porous support. Thin film polymerization was used to prepare a polyfuran membrane barrier layer on polysulfone. In this case, the monomer furfuryl alcohol is polymerized in situ by adjustment of pH and temperature. This membrane proved to be highly susceptible to oxidizing agents and is of limited value. By far the most valuable technique in the formation of membrane barrier layers is interfacial polycondensation. In this method, a polymer is formed on the porous support surface at the interface of organic and aqueous phases by reaction of specific molecules dissolved in each phase. It is by this method that a number of polyamides and polyurea membrane barrier layers have been formed on polysulfone. Elements containing these membranes are available commercially.

There has been very little progress in the last five years in improving the performance of single polymer asymmetric membranes. Meanwhile, the composite membranes have been improved and they exhibit a higher flux and better re-

jection at lower operating pressures than is available with the single component asymmetric membranes. The polyamide and polyurea composite membranes can withstand higher temperatures and larger pH variations than the cellulose acetate based membranes and they are immune to biological attack. On the other hand, as noted above, the cellulose acetate membranes can tolerate a limited concentration of residual chlorine while the polyamide and polyurea membrane barrier layers are subject to disintegration by residual chlorine and other oxidizing agents. Consequently, alternate methods of water disinfection or chlorination followed by dechlorination are employed in reverse osmosis systems using these membranes.

While the cellulose acetate membranes are compacted at the moderate pressures required for brackish water desalination, the thin film composite membranes exhibit no compaction at these pressures and a very low compaction rate at pressures of 1,000 psig.

The superior flux and rejection capabilities of the thin film composite membrane has been demonstrated at the municipal wastewater reclamation facility of the Orange County Water District in California. Both asymmetric cellulose acetate and thin film composite membranes were tested on lime clarified secondary effluent. The pilot plants were operated at 85% recovery and the rejections reported in Table 4.5 are the percent rejection of the constituents in the feedwater and not the rejection of the average concentration of the specific constituents in the feed/reject stream. Use of the average concentration would give a higher rejection in both cases.

Table 4.5: Rejection Comparison

Constituent	CA Membrane(9)	TFC Polyamide Membrane(10)
Na	93.8	99.0
NH_4	89.0	94.8
SO_4	99.3	99.8
Cl	93.3	95.2
NO_3	71.0	97.7
COD	93.6	>94.8
TDS	94.4	97.5

The thin film composite membrane exhibited superior overall rejection performance in these tests, with ammonia and nitrate rejection showing an outstanding improvement. It has also been reported that silica rejection by the thin film composite membranes is superior to that of cellulose acetate. While the above data indicates a marginal improvement in the rejection of chemical oxygen demand (COD), which is an indication of organic content, other tests conducted by membrane manufacturers show that the polyurea and polyamide membrane barrier layers exhibit an organic rejection that is clearly superior to that of cellulose acetate. Reverse osmosis element manufacturers should be contacted for rejection data on specific organic compounds.

MEMBRANE PACKAGING

Reverse osmosis membrane is produced in sheet form-up to 60 inches wide and lengths up to 1,500 feet-and as a hollow fine fiber. The asymmetric cellulose acetate was originally produced as a sheet and later as a hollow fine fiber. The asymmetric aromatic polyamide was originally produced as a hollow fine fiber and later in sheet form. The composite membranes with polyamide or polyurea membrane barrier layers are produced in sheet form as of the end of 1987, but research has been and will continue to be done to produce the composite reverse osmosis membranes as a hollow fine fiber.

The Office of Saline Water, U.S. Department of Interior, sponsored much of the development of membrane packaging configurations for reverse osmosis membrane. The configurations which have been developed and evaluated are as follows:

(1) plate and frame,

(2) spiralwound,

(3) tubular and

(4) hollow fine fiber.

Plate and Frame

The plate and frame configuration is much like the conventional plate and frame filtration concept except that, in reverse osmosis, a typically higher fluid operating pressure is used. Figure 4.7 is a schematic of the plate and frame approach. The membrane package is installed in a pressure vessel designed and fabricated to withstand operating pressures from 400 to 1,000 psig. A stack of parallel porous plates are used to support the membrane on each side of the porous plate. Feedwater under pressure enters the top of the pressure vessel and flows between the parallel stacks of membrane/porous plates. Product water passes through the membrane and into the porous plate to be routed to the product water collection system and then out of the pressure vessel. As the feed/reject stream passes across the membrane, it becomes concentrated and eventually leaves the pressure vessel as concentrate or reject. More advanced designs utilize external tie bolts which hold together sufficiently thick end plates which contain the pressurized feed/reject stream. The plate and frame packaging configuration has an advantage in that only the membrane must be replaced when a membrane becomes defective. It has disadvantages of complex flow patterns and high costs. The plate and frame configuration can achieve a packaging density of up to 150 square feet of active membrane area per cubic foot of pressure vessel. Overall, the plate and frame concept has not been economically competitive and there are no remaining manufacturers of this type of equipment in the United States.

Spiral Wound

The spiral wound membrane packaging configuration is shown in Figure 4.8. Basically, the spiral wound element consists of two sheets of membrane separated by a grooved, polymer reinforced fabric material. This fabric both supports the membrane against the operating pressure and provides a flow path

for egress of the product water. The membrane envelope is sealed with an adhesive on three sides to prevent contamination of the product water. The fourth side is attached to a product water tube which has perforations within the edge seal so that product water can be removed from the porous product water carrier material. The membrane envelope is rolled up around central product water tube, with a plastic mesh spacer between the facing membrane surfaces, in a spiral. The mesh spacer not only serves to separate membrane surfaces but it provides a flow path for and turbulence in the feed/reject stream of each element. The elements have an outer wrap to contain the feed/reject stream in the mesh passageway and brine seal to insure that the feed/reject stream goes through the element and not around it. Spiral wound elements are available in lengths from 12 to 60 inches and diameters from 2 to 12 inches. Packaging densities of up to 300 square feet of membrane to 1 cubic foot of pressure vessel have been attained. Reverse osmosis plants with a capacity from 100,000 to 5,000,000 gpd of product would normally use elements with an 8-inch diameter by a 40-inch or 60-inch length.

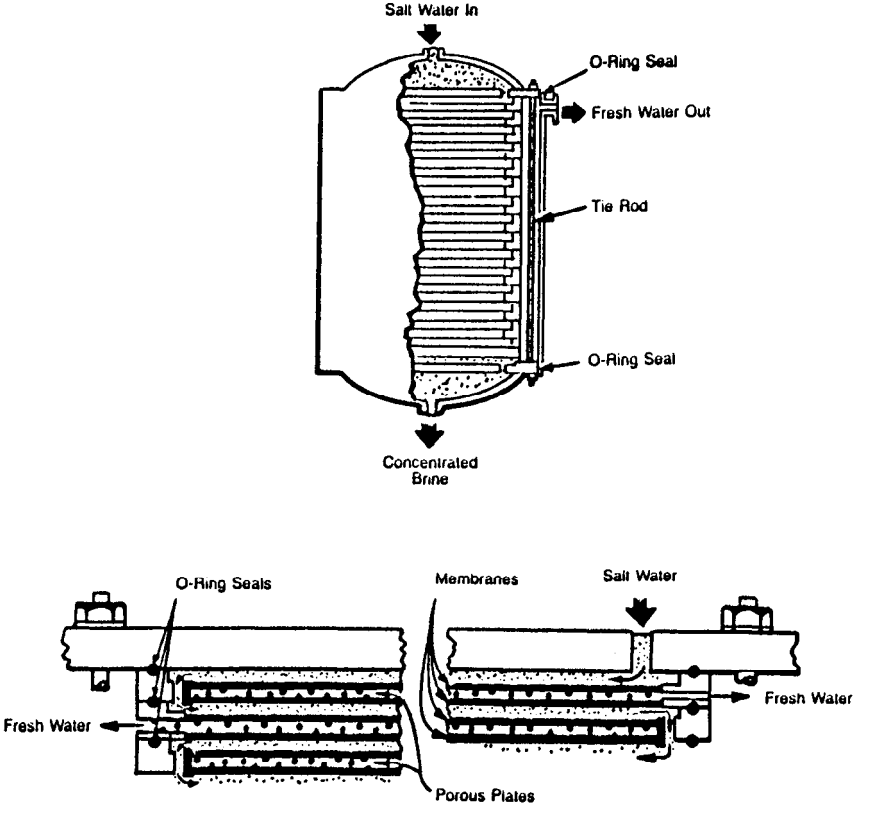
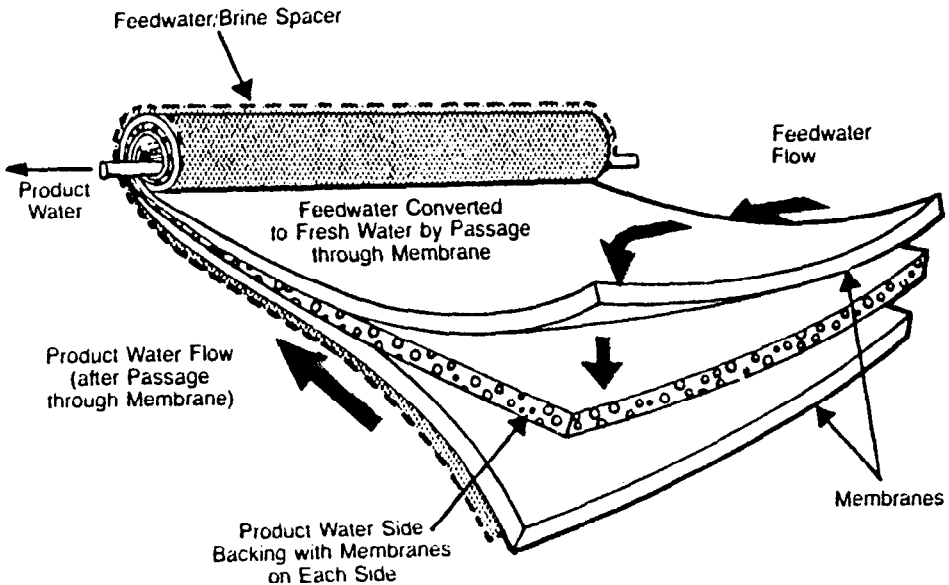


Figure 4.7: Plate and frame packaging.



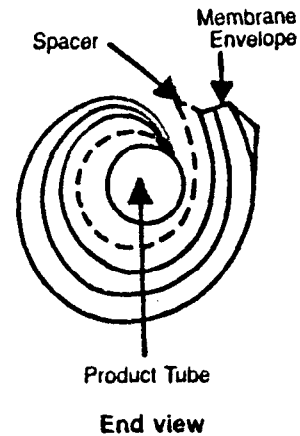


Figure 4.8: Spiral wound packaging.

Spiral wound elements are installed in a pressure vessel which is usually fabricated from fiberglass reinforced plastic. The pressure vessel inside diameter is sized to match the outside diameter of the element brine seal. The pressure vessels are designed and fabricated to accommodate from 1 to 6 elements and operating pressures from 50 to 1,000 psig. Figure 4.9 shows a pressure vessel with 6 elements installed. Feedwater enters one end of the pressure vessel and flows through the first element in which about 10% of the feed permeates through the membrane and flows through the product water carrier material into the product water tube. The reject from the first element flows to and through the second element and the reject from this element becomes the feed to the next element, etc. The reject from the last element is routed from the pressure vessel to the high pressure reject manifold. The first and sixth element product water tubes are sealed to the pressure vessel end caps by O-ring devices to prevent contamination by the high pressure feed or reject to the purified product water stream. The element product water tubes in the pressure vessel are connected to each other with interconnectors which again are O-ring devices whose seals prevent product water contamination. The product water can exit the pressure vessel, usually at near ambient pressures, from either end of the pressure vessel. In a single pressure vessel with six elements, between 40 and 60% of the feedwater to the pressure vessel is recovered as product water from a brackish water feed and from 25 to 35% is recovered from a seawater feed.

The advantages of the spiral wound elements are the high packing density and high flux which makes it one of the most cost effective elements. The disadvantage of the element is that a moderate amount of pretreatment is required for some feedwaters to prevent fouling of the mesh brine spacers.

Tubular

The tubular reverse osmosis device is shown in Figure 4.10. The tube serves as the pressure vessel and the membrane is installed inside the tube. Tubes with inside diameters of ½ and 1 inch have been used. Uniformly porous fiberglass reinforced plastic tubes have been used and nonporous but perforated copper, stainless steel and fiberglass tubes have also been successfully used. The membrane can be bonded to the tube in which case it is cast in situ or the membrane can be loose. The loose membrane is cast in sheet form and a cylindrical section is formed and placed in the tube. Packing densities for the ½-inch diameter tube are about 100 square feet per cubic foot and about 50 square feet per cubic foot for the 1-inch diameter tube.

Pressurized feedwater enters the tube through an end fitting which seals the membrane to the tube and prevents cross contamination of the product water. The feed water flows down the length of the tube and product water permeates through the membrane and weeps through the tubular pressure vessel into a collection basin. The reject flows through an end fitting and is routed to additional tubes in series or to waste.

The major advantages of the tubular reverse osmosis configuration are the ability to tolerate high suspended solids concentrations in the feed and the possibility of mechanical membrane cleaning. The disadvantages are the excessive number of tube end fittings in proportion to the active membrane area in each pressure vessel, the bulkiness of the reverse osmosis plant and the high cost.

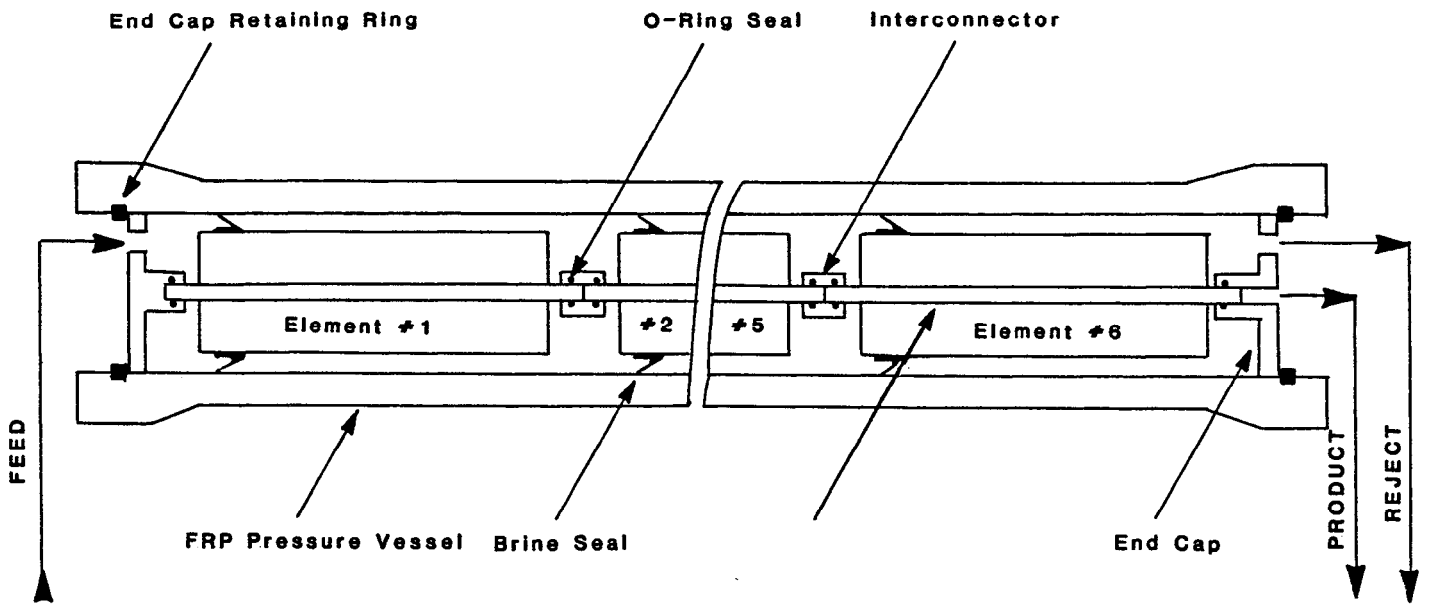


Figure 4.9: Spiral wound element pressure vessel assembly.

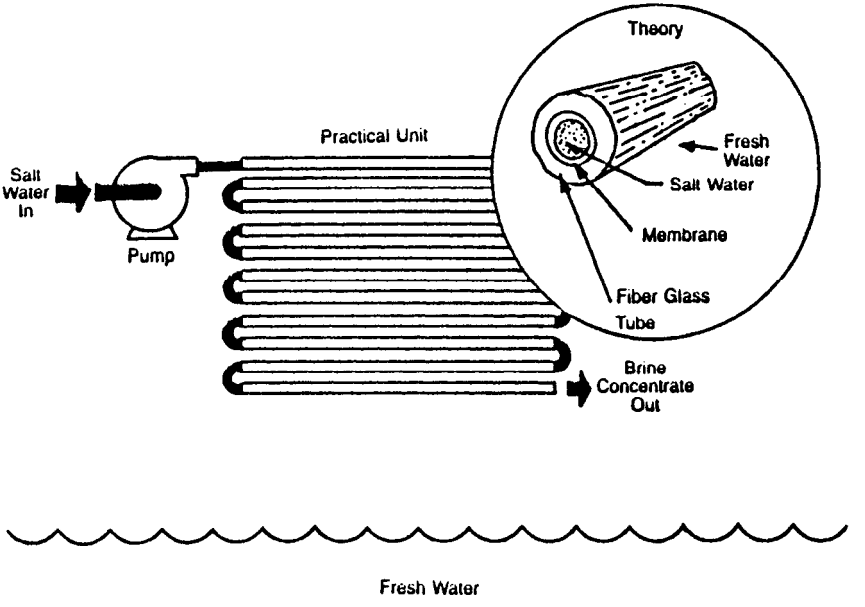


Figure 4.10: Tubular packaging.

There have been a number of attempts to commercialize tubular reverse osmosis systems in industrial applications. As of the end of 1987, there were no large scale tubular reverse osmosis manufacturers in the United States, although there are some in Europe and Japan.

Hollow Fine Fiber

Hollow fine fiber synthetic filaments have been prepared for use in the textile industry for a long time. This well-known technology was adapted to prepare polymers, which are suitable for reverse osmosis desalination, into hollow fine fibers. The most readily available polymers in hollow fine fiber elements are aromatic polyamide, cellulose diacetate and cellulose triacetate. The fibers are indeed very fine in that they approach the diameter of a single human hair. The aromatic polyamide hollow fine fiber has an outside diameter of 85 micrometers for the brackish water fiber and an outside diameter of 95 micrometers for the seawater fiber. Both of the fibers have an internal diameter of 42 micrometers.[11] The ratio of outside to inside diameter exceeds two. The fibers are thick walled cylinders that have the compressive strength necessary to withstand the operating pressures. This concept is capable of achieving a high packaging density of 3,000 square feet per cubic foot but the flux is considerably lower than with sheet membrane.

Figure 4.11 is a schematic of a typical hollow fine fiber element. A continuous fiber is looped into a bundle around a central feed tube. The central feed tube is sealed at the product water end and is perforated within the active membrane area. Both ends of the fiber bundle are potted in an adhesive. When cured, the adhesive and protruding fibers in the product water end are machined

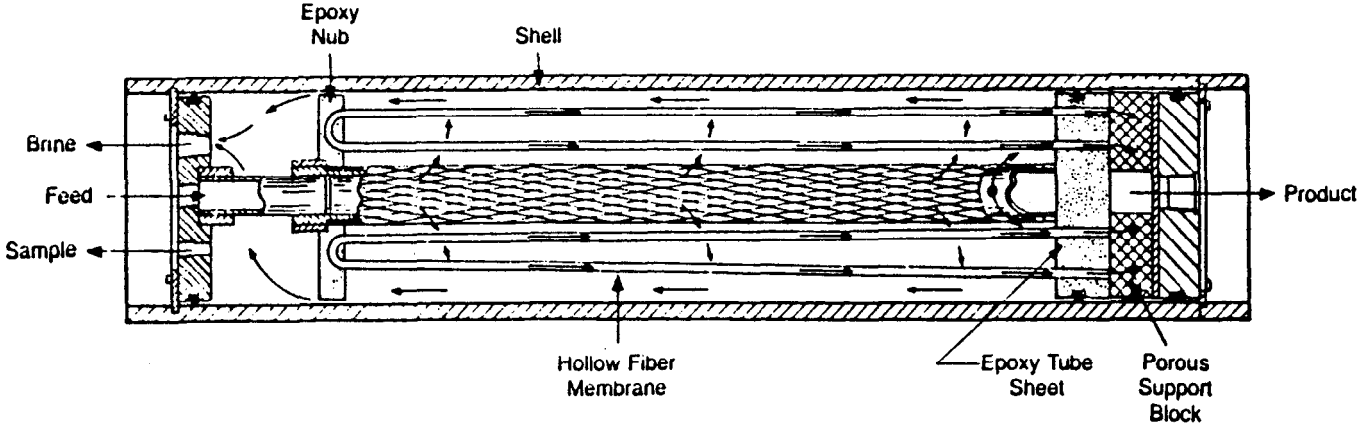


Figure 4.11: Hollow fine fiber packaging.

to open the fibers at that end. The fiber bundle is then installed in a pressure vessel and an O-ring in the product water end tube sheet seals against the pressure vessel wall to prevent the high pressure reject stream from contaminating the low pressure product stream. The element resembles a tube and shell heat exchanger. The pressure vessels are fiberglass reinforced plastic and they are designed and fabricated to accommodate operating pressures from 250 to 1,000 psig. Hollow fine fiber elements are available with nominal diameters of 4, 6 and 8 inches.

Pressurized feedwater enters the element through the central feed tube which is connected to the high pressure feed manifold. The feed flows through perforations in the tube and then radially between the spaces in the fiber toward the outer diameter of the bundle. Longitudinal feed flow is minimized by the reject end being potted. Product water permeates the membrane, enters the capillaries of the fiber bundle and flows to the tube sheet where it is discharged into the product water plenum and then into the product water manifold. The reject flows from the outer diameter of the fiber bundles, through the end cap and to waste via the high pressure reject manifolding. Normally, each hollow fine fiber element is capable of recovering from 40 to 75% of the feed water from brackish water and from 25 to 35% from seawater.

The advantages of the hollow fine fiber element are the high packaging density and the elimination of membrane support materials. The prime disadvantage is the need for an efficient feedwater pretreatment to remove suspended and colloidal solids.

Dynamic Membranes

Dynamic membranes are formed by flowing a feed solution containing 50 to 100 mg/ℓ of membrane-forming material tangential to a clean porous surface at velocities from 5 to 50 feet per second under pressures from 500 to 1,200 psi.[12] The dynamic membrane is formed within minutes and the optimum performance is usually achieved within an hour. The membrane-forming materials have been hydrous thorium, natural humic and fulvic acids, pulp mill wastes, municipal wastes, synthetic polyelectrolytes, zirconium oxide, and polyacrylic acid. One of the most successful membrane-forming materials has been a layer of polyacrylic acid deposited on top of a layer of zirconium oxide. The porous surfaces used have been carbon, ceramic and stainless steel tubes. Use of a stainless steel tube which had been pretreated with a filter aid and coated with a layer of polyacrylic acid over a layer of zirconium oxide achieved a sodium chloride rejection of 90% with a flux of about 60 gfd. Recently, several plants using dynamic membranes have been installed and there has been a renewed interest for such applications as orange juice concentration. These membrane promise a high flux with a lower rejection and a low membrane cost. However, the capital and operating costs have not always been commercially competitive.

PLANT DESIGN

The first step in the design of an industrial reverse osmosis plant is to determine the amount of water to be treated, peak demand, product water quality,

source of feedwater and reject discharge requirements. The next step is to obtain an accurate and representative analysis of the feedwater. This analysis should include determination of the concentration of the feedwater constituents shown in Table 4.6. Knowledge of the feedwater constituents in Table 4.6 will provide sufficient information for an experienced design engineer to successfully design a reverse osmosis plant in the majority of applications.

Table 4.6: Feedwater Analysis

Cations	Anions	Other
Calcium	Carbonate	Silica
Magnesium	Bicarbonate	Total Dissolved Solids
Sodium	Sulfate	Total Suspended Solids
Potassium	Chloride	Turbidity
Iron	Nitrate	Silt Density Index
Manganese	Phosphate	Temperature Range
Ammonia	Fluoride	Total Organic Carbon
		pH

The above determinations with the exception of the silt density index should be made in accordance with *Standard Methods for the Examination of Water and Wastewater.*[13] A schematic diagram of the silt density index apparatus is shown in Figure 4.12 and the silt density index (SDI) is determined as follows:

(1) Measure the amount of time required for 500 ml of feedwater to flow through a 0.45 micrometer Millipore filter (47 mm in diameter) at a pressure of 30 psig.

(2) Allow the feedwater to continue flowing at 30 psig applied pressure and measure the time required for 500 ml to flow through the filter after 5, 10 and 15 minutes.

(3) After completion of the test, calculate the SDI by using the equation below.

$$SDI = \frac{100\,(1 - T_i/T_f)}{T_t}$$

where SDI = Silt Density Index

T_t = Total elapsed test time (either 5, 10 or 15 minutes)

T_i = Initial time in seconds required to collect the 500 ml sample

T_f = Time in seconds required to collect the second 500 ml sample after test time T_t (normally after 15 minutes).[11]

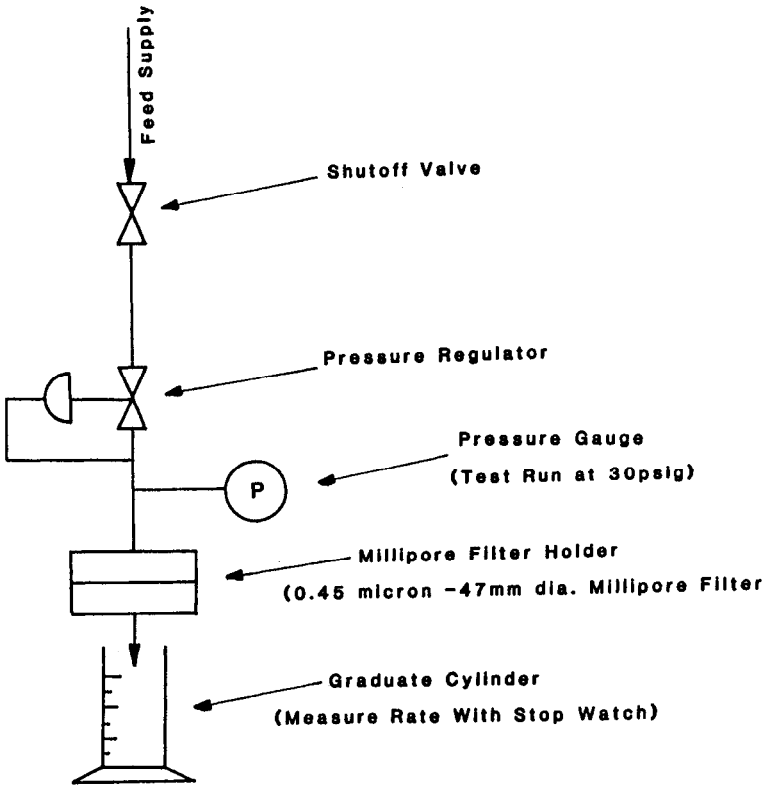


Figure 4.12: Silt density index apparatus.

Manufacturers of hollow fine fiber elements usually require that the pretreated feedwater have an SDI of 3.0 or below in order for the element warranty to be effective. One manufacturer of spiral wound element requires that the pretreated feedwater have a turbidity of less than 1.0 turbidity unit to maintain the element warranty. As a general rule, if hollow fine fiber elements are to be used, the pretreated feedwater should have an SDI of 3.0 or less and, if spiral wound elements are to be used, an SDI of 5.0 or less. However, spiral wound elements have been used to recover municipal wastes with an SDI in excess of 5.0 after pretreatment.

Pretreatment Section

The pretreatment section of a reverse osmosis plant is designed:

(1) to reduce suspended solids (1 micrometer or larger) to zero and to minimize the effects of colloids in membrane fouling,

(2) to adjust the pH of the feedwater,

(3) to add a threshold inhibitor to the feedwater and

(4) to remove oxidizing compounds in the feedwater if required.

In some applications, such as the desalination of a well water, suspended solids and colloids may be negligible and the pretreatment section may consist of pH adjustment and addition of a threshold inhibitor. At the other extreme is the desalination of surface waters, municipal wastes and industrial wastes which may require all of the steps outlined above.

The following techniques can be used to remove suspended solids or to mitigate the effects of colloids:

(1) If the feedwater is a municipal water supply or well water with an SDI of 6.0 or below it may only be necessary to filter the feed. There are a number of filters available that have been successfully employed and these are: diatomaceous earth, single media, dual media and mixed media. A properly designed filter in these applications should be able to reduce the suspended solids load to zero.

(2) In-line coagulation may be used to reduce colloidal membrane fouling. In this technique, coagulant aids such as alum, ferric chloride and/or a polyelectrolyte are added to the feed stream prior to filtration. It is necessary to conduct on-site jar tests in order to determine which coagulant aid is effective and what is the proper dose for that coagulant aid.

(3) In the case of a feedwater with a high suspended solids, turbidity and/or SDI, it may be necessary to use conventional coagulation followed by sedimentation prior to filtration. Again, on-site jar tests are required to determine the proper coagulant aid, dose and settling rate.

The feedwater pH is usually adjusted to a pH of between 4 and 6 for the following reasons:

(1) It is required (usually as a condition of warranty) to minimize the rate of hydrolysis of the cellulose acetate ester. Cellulose acetate hydrolysis reduces the useful life of the membrane by increasing the flux and reducing the rejection of the membrane.

(2) The flux and rejection of some composite membranes are a function of pH and the optimum pH is between 4 and 6.

(3) Many natural waters are saturated in calcium carbonate which is highly rejected by the membrane. Consequently, it is concentrated in the feed/reject stream during the reverse osmosis process and it will precipitate on the membrane decreasing the flux and rejection. Lowering the pH of the feedwater to between 4 and 6 converts some of the carbonate or bicarbonate ions to carbon dioxide and this prevents carbonate precipitation.

Some feedwaters contain compounds in addition to calcium carbonate that may become saturated in the feed/reject stream and when that stream is concentrated in the reverse osmosis process, these compounds will precipitate on the membrane with a resultant loss of membrane performance. Some of the more sparingly soluble compounds of concern are:

Calcium sulfate	Barium sulfate
Calcium phosphate	Strontium sulfate
Calcium fluoride	Silica

One method of preventing precipitation is to operate the reverse osmosis unit at a recovery which will not concentrate the feed/reject stream to the compound saturation level. Another method of preventing precipitation is to add a threshold inhibitor, such as sodium hexametaphosphate, certain polyacrylates, organophosphates or phosphonates, to the feedwater. The threshold inhibitors are added at the rate of 1 to 5 mg/ℓ of feedwater, and they serve to disrupt the formation of a crystalline precipitate during the residence time of the feedwater in the reverse osmosis unit. In doing this, they broaden the solubility limits of the sparingly soluble compounds.

As noted above, the polyamide and polyurea membranes cannot tolerate an oxidizing agent, such as residual chlorine in the feed. Consequently, if these membranes are used and the feed has a residual chlorine content, then it is necessary to remove it. This is usually done by adding a stoichiometric excess of sodium bisulfite or sodium thiosulfate in accordance with recommendations from the membrane manufacturer.

Even with the best of pretreatment schemes, membrane elements will foul over a long period of time and they must be cleaned. Each membrane packaging configuration has a different degree of susceptibility to fouling and an ease of cleaning.

The tubular element is the least susceptible to fouling and the easiest to clean. This element is widely used in ultrafiltration applications where the process streams contain suspended solids. The tubular element can be cleaned not only by chemical action but also by mechanical means. A sponge rubber ball is pumped through the tubular element with the chemical cleaning solution to scour the membrane surface.

The spiral wound element requires less pretreatment than the hollow fine fiber element or, stated in another manner, it is less susceptible to fouling. For instance, the hollow fine fiber has been tested and found to foul excessively on municipal wastewater reclamation applications while the spiral wound element has been operated successfully. The spiral wound element must be cleaned with chemical solutions, but there are no mechanical means available to clean this element.

The hollow fine fiber element, with the great number of close packed fibers, is an effective filter in itself. Consequently, it is the most easily fouled membrane configuration and requires the most pretreatment. The hollow fine fiber element can be cleaned with chemical cleaning solutions, but it is not amenable to mechanical cleaning. It is also more difficult to clean than the spiral wound element.

Element manufacturers have developed cleaning solutions for their specific membranes and elements. Generally, there are two types of cleaning solutions-one for removal of organic foulants and another for removal of metal hydroxides. A cleaning system should be provided with each reverse osmosis system and the cleaning system should consist of a tank to mix the cleaning solution and a pump with associated piping, valves and instruments to circulate the cleaning solution through the reverse osmosis elements.

Reverse Osmosis Section

Once the pretreatment study had been completed, it will be possible to decide on the type of elements to be used in the reverse osmosis unit. If the SDI of the pretreated feed is 3.0 or less, then either the spiral wound or hollow fine fiber elements can be used. The choice will depend on economics (element price) and desalination characteristics (flux and rejection). If the pretreated feed SDI is more than 3.0, then the spiral wound element should be used. When the decision as to element type is made, then it is appropriate to forward a copy of the pretreated feed water analysis to reverse osmosis element manufacturers to obtain a prediction of product water quality, recommended type of element, total number of elements required, possible problems with sparingly soluble compounds in the feedwater, allowable recovery, and price and delivery.

Figure 4.13 shows a flow diagram for a reverse osmosis unit with 75% recovery on a brackish feed. The pretreated feed is routed to the high pressure pump where the feed pressure is raised to between 250 and 400 psig as required for brackish water desalination. The pressurized feed is then pumped to the first pass pressure vessels where about 50% of the feed is recovered as product and 50% is reject. The reject from the first pass pressure vessels is then routed to the second pass pressure vessels where, again, about 50% of the first pass reject is recovered as product and 50% is reject which is sent to waste. Thus, the overall recovery of the unit is 75% as product. As can be seen, a normal array for a 75% recovery unit is two first pass pressure vessels feeding one second pass pressure vessel or a 2-1 array. If the system recovery were from 40 to 60%, all of the pressure vessels would be in parallel. However, if the system recovery were raised to between 85 and 90%, the pressure vessels would be arranged in a 4-2-1 array.

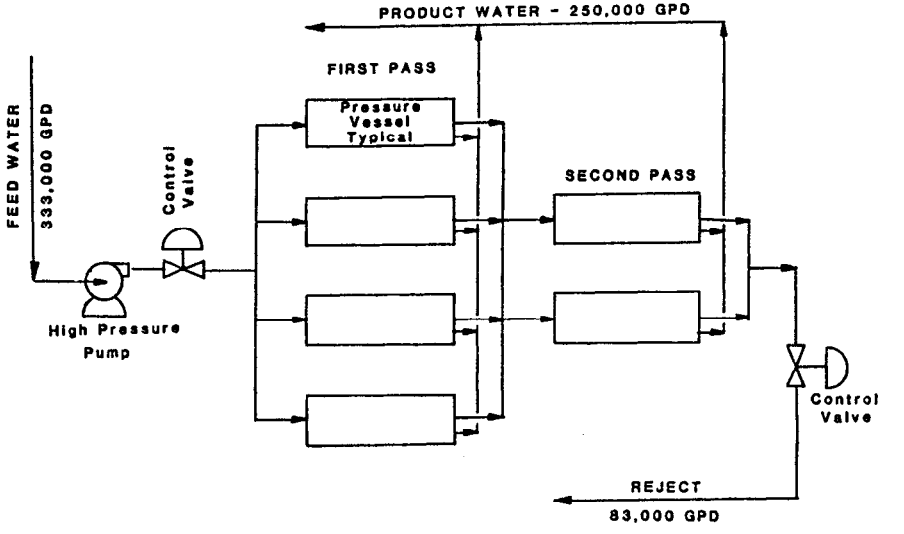


Figure 4.13: Reverse osmosis system.

The quality of the product water is a function of the rejection as shown in the following equation:

$$Cp = Cf * (1 - R)$$

where Cp = Concentration of the product
Cf = Concentration of the feed
R = Rejection

This equation produces accurate results for a membrane sample or a small element with a low recovery, e.g., 2% or less. However, a practical reverse osmosis system is designed to recover from 25 to 90% of the feedwater. This means that the concentration of the feed varies throughout the membrane system. At 90% recovery, the initial membranes will have a feed which is about 10 times less concentrated than the feed to the final membranes and the quality of the product water will vary incrementally throughout the system. The product water from the first membrane elements will be less concentrated than the product water from the last elements. The product water from the practical reverse osmosis system is combined in the product water manifold and its concentration is usually represented as the average product water concentration. The average product water concentration is determined by the following formula:

$$\overline{Cp} = \overline{Cf} * (1 - R)$$

where $\overline{Cp}$ = Average or total product water concentration
$\overline{Cf}$ = Average concentration of the feed and reject streams.

The average concentration of the feed and reject streams as represented by the following equation is not truly representative:

$$\overline{Cf} = \frac{\text{feed concentration} + \text{reject concentration}}{2}$$

As Figure 4.13 shows, there are more elements in the first pass of a 75% recovery reverse osmosis system than in the second pass and the first pass elements produce more product. Thus, a greater percentage of the total product water is derived from the first pass and the total product water will be nearer in concentration to the first pass average than to the second pass average.

Saltonstall[14] has derived an equation to determine the average concentration of the feed and reject streams accurately and this equation is as follows:

$$\overline{Cf} = Cf * \left[\frac{1 - (1 - Y)^{(1 - R)}}{(1 - R)\ Y}\right]$$

where $\overline{Cf}$, Cf and R are defined above and Y = system recovery.

The concentration of the total product then becomes:

$$Cp = Cf * \left[\frac{1 - (1 - Y)^{(1 - R)}}{(1 - R)\ Y} * (1 - R)\right]$$

$$= Cf * \left[\frac{1 - (1 - Y)^{(1 - R)}}{Y}\right]$$

Thus, the product water concentration is dependent on the feed concentration, membrane rejection and system recovery. Figure 4.14 shows the dependence of product concentration on these variables. It is possible to use a lower rejection membrane and a high recovery with a low TDS feedwater. On the other hand, a high TDS feedwater, such as seawater is limited to a low recovery and requires a high rejection membrane.

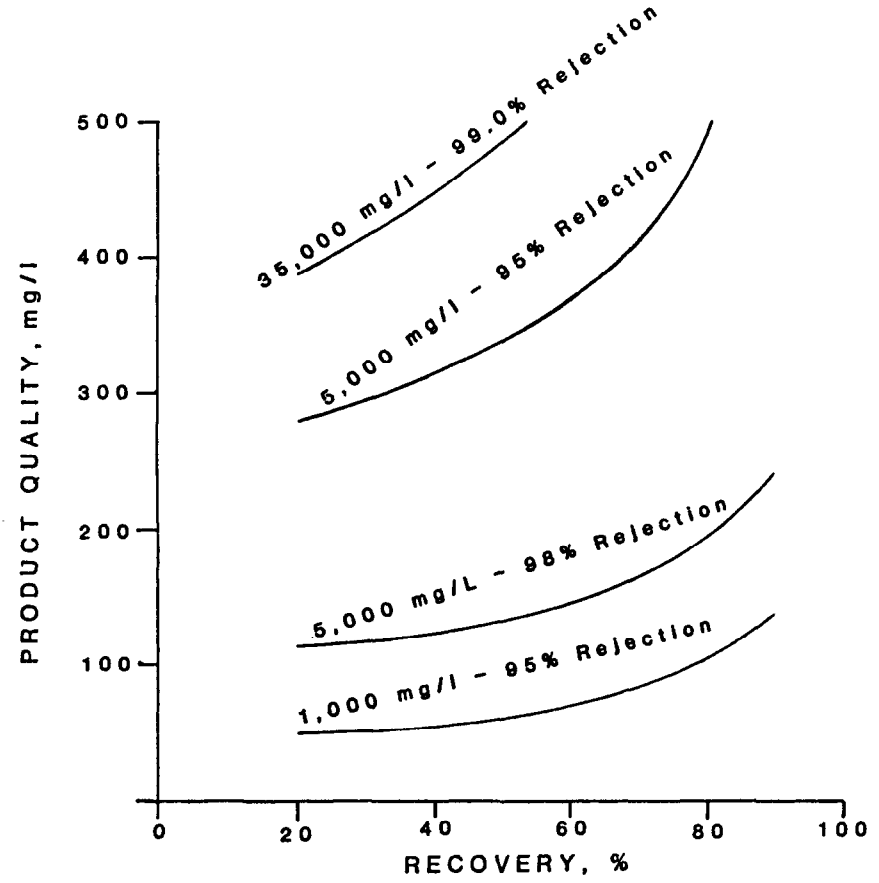


Figure 4.14: Product water vs. recovery.

The membrane flux is also dependent on recovery. The average feed/reject concentration increases with pressure and, since the osmotic pressure is proportional to concentration, the average osmotic pressure will increase with increased recovery. At constant applied pressure, the membrane flux will decrease with increased recovery. Figure 4.15 shows the increase in average osmotic pressure and the decrease in flux for a membrane which would produce 20 gfd at zero recovery operating on a feed of 5,000 mg/ℓ at 450 psi applied pressure. Concentration polarization is assumed to be constant at all recoveries.

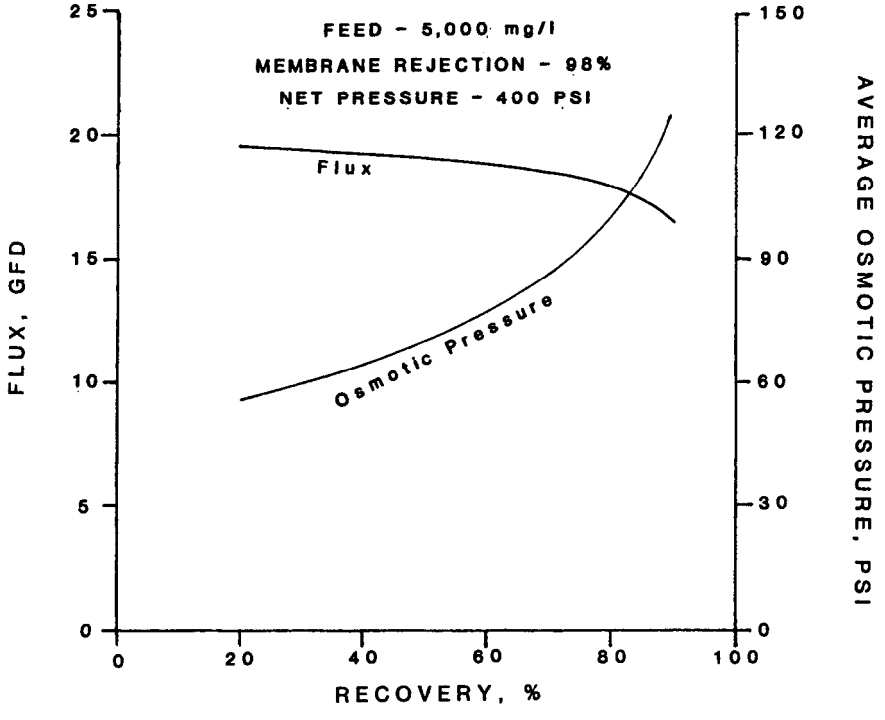


Figure 4.15: Flux and average osmotic pressure vs. recovery.

It is noted that the osmotic pressure of seawater is about 400 psig and an operating pressure of between 800 and 1,000 psig is required to obtain optimum flux and rejection. If a recovery of only 50% were used, the reject osmotic pressure would be in excess of 700 psig and the average osmotic pressure would be about 550 psig. This would present problems in obtaining a potable product of 500 mg/ℓ or less. Consequently, most seawater desalination reverse osmosis units are operated at a recovery of from 25 to 35%.

Since lowering of the feed pH usually means that the feed contains significant quantities of carbon dioxide, the feed and reject streams are extremely corrosive. In addition, the membrane does not reject carbon dioxide and, consequently, the product stream contains about the same concentration of carbon dioxide as the feed and reject streams, i.e., all three process streams are corrosive. General practice is to use PVC pipe and valves for low pressure piping (less than 100 psig) and 316 stainless steel pipe and valves for the high pressure (above 100 psig) process streams. The high pressure pump wetted parts should be either 316 stainless steel, corrosion resistant plastic or other corrosion resistant materials. The pressure vessels are fabricated with fiberglass reinforced plastic which is corrosion resistant.

The reverse osmosis process is relatively simple and instrumentation requirements are minimal. Following is a list of the minimum recommended parameters to be measured in a reverse osmosis system:

Feed	Product	Other
Flow	Flow	Differential Pressure
Temperature	Conductivity	across each array
Pressure		
Conductivity		
pH		

A variety of control schemes can be incorporated in the design of a reverse osmosis plant. However, this subject is beyond the scope of this manual.

Posttreatment Section

In most plants that use reverse osmosis in the preparation of process water, the reject stream is routed directly to waste discharge without any additional posttreatment. In industrial plants that use reverse osmosis to treat industrial wastes, the reject stream may contain valuable materials and this stream would be sent back to the process. In other applications of industrial waste treatment by reverse osmosis, the reject stream may require additional treatment prior to ultimate discharge. In this case, the reverse osmosis unit will have provided a large volume of water that is disposable or can be reused (the product) and a smaller volume of reject which can be treated more economically.

The product water from a reverse osmosis unit will have a low pH and most probably a high concentration of carbon dioxide. The carbon dioxide can be removed and the pH of the product increased by use of a decarbonator. A decarbonator is a packed column in which product water is introduced at the top while either forced or induced air is introduced at the bottom. The air and water flow countercurrently over and around the column packing. The carbon dioxide is stripped from the water and exits from the decarbonator at the top in the air stream. In a well-designed decarbonator, the carbon dioxide content can be reduced to about 5 mg/ℓ in the water effluent.

INDUSTRIAL REVERSE OSMOSIS AT A REFINERY

One of the most innovative industrial uses of reverse osmosis is at the Petromin Refinery in Riyadh, Saudi Arabia. The refinery takes an unusable municipal wastewater, secondary effluent from the Riyadh sewage treatment plant, and by using lime clarification, filtration, reverse osmosis and ion exchange demineralization, it converts that useless waste into the entire process water requirements for the refinery. Figure 4.16 is the process flow schematic for the refinery water treatment plant.

Chlorinated secondary effluent arrives at the pumping station, which is adjacent to the sewage treatment plant in Riyadh, through an open channel which flows to the pump station inlet basins. The 4.63 MGD of effluent is then pumped 19 kilometers to the refinery by either of two full capacity pumps which take suction from the inlet basins. The effluent is pumped through a

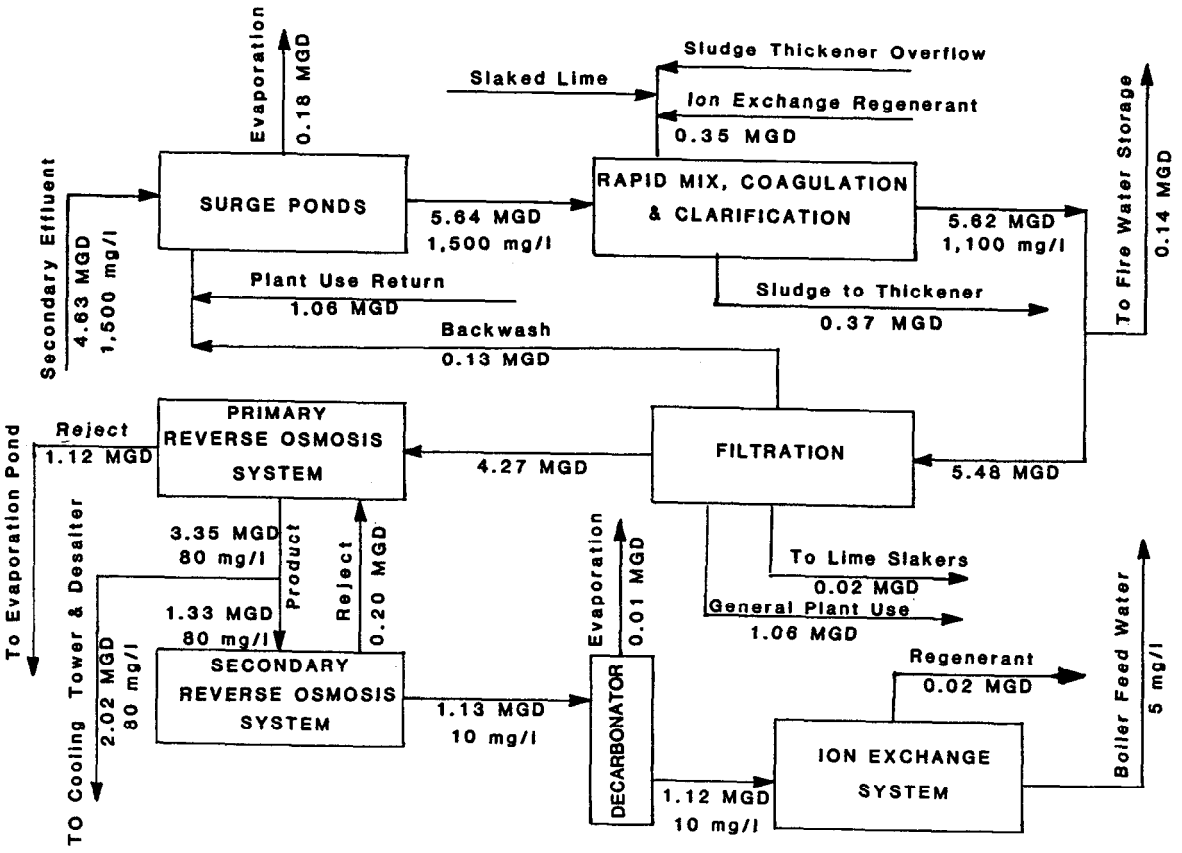


Figure 4.16: Industrial reverse osmosis at a refinery.

24-inch diameter cement lined carbon steel pipeline. The pipeline is equipped with vacuum relief valves and air-release safety valves at the two highest points in the line plus air-release safety valves at the third highest point in the line. The pipeline is also equipped with pigging facilities (for pipeline cleaning) which consist of 2 pigs, a pig launcher and pig receiver.

On arrival at the refinery, the effluent is discharged into a 2 compartment splitting box which divides the flow evenly for discharge into the two on-site surge ponds. The effluent flows from the splitting box by gravity into the surge ponds. At the same time, miscellaneous refinery plant streams and backwash from the refinery water treatment plant filter are returned to the surge ponds and mixed with the secondary effluent. The return stream flow is estimated to be 1.19 MGD with a quality similar to the secondary effluent. Each of the surge ponds is a concrete lined, earth basin with a capacity of 5.3 million gallons. The surge ponds have a static air diffusion system to prevent sewage septicity and improve homogeneity in the secondary effluent. Chlorine can be added to the secondary effluent either at the sewage treatment plant pump station or at the surge ponds at the refinery, if required.

All surface waters and municipal effluents contain suspended solids as well as dissolved solids and the presence of suspended solids dictates the need for a pretreatment section. Experience has shown that effective removal of the suspended solids in pretreatment is a prerequisite to efficient reverse osmosis membrane performance. Suspended solids in secondary effluent are primarily organic in nature and, due to their small size, it is difficult to remove them by settling. Therefore, it is necessary to aggregate the smaller particles into larger particles which can more easily be removed by settling and filtration.

For some time, it has been known that suspended solids or colloids in water possess an electrical charge which is predominantly negative. As a result of this electrical charge, the colloidal particles tend to repel each other and thereby limit the potential for aggregation and the colloidal suspension is said to be stabilized. Before the suspended particles can coalesce, the stabilizing forces must be neutralized and this is usually done by adding chemicals. Trivalent aluminum, ferric hydroxides, and/or lime have been used to destabilize colloidal suspensions and allow suspended particles to grow in size. Another means of particle destabilization is the use of natural or synthetic polymers which are long chain, high molecular weight polyelectrolytes with many active sites. The negatively charged colloids are adsorbed on the active sites with the resultant coagulation or growth of the particles.

The refinery clarification equipment has the capability of adding any of the chemicals mentioned above. However, lime clarification was chosen as the method to be used. The combined secondary effluent and the plant return streams (5.64 MGD) are pumped from the surge ponds to the rapid mix basin in the clarifier. The rapid mix basin has two compartments in series and each compartment has a high speed mixer. Lime and sodium hydroxide are added to the first compartment and these are vigorously mixed with the secondary effluent in both compartments. As a result, the pH of the effluent from the rapid mix basin is raised to between 10.8 to 11.0. At this pH, much of the bicarbonate in the water reacts with the lime and forms an insoluble calcium carbonate and the magnesium in the water reacts with hydroxyl ions to form insoluble magnesium hydroxide.

The water flows from the rapid mix basin to the flocculation basin which has four compartments. Each compartment is further divided into three sec-

tions and all twelve sections are equipped with a slow speed turbine mechanism. The gentle agitation provided in the flocculation basin promotes contact between the calcium carbonate, magnesium hydroxide and suspended matter which results in the formation of larger particles.

The water then flows by gravity from the flocculation basin to the sedimenor clarification basin. The enlarged floc particles settle to the bottom of this basin and they are removed as a 1% sludge by three circular rakes into a sludge basin or hopper. This amounts to about 0.37 MGD of sludge which is pumped to the sludge thickener tank. The sludge is thickened to about 6% in the sludge thickener and then filtered in a plate and frame filter press to about 50% solids. The filtered sludge may then be transported to a a landfill for disposal or sent to the on-site multiple hearth lime kiln for regeneration. Operation of the lime kiln is economically marginal. The overflow from the sludge thickener and the filter press filtrate are returned to the rapid mix basin for reclamation. In addition, part of the water used in the regeneration of the ion exchange demineralizers is also returned to the rapid mix basin for recovery. The total amount of water from these three sources is 0.35 MGD with variable quality.

Effluent from the clarifier is saturated in calcium carbonate and this would precipitate on the filter media to clog the filter which is the next step of pretreatment. Consequently, the clarifier effluent flows by gravity to the serpentine recarbonator basin where carbon dioxide is added to reduce the pH to between 7.5 and 8.0. The insoluble calcium carbonate and magnesium hydroxide are converted to soluble calcium and magnesium bicarbonate in the recarbonator basin. The 5.62 MGD of effluent from this basin has a suspended solids concentration of about 2 mg/ℓ and a TDS of about 1,100 mg/ℓ.

Following lime clarification and recarbonation, the treated water is pumped to the fire water storage tanks (0.14 MGD) and the remainder (5.48 MGD) is pumped to the water treatment plant cooling tower. The cooling tower is used to reduce reverse osmosis feedwater temperature when required. For a large part of the year, the cooling tower is inoperative. A static mixer is installed in the line upstream of the cooling tower. At this point, sulfuric acid can be added to the process stream to reduce the pH of the water in the event that carbon dioxide is unavailable to the recarbonation system. Chlorine can be added to the process water at the cooling tower influent line or at the chlorine diffuser of the filter aid basin. The water flows by gravity from the cooling tower to the filter aid mix station where it is possible to add coagulant aids to assist in the removal of suspended solids during filtration. Coagulant aids are not being added at the filter aid mix basin at this time. The water then flows by gravity to the dual media filters.

There are four separate filter basins with filter media as described in Table 4.7 below.

Table 4.7: Filter Media Description

	Height		
Media	mm	Inches	Size, mm
Coal	800	31.5	0.6 - 1.6
Sand	400	15.7	0.6 - 1.0
Gravel Support	400	15.7	3 - 35

The process water flows through the filter media by gravity to remove the remaining suspended solids. It then flows through a flow control valve to the filtered water reservoir by gravity. Backwash water overflows from the filtered water reservoir to the wash water storage tank. The filter effluent of 5.48 MGD provides 1.06 MGD of general use water to the refinery, 0.13 MGD of filter backwash water, 0.02 MGD of filtered water to the lime slakers at the rapid mix basin and the remaining 4.27 MGD flows by gravity to the reverse osmosis dechlorination basin.

Chlorine has been added to the feedwater upstream of reverse osmosis pretreatment. However, since chlorine will depolymerize the polyurea membrane barrier layer in the spiral wound element, with subsequent loss of desalination properties, the chlorine is removed in the pretreatment system dechlorination basin. This removal is chemically accomplished by the addition of sodium bisulfite. The chlorine level in the influent and effluent to the dechlorination basin is continuously monitored. The feedwater is then transferred from the dechlorination basin to the cartridge filter feed pumping station by gravity flow and it is then pumped to the cartridge filters.

Sulfuric acid and sodium hexametaphosphate (SHMP) are injected in the feedwater line upstream of the cartridge filters. The sulfuric acid is injected to adjust the feedwater pH to a level of between 4 and 6. The purpose of acid injection is twofold. The primary purpose is to mitigate the possibility of calcium carbonate deposition by conversion of bicarbonate to carbon dioxide. Coincidentally, the rejection performance of the thin film composite membrane is pH sensitive and the optimum performance is at the operating pH level. SHMP is added to the feedwater as a threshold inhibitor to inhibit the crystalline growth of sparingly soluble salts such as calcium sulfate.

After chemical addition, the feedwater is routed to cartridge filters which serve to mix the chemicals which have been added upstream and to insure that any particles that may have escaped the gravity filters, such as sand or other particulate matter is removed. In general, the cartridge filters do not improve the quality of the reverse osmosis feedwater to a large degree and they are not intended as continuous duty filters. The effluent from the cartridge filters is routed to the primary reverse osmosis feed pump wet well.

The primary reverse osmosis system contains five trains of equal capacity. Each train is operated independently and there is a vertical turbine high pressure pump for each train mounted on the primary feed pump wet well. The high pressure feedwater is pumped to the reverse osmosis train where the operating pressure of each train is adjusted by the pressure control valve upstream of the spiral wound element pressure vessels. The elements are located in fiberglass reinforced plastic pressure vessels with six elements per pressure vessel. The elements have nominal dimensions of 40 inches in length by eight inches in diameter and they contain composite membrane with a polyurea membrane barrier layer. Each primary train has 180 elements in 30 pressure vessels which are manifolded in a 20-10 array. The pressurized water is fed to 20 pressure vessels in parallel where about 50% of the feed is recovered as product and the reject from these pressure vessels is manifolded and fed to 10 pressure vessels in parallel. About 50% of the feed to these latter pressure vessels is recovered as product and the reject is manifolded through the flow control valve to waste. The product water from the primary reverse osmosis system is transferred to the cooling tower makeup and

desalt water storage tanks or to the secondary reverse osmosis system feed pump wet well. The overall recovery for each train is 75% and the design capacity of each train is 0.83 MGD of product for a total product water capacity of 4.10 MGD in the first stage. The daily requirements for product water are 3.35 MGD so there is an installed spare capacity of about 20%. The product water requirements are 2.02 MGD for the refinery cooling towers and the desalter and 1.33 MGD for the second stage reverse osmosis system. The reject (1.12 MGD) from the first stage reverse osmosis system is sent to the on-site solar evaporation pond for disposal.

The first stage product water concentration of 80 mg/ℓ is adequate for cooling tower makeup and desalter process water but it is not pure enough for moderate pressure boiler feed. Consequently, the first stage product must be further treated with ion exchange demineralization to achieve the desired purity. A second stage of reverse osmosis is used at the refinery to pretreat the first stage product prior to ion exchange demineralization. An improved quality feed to the ion exchangers will improve not only the quality of ion exchanger effluent but it will reduce the quantity of regenerative chemicals required by the ion exchangers.

The secondary reverse osmosis system contains three trains of equal capacity. As in the primary reverse osmosis system, each train is operatred independently and there is a vertical turbine high pressure pump associated with each train. The pressurized feedwater is pumped to the secondary trains where the operating pressure of each train is adjusted by the pressure control valve upstream of the element pressure vessels which are fabricated from fiberglass reinforced plastic. Each secondary train has 21 pressure vessels (126 elements) which are manifolded in a 12-6-3 array. The spiral wound elements in the secondary trains are identical to the elements in the primary stage. The pressurized feedwater is fed to the first 12 pressure vessels in parallel where about 50% of the feed is recovered as product and the remaining 50% is manifolded and fed to the next six pressure vessels in parallel. Product recovery in these pressure vessels is again about 50% and the reject is manifolded and fed to the last three pressure vessels where about 40% of the feed is recovered as product. The reject from the last three pressure vessels is manifolded through the flow control valve in each train to the dechlorination basin. The reject flow of 0.20 MGD from the secondary reverse osmosis trains is of better quality than the feed to the primary reverse osmosis system and, thus, it is used as feed to the primary system. The overall design recovery of each of the secondary trains is 85%. Each of the trains is rated at 0.57 MGD for a total capacity of 1.71 MGD. The total required capacity is 1.31 MGD which can be produced by two trains with one train in standby. The recovered product is routed to the forced air decarbonators in the ion exchange demineralization system.

The product water from the secondary reverse osmosis system contains a high concentration of carbon dioxide as a result of pH adjustment in the primary reverse osmosis system which converts bicarbonate and carbonate alkalinity to carbon dioxide. Since the membrane is "transparent" to carbon dioxide, it passes through both the primary and secondary reverse osmosis systems into the secondary system product water. Although the ion exchange resin would remove the carbon dioxide, it is more economical to do so in the decarbonator.

There are two degasifiers (decarbonators) in the refinery water treatment plant and each of these are in parallel and normally in operation, i.e., one de-

gasifier is not used as a standby. The secondary product is fed to the top of the degasifiers where it is allowed to cascade over the degasifier packing. Air is blown through the packed section from the bottom and it rises in the packed column countercurrent to the water. It is estimated that 0.01 MGD of product water are lost to evaporation in the decarbonator. Since the water is at a low pH, carbon dioxide is transferred from the liquid phase to the gas phase. The result is that the carbon dioxide concentration in the water is reduced to about 5 mg/ℓ. Two transfer pumps, both full capacity, are installed to pump the decarbonated water through the ion exchange system.

There are two full capacity ion exchange trains in the system and each train consists of a cation tank, an anion tank, instrumentation, and the necessary valves and piping for process control. The ion exchange demineralization is accomplished in a two-step process involving treatment with both cation and anion resins in separate process vessels. The water is first passed through the strong acid cation exchange resin (Amberlite IR-20) to exchange the cations for the hydrogen ion. The effluent is then passed through a Type I, strong base anion exchange resin (Amberlite IRA-410) where the anions are exchanged for the hydroxide ion. The result is that cations and anions are substituted by water molecules and a high purity effluent is available for use as boiler feedwater. When the ion exchange capacity of one train is depleted, this train is removed from service, the standby train is placed in operation and the depleted train is regenerated with acid and caustic. About 0.02 MGD of decarbonator effluent are used for regeneration of the resins and much of this is returned to the rapid mix basins for recovery.

REVERSE OSMOSIS AND ION EXCHANGE

The preceding example of a reverse osmosis industrial application at a refinery showed that the process is capable of:

(1) treating a feedwater with high suspended solids and dissolved solids concentrations;

(2) reclaiming a water that is considered by most as unusable; and

(3) developing a number of process streams with different quality requirements.

Reverse osmosis also has been used to treat municipal water supplies for industrial purposes even though these supplies are generally low in turbidity, suspended solids and dissolved solids. A large number of reverse osmosis systems have been installed in industrial plants to prepare industrial process water with municipal water as the feed source. A significant number of these industrial applications are to either replace ion exchange demineralization or to pretreat municipal supplies prior to ion exchange demineralization.

Reverse osmosis systems now commercially available will remove 95% or more of the dissolved solids normally removed in ion exchange, and as will be discussed later, a few that are not. The ionized solutes are not all removed to the same degree by reverse osmosis any more than ion exchange resins have the same effect on all solutes. Divalent and multivalent ions, such as calcium, magnesium, sulfate, iron and manganese, can be rejected to greater than 99%. So-

dium, potassium and chloride are normally rejected to the 95% level or better. The net effect is to reduce the number of regenerations required of the ion exchange columns by a factor of 20 or more. This results in a significant reduction in the amount of waste regenerant solutions that must be disposed of and a material reduction in the dissolved solids that might normally be discharged to the environment. A concentrate or reject is produced by reverse osmosis, but there is little change in the environmental salt budget. Concommitant results are a major decrease in the space and equipment necessary for regenerant storage and an extension of the useful life of the resins, owing to reduced resin attrition. In addition, substances difficult to remove from the resin, which also affect its performance, are greatly reduced or are removed by reverse osmosis pretreatment.

When reverse osmosis is used for preliminary demineralization, the variation in the quality of the ion exchange demineralized water is reduced. The amount of dissolved solids in the feed to the ion exchange beds is 5% or less than when the raw water is fed directly. It is, therefore, obvious that the variation in solids in the finished water will also be less when breakthrough occurs. As a result, the resins may be utilized more efficiently. Additional reliability and control can be gained by measuring the solids concentration following reverse osmosis treatment. This precaution virtually eliminates shock loadings on mixed bed polishing columns. Where small point of use polishing columns are used, such as in microelectronics manufacturing, the danger of a rapid breakthrough becomes considerably reduced, and there is an improvement in production and product quality.

An important factor to be remembered is that in some cases water supplies unsatisfactory for processing to high purity water may be the only sources available. Preliminary demineralization by reverse osmosis will make this water suitable for subsequent demineralization by ion exchange. It is thus apparent that such an economically important factor as plant site location, which may be dependent on the availability of suitable water, can be made more flexible through the use of reverse osmosis. It may be possible now to utilize seawater as a source of industrial process water.

During the 1960's, reverse osmosis was compared with other methods of demineralization. It was indicated in these comparisons that reverse osmosis could not compete favorably with ion exchange at dissolved solids concentrations below 700 mg/ℓ and that its most favorable area of use would be from about 1,200 to 5,000 mg/ℓ dissolved solids. This idea has been totally refuted because some of the most successful applications of reverse osmosis, particularly as part of the process to produce high purity water, have been in treating low dissolved solids water. Water containing 200 mg/ℓ dissolved solids or less has been treated at costs equal to or lower than those of ion exchange alone.

Two substances that are frequently of concern in ion exchange demineralization are silica and organics. The organics are frequently present in natural waters as aromatic polycarboxylic acid derivatives known as humic and fulvic acids. Silica may be the limiting factor in the efficiency of the anionic resins, and (particularly in boiler feedwater applications) the lower the concentration before ion exchange demineralization, the better. Reverse osmosis will frequently produce 90% or greater reductions in total silica concentrations. However, performance should be tested on the specific water to be treated since the results can be variable and the reason for differences between waters is not yet understood.

Where the silica concentrations in the raw water are high, reverse osmosis has been most effective. Even in trace quantities, humic and fulvic acids have been responsible for impairing the life of anionic resins and affecting performance of ion exchange columns. These organics are readily removed by reverse osmosis membranes.

REVERSE OSMOSIS AND POLLUTION CONTROL

Pollution control legislation has made industry aware of the economic penalty for inefficient use of raw materials. The plating industry was one of the first industries to experience this enforced awareness. Loss of raw materials in this industry[15] can result in five distinct costs:

(1) replacement of the plated material that was discharged to waste prior to initiation of pollution control practices;

(2) removal of that material from the wastewater after pollution control enforcement;

(3) disposal of the residue from item 2;

(4) replacing of the process water (at times quite expensive) lost in wastewater; and

(5) treatment of the wastewater in a publicly owned treatment works after discharge into a sewage system.

In response to the plating industry's increased awareness of the above costs, plating shops have modified their practices to reduce their material and economic losses. While pollution control was greeted by many with coolness, the resultant cost savings have shown that pollution control is not as onerous as expected.

Reverse osmosis has been installed in many plating shops as a way to resource recovery and minimizing the size of waste treatment equipment and volume. Reverse osmosis is particularly suited to waste treatment in the plating industry because most of the toxic ions in the plating solutions are well rejected by commercially available membranes. Table 4.8 shows the rejection ranges of some of the more common toxic materials in the plating industry.[16]

Table 4.8: Reverse Osmosis Rejection Range

Ion	Rejection Range, %
Nickel	98 - 99
Copper	98 - 99
Cadmium	96 - 98
Chromate	90 - 98
Cyanide	90 - 95
Zinc	98 - 99

The nickel plating industry is a typical candidate for the use of reverse osmosis in pollution control. Figure 4.17 shows a schematic of this industrial application. The workpiece travels from the plating bath with a concentration of 270,000 mg/ℓ to the rinse tanks. There are three rinse tanks in series and rinse water flows countercurrent to the workpiece. The work piece drags out plating bath to the first rinse tank, first rinse tank solution to the second rinse tank and second rinse tank solution to the third rinse tank. Consequently, the first, second and third rinse tanks have concentrations of 3,000 mg/ℓ, 333 mg/ℓ and 37 mg/ℓ, respectively.

About 100 gallons/hour (GPH) are pumped from the first rinse tank through a cartridge filter and into a reverse osmosis unit. The reject stream contains 99% (59,400 mg/ℓ) of the nickel in the feed stream with 1% (32 mg/ℓ) remaining in the product stream. The reject stream is routed through an activated carbon column to the plating bath. The reverse osmosis product stream is combined with 5 GPH of tap water makeup, which is added to compensate for surface evaporation in the plating tank, and the combined stream is returned to second rinse tank. The waste stream (10 GPH) is sent to waste treatment which is a precipitation process.

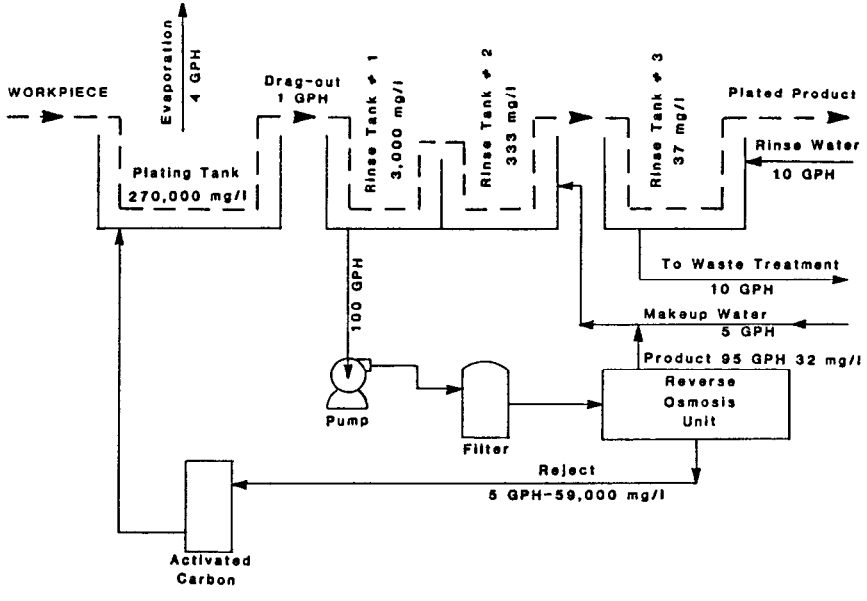


Figure 4.17: Reverse osmosis in nickel plating.

REVERSE OSMOSIS AND SEAWATER DESALINATION

It has been estimated that the oceans cover about 70% of the earth's area and contain about 80% of the water on or in the earth. Seawater concentration varies from 25,000 mg/ℓ of total dissolved solids up to over 50,000 mg/ℓ in the Arabian Gulf. The average composition of seawater is about 35,000 mg/ℓ with the major ions being shown in Table 4.9.

Table 4.9: Major Constituents of Seawater

Constituent	Concentration, mg/l
Sodium	10,500
Magnesium	1,350
Calcium	400
Potassium	380
Chloride	19,000
Sulfate	2,700
Bicarbonate	142
Bromide	65
Other Ions	33
Total	34,570

While seawater is abundant, it is to a large degree unusable and it is the constant dream of the desalination industry to desalt seawater in an economical manner that would allow the product to be used for agricultural purposes. This goal is a long way from reality. On the other hand, distillation and now reverse osmosis are desalting seawater efficiently enough to be used for preparing potable waters in affluent areas. Seawater, with a concentration of 35,000 mg/ℓ, has an osmotic pressure of almost 400 psig and this mandates a membrane element with high pressure capabilities. If the reverse osmosis seawater plant were required to deliver a product water of potable quality (500 mg/ℓ or less), then the membrane element would require a minimum rejection of 98.6% to attain that product quality at 0% recovery. At higher recoveries, both pressure and rejection must increase to obtain potable quality. Spiral wound and hollow fine fiber elements have been developed with the capability of operating at 800 to 1,000 psig and sodium chloride rejections up to 99.5%. This capability has placed reverse osmosis in the seawater desalination business and reverse osmosis is beginning to replace distillation as the result of the clear cut economic advantage of reverse osmosis.

An example of reverse osmosis seawater desalination for industrial purposes is the system installed in a thermoelectric power plant in Venezuela in 1980.[17] The original segment of the plant is designed to produce 800,000 GPD of boiler feedwater and potable water. A process flow diagram for this system is shown in Figure 4.18.

Seawater is pumped from an intake channel to the roughing filters which are the first part of the pretreatment process. Ferrous chloride and chlorine are added to the filter influent line. The chlorine disinfects the seawater and oxidizes the ferrous ion to the ferric ion which forms insoluble ferric hydroxide. The ferric hydroxide acts as a coagulant aid. A large percentage of the coagulated particles are removed in the roughing filter which reduces the feedwater SDI from 15 to about 3. There are five gravity roughing filters which have a dual media of sand and anthracite. Four of the filters are in operation while one is

in standby to be placed in operation when one of the operating filters is backwashed.

The effluent from the roughing filter clearwell is pumped to the pressurized polishing filters which further reduce the SDI to less than 3. There are four operating polishing filters and one standby filter. The filter media is anthracite and green sand.

Sodium bisulfite is added to the effluent from the polishing filters to remove residual chlorine which would be harmful to the polyamide reverse osmosis membrane. Sulfuric acid is then added to the filter effluent to adjust the pH to about 6.5 and the pretreated water is routed to the primary reverse osmosis system.

The first stage reverse osmosis systems consist of four trains which are capable of producing 200,000 GPD each of product water. Each train consists of a 5-μ cartridge filter with a high pressure pump feeding two subunits of 25 DuPont B-10 permeators each plus the necessary piping, valves and instrumentation. The first stage system reverse osmosis units are operated at 30% recovery with a pump discharge pressure of 900 psig. The total dissolved solids content of the feed was reported to be 37,000 mg/ℓ and the product concentration from this stage was 490 mg/ℓ. This product water is sent to a 262,000-gallon storage tank which provides feed to the two second stage reverse osmosis trains and it is the source of potable water for the power plant. The reject from the first stage is routed to waste. A high pressure recovery turbine is not used and a considerable amount of energy is wasted.

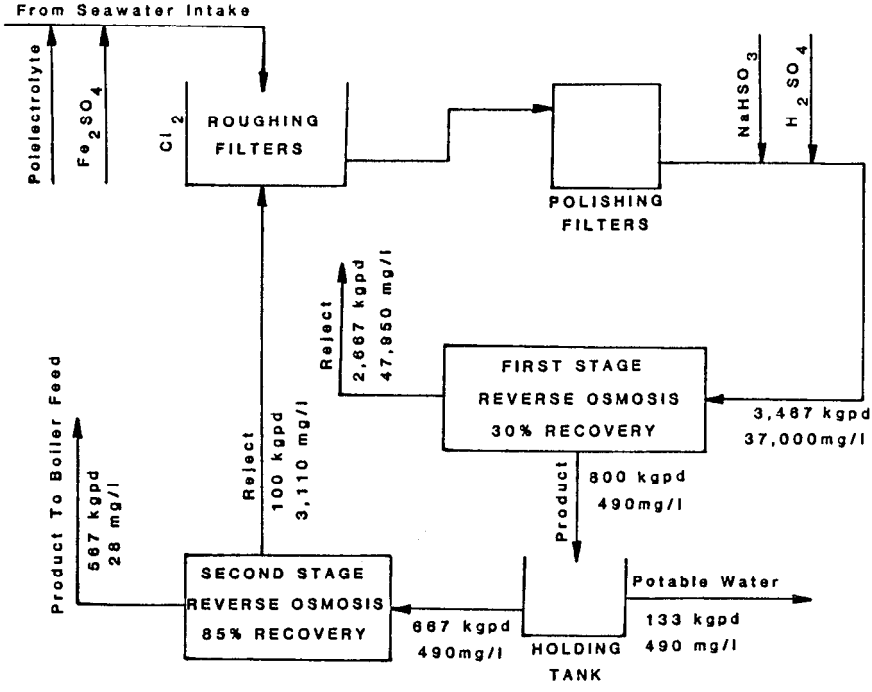


Figure 4.18: Power plant process water from seawater.

The first stage product quality meets potable standards but it is far from the quality required for boiler feedwater. Preparation of boiler feedwater is done in an ion exchange system and, with an influent of 490 mg/ℓ, the operating cycle would be short and chemical regenerant cost high. In this case, it is economical to further treat the first stage reverse osmosis product in a second stage reverse osmosis system to further decrease the load on the ion exchange resins.

About 85% of the first stage reverse osmosis system product water is pumped to the second stage reverse osmosis system which consists of two trains. Each train consists of a 5-μ cartridge filter, a high pressure pump, DuPont B-9 permeators, piping, valves and instrumentation. Each train has 22 permeators in a 12-7-3 array and it is operated at 85% recovery. The product from the second stage has a TDS of 28 mg/ℓ and this is sent to the ion exchange system. The reject from the second stage is of much better quality than the incoming seawater and this is routed to the roughing filter clearwell.

The reverse osmosis system has operated well and the capacity of the plant has been increased to twice that of the initial segment described above.

GENERAL APPLICATIONS OF REVERSE OSMOSIS

The above applications were specific examples that were chosen to demonstrate the versatility of the reverse osmosis process. The following list enumerates a wide variety of applications for which the reverse osmosis process may be considered:

(1) Municipal Potable Water
- General quality improvement of present supplies
  - Upgrade total municipal supply
- Potable water from degraded supplies
  - Brackish water desalination
  - Seawater desalination
  - Removal of nitrates, fluorides, heavy metals, etc.
- Bottled water production

(2) Industrial Water
- Provide usable water where none available
  - Brackish water desalination
  - Seawater desalination
- Pure water production
- Industrial rinse waters
  - Food industry
  - Electroplating
  - Power plant boiler feed
  - Beverage production
  - Medical
  - Ultrapure water production
  - Pharmaceutical

Electronics
Medical

(3) Municipal Wastes
Reclaim municipal wastewaters (sewage) for
Ground water recharging
Agricultural or landscape irrigation
Industrial process water
Improve effluent quality to meet discharge requirements

(4) Industrial Wastes
Reclaim industrial wastewaters for
Reuse within industrial plant
Zero discharge
Agricultural or landscape irrigation
Removal of toxic substances prior to discharge
Resource recovery
Separate or concentrate valuable materials
Electroplating industry
Dairy industry

(5) Miscellaneous
Production of pure water for high value crops
Recovery of agricultural irrigation drainage
Production of shipboard drinking water

COSTS OF REVERSE OSMOSIS

There is no such thing as the typical cost of a reverse osmosis system or of the product water from that system as these costs depend on a number of things:

Economic conditions	Power costs
Market conditions	Site preparation
Plant size	Product quality requirements
Local labor rates	Feedwater availability
Chemical costs	Accounting procedures

The DuPont Permasep Engineering Manual[11] has published a "guide" for the capital, operating and maintenance costs for both a brackish water system and a seawater system. The brackish water system costs are shown in Table 4.10. They are based on a large brackish water system built in the southern United States in 1982. The estimated capital cost of the plant is $1.25 per gallon per day of product water installed. This cost includes the cost of wells, a reverse osmosis system with pretreatment, a building for the reverse osmosis systems and office. The above installed capacity cost does not include the cost of land nor an independent power source.

Table 4.10: Total Water Cost for Brackish Water RO

	Cost/1,000 Gals. Product
Energy (0.06/KWH)	$0.36
Chemicals	0.09
Labor	0.12
Maintenance and Repair	0.05
Membrane Replacement	0.10
Amortization (12%/20 years)	0.48
Total	$1.20

Data are provided for a seawater system that will produce 10 million gallons per day of product water. The system is a two stage system similar to the one shown in Figure 4.18 where the product water from the first stage high pressure seawater system is treated in a second stage lower pressure brackish water system. The product water TDS is 200 mg/ℓ. The estimated 1982 cost for such a system was $45 million which includes the RO system with pretreatment and a building for the RO system, controls and office. It does not include the cost of land or an independent energy source. The total water cost for such a plant is shown in Table 4.11.

Table 4.11: Seawater RO System

	Cost/1,000 Gals.Product
Energy ($0.06/KWH)	$1.80
Chemicals	0.14
Labor	0.19
Maintenance	0.22
Membrane Replacement	0.90
Amortization (12%/20 years)	1.75
Total	$5.00

Both the brackish and seawater reverse osmosis product water costs are based on 1982 costs and they are indicative of specific plants in an assumed location in the southern United States. The cost of energy in the seawater system assumes that the reject from the first stage high pressure reverse osmosis system is sent to an energy recovery system which reduces the overall energy requirements for the total system by 31%.

FUTURE PROJECTIONS

The initial projections of 20 years ago have proven to be unrealistic in that reverse osmosis has not caused deserts to bloom, nor does every household contain a reverse osmosis unit to improve the tap water. Yet, the process has been of economic value in providing process water to industry, potable water to high income arid regions and a method of reclaiming municipal and industrial wastes. As of 1985, it was estimated that the worldwide market for reverse osmosis membrane elements (not total systems) was about $50 million.

The future of the process rests in the research that will result in the development of a product that will compete with and win over other separation processes that can do the same thing. Reverse osmosis has gone a long way toward becoming more economical than multistage flash distillation in the production of potable water from seawater. The development of membranes with higher fluxes and improved rejections will be incorporated into single stage seawater plants with lower operating pressures. This will not only permit reverse osmosis to win the competition for new seawater desalination capacity but it will allow the RO process to replace distillation plants that are being retired in the Middle East where the enormous capacity of these plants exists. The low pressure membranes which are being developed for brackish applications will also further potential municipal wastewater reclamation as an alternate source of potable and industrial water. The reduced costs which will result from lower pressure/higher rejection systems will effectively compete with pipelines, dams and other water supply schemes that proliferate in the western United States.

While not totally essential to progress, it is suggested that oxidizing-agent-resistant membranes will be developed in a thin film composite membrane. This will broaden the applications available to RO and, at the same time, reduce the cost and complexity of existing plants which presently use chlorine sensitive membranes.

An elusive goal has been the development of ion specific membranes. Based on limited knowledge of worldwide research programs, it appears that this goal will remain elusive for the forseeable future.

Finally, as the world becomes more aware of the environmental damage caused by indiscriminate waste disposal it is apparent the RO process will play a key role in mitigating that problem. It appears that the next market for the RO process will be in industrial waste treatment in the United States to be followed by application in other countries. Eventually, the world will be forced to use reverse osmosis to reclaim municipal wastewater on a large scale and to put the reclaimed water to a number of already demonstrated beneficial uses.

REFERENCES

1. El-Ramly, N.A. and Congdon, C.F., *Desalting Plants Inventory, Report No. 6*, United States Department of Interior (1977).
2. El-Ramly, N.A. and Congdon, C.F., *Desalting Plants Inventory, Report No. 7*, National Water Supply Improvement Association (1981).
3. Wangnick, K., *Desalting Plants Inventory, Report No. 8*, Water Supply Improvement Association (1984).

4. *Water Desalination Report* (M.C. Smith, Ed.), Vol. XXI, No. 37 (September 19, 1985).
5. Soltanieh, M. and Gill, W.N., *Chemical Engineering Communications*, Vol. 12, pp. 279-363.
6. Fluid Systems Division of UOP, Inc., *Product Catalog* (1984).
7. Beasley, J.K., "The Evaluation and Selection of Polymeric Materials for Reverse Osmosis Membranes," *Proceedings of the International Congress on Desalination and Water Reuse*, International Desalination and Environmental Association (1977).
8. Sudak, R.G. and McKee, M.E., "Low Pressure Composite Membranes," *Proceedings of the International Congress on Desalination and Water Reuse*, International Desalination and Environmental Association (1977).
9. Orange County Water District, *Evaluation of Membrane Processes and their Role in Wastewater Reclamation*, Vol. I (1979).
10. Orange County Water District, *Evaluation of Membrane Processes and their Role in Wastewater Reclamation*, Vol. II (1980).
11. E.I. DuPont de Nemours & Co., *Permasep Engineering Manual* (1982).
12. Sourrajan, S., Editor, *Reverse Osmosis and Synthetic Membranes*, National Research Council of Canada (1977).
13. American Public Health Association, American Water Works Association and Water Pollution Control Federation, *Standard Methods for the Examination of Water and Wastewater*, 16th Edition (1985).
14. Saltonstall, C.W., Jr., *Proceedings of the 10th Annual Conference of NWSIA* (1982).
15. Environmental Protection Agency, *Environmental Regulations and Technology—The Electroplating Industry* (1980).
16. Environmental Protection Agency, *Economics of Wastewater Treatment Alternatives for the Electroplating Industry* (1979).
17. Vera, I., "Operating Experiences on a Reverse Osmosis Plant Which Converts Seawater to Boiler Feedwater," Industrial Water Engineering (November 1981).

5

Thin Film Composite Reverse Osmosis Membranes

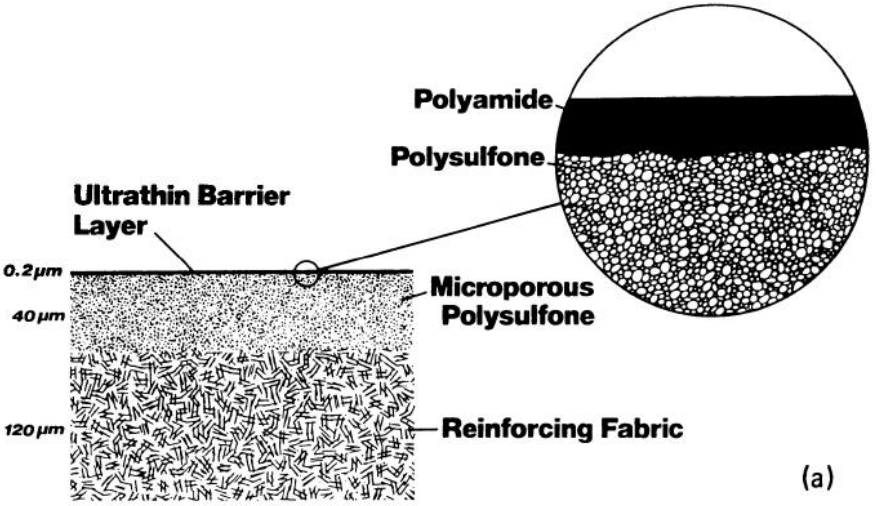
Robert J. Petersen and John E. Cadotte

A thin film composite reverse osmosis membrane can be defined as a multilayer membrane in which an ultrathin semipermeable membrane layer is deposited on a preformed, finely microporous support structure. This contrasts with asymmetric reverse osmosis membranes in which both the barrier layer and the porous substructure are formed in a single-step phase inversion process and are integrally bonded.

Figure 5.1 contains a schematic diagram illustrating the concept of a thin film composite reverse osmosis membrane. Alongside this is shown a photomicrograph of a fracture edge of an actual membrane of this type at 1,000 magnification. In this photomicrograph, the barrier layer is not actually visible other than as a smooth surface. Because its thickness is so small, it cannot be seen at the magnification shown.

Fabrication of a thin film composite membrane is typically a more expensive route to reverse osmosis membranes because it involves a two-step process versus the one-step nature of the phase inversion film casting method. However, it offers the possibility of each individual layer being tailor-made for maximum performance. The semipermeable coating can be optimized for water flux and solute rejection characteristics. The microporous sublayer can be optimized for porosity, compression resistance and strength. Both layers can be optimized for chemical resistance. In nearly all thin film composite reverse osmosis membranes, the chemical composition of the surface barrier layer is radically different from the chemical composition of the microporous sublayer. This is a common result of the thin film composite approach.

The term "thin film composite" has the connotation that the barrier layer is extremely thin, and hence quite fragile. Indeed, the barrier layer may be quite thin, varying to as low as 200 angstroms depending on the nature of the particular reverse osmosis membrane and its method of manufacture. But this does not necessarily result in fragility. Some of these membranes may be considerably



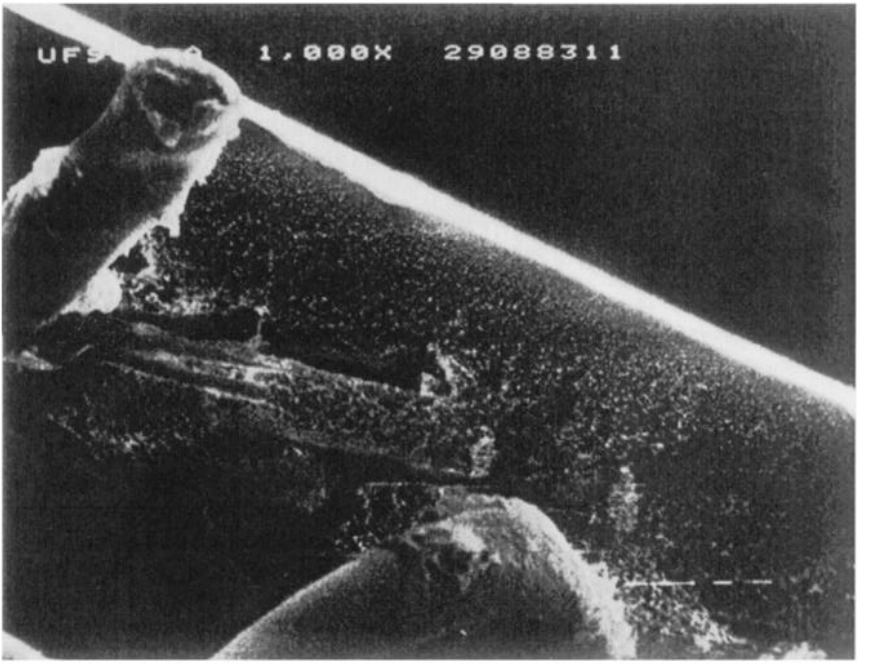


Figure 5.1: (a) Schematic diagram of the cross section of a composite reverse osmosis membrane; (b) scanning electron microscope photograph of the cross section of a composite reverse osmosis membrane.

more rugged and chemically resistant than the typical asymmetric cellulose acetate membrane in field service. It should be noted that the barrier layer in asymmetric cellulose acetate membranes is itself only about 2000 angstroms thick. Therefore, it may be more correct to refer to such membranes simply as "composite" reverse osmosis membranes.

There are several potential routes to the preparation of composite reverse osmosis membranes, whereby the ultrathin semipermeable film is formed or deposited on the microporous sublayer.[1,2] The film can be formed elsewhere, then laminated to the microporous support, as was done in the earliest work on this membrane approach. Or it can be formed in place by plasma polymerization techniques. Alternatively, membrane polymer solution or polymer-forming reactants can be applied in a dipcoating process, then dried or cured in place. The most attractive approach from a commercial standpoint, however, has been the formation of the semipermeable membrane layer in situ by a classic "non-stirred" interfacial reaction method. Several examples of membranes made by this last approach have reached commercial status.

CELLULOSE ACETATE MEMBRANES

The first composite reverse osmosis membrane to be developed and described consisted of an ultrathin film of secondary cellulose acetate deposited onto a porous Loeb-Sourirajan membrane.[3] The ultrathin film of cellulose acetate was fabricated by a water surface float-casting technique. This has been described to some extent in the published technical literature,[4,5] and in considerable detail in several reports on government-funded research projects.[3,6-8] Figure 5.2 illustrates this process schematically.

In float-casting, a polymer such as cellulose acetate is dissolved in an aqueous solvent, usually cyclohexanone, to a level of about 5% by weight. A solvent is preferred which has a slight solubility in water and a specific gravity of less than 1.0 g/cc. When a casting dope of this type is allowed to flow down an inclined plane onto a quiet water surface, it shows a pronounced tendency to spread over the water surface. Migration of the solvent into the water surface (as well as some loss by air evaporation) occurs, leaving behind a floating solidified polymer film. Continuous addition of the casting dope with mechanical drawing off of the solidified film, can be used to control the thickness of the ultrathin film. For reverse osmosis membranes, thicknesses of 200 to 5000 angstroms have been achieved. In a related application involving float-cast thin cellulosic membranes for hemodialysis, thicknesses of up to 2.5 μm (25000 angstroms) were developed and used.[5]

The free floating film is transferred to a microporous support by bringing a sheet of the support into contact with the underside of the ultrathin film, lifting it from the water surface.[9] Also, two layers can be simultaneously cast and laminated to a carrier web.[7,8] Numerous patents have appeared in recent years on the fabrication of gas separation membranes by float-casting, even including the double layer membrane technique.[10,11]

Ultrathin float-cast films exhibit visible light interference colors. These can be used as a general guide for thickness, blue being about 2000 angstroms in the case of cellulose acetate, gold being thinner, green and red being thicker. Actual

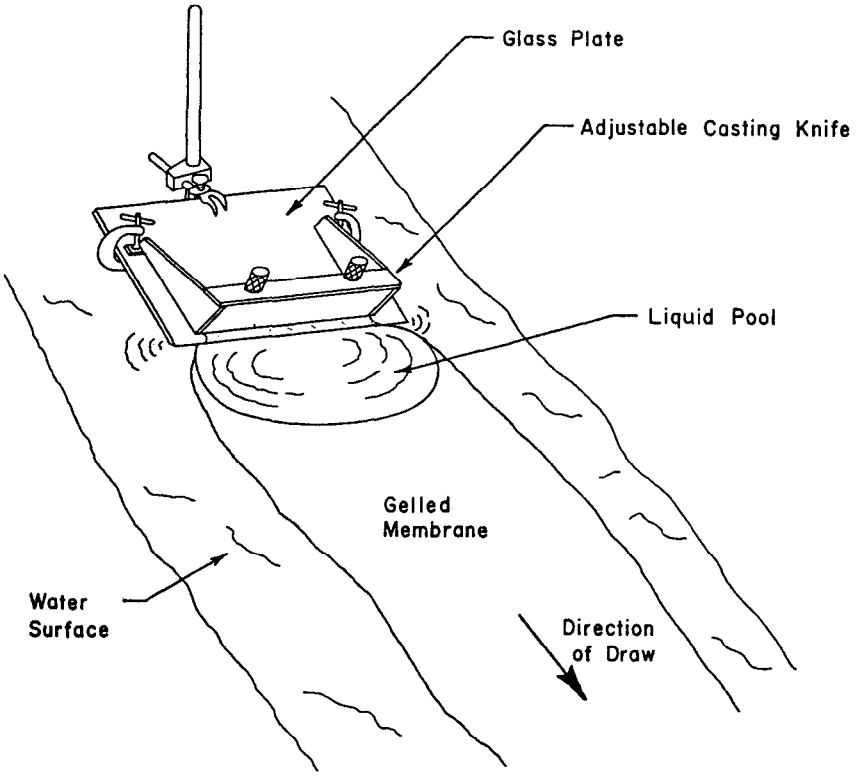


Figure 5.2: Schematic diagram of the float-casting of ultrathin cellulose acetate membranes.

measurements have been made by interferometric methods on films deposited and air-dried on glass plates.[12,13]

An alternate route to ultrathin cellulose acetate membranes exists via the Carnell-Cassidy technique.[14,15] In this method, a glass plate is mechanically withdrawn at a slow, careful rate from a dilute solution of the polymer. A thin, air-dried film is obtained, which could be released from the glass plate by immersion in water. The result can be achieved on a large scale by the meniscus coating approach, illustrated in Figure 5.3.[16] A commercial adaptation of this process was developed by Lonsdale and Riley.[17,18] A microporous sheet of a cellulose acetate/cellulose nitrate blend was first coated with a thin film of polyacrylic acid. This coating was temporary in nature, intended to protect the microporous sheet from solvent attack during overcoating with the semipermeable barrier film. The polyacrylic acid would dissolve in water and wash out during subsequent usage under reverse osmosis conditions. An ultrathin coating of cellulose triacetate dissolved in chloroform was meniscus-coated onto the polyacrylic acid surface, and dried. These membranes exhibited salt rejections of as high as 99%.

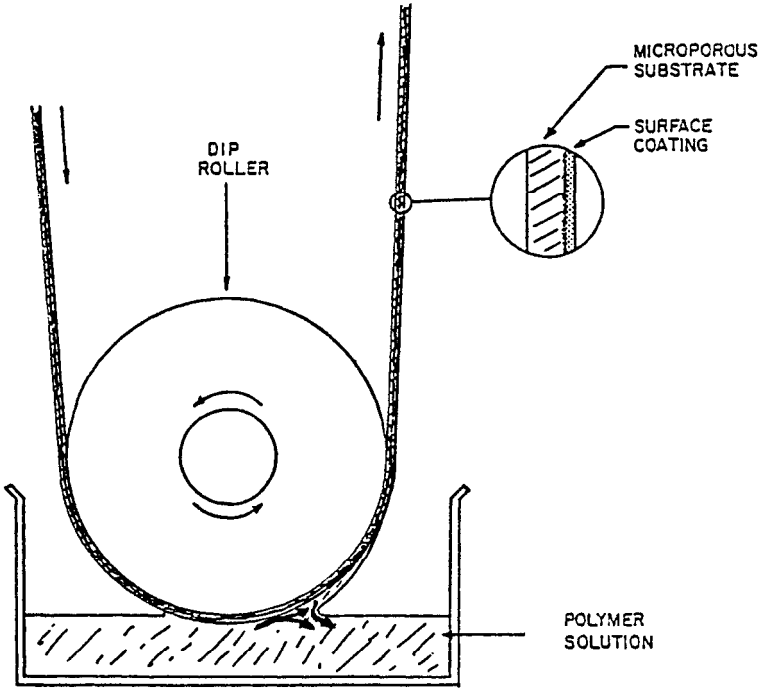


Figure 5.3: Schematic diagram illustrating the meniscus coating technique.

During the period of 1965 to 1972, the best data on flux and salt rejection for cellulose acetate membranes were exhibited by the composite membranes. However, these membranes never reached commercial viability; efforts on them died out completely by 1975. Reasons for this appear to be threefold. First, composite cellulose acetate membranes were technically difficult to scale up. Second, the advent of noncellulosic composite membranes in 1972 (the NS-100 membrane) offered much more promise for high performance (salt rejection and water flux), especially for seawater desalination. Third, continual improvements in asymmetric cellulose acetate membrane casting technology (such as the development of swelling agents and of blend membranes) brought the performance of asymmetric membranes to full equality with composite cellulose acetate membranes.

MICROPOROUS POLYSULFONE SUPPORTS FOR COMPOSITE MEMBRANES

Early examples of cellulose acetate composite membranes used cellulose ester sheet materials as the porous underpinnings for the float-cast films. These sheet materials included: (a) Loeb-Sourirajan asymmetric cellulose acetate mem-

branes formulated to have loose, high flux structures and (b) mixed cellulose ester microfiltration membranes in the tightest grades. These were concluded to be far from optimum because of their susceptibility to compaction at the seawater test condition of 1,500 psi prevalent at that time.

In the fall of 1966, researchers at North Star Research Institute began a search for compression-resistant microporous substrates.[19] This effort resulted in the development of microporous sheets of polycarbonate (Lexan) and polysulfone (Udel).[20] Figure 5.4 shows a graph comparing the flux levels and flux stability for three membranes made at that time: (a) float-cast cellulose acetate on microporous polysulfone, (b) float-cast cellulose acetate on a mixed cellulose ester microfilter support and (c) a standard asymmetric cellulose acetate membrane. The improvement in membrane fluxes was readily apparent, when switching from cellulosic substrates to the microporous polysulfone substrate.

The structure of a microporous polysulfone sheet, optimized for composite reverse osmosis membranes, is illustrated in Figure 5.5. These pictures were obtained using freeze fractured samples in a Hitachi Model H-600 STEM electron microscope. The SEM photographs show an asymmetric cross section of graded porosity-very dense at the top surface and highly porous at the bottom surface. High magnification views of the dense top layer show the anticipated nodular structure, which has also been observed in asymmetric aromatic polyamide and cellulose acetate membranes prepared by phase inversion methods. Surface views of the microporous polysulfone indicate pores of 200 to 300 angstroms.

Polysulfone was recognized as a major improvement in the state-of-the-art of composite membranes at that time. But the broad scope of its usefulness was never fully appreciated until later. It has since become widely useful in its own right as an ultrafiltration membrane. It was subsequently included in a U.S. patent on ultrafiltration membranes by Michaels that issued in 1971.[21] Concerning reverse osmosis membranes, it represented a *key development* that later enabled rapid progress to take place in noncellulosic composite membranes.

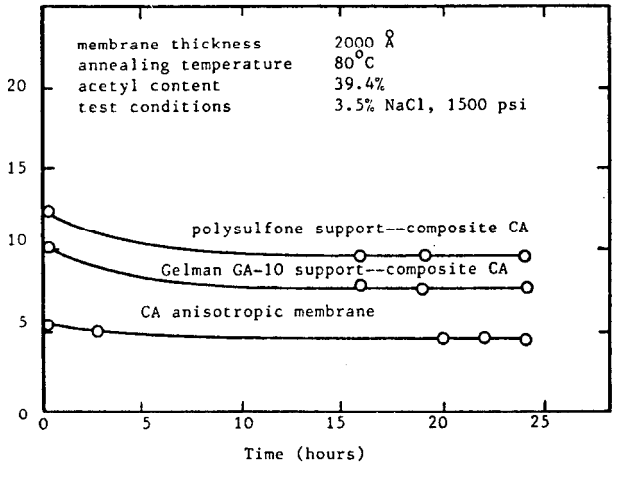


Figure 5.4: Effect of support films on the reverse osmosis water flux of cellulose acetate membranes.

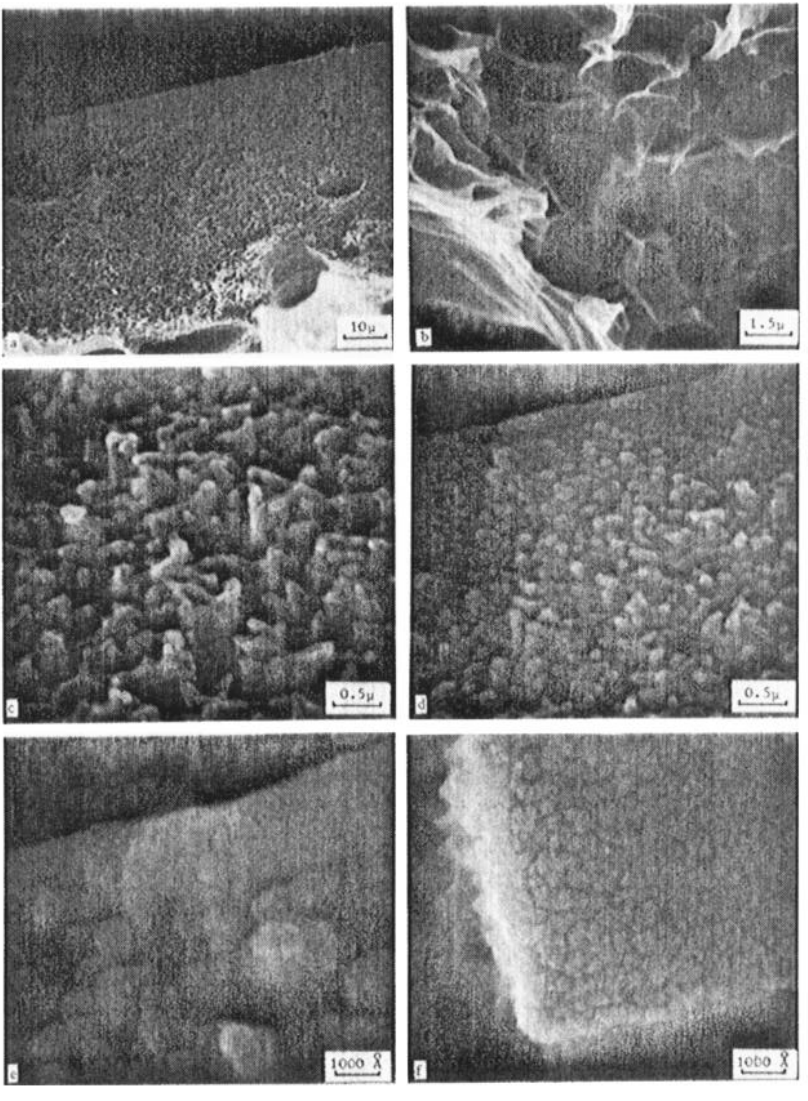
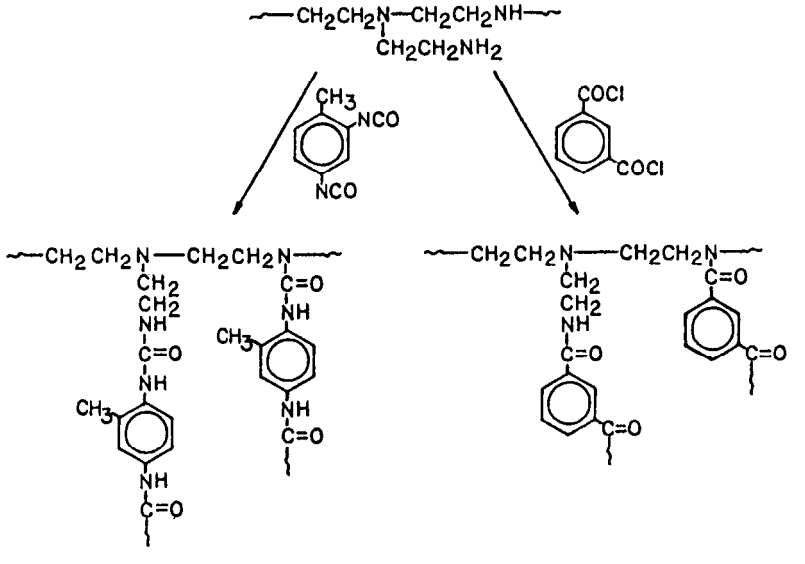


Figure 5.5: Cross section and surface of a microporous polysulfone sheet used in composite reverse osmosis membranes: (a) total cross section of a polysulfone sheet cast on a nonwoven polyester fabric, then delaminated prior to freeze-fracture for SEM (note fiber tracks on backside of the sheet); (b) backside of sheet showing cellular structure, which extends through 85% of the sheet thickness; (c) transition region from cellular to nodular structure near film surface; (d) dense nodular structure at the surface; (e) high magnification of the extreme top surface cross section; (f) high magnification view of the surface structure showing the texture of the top surface.

NS-100 COMPOSITE MEMBRANE

The NS-100 membrane (initially designated as NS-1) was the first noncellulosic composite membrane to appear in the published literature and have an impact on the reverse osmosis scene.[22,23] This membrane, invented by Cadotte,[24] consisted of a microporous polysulfone sheet coated with polyethylenimine, then interfacially reacted with either 2,4-toluenediisocyanate (TDI) or with isophthaloyl chloride (IPC). In the first case, a polyurea is formed; in the second case, a polyamide. The chemistry of this membrane is as follows:



Strictly speaking, the descriptors NS-1 and NS-100 (North Star Research Institute) in the technical literature refer to the TDI-based polyurea membrane. MSI-400 (Membrane Systems, Inc.) refers to the same composition.[25] PA-100 (UOP, Fluid Systems Division) and NS-101 have been used to name the corresponding IPC-based polyamide. The polyamide analog exhibits somewhat higher flux and slightly lower salt rejection than the polyurea form of the membrane. A low pressure version of PA-100/NS-101 membrane, optimized for brackish water operation on Mohawk-Wellton (Yuma) agricultural drainage water, was developed by UOP under the name TFC-202.[26]

Polyethylenimine is a product of the self-condensation of the strained-ring compound ethylenimine (aziridine, azacyclopropane). It is a globular molecule having a not quite statistical distribution of amine groups (30% primary, 40% secondary and 30% tertiary amine). The most effective molecular weight range for this water-soluble polymer in composite membrane fabrication has been 10,000 to 60,000.

Figure 5.6 illustrates the preparation of the NS-100 membrane. A microporous polysulfone sheet is saturated with a water solution of the polymeric amine (0.5 to 1.0% solution of polyethylenimine). Excess solution is drained off

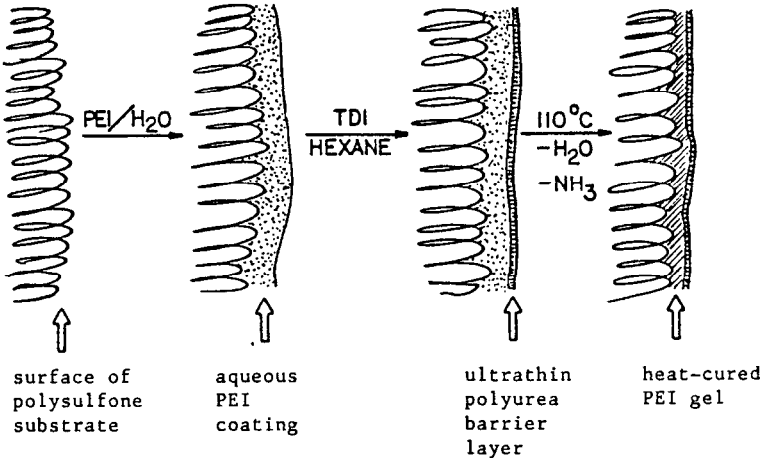


Figure 5.6: Steps in the preparation of the NS-100 composite membrane.

by positioning the film vertically. The amine-impregnated film is then immersed in a solution of 0.1% tolylene diisocyanate in hexane for 30 to 60 seconds. This forms a very thin crosslinked polyurea zone on the surface of the wet polyethylenimine layer. The film is then heated in an oven at 110°C for up to 15 minutes. This treatment not only dries and anneals the film, but performs the crucial step of crosslinking the residual unreacted polyethylenimine. Internal crosslinking of the polyethylenimine takes place via ammonia elimination from adjacent amino groups. If the polyethylenimine were not insolubilized such as by this treatment, it would wash out later during use of the membrane. The polyurea layer itself is too thin to withstand high pressures without the help of the polyamine gel sublayer as an intermediate level support.

The NS-100 membrane is capable of giving salt rejections in excess of 99% in tests on salt solutions simulating seawater (18 gfd, 3.5% synthetic seawater, 1,500 psi, 25°C). If the polyurea interfacial reaction step is omitted, and the polyethylenimine-coated polysulfone film is heat-cured as usual, a crosslinked polyethylenimine semipermeable barrier film is generated. This membrane gives 70% salt rejection and 55 gfd water flux under the same test conditions as above. Also, if the fully formed NS-100 membrane is dried at 75°C, which is too low a temperature to effectively crosslink the amine layer, the resulting film will exhibit a salt rejection of 96% or less.

This membrane is highly sensitive to chemical attack by hypochlorite ion and hypochlorous acid in chlorinated feedwaters. Wrasidlo prepared a variation of the NS-100 membrane in which the primary amine groups of polyethylenimine were cyanoethylated before reaction with isophthaloyl chloride.[27] This membrane was claimed to be chlorine-resistant, but was probably not so.

Optimization studies on the NS-100 membrane were carried out by other groups in addition to North Star Research Institute. Fang and Chian used a statistically designed set of 33 experiments to produce a membrane with

10.30±1.95 gfd and 99.30±0.18% rejection tested on 5,000 ppm sodium chloride at 600 psi.[28] Sudak and coworkers at Membrane Systems, Inc., also used statistically designed experiments to develop a membrane (MSI-400) capable of low pressure operation.[25] This membrane demonstrated a flux of 20 gfd and a salt rejection of 97% when operated at 250 psi on a 5,000 ppm sodium chloride feedwater. Modification of fabrication conditions produced a seawater version of MSI-400 capable of generating 17 gfd and 99% salt rejection on 35,000 ppm sodium chloride at 800 psi and 24°C.

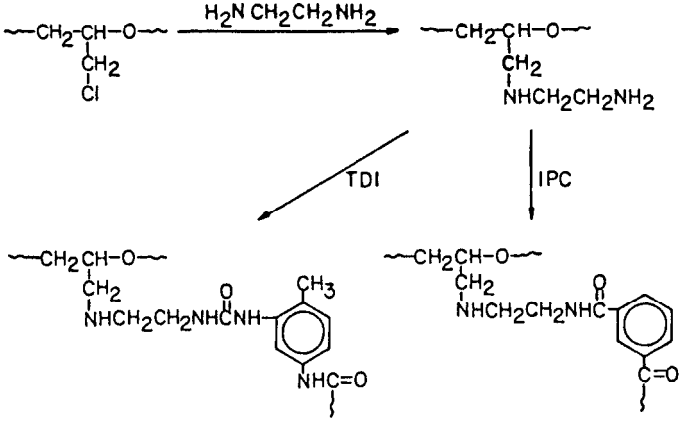
Chian and coworkers have also published studies on the organic solute rejections of the NS-100 membrane[29] and its potential for pesticide removal from water.[30]

PA-300 AND RC-100 MEMBRANES

The NS-100 membrane, being the first of a kind, was by no means optimum in chemistry and performance. Flux was only marginally attractive for desalination, sensitivity to chlorine was extreme, and the barrier surface was thin and brittle. In commercial fabrication trials, overcoating of the membrane surface with a layer of water-soluble polyvinyl alcohol was practiced in order to overcome its brittleness and susceptibility to abrasion damage during handling and spiral element fabrication.

A broad-based effort in both the United States and Japan has since taken place to find other polymeric amine reactants that would contribute to better properties. Perhaps the most significant outcome of this effort to date has been the discovery of composite interfacial membranes based on "polyepiamine" by Wrasidlo,[31] and their development into the PA-300 and RC-100 commercial forms by Riley and coworkers.[32,33]

Polyepiamine, also called polyetheramine, is the reaction product of polyepichlorohydrin with an excess of ethylenediamine. Its idealized structure and its reaction products with isophthaloyl chloride (PA-300) and 2,4-toluenediisocyanate (RC-100) are shown below:



Reaction would take place on both the primary and secondary nitrogen groups, of course. The end result would be a highly crosslinked structure, yet retaining some ductility because of the flexible polyether backbone chains.

Initial data on the PA-300 analog were excellent.[32] In tests on 35,000 ppm sodium chloride at 1,000 psi, fluxes of 20 to 25 gfd and salt rejections in excess of 99.4% (at pH 5.0 to 6.0) were observed. Similarly, in a brackish water test on 5,530 ppm sodium chloride at 400 psi, a water flux of 20 gfd at 98% salt rejection was observed. These data represented major decreases in operating pressure while maintaining effective permeate production rates.

In other respects, it also shared the favorable characteristics of the NS-100 membrane. That is, it was resistant to pH 3 to 12, and showed far better compaction resistance than cellulose acetate. Also, it possessed the capability to operate at elevated temperatures, though some irreversible flux decline could still occur.[34] Rejections of various organics were also good, as shown in Table 5.1 These were in sharp contrast to organic rejection data on cellulose acetate membranes. Initially, PA-300 was also postulated to possess good chlorine resistance.[31] Subsequent experience showed it to be equally sensitive to chlorine as NS-100.

Table 5.1: Reverse Osmosis Performance of the PA-300 Composite Membrane Toward Various Organic Solutes

Solute	Concentration (ppm)	pH	Solute Rejection (%)*
acetaldehyde	600	5.8	70-75
acetic acid	190	3.8	65-70
acetonitrile	425	6.3	25
Alcozyme (soap)	2,000	9.3	99.3
aspartic acid	1,500	3.2	98.3
2-butanone	465	5.2	94
butyl benzoate	220	5.8	99.3
citric acid	10,000	2.6	99.9
2,4-dichlorophenoxy-acetic acid	130	3.3	98.5
dimethyl phthalate	37	6.2	95
ethanol	700	4.7	90
ethyl acetate	366	6.0	95.3
glycine	1,400	5.6	99.7
phenol	100	4.9	93
phenol	100	12.0	99
tetrachloroethylene	104	5.9	93
trichlorobenzene	100	6.2	99

* Conditions: 1000 psi, 25°C

Both PA-300 and NS-100 exhibit mild cationic behavior because of the excess unreacted amino groups present in the barrier layer. One manner in which this is evident is their propensity to absorb anionic surfactants and lose flux

thereby.[34] Consequently, wastewaters containing anionic surfactants cannot be economically treated with this particular type of composite membrane.

Some difficulty was encountered in reliably producing this membrane during its earlier history. A major problem was due to the nature and supply of polyepiamine itself. It was originally developed by Dow Chemical Company as a cationic coagulant for water treatment purposes. Membrane manufacture accounted for only a tiny fraction of its usage. The polyepiamine polymer was observed to be unstable in shelf storage, undergoing a continuous change in viscosity, and sometimes turning into insoluble gel. Eventually, Dow Chemical ceased production of this chemical, and membrane manufacturers desiring to use it were forced to develop their own preparative methods for the polyepiamine.

The PA-300 membrane was the first composite reverse osmosis membrane to be used successfully in a major seawater desalination facility–the 3.2 MGD plant at Jeddah, Saudi Arabia.[35] Much of the original membrane in this plant, as well as replacement membrane, is believed to be RC-100 (the TDI-based analog) because of its greater stability and retention of salt rejection. The Jeddah plant was truly a pioneer installation for spiral-wound composite membranes. Even though it was attended by a variety of start-up and operating problems, mostly unrelated to the membranes,[36] it continues to operate successfully at this date.

A low pressure version of PA-300, designated LP-300 membrane, has also been developed for brackish water applications.[26] This membrane provided up to 24 gfd and 98.5% salt rejection operating on a simulated Yuma feedwater at 200 psi. A summary of UOP developments in the area of these various composite membranes as of the end of 1980 has been published by Riley and coworkers.[37]

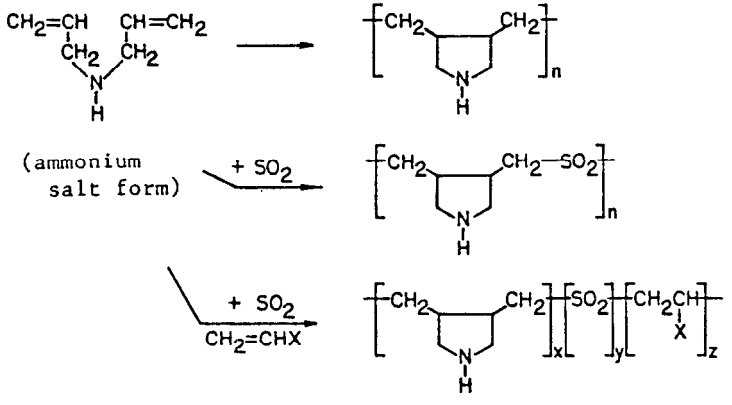
OTHER INTERFACIAL MEMBRANES BASED ON POLYMERIC AMINES

Various polyamines have been synthesized and evaluated in the fabrication of the NS-100 type of membrane. These various compositions are described in the patent literature. Some of these efforts have involved polymeric amines containing only secondary amino groups to reach a goal of improved chlorine resistance. Whether any of them have reached commercial status cannot be determined because of the current trend to avoid publication of the compositions of new commercial reverse osmosis membranes.

Kurihara and coworkers at Toray Industries prepared several aminated derivatives of polyepichlorohydrin, then formed composite polyamide membranes by interfacial reaction with isophthaloyl chloride.[38] Polyepichlorohydrin was converted to polyepiiodohydrin, then reacted with either 4-(aminomethyl)piperidine, 3-(methylamino)hexahydroazepine, or 3-(amino)hexahydroazepine. Also, polyepiaminohydrin was prepared by reduction of the azide derivative of polyepiiodohydrin. Best salt rejections were obtained if the polymeric amine formulation contained a substantial proportion of the monomeric amines as coreactants in the interfacial reaction. In tests on 3.5% sodium chloride at 800 psi and 25°C, salt rejections of 99.5% at fluxes of 8 to 9 gfd were characteristic. A three-zone barrier layer was produced, consisting of a heat-crosslinked polyamine gel (as in NS-100), a polyamide layer incorporating both the polymeric

and monomeric amine reactants, and an additional surface polyamide layer comprised almost solely of the monomeric amine reactant combined with the acyl halide. Toray has recently announced the commercial introduction of a new, high rejection polyamide composite membrane, which may or may not correspond to this patented composition.

Kawaguchi and coworkers at Teijin have prepared a series of polymers based on poly(diallyl amine), its copolymer with sulfur dioxide, and various terpolymers.[39] The chemistry of this polymer synthesis is shown below. The patent description shows the diallylamine polymers to be polypiperidine (six-membered ring) derivatives, but there are a number of publications that show this monomer to produce preferably polypyrrolidine (five-membered ring) structures:



These polymers were then interfacially reacted with di- and trifunctional aromatic acyl halides to give polyamides. Because the only reactive amine groups in these polymers were of the secondary amine type, such polymers should be chlorine-resistant. Dynamic chlorine tests (5 ppm, pH 6.0 to 6.5, 0.5% NaCl, 600 psi, 25°C) of 40 to 80 hours duration appeared to uphold this inference.

Interestingly, the best salt rejections were observed for the polyurea analogs, formed by crosslinking the polymers with isocyanates instead of acyl halides. For instance, poly(diallyl amine) reacted with 2,4-toluenediisocyanate gave membranes with 96.9 and 99.7% salt rejection (50 and 20 gfd flux respectively) under the above test conditions. Salt rejections for the polyamide examples rarely exceeded 95% in the patent examples. The polyurea analogs would not be resistant to chlorine.

Several other systems of polymeric amine-based interfacial polyamide membranes have appeared in patents by Kawaguchi and coworkers. One patent describes the use of amine-terminated oligomers prepared by reaction of polyepoxides with polyfunctional amines.[40] Another patent describes the attachment of polyfunctional amines as side groups onto linear soluble polymers via carboxamide or sulfonamide linkages.[41] A third patent covers the use of additives to the polymeric amine phase, these additives bringing about additional crosslinking of the residual amino groups through heat-curing after interfacial formation

of the barrier layer.[42] Examples of such additives include esters, chlorohydrins, imidazoamides and carbamates. Finally, one patent describes the preparation of amphoteric polyamide barrier layers containing both free carboxylate groups and ammonium groups.[43] Such membranes show high rejection levels towards sucrose (92 to 99%) while freely passing sodium chloride (15 to 25% rejection).

Yaginuma patented interfacial membranes made by condensation of polyalicyclic diisocyanates and diacyl halides with polyethylenimine or polyepiamine.[44] This approach was claimed to provide high organic rejections simultaneously with low salt rejections, whereas comparative data for typical aromatic diisocyanates or diacyl halides showed high rejections for both types of solutes. However, only a wastewater product, naphthalenesulfonic acid/formaldehyde condensate, was used in the testing of such membranes.

No commercially available membranes corresponding to any of the above series of patents have as yet been reported, with the possible exception of the Toray patent.

INTERFACIAL POLYMERIZATION WITH MONOMERIC AMINES: NS-300 MEMBRANE

The initial studies by Cadotte on interfacially formed composite polyamide membranes indicated that monomeric amines behaved poorly in this membrane fabrication approach. This is illustrated in the data listed in Table 5.2, taken from the first public report on the NS-100 membrane.[22] Only the polymeric amine polyethylenimine showed development of high rejection membranes at that time. For several years, it was thought that polymeric amine was required to achieve formation of a film that would span the pores in the surface of the microporous polysulfone sheet and resist blowout under pressure. However, in 1976, Cadotte and coworkers reported that a monomeric amine, piperazine, could be interfacially reacted with isophthaloyl chloride to give a polyamide barrier layer with salt rejections of 90 to 98% in simulated seawater tests at 1,500 psi.[45] This improved membrane formation was achieved through optimization of the interfacial reaction conditions (reactant concentrations, acid acceptors, surfactants). Improved technique after several years of experience in interfacial membrane formation was probably also a factor.

A typical formula for membrane fabrication consisted of an aqueous phase containing 1:1:0.5 weight percent piperazine:sodium hydroxide:dodecyl sodium sulfate, and a hexane phase containing 1.0 percent weight/volume of isophthaloyl chloride. This membrane exhibited up to 26 gfd and 98% seawater rejection (3.5% synthetic seawater, 1,500 psi, 25°C) and up to 4 gfd and 99.2% magnesium sulfate rejection (0.5% magnesium sulfate, 200 psi, 25°C). Unfortunately, seawater salt rejections in excess of 96% could not be produced routinely, and brackish water fluxes were too low to be attractive.

To increase the flux of this membrane, partial or complete substitution of isophthaloyl chloride with trimesoyl chloride was examined.[46,47] Dramatic changes in membrane flux and salt rejection were observed. Table 5.3 lists the results of this approach. As the trimesoyl chloride content of the acyl halide reactant was increased from 0 to 100%, seawater salt rejection dropped while

Table 5.2: Reverse Osmosis Performance of Membranes from Various Diamines or Polyamines Reacted with Terephthaloyl Chloride

Polyamine	Reverse Osmosis Performance* Water Flux (gfd)	Salt Rejection (percent)
hexanediamine	104	8.2
1,3-diaminopropane	233	30.6
ethylenediamine	Too brittle to test	
hydrazine	Too brittle to test	
p-phenylenediamine	53	38
m-phenylenediamine	26.9	12
piperazine	59.8	74
polyethylenimine	29.3	96.3

* Test Conditions: 3.5% synthetic seawater, 1500 psi, 25°C

Table 5.3: Seawater and Brackish Water Test Data on Membranes of Poly-(piperazineamides)

Acid Chloride IPC	Acid Chloride TMC	Acid Acceptor*	Seawater Test** Flux (gfd)	Seawater Test** Rejection (%)	Brackish Water Test*** Flux (gfd)	Brackish Water Test*** Rejection (%)
1.0	0.0	1.0% NaOH	26	98	4	99.2
0.9	0.1	0.9% Na_3PO_4	33	96	18	99.0
0.8	0.2	0.9% Na_3PO_4	73	78	58	99.9
0.67	0.33	0.9% Na_3PO_4	94	65	77	99.6
0.5	1.5	0.9% Na_3PO_4	96	64	31	99.9
0.0	1.0	1% DMP	80	68	26	99.3

* Key: NaOH=Sodium hydroxide, Na_3PO_4=trisodium phosphate, DMP= N,N'-dimethylpiperazine

** Test Conditions: 3.5% synthetic seawater, 1500 psi, 25°C

*** Test Conditions: 0.2% magnesium sulfate, 200 psi, 25°C

magnesium sulfate rejection remained constant. Furthermore, flux rose to a peak value at a 2:1 isophthaloyl:trimesoyl ratio of acyl halides, then dropped off. Note that the acid acceptor was changed in this series from sodium hydroxide to sodium phosphate to N,N'-dimethylpiperazine. These changes were made to achieve the highest combination of flux and magnesium sulfate rejection at each acyl chloride combination.

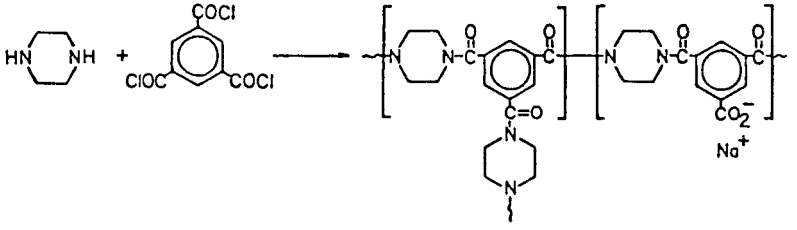
The combination of piperazine with trimesoyl chloride in composite membrane form was named NS-300. Trimesoyl chloride leads to a crosslinked polyamide structure. Apparently, however, considerable formation of hydrolyzed carboxylate groups also occurs. This is evidenced by the anion selectivity of the membrane, demonstrated by the sequential salt rejection data in Table 5.4 for a series of salts on test with a single set of membrane specimens.

Table 5.4: Effect of Cation and Anion Valence on Rejection of Various Salts by a Piperazine Trimesamide Interfacial Polyamide Membrane

Solute Used in Test Loop	Reverse Osmosis Test Data* Salt Rejection (%)	Flux (gfd)
0.1% $MgSO_4$	98.0	35
0.1% NaCl	70	31
0.5% NaCl	50	42
0.5% Na_2SO_4	97.8	41
0.5% $MgCl_2$	46	32
0.5% $MgSO_4$	97.9	32

* Test conditions: 200 psi, 25°C

The Donnan ion effect is also reflected in the lower rejection of sodium chloride at the higher salinity level (0.5% vs. 0.1%). The chemistry of this membrane is shown as follows:



Synthesis of piperazine-terminated oligomers as prepolymers for interfacial membrane formation was also examined.[46,48] Excess piperazine was reacted with di- and triacyl chlorides in an inert solvent such as 1,2-dichloroethane. The resulting amine-terminated polyamide oligomers had low solubility in the solvent system and precipitated. This served to limit the degree of polymerization of the oligomer. Even so, a portion of the product was insoluble in water and was filtered out during preparation of the aqueous oligomeric amine solution for the interfacial reaction step.

Table 5.5 lists the best performance data obtained for some piperazine oligomer membranes interfacially reacted with isophthaloyl chloride. The objective of these tests was to achieve single-pass seawater desalination membranes. As such, the presence of free carboxylate groups was avoided. Use was made of the trimesoyl chloride or alternate triacyl halides in the oligomer formation step, and diacyl chlorides in the interfacial reaction step. A few examples of seawater desalination membranes were obtained. Best results were seen for piperazine-cyanurate prepolymers interfacially crosslinked by isophthaloyl chloride, but fluxes were low in view of the operating test pressure of 1,500 psi.

Table 5.5: Reverse Osmosis Properties of Interfacial Membranes Formed of Piperazine Oligomers and Isophthaloyl Chloride

Reactant used to prepare Piperazine Oligomer	Acid Acceptor	Reverse Osmosis Test Data* Flux (gfd)	Rejection (%)
trimesoyl chloride	NaOH	13	99.0
trimesoyl chloride	triethylamine	58	93.8
cyanuric chloride	NaOH	14	99.2
cyanuric chloride	triethylamine	24	98.0
phosphorus oxychloride	N,N'-dimethyl-piperazine	45	93.9
1:1 trimesoyl chloride: isophthaloyl chloride	triethylamine	34	92.4

* Test conditions: 3.5% synthetic seawater, 1500 psi, 25°C

The use of piperazine-terminated oligomers in composite membrane formation has been explored by several working groups. Even high polymers containing piperazine pendant groups have been made. The interest in piperazine stems in part from the work by Credali and Parrini on asymmetric poly(piperazine-amide) membranes, wherein this type of polyamide membrane is reported to be resistant to chlorine in chlorinated feedwaters.[49,50] It is of some surprise to note that an interfacial polyamide membrane formed from piperazine and acyl halides is not fully chlorine resistant.[51] In a long term supervised test on brackish water at the Roswell Test Facility, some chlorine damage was beginning to appear within 2,000 hours continuous exposure to 0.75 ppm active chlorine at pH 5.5, as shown in Figure 5.7.

NF-40 COMPOSITE MEMBRANE

A reverse osmosis membrane is commercially available, named NF-40 (FilmTec Corporation), which is closely based on the NS-300 membrane technology. Typical solute rejection data for this membrane are as follows: sodium chloride, 45%; calcium chloride, 70%; magnesium sulfate, 93%; sucrose, 98%. Water flux of the membrane averages about 23 gfd at 225 psi and 25°C. As already noted for NS-300, the sulfate anion is associated with high rejection; the chloride anion, low rejection. Partial discrimination between monovalent and divalent cations (sodium versus calcium) has also been observed for NF-40. The membrane can be operated at temperatures to 45°C and in a pH range from 3 to 11. In this respect, it would find probable use in industrial separations where

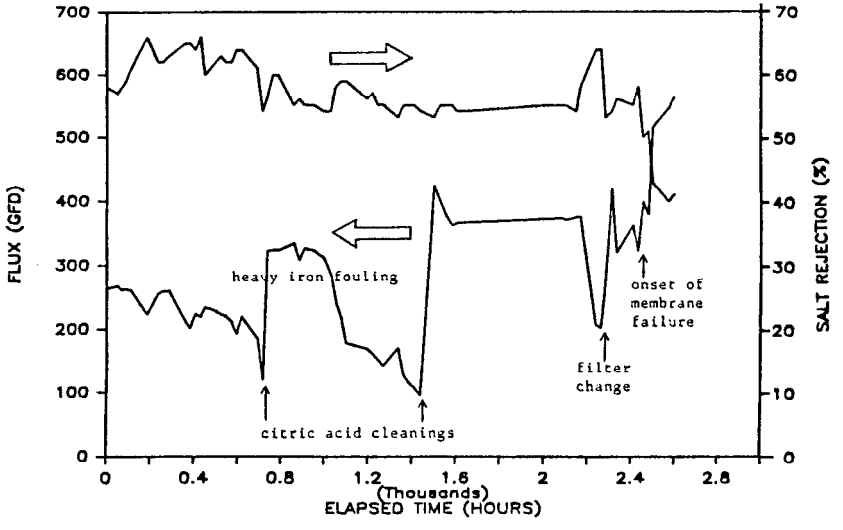


Figure 5.7: Long term test of NS-300 membrane on chlorinated brackish water showing onset of membrane failure at 2,500 hours due to chlorine attack.

the temperature and pH limitations of "loose" cellulose acetate asymmetric membranes are a problem.

An interesting behavior of this kind of membrane is its response to feedwater salinity and operating pressure. This type of membrane will show changes in flux and salt rejection as ionic strength of the feedwater is varied. This is illustrated in Figures 5.8 and 5.9 for two types of salts, sodium chloride and magnesium sulfate. The changes in membrane flux as a function of feedwater salinity are not explained by osmotic pressure differences across the membrane.

Among other applications, this membrane is being used in the treatment of salt whey, a waste stream product of cheese making in which the sodium chloride content is very high (up to 7%). The salt whey protein and lactose can be both concentrated and desalted in a single membrane operation (requires some diafiltration).

NTR-7250 COMPOSITE MEMBRANE

A similar type of membrane, named NTR-7250, is being marketed by Nitto Electric Industrial Company.[52] This membrane exhibits high rejection of sodium and magnesium sulfates (95 to 98%) and low rejection of sodium chloride. Compared to NF-40 membrane, its water flux and sulfate rejections are both higher, and long term chlorine resistance is claimed. It has been operated successfully for 4,500 hours on a chlorinated tapwater containing about one part per million average chlorine content, as shown in Figure 5.10.

Potential applications exist in industrial separations, water softening, and point-of-use filtration for high purity water in semiconductor chip manufactur-

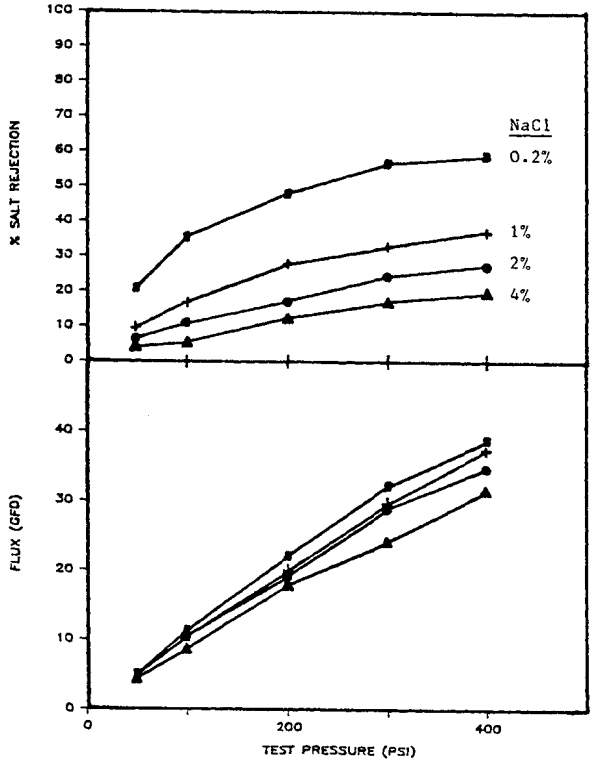


Figure 5.8: Salt rejection and flux of NF-40 membrane as a function of sodium chloride concentration and feedwater pressure.

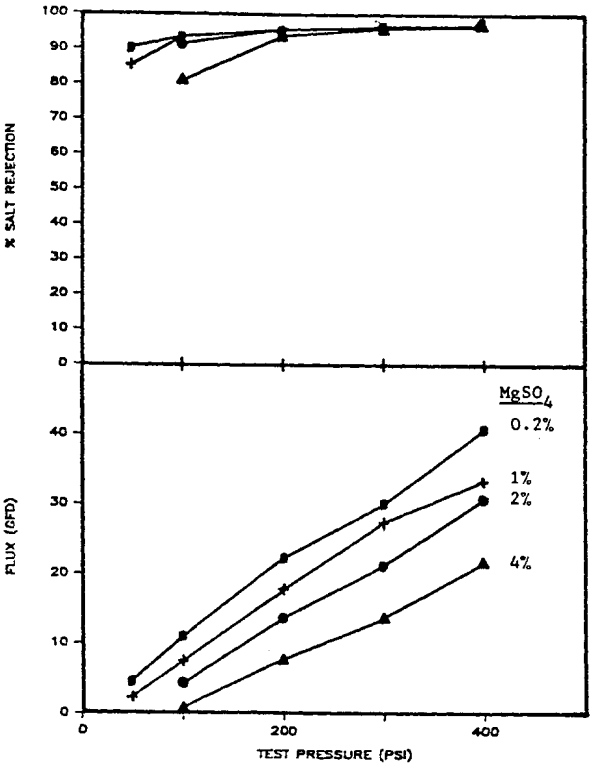


Figure 5.9: Salt rejection and flux of NF-40 membrane as a function of magnesium sulfate concentration and feedwater pressure.

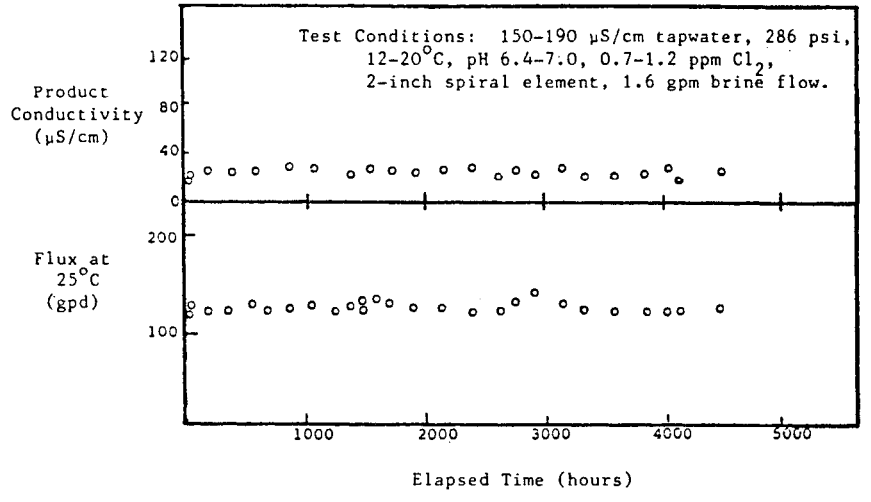
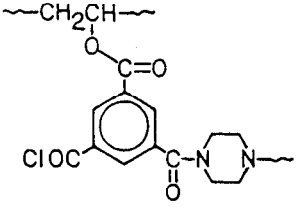


Figure 5.10: Long term performance of NTR-7250 during exposure to chlorinated tapwater.

ing. It has one potential drawback in that pH resistance is limited to pH 9 on the alkaline side. This limits its applications where alkaline feedwaters and alkaline cleaning are involved.

Although its composition has not been revealed, it may consist of, or be related to, the composition described in a German patent application by Kamiyama and coworkers.[53] This patent application describes a membrane made by interfacial reaction between a 1.0% hexane solution of trimesoyl chloride and an aqueous solution containing 0.25:0.25:0.5% by weight polyvinyl alcohol:piperazine:sodium hydroxide. This membrane, after curing at 110°C for 10 minutes, exhibited 30 gfd water flux and a magnesium sulfate rejection of 98.9% at 200 psi on a 500 ppm salt solution. In a recent review by Ohya on current progress in reverse osmosis membranes,[54] a (somewhat overly simplified) composition is given for the NTR-7250 membrane consisting of both ester and piperazineamide groups. This composition, shown below, is consistent with the patent application and with the pH 9 upper limit for alkaline stability:



FT-30 COMPOSITE MEMBRANE

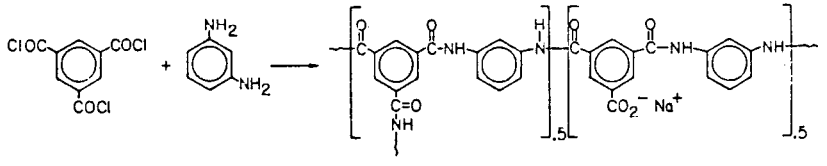
Cadotte discovered that aromatic diamines, interfacially reacted with triacyl halides, gave membranes with dramatically different reverse osmosis performance characteristics than membranes based on aliphatic diamines.[55,56] Before that time, the area of aromatic amines in interfacial membrane formation had been neglected because of two factors: (a) the emphasis on chlorine-resistant compositions, which favored use of secondary aliphatic amines such as piperazine, and (b) poor results that had been observed in early work on interfacial aromatic polyamides. The extensive patent network in aromatic polyamide (aramid) technology may also have been a limiting factor.

A typical recipe for an interfacially formed aromatic polyamide composite membrane comprised a 2.0% aqueous solution of the aromatic diamine and a 0.1% nonaqueous solution of trimesoyl chloride. This recipe was extraordinarily simple, and ran quite contrary to experience with piperazine-based membranes. For example, surfactants and acid acceptors in the aromatic diamine solution were generally not beneficial, and in many cases degraded membrane performance by lowering salt rejection. In contrast, surfactants and acid acceptors were almost always beneficial in the NS-300 membrane system. In the nonaqueous phase, use of isophthaloyl chloride as a partial replacement for trimesoyl chloride had relatively little effect on flux, but tended to decrease salt rejection and increase susceptibility to chlorine attack.

Another feature of this type of membrane was the rough surface of the membrane on a microscopic scale. As illustrated in Figure 5.11, interfacial aromatic polyamides from trimesoyl chloride and various aromatic diamines all showed a well developed "ridge and valley" structure. For aliphatic polyamines such as polyethylenimine, 1,6-hexanediamine, piperazine, and even α,α'-diaminoxylene, this ridge-and-valley structure was absent; instead, a flat surface–sometimes smooth, sometimes grainy–was observed. The thicker sections of this aromatic polyamide membrane are apparently about as active in water permeation as the thinner sections. The backside of the barrier layer, shown in Figure 5.12, contained numerous micropores or passageways for exit of permeate water from the depths of the interfacial membrane.

Average thickness of the polyamide barrier layer is about 2000 angstroms. Thus, this type of membrane has a barrier layer thickness approximately equivalent to the skin thickness in asymmetric reverse osmosis membranes. The ridge-and-valley structure does not appear to cause any increased susceptibility to membrane fouling. Deposition of foulants to the point restricting flux and increasing salt rejection has been found to be controlled by feedwater quality, element design, and hydrodynamic parameters rather than the surface topography of the membrane.[57]

FT-30 membrane is made from one of the simplest aromatic diamines: 1,3-benzenediamine. The final chemical structure of the membrane is believed to be as follows:



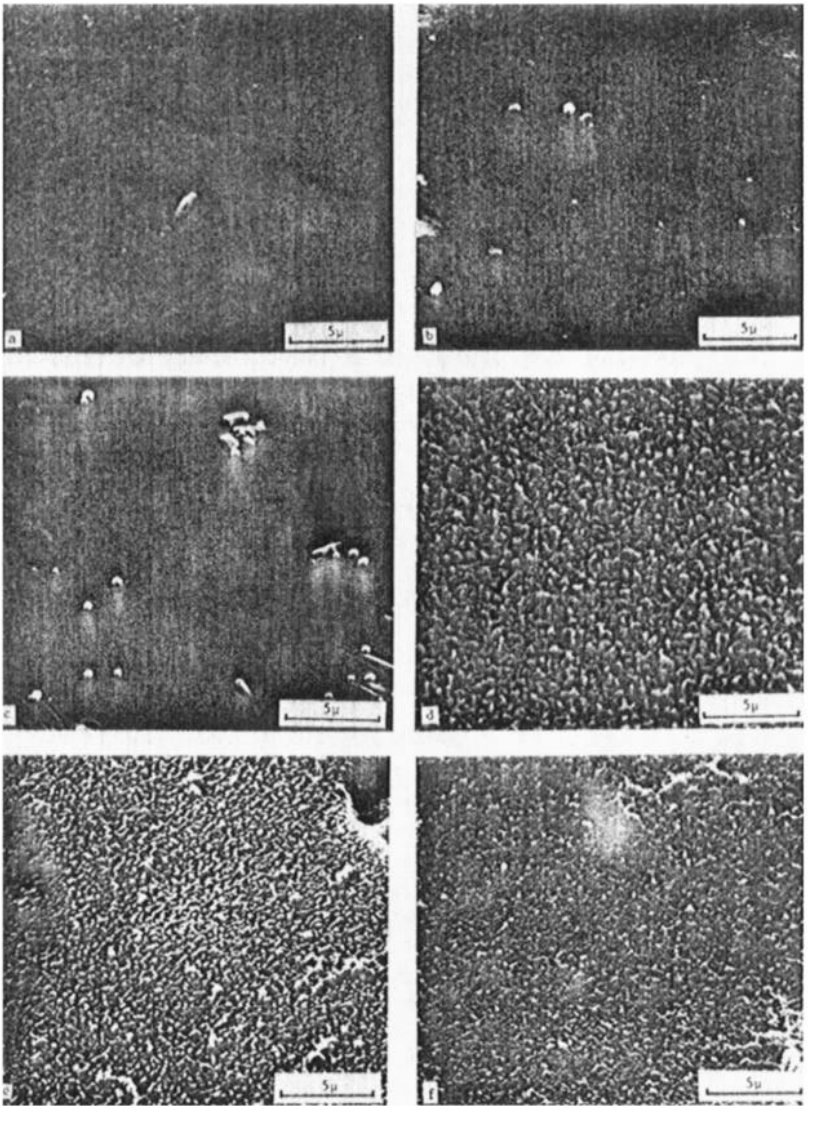


Figure 5.11: SEM photographs of the surface texture of composite polyamide membranes from aliphatic and aromatic amines: (a) uncoated microporous polysulfone; (b) polyamide from polyethylenimine and trimesoyl chloride; (c) triethylenetetramine and trimesoyl chloride; (d) 1,3-benzenediamine and trimesoyl chloride; (e) 2,4-toluenediamine and trimesoyl chloride; (f) 4-methoxy-1,3-benzenediamine and trimesoyl chloride. Note the smooth surface for aliphatic amine-based interfacial trimesamides and the coarse ridge-and-valley structure for aromatic amine-based interfacial trimesamides.

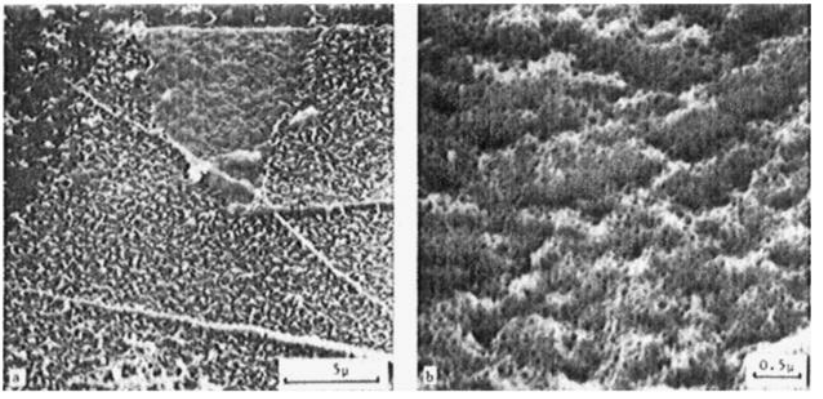
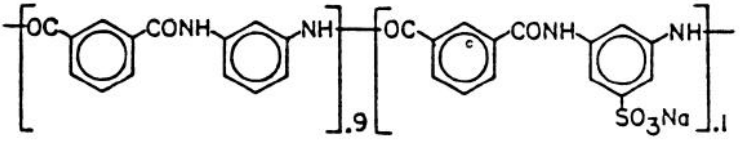


Figure 5.12: Topside and underside of the FT-30 composite reverse osmosis membrane: (a) topside showing well-developed ridge-and-valley structure, and also an area of membrane barrier layer folded over upon itself; (b) underside of the barrier layer (foldover zone) showing the network of micropores inside the ridge-and-valley structure.

Some hydrolysis of the trimesoyl chloride takes place during membrane fabrication. ESCA studies indicated that approximately one-sixth of the carboxyl groups are present as ionic carboxylate and five-sixths of the carboxyl groups are present as amides, leading to the above structure. The FT-30 barrier layer is insoluble in sulfuric acid and in all organic solvents, in agreement with the crosslinked nature indicated above. Its chemical structure is somewhat similar to the composition of the duPont Permasep B-9 hollow fiber polyamide, believed to be approximately as follows:



Both membranes show similar behavior toward oxidants such as chlorine and bromine,[58] and both membranes show approximately equivalent behavior in organic rejections.[59] The crosslinking inherent in the FT-30 membrane barrier layer appears to confer greater membrane stability towards compaction, halogen oxidation and pH extremes. The FT-30 membrane also appears to have a uniquely high rejection (95% or higher) of soluble reactive silica, which is advantageous in ultrapure semiconductor water preparation. The high silica rejection may be a function of the combination of the carboxylate ionic groups and the degree of polymer crosslinking.

The properties of FT-30 membranes have been reviewed in several publications, including reverse osmosis performance under seawater and brackish water test conditions.[60-62] In commercially produced spiral-wound elements , the FT-30 membrane typically gives 99.1 to 99.3% salt rejection at 24 gfd flux in seawater desalination at 800 psi and 25°C. In brackish water applications, FT-30 spiral elements can be operated at system pressures of as low as 225 psi while producing water at 22 to 24 gfd. Similar flux levels are possible with the TFC-202 and LP-300 membranes, as mentioned earlier. But it is notable that those membranes achieve such high fluxes through use of extremely thin surface barrier layers about only one-tenth the thickness of the FT-30 barrier layer.

Applications for FT-30 membrane have appeared in all reverse osmosis fields from seawater desalination to home tapwater systems operating on line pressure. At this date, it is the only commercial reverse osmosis membrane other than cellulose acetate that has specific FDA approval for food contact usage.[63] Versions of this membrane, manufactured under license to FilmTec, are available in tubular form (ZF-99, Patterson Candy International) and plate-and-frame design (HR-95, HR-98, De Danske Sukkerfabrikker).[64,65]

Chlorine resistance tests on FT-30 membranes, whether static jar storage tests or dynamic tests with chlorine added to the feedwater, showed a much lower rate of oxidation compared to other polyamide membranes such as the NS-100. A peculiar property of the FT-30 membrane in regard to chlorine attack was that the rate of oxidation was lowest in an acid pH range of 5 to 6 and higher in the alkaline pH range.[1] This is illustrated in Figure 5.13. This effect has also been observed by Glater and coworkers.[58] The pH effect on chlorine oxidation of FT-30 membrane was opposite of that normally observed with other membranes, because the hypochlorous acid at pH 5 to 6 would have a higher oxidation potential than sodium hypochlorite in the alkaline pH range. At pH 3, the effect of hypochlorous acid on FT-30 membrane lifetime could not be measured because the underlying polysulfone support layer was instead rapidly attacked and weakened.

Chlorine attack on reverse osmosis membranes is believed to be catalyzed by transition metal ions such as iron, manganese and cobalt. Figure 5.14 shows the effect of ferric ion in promoting chlorine attack, using in this case FT-30 membranes preimpregnated with ferric chloride. The presence or absence of these heavy metal ions may explain the discrepancies in chlorine resistance that have been reported for basically identical membranes such as NS-300 and NTR-7250.

The prepolymer approach which worked well for piperazineamide interfacial membranes was not useful in the case of FT-30 and its analogs. Poor solubility of aromatic amide precursors in aqueous media was the main obstacle. A patent application has appeared on the use of prepolymer formed from 1,3-benzenediamine and trimellitic anhydride acid chloride.[66] This prepolymer contains a free carboxylate group and is soluble in water as the sodium salt. A membrane is obtained by reaction of this intermediate with trimesoyl chloride, followed by a curing step at 110° to 130°C. Salt rejections of 98.5 to 99.1% on 2,000 ppm sodium chloride solution at 200 psi were obtained; fluxes were 4 to 11 gfd.

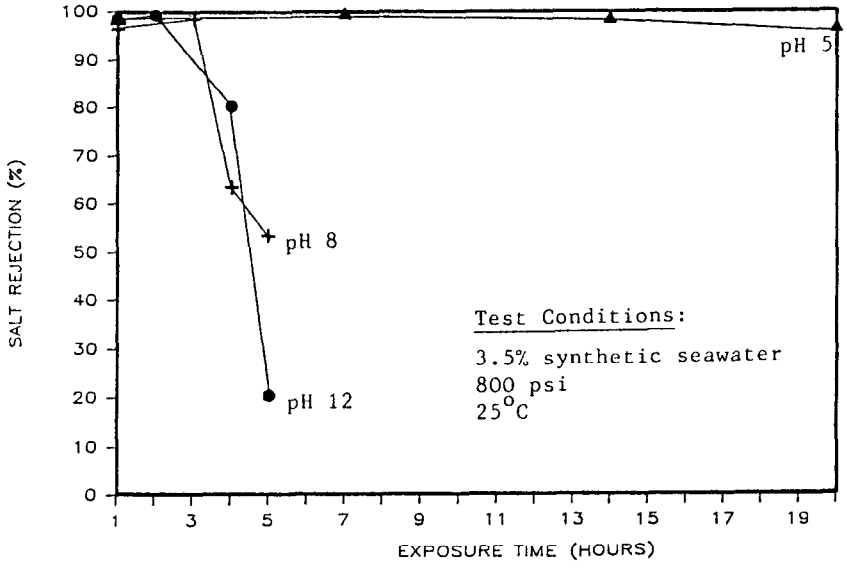


Figure 5.13: Effect of pH on the chlorine resistance of the FT-30 composite membrane.

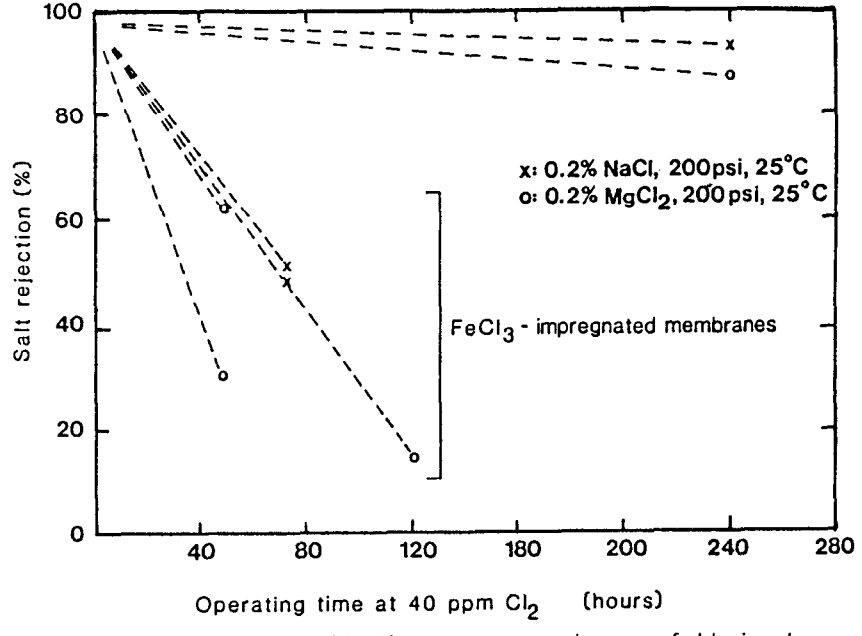


Figure 5.14: Effect of ferric chloride treatment on the rate of chlorine damage to FT-30 polyamide membrane.

NF-50 COMPOSITE MEMBRANE

A new variation related to the FT-30 membrane is being developed–the NF-50 composite membrane–which would appear to occupy a unique place in membrane technology. The NF-50 membrane has approximately the same characteristics as NTR-7250 and NF-40, but possesses an extremely high water flux. Reverse osmosis operation in large systems at a pressure of 35 to 50 psi is possible. The NF-50 membrane thus becomes the first example of a reverse osmosis membrane capable of operation at ultrafiltration membrane pressures.

Characteristics of this membrane include 30 to 40% sodium chloride rejection, 85 to 90% magnesium sulfate rejection, 98% sucrose rejection, and 99% raffinose rejection. Water flux is 15 to 25 gfd at 35 to 50 psi, depending on feedwater composition. The effect of increasing salinity on salt rejection and water flux is similar to the behavior observed for NF-40 membrane as was illustrated in Figures 5.8 and 5.9.

Applications for NF-50 membrane potentially include industrial separations, partial water softening, removal of trihalomethane precursors from groundwaters, and point-of-use filtration of high purity water for semiconductor chip manufacturing.

MECHANISM OF INTERFACIAL MEMBRANE FORMATION

In the book, *Condensation Polymers: By Interfacial and Solution Methods*, by P.W. Morgan,[67] interfacial polyamide formation is stated to occur in the organic phase, that is, on the organic solvent side of the interface. Several proofs are presented in support of this statement. For instance, monofunctional acyl halides added to the difunctional acyl halide in the organic phase always lowered polymer molecular weights. However, monofunctional amines added to the difunctional amines in the aqueous layer did not always show this effect. In this latter case, partition coefficients became a factor, particularly when relative reactivities of the amines were comparable. Mass transfer rate of diamine across the interface into the organic phase was noted to be the rate-controlling step at all concentrations of diamine.

A visually graphic display of this mechanism is illustrated in Figure 5.15. An insoluble colored powder, deposited on the face of an interfacial polyamide film, becomes incorporated into the polyamide film if the powder is introduced on the organic phase side. However, if the powder is deposited on the aqueous phase side of the growing interfacial film, it remains loose and unattached.

In the case of a polymeric amine such as polyethylenimine or polyepiamine, the solubility of the polymer in the organic phase would be very low. Reaction would take place at the interface to form an extremely thin, crosslinked network. This network would block the transport of further polymeric amine from the aqueous phase into the organic phase. Continued buildup of the membrane material on the organic side becomes impossible. Thereafter, the growth in thickness of the barrier layer is controlled by the much slower diffusion of acyl halide or isocyanate into the aqueous phase. As a result, composite membranes made by the NS-100/NS-101 type of approach will naturally tend to have very thin barrier layers–typically 200 to 250 angstroms thick.

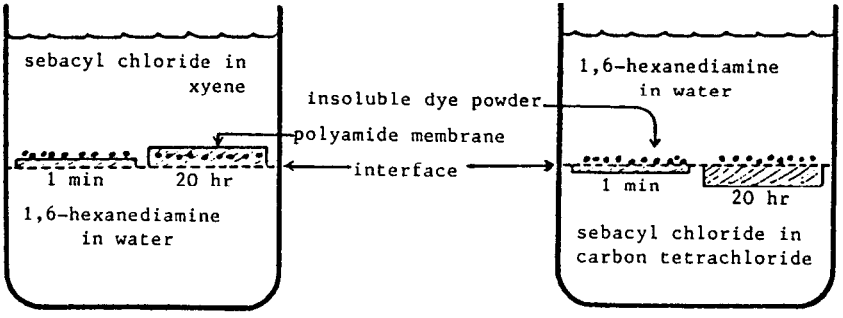


Figure 5.15: Visual demonstration of the direction of growth of a polyamide film at the solution interface.

In the case of monomeric amines such as piperazine or 1,3-benzenediamine, transport of the amine across the water-solvent interface takes place readily. Furthermore, the interfacially formed polymer film remains rather porous to salts and small molecules (until dried or heat-cured), so that membrane material continues to form on the organic side. Therefore, barrier layer thicknesses as high as 2500 angstroms are readily produced.

Monomeric amines have two advantages over polymeric amines in interfacial composite membrane fabrication. First, monomeric amines can be obtained in most cases as pure crystalline compounds, identical in lot after lot. Polymeric amines, on the other hand, will show variations in purity, molecular weight, chain branching and viscosity from lot to lot. This adds an element of variability to the membrane fabrication process. Second, monomeric amines lead to thicker barrier layers, which consequently tend to show better abrasion resistance and greater tolerance to chemical attack. By contrast, a membrane such as PA-300 is normally overcoated with a protective layer of water-soluble polyvinyl alcohol to minimize abrasion and salt rejection losses during spiral element assembly.

In the patent by Kurihara, Uemura and Okada,[38] combinations of a polymeric amine with a monomeric amine were used to produce composite polyamide membranes having high salt rejections. The membranes were described as having a bilayer polyamide barrier film: a surface polyamide zone rich in monomeric amine, and a subsurface polyamide zone incorporating both monomeric and polymeric amine. This patent disclosure demonstrated an understanding of the mechanism of interfacial polyamide barrier layer formation.

A patent has also appeared by Fukuchi and coworkers on the combination of polyethylenimine and several monomeric amines (including piperazine, 2,5-dimethylpiperazine, and 4-aminomethylpiperidine) in interfacial polyamide membranes. This patent also claimed very high salt rejections.

SULFONATED POLYMER COMPOSITES: NS-200 MEMBRANE

Several composite membranes have been prepared based on sulfonated polymers. These are typically formed on microporous polysulfone supports by solu-

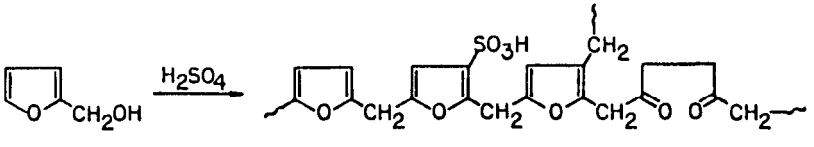
tion-coating techniques. One of the earliest and most unique examples of this type of membrane was the NS-200 membrane. This membrane was discovered by Cadotte,[69] and was characterized in government-sponsored research programs.[70,71,45] The NS-200 membrane in its optimized formulation[71] was prepared by dipping a microporous polysulfone sheet in a 2:2:1 solution of furfuryl alcohol:sulfuric acid:Carbowax 20M (Union Carbide) polyethylene oxide dissolved in 80:20 water:isopropanol. Excess coating solution was drained away, followed by an oven curing step at 125° to 140°C. The high oven temperature, in addition to drying the membrane, generated a black sulfonated polyfurane resin that was embedded in the surface of the polysulfone.

When the NS-200 membrane was initially discovered,[70] only furfuryl alcohol and sulfuric acid in water were used. The furfuryl alcohol was fairly rapidly converted to a resinous product in the aqueous solution; isopropanol was eventually added as a cosolvent to prolong the usable life of the dip-coating solution. Various water-soluble additives were also evaluated for their effects on formation of the sulfonated polyfurane resin and its subsequent reverse osmosis performance. Examples of additives included saccharides, polyalcohols, polycarboxylic acids and polyethylene glycols. Of these, the 20,000 molecular weight polyethylene oxide was singularly beneficial in increasing membrane flux quite significantly without disturbing salt rejection. It is probably severely degraded by sulfuric acid during the oven treatment step, and may be mostly absent in the final membrane after washout.

The most outstanding property of the NS-200 membrane was its extremely high salt rejection. In simulated seawater tests, salt rejection levels of 99.8 to 99.9% were rountinely observed. Typical performance in a 1,500 psi test on 3.5% synthetic seawater at 25°C was 20 gfd and 99.9% salt rejection. In a few instances, laboratory samples of NS-200 membranes with fluxes of 40 to 50 gfd under these same test conditions were obtained.

In subsequent efforts on the commercialization of this membrane, in flat sheet form, water fluxes of up to 23 gfd (99.6% salt rejection) at 800 psi on simulated seawater[72] and 50 gfd (98% salt rejection) on 0.5% sodium chloride at 250 psi[73] were achieved.

The freshly prepared membrane is glossy black in appearance, turning brown in the wet state, and partially decolorizing in exposure to the bleaching effects of sunlight. The chemistry of the NS-200 barrier layer in its early stages of formation is believed to be approximately as shown below. But the barrier layer composition is believed to be ultimately quite complex due to ring opening crosslinking and other side-reactions.



Membrane instability was believed to result from hydrolytic cleavage of sulfate and sulfonate esters in the sulfonated polyfurane resin. This hydrolysis would entail some depolymerization of the resin and concurrent formation of ionic sulfonate groups, causing the membrane to absorb water and swell in monovalent salt solutions. Oxidation by dissolved oxygen is another potential

mechanism that was not fully considered during attempted development of the NS-200 membrane, but which may have been an important factor (cf. PEC-1000 membrane). Further studies by other groups attempting to commercialize the membrane were unsuccessful in solving the NS-200 membrane instability problem.[72-74]

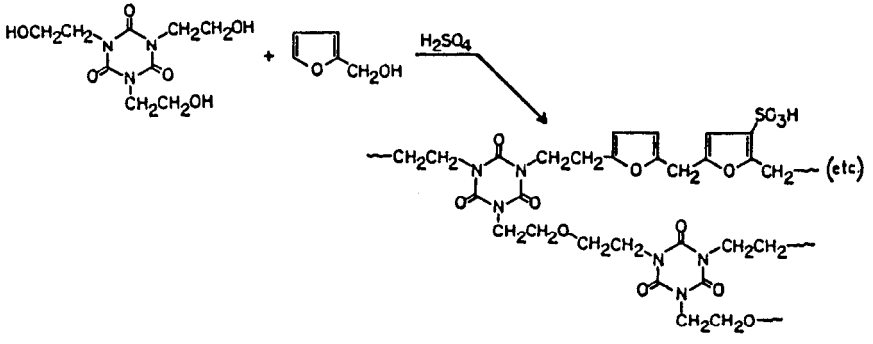
PEC-1000 MEMBRANE

The PEC-1000 membrane, developed by Toray Industries, has many similarities to the NS-200 membrane. This membrane has been described by Kurihara and coworkers as a thin film composite membrane in which the barrier layer was formed by an acid-catalyzed condensation reaction on the surface of microporous polysulfone.[75] The cross section of this membrane, under high magnification in a scanning electron microscope is quite similar in structure to the NS-200 membrane. The barrier layer is 300 angstroms thick.

The composition of the PEC-1000 membrane has not been specifically published. However, it is covered by U.S. Patent 4,366,062.[76] This patent describes membranes formed by acid-catalyzed condensation of the monomer 1,3,5-tris-(hydroxyethyl)isocyanuric acid (THEIC). By itself or in combination with additives such as sorbitol or polyethylene glycol, this monomer leads to membranes with 95 to 97% sodium chloride rejection (0.25% NaCl, 570 psi, 25°C), but at extremely low fluxes (0.5 to 1.0 gfd). Organic rejections were very good.

When furfuryl alcohol was added as a comonomer to the THEIC, water fluxes were increased tenfold. In addition, the extremely high salt rejections characteristic of NS-200 were obtained, while the high organic rejections characteristic of the isocyanurate moiety were retained. A typical patent example of membrane fabrication uses a water solution of 1:2:2:1 weight percent THEIC:furfuryl alcohol:sulfuric acid:dodecyl sodium sulfate, deposited on microporous polysulfone and cured at 150°C for 15 minutes. This membrane, possessing a thin active layer 100 to 300 angstroms thick, showed 99.9% rejection and 12 gfd flux under seawater test conditions at 1,000 psi.

The chemical structure of the PEC-1000 membrane is probably quite complex. This membrane, in its early stages of formation, may involve some of the following types of chemical structures, for example:



Basic characteristics of the PEC-1000 membrane include very high salt rejections, high organic rejections, and maintenance of high salt rejections over a pH range of 1 to 13 (in short term tests).[77] The membrane is not chlorine-resistant, and, indeed, has been found to suffer damage from dissolved oxygen in the feedwater. This has been alleviated by using sodium bisulfite as a feedwater additive, and by use of a vacuum deaerator as a pretreatment step in a large seawater plant design.[78] Flux of the PEC-1000 membrane is low relative to polyamide composite membranes; but for organic chemical concentration and seawater desalination applications, the high rejection characteristics offset this disadvantage.

Figure 5.16, adapted from Kurihara,[79,80] shows a comparison of several types of commercial reverse osmosis membranes in terms of salt rejection and permeate flow rate under seawater test conditions (35,000 ppm, 800 psi, 25°C). This chart emphasizes the capability of PEC-1000 to provide complete single-stage seawater desalting. In a test at Toray's Ehime desalination test facility on 42,000 ppm seawater (equivalent to Red Sea salinity), PEC-1000 spiral elements operated at 35% recovery produced a permeate having an average salinity of only 220 ppm, well below WHO standards. Average salt rejection was 99.5%.

The type of display in Figure 5.16 has been adapted and altered by others, such as Kamiyama and coworkers.[81] It should be noted that flux is shown on a logarithmic scale in Figure 5.16, and this presents a visual bias to the reader. If

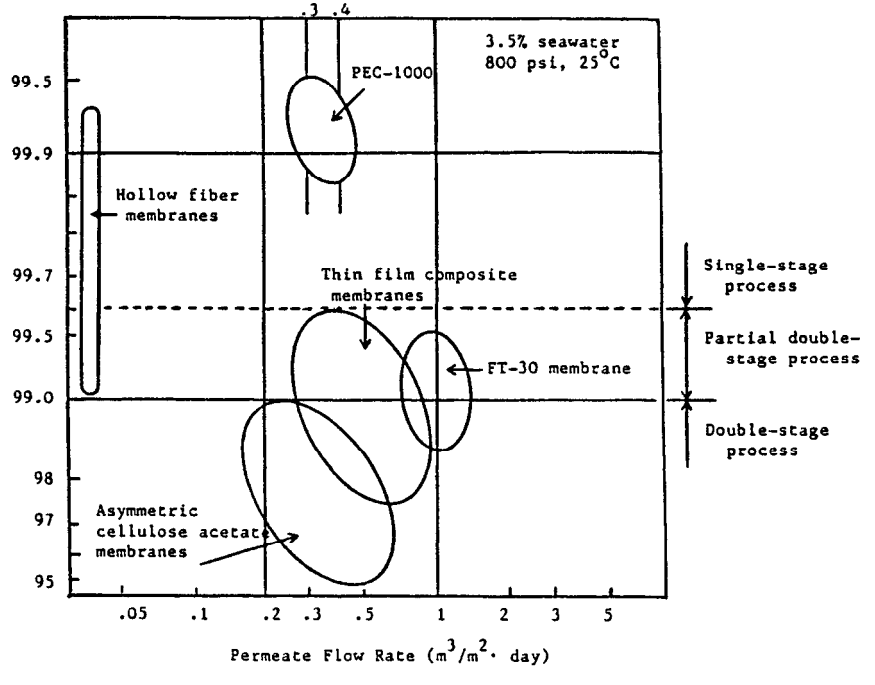


Figure 5.16: Comparison of desalination performance of different commercially available membranes for seawater.

the flux axis were changed to an arithmetic scale, the flux advantages of polyamide composite membranes would become visually more evident. In the case of seawater desalination plants, two stage systems become economically feasible at the higher fluxes. In tapwater and brackish water purification systems, absolute flux is normally more important than small differences in rejection.

In terms of organic rejections, PEC-1000 membrane shows the highest values among all commercial reverse osmosis membranes. Table 5.6 lists rejection data for a variety of organic compounds. In most cases, these were measured at solute concentrations of 4 to 5%, which represents a severe test protocol. Organic solute rejections determined for other commercial membranes were typi-

Table 5.6: Reverse Osmosis Performance of PEC-1000 Membrane for Various Organic Solutes in Aqueous Solutions

			Performance*		Operating Conditions	
Functional Group	Solute	Molecular Weight	Rejection (%)	Flux (gfd)	Concentration (%)	pH
Alcohol	Methanol	32	41	9.7	5	6.9
	Ethanol	46	97	5.9	6	6.9
	Isopropanol	60	99.5	8.1	5	6.5
	n-Butanol	74	99.4	6.6	4	7.0
	Benzylalcohol	108	82	2.5	4	7.0
	Ethylene glycol	62	94	9.2	5	6.8
	Propylene glycol	76	99.4	3.1	10	7.0
	Glycerine	92	99.8	9.7	5	7.0
	Phenol	94	99	6.1	1	5.2
Carboxylic acid	Acetic Acid	60	86	9.7	6	2.6
	Propionic acid	74	98	7.9	10	3.4
	Oxalic acid	90	99.1	18	0.5	1.8
Aldehyde	Formaldehyde	30	66	5.3	6	5.3
Ketone	Acetone	58	97	7.4	4	6.7
	2-Butanone (MEK)	72	98	5.3	4	6.6
Ester	Ethyl acetate	88	99.2	4.6	4	6.8
	n-Butyl acetate	116	99.6	9.7	1	6.9
Ether	Tetrahydrofuran	72	99.8	7.1	5	6.7
	1,4-Dioxane	88	99.9	10	5	6.6
Amine	Ethylenediamine	60	99.5	2	5	12.1
	Aniline	93	95	2.8	1	8.3
	n-Butylamine hydrochloride	109	99.9	3.3	1	7.0
Amide	Urea	60	85	14	1	6.9
	N,N-Dimethyl-formamide	73	98	8.1	5	6.5
	N,N-Dimethyl-acetamide	87	99.6	7.6	5	6.5
	ε-Caprolactam	113	99.9	9.7	5	6.5
Sulfoxide	Dimethylsulfoxide	78	99.6	8.6	5	6.4

* Test Conditions: 800 psi, 25°C, pH and concentrations as indicated.

cally at solute concentration levels of 0.1 to 1.0%. Figure 5.17 gives a capsule illustration of the differences in organic rejections for four commercial membranes: PEC-1000, FT-30, Permasep B-9 polyamide and asymmetric cellulose acetate. The superior organic rejection characteristics of PEC-1000 are quite evident in this graph.

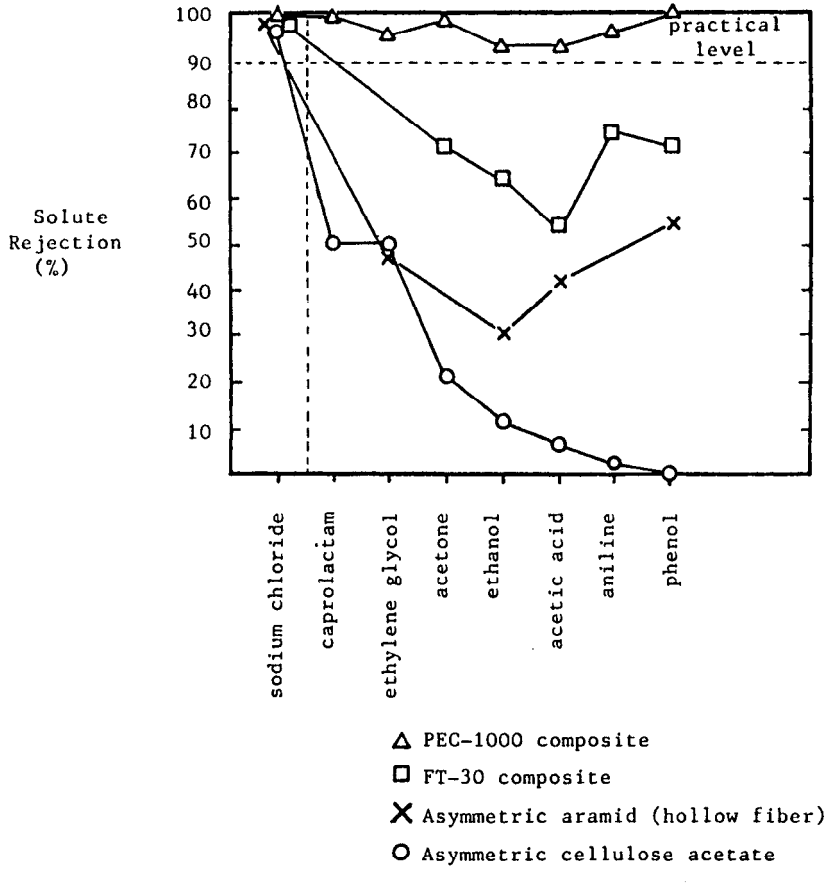


Figure 5.17: Comparison of organic solute rejections of various membranes.

SULFONATED POLYSULFONE MEMBRANES

Sulfonation of aromatic polymers has been explored as a method to produce hydrophilic polymers with water permeability and salt rejection characteristics. These have been of interest because of their potentially high degree of chlorine resistance. The use of sulfonated aromatic polymers for reverse osmosis membranes began in the late 1960's with the work of Plummer, Kimura and LaConti of General Electric Company.[82] Polyphenylene oxide [poly(2,6-di-

methylphenyleneoxy)] were cast from a chloroform/methanol solvent. The degree of sulfonation was limited so that the product would be water-insoluble. Later, composite membranes of this polymer were prepared by meniscus coating onto Celgard microporous polypropylene film and eventually onto microporous polysulfone sheeting.[83] In the latter case, a solvent blend was developed for the sulfonated polyphenylene oxide, consisting of nitromethane/methanol/butanol, which did not dissolve the polysulfone substrate. While this membrane appeared useful for several difficult applications involving highly acidic or high temperature feedwaters, its stability and performance characteristics were not sufficient to result in its commercialization.

After the initial work on asymmetric sulfonated polyphenylene oxide membranes, sulfonated polysulfone was subsequently examined by several research groups. However, the appearance of patents in 1973 and 1977 by Rhone-Poulenc[84,85] covering asymmetric membranes of sulfonated polysulfones appeared to dampen such research efforts. Also, a basic problem with sulfonated polysulfone was the fact that salt rejections fell rapidly when a critical level of sulfonation was exceeded, but water fluxes were too low until this sulfonation level was exceeded.

Beginning in late 1976, Cadotte and coworkers developed a composite sulfonated polysulfone membrane, using a slightly different approach.[46] Polysulfone was sulfonated to a degree sufficient to produce complete water solubility. Solutions of this polymer dissolved in aqueous or water-alcohol media were coated onto microporous polysulfone sheets, then oven-dried at 100 to 140°C. This temperature treatment served to insolubilize the sulfonated polymer. Intramolecular sulfone crosslinks were assumed to be formed, though this was never specifically proven. Additives such as polyols and polyphenols could be added for additional crosslinking. These and other sulfonated membranes often showed good rejection toward dilute salt solutions such as tapwater or 0.1% aqueous sodium chloride. At increasing salinities, however, salt rejection levels showed a rapid fall off. The composite sulfonated polysulfone membrane described by Cadotte, for instance, exhibited 80% or less salt rejection in seawater reverse osmosis tests.

In sulfonated aromatic polymer membranes, therefore, Donnan ion exclusion appears to be an important contributor to performance. In contact with dilute feedwaters, these strongly anionic membranes exclude feedwater anions from entering the membranes by charge repulsion effects, thus inhibiting salt passage. In more concentrated salt solutions, the charge repulsion effects are shielded by the high ionic activity of the feedwater.

A sulfonated polysulfone membrane with commercial potential has been developed in the form of a hollow fiber by workers at Albany International Corporation.[86,87] In a 5,000-hour test on 3,500 ppm brackish water at 400 psi, this membrane exhibited 98% salt rejection at 1 gfd. Flux and salt rejection remained constant even with addition of 100 ppm chlorine. In a 12,000-hour test on seawater at the Wrightsville Beach Test Facility, this membrane exhibited 98+% salt rejection and an average flux of 1.5 gfd at 1,000 psi operating pressure. Thus, it is possible to make a high rejection membrane from sulfonated polysulfone. Flux was rather low in this particular case, but suitable for hollow fiber membrane use.

PLASMA POLYMERIZATION IN COMPOSITE MEMBRANE FABRICATION

Plasma polymerization has been explored in considerable detail as a potential route to composite reverse osmosis membranes. Yasuda has written an excellent review covering the fundamentals and progress of plasma polymerization through 1974.[88] Advances since then have not been particularly promising from a commercial standpoint, with the exception of the Solrox membrane (see below).

Monomer polymerization by gas plasma techniques is quite complex, involving considerable fragmentation of vaporized monomers, and considerable crosslinking and grafting of deposited films. Vinyl unsaturation is not necessarily required for monomers to be polymerizable. Plasma polymers generally have short chain lengths, coupled with a high degree of branching and crosslinking, and containing a high concentration of residual free radicals. Monomers containing oxygen-based functional groups (such as carboxylic acids, ketones and esters) lose much of their oxygen content during polymer deposition. Nitrogen-containing monomers such as amines, on the other hand, show high levels of nitrogen incorporation into the deposited polymer films. Nitrogen gas and water vapor, added to the gas plasma of an organic monomer, tend to show finite rates of incorporation into the polymer deposits. To obtain good reverse osmosis characteristics, sufficient polymer must be deposited to "plug" the holes on the surface of a microporous substrate. Substrates having surface pore sizes of 200 to 300 angstroms appeared to be optimum in this regard.

Early work by Buck and Davar[89] examined the plasma polymerization of several monomer systems. Best results in terms of reverse osmosis performance were achieved with vinylene carbonate/acrylonitrile and vinyl acetate/acrylonitrile.

Wydeven and his coworkers examined the plasma polymerization of several amine monomers and obtained the best reverse osmosis membranes using allylamine.[90,91] Reverse osmosis performances of 98 to 99% salt rejection and 4 to 8 gfd flux were achieved at test conditions of 1.0% sodium chloride, 600 psi, 20°C. ESCA spectra showed the nitrogen groups in the plasma-formed polymer to be nitrile or imine groups, but not amine groups. Oxygen was also present in the ESCA analysis. Elemental analysis showed a membrane stoichiometry of $C_3H_{3.8}N_{0.9}O_{0.1}$.

Yasuda obtained membranes with good reverse osmosis properties by polymerizing gas plasma mixtures of acetylene/water/nitrogen and acetylene/water/carbon monoxide.[92,93] Elemental analysis of the acetylene/water/nitrogen membrane was not given, but it was likely approximately equivalent to the allylamine-derived composition. Yasuda has observed membrane performance levels as high as 99% salt rejection and 38 gfd, tested on 3.5% sodium chloride at 1,500 psi.

To date, no commercial examples of these membrane compositions have appeared in the marketplace.

SOLROX 0200 MEMBRANE

Sano and coworkers at Sumitomo Chemical Company developed the Solrox

membrane, which is technically a cross between asymmetric and composite membrane technologies.[94-96] An asymmetric polymer membrane is formed from a polyacrylonitrile copolymer. This membrane contains discrete micropores, being more like an ultrafiltration membrane rather than a reverse osmosis membrane. It is dried, then exposed to a helium or hydrogen gas plasma. The plasma treatment forms a tight, crosslinked surface skin on the asymmetric polyacrylonitrile support. Some vaporization and redeposition of the film components most likely occurs in this step. When placed on test, this plasma-modified membrane develops good salt rejection and flux in about 24 hours of continuous use. Analogs were also prepared using an organic monomer such as 4-vinylpyridine in the gas plasma. Data in a 1979 patent show a water flux of 87 gfd at 140 psi for the unmodified asymmetric film substrate.[95] After plasma treatment, this film exhibited 11 gfd and 98.3% salt rejection on a 0.55% sodium chloride feedwater at 700 psi.

Table 5.7, taken from a July 1982 technical bulletin by Sumitomo Chemical, lists performance data for a series of Solrox membrane grades that can be made by this process. Of these, the Solrox SC-0200 has been manufactured in tubular form on a semicommercial basis and used within the Sumitomo organization on organic chemical concentration applications. Table 5.8 lists organic rejections for the SC-0200 membrane.

These organic rejections, while greatly exceeding the capabilities of cellulose acetate membranes, are not appreciably different than rejection levels exhibited by aromatic polyamide membranes (FT-30, Permasep B-9). Nor do they match the organic rejection characteristics of the PEC-1000 membrane. The Solrox membrane is not resistant to chlorine, and its water flux is somewhat low (about 25 gfd at 650 psi net driving pressure). Consequently, it has not become a significant competitive membrane in the world marketplace.

Table 5.7: Available Types of Solrox Membranes

	Reverse Osmosis Performance*	
Membrane Type	Salt Rejection (%)	Flux (gfd)
SC-0100	99.0+	18
SC-0200	97.5-98.5	27-32
SC-0500	94-96	35-41
SC-1000	88-92	41-47
SC-2000	75-85	50-71

* Test conditions: 0.5% NaCl, 710 psi, 25°C

Table 5.8: Organic Solute Rejections of SOLROX SC-0200 Membrane in Comparison with Cellulose Acetate Membrane

Solute	M_w	Solrox SC-0200 (% rej.)*	Cellulose Acetate (% rej.)*
Sodium chloride	58	98	98
Methanol	32	15	5
Ethanol	46	61	10
n-Propanol	60	79	25
n-Butanol	74	90	15
sec-Butanol	74	97	35
Isobutanol	74	97	40
tert-Butanol	74	99	80
Ethylene glycol	62	78	--
Glycerol	92	98	--
Phenol	94	89	0
Ethyl cellosolve	90	96	--
Acetone	58	82	21
Urea	60	57	35
Acetic acid	60	51	25
Adipic acid	146	88	--
Aniline	93	94	8

*Test conditions: 1.0% aqueous solution, 710 psi, 25°C

MISCELLANEOUS COMPOSITE REVERSE OSMOSIS MEMBRANES

The emphasis in this chapter has been on commercially significant membranes. Historical technical events leading to the successful development of these membranes, and information on closely related membranes appearing in the technical literature have also been presented. Other composite membranes have appeared in the technical and patent literature, that have been omitted for lack of time and space. Perusal of the U.S. government-supported research project reports published by Cadotte, for instance, will reveal composite membranes based on polyacrolein, styrene-maleic anhydride condensates, metaphenylene-diamine-formaldehyde polymers, hydrophilic aromatic polyesters, sulfonated polymers, terephthaloyl oxalic-bis-amidrazone polymers, and crosslinked polyvinyl alcohol derivatives. A few other interesting examples are given below, illustrating the versatility of the composite membrane approach.

Strathmann prepared an all-polyimide composite membrane–both bottom and top layers.[97] A microporous asymmetric film of the polyamic acid intermediate was cast by quenching in acetone, then dried and thermally cyclized to the polyimide at 300°C. The microporous polyimide sheet was then overcoated with a dilute solution of the same polymer, which was allowed to evaporate to give a 300-angstrom-thick coating. This was also cyclized to the polyimide to generate a fully solvent resistant reverse osmosis membrane.

Taketani and coworkers at Teijin have sought to produce a stable flux polybenzimidazolone (PBIL) membrane by producing it as an ultrathin coating on

microporous polysulfone.[98] The key to this effort was the discovery that the PBIL polymer was soluble in water containing 5% or more of a water-miscible aliphatic amine. Thus, the solvent sensitivity of polysulfone could be sidestepped.

Koyama, Okada and Nishimura prepared composite reverse osmosis membranes containing an interpenetrating polymer network of polyvinyl alcohol with poly(styrenesulfonic acid).[99] The barrier layer was insolubilized by heating at 120°C for 2 hours. Salt rejections in the low 90's and rather low fluxes were observed. The long time length of heat-curing at 120°C was probably a factor in producing low fluxes. Kawahara and Yasuda obtained composite reverse osmosis membranes by acid-catalyzed crosslinking of methylolated poly(4-vinylphenol) coatings on polysulfone substrates.[100]

ADVANTAGES OF THE COMPOSITE MEMBRANE APPROACH

The numerous examples of composite membranes that have appeared in the technical literature exemplify the versatility of this approach. To the chemist attempting to develop new reverse osmosis membranes, the composite approach has three major advantages.

First, large quantities of monomers or polymers are not required to fabricate the barrier layer. At surface thicknesses of 200 to 2000 angstroms, roughly 0.02 to 0.2 grams of barrier layer polymer per square meter of membrane is required (excluding excess chemicals used in membrane fabrication). These are orders of magnitude smaller than required in asymmetric membrane manufacture. Thus, very expensive chemicals are not a deterrent to composite membrane fabrication. Furthermore, one avoids the need for expertise in producing large quantities of high polymers in a reproducible manner. Small companies that are not basic in plastics production can emerge and compete effectively in this membrane market.

In this context, only two polymers have ever been used on a large scale in asymmetric membranes: cellulose acetate and Permasep B-9/B-10 aramids. The former polymer predates the era of reverse osmosis membranes. The latter polymer has been used in hollow fiber membranes for 15 years. Attempts to bring other new polymers into *asymmetric* membrane production have been few (PBIL, PBI, polypiperazineamides), generally without particular success.

Second, insoluble crosslinked barrier layer compositions are possible, and, in fact, are almost universal in the composite membrane approach. Optimum reverse osmosis performance and chemical stability can be achieved, in part, due to preparation of crosslinked compositions. This is readily possible by the composite membrane approach, but not so simple by the asymmetric membrane approach. The PA-300, FT-30, and PEC-1000 barrier layer compositions, for example, are simply not feasible to prepare by asymmetric film casting techniques. The composite approach, therefore, is far more versatile.

Water flux through reverse osmosis membranes is considerably dependent on the hydrophilic character of the barrier layer. In the composite membrane approach, highly hydrophilic barrier layer compositions can be used, suitably insolubilized by crosslinking. To a large extent, water flux and salt rejection can be controlled by the type and extent of crosslinking.

Third, each layer of a composite membrane can be optimized. The barrier

layer can be developed to display single pass seawater desalination characteristics, on the one hand, or to selectively pass monovalent salts, on the other hand. The microporous substructure can be optimized for mechanical strength. The combination can be optimized for maximum water permeation rates.

These advantages are reflected in the intense activity in filing patents on composite reverse osmosis membranes, and in the growing selection of commercially available types. Because of these advantages, many new examples of such membranes are likely to reach commercial status in the future, whereas very few new asymmetric membranes can be anticipated.

REFERENCES

1. Cadotte, J.E. and Petersen, R.J., "Thin-Film-Composite Reverse Osmosis Membranes: Origin, Development, and Recent Advances", in *Synthetic Membranes: Vol I. Desalination*, A.F. Turbak, Ed., American Chemical Society, Washington, D.C., 1981, p. 305.
2. Cadotte, J.E., "Evolution of Composite Reverse Osmosis Membranes", in *Materials Science of Synthetic Membranes*, D.R. Lloyd, Ed., American Chemical Society, Washington, D.C., 1985, p. 273.
3. Francis, P.S., "Fabrication and Evaluation of New Ultrathin Reverse Osmosis Membranes", NTIS Report No. PB-177083, available from National Technical Information Service, U.S. Department of Commerce, Springfield, VA 22161 (Feb. 1966).
4. Rozelle, L.T., Cadotte, J.E. and McClure, D.J., "Ultrathin Cellulose Acetate Membranes for Water Desalination" in *Membranes from Cellulose and Cellulose Derivatives*, A.F. Turbak, Ed., Interscience Publishers, New York, 1970, p. 61.
5. Rozelle, L.T., Cadotte, J.E., Senechal, A.J., King, W.L. and Nelson, B.R., "Tubular Ultrathin Membranes for Water Desalination" in *Reverse Osmosis Membrane Research*, H.K. Lonsdale and H.E. Podall, Ed., Plenum Press, New York, 1972, p. 419.
6. Rozelle, L.T., Cadotte, J.E. and McClure, D.J., "Development of New Reverse Osmosis Membranes for Desalination", NTIS Report No. PB-201016, loc. cit. (June 1970).
7. Rozelle, L.T. and Petersen, R.J., "Development of a New Concept in Membrane Structure for Application in Hemodialysis", Sixth Ann. Prog. Report, NTIS Report No. PB-230997, loc. cit. (Jan. 1974).
8. Rozelle, L. T. and Petersen, R.J., "Ultrathin Membranes for Blood Oxygenators", Second Ann. Prog. Report, NTIS Report No. PB-231324, loc. cit. (Jan. 1974).
9. Forester, R.H. and Francis, P.S., U.S. Patent 3,551,244 (Dec. 29, 1970).
10. Ward, W.J. III, U.S. Patent 4,374,891 (Feb. 22, 1983).
11. Salemme, R.M. and Browall, W.R., U.S. Patent 4,155,793 (May 22, 1979).
12. Tolansky, S., *An Introduction to Interferometry*, Longmans Green, London, 1965.
13. Nomarski, M.G., *J. Phys. Rad.*, 16, 95 (1955).
14. Carnell, P.H. and Cassidy, H.G., *J. Appl. Polym. Sci.*, 9, 1863 (1965).

15. Riley, R.L., Lonsdale, H.K., Lyons, C.R. and Merten, U., *J. Appl. Polym. Sci.*, 11, 2143 (1967).
16. Petersen, R.J. and Johnston, P., "Evaluation of Nonthrombogenic Fluoropolymer Membranes in Blood Oxygenators", NTIS Report No. PB-251585, loc. cit. (Feb. 1976).
17. Riley, R.L., Lonsdale, H.K., La Grange, L.D. and Lyons, C.R., "Development of Ultrathin Membranes", NTIS Report No. PB-207036, loc. cit. (Jan. 1969).
18. Riley, R.L., Lonsdale, H.K. and Lyons, C.R., *J. Appl. Polym. Sci.*, 15, 1267 (1971).
19. Cadotte, J.E. and Francis, P.S., "Development of New Reverse Osmosis Membranes for Desalination", First Quarterly Report on Contract No. 14-01-0001-1143 to Office of Saline Water, U.S. Department of the Interior; *Desalination Abstracts,* Vol 1/2, Abstract No. C-395 (p. 133) 1966/1967.
20. Rozelle, L.T., Cadotte, J.E., Corneliussen, R.D. and Erickson, E.E., "Final Report on Development of New Reverse Osmosis Membranes", NTIS Report No. PB-206329 (June 1968).
21. Michaels, A.S., U.S. Patent 3,615,024 (Oct. 26, 1971).
22. Cadotte, J.E. and Rozelle, L.T., "In-Situ-Formed Condensation Polymers for Reverse Osmosis Membranes", NTIS Report No. PB-229337, loc. cit. (Nov. 1972).
23. Rozelle, L.T., Cadotte, J.E., Cobian, K.E. and Kopp, C.V., Jr., "Nonpolysaccharide Membranes for Reverse Osmosis: NS-100 Membranes", in *Reverse Osmosis and Synthetic Membranes*, S. Sourirajan, Ed., National Research Council of Canada, Ottawa, 1977, p. 249.
24. Cadotte, J.E., U.S. Patent 4,039,440 (Aug. 2, 1977).
25. Sudak, R.G., Bott, J.B., Fox, R.L., Gagner, S.J. and McKee, M.E., "Development of Reverse Osmosis Membrane for Seawater Desalination", NTIS Report No. PB80-182090, loc. cit. (Sept. 1979).
26. Milstead, C.E. and Riley, R.L., "Low Pressure Brackish Water Reverse Osmosis Membrane Development", NTIS Report No. PB80-153539, loc. cit., (Feb. 1980).
27. Wrasidlo, W.J., U.S. Patent 3,951,815 (April 10, 1976).
28. Fang, H.H.P. and Chian, E.S.K., *J. Appl. Polym. Sci.*, 20, 303 (1976).
29. Fang, H.H.P. and Chian, E.S.K., *Environ. Sci. Technol.*, 10, 364 (1976).
30. Chian, E.S.K., Bruce, W.N. and Fang, H.H.P., *Environ. Sci. Technol.*, 9, 52 (1975).
31. Wrasidlo, W.J., U.S. Patent 4,005,012 (Jan. 25, 1977).
32. Riley, R.L., Fox, R.L., Lyons, C.R., Milstead, C.E., Seroy, M.W. and Tagami, M., *Desalination*, 19, 113 (1976).
33. Riley, R.L., Milstead, C.E., Lloyd, A.L., Seroy, M.W. and Tagami, M., *Desalination*, 23, 331 (1977).
34. Leban, M.I. and Wydeven, T.J., *Environ. Sci. Technol.*, 18, 778 (1984).
35. Hickman, C.E., Jamjoom, I., Riedinger, A.B. and Seaton, R.E., *Desalination*, 30, 259 (1979).
36. Kutbi, I.I., Metwally, A.M., Zabri, Z.A. and Husseiny, A.A., *Desalination*, 39, 179 (1981).

37. Riley, R.L., Case, P.A., Lloyd, A.L., Milstead, C.E. and Tagami, M., *Desalination*, 36, 207 (1981).
38. Kurihara, M., Uemura, T. and Okada, K., U.S. Patent 4,387,024 (June 7, 1983).
39. Kawaguchi, T., Taketani, Y., Minematsu, H., Sasaki, N., Hayashi, Y. and Hara, S., U.S. Patent 4,242,208 (Dec. 30, 1980).
40. Kawaguchi, T., Taketani, Y., Hayashi, Y., Ono, T. and Mori, K., U.S. Patent 4,265,745 (May 5, 1981).
41. Kawaguchi, T., Taketani, Y., Sasaki, N., Minematsu, H., Hayashi, Y. and Hara, S., U.S. Patent 4,302,336 (Nov. 24, 1981).
42. Kawaguchi, T., Minematsu, H., Hayashi, Y. and Hara, S., U.S. Patent 4,388,189 (June 14, 1983).
43. Kawaguchi, T., Minematsu, H., Hayashi, Y., Hara, S. and Ueda, F., U.S. Patent 4,360,434 (Nov. 23, 1982).
44. Yaginuma, H., U.S. Patent 4,244,817 (Jan. 13, 1981).
45. Cadotte, J.E., Cobian, K.E., Forester, R.H. and Petersen, R.J., "Continued Evaluation of In Situ-Formed Condensation Polymers for Reverse Osmosis Membranes", NTIS Report No. PB-253193, loc. cit. (Apr. 1976).
46. Cadotte, J.E., Steuck, M.J. and Petersen, R.J., "Research on In Situ-Formed Condensation Polymers for Reverse Osmosis Membranes", NTIS Report No. PB-288387, loc. cit. (March 1978).
47. Cadotte, J.E., King, R.S., Majerle, R.J. and Petersen, R.J., *J. Macromol. Sci. Chem.*, A15, 727 (1981).
48. Cadotte, J.E., U.S. Patent 4,259,183 (March 31, 1981).
49. Credali, L., Chiolle, A. and Parini, P., *Desalination*, 14, 137 (1974).
50. Parrini, P., *Desalination*, 48, 67 (1983).
51. Petersen, R.J., Cadotte, J.E. and Buettner, J.M., "Development of FT-30 Membranes in Spiral Wound Modules", NTIS Report No. PB83-191775 loc. cit. (Oct. 1982).
52. Brady, M.F., Iwahori, H. and Murata, K., "New Thin-Film Composite Reverse Osmosis Membranes and Spiral Wound Modules", Technical Proceedings of the 12th Ann. Conf. of the Water Supply Improvement Assoc., Volume II: Capsule Presentations, Orlando, Florida, May 13-18, 1984, available from WSIA, P.O. 387, Topsfield, MA.
53. Kamiyama, Y., Yoshioko, N. and Nakagome, K., Ger. Offen. DE 3,129,702 (Feb. 11, 1982).
54. Ohya, H., *Maku (Membrane)*, 10, 101 (1985).
55. Cadotte, J.E., U.S. Patent 4,277,344 (July 7, 1981).
56. Cadotte, J.E., Petersen, R.J., Larson, R.E., and Erickson, E.E., *Desalination*, 32, 25 (1981).
57. Koo, J-y., Reitz, J.M., Cadotte, J.E. and Petersen, R.J., "Nonfouling Coatings for Thin Film Composite Membranes", final report on Contract No. 14-08-0001-2288 submitted to U.S. Department of the Interior, in press.
58. Glater, J., McCutchan, J.W., McCray, S.B. and Zachariah, M.R., "The Effect of Halogens on the Performance and Durability of Reverse-Osmosis Membranes", in *Synthetic Membranes: Vol I Desalination*, A.F. Turbak, Ed., American Chemical Society, Washington, D.C., 1981, p. 171.

59. Bhattacharyya, D., Jevtitch, M., Ghosal, J.K. and Kozminski, J., *Environ. Prog.*, 3(2), 95 (1984).
60. Larson, R.E., Cadotte, J.E. and Petersen, R.J., "Development of the FT-30 Thin Film Composite Membrane for Seawater Desalting Applications," *NWSIA Journal*, Vol. 8, No. 1, p. 15 (Jan. 1981).
61. Larson, R.E., Cadotte, J.E. and Petersen, R.J., *Desalination*, 38, 473 (1981).
62. Larson, R.E., Petersen, R.J. and Eriksson, P.K., *Desalination*, 46, 81 (1983).
63. Federal Register, Vol. 49, No. 246, p. 49448 (Dec. 20, 1984).
64. Hedges, R.M. and Pepper, D., *Filtration & Separation*, March/April 1984, p. 112.
65. Nielsen, W.K. and Kristensen, S., Proceedings–Int. Conf. on Desalination and Water Reuse, Vol. 1, p. 383 (1981); *Desalination*, 38 (1), 605 (1981).
66. Rak, S.F. and Ward, K., U.K. Patent Application 2,139,113A (Nov. 7, 1984).
67. Morgan, P.W., Condensation Polymers: By Interfacial and Solution Methods, Interscience Publishers, 1965, p. 22.
68. Fukuchi, S., Hayashi, T., Kobayashi, H. and Oshiumi, R., U.S. Patent 4,337,154 (June 29, 1982).
69. Cadotte, J.E., U.S. Patent 3,926,798 (Dec. 16, 1975).
70. Cadotte, J.E., Kopp, C.V., Jr., Cobian, K.E. and Rozelle, L.T., "In Situ-Formed Condensation Polymers for Reverse Osmosis: Second Phase", NTIS Report No. PB-234198, loc. cit. (June 1974).
71. Cadotte, J.E., Cobian, K.E., Forester, R.H. and Petersen, R.J., "In Situ-Formed Condensation Polymers for Reverse Osmosis Membranes", NTIS Report No. PB-248670, loc. cit. (Feb. 1975).
72. Graefe, A.F., "Development of a Composite Reverse Osmosis Membrane for Single Pass Seawater Desalination", NTIS Report No. PB80-124852, loc. cit. (Feb. 1979).
73. Graefe, A.F. and Schell, W.J., "Development of Low Pressure Brackish Water Reverse Osmosis Membranes", NTIS Report No. PB80-126204, loc. cit. (May 1979).
74. Schiffer, D.K., Davis, R.B. and Coplan, M.J., "Development of Composite Hollow Fiber Reverse Osmosis Systems", NTIS Report No. PB80-213044, loc. cit. (June 1979).
75. Kurihara, M., Kanamaru, N., Harumiya, N., Yoshimura, K. and Hagiwara, S., *Desalination*, 32, 13 (1980).
76. Kurihara, M., Watanabe, T. and Inoue, T., U.S. Patent 4,366,062 (Dec. 28, 1982).
77. Kurihara, M., Harumiya, N., Kanamaru, N., Tonomura, T. and Nakasatomi, M., *Desalination*, 38, 449 (1981).
78. Kurihara, M., Nakagawa, Y., Takeuchi, H., Kanamaru, N. and Tonomura, T., *Desalination*, 46, 101 (1983).
79. Kurihara, M., *Maku (Membrane)*, 8 (2), 97 (1983).
80. Chen, J-y., Kurihara, M. and Pusch, W., *Desalination*, 46, 379 (1983).
81. Kamiyama, Y., Yoshioka, N., Matsui, K. and Nakagome, K., *Desalination*, 51, 79 (1984).

82. Plummer, C.W., Kimura, G. and La Conti, A.B., "Development of Sulfonated Polyphenylene Oxide Membranes for Reverse Osmosis", NTIS Report No. PB-201034, loc. cit. (May 1970).
83. La Conti, A.B., "Advances in Development of Sulfonated PPO and Modified PPO Membrane Systems for Some Unique Reverse Osmosis Applications", in *Reverse Osmosis and Synthetic Membranes*, S. Sourirajan, Ed., loc. cit., p. 211.
84. Quentin, J-P., U.S. Patent 3,709,841 (Jan. 9, 1973).
85. Bourganel, J., U.S. Patent 4,026,977 (May 31, 1977).
86. Schiffer, D.K. and Coplan, M.J., "Development of Hollow Fiber Reverse Osmosis Membranes", NTIS Report No. PB81-167215, loc. cit. (Nov. 1980).
87. Davis, R.B., Schiffer, D.K. and Kramer, C.E., "Hollow Fiber Reverse Osmosis Composite Membranes: Process and Properties", in *Synthetic Membranes: Vol I. Desalination*, A.F. Turbak, Ed., American Chemical Society, Washington, D.C., 1981, p. 367.
88. Yasuda, H., "Composite Reverse Osmosis Membranes Prepared by Plasma Polymerization", in *Reverse Osmosis and Synthetic Membranes*, S. Sourirajan, Ed., loc. cit., p. 263.
89. Buck, K.R. and Davar, V.R., *Br. Polymer J.*, 2, 238 (1970).
90. Bell, A.T., Wydeven, T. and Johnson, C., *J. Appl. Polym. Sci.*, 19, 1911 (1975).
91. Hollahan, J.R. and Wydeven, T., *J. Appl. Polym. Sci.*, 21, 923 (1977).
92. Yasuda, H., Marsh, H.C. and Tsai, J., *J. Appl. Polym. Sci.*, 19, 2157 (1975).
93. Yasuda, H. and Marsh, H.C., *J. Appl. Polym. Sci.*, 19, 2981 (1975).
94. Sano, T., Shimomura, T., Sasaki, M. and Murase, I., U.S. Patent 4,107,049 (Aug. 15, 1978).
95. Sano, T., Shimomura, T., Sasaki, M. and Murase, I., U.S. Patent 4,147,745 (April 3, 1979).
96. Sano, T., Shimomura, T., Sasaki, M. and Murase, I., U.S. Patent 4,272,378 (June 9, 1981).
97. Strathmann, H., U.S. Patent 4,071,590 (Jan. 31, 1978).
98. Taketani, Y., Kawaguchi, T., Ono, T. and Mori, K., U.S. Patent 4,260,652 (April 7, 1981).
99. Koyama, K., Okada, M. and Nishimura, M., *J. Appl. Polym. Sci.*, 27, 2783 (1982).
100. Kawahara, H. and Yasuda, T., U.S. Patent 4,326,958 (April 27, 1982).

6

Process Design and Optimization

Robert Rautenbach

INTRODUCTION-MASS TRANSPORT AT THE MEMBRANE SURFACE

The Local Mass Transport

It is understood that the economical success of any membrane process depends primarily on the quality of the membrane, specifically on flux, selectivity and service lifetime. Consideration of only the transport mechanisms in membranes, however, will in general, lead to an overestimation of the specific permeation rates in membrane processes. Formation of a concentration boundary layer in front of the membrane surface or within the porous support structure reduces the permeation rate and, in most cases, the product quality as well. For reverse osmosis, Figure 6.1 shows how a concentration boundary layer (concentration polarization) forms as a result of membrane selectivity. At steady state conditions, the retained components must be transported back into the bulk of the liquid. As laminar flow is present near the membrane surface, this backflow is of diffusive nature, i.e., is based on a concentration gradient. At steady state conditions, the concentration profile is calculated from a mass balance as

$$\frac{c_2 - c_3}{c_1 - c_3} = e^{V_w / k} \quad (1)$$

where k is the mass transfer coefficient which can be assumed, at least with a good approximation, to be independent of the permeate flux V_w. For this reason, the analogy between heat and mass transfer is valid and k can be calculated using the well-known heat transfer equations. This has been tested experimentally for a number of cases.[1]

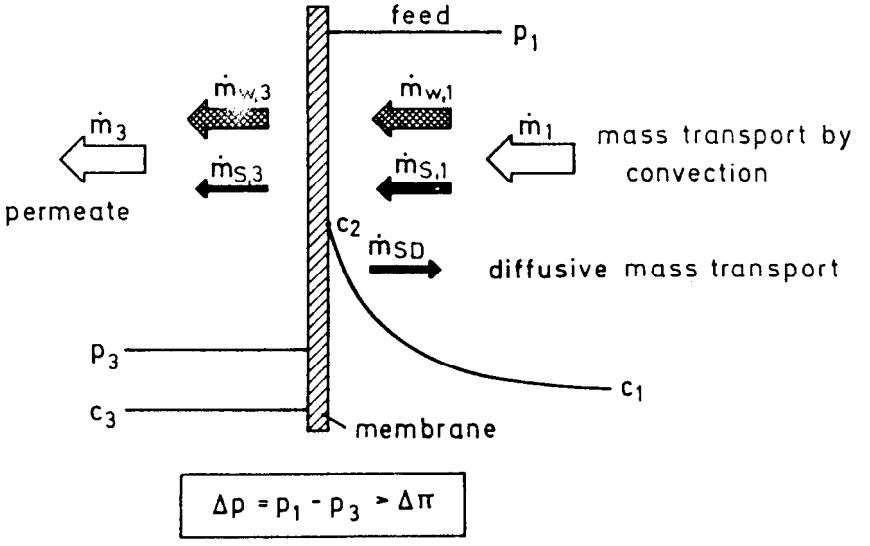


Figure 6.1: Concentration polarization.

Figures 6.2 and 6.3 indicate the order of magnitude of concentration polarization for laminar and turbulent flows through tubular membranes. The diagrams illustrate the dependence of the concentration boundary layer on flow conditions along the membrane (Re) and on the permeation flux (Pe_w).

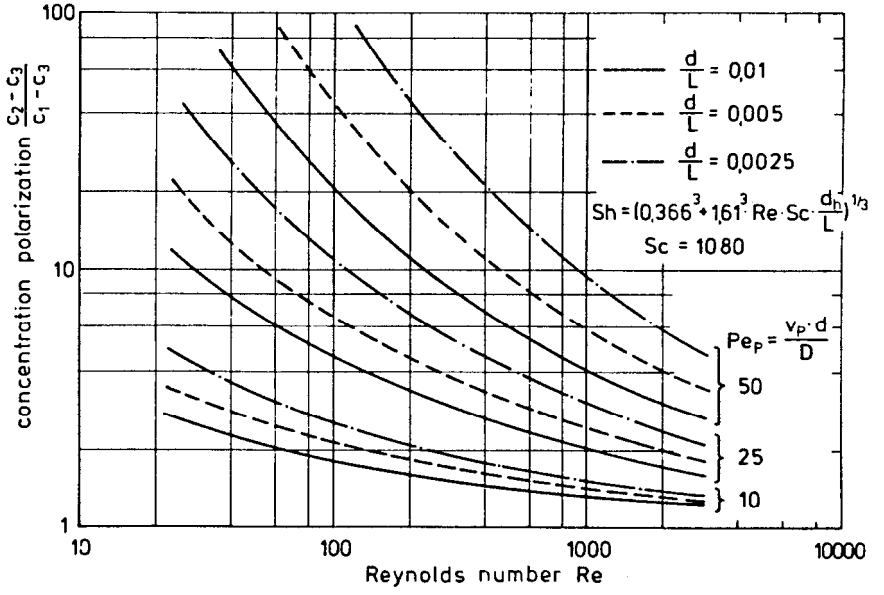


Figure 6.2: Concentration polarization in laminar flow.

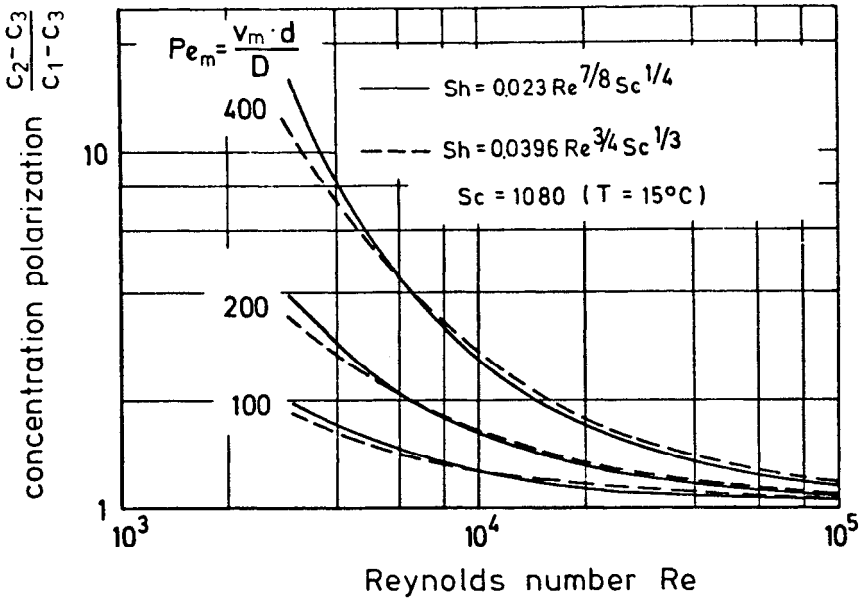


Figure 6.3: Concentration polarization in turbulent flow.

According to Figures 6.2 and 6.3, turbulent flow is more advantageous. Furthermore, these diagrams explain why, in the case of gas permeation, in contrast to separation processes in the liquid state, the resistance due to a boundary layer can be neglected: the diffusion coefficients of gases, for example O_2/N_2 are 10^4 times larger than those of dissolved components in liquids such as $NaCl/H_2O$ which, in combination with the permeation rates reported in literature, leads to Pe numbers of less than unity.

Influence of the Asymmetric Structure of Membranes

While it is possible to enhance mass transfer in the boundary layer by improving the flow conditions, this is impossible if a concentration profile exists within the porous support structure.

For reverse osmosis, Figure 6.4 shows the predicted concentration profile in the porous structure of an asymmetric membrane. According to Figure 6.4, in liquid systems, the concentration c_3, which affects permeate flux and product quality, cannot be influenced significantly by the concentration of the liquid on the product side. Conditions are nearly always favorable for the permeate to flow unhindered. Even in the extreme case of local concentration on the permeate side being equal to that of the liquid on the high pressure side of the membrane ($c_1 = c_5$), the error made in calculating the solvent flux V_W and the salt flux J_s is only 2% or 5% respectively, if the effect of c_5 is neglected.

Again, the situation is different in the case of gas permeation. Here, the local concentration affects the (local) permeate fluxes of the mixture components and, for this reason, the type of flow for gas permeation on the permeate side is

much more important than for liquid separation processes such as reverse osmosis. Figure 6.5 shows theoretical results of Blaisdell and Kammermeyer.[2] Mol fraction of oxygen is plotted against the yield during fractionation of air for different flow configurations and cases of mixing. The diagram demonstrates that (1) countercurrent flow provides the best results and (2) marked differences exist between the perfect mixing and plug flow.

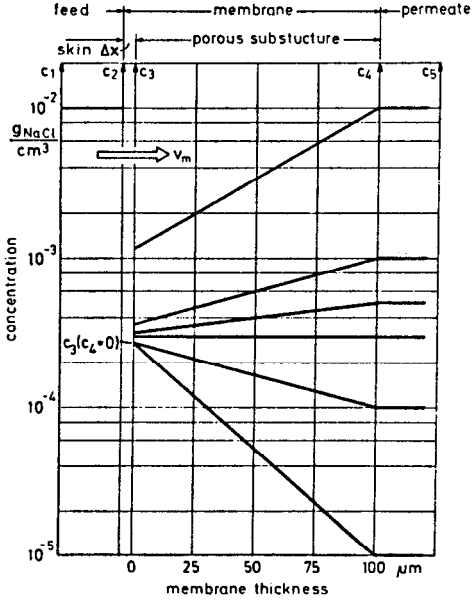


Figure 6.4: Concentration profile in porous substructure of asymmetric membranes.

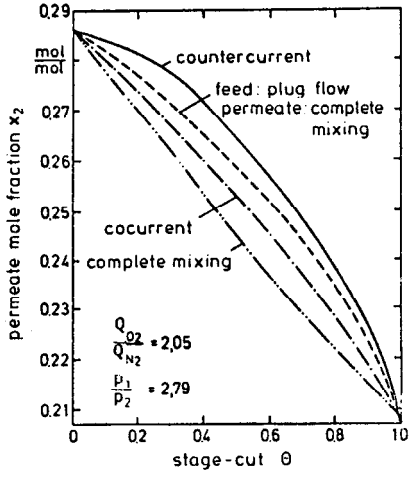


Figure 6.5: Effect of flow configuration in gas permeation.

Change of Conditions Along the Membrane

As a consequence of the permeate flux, the pressure gradient as well as the mean velocity and concentration will vary along the membrane surface–in principle at the feed side as well as at the product side. Depending on module design, this has to be taken into account for one or both sides. If, for example, the membrane is of tubular design with feed-flow inside, the following has to be expected along the tube-axis:

(1) Decrease of the transmembrane pressure-difference as a consequence of the drop in pressure due to friction (→ decrease of permeate flux).

(2) Increase of the mean concentration of the feed solution (→ increase of osmotic pressure → decrease of permeate flux and increase of salt flux).

(3) Decrease of the mean velocity (→ increase of concentration polarization → decrease of permeate flux and increase of salt flux).

For these reasons, the overall permeation rate and the product quality of a membrane channel have to be calculated by integrating over the length elements employing, in addition to the equations discussed above,

(1) the mass balance

(2) the material balance

(3) the energy balance.

The equations necessary for the calculation of tubular RO-membrane channels (flow of permeate unhindered, no influence of the porous support-layer) are:

mass transfer at the membrane surface

concentration polarisation $\frac{c_2 - c_3}{c_1 - c_3} = e^{V_w/k}$

equation for mass transfer $Sh = \frac{k\,d}{D} = Sh(Re, Sc)$

mass transfer in the membrane

permeate flux $V_w = A \cdot [\Delta p - b(c_2 - c_3)]$; $\Delta p = p_n - p_{3,n}$

salt flux $J_S = B \cdot (c_2 - c_3)$

salt concentration $c_3 = \frac{J_S}{V_W}$

balance for a length element

mass balance $\bar{v}_{x,n+1} = \bar{v}_{x,n} - \frac{4\Delta x}{d} V_{w,n}$

material balance (salt) $\bar{v}_{x,n+1} \cdot c_{1,n+1} = \bar{v}_{x,n} \cdot c_{1,n} - \frac{4\Delta x}{d} \cdot V_{w,n} \cdot c_{3,n}$

energy balance (ρ = const) $p_{n+1} = \frac{\bar{v}_{x,n}}{\bar{v}_{x,n+1}} \left[p_n + \frac{1}{2}\rho \bar{v}_{x,n}^2 \left(1 - \xi \frac{\Delta x}{d}\right)\right] - \frac{4\Delta x \cdot V_W}{d\,\bar{v}_{x,n+1}} \cdot p_n - \frac{1}{2}\rho \bar{v}_{x,n+1}^2 - \Delta p_V$

This set of equations has to be solved numerically.

Figure 6.6 discusses the results of such a numerical calculation of a long tubular RO-membrane channel for seawater desalination. It clearly demonstrates the decrease of permeate (mass) flux J_W and, at the same time, the increase of local and mean product concentration c_3 and $\bar{c}_3$.

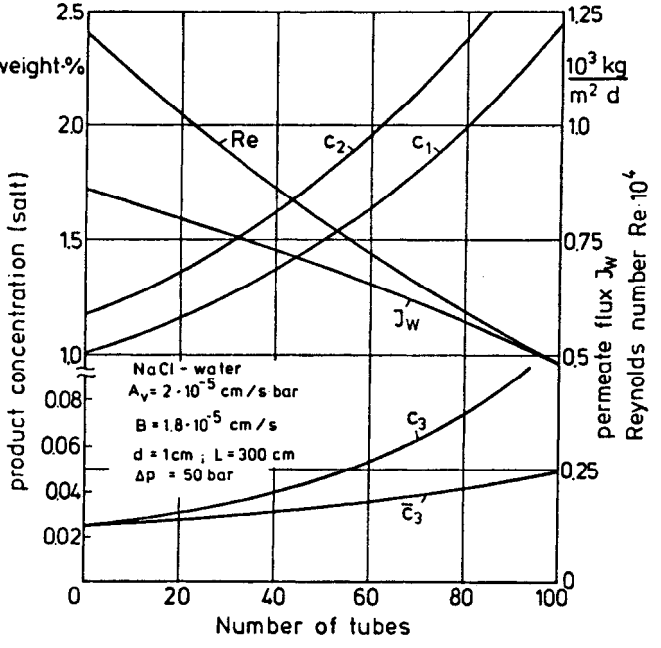


Figure 6.6: Calculation of a tubular module.

MODULE CONCEPTS AND DESIGN

The module, i.e., the industrial configuration of membranes, has to meet a variety of requirements which are sometimes even contradictory. Points of major importance are: (1) flow conditions along the membranes, (2) ratio of membrane area to pressurized vessel volume, (3) price of module and (4) the possibility of cleaning the membrane.

Depending on the process application, one or the other of these requirements is of primary importance and, for this reason, a number of different modules have been designed. The most important designs are the plate and frame, the spiral wound and the hollow fiber module. Optimization procedure and some of its results will be discussed for only one module configuration, the hollow fiber module-and for only one application-RO.

The Hollow Fiber Module

Hollow fiber modules contain very fine fibers forming asymmetric or symmetric membranes and capable of withstanding pressure differences (high-pres-

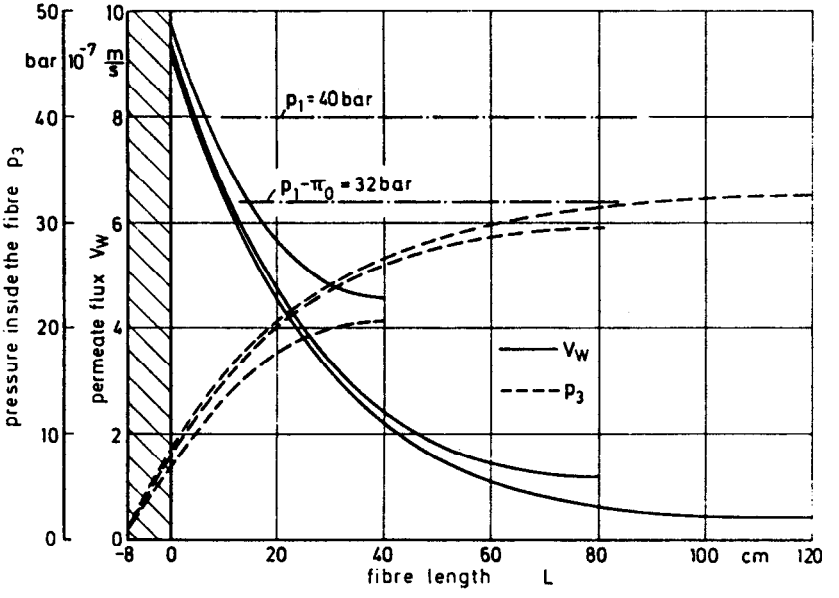


Figure 6.8: Permeation behaviour of hollow fibers.

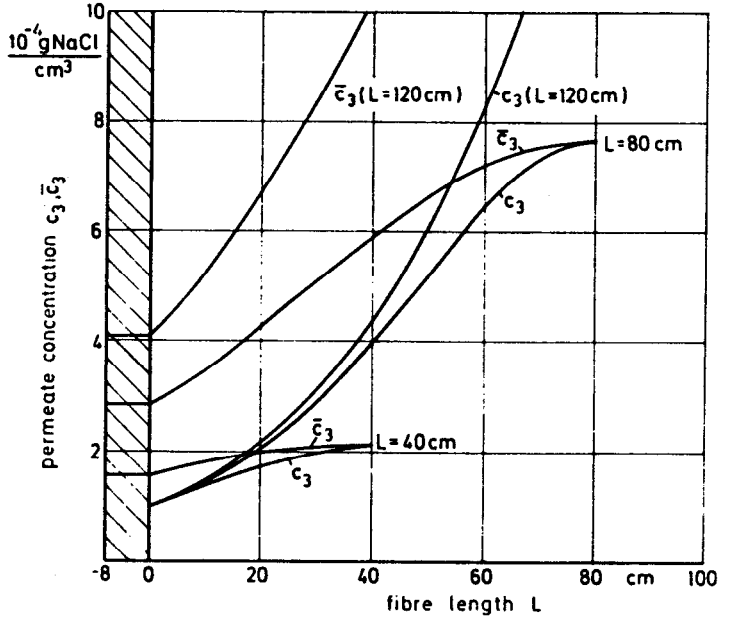


Figure 6.9: Concentration profiles in hollow fibers.

In theory, larger fiber diameters should increase the flux, i.e., the performance of a single fiber. However, at the same time, the membrane area per unit volume decreases. For some simplifying assumptions, it can be easily discussed how fiber diameter and fiber length have to be chosen in order to maximize the "yield" per unit volume of the bundle.

Neglecting (1) the radial pressure losses in the feed and (2) the influence of osmotic pressure on flux, the specific yield of the fiber bundle is given by:

$$\frac{\dot{Q}}{V} = \frac{\dot{Q}_{FA}}{F_A} \cdot \frac{F}{V} = \frac{\dot{Q}_{FA}}{\pi d_a L} \cdot \frac{4(1-\varepsilon)}{d_a}$$

$$\frac{\dot{Q}}{V} = \frac{4(1-\varepsilon)}{d_a} \cdot \frac{A \cdot \Delta p}{H \cdot L} \cdot \frac{\tanh\ (HL)}{1+H \cdot l_s \cdot \tanh\ (HL)} \tag{8}$$

For a fixed ratio of $\frac{d_a}{d_i} = 2$, Equation 8 is discussed in Figure 6.10.

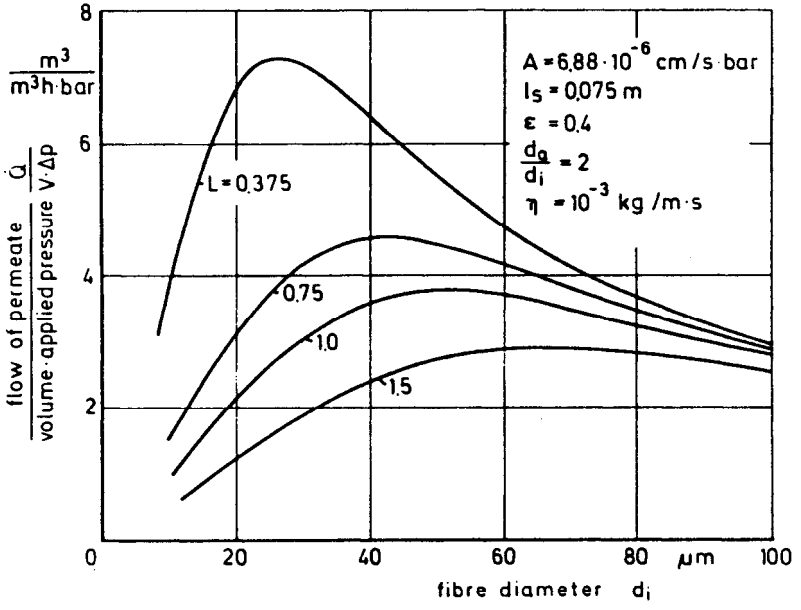


Figure 6.10: Optimum design of hollow fibers.

According to Figure 6.10, an optimal fiber length exists for a given fiber diameter. Figure 6.8 clearly indicates that hollow fiber modules for reverse osmosis should be made as short as possible. It should be noticed that a simple correlation between yield of the single fiber and yield of the bundle can be derived in any case only if the concentration and the pressure in the shell (outside of the bundle) are considered to be constant! In principle, the concentration of the feed increases between entrance and outlet while the pressure of the feed

decreases. A numerical solution taking this into account can be achieved if the bundle is considered as a continuum containing sinks (Figure 6.11). In this case, the following equations have to be solved:

mass balance (ρ_L = const):

$$\frac{d}{dr}\left(\frac{\dot{Q}}{2\pi}\right) = \frac{d}{dr}\left(r\,\bar{v}_1(r)\right) = \sqrt{\frac{r\,n_{(F)}\dot{Q}_{FR}}{L}} \tag{9}$$

material balance:

$$\frac{d}{dr}\left(\frac{\dot{Q}c_1}{2\pi}\right) = \frac{d}{dr}\left(r\,\bar{v}_1(r)c_1(r)\right) = \sqrt{\frac{n_{(F)}\dot{Q}_{FR}c_{30}r}{L}} \tag{10}$$

energy balance:

$$\frac{dp_1(r)}{dr} = -K_o\,\eta F^2_{(v)}\,\frac{(1-\varepsilon)^2}{\varepsilon^3}\,\bar{v}_1(r) \tag{11}$$

K_o has to be varied according to the fiber arrangement. $K_o = 30$ is valid for fibers in parallel.

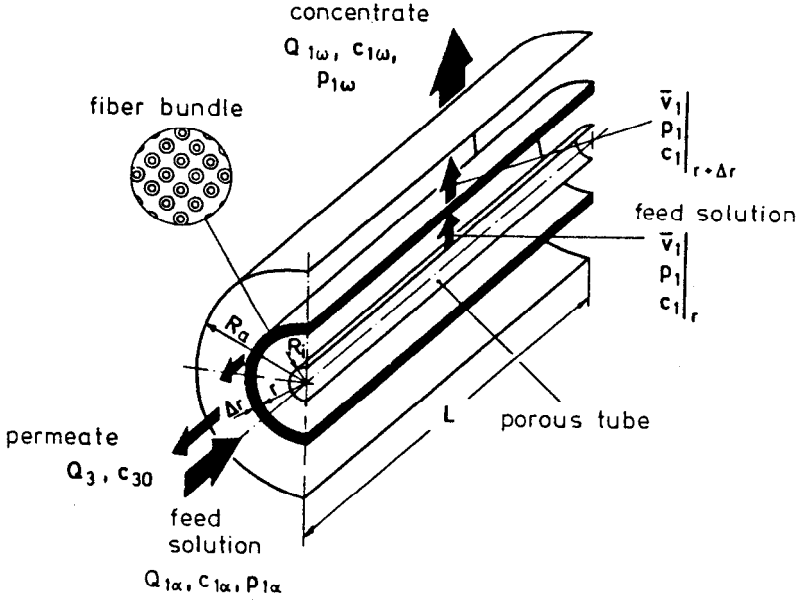


Figure 6.11: Balance element in the fiber bundle.

In the case of reverse osmosis, the relative flow configuration does not affect the performance to any large extent. As already indicated, the situation is quite different for gas permeation. While countercurrent flow improves the separation efficiency of hollow fiber modules in reverse osmosis only slightly, as far

as gas permeation is concerned, countercurrent flow produces the best results. A consequent application of the countercurrent principle led to the concept of Hwang,[4] i.e., the membrane column (Figure 6.12). This column consists of a rectification and a stripping section and permits binary mixture to be fractionated into its components. For a given geometry of the membrane fractionating column (length of each section, membrane area per unit length), the product quality is determined by the flow rate of the gas being recirculated.

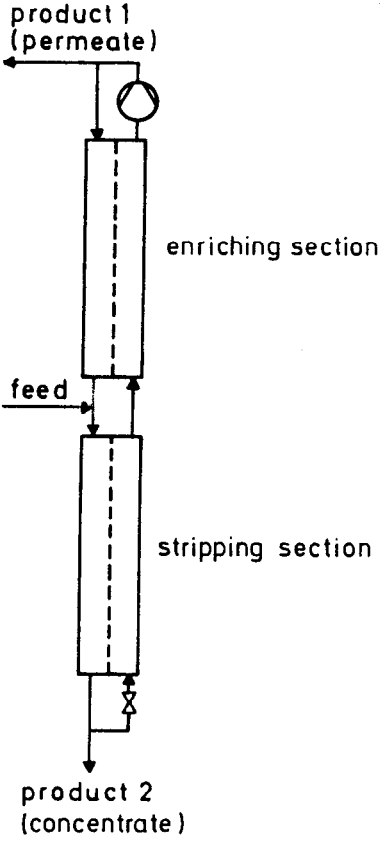


Figure 6.12: Membrane column for gas separation.

The modules employed in a membrane fractionating column must be different from those used in cascades: in hollow fiber modules, for example, the fibers cannot be U-shaped and must be open at both ends. In Reference 5, a module is described based on this principle.

CASCADES

There are cases where it is impossible to fractionate a given mixture in one

stage to the desired degree of purity; the separation process will consist of several stages. These stages can be realized in several ways, for example, by employing the countercurrent flow principle as much as possible within one unit like in packed towers for absorption or rectification or by combining definite separation units in the form of a cascade. The best known examples of this case are fractionating towers employing trays.

In fractionating towers, the trays are still incorporated in one vessel, i.e., part of one unit. In other cases, for example, cascades of hydrocyclones, gas centrifuges and-last not least-membrane modules, the unit itself will be the stage of the cascade.

In membrane technology, processes consisting of more than one stage are known in gas permeation and for the production of boiler feed water from seawater. Furthermore, cascades will be necessary if organic mixtures are to be separated by membrane processes only.

The best known example of a membrane cascade consisting of a high number of stages is the Oak-Ridge plant for enriching U-235 in the gaseous phase (employing porous membranes).

Definitions

Separation Unit. The elements of a separation process. Separation units of a separation process could be, for example, a gas centrifuge, a membrane module, a tray of distillation column or the evaporator of a multiple effect plant. It should be kept in mind, however, that in plate-and-frame modules as well as in modules of the spiral-wound-type usually every block or pressure-vessel contains more than one separation unit!

Stage. The element of a cascade will be named "stage" and the stage itself might contain several separation units connected in series and/or in parallel. Separation units are considered part of a stage as long as they are connected only at the feed and/or retentate side!

The elements of a stage can be arranged according to Figure 6.13 (this is sensible with respect to mass transfer in the boundary layer because of the decreasing volume flow at the feed side along the "axis" of a stage), in a "tapered" fashion or in a "squared-off" fashion.

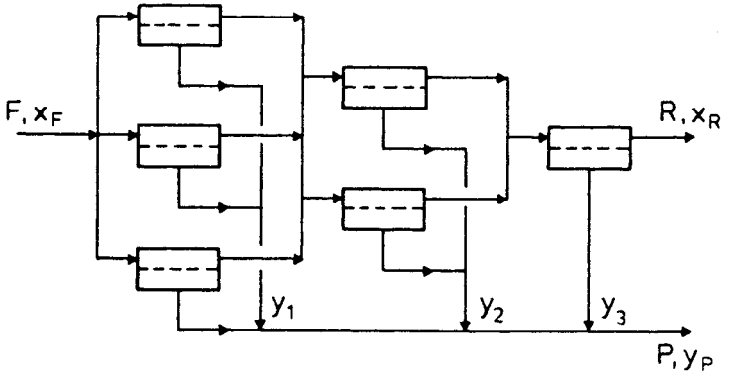


Figure 6.13: "Tapered" module arrangement.

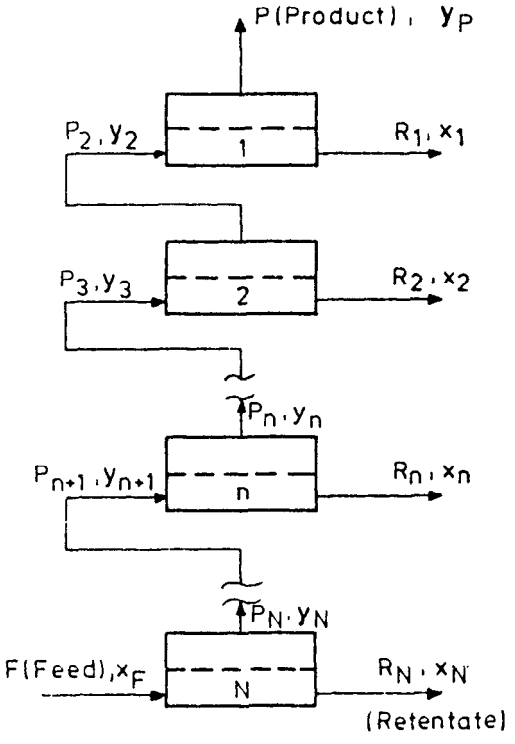


Figure 6.14: Cascade without reflux.

Cascade. A combination of stages where the permeate of a stage will be the feed of the next stage.

Yield. Yield is defined as the ratio of a certain (key) component in the product and in the feed:

$$\eta = \frac{\dot{m}_{AP}}{\dot{m}_{AF}} = \frac{P_A}{F_A} \tag{12}$$

Selectivity. Selectivity in general is defined as the quotient of ratios of conveniently chosen concentration measures. Convenient measures for a concentration are, for example, the partial pressure p_i and the molar fraction x_i or a mass fraction w_i. Accordingly, the selectivity is defined as:

$$S_1 \equiv \frac{P_A/P_B|\ \text{Prod}}{P_A/P_B|\ \text{Feed}} = \frac{x_A/x_B|\ \text{Prod}}{x_A/x_B|\ \text{Feed}} \tag{13}$$

or

$$S_2 = \frac{w_A/w_B|\ \text{Prod}}{w_A/w_B|\ \text{Feed}} \tag{14}$$

For the permeation of ideal gases, where

$$\dot{n}_i = Q_i \quad (p_1 x_i - p_2 y_i)$$

describes the transport mechanism (in sorption-diffusion) membranes, Equation 13 is reduced to

(15) $$S = \frac{Q_A}{Q_B} = \frac{1}{\alpha} \qquad , 0 < \alpha < 1$$

(in cases, where $p_2 y_i \ll p_1 x_i$ and, consequently, $n_i \sim Q_i p_1 x_i$ is valid).

Another entity which is often employed because of its simplicity is defined as:

(16) $$\lambda = \frac{x_A \mid \text{Permeate}}{x_A \mid \text{Retentate}} = \frac{y_A}{x_A}$$

or

$$\lambda_n = \frac{y_{AP} \mid \text{module permeate, stage n}}{x_{AR} \mid \text{module retentate, stage n}} = \frac{y_n}{x_n}$$

if characterizing the selectivity of the entire module.

"Cut-Rate" (Split-Factor). The cut-rate, sometimes called "split-factor", is defined as the ratio of permeate flow and feed flow. There will be, however, a difference between the cut-rate defined for molar flows and for mass flow.

(17) $$\Theta_1 = \frac{\dot{m}_P}{\dot{m}_F}$$

or

(18) $$\Theta_2 = \frac{P}{F}$$

Operating Line and "Equilibrium" Curve. Both terms are of importance for the graphical solution of a separation problem, i.e., for the graphical determination of the number of stages of a cascade. This method has been developed for the design of distillation columns by MacCabe and Thiele and should be well known. For all cases, the *operating line* represents the *mass and material balances*. In distillation, the equilibrium curve represents the thermodynamical vapor/liquid equilibrium. For an ideal binary system, the equilibrium curve can be calculated from Raoult's law and the saturation-pressure curves of the pure components of the mixture. In all other cases, however, for example, for all membrane processes, the equilibrium curve does not represent a thermodynamical equilibrium at all but will represent the separation characteristics of the module or that of the stage.

Cascades Without Reflux

Such cascades are only sensible in cases where the retentate is practically worthless. Norsk-Hydro, for example, is operating an electrolysis-heavy-water-production-plant where the deuterium is separated in a cascade without reflux (at least in the lower part of the cascade). Figure 6.14 illustrates the principle of a cascade without reflux.

Reflux Cascades

The inevitable losses of product with the retentate of cascades without reflux can be avoided by recycling the retentate according to Figure 6.15. This advantage, however, has to be weighed against the higher capital costs of reflux cascades. Only a detailed calculation of the specific separating costs will lead to a sound decision on whether a separation process should operate with or without reflux. In principle, there are four possible modes of operation:

(1) Constant reflux R/P

(2) Constant cut rate and variable reflux

(3) Variable cut rate and variable reflux

(4) "Ideal" cascade operation ($x_{n-1,R} = x_{n+1,p}$).

Here, only the first two cases will be discussed because with modern computers at hand, for these two cases only a graphical solution will be of value.

Constant Reflux. In general, the operating line of a cascade follows from a mass/molar balance and a material balance between the top and a certain stage n of the cascade. For constant reflux R = const resp. $R/P_1 = v$ = const,

the molar balance:

$$P_{n+1} - R_n - p_1 = 0 \tag{19}$$

and the material balance:

$$P_{n+1}\ y_{n+1} - R_n x_n \quad P_1\ y_1 = 0 \tag{20}$$

result in:

$$y_{n+1} = \frac{v}{v+1} x_n \quad \frac{1}{v+1}\ y_1 \tag{21}$$

The operating line is a straight line with the slope $\frac{v}{v+1}$

If the "equilibrium curve" is known, the number of stages necessary to achieve a certain product quality can be easily found according to Figure 6.16 by a step-by-step graphical procedure.

Constant Cut Rate, Variable Reflux. When the molar balance:

$$P_{n+1} - R_n - P_1 = 0 \tag{22}$$

is developed for several stages, a pattern can be noticed if the (constant) cut rate is introduced:

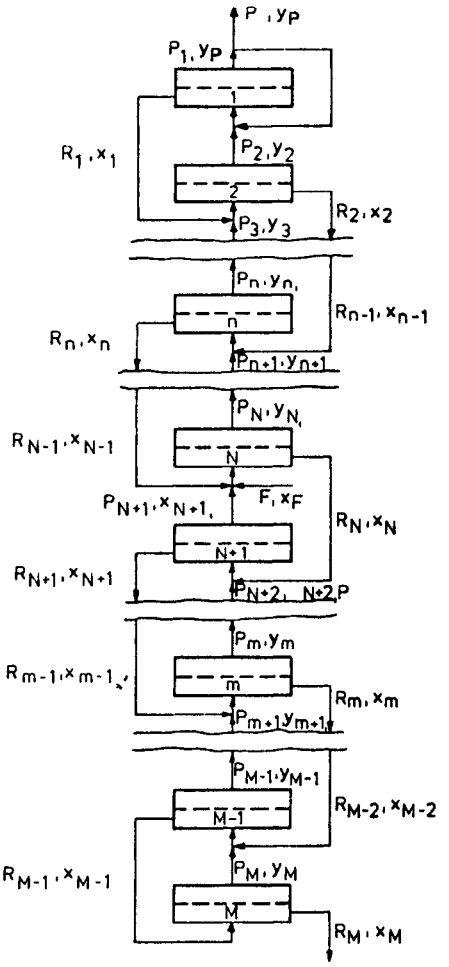


Figure 6.15: Reflux cascade.

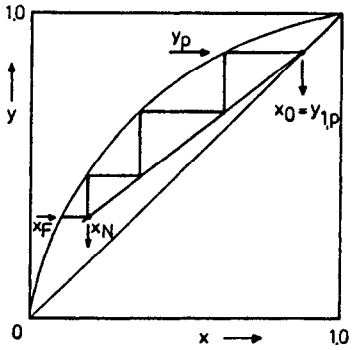


Figure 6.16: Graphical evaluation of the number of stages for a reflux cascade (enriching section), operated with constant reflux.

(23) $$P_2 = P_1 + R_1 = P_1 \ (1+\gamma)$$

Here, $\gamma = R/P$ is used instead of $\theta = P/F$. θ and γ are related by the molar balance of a stage: $\gamma = (1 - \theta)/\theta$.

$$P_3 = P_1 + R_2 = P_1(1+\gamma \ (1+\gamma))$$

$$P_n = P_1 \ (1+ \gamma +\gamma^2 + \ldots \ \gamma^{n-1})$$

(24) $$P_n = P_1 \frac{1 - \gamma^n}{1 - \gamma}$$

With the material balance:

(25) $$y_{n+1} = \frac{R_n}{P_{n+1}} x_n + \frac{P_1 y_1}{P_{n+1}}$$

the operating line follows:

(26) $$y_{n+1} = \frac{\gamma - \gamma^{n+1}}{1-\gamma^{n+1}} x_n + \frac{1-\gamma}{1-\gamma^{n+1}} y_1$$

Quite obviously, the slope of the operating line differs from stage to stage! The number of stages follows according to Figure 6.17. It should be noticed that all operating lines will intersect at $y_1 = x_1$.

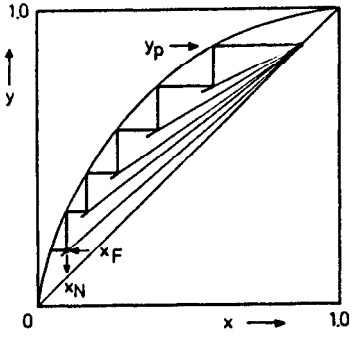


Figure 6.17: Graphical evaluation of the number of stages for a reflux cascade (enriching section), operated with constant cut-rate, variable reflux.

Once the necessary number of stages is known, the product rate P_1/F can be calculated according to:

(27) $$\frac{P_1}{F} \equiv \frac{P_1}{P_{N+1}} = \frac{1 - \gamma}{1 - \gamma^{N+1}}$$

The "Equilibrium Curve"

As mentioned above, the "equilibrium curve" in the case of membrane cascades is not at all a thermodynamic equilibrium but will represent the separation characteristics of the module or of the stage. This separation characteristic is in general a function of:

(1) the selectivity of the membrane

(2) the fluid dynamics in the module

(3) the driving force

(4) the concentration level (because the membrane selectivity is or might be concentration dependent)

(5) the flow pattern in the module, for example, co- or countercurrent flow.

With respect to flow pattern, five different patterns are possible:

(1) complete mixing at both sides of the membrane (Weller Steiner Case 1[6])

(2) Cross-plug flow, i.e., plug flow at the feed side and permeate flow orthogonal to the membrane without mixing (Weller Steiner Case 2,[6] Naylor-Baker[7])

(3) Parallel plug flow, cocurrent flow (Blaisdell-Case[8])

(4) Parallel plug flow, countercurrent flow

(5) Partial (incomplete) mixing of feed and permeate (Breuer Case[9]).

Here, only the first case will be discussed. A detailed discussion of the other cases can be found elsewhere.[10,11]

Complete Mixing of Feed and Permeate. In this case (Figure 6.18), the material balances for a binary mixture are:

$$P_n\, y_n = Q_A\, (p_1\, x_n - p_2\, y_n) \tag{28}$$

$$P_n(1-y_n) = Q_B\, (p_1(1-x_n) - p_2(1-y_n)) \tag{29}$$

Combining of both equations and introducing $\delta = p_2/p_1$ and $\alpha = Q_B/Q_A$ leads to:

$$\frac{x_{pn}}{1-x_{pn}} = \frac{1}{\alpha}\, \frac{x_n - y_n\,\delta}{(1-x_n)-(1-y_n)\delta} \tag{30}$$

As Equation 30 indicates, the equilibrium curve in this case is influenced by the ideal separation factor S_α and the pressure ratio r_δ.

For large pressure ratios, the equilibrium curve simplifies to:

$$y_n = \frac{x_n}{\alpha+(1-\alpha)x_n} \tag{31}$$

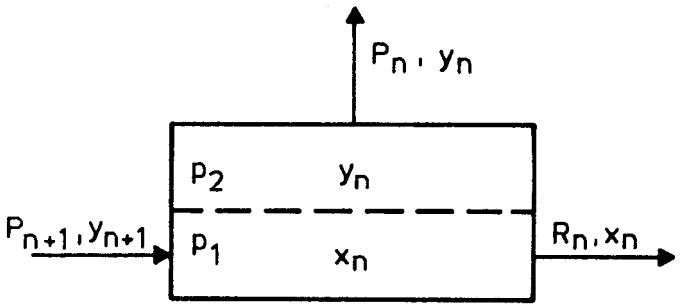


Figure 6.18: Complete mixing.

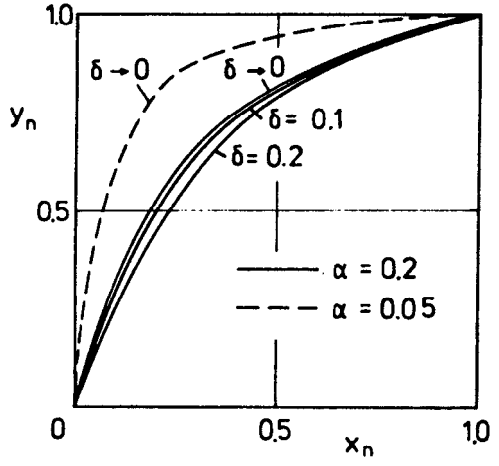


Figure 6.19: Separation characteristics (complete mixing).

Membrane Column

The membrane column can be an alternative to membrane cascades.[12-14] The membrane column consequently utilizes the countercurrent flow principle (Figure 6.20) and, for this reason, is restricted to cases where concentration polarization is negligible. (It has been suggested that the membrane-column concept be applied to the separation of liquid mixtures. However, this concept must fail here-at least for asymmetric membranes because of the concentration polarization within the support layer.) Membrane columns utilize the maximal driving forces because of the countercurrent flow at both sides of the membrane. The preferably permeating component is depleted on the high-pressure-side in the direction of the flow. The preferably permeating component can be withdrawn at the top of the column, the slower permeating component of the mixture at the bottom. At present, all modules for membrane columns described in the literature employ hollow fiber membranes.

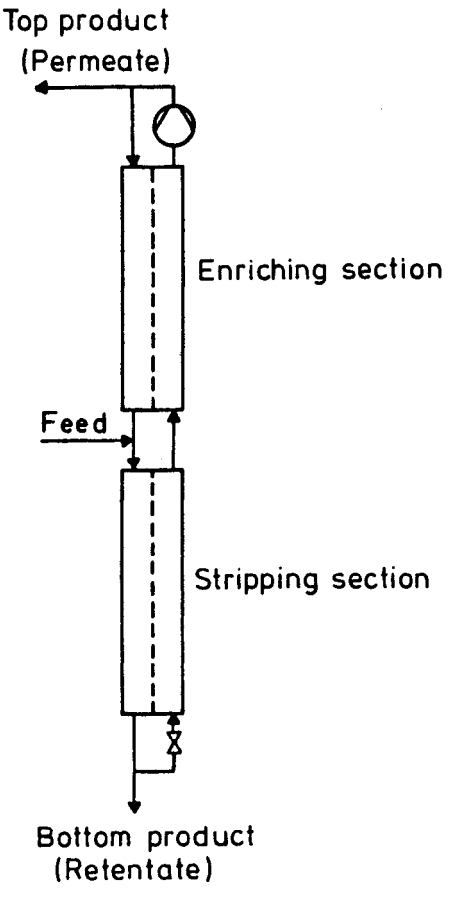


Figure 6.20: Membrane column.

The design equations for a membrane column are:

(1) the transport equation for material transport in the membrane

(2) mass, material and energy balances (pressure losses), formulated for the differential element of the membrane channel.

Material transport in the membrane:

$$\dot{n}_i = Q_i \, (x_i \, p_1 - y_i \quad p_2) \tag{32}$$

Mass (molar) balance (M = constant) combined with Equation 32:

$$\frac{d\dot{N}}{dz} = \pi d \left[Q_i (x_i \, p_1 - y_i \, p_2) + Q_j \left[(1-x_i) \, p_1 - (1-y_i) \, p_2 \right] \right] \tag{33}$$

Material balance:

$$(34)\quad \frac{d^2x_i}{dz^2} + \frac{\dot{N}\ RT\ 4}{p_1 D_{ij} \pi d^2}\ \frac{dx_i}{dz} = \frac{4\pi d\ RT\ Q_i}{D_{ij}\ \pi d^2}\left[x_i - \frac{p_2}{p_1}\ y_i - x_i\ (x_i - y_i\ \frac{p_2}{p_1})(1-\frac{Q_j}{Q_i}) - x_i\ \frac{Q_j}{Q_i}\ (1-\frac{p_2}{p_1})\right]$$

For a membrane column, it is essential that axial backmixing by diffusion (dispersion) be negligible compared to convective transport. In this case, Equation 34 is reduced to:

$$(35)\quad \frac{d}{dz}\ (x_i\ \dot{N}) = \pi\ d\ Q_i\ (x_i\ p_1 - y_i\ p_2)$$

Combining Equation 35 with Equation 32 (transport in the membrane) leads to:

$$(36)\quad \frac{dx_i}{dz} = \frac{\pi\ d\ Q_i p_1}{\dot{N}}\left[x_i - \frac{p_2}{p_1}\ y_i - x_i\ (x_i - y_i\ \frac{p_2}{p_1})(1-\frac{Q_j}{Q_i}) - x_i\ \frac{Q_j}{Q_i}\ (1-\frac{p_2}{p_1})\right]$$

Energy-balance: For the calculation of pressure losses, it must be taken into account-besides the compressibility of gases-that hollow fibers are elastically deformed (widened) by the higher pressure inside the fiber. According to Hwang and Thorman,[13] in the case of a deforming fiber, the pressure losses can be calculated by:

$$(37)\quad \frac{dp}{dz} = \frac{16K_1\,\eta\,\dot{N}\,RT}{\pi\,d^4\,p_1}\left(\frac{1}{K_2} - \frac{8\ Re_{w\,z}}{Re_z \cdot d}\right) - \frac{8}{d}\ \frac{1}{\frac{Re_z}{3p_1} - \frac{\pi d^3 p_1}{16\,\eta\,\dot{N}RT}} - \frac{128\,\eta\,\dot{N}RT}{\pi d^4\,p_1}$$

$$\text{with } Re_w = \frac{\rho v_w d}{2\,\eta}\ ;\ Re_z = \frac{\rho v_z d}{2\,\eta}$$

$$K_1 = 8\ (1+0.75 \cdot Re_e - 0.0407\ Re_w^2 + 0.0125\ Re_w^3)$$

$$K_2 = 1 + 0.056\ Re_w - 0.0153 \cdot Re_w^2$$

The set of Equations 32 ÷ 37 has to be solved numerically. For the special case of total reflux, however, an analytical solution for the concentration profile along the membrane column can be derived if the pressure losses are neglected. In the case of total reflux, for every section of the column (Figure 6.21):

$$(38)\quad x_i = y_i$$

is valid.

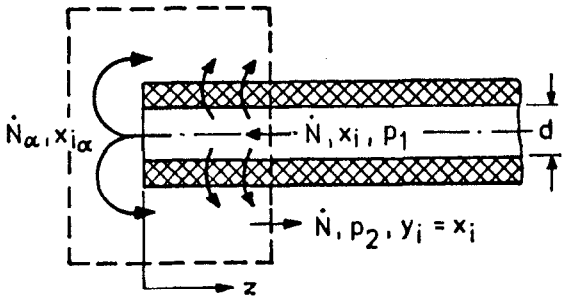


Figure 6.21: Membrane column, material balance around a fiber end (total reflux).

With the boundary conditions:

(39) $$z = 0: \; x_i = x_{i\alpha} \; ; \quad \dot{N} = \dot{N}_\alpha$$

Equation 36 can be integrated:

(40) $$z = \frac{\dot{N}_\alpha \cdot x_{i\alpha} \frac{1-x_{i\alpha}}{x_{i\alpha}}^{\frac{1+Q_j/Q_i}{1-Q_j/Q_i}}}{\pi d Q_j \; p_1 (1-\frac{p_2}{p_1})} \left[\left\{ \frac{x_i}{x_{i\alpha}} \frac{1-x_{i\alpha}}{1-x_i}^{\frac{Q_j/Q_i}{1-Q_j/Q_i}} - 1 \right\} + \frac{x_{i\alpha}}{1-x_{i\alpha}} \left\{ \frac{x_i}{x_{i\alpha}} \frac{1-x_{i\alpha}}{1-x_i}^{\frac{1}{1-Q_j/Q_i}} - 1 \right\} \right]$$

(41) $$\dot{N} = \dot{N}_\alpha \left(\frac{x_i}{x_{i\alpha}}\right)^{\frac{Q_j/Q_i}{1-Q_j/Q_i}} \left(\frac{1-x_{i\alpha}}{1-x_i}\right)^{\frac{1}{1-Q_j/Q_i}}$$

The separation process is determined (among other parameters) by the reflux ratio. Similar to fractionating by distillation, the calculation with total reflux leads to the minimal necessary column length. For a given column length, on the other hand, Equations 40 and 41 indicate the maximum possible purities of top and bottom product. For these reasons, a discussion of Equations 40 and 41 is useful for a first estimate of the column length and the operating conditions.

Column length depends on the recycled molar flow rate $\dot{N}_\alpha$. Figure 6.22 indicates that a specific molar flow rate (molar flow per fiber) as low as possible should be chosen. The lower limit is set by the condition that diffusive axial backmixing must be negligible with respect to the convective mass transport. On the other hand, the volume-specific yield (yield per unit-volume of fiber bundle) should be high.

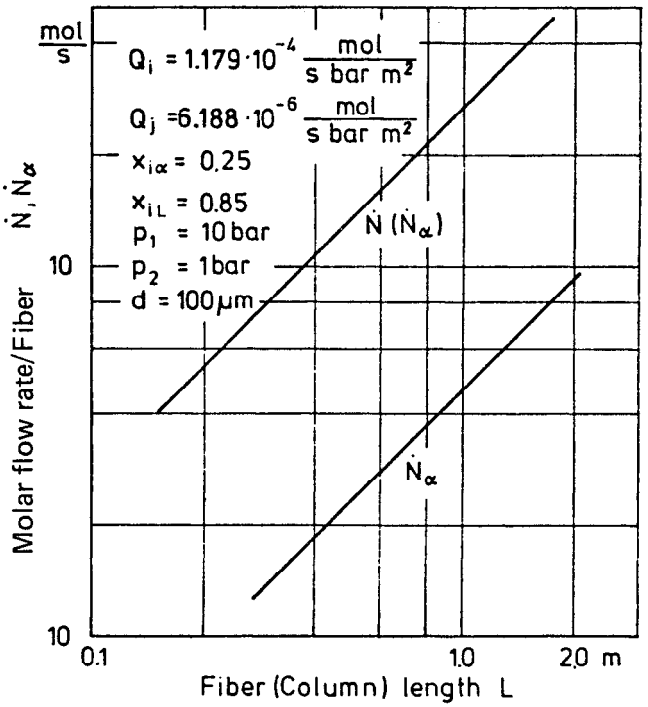


Figure 6.22: Membrane column, influence of reflux (recycled molar flow rate) on column length.

In general, the optimization of a membrane column must consider molar flow rate $\dot{N}_\alpha$, reflux ratio and the pressure losses. The mutual dependencies, which have been only shortly discussed here, are the reason why hollow fiber modules for the membrane column are relatively long ($L/d_1 \sim 20{,}000$) compared to hollow fiber modules for the separation of liquid mixtures.

Figure 6.23 shows the concentration profile of a membrane column as calculated by Equations 40 and 41 (total reflux). The concentration profile is very similar to the profile calculated by a numerical solution of the set of Equations 37 for the separation of CO_2/N_2 (Figure 6.24), taking into account the pressure losses and a finite reflux ratio. Figures 6.23 and 6.24 clearly indicate that a membrane column is especially effective in the stripping section. For the enriching section, especially for high concentrations of the preferably permeating component, the necessary membrane area and the reflux ratio (pressure losses) are increasing rapidly. It should be emphasized that a membrane column represents a multi-stage process just as a reflux cascade. The question, whether a membrane column or a reflux cascade is superior cannot be answered in general but must be evaluated for every individual case. It seems doubtful, however, whether multistage membrane processes will be often employed. According to our opinion[15], only one stage or, at the most, two-stage cascades seem to be competitive compared to proven processes like pressure swing adsorption, absorption, or low-temperature distillation.

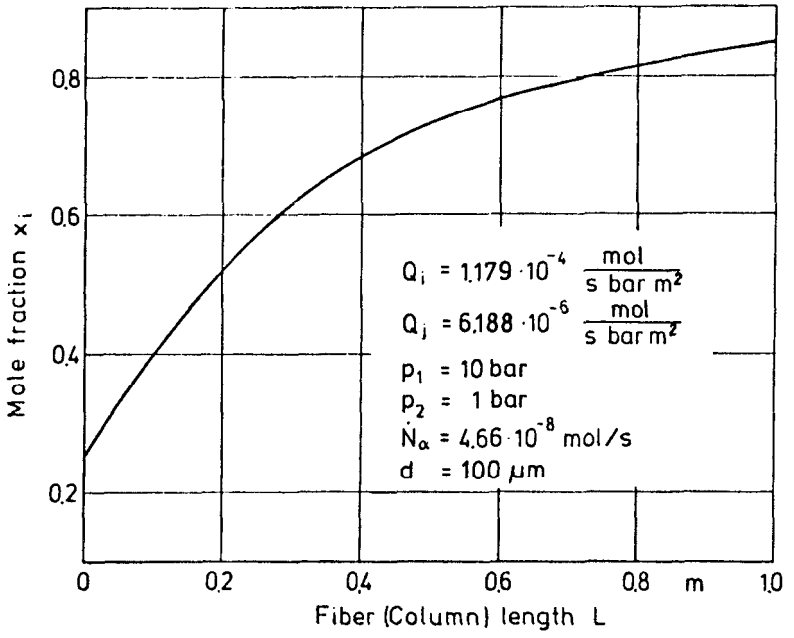


Figure 6.23: Calculated concentration profile of a membrane column, total reflux.

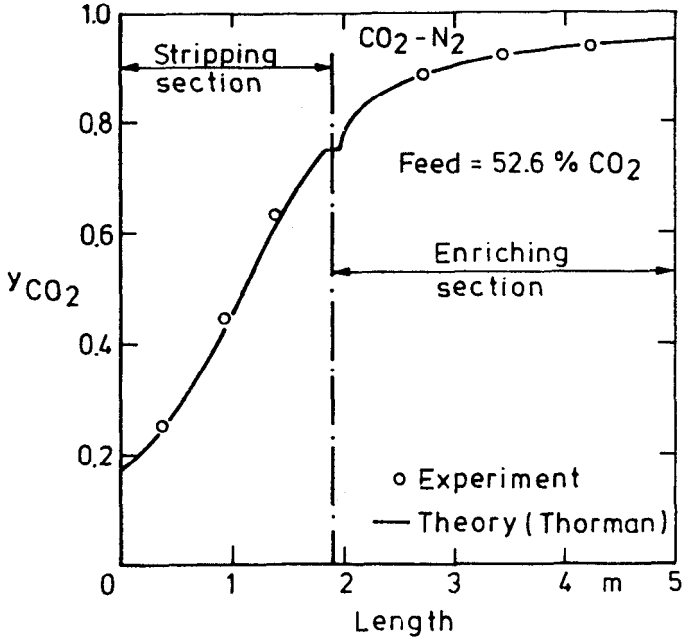


Figure 6.24: Concentration profile of a membrane column, comparison between theory and experiment.[13]

PROCESSES

Any application of membrane processes will be ultimately determined with respect to economic reasons, when compared to proven separation processes such as distillation. Strictly speaking, membrane processes will not replace conventional processes but, in the main, a combination of membrane processes and conventional processes will be the optimal solution. This trend can be noticed at least partly in the following examples.

Seawater Desalination by RO

At present, nearly all seawater desalination plants are distillation plants. Since low pressure steam can be utilized for heating, all major plants are combined with power plants–the heat input section of the desalination units replacing the condensor in the Rankine cycle. By this combination, the primary energy consumption of seawater desalination can be kept low[16] which is one of the reasons that thermal processes will always have their place in seawater desalination although the relatively rigid coupling of power and water production is sometimes disadvantageous.

Modern distillation plants have unit capacities of about 25,000 t/d. The energy consumption is approximately 95 KWh/to distillate in the form of saturated steam of a pressure of about 2.2 bar and 4 to 5 KWh/to distillate in form of power for the pump drives. All distillation processes produce a distillate containing only 20 to 30 ppm salts (total dissolved solids). Reverse osmosis (RO) will be *the* alternative to distillation. The modules which are successfully employed are of the "spiral wound" or the "hollow fiber" configuration. Under favorable conditions, the economic service lifetime of the modules resp. the membranes is about 5 years and warranties for such a figure are given by manufacturers.

RO plants are, however, much more sensitive to insufficient feedwater pretreatment than thermal plants. For this reason, it is accepted technology to use well water from wells drilled at the seashore rather than surface water as in thermal desalination.

As an example of the present state of the art in RO-seawater desalination, some data of the Malta facility shall be discussed.[17] The entire plant, consisting of 10 trains of hollow fiber modules (B10 Permeators of DuPont), produces 20,000 t/d fresh water at a specific power consumption of 6.3 KWh/to fresh water. This very low registered figure includes the power consumption for the feed pretreatment and is a direct consequence of the installed energy recovery system (Guinard integrated turbo pumps). Figure 6.25 shows the process flow sheet of the plant. The feed pretreatment is simple: sand-filtration (well water) followed by a settling tank, acid dosing and cartridge filtration. Feedwater temperature is not a critical factor in this case (in general, the manufacturer limits the maximum temperature to about 30°C despite the fact that the membrane itself can withstand higher temperatures). Table 6.1 summarizes the major operating data of the plant; Table 6.2 is a breakdown of cost.

In general, the following measures have to be considered for feed pretreatment of RO seawater plants:[18]

- pH-adjustment by acid dosing against carbonate scaling
- chlorine dosing against marine life in the plant

- polyphosphate dosing against calcium sulfate scaling
- cartridge filtration.

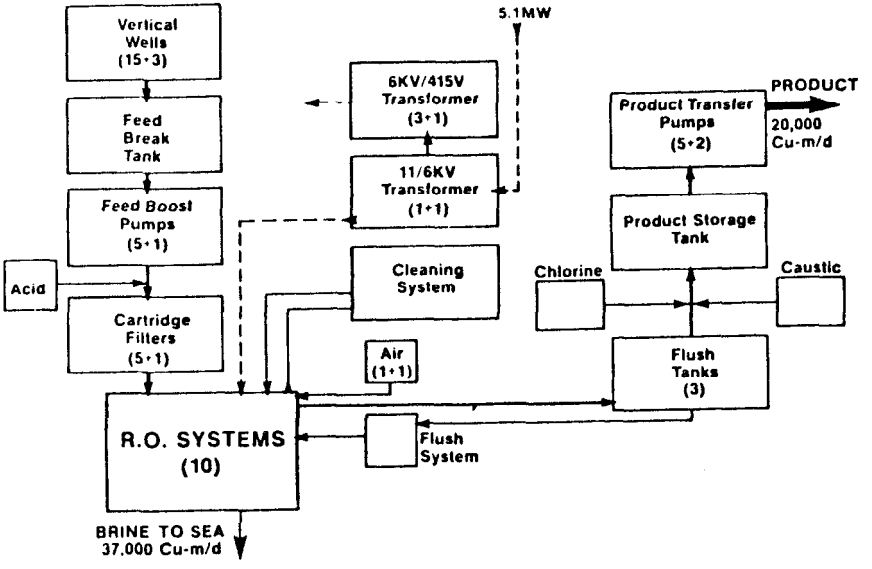


Figure 6.25: 20,000 cu-m/d seawater R.O. plant, Ghar Lapsi, Malta–process flow.

Table 6.1: Malta Seawater RO Plant Initial Operating Data

ITEM	UNITS	ACTUAL DATA[a]	DESIGN BASIS
FEEDWATER			
Total Dissolved Solids	ppm	36,500	39,200
Temperature	°C	17	21
Pressure	bar	70	70
Recovery	%	33	35
Silt Density Index[b]	-	2-4	0-3
PRODUCT			
Flowrate	m^3/d	18,600[c]	20,000
Total Dissolved Solids	ppm	380	500
CONSUMABLES			
Electricity	KWh/m^3	6.30	6.12
Sulfuric Acid	ppm	6.6	6.6
Caustic Soda	ppm	3.2	3.2
Chlorine	ppm	1.0	1.0

[a] 13 March 1983 (400 Operating Hours)

[b] Before cartridge filters

[c] 80% of permeators installed

Table 6.2: Production Cost Summary Malta Seawater RO Plant

	$/m³	$/Kgal
Electricity	0.43	1.62
Permeators	0.11	0.43
Labor & Overhead	0.05	0.20
Spare Parts	0.04	0.14
Chemicals	0.01	0.03
Filters	0.01	0.04
Total Operating	0.65	2.46
Total Investment costs RO-plant	1.250.000	
Civil works	5.000.000	
Total production	1.08	4.07

Furthermore, a flushing and cleaning system is necessary. For membranes which are sensitive to oxidizing agents, active charcoal filtration and/or sodium bisulfite dosing is mandatory if chlorine has been used in the pretreatment. Note that the product of any one-stage RO seawater plant contains about 300 to 500 ppm total dissolved solids, i.e., much more than the distillate from thermal desalination plants. Higher product purities-for chemical processes or for boilers-can only be achieved by a (2-stage) RO cascade. The second stage can be equipped with a different type of membrane (high-flux) than the first stage and certainly must be operated at a different transmembrane pressure difference. The module arrangement in each stage, i.e., the number of modules in series and/or in parallel is determined for a given type of module by the desired yield of the stage and a necessity to maintain optimal flow conditions in the modules (concentration-polarization). In general, these requirements lead to a so-called "tapered design" (see Figure 6.13) In any case, the designer faces on optimizing problem which can be solved numerically by a relatively simple computer program based on the general flow sheet indicated in Figure 6.26. One result of numerical calculations which seems to be generally valid is that recycling pumps (ZP in Figure 6.26) for the improvement of the flow conditions in the modules and/or pumps between the module-banks of a single stage (DEP in Figure 6.26) are not economical. More details about seawater desalination by RO can be found in the literature, especially in the proceedings of the IDEA conferences and of the symposia "Fresh water from the Sea".[19,20]

Total Desalination of Brackish Water

When desalting brackish water far inland, the discharge of the concentrated brine may pose a serious problem. For the case where neither deep-well-injection nor a discharge into a river or canal is possible, a hybrid plant consisting of a reverse osmosis process as a first stage and a special crystallization process as a second stage seems to be feasible (Figure 6.27).

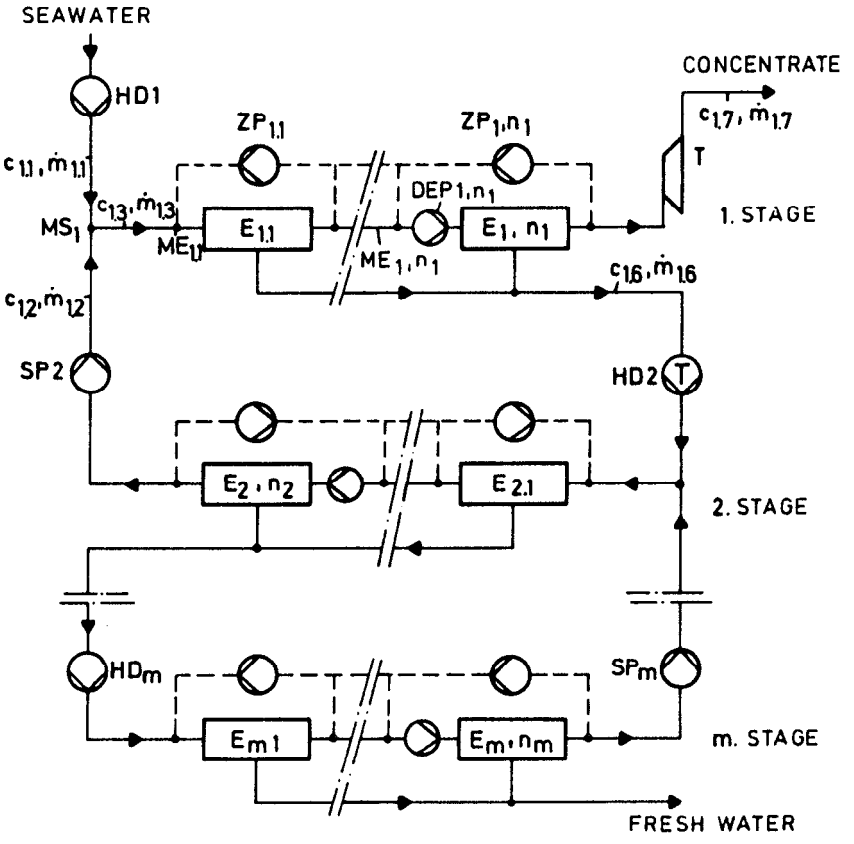


Figure 6.26: General flow sheet of an m-stage RO cascade.

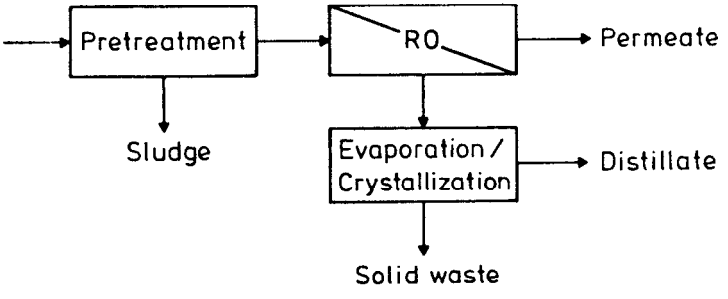


Figure 6.27: Total desalination of brackish water by a combination of RO and crystallization.

Studies on three real brackish waters of different sources indicated that for the RO stage the optimum pressure will be between 40 and 50 bar. If modules of the spiral wound type are employed, for example ROGA 4160 HR, the Reynolds number, $Re = h \cdot v_\alpha / \nu_\alpha$, at the inlet should be about 80. Although the

Reynolds number has a significant influence on the plant structure, i.e., on the ratio of modules in series and in parallel, its influence on the minimum specific cost of permeate is nil in a wide range (Figure 6.28).[21] Furthermore, the calculations clearly indicate that internal recirculations and/or repressurizing pumps between the module banks of a single stage will not pay off (see Figure 6.26). For spiral wound modules (Figure 6.29) as well as for hollow fiber modules (Figure 6.30), the lowest costs are obtained without recirculation ($z = 0$) and without repressurizing pumps (in Figures 6.29 and 6.30). Costs due to frictional losses and additional pumps are higher than the possible gain in permeate-flux by improved flow-conditions.

The second stage of the hybrid-process is essentially a crystallization capable of crystallizing all solids dissolved in the feed resp. the brine of the RO stage. Parts of these substances tend to heavy scaling and, therefore, the choice of the crystallization equipment is limited. A proven solution is, of course, the agitated thin film evaporator. However, this type of equipment must lead to high specific treatment costs for two reasons:

(1) An agitated thin-film evaporator is costly and limited in size.

(2) Because of its high capital cost, it is in general out of the question to combine agitated thin film evaporators to an energy saving multiple effect evaporation process.

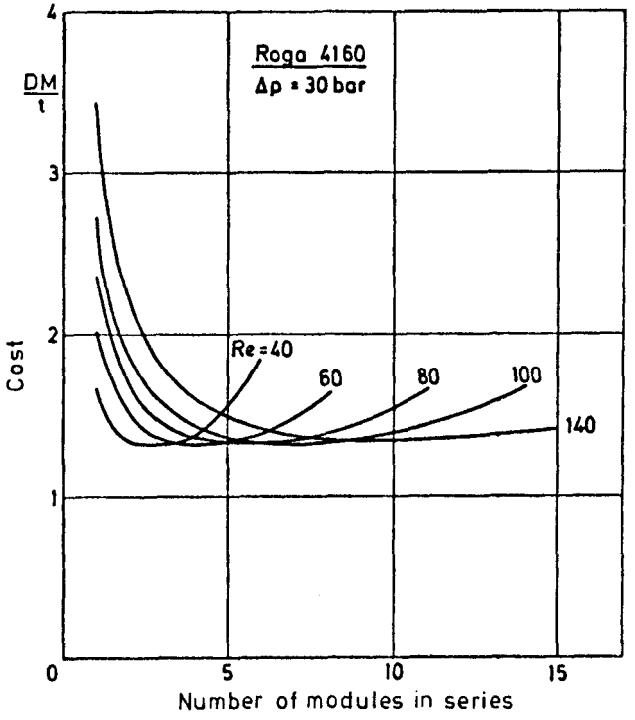


Figure 6.28: Influence of flow conditions in the modules on the specific cost of RO (tapered arrangement).

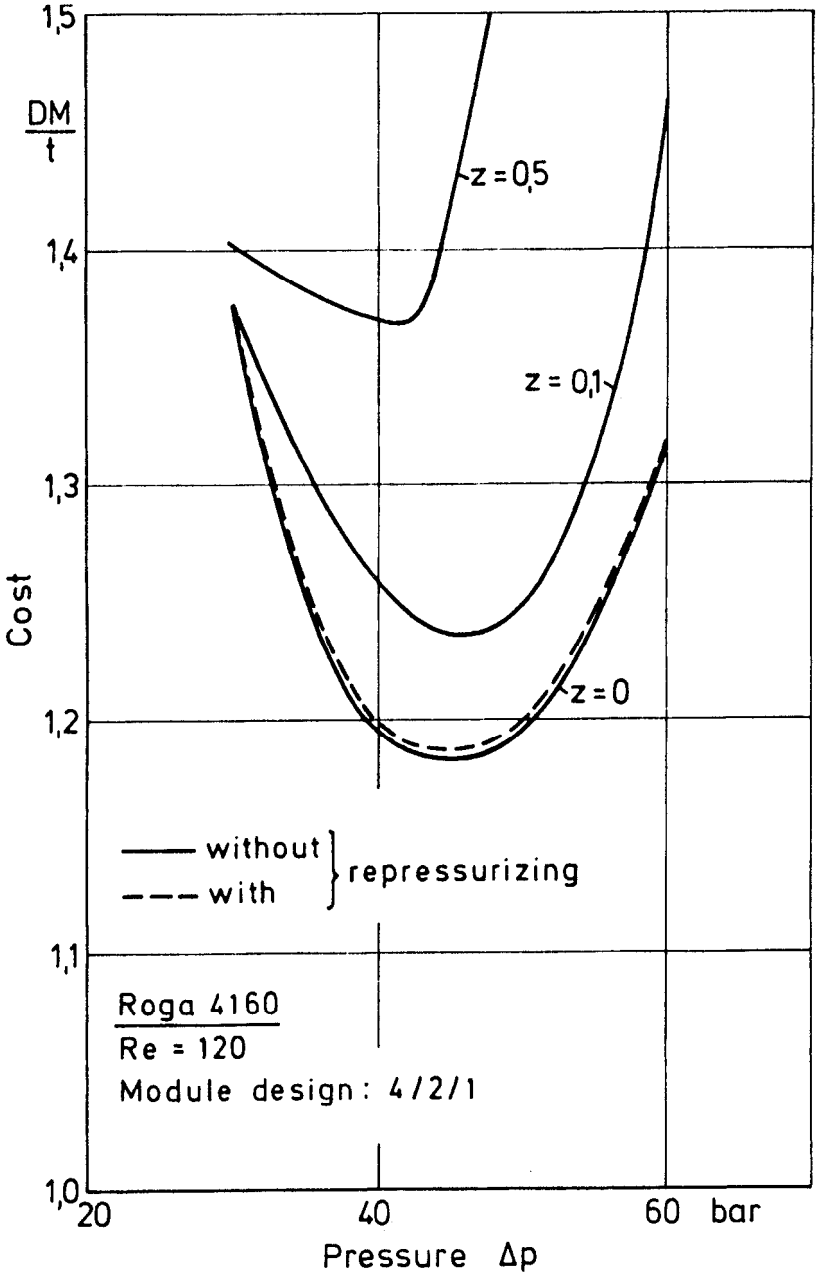


Figure 6.29: The influence of brine recirculation within each bank of modules ($\dot{m}_{Rec}/\dot{m}_F = z > 0$) on specific cost of RO (spiral-wound).

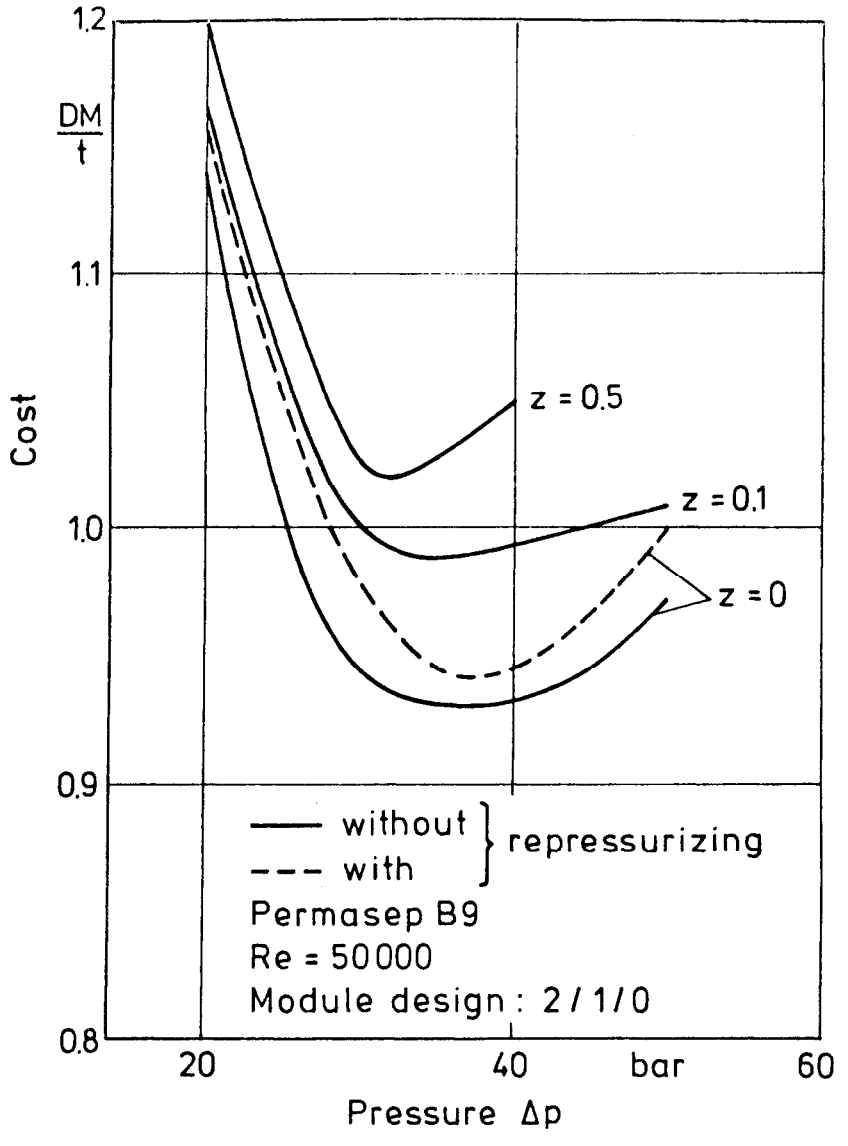
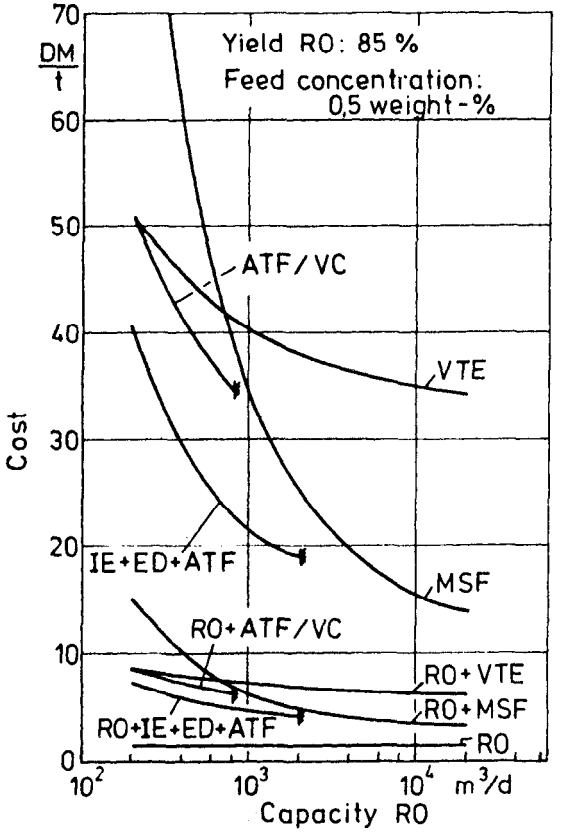


Figure 6.30: Influence of brine recirculation within each bank of modules ($\dot{m}_{Rec}/\dot{m}_F = z > 0$) on specific cost of RO (hollow fiber).

Low treatment costs for the brine can only be expected if the heat transfer surfaces can be designed as tube bundles and if energy saving concepts like MSF, ME or VC can be applied.

Promising crystallization processes like the seeding process and a modified MSF process, employing an inexpensive oil as heat carrier, are discussed in Reference 22.

One of the most important variables for the hybrid process is the concentration of the RO brine. In principle, the specific treatment costs of each stage must increase with increasing concentration of the RO brine. For the RO stage, this is mainly due to the rising osmotic pressure. For the crystallization step not concentration per se, but the fact that a rising brine concentration in the RO stage is equivalent to a decrease in feed flow for the crystallization step, results in smaller but specifically more costly crystallization units. However, because the specific treatment cost of the crystallization is in any case higher by an order of magnitude than the specific treatment cost of the RO step, it is easily understood that the optimum of the hybrid plant is determined by the maximum concentration which can be achieved with the RO modules! This result is demonstrated by Figure 6.31 comparing specific costs of different process combinations.



ATF: Agitated Thin Film Evaporator
VTE: Vertical Tube Evaporator
MSF: Multi Stage Flash

Figure 6.31: Water cost of alternative hybrid plants.

In any case, the specific costs of fresh water for a 2-stage hybrid process will be 3 or even 4 times higher than for a single-stage RO process. This is a direct consequence of the specific costs of the second stage, regardless of whether a VTE-seeding process, a modified MSF-process or vapor compression is considered. (VTE = Vertical Tube Evaporator, here in combination with a seeding technique, MSF = Multi-Stage-Flash, ATFE/VC = Agitated-Thin-Film-Evaporator in combination with Vapor Compression). Because of these high treatment costs, the chances for such a hybrid process are very limited with respect to brackish water desalination. The situation seems to be different for wastewater treatment and it is not surprising, that a process as described has been realized for the treatment of the effluents of a power plant (San Juan, New Mexico, USA).

The process is designed to handle 10.000 m^3/d wastewater from the flue gas scrubber and the cooling towers (Figure 6.32). The mechanically pretreated effluents are fed to a RO unit, designed for a recovery rate of 80%. The concentrate of the RO unit is fed to the crystallization stage, designed as vertical tube evaporator combined with vapor compression. Scaling in the evaporator is prevented by the application of a (calcium-carbonate) seeding technique.

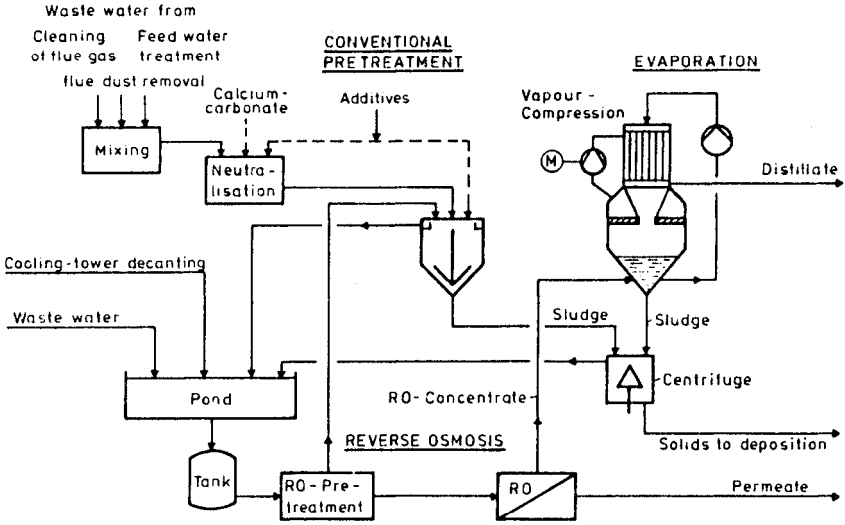


Figure 6.32: Treatment of power-plant wastewater; combination of RO and crystallization.

Automotive Industry-Combination of UF, Cross Flow Filtration and Evaporation for Recycling of Detergents and Process Water

The final step in the production of automotive parts such as pistons, axles, etc. is usually a rinse. The spent wash water of such a process contains, in addition to the detergents, cutting oil and suspended matter and it is impossible to discharge it into the canalization without further treatment. Fractionating the wastewater into a concentrate containing the oil and the suspended particles and into a premeate containing practically no oil is possible by UF.

The detergent concentration of the permeate and, consequently, its biological oxygen demand (BOD) is high, leading to further treatment costs if discharged into the canalization. For two obvious reasons, the question arises whether such a permeate could be recycled:

(1) a further treatment or further treatment costs would be obsolete and

(2) the recycling would lead to substantial savings in process water and in detergents.

The savings in detergents are of prime importance and it must be the aim of process development to maximize the detergent concentration in the permeate without increasing the oil-concentration to an intolerable amount.

In on-line experiments with a plant effluent containing 2% detergents, 1% oil and 0.8% suspended solids (metal, dirt, etc.), tubular modules equipped with UF membranes of different pore-sizes and a microfiltration membrane have been tested. (The experiments were carried out in the gear and axle production of Daimler Benz AG.) As expected, the MF membrane produced the highest flux for detergents. Because of th relatively low retention capacity for oil, however, the use of MF membranes is limited to a maximum oil concentration of about 10% in the concentrate. In this case, the oil concentration of the permeate is about 50 mg/ℓ, contrary to the UF membranes, where the oil concentration of the permeate is independent of the oil concentration of the concentrate up to the phase inversion concentration of about 41%.

For ultrafiltration as well as microfiltration the permeate flux is controlled by a gel layer-not by the membrane itself. This must be concluded from Figure 6.33 because the permeate flux for steady state conditions is almost exactly the same for the three tested membranes (for comparison, the data of Figure 6.33 have to be corrected for the same temperature and the same flow conditions).

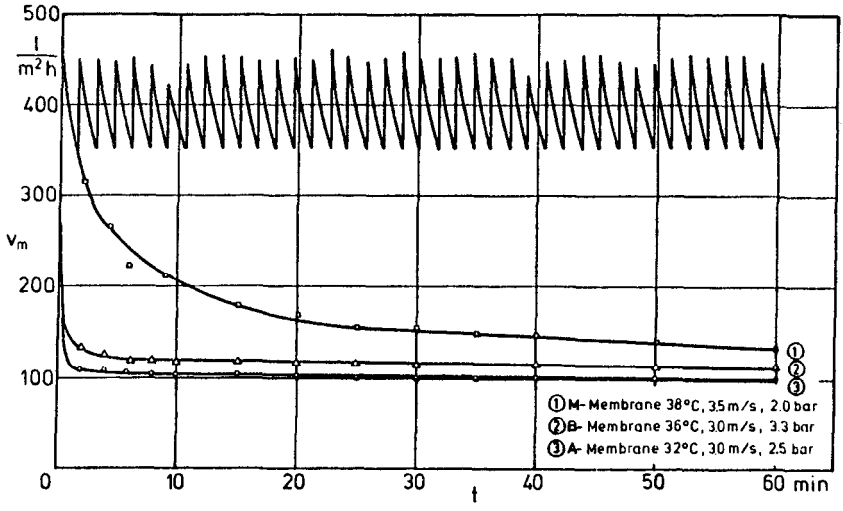


Figure 6.33: Gel-layer controlled flux in UF and MF (MF-membranes with and without backflushing).

Quite often, the formation of a gel layer is reversible; the gel layer can be removed by cleaning. In every case, periodic cleaning and a higher average flux have to be weighed against the time for cleaning. Microfiltration is advantageous compared to UF because microfiltration membranes are available in the form of tubes withstanding outer or inner pressure of several bars which can be easily cleaned by reversing the flux for a short time. Despite the advantages with respect to flux and yield of detergents, microfiltration alone will not be a solution for the described effluent-treatment problem since the retention capacity for oil at higher feed concentrations is too low. The optimal process is a combination of microfiltration and ultrafiltration according to Figure 6.34.[24]

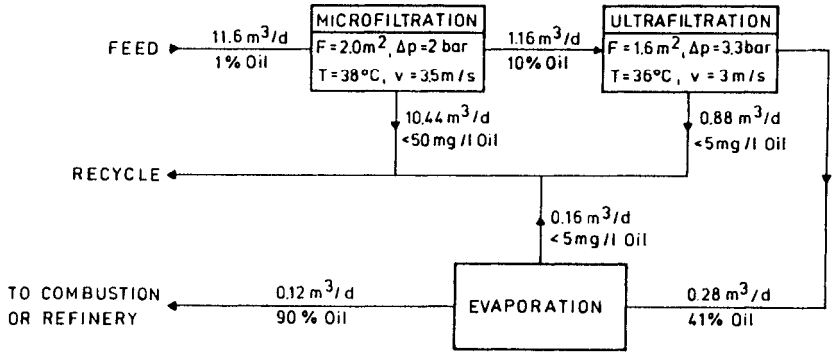


Figure 6.34: Flow sheet for a combination of micro- and ultrafiltration for the treatment of oily wastewater.

The recovery of detergents of such a process has been determined to an average of 85%. It should be noted, that the permeabilities of the individual components of a detergent differ and that the upgrading of the recycled permeate must be based on the selectivity of the process.

The limiting oil-concentration for the first stage, microfiltration, is determined by the tolerable concentration of oil in the recycled product. Since the oil retention capacity of the ultrafiltration stage is independent of feed concentration, the final concentration of the retentate is solely determined by the phase inversion "oil/water → water/oil". At this concentration, the overall water recovery of the process is above 97.5%. However, the retentate of the process still contains too much water if incineration or refining is considered. Therefore, an evaporation step must be included in the process. Almost certainly evaporation will not be economical for the small capacities indicated in Figure 6.34 and a central evaporation station for the tentates from several production lines should be considered.

Galvanic Industry–Treatment of Effluents

In the galvanic industry, a treatment of the effluents is mandatory. A process which is not only capable of water treatment but, at the same time, of reclaiming metals which would otherwise be lost would be most favorable. RO is such a process. In the U.S., more than 200 RO plants are installed in the gal-

vanic industry and, according to reported data, these plants are very profitable because of the reclaimed metals.

Figure 6.35 is a flow sheet of a galvanic production line completed by RO. The modules are of the spiral wound type and the membrane material is cellulose acetate in this case.[25]

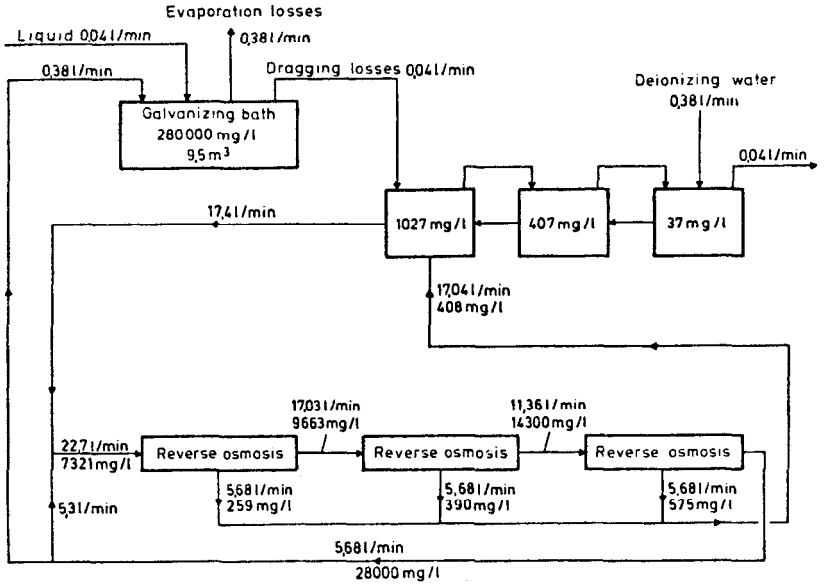


Figure 6.35: Flow sheet of nickel plating, including RO for wastewater treatment.

By recycling of the permeate into the first stage of the rinsing cascade and recycling the concentrate into the galvanic bath, the recycling is complete; the evaporation losses of the plant are balanced by the deionized water necessary in the last stage of the rinsing cascade. Depending on the permeate concentration which, in turn, depends on membrane retention and on the required recovery rate of the RO unit, the permeate must be added to the first or second stage of the rinsing cascade. Table 6.3 shows the (average) composition of the galvanizing bath; Figure 6.36 shows flux and selectivity (retention rate) of the modules.

Table 6.3: Composition of Watts-nickel bath

	concentration
total nickel ratio	82 g/l
nickel sulfate 6 H_2O	255 g/l
nickel chloride 6 H_2O	105 g/l
boric acid	45 g/l
brightening agent	not analyzed
pH-value	4.3
temperature	60 °C

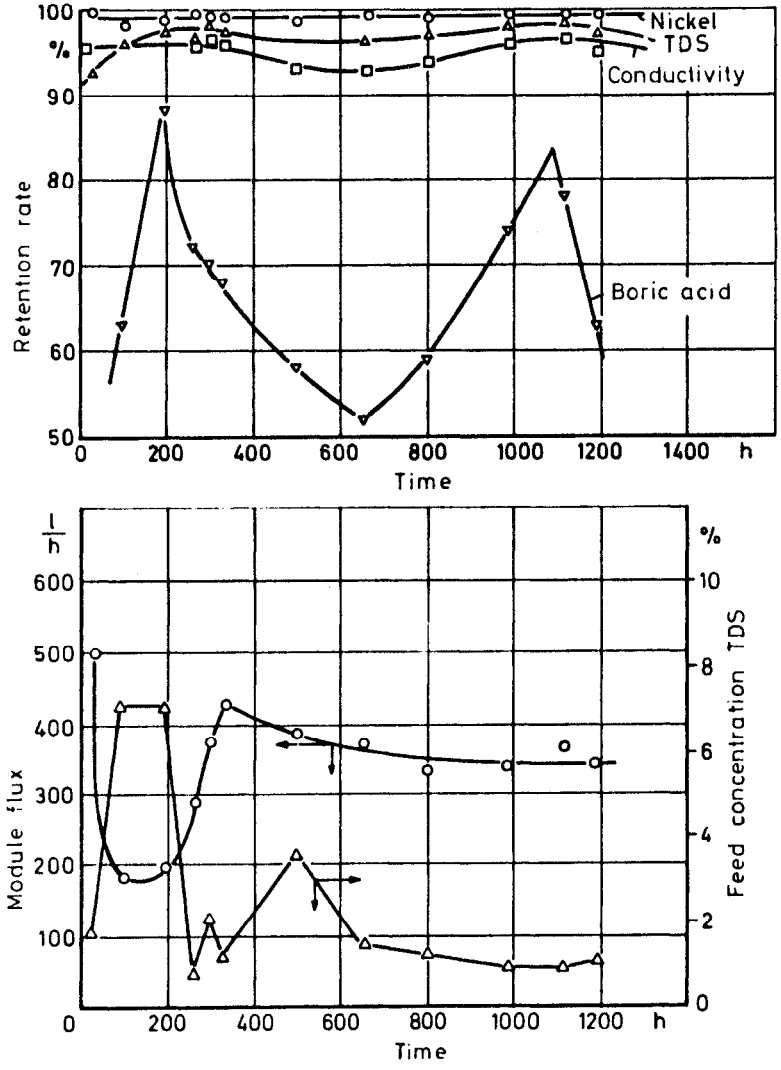


Figure 6.36: Treatment of nickel-plating effluents by RO, module flux and selectivity.

Figure 6.36 indicates the high retention capacity of the membranes for nickel and solubles whereas the retention for boric acid is not quite satisfactory (no explanation could be found for the concentration fluctuations in time).

Payback time of the RO units is given as 8.1 years for single shift operation, 2.4 years for a two shift operation and 1.4 years for a three shift operation.

An analysis of the RO units installed in the galvanic industry demonstrates

that presently RO units are mainly installed in the nickel plating industry for two reasons:

(1) the pH value of Watts nickel baths is between 3 and 5 permitting the installation of cellulose acetate membranes (cellulose acetate, still being a very common membrane material). It should be mentioned that more recently synthetic membranes have been developed (i.e., the PA 300 of UOP, San Diego, the NS 100 of Abcor Inc. Wilmington or the PBIL of Teijin Ltd., Tokyo) which proved to be resistant to chromium acid, copper cyanide and zinc cyanide baths at extreme pH values.

(2) the temperature of the Watts nickel bath is 50° to 70°C. At this temperature, the evaporation losses of the bath are such that no additional evaporators for further concentration of the RO concentrate are necessary.

Gas Permeation

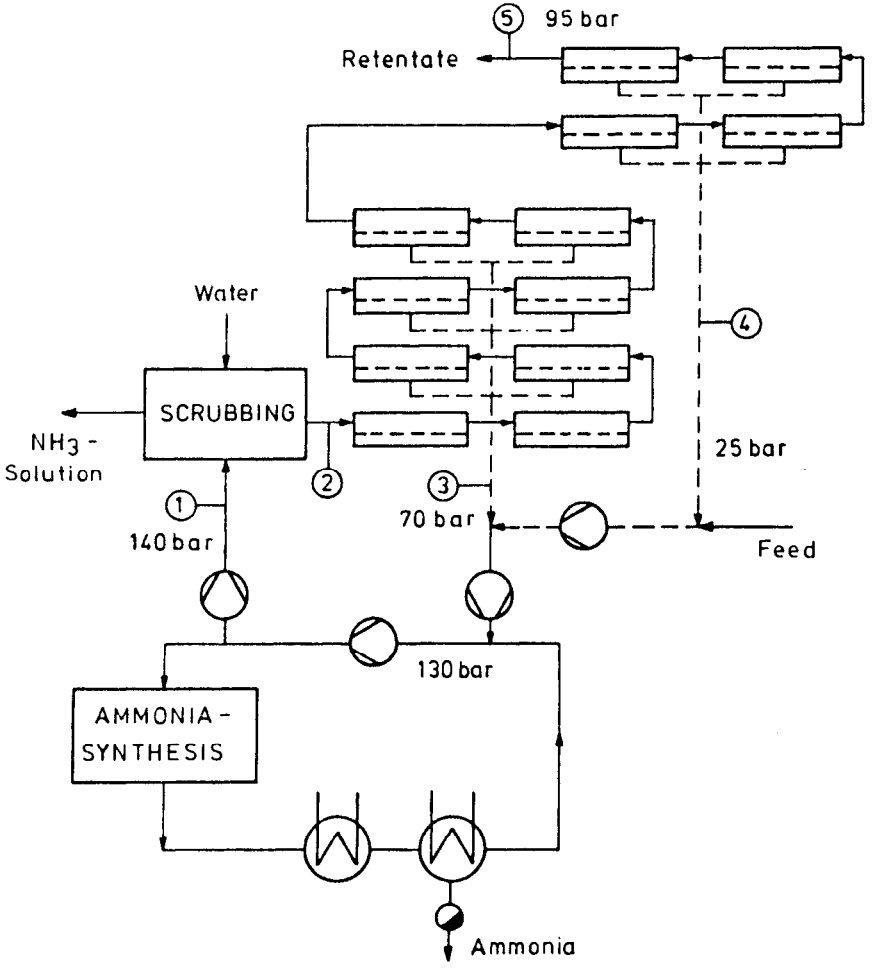
With few exceptions, gas permeation on a technical scale employs membranes of the sorption diffusion type. In this case, the flux of a permeating component is proportional to the difference of the partial pressures at both sides of the membrane.

$$J_i = Q_i \quad (p_1 x_i - p_2 y_i) \tag{42}$$

at least as long as the conditions of the gases are well above the critical point. On a commercial basis, gas separation started with the recovery of H_2 from the bleed of (high pressure) synthesis loops, employing in most cases a composite membrane "silicon/polysulfone" in the form of hollow fibers.

Asymmetric phase-inversion membranes like the membranes employed in reverse osmosis are difficult to prepare as gas permeation is much more sensitive to micropores than RO due to the much higher diffusion coefficients of gases. For the same reason, the composite membrane differs from RO composite membranes: in gas permeation, the top layer of the asymmetric support structure is responsible for the separation while it is the sole duty of the coating to plug the micropores. Consequently, the material of the coating chosen (silicone) has a high permeability but a low selectivity while the membrane material (polysulfone) has a high selectivity (and a much lower permeability).

Figure 6.37 shows the flow sheet for the recovery of H_2 from the bleed of the synthesis loop of ammonia plants. In ammonia synthesis, a recycling of the unreacted components is mandatory because of its low equilibrium conversion rate. In all technical processes, however, a bleed is necessary because otherwise the concentration of impurities would increase to an intolerable level. Normally, the bleed is utilized for heating purposes in the reforming stage. Here, the bleed is fed to a conventional separation unit first-a scrubber for recovering ammonia. Behind the scrubber, the modules for the recovery of H_2 are arranged in a "one-stage-two unit" form. The first unit, consisting of 8 hollow fiber modules (total feed capacity 3,800 Nm^3/h) is operated with a transmembrane pressure difference of 60 bars, the permeate leaving at a pressure of about 70 bars. At this pressure, the permeate can be fed to the second stage of the synthesis feed compressor.



	1	2	3	4	5
H_2 [mol - %]	61,0	62,2	87,3	84,8	20,8
N_2 [mol - %]	20,5	20,9	7,1	8,4	43,8
CH_4 [mol - %]	10,5	10,7	3,6	4,3	22,5
Ar [mol - %]	6,0	6,1	2,0	2,5	12,9
NH_3 [mol - %]	2,0	< 0,02	< 0,02	< 0,02	< 0,02
Flow [m^3_N / h]	3868	3821	1591	820	1410

Figure 6.37: Flow sheet for the recovery of H_2 from the synthesis loop of an ammonia plant.

The retentate of the first unit is fed to the second unit (and for this reason, it cannot be considered a two stage cascade), the permeate leaving at 25 bars as an additional feed to the first stage of the compressor. The retentate is utilized for heating purposes.[26]

Since flux and selectivity increase with increasing transmembrane pressure difference and the modules can tolerate pressure differences of about 100 bars, the reader might question why the first unit is operated with a transmembrane pressure difference of only 60 bars. The reason is that the H_2 recovery system has been added to an existing plant and that the first stage of the synthesis compressor would not accept the permeate flux of both units.

Figure 6.38 shows another example of H_2 recovery; here from the tail gas of a high pressure synthesis (UOP Butamer process). In this case, the tail gas leaving the conventional fractionating system contains about 70% H_2. The membrane unit placed behind the fractionating system recovers about 90% with a purity of >96%.[27] This process seems to be interesting for two reasons:

(1) spiral-wound modules are employed with dry asymmetric phase inversion (cellulose-acetate) membranes.

(2) the feed contains small amounts of HCl.

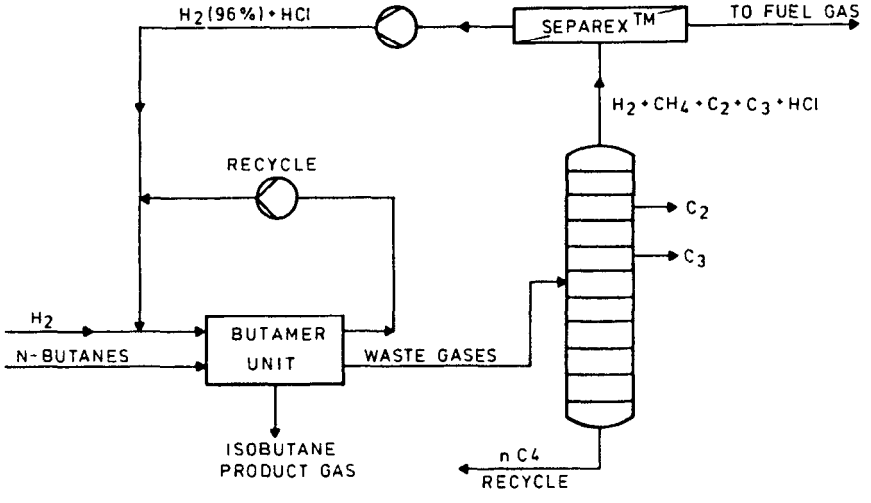
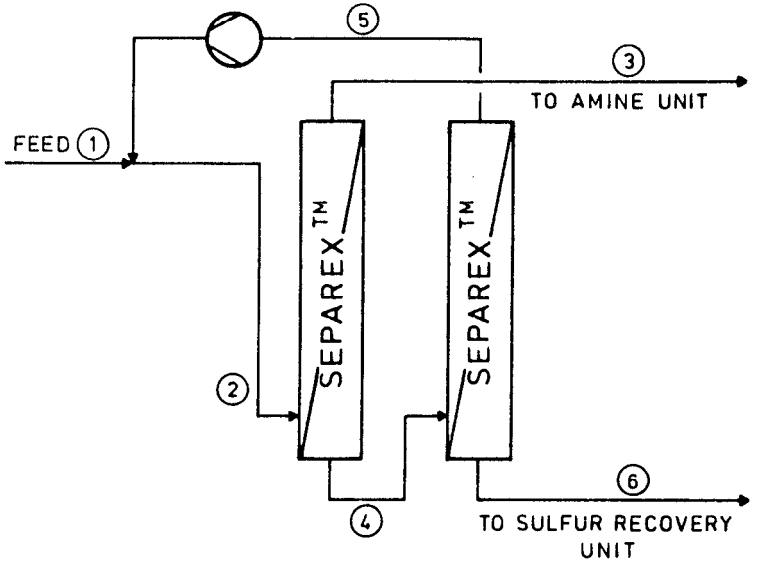


Figure 6.38: Hydrogen recovery from the tail gas of the UOP Butamer process.[27]

Figure 6.39[27] shows a two-stage cascade for the purification and dehydration of sour gases, mainly removing CO_2 and H_2S. Again, spiral wound modules with asymmetric cellulose acetate membranes are employed. It should be noted, that in this case as in all other cases discussed here, no compressors had to be installed. This is the main reason why these applications show excellent payback times.



STREAM / COMPONENT	1	2	3	4	5	6	
CO_2	10	11,5	2	16	13,7	23	
CH_4	64,9	64,2	86,49	48,8	63,19	4,8	
C_2	5	4,2	8,6	2,4	3,1	0,1	
H_2S	20	20	3	32,7	20	71,6	ξ_{CH_4} 98%
H_2O	0,1	0,1	0,01	0,1	0,01	0,5	
VOLUME FLUX [Nm3/h]	17110	29830	12625	16872	12742	4130	
MOLAR FLUX [kmol/h]	763	1331	563	753	568	184	
PRESSURE [bar]	66,5	66,5	65,5	18,2	17,2	1,35	

Figure 6.39: Purification of sour gas by a two-stage stripping cascade.[27]

Pervaporation

Pervaporation differs from all other membrane processes because of the phase change of the permeate. Mass transport across the membrane is not achieved by elevated pressures at the feed side as in RO and in gas permeation but by lowering the activity of the permeating components at the permeate side. This can be achieved by applying either a vacuum at the permeate side or by sweeping the permeate side with a carrier like air or H_2O vapor (Figure 6.40). Phase change occurs because the partial pressure of the permeating components is lower than the corresponding saturation pressure.

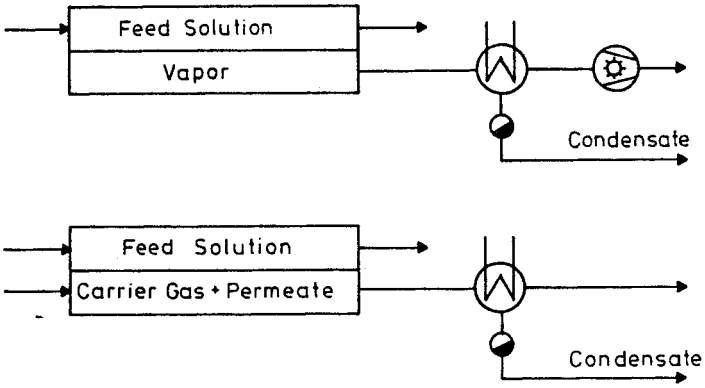


Figure 6.40: Schematic of pervaporation.

In general, the selectivity of pervaporation is high, as demonstrated in Figure 6.41 for the system "benzene-cyclohexane, polyethylene membranes". The separation characteristic is shifted to much more favorable figures compared to the thermodynamic equilibrium curve; the azeotropic point can be suppressed.[28-30] Parameter in the diagram is the ratio of total pressure p at the permeate side to saturation pressure $P_L^\circ = \gamma_i x_i P_i + \gamma_j x_j p_j^\circ$.

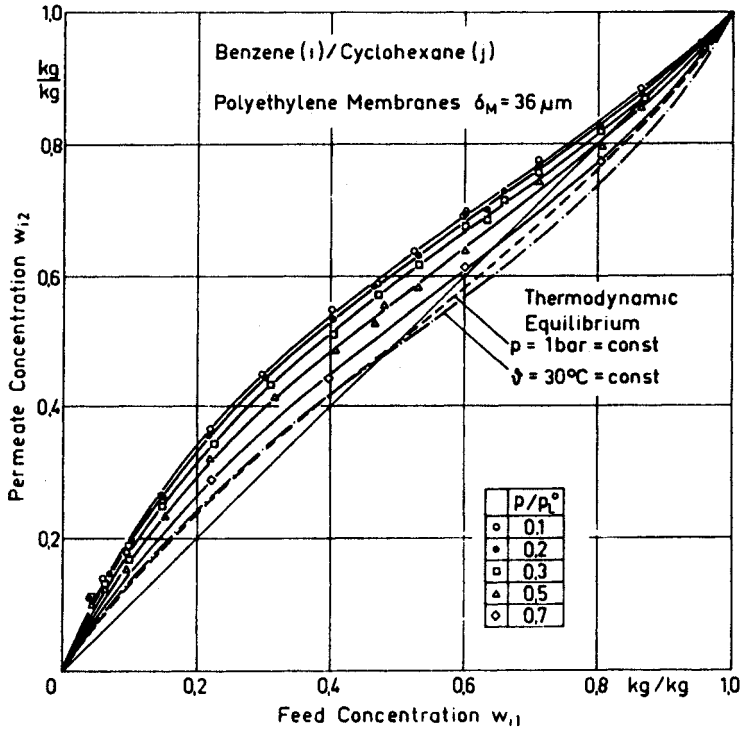


Figure 6.41: Influence of permeate pressure on selectivity.

Figure 6.41 shows that the selectivity decreases with increasing pressure at the permeate side. For a ratio of $p/p_L^\circ = 1$ finally, the separation characteristic is identical to the thermodynamic equilibrium curve (for ϑ = constant). Pervaporation will always be a process which is relatively expensive compared to other membrane processes for two reasons:

(1) The modules must be designed for a low pressure drop at the permeate side despite the increasing volume of the permeate due to the phase change since the principle of pervaporation is very sensitive to such pressure losses.

(2) The process requires heat transfer surfaces because the heat of evaporation necessary for the phase change of the permeate must be supplied to the process (and must be rejected by condensation of the permeate).

The necessary heat-flux

$$\dot{q} = \Sigma J_i \, (\Delta h_{vi} + c_{piv} \, \Delta\vartheta)$$

is usually drawn from the feed and will inevitably lead to temperature gradients-orthogonally to the membrane as well as in the dirction of flow. Especially in pervaporation of water mixtures with water as the preferably permeating component, heat transfer between the bulk of the liquid and the membrane surface (permeate-side) can become the rate-controlling step.

Figure 6.42 shows the temperature drop orthogonally to the membrane as a function of heat flux for water/isopropanol flowing in a rectangular channel (laminar flow, $Re_h = 498$, $d_h = 4$ mm). According to Figure 6.42, the correlation between measurements and calculations (straight line) based on

$$\dot{q} = k_q \, \overline{\Delta\vartheta}$$

$$\frac{1}{k_q} = \frac{1}{\alpha} + \frac{\delta_M}{\lambda_M}$$

is fairly good.[31] Quite often the heat-flux is small and, therefore, the temperature drop orthogonally to the membrane can be neglected. In any case, the temperature decrease in the direction of flow has to be taken into account.

Figure 6.43 shows, for the pervaporation of benzene/cyclohexane and for symmetric PE-membranes, the temperature decrease along the membrane. The temperature distribution has been calculated numerically assuming laminar flow in a rectangular channel with membranes at only one side. Due to the laminar flow, heat transfer orthogonally to the membrane is only achieved by heat conduction and, for this reason, the channel height should be small. The dotted lines in Figure 6.43 are valid for external heating of the channel wall opposite to the membrane. Such a design is expensive. In most cases, it will be the far better solution to achieve a quasi-isothermal operation by a combination of modules and heat exchangers connected in series.

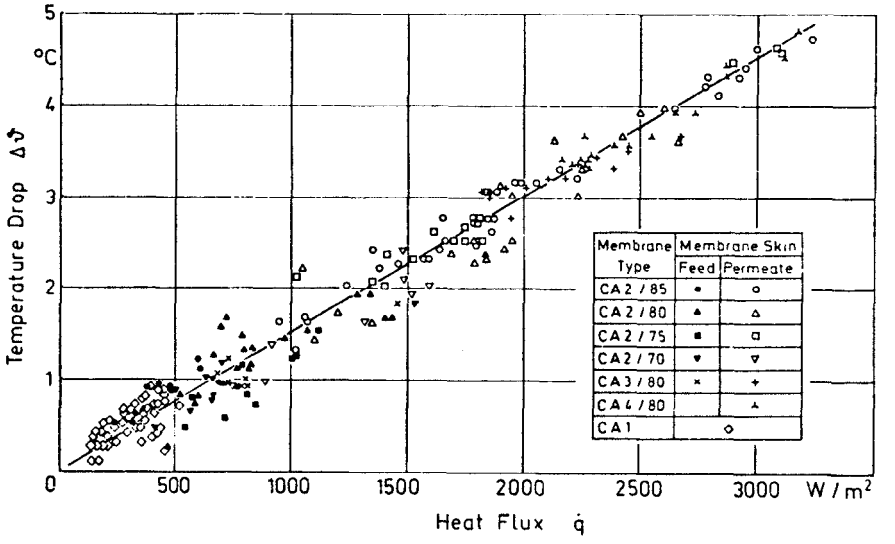


Figure 6.42: Temperature difference orthogonally to the membrane between bulk of feed and permeate.

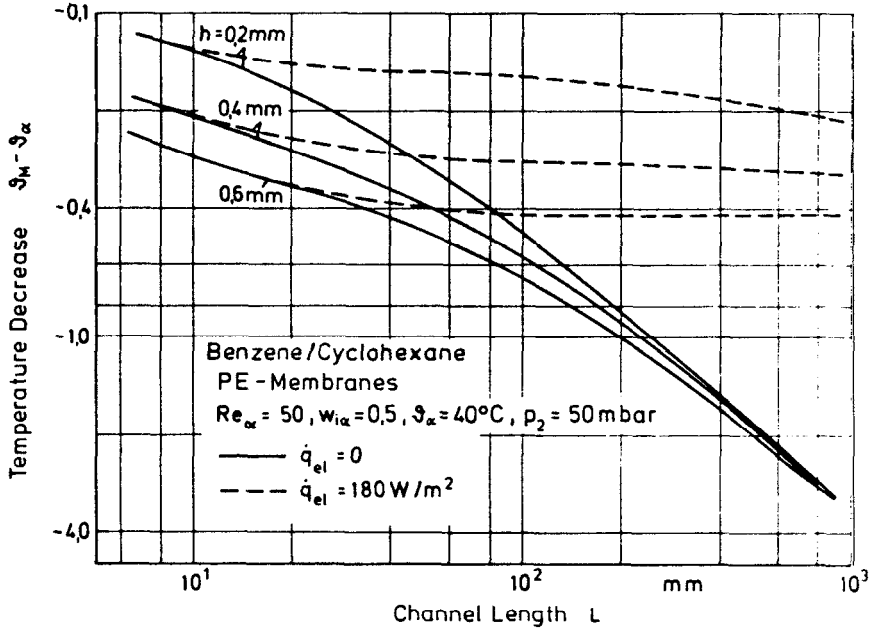


Figure 6.43: Temperature distribution of the feed along a membrane channel.

The major field of application for pervaporation will be either the separation of organic components with almost identical boiling characteristics or azeotropic mixtures. In most cases, the desired product quality cannot be achieved in a single step-either a combination of different processes or a "multi-stage" process will be necessary. In this case, a reflux-cascade has to be designed.

Figure 6.44 shows some results of a numerical optimization of pervaporation cascades.[32] Assumptions: (1) the selectivity is constant and equal for all stages; (2) the fluxes are small enough to neglect concentration polarization.

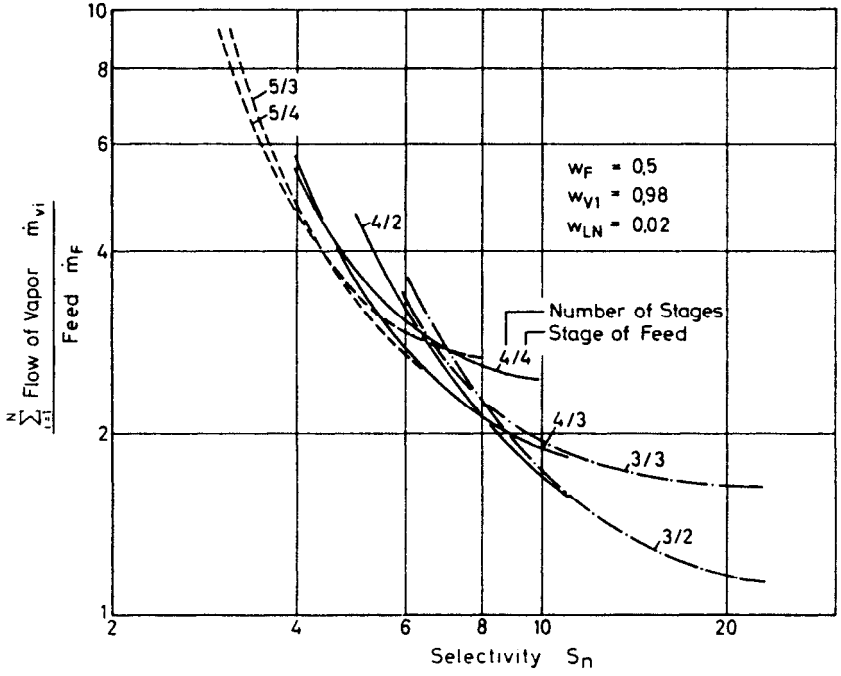


Figure 6.44: Optimisation of a reflux cascade for pervaporation: influence of selectivity on total permeate flow and number of stages.

Mostly, cascades are designed for either constant reflux, or constant cut rate or as a so-called "ideal cascade". Here, a different optimization procedure has been chosen: with respect to costs, the permeate flows are of prime importance and, therefore, the calculation was aimed at minimizing the sum of all permeate flows in the cascade.

Figure 6.44 clearly indicates that for a decreasing selectivity of the module the specific process costs will increase for two reasons:

(1) the number of stages increases and

(2) the membrane area increases because the internal permeate (reflux) flows increase.

There already exist applications of pervaporation on a technical scale. A

hybrid process (Figure 6.45) for the production of pure alcohol, combining distillation and pervaporation, proved superior to the conventional approach (extractive distillation) with respect to specific energy consumption (1 kg/kg ing to Figure 6.45, the alcohol concentration is increased from about 80% to 99.5% by only one pervaporation stage.[33] It should be noticed, that for this range of concentrations membranes for which water is the preferable permeating component must be used.

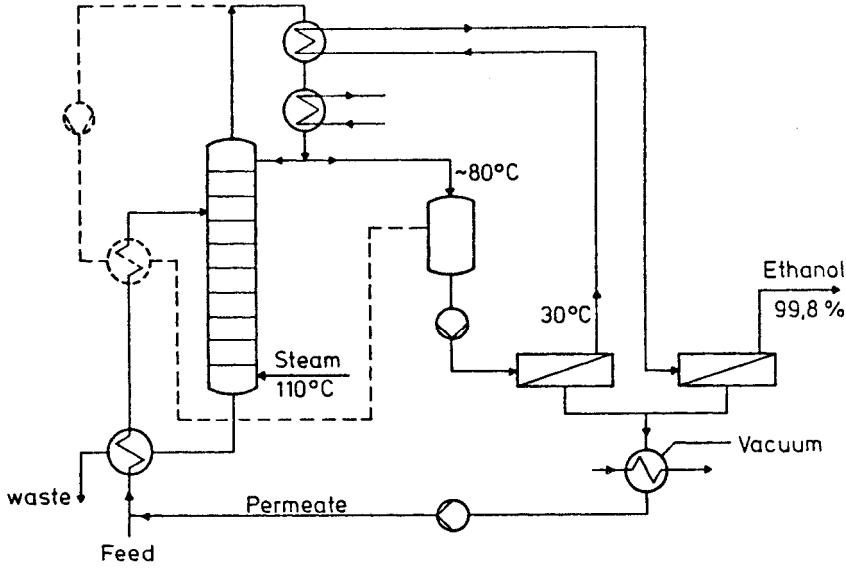


Figure 6.45: Hybrid-plant for production of pure alcohol.

Although the high separation potential of permeation has been demonstrated for a number of systems in laboratory experiments,[30] pervaporation seems to be economical only in cases where high product purities are required–and in combination with a conventional separation process. This statement is based at present only on a detailed analysis of the separation of benzene/cyclohexane and corroborated by the abovementioned production of pure alcohol, but there can be no doubt that the results are valid for many other systems as well.

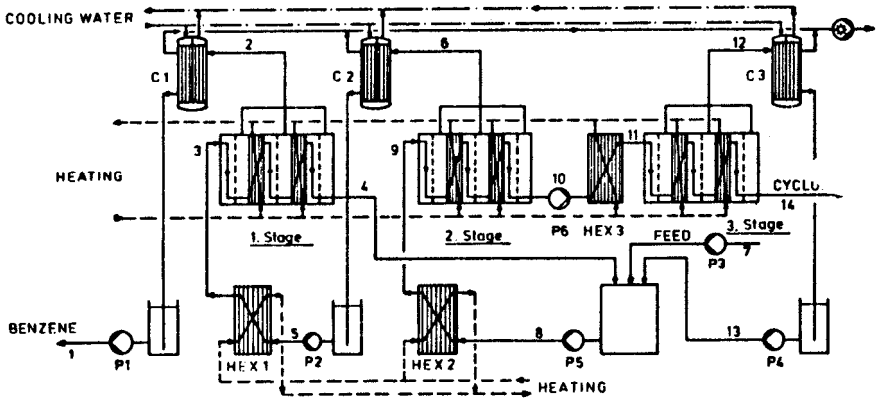
The fractionating of a 50% benzene-cyclohexane mixture into products of 98% purity is normally achieved by extractive distillation with furfural as a carrier. If pervaporation is to be employed instead, at best a three stage cascade with the refluxes indicated in Figure 6.46 is needed, where each stage consists of a combination of membrane-modules and heat exchangers. In a numerical calculation, the temperature decrease "along" each module is a free parameter. In Figure 6.46, this temperature decrease is set equal for each module (7.5 K). This leads directly to the necessary number of heat exchangers and membrane units per stage and to the necessary heat transfer area.

The flow-sheet indicates a major difficulty of the process: if the membrane selectivity is high, fluxes will vary markedly with the feed concentration of the

preferably permeating component. Permeate fluxes might differ by a factor of 10 between the first and the last stage if the same membrane is employed throughout the cascade. Compared to extractive distillation, a pervaporation cascade will not be competitive (Table 6.4); investment costs as well as operating costs are much higher. Especially noted should be the high costs for condensation–a direct consequence of the low pressure (150 mbar) at the permeate side. (Entrance temperature of the cooling water was assumed to be 20°C.)

The situation is different if product purities of about 99.5% are required. In this case, the energy consumption of the extractive distillation is very high because of the high reflux ratio (in the extractive distillation tower, the effectiveness of the carrier is rapidly decreasing in the section above the feed tray for the carrier and as a consequence, benzene will "enrich" in this section).

	1 Stage	2 Stage	3 Stage
$\dot{J}$ [kg/m²h]	2,83	1,43	0,16
ξ_{ij} —	7,48	8,94	7,92
ϑ [°C]	70,9	70,5	70,8
F_M [m²]	621	4940	6998
n_{HEX} —	6	26	10
F_{HEX} [m²]	9,5	41	6,2



	1	2	3	4	5	6	7	8	9	10	11	12	13	14
$\dot{m}$ [kg/h]	1760	1760	7040	5280	7040	7040	3520	9905	9905	2865	2865	1105	1105	1760
w_i [Gew-%]	98	98	88,2	85	88,2	88,2	50	67,5	67,5	16,4	16,4	39,3	39,3	2
ϑ [°C]	29,1	70,9	75	68,1	27,5	70,5	75	66,9	75	67,5	75	70,8	25,9	67,7

Figure 6.46: Flow sheet of an optimized cascade for the separation of a 50% benzene-cyclohexane mixture, product quality 98% benzene and cyclohexane. ($\Delta\vartheta$ = 7.5 K per membrane unit).

A hybrid process according to Figure 6.47 with a one-state pervaporation for final purification of the top product of the extractive distillation shows a cost advantage of 20%, compared to pure extractive distillation, even for very conservative assumptions. The calculations are based on the following assumptions:

(1) Capacity N_F = 40 kmol/h

(2) Equimolar feed of benzene (1) - cyclohexane (2)

(3) Product purities x_{21} = 0.992 and x_{12} = 0.995

(4) Effective thickness of the membrane = 8 μm

The optimal feed concentration of the pervaporation unit depends on carrier flow rate, reflux ratio and number of theoretical trays of the extractive distillation. Retentate concentration and cut rate of the pervaporation stage follow from the requested product quality $x_{11} + x_{31} \leqslant 0.008$. For the design of the pervaporation stage, the worst case has been assumed that only benzene and no furfural (3) will pervaporate. The major factor for the cost reduction is the much lower energy consumption of the hybrid process of 1.18 t/h heating steam against 1.7 t/h for the conventional process.

Table 6.4: Extractive Distillation vs. Pervaporation–Cost Analysis

		spec. costs $\frac{DM}{t_{product}}$	
		extractive distillation	pervaporation
Investment costs	sieve-tray column	6,11	--
	module	--	4,85
	evaporator/heat exchanger	4,43	2,67
	condensor	1,41	6,33
	pumps	0,45	0,72
	piping	1,86	2,19
Operating costs	membranes (DM 100/m²)	--	43,65
	steam	18,81	14,44
	cooling water	1,38	12,69
	power	0,09	0,04
total costs		34,54	87,58

Assumptions

1) membrane service lifetime 20 months
2) cost of piping = 15 % of cost of main items
3) linear amortization within 5 years, 10 % interest
4) Pervaporation: ϑ_α = 75 °C
   $\vartheta\nu$ = 3 K per membrane unit (optimal $\Delta\vartheta$)
   δ_M = 8 µm
   reflux ratio in stage 1: $\frac{\dot{L}_{1\omega}}{\dot{L}_{1\alpha}}$ = 0.75
   p_2 = 150 mbar
   extractive distillation: reflux ratio
   column I: v_I = 2.5, column II: v_{II} = 1

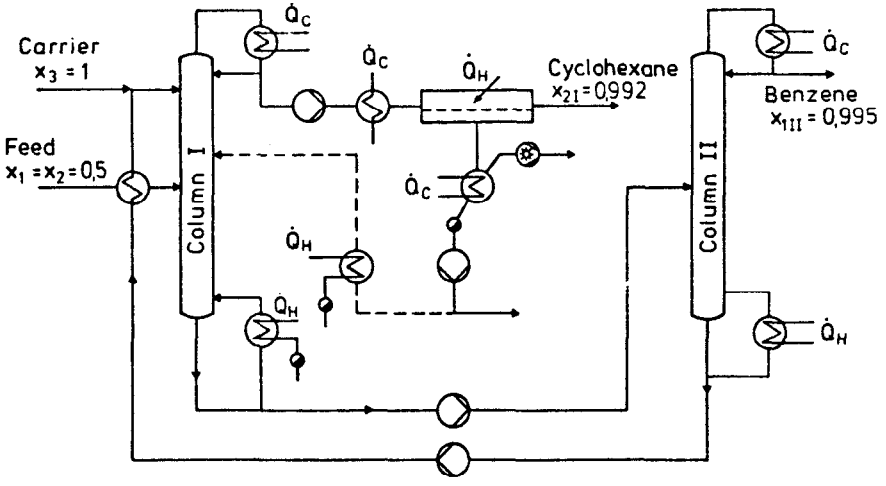


Figure 6.47: Flowsheet of a hybrid-process "extractive distillation-pervaporation" for the production of 99.2% cyclohexane.

According to Table 6.5, a further reduction of the specific separation costs is feasible if the effective membrane thickness can be reduced, for example, by employing "optimized" asymmetric membranes.[31] It should be noted, that the optimal feed concentration of the pervaporation unit is not only determined by the design of the extractive distillation but by the effective membrane thickness (or specific membrane costs) as well. With increasing permeate fluxes, or lower specific membrane costs, the optimal feed concentration is shifted to higher benzene concentrations.

Table 6.5: Hybrid-Process. Influence of Membrane Thickness on Process Costs and Optimal Intermediate Concentration $x_{1\alpha}$ of the Hybrid Process

Feed Concentration			Product Concentration			δ_{Ma}	Costs [DM/t]		
$x_{1\alpha}$	$x_{2\alpha}$	$x_{3\alpha}$	$x_{1\omega}$	$x_{2\omega}$	$x_{3\omega}$	[µm]	PV +)	Dist.	Total
0,0062	0,9911	0,0027	0,0052	0,9920	0,0028	8	10,55	63,96	74,51
0,0071	0,9899	0,0030	0,0048	0,9920	0,0032	4	11,41	53,39	64,80
0,0100	0,9865	0,0035	0,0039	0,9920	0,0041	2	14,25	41,18	55,43
Extractive Distillation			0,0055	0,9920	0,0025			93,65	

+) Reference-Stream: Retentate + Distillate of Column II

REFERENCES

1. Sherwood, T.K., Pigford, R.L., Wilke, C.R., *Mass Transfer*, McGraw-Hill Kogakusha, Ltd., Tokyo, 167/169 (1975).
2. Blaisdell, C.T., Kammermeyer, K., *Chem. Eng. Sci.*, 28, 1249 (1973).
3. Gill, W.N. and Bansal, B., *AIChE J.*, 19, 823/831 (1973).
4. Hwang, S.T. and Thorman, J.M., *AIChE J.*, 26, 558/566 (1980).
5. Kammermeyer, K., *Chem.-Ing.-Tech.*, 48, 672/675 (1976).
6. Weller, S. and Steiner, W.A., *J. Appl. Phys.*, 21, S. 279 (1950).
7. Naylor, R.W. and Backer, P.O., *AIChE J.*, 1, S. 95 (1955).
8. Blaisdell, C.T. and Kammermeyer, K., *Chem. Eng. Sci.*, 28, S. 1249 (1973).
9. Breuer, M.E. and Kammermeyer, K., *Seperation Science*, 2, 319 (1967).
10. Hwang, S.-T. and Kammermeyer, K., "Membrane in Separations", *Techniques of Chemistry*, Volume VII, John Wiley & Sons (1965).
11. Walawender, W.P. and Stern, S.A., *Separation Science*, 7, 5, S. 553-584 (1972).
12. Thorman, J.M., Engineering Aspects of Capillary Gas Permeators and the Continuous Membrane Column., Dissertation, University of Iowa (1979).
13. Hwang, S.T. and Thorman, T.M., *AIChE J.*, 26, 4, 558/566 (1980).
14. Hwang, S.T. and Ghalchi, S., *J. Membr. Sci.*, 11, 187/198 (1982).
15. Rautenbach, R. and Dahm, W., *Chem. Eng. Technol.* 10, 256-261 (1987).
16. Rautenbach, R. and Arzt, B., *The Arabian Journal for Science and Engineering*, Vol. 8, No. 3 (1983).
17. Andrews, W.T. and Berman, R.A., "The Malta Seawater RO Facility" presented at the First World Congress on Desalination and Water Re-Use, Florence (Italy) 23-27 (May 1983).
18. GVC, *Seawater Desalination—Water Pretreatment and Conditioning*, Editor: VDI-Gesellschaft Verfahrenstechnik und Chemie-ingenieurwesen, Düsseldorf (FRG).
19. First World Congress on Desalination and Water Re-Use, Florence (Italy) (May 1983).
20. Proceedings of the 7th International Symposium on Fresh Water from the Sea, Amsterdam, 23-26 (September 1980).
21. Henne, K.-H., Ph.D. Thesis, RWTH Aachen (1981).
22. Rautenbach, R. and Henne, K.-H., "Total Desalination of Brackish Water," Proceedings of the 7th International Symposium on Fresh Water from the Sea, Amsterdam, Vol. 1, 163-171 (1980).
23. Paul, H., Schock, G. and Rautenbach, R., *Maschinenmarkt*, 89, S. 1785-1988 (1983).
24. Rautenbach, R., Schock, G. and Paul, H., *Fette, Seifen, Anstrichm.*, 86, 1, 1-46 (1984).
25. McNulty, K.J. and Goldsmith, A.Z., Gollan, US-NTIS-Rep. PB 266919 (Feb. 1977).
26. Monsanto-Communications, Symposium in Scheveningen (NL) 24.03. (1982).
27. Schell, W.J. and Houston, C.D., *Use of Spiral-Wound Gas Permeators for Purification and Recovery* (1982).
28. Heisler, E.G., *Science*, 124, 77/78 (1956).

29. Binning, R.C. and James, F.E., *Petroleum Refiner*, 37, 5, 214-216 (1958).
30. Aptel, P., Cuny, J., Challard, N. and Neel, J., *J. Membr. Sci.*, 1, 271-287 (1976).
31. Rautenbach, R. and Albrecht, R., On the Behavior of Asymmetric Membranes in Pervaporation, European Workshop on Pervaporation, Nancy, 21-22.9 (1982).
32. Albrecht, R., Pervaporation–Beiträge zur Verfahrensentwicklung, Ph.D. Thesis, RWTH Aachen (FRG) (1983).
33. Ballweg, A.H., Brüschke, H.A., Schneider, W., Tusel, G.F., et. al., Pervaporation Membranes–An Economical Method to Replace Conventional Distillation and Rectification Columns in Ethanol Distilleries, 5th Int. Symp. on Alcohol Fuel Techn., Auckland, New Zealand (1982).

7

Enzyme Membrane Reactors and Membrane Fermentors

Enrico Drioli, Gabriele Iorio and Gerardo Catapano

INTRODUCTION

A growing interest in the use of purified enzymes as biocatalysts in laboratory scale and industrial applications is being developed as an alternative to more traditional approaches, generally based on fermentation processes.

The number of papers and patents appearing in this field in recent years clearly indicate the existence of a new branch of biotechnology, known as "enzyme engineering," dealing with enzyme production, separation, purification and the development of their applications in enzymatic reactors.

Referring to specific literature[1,2] for a detailed presentation of enzymes and their properties, suffice it to say that enzymes are globular proteins which catalyze the complex of biological reactions of a living organism known as "metabolism". They are usually confined within living cells, often bound to cellular membranes. Enzymes are organized in colonies and synergistically cooperate; they catalyze specific reactions contributing to the energy balance of living cells and at the same time regulate their metabolic state.

Although enzymes play, in a specific reaction, a role similar to that of synthetic catalysts, leading to a substantial reduction of reaction activation energy, their catalytic action is extremely efficient and selective, well beyond the performances of synthetic catalysts. It is not surprising, therefore, that prospects of their possible applications has prompted an enormous interest both in universities and industries leading to a series of related developments, such as:

(a) Enhancement of the techniques to induce microorganisms to produce selected enzymes;

(b) Improved enzyme purification techniques;

(c) Engineering of techniques to immobilize enzymes or whole cells on or in solid supports;

(d) Development of techniques for enzyme usage in continuous flow reactors;

(e) Development of techniques toward the solid phase synthesis of peptides.

Enzymes produced by microorganisms such as fungi or bacteria have been used for years in batch fermentation plants for the production of pharmaceuticals, beverages, foods, etc. The availability of almost pure enzymes enables one to carry out specific reactions under mild conditions, to limit side-product formation and to perform the synthesis of chemically active compounds which would otherwise require extremely long reaction time, with low yields.

The use of enzymes as biocatalysts can therefore be of extreme interest for individual applications mainly for the advantages it implies in terms of energy consumption, safety, pollution prevention and materials preservation.

The traditional use of enzymes in batch stirred and similar reactors is however limited for the following reasons:

(a) High enzyme purification costs;

(b) Low productivity per reactor, per unit time;

(c) Difficult and expensive recovery and reuse of enzymes or cellular microorganisms;

(d) Product pollution;

(e) Difficulties in maintaining standard product quality.

Most of the above problems could be overcome using "immobilized enzymes", or in other words "enzymes confined or compartmentalized in a well defined region of space, which retain their catalytic properties and can be repeatedly and continuously used".[3] Several advantages can derive from the use of immobilized enzymes or microbial cells, such as:

(a) Opportunity to design processes in a more rational way;

(b) Cost cut-off in enzyme consumption;

(c) More compact plants;

(d) Operating costs cut-off;

(e) High productivity per unit time per equipment, with small amounts of side-products.

A lot of research work has therefore been performed in order to optimize immobilization techniques and procedures in view of the development of enzyme reactor engineering.

Traditional immobilization techniques include:

(a) Confinement in a gel;

(b) Encapsulation in a membrane shell;

(c) Adsorption on a surface;

(d) Covalent binding to an insoluble support;

(e) Copolymerization with a proteic carrier.

In Japan, a leading country in the development of enzymatic engineering, more than seventy enzymes have already been immobilized, but only ten of them are used in most existing applications. This limitation, compared to the great potential of immobilized enzyme systems, requires that research efforts be directed towards the realization of more efficient immobilization techniques characterized by low carrier costs, and the development of practical equipment.[4]

Membrane science can strongly contribute, in this sense, to further developments of immobilized enzyme reactors for industrial processes. This well assessed technology seems, in fact, very promising for the design of compact and flexible apparatus and particularly useful when a separation step is to be coupled to the chemical reaction.[5] A number of applications of membrane processes to biotechnology are already in operation.[6]

Insoluble carrier-fixed enzymes can be continuously used in stirred vessels or tubular reactors without catalyst loss, and can then be recovered by means of sedimentors, magnetic fields or similar apparatus.

On the other hand, in nature a continuous uptake of substrate and release of product without loss of biocatalysts is not achieved by carrier fixation but by means of cellular membranes. Efficient immobilized enzyme reactor systems for technical applications can therefore be established replacing cellular membranes by ultrafiltration or reverse osmosis synthetic membranes, and the activated transport through the cellular wall by a forced flow across the membrane.[7]

Ultrafiltration membranes can be used to retain enzymes in the reaction vessel due to size difference between the usual high molecular weight enzymes and most of the low molecular weight substrates and products; a homogeneous continuous catalysis can thus be achieved. Some membrane reactor configuration do not allow a homogeneous distribution of catalyst in the vessel so that the reactor acts in a more heterogeneous way. Depending on enzyme kinetics, different reactor configurations exist which are able to optimize system yield; systems where product concentrations are kept low and a continuous product removal occur are particularly interesting when dealing with product-inhibited enzymes, for instance see References 8–26.

Enzymatic systems in which membranes are simply used as separation media and not as catalyst carriers are traditionally called "enzyme membrane reactors" (EMR). Concentration polarization phenomena severely affect the performance of such reactors so that it is necessary to control the polarization layer onto membrane pressurized side by means of reactor fluid dynamics or design tricks. Fluid dynamic conditions in some of these reactors make them especially suitable for enzymatic systems for which a homogeneous catalyst distribution is particularly important, such as cofactor-requiring mono- and multi-enzyme systems.

Concentration polarization phenomena, which are the main drawbacks of the aforesaid enzyme membrane reactors, can nevertheless be used to form, either in dynamic or in static conditions, a gel layer of enzyme proteins on a membrane.[27-41] It is even possible to establish more than one enzyme layer and no coupling agent is needed to carry out the immobilization. Due to high protein

concentration on the membrane surface, enzyme stability can be improved over that in systems using enzymes homogeneously distributed in the reacting solution.[106] Reduced catalytic efficiency due to mass transport limitations and the possibility of preferential pathways in the enzyme gel layer can be typical system disadvantages.

Asymmetric hollow fiber membranes can also be used as selective supports for enzymes. A biocatalyst suspension can in fact be forced through the unskinned surface of asymmetric membranes so that biocatalysts, either enzymes or whole cells, although still suspended, are effectively immobilized within the macroporous spongy part of the membranes.[42–53] The enzymatic activity can thus be spread over a large surface, although substrates and products can only diffuse to and from the biocatalyst.

In certain applications, the size of the biocatalyst is not suitable for entrapment into the supporting sponge layer of asymmetric membranes. In these cases, the membrane acts mainly as a selective barrier; it defines a reactive zone in the vessel, usually the shell, accessible to substrates and products mainly by diffusive mass transfer preventing the catalyst from pollution or inhibition possibly caused by other species in solution.[54–69]

Enzymes can still be absorbed within symmetric macroporous membranes in order to establish high catalyst concentrations, cross-linked to prevent them from elution, or simply covalently or ionically bound either to symmetric or asymmetric membranes. In spite of short residence times, high conversions can be achieved in most kinds of enzyme membrane reactors.[70–83]

Last but not least, viable cells are grown and used in membrane fermentors for a wide range of applications.[84–98]

Our analysis of enzyme membrane reactors will range from systems proposed at bench scale to equipment already in operation at the industrial level, and from systems where enzymes are bound to membranes to apparatus where enzymes are simply confined in well-defined regions of the reaction vessel. In the following sections, we will refer to five main reactor configurations:

(a) Enzyme membrane reactors, where enzymes are continuously flushed along membranes;

(b) Dynamic enzyme gel layer reactors, where enzymes are immobilized in a proteic gel layer, dynamically or statically formed;

(c) Membrane segregated enzyme reactors;

(d) Membrane bound enzymes in continuous-flow systems;

(e) Membrane fermentors.

LIST OF SYMBOLS

The following symbols are used throughout this chapter.

A	Membrane surface area, L^2
a	Inner radius of the fiber, L

b	(b-a) is the thickness of the dense membrane region of the fiber wall, L
C	Concentration factor
C_g	Solid concentration in the gel, $M\ L^{-3}$
D	Diffusion coefficient, $L^2\ T^{-1}$
D'	Dilution rate, T^{-1}
D_e	Enzyme diffusion coefficient, $L^2\ T^{-1}$
D^L	Diffusion coefficient in the bulk liquid phase, $L^2\ T^{-1}$
D^S	Diffusion coefficient in the catalyst annulus, $L^2\ T^{-1}$
d	Outer radius of the fiber, L
E	Enzyme concentration, $M\ L^{-3}$
E_{diff}	Diffusive efficiency
E_{kin}	Kinetic efficiency
E_o	Initial enzyme concentration, $M\ L^{-3}$
E_S	Enzyme concentration in the bulk liquid phase, $M\ L^{-3}$
E_w	Enzyme concentration at membrane surface, $M\ L^{-3}$
F	Feed flow rate, $L^3\ T^{-1}$
J	Volumetric flux, $L^3\ L^{-2}\ T^{-1}$
K	Enzyme kinetic constant, T^{-1}
K_d	Enzyme activity decay constant, T^{-1}
K'_M	Enzyme Michaelis constant, $M\ L^{-3}$
K_s	Overall mass transfer coefficient, $L\ T^{-1}$
L	Reactor length, L
L_c	Critical reactor length, L
L_p	Membrane hydraulic permeability, $L^2\ T\ M^{-1}$
$M = K'_M/S_f$	Dimensionless Michaelis constant
$M' = K'_M/(\gamma_2(0)\ S_f)$	Dimensionless Michaelis constant for the segregated region
N	Overall enzyme amount in the reactor, M
N_f	Number of capillary membranes in a bundle
P	Product concentration, $M\ L^{-3}$
$Pe = v\ \delta\ /D$	Peclet number

$Pe' = v_{max}\ a\ /D_1$	Peclet number
P_f	Feed product concentration, $M\ L^{-3}$
P_o	Initial product concentration, $M\ L^{-3}$
P_r	Reactor productivity, or product moles (grams) per unit time, membrane area (reactor volume) and enzyme concentration, T^{-1}
Q	Flow rate, $L^3\ T^{-1}$
Q_{f1}	Fiber-to-shell permeate flow rate, $L^3\ T^{-1}$
Q_{f2}	Shell-to-fiber permeate flow rate, $L^3\ T^{-1}$
R	Reaction rate, $M\ T^{-1}\ L^{-3}$
r	Radial coordinate, L
$r' = r/a$	Dimensionless radial coordinate
$r'' = (r-a)/(d-a)$	Dimensionless position in the annular catalyst
r_e	Equivalent radius of the shear-free surface, L
S	Substrate concentration, $M\ L^{-3}$
S_f	Feed substrate concentration, $M\ L^{-3}$
$S^L = S/S_f$	Dimensionless substrate concentration in the bulk bulk liquid phase
S_o	Substrate initial concentration, $M\ L^{-3}$
$S^S = S/S_f$	Dimensionless substrate concentration in the catalyst annulus
S_w	Substrate concentration at membrane wall, $M\ L^{-3}$
s	Laplace coordinate
T_1	Downstream time constant (time lag), T
T_2	Downstream time constant (segregated region), T
TSS	Total suspended solids, $M\ L^{-3}$
t	Time, T
$u(t)$	Unit step function
V	Reactor volume, L^3
$V_{max} = K\ E$	Enzyme reaction rate at saturating substrate concentration, $M\ L^{-3}\ T^{-1}$
V_{maxo}	Initial value of V_{max}

V_{max}^{S}	Enzyme reaction rate at saturating substrate concentration, M L^{-2} T^{-1}
VSS	Volatile suspended solids, M L^{-3}
v	Linear velocity, L T^{-1}
$\bar{v} = v/v_{max}$	Dimensionless linear velocity
v_{max}	Maximum linear velocity, L T^{-1}
$X = (S_f-S)/S_f$	Conversion degree
$\bar{X}$	Anaerobic reactor VSS or TSS, M L^{-3}
X'	Cell concentration, M L^{-3}
X'_1	Cell concentration entering the membrane module, M L^{-3}
X'_2	Cell concentration in the recycle stream, M L^{-3}
x	Space coordinate, L
x_e	Enzyme penetration depth, L
Y	Organism yield coefficient, i.e. mass of cells formed/mass of nutrients
Z	Axial distance from the inlet of the reactor to achieve a given conversion, L
$Z' = D^L x/(2 v_{max} a^2)$	Dimensionless axial coordinate
Z_{diff}	Dimensionless reactor length characteristic of operation under diffusion control
Z_{kin}	Dimensionless reactor length characteristic of operation under kinetic control
z	Dimensionless transversal coordinate
$z' = x/(a\ Pe')$	Dimensionless axial coordinate.

Subscripts

a, b	Refer to region A, B, respectively
1, 2, 3, 4	Refer to region 1, 2, 3, 4, respectively

GREEK SYMBOLS

$\alpha = \delta\ A/V$	
α'	Recycle ratio
$\alpha_0 = V_{max}^S /(S_0\ v)$	Dimensionless zeroth order kinetic parameter
$\alpha_1 = V_{max}^S/(K'_M\ v)$	Dimensionless first order kinetic parameter
$\beta = J\ /(D/\delta)$	
$\beta^* = S_f\ /K'_M$	Reciprocal dimensionless Michaelis constant
$\gamma = S\ /S_f$	Dimensionless substrate concentration
γ'	Membrane partition coefficient
$\gamma^* = K'_M\ D^S\ /[V_{max}\ (d-a)^2]$	Thiele modulus
$\gamma_p = P/P_0$	Dimensionless product concentration
γ_p	Laplace transform of dimensionless product concentration
$\gamma_S = S/S_0$	Dimensionless substrate concentration
δ	Gel layer thickness, L
η	Effectiveness factor
$\theta = t\ v^2\ /D$	Dimensionless time
$\theta^* = (\theta - \tau_1)$	Dimensionless time
$\theta' = K'_M\ /S_f$	Dimensionless Michaelis constant
λ	Length of the characteristic dimension of the segregated gel region, L
$\lambda' = \left(\frac{V_{max}\ a^2}{K'_M\ D}\right)^{1/2}$	Thiele modulus
μ^*	Specific cell growth rate, T^{-1}
μ	Solution viscosity, $M\ T^{-1}\ L^{-1}$
$\xi = x\ v\ /D$	Dimensionless space coordinate
$\xi' = x\ /\delta$	Dimensionless space coordinate
Π	Pressure, $M\ L^{-1}\ T^{-2}$
Π_b	Pressure of the bulk phase within the capillary membrane, $M\ L^{-1}\ T^{-2}$
Π_{bi}	Pressure of the bulk phase at the inlet of the capillary membrane, $M\ L^{-1}\ T^{-2}$

Π_{onc} Oncotic pressure, $M\ L^{-1}\ T^{-2}$

Π_S Shell side pressure, $M\ L^{-1}\ T^{-2}$

ρ Dimensionless reaction rate,

$\rho = \alpha_1\ \gamma_S$ for first order kinetics

$\rho = \alpha_0$ for zero order kinetics

$\tau = V/Q$ Reactor time constant, T

$\tau_1 = T_1\ v^2\ /D$ Downstream dimensionless time constant (time lag)

$\tau_2 = T_2\ v^2\ /D$ Downstream dimensionless time constant (segregated region)

$\Phi = \left(\frac{K\ E\ \delta^2}{D\ S_f}\right)^{1/2}$ Thiele modulus

$\Phi'' = \left(\frac{K\ E\ \lambda^2}{D\ \gamma_2(0)\ S_f}\right)^{1/2}$ Heterogeneous gel model Thiele modulus

$\phi = \lambda'^2\ \theta'$

$\chi = S\ /\gamma_2(0)\ S_f$ Dimensionless substrate concentration within the gel layer

$\psi(z) = e^{-z^2} \int_0^z e^{u^2}\ du$ Dawson's integral

$\omega = (d-a)\ D^L/(a\ D^S)$ Ratio of diffusion rate in the bulk phase to that in the porous catalyst

ENZYME MEMBRANE REACTORS (EMR)

During the last ten years enzyme technology has moved mainly towards the development of new immobilization techniques and the improvement of those already existing. In turn, the attention of applied research has been focused on the engineering of systems based on immobilized biocatalysts. Enzymes involved in this development were enzymes catalyzing simple reactions that normally require no cofactors. A number of drawbacks affected the use of immobilized enzymatic preparations. An often dramatic reduction of initial enzyme activity due to the binding process, and the existence of diffusional resistances limits this approach with low activity enzymes, with macromolecular substrates and in general with enzymes whose cata-

lytic behavior is strongly dependent on a good mixing of catalyst and substrate. Biotechnological processes based on immobilized biocatalysts have not been successful with coenzyme-dependent reactions. Moreover, removal of deactivated enzymes or cells from the solid support often raises serious problems and sometimes is not convenient.

Instead of being immobilized, enzymes or cells can be confined in the vessel of dialytic or ultrafiltration cells, in a configuration that is commonly called "enzyme membrane reactor" (EMR). An EMR is a reactor system where ultrafiltration or dialysis membranes with a suitable molecular weight cut-off are used in order to keep larger components in the reactor vessel, i.e. enzymes and/or macromolecular substrates, while low-molecular-weight molecules, e.g., products and/or inhibitors, are allowed to pass freely through the membrane, thus leaving the reactor as permeate. In this set-up, typical advantages of immobilized preparations, together with easy recovery of deactivated enzymes and replacement with fresh catalysts are achieved; inhibitors are moreover continuously removed from the reaction vessel. The direct and deep contact between substrates and biocatalysts limits diffusional resistances, while no activity losses due to fixation to the carrier occur, thus maximizing the activity of the biocatalyst.

Depending on the flow dynamics of the reaction vessel, it is possible to distinguish between reactors equipped with flat UF membranes or hollow fibers.

So far, both dead-end and CST UF cells with flat membranes have been proposed as enzymatic reactors (Figure 7.1).

Performance of dead-end units is largely affected by the flow dynamics of the system; in fact, mixing of substrates and catalysts is not fully accomplished, and concentration polarization phenomena strongly limit reactor performance. On the one hand, the existence of a polarization layer above the membrane surface significantly reduces permeate flow rates; on the other hand, enzymatic conversion is achieved mostly inside a highly concentrated polarization layer giving lower conversions as compared to those obtained with the same amount of enzyme uniformly distributed within the reactor.

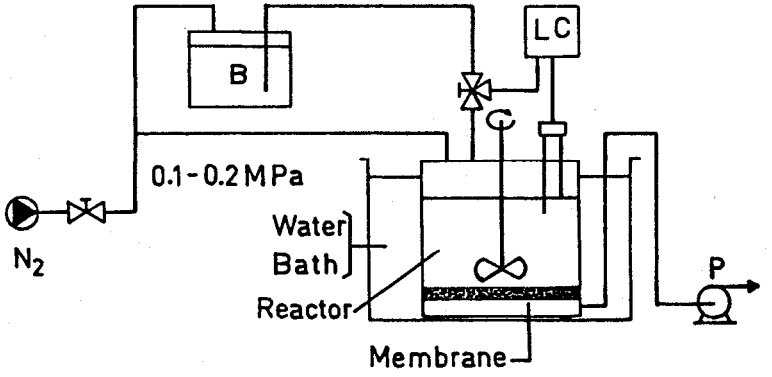


Figure 7.1: Experimental set-up of an enzyme membrane reactor.[11] P: peristaltic pump; LC: level controller.

CST reactors have been more widely adopted, partly due to the possibility of concentration polarization control, and partly due to the easy modeling of enzyme kinetic behavior. In the literature, comprehensive mathematical descriptions of the kinetic behavior of enzymes located in CSTR UF units are reported[8,9,10] as far as low-molecular-weight substrates are concerned.

Assuming complete mixing within the reactor so that enzyme and substrate concentration in the reactor vessel are uniform, and the latter is equal to its value in the permeate, substrate mass balance in molar form generally looks like:

$$(S_f - S)/\tau = R(S,P) \tag{1}$$

Product steady state mass balance similarly appears as:

$$(P - P_f)/\tau = R(S,P) \tag{2}$$

Assuming that substrate conversion obeys the simple Michaelis-Menten model, substrate steady state mass balance reduces to:

$$XS_f + [X/(1 - X)]\, K'_M = KEV/Q \tag{3}$$

R being expressed as $K\ E\ S/(K'_M + S)$.

The equation in this form is a useful tool to estimate parameters of reaction kinetics. Instead of performing nonlinear parameter estimation procedures, the functional dependence of XS_f on $X/(1 - X)$ can be plotted. The plot should look like a straight line whose slope is $(-K'_M)$ and whose intersection with the XS_f axis is given by the point of coordinate $(V_{max}\tau)$. Hence, it furnishes a rapid graphic procedure to obtain rough estimates of kinetic parameters.

When more complex kinetics are involved, so that the substrate rate of conversion is dependent on both substrate and product concentrations, combining Equations 1 and 2 with the rate equation eventually leads to an implicit Equation:[9]

$$(P - P_f)/\tau = R(P) \tag{4}$$

Product concentration in the permeate can then be determined either with numerical procedures or with graphic techniques. True reactor operating point at steady state is given by the intersection point of the straight line representing mass balance and the curve of the reaction term.[8,10,99] As can be seen from Figure 7.2, for α-ketoisocaproate conversion to L-leucine, the slope of the convective term is reciprocally proportional to the mean residence time. If multienzymatic systems are used as the biocatalyst, it must be outlined that the reaction term is the course of the reaction rate relative to the substrate conversion of the key component.[10]

Enzyme activity is usually not constant with time.

Physiochemical changes in enzyme structure, thermal denaturation and microbial contamination cause enzyme activity to continuously decrease with time. When enzymes or cells are compartmentalized in UF cells, biocatalyst losses can even occur due to the wrong choice of membrane molecular weight cut-off. It is conventional to measure the enzyme stability in terms of its half-life, $t_{½}$, that is the time at which enzyme activity is reduced to half its initial

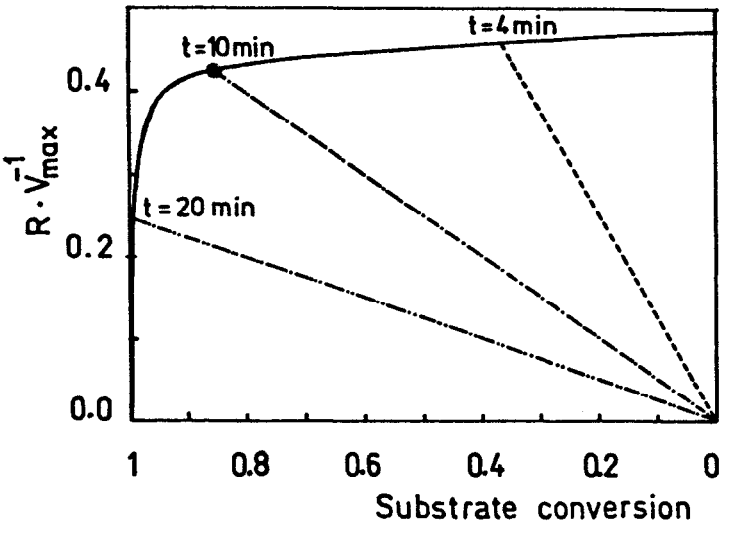


Figure 7.2: Relative reaction rate of the formate dehydrogenase-leucine dehydrogenase (FDH-LEUDH) system as a function of substrate conversion.[10] FDH = 20 U/ml; LEUDH = 20 U/ml.

value. Since biotransformations by means of enzymes are continuous processes, as long as the reactor working life is longer than the native enzyme half-life, enzyme activity decay with time must be taken into account in order to correctly assess reactor performance, or a strategy in reactor operation. A transient substrate mass balance on the CST reactor leads to the Equation:[8]

$$V[dS(t)/dt] = Q[S_f - S(t)] - V_{max}V \qquad (5)$$

Let us assume that substrate inlet concentration is much higher than the enzyme's apparent Michaelis constant, K'_M, so that enzyme kinetics is expressed according to zero order kinetics, i.e., $R = KE = V_{max}$.

Enzyme activity decay can be expressed in terms of the Arrhenius Equation:

$$E = E_o \exp(-K_d t) \qquad (6)$$

where K_d is the deactivation constant. Equation 5 then takes the form

$$[S_f - S(t)]/\tau - dS(t)/dt = V_{maxo} \exp(-K_d t) \qquad (7)$$

Integration of the differential Equation 7 leads to estimate the outlet substrate concentration:[8]

$$S(t) = V_{maxo} [\exp(-t/\tau) - \exp(-K_d t)]/(1/\tau - K_d) + S_f \qquad (8)$$

Figure 7.3 shows good agreement of experimental data and theoretical predictions for benzaldehyde conversion by *Rhodotorula Mucilaginosa.*[8]

For $t>5\tau$, $\exp(-t/\tau)$ contribution can be neglected so that enzyme half life time, $t_{1/2}$ can be expressed as:

$$t_{1/2} = \ln[V_{maxo}/[(1/\tau - K_d)\ (S_f - S_o)/2]]/K_d \qquad (9)$$

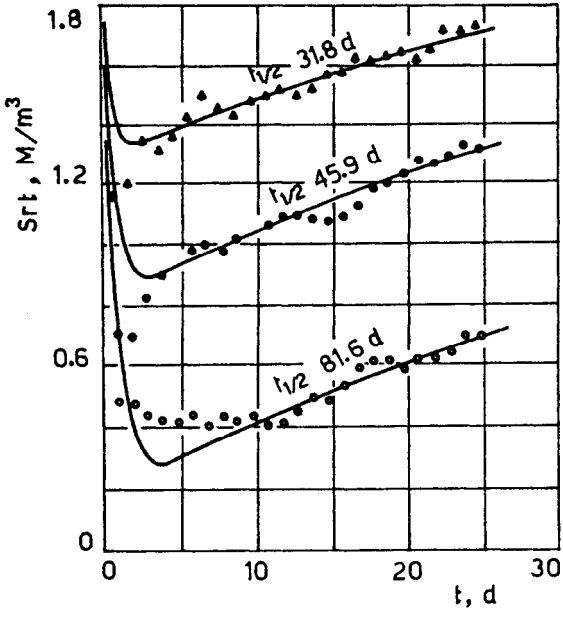


Figure 7.3: Experimental and (solid lines) theoretical plots of substrate concentration (S) as a function of time, for various retention times: (△) 0.417 days, (●) 0.520 days, (○) 0.695 days.[8]

Estimate of the deactivation constant can be graphically carried out from Equation 7 plotting $\ln[[S_f - S(t)]/\tau - dS(t)/dt]$ vs t (Figure 7.4). A straight line is thus obtained whose slope is given by $(-K_d)$ and the line intersects the vertical axis at the point of coordinate $(\ln V_{maxo})$.

When the reacting solution is fed to the system, low-molecular-weight products leave the reactor permeating the membrane, whereas enzymes are partially or totally rejected. Then, enzymes tend to accumulate in a thin layer immediately upstream from the membrane causing polarization phenomena to occur. The extent to which concentration polarization affects reactor performance depends on the balance of rejected solutes, e.g., enzymes or cells, accumulation due to membrane rejection and back diffusion to the bulk phase, and eventually on the flow dynamics of the reacting vessel.

For macromolecules (like most biocatalysts), if membrane properties are carefully chosen, membrane rejection is usually very good, while biocatalyst

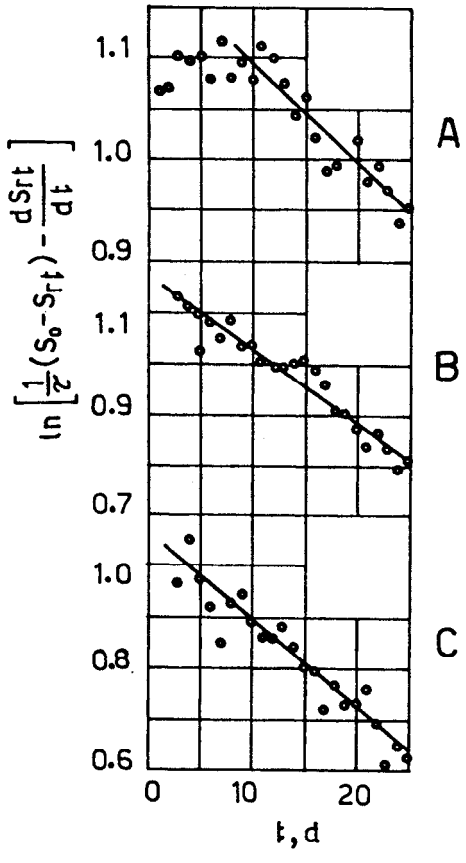


Figure 7.4: Values of V_{maxo} and K_d for various retention times: (A) 0.695 days; (B) 0.520 days; (C) 0.417 days. Straight lines are approximations of experimental data to a straight line calculated from Equation 7.[8]

back diffusion towards the bulk phase is extremely slow. The effect of concentration polarization on such reactor performances can then be significant. Figure 7.5 shows a schematic of the situation. Applying the thin film theory to a region immediately upstream from the membrane results in the following steady state mass balance equation:[100,101]

$$J E = - D_e dE/dx \qquad (10)$$

under the B.C. $x \rightarrow \infty \quad E = E_S$.

Under the assumption of totally rejected enzyme macromolecules, integration of Equation 10 allows one to express the ratio of enzyme concentration in the bulk solution in the presence of concentration polarization, to its

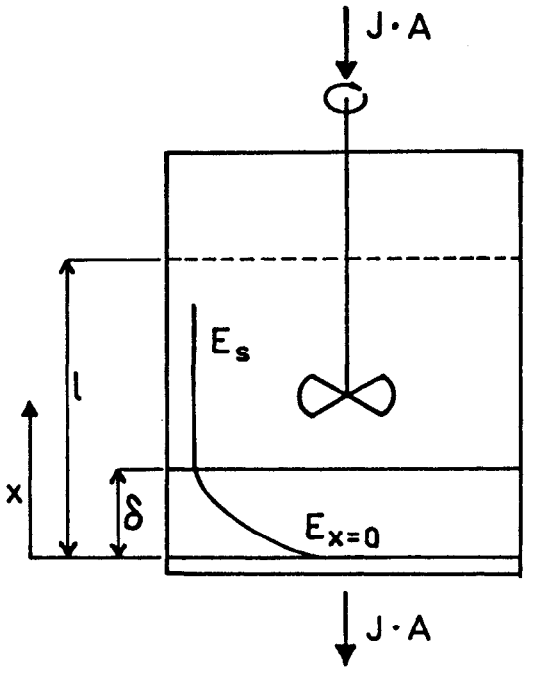


Figure 7.5: Schematic diagram of enzyme membrane reactor.[9]

value in the absence of concentration polarization phenomena as:[9]

$$E_S/E_o = 1/[(1-\alpha) + (\alpha/\beta)\,[\exp(\beta)-1]] \qquad (11)$$

Enzyme concentration at the membrane-solution interface can thus be related to enzyme concentration in the bulk phase by the following equation:

$$E_w = E_S \exp(\beta) \qquad (12)$$

where the dimensionless parameter β is a measure of convective mass transfer, J, relative to the overall mass transfer, D/δ, more generally K_s.[102] Figure 7.6 shows how dramatic the change of enzyme bulk concentration can be, with changes in permeate flow rate, and hence applied pressure. Doubling flow rate from 4 to 8 ml/min results in an 8-fold decrease of fractional bulk concentration of soluble enzyme, from 97% to 12% for the cellobiose/cellobiase system.

Changes in enzyme bulk concentration may induce a large reduction in reaction rate within the membrane reactor. Figures 7.7 and 7.8 give evidence of the existence of enzyme deactivation phenomena which can be misleading in the evaluation of reactor performances, and/or of the thickness of the boundary layer close to the membrane surface in accordance with Equation 12.

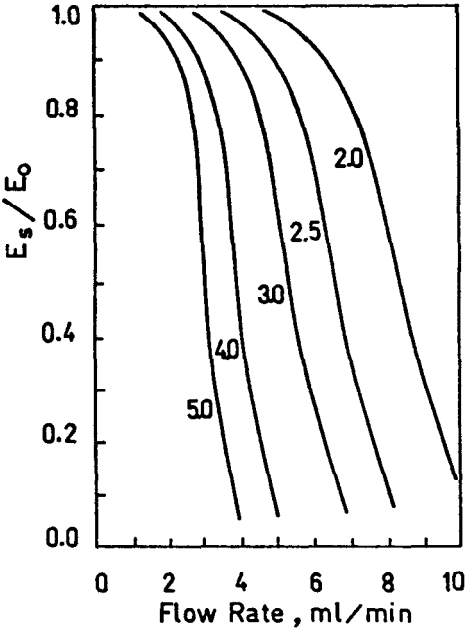


Figure 7.6: Dimensionless bulk concentration (E_s/E_o) versus flow rate for a membrane reactor with a PM 10 membrane.[9] V = 300 ml, A = 39.2 cm^2, D = 6.8 x 10^{-7} cm^2/s. The parameter is gel thickness times 1,000 cm.

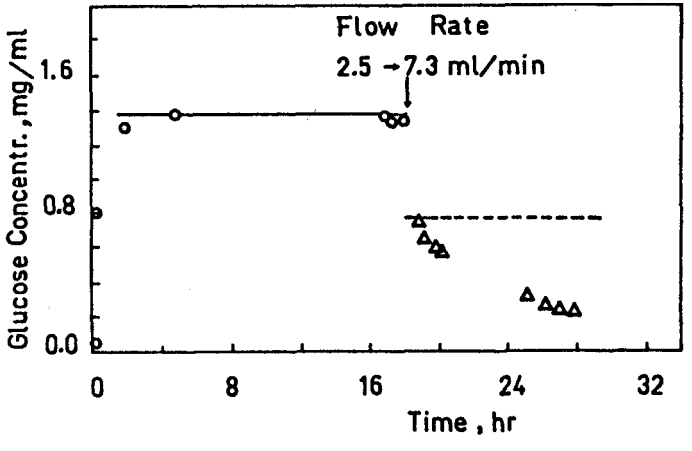


Figure 7.7: Concentration of glucose in permeate versus reaction time: (○) at flow rate of 2.5 ml/min, solid line is expected level for ideal operation (1.37 mg/ml); (△) at flow rate of 7.3 ml/min; dotted line is expected level for ideal operation (0.77 mg/ml).[9]

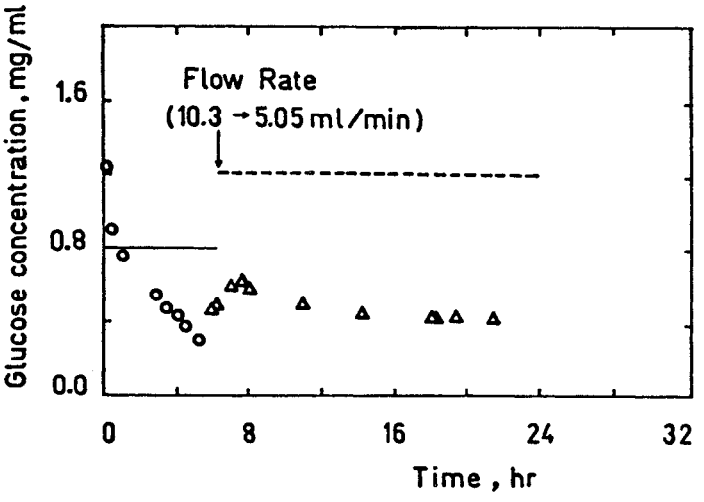


Figure 7.8: Concentration of glucose in permeate versus reaction time: (○) at flow rate of 10.3 ml/min; solid line is expected level for ideal operation (0.8 mg/ml); (△) at flow rate of 5.05 ml/min; dotted line is expected level for ideal operation (1.21 mg/ml).[9]

Under given stirring conditions, therefore, a critical value of flow rate and hence of applied pressure does exist. At flow rates lower than the critical value, the reactor always attains steady operation conditions; and correspondingly outlet product concentration is constant. Beyond the critical value, concentration polarization phenomena promote the localization of a large fraction of enzymes near the membrane surface, seldom leading to an enzymatic gel formation.[9] Correspondingly, an accelerated deactivation of enzyme activity is superimposed on reactor performance thus hindering the attainment of steady state conditions. Experimental evidence suggests that the contribution of polarized enzymes to overall conversion can be negligible, due to the consistency of product concentration in the bulk phase of the reactor and in the permeate. As suggested by Tsao et al,[9] a continuous conversion decrease, as concentration polarization occurs, can be attributed to the localization of large amounts of enzymes in a region immediately upstream from the membrane; in a stirred UF unit proteic coiled macromolecules in the polarization layer are subjected to a high shear field due to stirring, which can result in protein unfolding and consequent denaturation. Overall enzyme deactivation is moreover accelerated by the exchange of deactivated enzymes in the polarization layer with fresh enzymes in the bulk solution via a coupled diffusion-convection mechanism. Irreversible enzyme deactivation is confirmed by the discrepancy between the expected values of conversion and experimental data as applied pressure is slowed down from hypercritical to subcritical values (Figure 7.8). Boundary layer thickness under such conditions cannot be easily estimated from the conversion at various permeate flow rates. Enzyme deactivation, being

superimposed on the enzyme concentration decrease in the bulk phase, can be misleading. It is to be noted that deactivation phenomena are less prominent for enzymes stable to shear stresses.

When macromolecular substrates are involved in the transformation under study, concentration polarization phenomena affect the EMR performance more severely. Diffusion limitations of macromolecular substrates hamper the use of immobilized enzymes in the hydrolysis of high-molecular-weight substrates. By selecting membranes with an appropriate molecular weight cut-off, both enzyme and substrate are retained in an EMR in touch with each other, and hydrolysis products and/or inhibitors are continuously removed from the system. Soluble enzymes can then act directly on substrate macromolecules without diffusion limitations and steric hindrance imposed by enzyme fixation to a solid support. The stirring features of CST EMRs moreover assures that substrates and/or inhibitors within the reactor vessel are maintained at the lowest possible concentration level. Such reactor configuration is then extremely useful when substrate inhibited reaction patterns are involved, or when inhibiting species are assumed to exist in the feed stream.

Diafiltration,[11] semicontinuous[12] and continuous operational modes[13-15] have been proposed and applied for saccharification of cellulose[11,12,14,15] and protein hydrolysis.[9] As far as the first two operational modes are concerned, Figure 7.9 shows typical curves of product concentration as a function of time for the hydrolysis of cellulose according to a diafiltration operational strategy, at different space velocities. A peak is always observed in the first period of operation, more marked for lower residence times, followed by a slow decay. Initial sudden increase in product concentration in the permeate occurs earlier at lower residence times, i.e., higher flow rate. Such findings confirm that enzymatic hydrolysis of cellulose is strongly product inhibited and that suitable flow dynamic conditions greatly improve reactor performances, as shown in Figure 7.10.

Operating the reactor in a semi-continuous condition and adding substrate so as to keep its bulk concentration constant, leads to meaningful changes in reactor performance as compared to the diafiltration mode. Under either operational mode permeate flow rate continuously decreases with time.

When EMRs are operated continuously, feeding a slurry of substrate macromolecules to the reactor, concentration polarization phenomena play a dominant role. The presence within the reaction vessel of contaminants or intermediate products, e.g., dextrins in starch hydrolysis,[13] which are not fully hydrolyzed by the enzymatic system under study can lead to membrane fouling[12] or to the formation of a gel layer at the membrane surface. Under such conditions, the filtration rate continuously decreases with time, and it may happen that, after a sudden increase in the early stages, substrate conversion does not attain steady state conditions, Figure 7.11. The addition of enzymes capable of hydrolyzing such foulants to low-molecular-weight compounds usually improves reactor performance, eventually approaching steady state conditions in terms of both permeate flow rate and substrate conversion.[16,17] In addition, antifouling procedures including suitable feed pretreatment or procedures to reduce concentra-

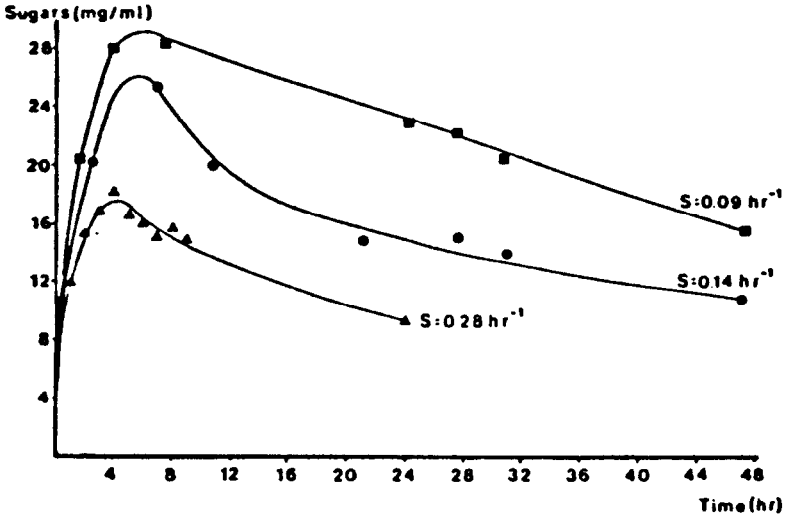


Figure 7.9: Concentration of soluble sugars (cellobiose and glucose) in permeate from an enzyme membrane reactor as a function of time for various space velocities (S).[11]

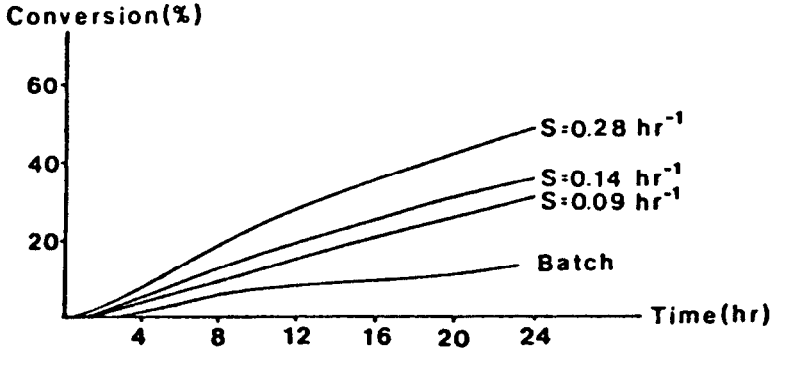


Figure 7.10: Conversion of cellulose to soluble sugars as a function of time for various space velocities (S).[11]

tion polarization can be used.[101] Equation 12 demonstrates the dependence of enzyme concentration at the upstream membrane surface on the flow dynamics of the reaction vessel. Due to the monotonicity of the exponential function, at given applied pressure, i.e., J, operational conditions improving mass transfer in the bulk phase, i.e., K_S or D/δ, diminish concentration polarization.[101] Figure 7.12[84] shows how high stirring speeds usually improve filtering performance of a CST flat membrane reactor, albeit at the expense of partial enzyme deactivation, as discussed earlier.

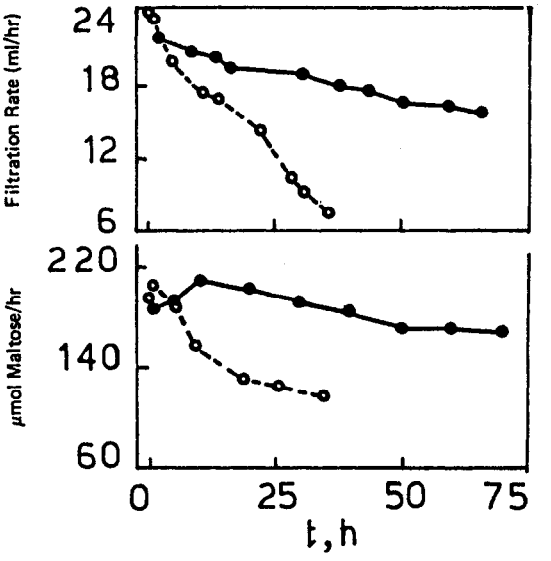


Figure 7.11: Effect of adding crystalline sweet potato β-amylase (87 μg protein/ml reaction mixture) on the filtration rate (ml/h) and on the reducing sugar content (measured as maltose) in the filtrate at 50°C, 15 psi, in a stirred cell system. Enzyme added (●); no enzyme added (○).[13]

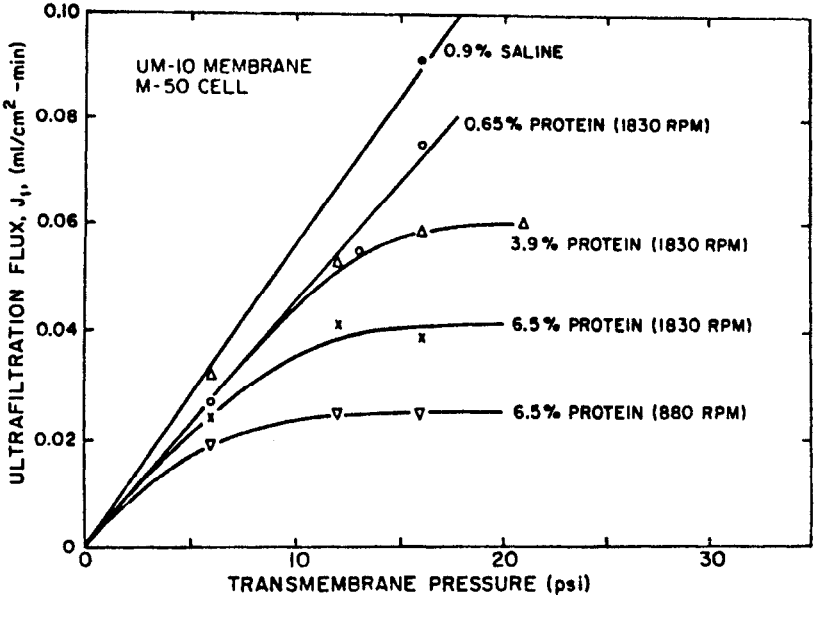


Figure 7.12: Flux-pressure relationship for bovine-serum albumin solutions in a stirred batch cell at various stirring rates and protein concentrations.[101]

Reactor configurations other than dead end or CSTR can offer improvements. In Figure 7.13, the performance of a thin channel flat membrane reactor for the hydrolysis of sweet potato by means of α-amylase is reported in terms of filtration rate and product concentration vs time plots. A comparison to Figure 7.11 shows how great the improvements due only to the change of configuration can be. At an appreciably high flow rate and product concentration level, a steady state is also attained.

The use of hollow fiber ultrafiltration modules strongly improves both reactor performance and economics. Capillary membranes are characterized by a favorable surface to volume ratio; advantages from this feature are not only related to lower overall plant size, but also to the increase of the surface to price ratio. Flushing enzyme/substrate solution from a reservoir to an HF module in a semiclosed loop at a high linear velocity reduces the extent of concentration polarization avoiding the formation of a secondary enzymatic gel membrane, in spite of product flux through the membrane.[101,102] Provided that the volume of the UF module is small relative to the total volume, and that recirculation flow rate is much larger than permeate flux, system kinetic behavior can be modeled in terms of a CST reactor. Assuming biocatalyst kinetics are described by the simple Michaelis Menten model, the substrate mass balance can be expressed according to Equation 3.[18] Reactor productivity as a function of time can be related to flux and enzyme concentration according to the following equation:

$$P_r = X(t)\, S_f\, J(t)/E\, V \qquad (13)$$

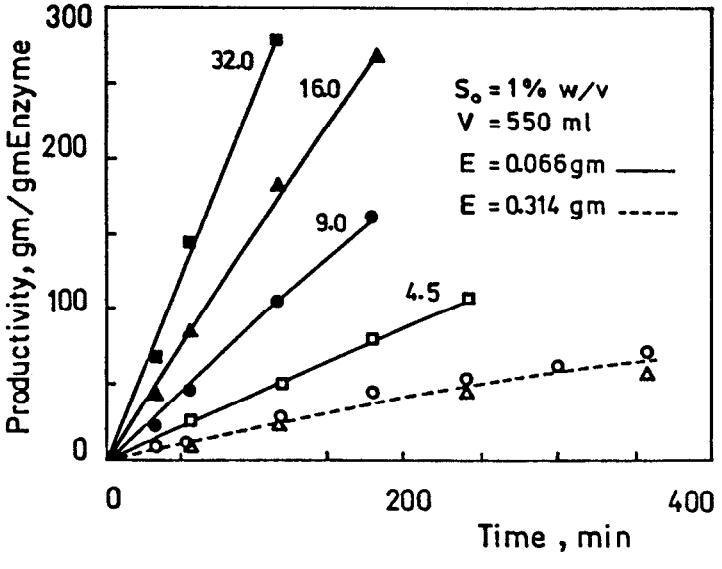


Figure 7.13: Effect of adding crystalline sweet potato β-amylase (87 μg protein/ml reaction mixture) on the filtration rate (ml/h) and on the reducing sugar content (measured as maltose) in the filtrate at 50°C, 15 psi, in a stirred cell system. Enzyme added (●); no enzyme added (○).[13]

Figure 7.14 shows how reactor productivity (g product/g enzyme) is affected by flux and enzyme concentration, for soy protein hydrolysis performed by *Pronase* enzyme. Maximum productivity can be obtained by operating the reactor at the highest flux and the lowest enzyme concentration.

Figures 7.15–7.18 show how reactor capacity (i.e., maximum productivity, g product/g enzyme/min) is affected by operational parameters. Enzyme and substrate concentration appear to affect reactor capacity to a large extent (Figures 7.15 and 7.16) especially at lower enzyme concentrations. Effects of permeate flux and reactor volume on conversion are related to each other by means of substrate residence time in the reaction vessel. Increasing residence time, that is increasing reactor volume or lowering fluxes, results in higher conversions at the expense of lower capacities (Figures 7.17 and 7.18).

Comparisons of EMRs operated in the diafiltration mode[11] and in the continuous mode[19] to batch reactor performances are reported in Figure 7.10 and 7.19. Figure 7.10 shows how conversion rate is improved by continuous removal of inhibiting products. Figure 7.19 (reactor continuously operated) shows that productivity levels are higher the longer the reactor is operated before shutting down for cleaning, recharging or backflushing. In the continuous process, enzymes are charged at the beginning of the process, and the system is kept working until enzyme activity drops down to a given limit established on the base of enzyme half life and plant economics. In batch reactors, the enzymes must be replaced at the end of each cycle. Hence the longer the reactor is operated, the greater is the productivity and the larger the difference between continuous and batch system performance. Moreover, batch processes require added expenses for enzyme inactivation and product purification, as well as more labor.

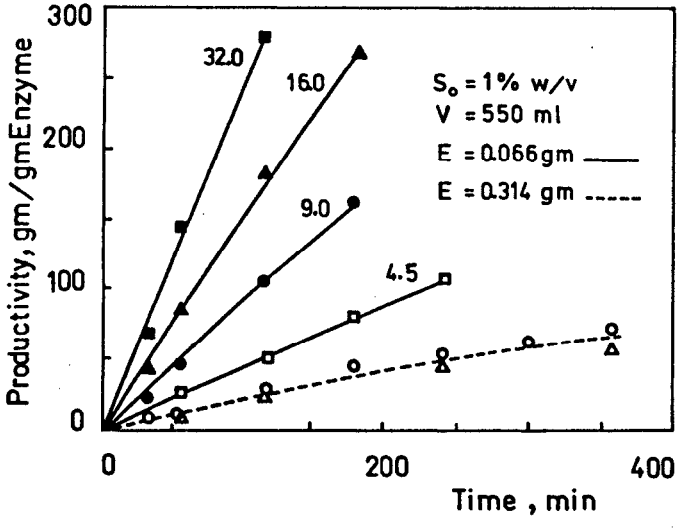


Figure 7.14: Effect of flux and enzyme concentration on UF reactor productivity. E = weight of enzyme added to reaction vessel (flux at E = 0.314 g: (○) = 9 ml/min; (△) = 16 ml/min).[19]

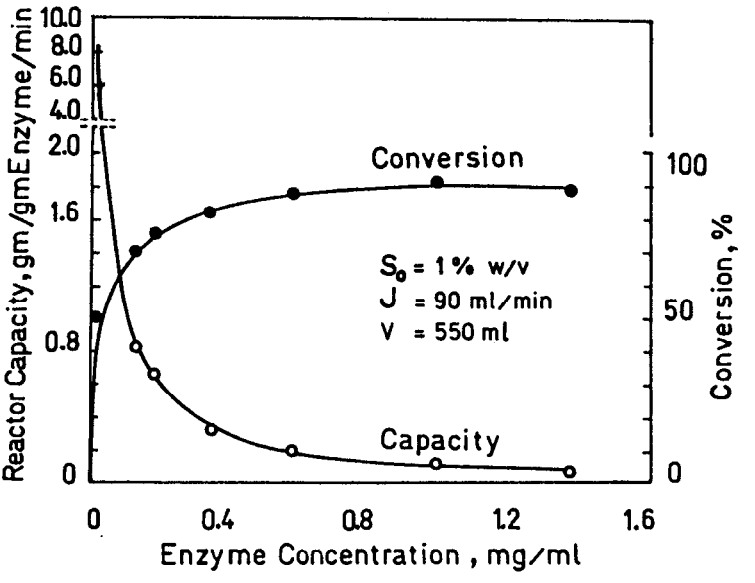


Figure 7.15: Effect of enzyme concentration on conversion and capacity of a UF reactor. Pronase-Promine D at pH 8.0, 50°C.[19]

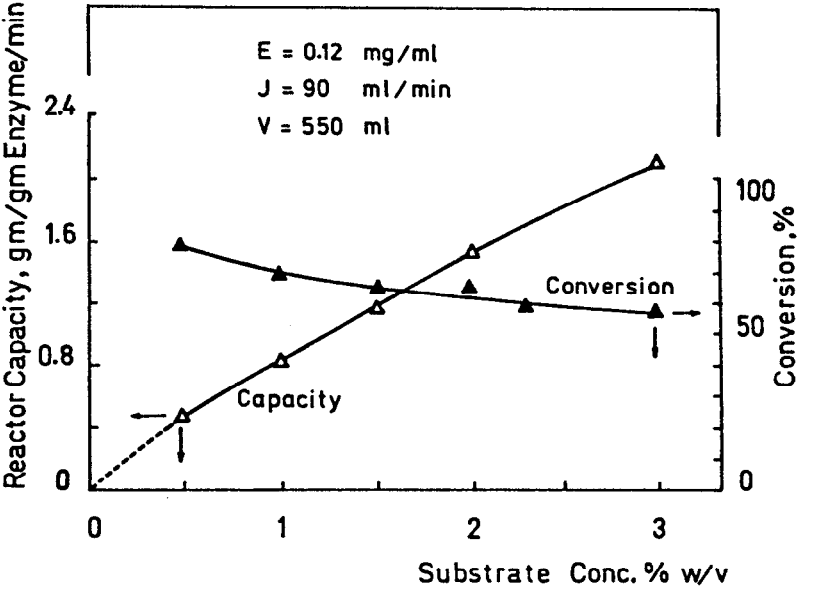


Figure 7.16: Effect of substrate concentration on conversion and capacity of a UF reactor.[19]

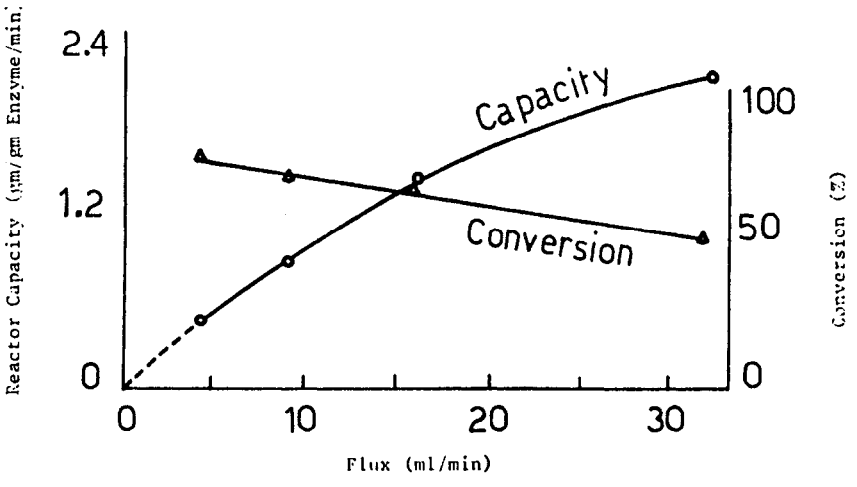


Figure 7.17: Capacity and conversion of a UF reactor as a function of flow rate through the system (flux).[19]

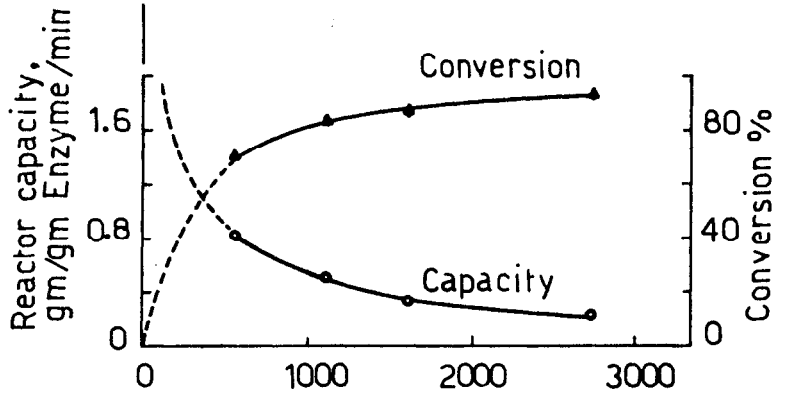


Figure 7.18: Effect of reactor volume on UF reactor capacity and conversion.[19]

The real potential of membrane reactors becomes evident with coenzyme dependent enzymatic systems.[10,20,21] Coenzymes, like NAD^+ or $NADP^+$, usually have a long term effect on enzyme activity only if they can move from one enzyme, able to oxidize them, to another, able to reduce them, in loop kinetics. Continuous homogenous catalysis is then a prerequisite to achieving high reaction yields. Enzyme membrane reactors offer a suitable reaction environment provided that coenzymes are retained in the reaction system. Such compounds are in fact quite expensive, which limits the use of coenzyme dependent enzymes. Reverse osmosis (RO) membranes could be helpful in retaining native

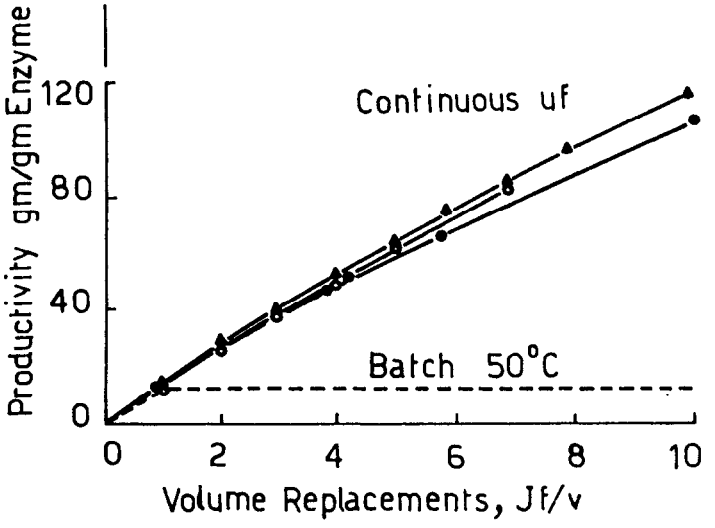


Figure 7.19: Comparison of productivity of a continuous UF reactor and a batch reactor for the Promine D-Pronase system at pH 8.0. Volume replacement for the continuous UF reactor calculated as J t/V.[19]

coenzymes in a given vessel on the basis of their size. Unfortunately, permeability of such membranes towards water is poor as compared to UF membranes, thus limiting overall fluxes. Moreover, the presence of product in the permeate implies coenzyme loss due to the usually small differences of their molecular weight. In the early 1970s, some procedures were proposed in order to increase coenzyme molecular weight by covalently binding the coenzyme to a high-molecular-weight soluble polymer such as polyethylene glycol or dextran.[10,103,104] Choosing the membrane molecular weight cut-off so as to reject the soluble polymers results in retaining the coenzymes within the reaction vessel. If a suitable pair of enzymes is charged into the reactor together with the macromolecularized coenzymes, the latter are continuously regenerated and long term operation is assured. Laboratory and plant scale experiments[10,20] show the importance of a careful choice of the enzymatic system, as well as the ratio of oxidizing to reducing enzymes. Differences in enzyme cofactor requirements, half life, and optimum pH and temperature can in fact render one enzymatic system rate limiting thus reducing reactor performance.

Patents already exist such as for amino acid production from α-ketoacids,[22] which confirm the potential of scale-up for EMR plants. For this particular process, resolution, derivatization and racemization steps can be avoided, thus reducing overall costs.

EMRs have a number of advantages over other immobilized preparations. In summary:

(a) Homogeneous catalysis

(b) No diffusion limitations

(c) No activity losses due to carrier fixation
(d) Absence of enzyme fixation costs
(e) High activity per unit volume
(f) Sterilizability of the plant
(g) Constant productivity assured by enzyme dosage
(h) Absence of contaminants
(i) Interchangeability of substrate/enzyme systems
(j) Use of multienzyme systems.

Efficient circulation, however, is required to prevent concentration polarization, which becomes quite a problem as enzymes are added to keep conversion constant. A large membrane area and sterile filtration are also needed to assure high yields over long periods of time. If the enzyme solution is to be flushed at high linear velocity near the membrane surface, shear forces may deactivate enzyme molecules.

Thus far, EMRs have been successfully used with macromolecular substrates, as for the saccharification of cellulose[11–13,15,26] and protein hydrolysis,[19] or with low molecular weight substrates, as for cellobiose hydrolysis[9] and L-malic acid production from fumaric acid.[20] Bench and large scale plants are already in operation for the preparation of N-acetyl-D,L derivatives from L-amino acids by means of acylase and the production of L-malic acid from fumaric acid by means of fumarase.[20] In the case of fumarase, conversions of up to 86% with resolution rates of up to 85% have been attained.

In conclusion, flexibility of such systems can be considered to be limited only by the number of active compounds which can be synthesized via an enzymatic route.

DYNAMIC ENZYME GEL LAYER REACTORS

Ultrafiltration of protein solutions is a proven unit operation[105] for obtaining purified enzymes from cell cultures. Under certain circumstances, such processes can provide an interesting technique for enzyme immobilization which takes advantage of concentration polarization phenomena. If an enzyme solution is flushed under pressure through a UF membrane that completely rejects enzyme molecules, these molecules will accumulate on the active membrane surface and possibly deposit there as a thin gel layer characterized by enzymatic catalytic activity.[27,28] Actual gelation of enzyme proteins, and hence their dynamic immobilization, depends strictly on enzyme concentration at the membrane-liquid interface,[29] (Figure 7.20). When the maximum enzyme concentration is lower than the gel concentration value, enzymes are not immobilized. Although they are confined near the membrane surface at fairly high concentration levels, they are still in soluble form.[30]

If gel formation occurs, enzymes are effectively immobilized without meaningful changes in their microenvironment.[31] Moreover, their settlement is partic-

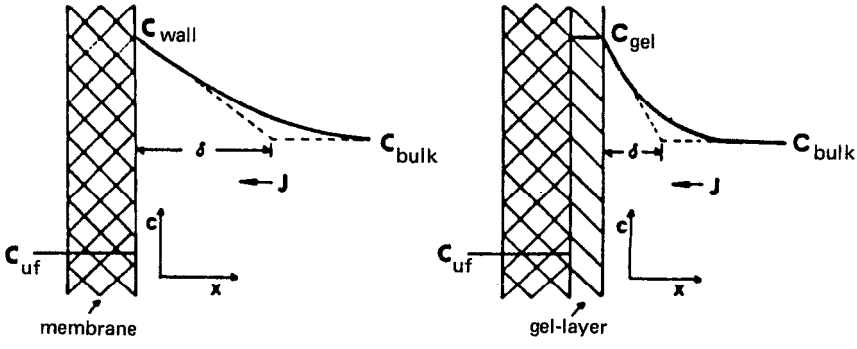


Figure 7.20: Gel layer formation ultrafiltering a protein solution through a semipermeable membrane. x is the distance from the membrane wall.[31]

ularly attractive due to the high enzyme and protein concentrations in the gel, the latter strongly enhancing enzyme stability.[106]

Enzyme gel layers can be built up under a number of fluid dynamic conditions. Unstirred and stirred batch reactors have been used as well as systems where the enzymatic solution is kept continuously flowing along semipermeable membranes until gel formation sets in.

When unstirred batch membrane units are used as reacting vessels, a steady state mass balance on retained species, i.e., enzymes, leads to the evaluation of their concentration as a function of the distance from the membrane surface, x. Taking into account both convective and diffusive mass transfer mechanisms, the enzyme mass balance equation at steady state is as follows:

$$D_e\, d^2E/dx^2 + v\, dE/dx = 0 \qquad (14)$$

Proper boundary conditions can be derived assuming (a) complete enzyme rejection and (b) no enzyme loss, that is:

B.C.1 $$x = 0 \quad D_e\, dE/dx + v\, E = 0 \qquad (15)$$

B.C.2 $$\int_0^\infty E(x)\, A\, dx = N$$

Upon integration of Equations 14 and 15, the enzyme concentration profile appears to be:[30,32]

$$E(x) = [Nv/(AD_e)] \exp[-vx/(D_e)] \qquad (16)$$

Maximum enzyme concentration occurs at the upstream membrane surface, (for x = 0) and it can be expressed as:

$$E_w = Nv/(AD_e) \qquad (17)$$

Enzyme depth of penetration, defined as the ratio of gel volume (in which

99% of the initial amount of enzyme is contained) to membrane cross-sectional area, can be estimated to be:[30]

$$x_e = 4.6\ D_e/v \qquad (18)$$

Enzyme average concentration in the gel is therefore 21% of enzyme concentration at the gel-membrane interface.

With the enzyme gel concentration known, Equation 16 can be used as a design equation in order to estimate the amount of enzyme, N, required to build up an enzymatic gel layer of thickness x.

Similar equations under different fluid dynamic conditions can be derived from Michaels' gel formation theory[100] or from similar theories modeling concentration polarization phenomena.[101,102,107,108]

Unfortunately for most substances, an accurate knowledge of gel concentration is not available, and only order of magnitude estimates can be gained from the literature.[101] Protein gelation, for instance, is thought to occur at concentration levels ranging from 20% to 40% by weight. Criteria need to be developed in order to experimentally detect enzyme gel build-up.

Ultrafiltration of protein solutions usually results in a time progressive decay of permeate flow rate, which after a period of time attains a steady state constant value for a given transmembrane pressure. Such a decay can be attributed either to gel formation, or to an increase in osmotic pressure of the ultrafiltered solution as a result of macromolecule accumulation at the membrane-solution interface which lowers the pressure driving force. If a gel is formed, any further transmembrane pressure increase does not enhance permeating fluxes correspondingly. In some cases,[30] permeate flux decay associated with gel formation is negligible thus ruling out the possibility of detecting eventual gel formation.

The steady state kinetic behavior of such an enzyme membrane reactor is only related to the kinetic behavior of enzymes in the gel or in the soluble state. Unless knowledge of intrinsic enzyme kinetics both in the gel and in the soluble form is available, a steady state analysis is not useful for determining whether gel formation has occurred.

An effective distinction between enzymes in gel form and enzymes in the soluble state can be achieved by the analysis of the transient behavior of the enzymatic reaction.[30,33]

Figures 7.21 and 7.22 show typical results for the two cases–with enzymatic gel layer formation and when soluble enzymes are confined only near the membrane surface. Comprehensive models for an immobilized enzyme batch membrane reactor (IEMR) and for a soluble enzyme batch membrane reactor (SEMR) are proposed in References 33 and 30, respectively, for a flat slab membrane configuration.

As far as an IEMR is concerned, analytical closed-form solutions are available for limiting first and zero order kinetic rate equations.[33]

The unstirred reacting vessel is divided into two sections–upstream and downstream of the membrane supported enzyme gel layer. Referring to the upstream region, the mass balance must take into account both diffusion and convection due to the usual low permeating fluxes. Assuming that neither reactant nor product is rejected by the membrane and that diffusion coefficients of

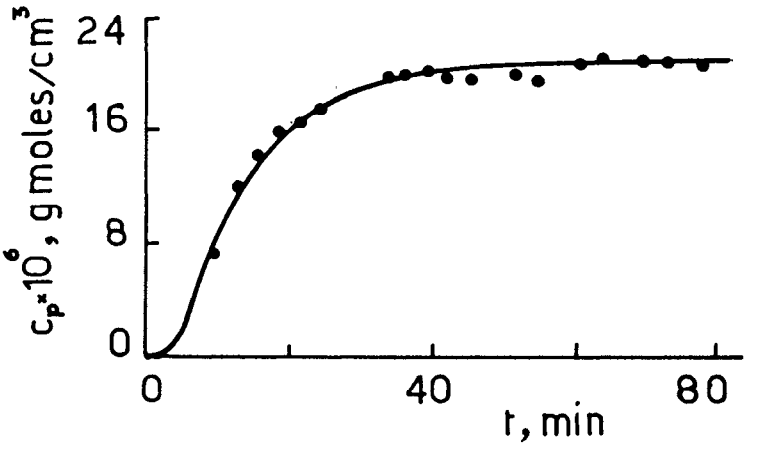


Figure 7.21: Hydrolysis of 1.5 mM sucrose by cogelled invertase in an immobilized enzyme membrane reactor (IEMR). Comparison between experimental data in terms of glucose outlet concentration (C_p) vs. reaction time (t) and theoretical predictions (–). Enzyme amount, 0.398 x 10^{-5} g/cm^2; reaction temperature, 30°C; pH 4.65; flow rate 1.13 x 10^{-3} ml/s.[30]

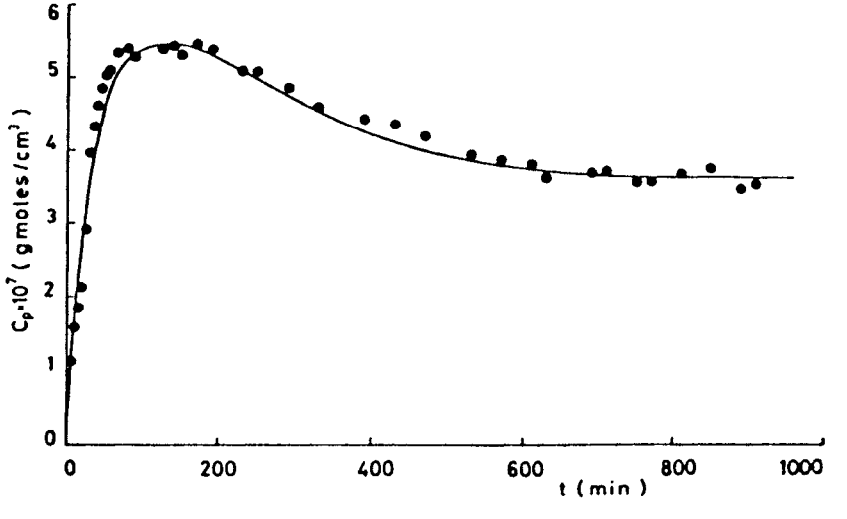


Figure 7.22: Hydrolysis of 1.0 mM sucrose by soluble invertase in a soluble enzyme membrane reactor (SEMR). Comparison between experimental data in terms of glucose outlet concentration (C_p) vs. reaction time (t) and theoretical predictions (–). E = 1.06 x 10^{-11} mols/ml; S_f = 10 mols/ml, V = 70 ml, flow rate = 1.6 x 10^{-2} ml/s, T = 30°C, pH = 4.65.[30]

either compound are constant and close to each other, mass balance equations in dimensionless form can be written

$$\frac{\partial^2 \gamma_s}{\partial \xi^2} + \frac{\partial \gamma_s}{\partial \xi} = \frac{\partial \gamma_s}{\partial \theta} \tag{19}$$

$$\frac{\partial^2 \gamma_p}{\partial \xi^2} + \frac{\partial \gamma_p}{\partial \xi} = \frac{\partial \gamma_p}{\partial \theta} \tag{20}$$

with the following boundary conditions:

I.C. $\theta = 0 \qquad \gamma_s = 1 \; ; \quad \gamma_p = 0$ (21)

B.C.1 $\xi \to \infty \qquad \gamma_s = 1 \; ; \quad \gamma_p = 0$

B.C.2 $\xi = 0 \qquad \frac{\partial \gamma_p}{\partial \xi} + \rho = \frac{\partial \gamma_s}{\partial \xi} - \rho = 0$

Boundary condition B.C.1 states that the height of the region where substrate and product concentrations appreciably differ from their feed values is negligible compared to cell height. B.C.2 stems from the assumption that enzymatic reaction takes place only on the enzyme layer free surface.

The downstream region of the UF test can be modeled in terms of a first order system in series to a pure time lag. Dimensionless product concentration at the UF cell outlet is then related to that immediately downstream of the membrane by the system transfer function.

$$\frac{\bar{\gamma}_p(s)}{\bar{\gamma}_p(0,s)} = \frac{e^{-\tau_1 s}}{(1 + \tau_2 s)} \tag{22}$$

Overall system response in time domain can then be evaluated from the system response in Laplace domain for first and zero order kinetics:

$$\gamma_p(\theta) = \left\{ \frac{\alpha_1 + 0.5}{\alpha_1 + 1} \left(1 - e^{-\frac{\theta^*}{\tau_2}} \right) - \frac{0.5}{\alpha_1 + 1} \operatorname{erf} \sqrt{0.25\,\theta^*} + \Phi(\theta^*) + \right. \tag{23}$$

$$+ \frac{(\alpha_1 + 0.5)\ e^{-\frac{\theta^*}{\tau_2}}}{\tau_2\ (\alpha_1+1)\ (\ \alpha_1^{\,2} + \alpha_1 + \frac{1}{\tau_2}\ )} \cdot$$

$$\cdot\ (1 - e^{((\alpha_1^{\,2} + \alpha_1 + \frac{1}{\tau_2})\ \theta^*)}\ \mathrm{erfc}\ ((\alpha_1 + 0.5)\ \sqrt{\theta^*}\ )\ \}\ u(\theta^*)$$

and

$$\gamma_p(\theta) = \alpha_0\ \{0.5\ (\ \tau_2 - \theta^*)\ \mathrm{erfc}\ \sqrt{0.25\ \theta^*} + \mathrm{erf}\ \sqrt{0.25\ \theta^*} +$$

$$+ \sqrt{\theta^*/\pi}\ e^{-0.25\ \theta^*} - 0.5\ \tau_2\ e^{-\frac{\theta^*}{\tau_2}} + \Psi(\theta^*)\ \}\ u(\theta^*) \qquad (24)$$

respectively, with

$$\Phi(\theta^*) = \frac{\alpha_1\ e^{-\frac{\theta^*}{\tau_2}}\ \mathrm{erf}(((\ 0.25 - \frac{1}{\tau_2}\ )\ \theta^*)^{\frac{1}{2}}\ )}{(\ \alpha_1^{\,2} + \alpha_1 + \frac{1}{\tau_2}\ )}\ (0.25 - \frac{1}{\tau_2})^{\frac{1}{2}}$$

$$\tau_2 > 4$$

$$\Psi(\theta^*) = \frac{0.25\ \tau_2}{(\ 0.25 - \frac{1}{\tau_2}\ )^{\frac{1}{2}}}\ e^{-\frac{\theta^*}{\tau_2}}\ \mathrm{erf}\ ((\ 0.25 - \frac{1}{\tau_2}\ )^{\frac{1}{2}}\ \theta^{*\,\frac{1}{2}}\ )$$

and (25)

$$\Phi(\theta^*) = -\frac{2\ \alpha_1\ (\ \frac{1}{\tau_2} - 0.25\ )^{\frac{1}{2}}\ e^{-0.25\ \theta^*}}{\sqrt{\pi}\quad (\ \alpha_1{}^2 + \alpha_1 + \frac{1}{\tau_2}\ )}\ \psi(((\ \frac{1}{\tau_2} - 0.25\ )\theta^*\ )^{\frac{1}{2}}\ )$$

$$\tau_2 < 4$$

$$\Psi(\theta^*) = \frac{0.5\ e^{-0.25\ \theta^*}}{(\ \frac{1}{\tau_2} - 0.25\ )^{\frac{1}{2}}}\ \frac{\tau_2}{\sqrt{\pi}}\ \psi(((\ \frac{1}{\tau_2} - 0.25\ )\ \theta^*\ )^{\frac{1}{2}}\ )$$

Figure 7.23 depicts a model fitting experimental data for the enzyme invertase for both kinetic orders.[32]

An overall steady state mass balance relates kinetic parameters of either rate equation to the ultimate value of the dimensionless product concentration yielding:

$$\lim_{\theta \to \infty} \gamma_p(\theta) = \frac{\alpha_1}{(\alpha_1 + 1)} \tag{26}$$

and

$$\lim_{\theta \to \infty} \gamma_p(\theta) = \alpha_0$$

When the amount of enzyme is insufficient to ensure that the enzyme concentration at the membrane surface attains the gel value, Equation 17 indicates that the enzyme is confined in soluble form at a fairly high concentration in a region immediately upstream from the membrane. A soluble enzyme membrane reactor (SEMR) is thus defined. As soon as the substrate stream is fed to the system, enzyme remixing occurs throughout the vessel and reaction then starts throughout the whole cell. As time goes by, enzyme macromolecules are pressure driven towards the membrane surface; thus reaction rate in most of the cell volume progressively decreases due to an enzyme concentration decrease. Immediately upstream of the membrane, the reaction rate increases due to an enzyme concentration increase. Once steady state conditions are attained, reaction takes place only in the region where enzymes are confined and whose thickness is determined by Equation 18.

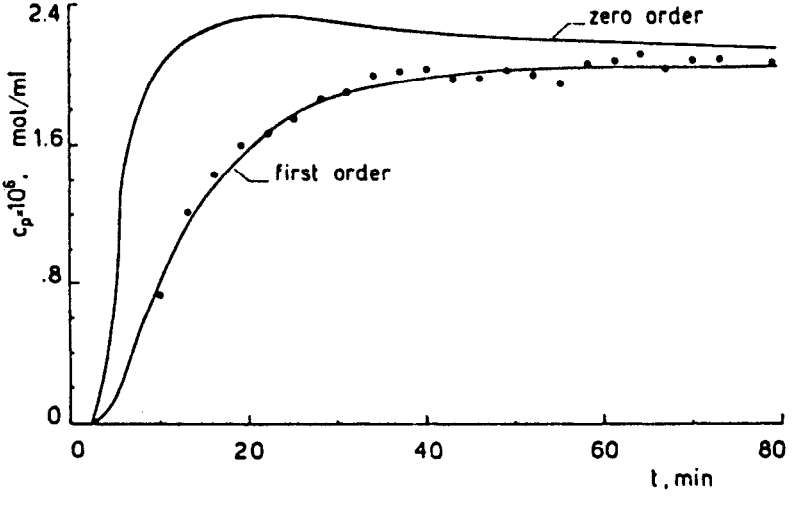


Figure 7.23: Hydrolysis of sucrose (3×10^{-6} mols/ml) by immobilized invertase operating in an IEMR. Comparison between experimental data (expressed in terms of glucose, C_p) and theoretical curves (solid lines) calculated according to Equations 23 and 24.[32]

Simple mathematical modeling of this situation is reported in Reference 30 referring to the equivalent lumped parameters system in Figure 7.24. Also in this case the reacting volume is modeled as two separate regions in series to each other. Region A, where a time dependent enzyme depletion occurs, virtually coincides with the cell as a whole except for the negligible liquid volume where enzymes accumulate, namely region B. Each region is modeled in terms of a single well mixed tank. As far as region A is concerned, for a particular UF test cell this assumption can be verified simply by a tracer step response test performed on the system itself.

Assuming a uniform enzyme distribution within the cell volume at system start-up, the functional dependence of enzyme concentration in region A on the reaction time is obtained upon integration of the mass balance equation:

$$E_a = \tau_a \, dE_a/dt \tag{27}$$

subject to the initial condition

$$\text{I.C.} \quad t = 0 \qquad E_a = N/V_a$$

to give

$$E_a(t) = (N/V_a)\exp(-t/\tau_a) \tag{28}$$

Regarding region B as a lumped parameter system of volume V_b (with $V_b = X_e$ A) fed by the outlet from region A, the average enzyme concentration

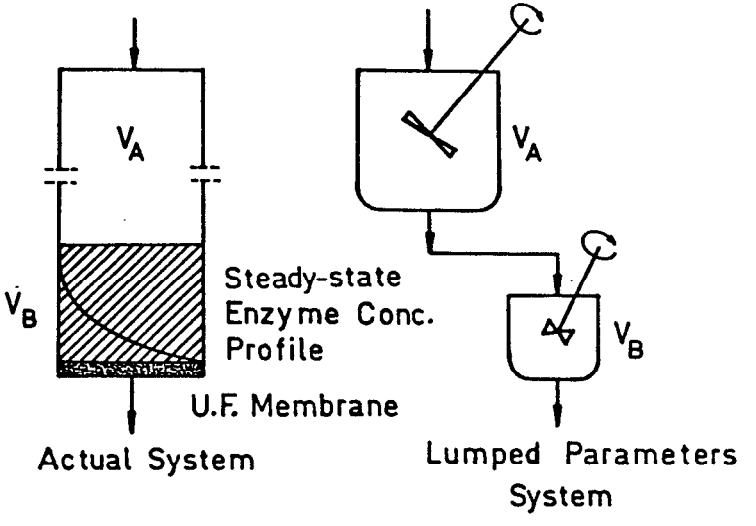


Figure 7.24: Actual and lumped parameters system. V_A is the dominating volume portion where enzyme depletion takes place; V_B is the constant volume in which enzyme accumulation occurs.[30]

in region B can be expressed as follows:

$$E_b(t)=(N/V_a)\ [1+\frac{V_a}{V_b}\ (1-\exp(-t/\tau_a)] \qquad (29)$$

Similarly, substrate mass balance in region A looks like

$$S_f - S_a - R_a\ \tau_a = \tau_a \frac{dS_a}{dt} \qquad (30)$$

The kinetic equation describing region A, R_a, can be assumed identical to the rate equation for enzymes in homogeneous solution.

Referring to region B, it has been shown[33] that the ratio between substrate and enzyme depths of penetration, x_e, is equal to the ratio between the corresponding diffusivities. In most cases, enzyme depth of penetration, i.e., thickness of region B, can then be assumed to be one order of magnitude lower than that for the substrate. Substrate concentration is, therefore, virtually constant over the whole region B. Hence, substrate mass balance in this region is expressed according to the dynamics of a stirred tank reactor of volume V_b, that is:

$$S_a - S_b - R_b\ \tau_b = \tau_b \frac{dS_b}{dt} \qquad (31)$$

An overall product mass balance at steady state yields the proper rate equation for region B:

$$R_b = (Q/V_b)P_b \qquad (32)$$

P_b being product concentration in the permeate. Once steady state conditions are attained, all enzyme is virtually confined within region B at a concentration $E_b=N/V_b$. Therefore, enzyme kinetics in region B can be experimentally determined through Equation 32. For details on the initial conditions and integration of the set of Equations 30 and 31 readers are referred to Reference 30.

Ultrafiltration of an enzyme solution through a UF membrane does not always result in gel layer formation. Unless a gel layer is formed, this immobilization technique cannot be used for flow systems lacking effective enzyme immobilization. In any event, soluble enzyme membrane reactors can be useful in order to perform kinetic analysis at high enzyme concentrations. Once steady state is attained, the theoretical model permits calculation of reaction rates in both regions. Once the layer is formed it behaves like a secondary membrane,[34] capable of separating compounds of different molecular weight in the mixture as well as catalyzing a chemical reaction.

Enzyme immobilization via dynamic formation of an enzyme gel layer has been applied both to flat and tubular membrane reactors, either recirculating the permeate or the axial stream.

The kinetic behavior of these immobilized systems is to be analyzed taking into account:

(1) The rate equation for native enzymes and for enzymes in gel form is not necessarily the same due to microenvironmental and shear stress effects;

(2) Within the gel layer, substrate mass transfer and reaction occur simultaneously giving rise to substrate concentration profiles at levels lower than the feed concentration;

(3) External mass transfer resistances have to be taken into account occasionally, depending on operating conditions and reactor configuration.

Experimental kinetic data at different temperatures and at saturating substrate concentrations can be used to evaluate the relative importance of all the aforesaid phenomena.

Plotting such data in terms of the logarithm of the specific reaction rate vs the reciprocal of the absolute temperature (i.e., an Arrhenius plot) is helpful in assessing which step is rate controlling. A reduction in the activation energy relative to that of the native enzyme, indicates that kinetics are not rate limiting.

If external resistance is rate controlling, a mass transfer coefficient, K_s, can be introduced. From the fluid dynamics of the reaction vessel, it is possible to estimate substrate concentration at enzyme catalytic sites according to the steady state relationship:

$$K_s(S_f - S) = R(S) \tag{33}$$

which for a Michaelian enzyme reduces to:[3]

$$K_s(S_f - S) = V_{max}S/(K'_M + S) \tag{34}$$

When the internal mass transfer/reaction step is rate limiting, an effectiveness factor, η, is usually introduced related to dimensionless parameters characteristic of the reacting system as a Thiele modulus.[109] It is worthwhile noting that most of the available correlations are based upon theoretical models assuming diffusion as the only mass transfer pattern. Hence, effects related to external mass transfer resistances are neglected.

Comprehensive models of unstirred enzyme gel flat membrane reactors have been proposed.[30,32,33,35]

The analysis of unstirred membrane systems in flat slab configuration is carried out in two different cases:

(1) The gel formed on the flat membrane is homogenous,

(2) The gel is heterogenous, i.e., preferential flow patterns exist for the substrate flowing under pressure through the gel.

Case 1: If a homogenous enzyme gel is formed above the membrane surface, no segregated regions exist; substrate permeation and conversion to products occur throughout the whole gel layer so that both convection and diffusion concur in determining mass transfer through the gel. Since the reaction vessel is unstirred even external mass transfer resistances must be taken into account. Thus, substrate steady state mass balance equations upstream and within the gel have to be simultaneously integrated. Expressing equations in dimensionless form pulls out three dimensionless parameters, namely the Peclet number, the Thiele modulus and the dimensionless Michaelis constant.

$$\frac{d^2\gamma_1}{d\xi'^2} + Pe\,\frac{d\gamma_1}{d\xi'} = 0 \qquad \text{upstream} \qquad (35)$$

$$\frac{d^2\gamma_2}{d\xi'^2} + Pe\,\frac{d\gamma_2}{d\xi'} = \Phi^2\,\gamma_2^2\,/(M + \gamma_2) \qquad \text{within the gel} \qquad (36)$$

with the following boundary conditions:

B.C.1 $\xi' \to \infty$ $\gamma_1 = 1$ cell inlet (37)

B.C.2 $\xi' = 1$ $\gamma_1 = \gamma_2$; $\frac{d\gamma_1}{d\xi'} = \frac{d\gamma_2}{d\xi'}$ upstream gel surface

B.C.3 $\xi' = 0$ $\frac{d\gamma_2}{d\xi'} = 0$ downstream gel surface (Dankwaerts conditions).

In most cases, enzyme kinetic behavior can be assumed to be Michaelian. The assumption of a semiinfinite slab for the fluid reacting volume, B.C.1, holds that gel height, x_e from Equation 19, is negligible relative to cell height.

In B.C.2 and 3, both the gel layer and the supporting membrane are assumed to be completely permeable both to substrate and product, and enzymes are uniformly distributed throughout the gel.

An effectiveness factor is then introduced, defined as the ratio between the overall reaction rate and the rate one would obtain if substrate concentration within the gel were uniform at the feed level. An overall substrate mass balance relates this factor to the Thiele modulus, Φ:[35]

$$\eta = (1 + M)\,\frac{(1 - \gamma_2(0))}{\Phi^2} \qquad (38)$$

The existence of convective fluxes rules out the possibility of using correlations already existing. Decreasing substrate concentration is responsible for efficiency factors less than unity across membrane thickness. Minimum concentration is, therefore, the cell output value which can be easily estimated; evaluation of the dimensionless parameters is possible and correlations are not necessary.

Case 2: If gel structure is assumed heterogenous, substrate convection occurs through preferential pathways, while simultaneous substrate diffusion and reaction occur in segregated regions. Minimum substrate concentration is now attained in the core of the segregated region and cannot be readily measured.

Within a segregated region, the steady state substrate mass balance equation can be written as:[35]

$$\frac{d^2\chi}{dz^2} = \Phi''^2 \frac{\chi}{(M' + \chi)} \tag{39}$$

with the following B.C.s:

$$\text{B.C.1} \quad z = 1 \quad \chi = 1 \qquad \text{segregated region/preferential flow pattern interface} \tag{40}$$

$$\text{B.C.2} \quad z = 0 \quad d\chi/dz = 0 \qquad \text{center of segregated region}$$

in dimensionless form.

The modified Thiele modulus, Φ'' is expressed as a function of the characteristic dimension of the segregated region and external substrate concentration,[35]

$$\Phi'' = \left(\frac{K E \lambda^2}{D \gamma_2(0) S_f}\right)^{1/2} \tag{41}$$

With reference to the homogenous phase reaction rate, and to the feed substrate concentration, the effectiveness factor can be estimated to be:[35]

$$\eta = (1 + M) \frac{\left.\frac{d\chi}{dz}\right|_{z=1}}{\Phi''^2} \tag{42}$$

For preferential pathway geometries other than the flat slab model, λ has to be regarded as the characteristic dimension of the segregated regions corrected by a suitable shape factor.

As far as Michaelis-Menten enzymes are concerned, η vs Φ diagrams have been produced[109] for various immobilized enzyme configurations. They can, therefore, be used provided that the geometry of the segregated regions is defined and that external resistances are taken into account.

Modeling of unstirred UF cells equipped with flat membranes and interpretation of experimental data is then relatively simple. It is interesting to note that transmembrane pressure plays a different role from that which it plays in the usual UF membrane separators. On the one hand, increasing pressures lead to increasing permeating fluxes, thus enhancing reactor productivity; on the other hand, high effluent flow rates strongly reduce the substrate conversion.[29] Moreover, the ultrafiltering surface area per unit reactor volume is quite small.

As for membrane UF units, tubular membranes fitted in cylindrical shells in a "tube-and-shell" configuration help in improving the performance of en-

zyme gel reactors. The ratio of filtering area to volume is an order of magnitude higher than that for membranes in a flat slab configuration, and the flow dynamic conditions are more easily controlled.[34,36] An enzymatic gel layer can be built up on the inner wall of tubular membranes either by filtering proteic solutions in a batch mode, or flushing them along the membrane wall until the gel layer is eventually formed. In both cases, industrial operations require the enzymatic reactor to be continuously operated. Feeding an axial substrate stream to the reactor gives rise to new flow dynamic conditions. High shear stresses may in fact develop on the gel layer surface leading to partial or total removal of the enzyme.[34,36] There is evidence of stable systems, at least under laminar flow conditions.[37] Moreover, under a fluid shear field enzyme molecules can be oriented and thereby denatured.[38] In order to develop this immobilization technique for large scale and industrial applications, work is in progress to guarantee mechanical stability of the gel layer. This goal can be achieved, first of all, by strictly controlling the axial flow rate. The enzyme gel layer can also be protected by applying layers of water soluble or insoluble macromolecular compounds or by forming the gel within the porous structure of the membrane where it is less subject to shear stresses.

Flushing the substrate solution along the enzymatic gel causes the substrate to be converted to product even in the axial stream. When the enzyme is product inhibited and the effluent from the reactor is recycled, product accumulates in the feed stream thus inhibiting gelled enzymes. High axial flow rates may reduce conversion of substrate to product in the axial stream and enzyme inhibition, while product conversion in the permeate remains unaltered at a given transmembrane pressure.[29,34,36] Under such conditions, the axial flow rate needs to be optimized since it plays an opposite role.

Yeast invertase,[30,32,33] acid phosphatase,[29,32,35,37,39] urease,[29] β-glucosidase,[29] dCMP-amino hydrolase[31] and malic enzyme[34,36] have been immobilized in gel form on both flat and capillary membranes. Cellulosic and polyamide polymers have been used as supporting membrane matrices. In all instances, immobilized enzymes behave in a manner almost identical to their behavior in homogenous solution, independent of the nature of the polymer. Neither allosteric nor pseudo-allosteric enzymes, proteins whose kinetic behavior is affected by the presence of particular compounds in the reaction environment (ligands), show different kinetic behavior, as they do when subjected to less gentle immobilization procedures.[31,34,36]

A number of procedures have been suggested in order to improve enzyme gel kinetic and mechanical stability.

Under ultrafiltration at suitable conditions any proteic solution can give rise to a gel layer. Besides simple enzyme ultrafiltration, two other gel formation procedures have been proposed, namely cogelation and copolymerization/gelation. In the first case, solutions consisting of both enzymes and high molecular weight inert compounds are ultrafiltered through semipermeable membranes. For example, polyalbumines (inert proteins),[37,39] water soluble and insoluble compounds,[40] have been used as cogelling agents. In the second case, before the UF step, enzymes are chemically linked to high molecular weight inert substances by means of bridge molecules.[33,41] In both cases, the enzyme microenvironment in the gel layer is characterized by a relevant protein concen-

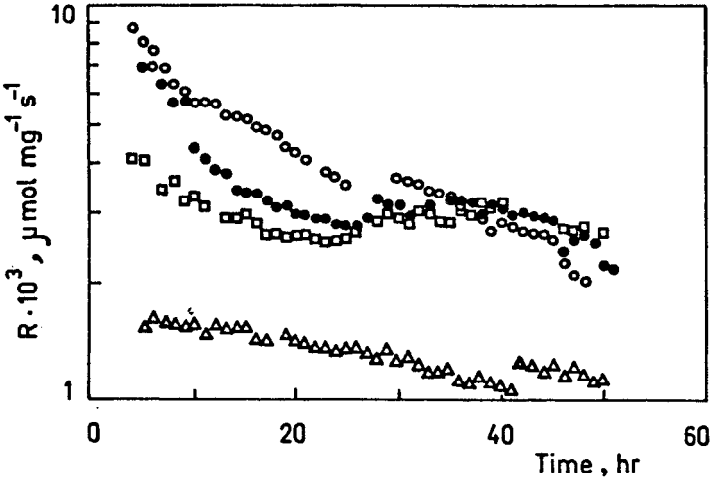


Figure 7.25: Effect of gel layer thickness on the stability of cogelled acid phosphatase at 40°C. Human serum albumin (HSA) polymers: (○) 2 mg, (●) 4 mg, (□) 8 mg, (△) 16 mg.[37]

tration. Enzyme kinetic stability is enhanced as protein concentration increases (Figure 7.25);[37,106] enzyme settlement is then particularly favorable. Copolymerized/gelled and cogelled enzymatic layers appear to be mechanically stable over a fairly wide range of temperatures and flow rates in the laminar regime.[37] Due to the covalent linking procedure, copolymerized/gelled enzymes can lose most of their original activity. Furthermore, the deactivation rate of cogelled enzymes appears to be less temperature-dependent than that of copolymerized/gelled preparations. These features suggest that in many cases immobilization by cogelation is preferred, provided that it also gives satisfactory mechanical stability.

The flexibility of enzyme gel layer reactors is fully exploited when multienzymatic reactions are to be performed. It may happen that enzymes involved in a given transformation cannot be subjected to the same immobilization procedure. Sequential enzyme gel layers can then be built up on the surface of a membrane in the proper sequence. Series reactions can be performed in such a set-up; products from one enzymatic layer being fed to the following ones for further transformation.[28,41]

In addition, enzyme gel reactors are inexpensive and easily controlled. Deactivated enzyme may be easily replaced.

MEMBRANE SEGREGATED ENZYME REACTORS

In these reactors, enzymes or cells are not immobilized, but only confined to a well defined region of space. The segregation of biocatalyst in the reaction vessel is achieved by means of an ultrafiltration or microfiltration membrane

with a suitable molecular weight cut-off. In this way, enzymes and bacterial cells are not lost in the effluent stream, and low-molecular weight products and inhibitors can be removed through the membrane. Enzyme segregated membrane reactors retaining the biocatalyst in the reaction system offer an economically attractive alternative to the design of continuous-flow equipment.

Organic synthetic membranes, either in hollow fibers or in flat slab configurations, have been extensively used in ultrafiltration units as enzyme or cell reactors for a number of applications. Starch and maltose hydrolysis,[42] sugar production,[43] cellulose hydrolysis[44] and steroid bioconversion[45] seem to be the most promising industrial applications of such systems. There is also growing interest in therapeutic applications of compartmentalized cells or microsomes functioning as a bioartificial pancreas or extracorporeal detoxification device.[57-60]

The development of hollow fibers with diameters down to about 100 microns makes possible "tube-and-shell" reactors with a high surface-to-volume ratio. Biocatalytic reactors can segregate enzymes or cells either within the hollow fiber lumen,[46] within the shell surrounding the outer surface of the fibers,[44,45,57-59] or within the porous membrane support.[42,45,47,53]

Segregated enzyme reactors avoid the negative aspects of immobilization techniques such as steric hindrance and enzyme deactivation due to coupling.

Reactors with Enzymes Segregated in the Lumen of Hollow Fibers

In 1971, Rony first suggested "immobilizing" enzymes within the lumen of hollow fiber membranes.[46] "Cylindrical microcapsules" were prepared by filling the core of hollow fibers of a suitable molecular weight cut-off with an enzyme solution, by capillary action for instance, and then sealing both ends. Bundles of such loaded fibers were then assembled in a "tube-and-shell" reactor configuration (Figure 7.26) flushing substrate solution into the shell-side, i.e., over the outer surface of the fibers. Substrate conversion into products can be accomplished if membranes are permeable to both substrate and products.

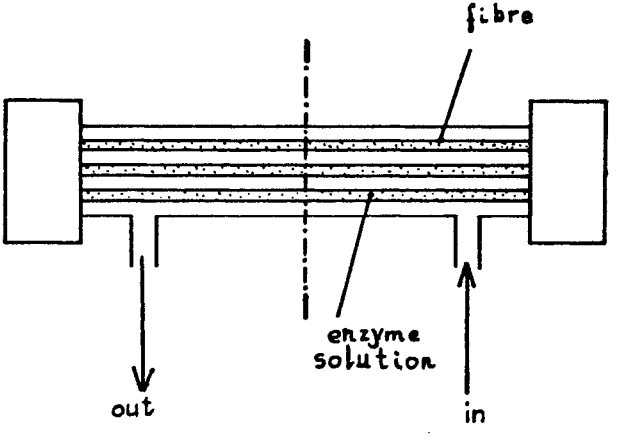


Figure 7.26: "Tube-and-shell" reactor configuration.

A theoretical analysis of such enzyme membrane reactors was carried out by Rony[46] and Waterland et al.[47] In the Waterland model, which refers to asymmetric hollow fibers, each fiber is assumed to be at the nodal position in an equilateral triangular mesh, so that it is equidistant from six adjacent fibers.

In the absence of pressure driven fluxes through the membrane and assuming a laminar flow pattern, a hexagonal free shear layer should sheath each fiber; the hexagon is approximated by an equivalent circle of radius Re.

Four different regions can be distinguished in the reacting system (Figure 7.27):

(1) The core of the fiber where enzyme solution is retained,

(2) The dense thick layer,

(3) The porous spongy part of the membrane,

(4) The shell region where substrate solution flows.

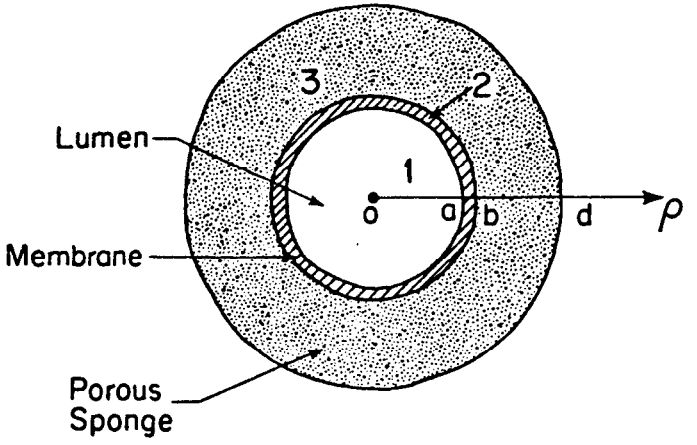


Figure 7.27: Asymmetric hollow fiber schematic: radial cross section.[47]

The equations of fluid flow in region 4 are then similar to those of a liquid film falling around a cylinder:

$$\frac{1}{r'}\frac{d}{dr'}\left(r'\frac{dv}{dr'}\right) = 4k \tag{43}$$

B.C.1 $\quad r' = d/a \quad \bar{v} = 0$

B.C.2 $\quad r' = r_e/a \quad \frac{d\bar{v}}{dr'} = 0$

where k is a constant proportional to the Reynolds number and to axial pressure drop. B.C.1 states that there is no slipping at the fiber-fluid boundary. B.C.2 detects the shear free surface. The solution to the set of equations is given by:

$$v = k\left(r'^2 - \frac{d^2}{a^2} - 2\frac{r_e^2}{a^2}\ln\left(r'\frac{a}{d}\right)\right) \tag{44}$$

with

$$k = \frac{3\,r_e^2 + d^2}{2\,a^2} - \frac{2\,r_e^2}{r_e^2 - d^2}\ln\left(\frac{r_e}{d}\right)$$

The mass transport equations for substrate concentration can be expressed as follows:

$$\frac{1}{r'}\frac{\partial}{\partial r'}\left(r'\frac{\partial S_4}{\partial r'}\right) - \left(r'^2 - \frac{d^2}{a^2} - 2\frac{r_e^2}{a^2}\ln\left(r'\frac{a}{d}\right)\right)\frac{\partial S4}{\partial z'} = 0 \tag{45}$$

$$\frac{1}{r'}\frac{\partial}{\partial r'}\left(r'\frac{\partial S_3}{\partial r'}\right) = 0 \tag{46}$$

$$\frac{1}{r'}\frac{\partial}{\partial r'}\left(r'\frac{\partial S_2}{\partial r'}\right) = 0 \tag{47}$$

Assuming a Michaelis-Menten rate equation, substrate mass transport through region 1 is governed by:

$$\frac{1}{r'}\frac{\partial}{\partial r'}\left(r'\frac{\partial S_1}{\partial r'}\right) = \frac{\phi\, S_1}{(\theta' + S_1)} \tag{48}$$

with the following boundary conditions:

$$S_4(r', z') = 1 \qquad z' < 0$$

$$S_4\left(\frac{d}{a}, z'\right) = S_w(z') \qquad z' > 0$$

$$\frac{\partial S_4}{\partial r'}\left(r' = \frac{r_e}{a}\right) = 0$$

$$S_3\left(\frac{d}{a}, z'\right) = S_w(z')$$

$$D_3 \frac{\partial S_3}{\partial r'}\left(r' = \frac{d}{a}\right) = D_4 \frac{\partial S_4}{\partial r'}\left(r' = \frac{d}{a}\right)$$

$$\gamma' S_2\left(\frac{b}{a}, z'\right) = S_3\left(\frac{b}{a}, z'\right)$$

$$D_2 \frac{\partial S_2}{\partial r'}\left(r' = \frac{b}{a}\right) = D_3 \frac{\partial S_3}{\partial r'}\left(r' = \frac{b}{a}\right)$$

$$S_1(1, z') = \gamma' S_2(1, z')$$

$$D_1 \frac{\partial S_1}{\partial r'}(r'=1) = D_2 \frac{\partial S_2}{\partial r'}(r'=1)$$

$$\frac{\partial S_1}{\partial r'}(r'=0) = 0$$

Dimensional analysis of the problem for this reactor configuration pulls out three dimensionless parameters, the Peclet number, Pe, θ' and ϕ defined as:

$$Pe = \frac{k\, Q\, a}{\pi\,(r_e^2 - d^2)\, D_4} \tag{49}$$

$$\theta' = K_M / S_f$$

$$\phi = \lambda'^2\ \theta'$$

The set of the above equations leads to a nonlinear problem which can be solved by an iterative numerical technique.[47] Substrate concentration profiles, and therefore substrate bulk concentration, are then a function of seven dimensionless parameters λ'^2, z', b/a, d/a, D_1/D_3, $D_1/\gamma' D_2$, θ'. Essential predictions of the model have been estimated by Waterland et al in terms of substrate bulk concentration as a function of λ'^2, θ', and z', the main dimensionless parameters.[47] Partition coefficients were kept equal to unity and geometrical parameters were set according to the dimensions of a typical hollow fiber, that is a = 100 μm, b = 100.5 μm, d = 175 μm; diffusion coefficients in region 1, 3 and 4 were assumed equal to each other, while the substrate diffusion coefficient in region 2 was assumed one order of magnitude lower.

A plot in shell coordinates of dimensionless length z' vs the Thiele modulus λ'^2 with θ' and the degree of conversion at given values (Figure 7.28) helps in predicting reactor performance at different operating conditions. As the Thiele modulus increases, the reaction rate becomes diffusion controlled where the dimensionless length required for a given conversion is independent of λ'^2. Under these conditions an increase in the activity or the amount of catalyst has little or no effect on the dimensionless length necessary for a given conversion. Accordingly, if a reactor is operated in a diffusion controlled regime enzyme activity decays, down to 10% or even to 1% of initial activity, negligibly affect reactor conversion. Operation of such enzyme reactors in a totally or partially diffusion controlled regime can therefore lead to an incorrect determination of biocatalyst stability.

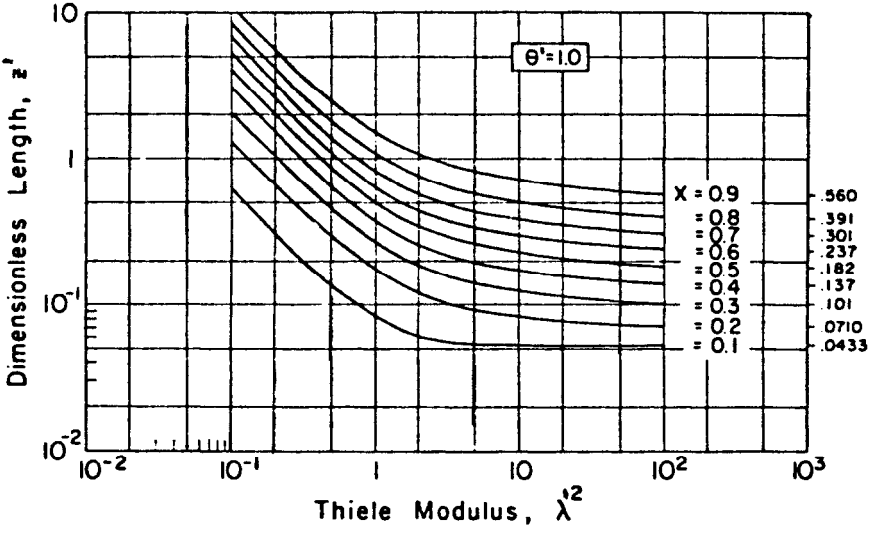


Figure 7.28: Reactor dimensionless length (z') as a function of the Thiele modulus. The parameter X is substrate conversion.[47]

As the Thiele modulus decreases, the reaction becomes kinetically controlled.

Transition from one regime to the other and the Thiele modulus value above which the reaction is diffusion controlled is strongly dependent on the parameter θ', i.e., on the initial substrate concentration. As S_f increases, the region under kinetic control is shifted towards larger Thiele moduli. Therefore, increases in catalyst activity or in the amount of catalyst are effective only at high substrate feed concentrations.[47-49]

Plots of substrate bulk concentration vs the dimensionless reactor length[47] show how steep the descent of profiles can be when large Thiele moduli are approached. Substrate conversion is therefore more rapid in the diffusion controlled regime, and reactors are better operated in this regime.

Furthermore, in applications where products can be easily separated from the effluent stream, it can be convenient to operate at small dimensionless lengths at the expense of lower conversions. Product mass flow rate will increase, more than compensating for this reduction in conversion.

Evaluation of stability and catalytic properties of the immobilized system must take into account possible pH differences between the inner core of the fiber, where the reaction takes place, and the bulk of the feed solution. The production of compounds which alter the pH, like ammonia produced from urea via immobilized urease,[48] and the partition properties in hollow fiber membranes can result in creating such pH gradients. Experimentally, these differences produce more or less pronounced shifts in the optimum pH dependence of enzyme activity relative to its free form dependence and thereby affect the activity of the enzyme at work.[2,3,48]

Urease, uricase,[48] alcohol dehydrogenase,[50] and alkaline phosphatase[51] have been used in such reactors.

Given the availability of hollow fiber membranes adequately permeable to substrates and products, and the control of fluid flow all around the fibers in the bundle in order to assure uniform flow distribution and to avoid stagnation (in order to reduce mass transfer diffusional resistances), the technique offers several advantages. Enzyme proteins can be easily retained within the core of the fibers with no deactivation due to coupling agents or to shear stresses, and the enzyme solution can be easily recovered and/or recycled.

Similar reactor configurations using flat membranes in place of hollow fibers have even been used with urease, uricase, glucose oxidase and creatinine kinase.[49] An enzyme solution is, in this case, introduced into one of the membrane-separated chambers of a flat-membrane dialyzer. Operating the reactor at high feed flow rates leads to a reduction of mass transfer resistances, which can also be achieved using suitable turbulence promoters. The overall behavior of such systems appears to be similar to that of the hollow fiber enzyme reactors, except for an apparent higher efficiency.[49]

Reactors with Enzymes within the Pores of Asymmetric Membranes

Asymmetric synthetic hollow fiber membranes designed for use in ultrafiltration/dialysis processes can provide an interesting support for immobilizing enzymes.

The term asymmetric refers to membranes comprised of a porous spongy wall supporting a very thin dense layer. The thin skin layer, approximately 0.5

μm thick, with pore sizes in the range of 10 to 2000 Å, determines the separation properties of the membrane with little hydraulic resistance to mass transport. This skin layer is fully surrounded by a spongy structure, approximately 75 μm thick, with pore sizes of 5 to 10 μm, and 80 to 90% porosity which has a very high hydraulic permeability. This porous spongy wall acts as a mechanical support for the semipermeable thin layer.

The use of these fibers in bioreactors can eliminate some of the disadvantages of the previously discussed reactor systems.[42,47,53]

Enzymes can be entrapped within the outer sponge layer of the fibers by saturating their pores with an enzyme solution (Figure 7.29). The wet catalytic fibers can then be organized in bundles and assembled in a "tube-and-shell" reactor configuration. If the pores in the dense layer are small enough to retain enzyme molecules but large enough to freely pass substrates and products, the enzymes are effectively immobilized or segregated within the spongy annular section. The reactor can then be operated by feeding substrate solution through the lumen of the fibers, in a reverse configuration than that previously sketched. If substrate molecules are small relative to the membrane's molecular weight cut-off, they diffuse across the dense layer from the fiber lumen into the enzyme solution where the reaction takes place. In turn, product molecules diffuse back into the substrate solution, or, if gaseous, leave the fiber through the shell side.

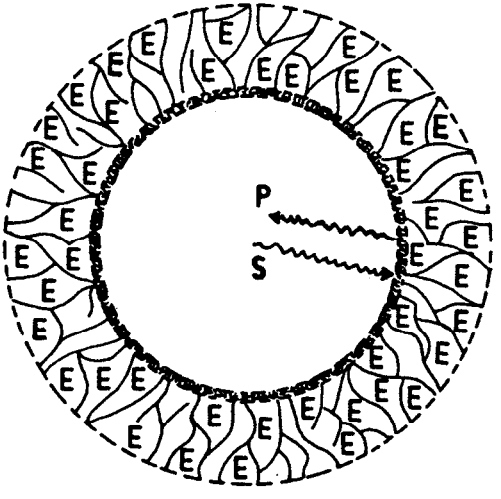


Figure 7.29: Schematic of the cross section of a hollow fiber in whose macropores enzymes are immobilized.[42]

The dynamics of substrate conversion therefore depend on enzyme kinetics as well as on mass transport conditions. Diffusion through the membrane matrix and within the flowing solution, play the most important roles in transport mechanisms. Since the flow is laminar in most cases, substrate and product transport resistances through the dense layer are exceedingly small relative to diffusional resistances in the flowing solution. The rate-limiting step in sub-

strate conversion is therefore either simple diffusion or the intrinsic kinetics of the reaction itself.

Mathematical modeling of such reactors has been extensively investigated.[47,53] Referring to the model presented in the previous section (Figure 7.27), the reaction system may be divided into only three regions; namely the previously defined regions 1, 2, and 3, with substrate solution flowing in region 1. It is assumed we have:

- Laminar flow in region 1, with substrates and products diffusing through all three regions
- Steady state conditions
- Chemical reaction confined to region 3, where fluid is assumed to be stagnant
- Constant fluid properties.

Using a set of cylindrical coordinates as in Figure 7.30, the set of mass transfer differential equations defining substrate concentration in each region is:

$$D_3 \frac{1}{r} \frac{\partial}{\partial r} \left(r \frac{\partial S_3}{\partial r} \right) = R \tag{50}$$

$$D_2 \frac{1}{r} \frac{\partial}{\partial r} \left(r \frac{\partial S_2}{\partial r} \right) = 0 \tag{51}$$

$$D_1 \frac{1}{r} \frac{\partial}{\partial r} \left(r \frac{\partial S_1}{\partial r} \right) = v \frac{\partial S_1}{\partial x} \tag{52}$$

Assuming a laminar flow pattern, the radial velocity profile in region 1 can be expressed as:

$$v(r) = v_{max} \left(1 - \frac{r^2}{a^2} \right) \tag{53}$$

with enzyme kinetic behavior still modeled by the Michaelis-Menten rate equation.

$$R = \frac{V_{max} \; S_3}{K'_M + S_3}$$

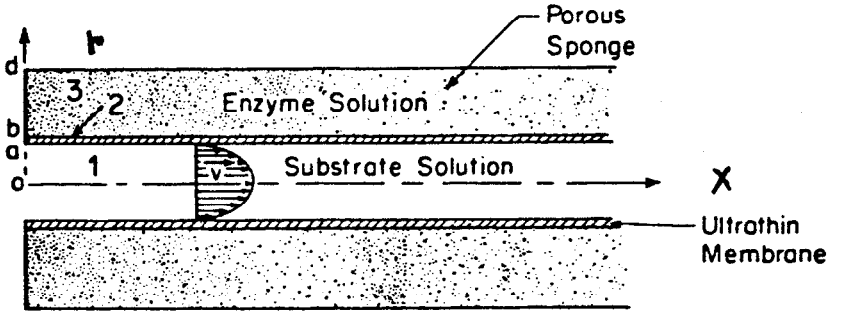


Figure 7.30: Axial section of an asymmetric hollow fiber. The substrate solution is fed to the lumen of the membrane under laminar regime.[47]

The intrinsic nonlinearity of this set of equations does not permit an analytical solution. Lewis et al[53] and Davis[110] have proposed an analytical solution to the problem in the case of low feed substrate concentration, that is for a linear rate equation. An iterative numerical solution for the nonlinear problem was fully developed by Waterland et al.[47]

Dimensional analysis of the equations relates the concentration profile, both along the lumen and the radius of the fiber, to seven dimensionless parameters: Thiele modulus, λ'^2, dimensionless length, z', dimensionless Michaelis constant, θ' and the following dimensionless quantities: b/a, d/a, D_1/D_3 and $D_1/\gamma' D_2$.

General correlations of bulk concentration as a function of Thiele modulus, dimensionless Michaelis constant and the dimensionless length in the entire range of practical operating conditions are available under the same assumptions as the previously described reactor configuration.[47,53]

Plots of the dimensionless length required to achieve a certain given conversion as a function of the Thiele modulus, with the dimensionless Michaelis constant as a parameter, are qualitatively in agreement with those obtained with the reactor operated in the reverse configuration. Regions under diffusion or kinetic control are approached as the Thiele modulus is increased or decreased, respectively (Figure 7.31). When the dimensionless Michaelis constant θ' (i.e., the reciprocal of the feed concentration) is decreased, transition between the kinetic and diffusion controlled regimes occurs over a narrower range of the Thiele modulus. Kinetic control holds for larger Thiele moduli, and the slope of the linear dependence of the dimensionless length z' on the Thiele modulus (in a log-log plot) increases. An increase in feed substrate concentration may therefore shift reactor operation from a mainly diffusion controlled regime to a mainly kinetic controlled regime, with a consequent decrease in reactor conversion. From another point of view, one might say that increases in feed concentration require sensible increases in the reactor dimensionless length to achieve the same conversion as before the change.

Comparisons between the performance of the reactor operated in this configuration and in the reverse one evidence[47] that both behave in a similar way

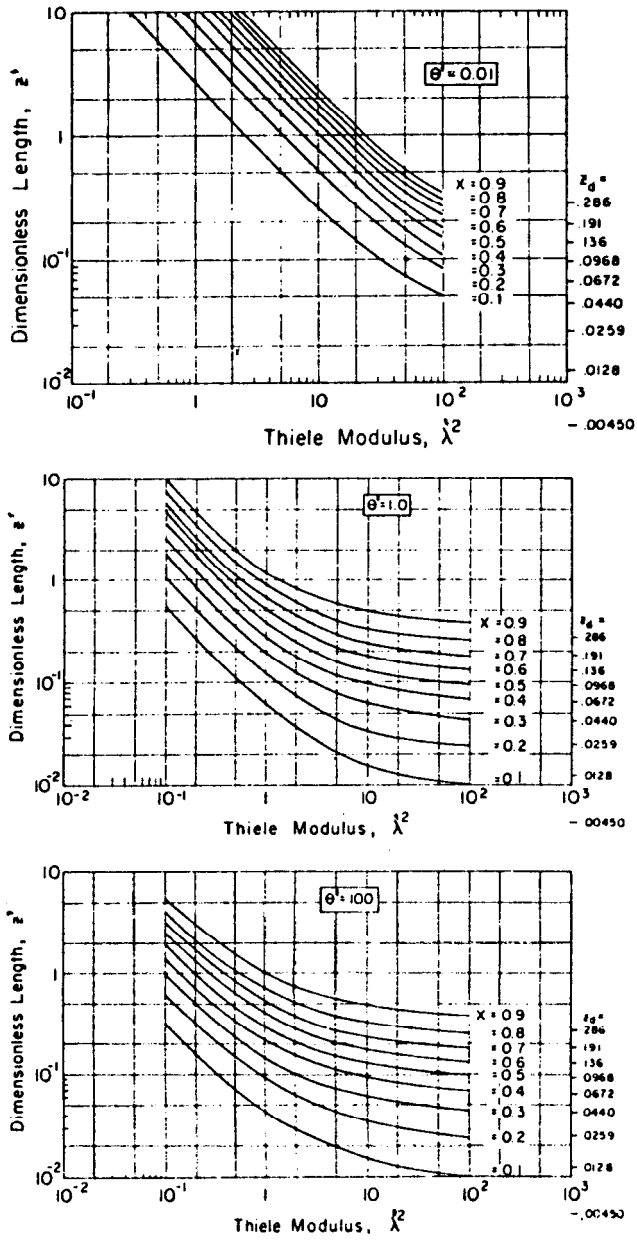


Figure 7.31: Reactor dimensionless length (z') as a function of the Thiele modulus at various dimensionless times. The parameter X is substrate conversion.[47]

under conditions of kinetic control. When the Thiele modulus is increased and the enzymes loaded into the sponge of the hollow fibers, the dimensionless reactor length required to achieve a given conversion is smaller than that necessary for a reactor where enzymes are encapsulated within the lumen of the fibers themselves. Reactors with enzymes entrapped in the macroporous region of the membrane wall appear to be better whenever they are operated in the diffusion controlled regime.

Experimental work in which enzymes with relatively simple kinetics were immobilized in the sponge of hollow fibers, e.g., α-galactosidase,[54] invertase,[54] glucose isomerase,[55] and urease,[53] are in good agreement with predictions of the theoretical model.[47,53] Quick graphical procedures are available in the literature for evaluating the extent to which external and internal diffusion affect immobilized enzyme kinetics.[43] Agreement between experimental results and predictions of the more comprehensive proposed model suggests that it might be used to predict reactor performances in the case of simple kinetics and when the kinetic and transport parameters are known.

When complex kinetics are involved in substrate conversion, as with product-inhibited enzymes (like amyloglucosidase which catalyzes maltose conversion to glucose[42]) or with reactions involving a number of intermediates (like starch hydrolysis by means of amyloglucosidase[42]) definite information on enzyme kinetics is rarely available. Moreover, when solutions of macromolecular compounds, like starch, are fed to the reactor, diffusional resistances are more pronounced and may hinder the possibility of using such reactors for analytical purposes. A thorough knowledge of the chemical mechanisms through which substrates are converted to products and of the coupling of transport phenomena to enzyme reactions appears to be a prerequisite for the design of such biochemical reactors.

Different operating conditions may require some modification of the performed analysis. Ultrafiltration and/or osmosis can promote convective solute or water flux through the membrane wall. Should it happen, radial convection could compete with diffusion as the main substrate and product transport mechanism. The relative importance of the two transport mechanisms can be evaluated by comparing the radial convective velocity to the diffusive velocity, that is the ratio of the diffusion coefficient to the wall thickness. When the first one is negligible relative to the latter, the model applies without modification. The second possible effect of the radial flux is to remove enzymes from the fiber wall, resulting in the reduction of reactor efficiency.

This reactor configuration is particularly attractive since substrates are physically separated from the enzyme solution only by a very thin membrane layer, the dense skin, thus minimizing mass transfer diffusional resistances. A number of other advantages make this reactor configuration feasible for many applications. The use of small diameter fibers leads to large area-to-volume ratios, with high enzyme loading capacity per unit of reactor volume. The enzyme microenvironment is fully shear free. Moreover, membranes act as selective barriers protecting enzymes from macromolecular contaminants such as proteolytic enzymes, or selecting substrates on the basis of their permeability or electric charge. Many enzymes can even be coimmobilized with the macroporous region of asymmetric membranes. The procedure itself does not exclude the possibility of crosslinking enzymes directly to the porous polymeric matrix of the fibers, nor that

of compartmentalizing within the same region enzymes previously coupled to soluble polymers or inactive proteins. Such binding procedures might in fact result in a greater stability, that is a slower decay of enzyme activity with time.

In this reactor configuration, once products are formed they diffuse back towards the stream flowing in the core of the fibers. Such configuration is therefore feasible for all those applications in which products at relatively high concentration are tolerated in the circulating stream.

Tube and Shell Membrane Reactors with the Biocatalyst on the Shell Side

As with enzymes, whole active microorganisms can be segregated in a definite region of space by means of membranes in order to catalyze specific reactions. Microsomes[57-60] and bacteria[61] have been and are currently employed in membrane reactors in order to perform complex multienzymatic reactions or to reduce overall reactor costs, avoiding enzyme purification. When the size of the biocatalyst exceeds the dimensions of the pores in the sponge of the asymmetric membranes,[44] previously examined reactor configurations are not applicable. Nevertheless, the problem can be overcome allowing the biocatalyst to stay on the shell side, while the substrate solution is kept flowing within the lumen of the fibers.

Apparently the main transport mechanisms through which substrate conversion takes place are:

- Diffusion of substrates from the bulk fluid phase to the membrane
- Diffusion of substrates within membrane pores
- Diffusion of substrates within the shell-side of the reactor to the biocatalyst

Referring to one fiber alone, the scheme of the reacting system is similar to those examined so far. However, the reaction does not occur in either regions 1, 2 or 3. The set of differential mass transfer and continuity equations defining substrate and product concentration in these regions are equal to those previously examined. The description of mass transport in the shell-side region is somewhat more complicated. Differences in the environment surrounding each fiber, the position of fibers in the bundle, and the ultrafiltration fluxes make both the analytical and the numerical approach quite difficult.

Models proposed[57,58,62] often deal with simpler systems, assuming good mixing conditions both in the shell and within the lumen of the fiber, and pure diffusive fluxes. In some particular configurations, as in the artificial pancreas, such assumptions hold and the models work quite well, especially in the case of membrane units using one large hollow fiber alone.[57,63] In cases where a quick transient response is needed, the only way to circumvent the slow transient behavior of the device is to reduce the volume where the catalyst is compartmentalized.[57] Even though diffusion appears to play an important role in substrate and product transport, there is experimental evicence that the bundles of hollow fibers assembled in a "tube-and-shell" configuration respond more quickly than could be predicted by assuming purely diffusive fluxes across the membrane walls.[62] Pressure drop along the length of each fiber should therefore produce a transmembrane pressure across the membrane wall such that at

the inlet of the reactor, the pressure difference promotes an ultrafiltration flux towards the shell side, where the catalyst is, and at the outlet it promotes a backward flux from the shell towards the lumen of the fiber (there is only a small pressure drop in the shell[44]). These pressure profiles promote fluxes which improve the performances of the system as compared to those exhibited by pure diffusive reactors.

A quantitative analysis of such ultrafiltration flux[59,62] can be approached referring to a single fiber device (Figure 7.32). At a distance, x, from the inlet of the reactor local ultrafiltration flux, J, can be related to local transmembrane pressure, $\Delta\Pi$, according to the following equation:

$$J(x) = L_p \quad \Delta\Pi(x) \tag{54}$$

where the coefficient L_p is the hydraulic permeability of the membrane to the substrate solution. In turn, the local transmembrane pressure can be expressed as:

$$\Delta\Pi(x) = \Pi_b(x) - \Pi_{onc} - \Pi_s \tag{55}$$

where Π_{onc} and Π_s are the local oncotic pressure and shell-side pressure. Assuming that the feed solution is newtonian with a laminar flow pattern, pressure in the fiber at distance x from the fiber inlet can be evaluated from Poiseuille's law to be:

$$\Pi_b(x) = \Pi_{bi} - \left(\frac{8\,\mu\,Q}{\pi\,a^4\,N_f}\right) x \tag{56}$$

where Π_{bi} = inlet pressure

μ = substrate solution viscosity

N_f = the number of fibers in the bundle.

Introducing $B = \Pi_{bi} - \Pi_{onc} - \Pi_s$

and $$C = \frac{8\,\mu\,Q}{\pi\,a^4\,N_f}$$

and substituting the expression for flux as a function of transmembrane pressure one obtains:

$$J(x) = L_p\,(B - Cx) \tag{57}$$

A decrease in hydrostatic pressure along the fiber due to resistance to substrate solution flow occurs so that at a definite distance from the inlet, say L_c, transmembrane pressure is nil. Fiber-to-shell solution flux from that point on is negative and becomes a shell-to-fiber flux. Neglecting the shell pressure drop, the overall fiber-to-shell ultrafiltration net flow rate can then be obtained upon integration of the flux equation over the length of the fiber from the inlet to L_c, that is:

$$Q_{f1} = 2\,\pi\,a\,N_f\,L_p \int_0^{L_c} (B - C\,x)\,dx = \tag{58}$$

$$= 2\,\pi\,a\,N_f\,L_p \left(B\,L_c - C\,\frac{L_c^2}{2}\right)$$

But at a distance L_c from the inlet $\Delta\Pi = 0$, so that $L_c = B/C$ and consequently:

$$Q_{f1} = \pi\,a\,N_f\,L_p\,\frac{B^2}{C} \tag{59}$$

The overall shell-to-fiber flux can be obtained in a similar way, upon integration of the flux equation between L_c and the reactor outlet, as follows:

$$Q_{f2} = -\,2\,\pi\,a\,N_f\,L_p \int_0^{L-L_c} C\,x\,dx = -\,\pi\,a\,N_f\,L_p\,(L - L_c)^2\,C \tag{60}$$

The shell volume is constant, therefore $Q_{f1} + Q_{f2} = 0$ (61)

or in other terms $\pi\,a\,N_f\,L_p\,B^2/C = \pi\,a\,N_f\,L_p\,(L - L_c)^2\,C$

that is $B^2/C = (L - L_c)^2\,C$ and $L = 2\,B/C = 2\,L_c$

The expression for B can be substituted in the expression of the overall fiber-to-shell flux to give:

$$Q_{f1} = 2\,\mu\,L_p\,L^2\,Q/\,a^3 \tag{62}$$

Upon imposition of the pressure drop along the fibers, the flow rate Q can be evaluated from Poiseuille's law to give a relation where the net ultrafiltration flow rate, Q_{f1}, is related to the total membrane area, A, and pressure drop along the fibers:

$$Q_{f1} = A\,L_p\,\Delta\Pi/8 \tag{63}$$

The characteristic time of this reacting system is $\tau = V/Q_{f1}$, where V is the shell-side void volume. The previous equation can be rewritten to relate the characteristic response time of the device and the volume where the biocatalyst is confined to give:

$$V = A\,L_p\,\Delta\Pi\,\tau\,/8 \tag{64}$$

Given the membrane surface area, A, its hydraulic permeability, L_p, and pressure drop along a fiber, $\Delta\Pi$, it is possible to estimate the minimum volume required in order to obtain the necessary response time.[59]

This reactor configuration is often appropriate for complex catalytic systems. The use of cofactors with the enzymes in continuous flow systems has of-

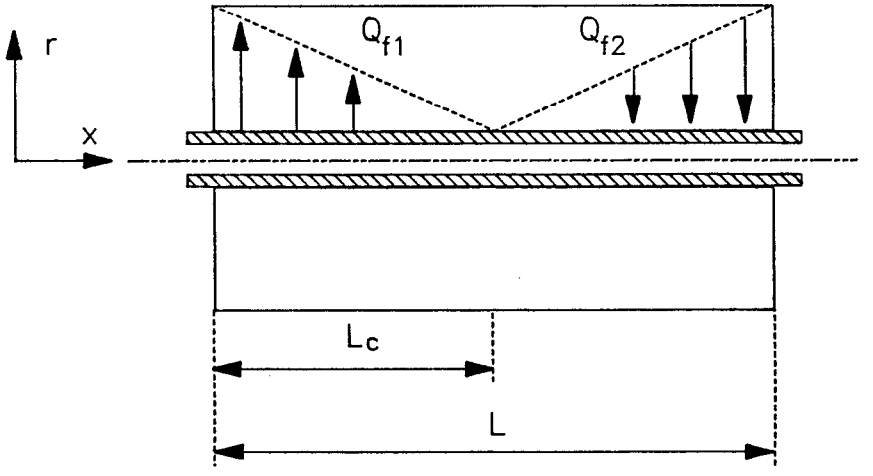


Figure 7.32: Schematic of a hollow fiber encased in a closed shell. The occurring absorption and reabsorption fluxes along membrane axis are Q_{f1}/Q_{f2}, respectively. No transmembrane flux occurs at membrane half length.[59]

ten been limited by the need to supply large amounts of fresh cofactor, usually an expensive compound. Many procedures have been suggested in order to confine these low-molecular-weight compounds in a well defined region of space where they are continuously used and regenerated.[103,111] When the biocatalyst is compartmentalized in this way, cofactor costs are reduced. In the presence of a suitable regeneration system, only low cofactor additions are needed to maintain excess concentration levels thus assuring maximum rates of conversion.[60,64]

Membranes which retain high-molecular-weight biocatalysts in the shell, but allow the passage of low-molecular-weight products or inhibitors, may also allow the segregation of biocatalysts in the shell capable of transforming inhibitors into nonactive compounds, thereby keeping their concentration low in the effluent reacting stream. This concept has been used in the enzymatic hydrolysis of cellulose.[44,65] A blend of cellulose, substrate, and cellulase, a suitable enzyme mixture, is kept flowing within the lumen of the fibers assembled in the bundle. When cellulose is converted to glucose, cellobiose (an intermediate product) is formed which acts as an inhibitor for some cellulase enzymes. The presence of a suitable biocatalyst, such as the enzyme β-glucosidase[44] or the cells of Hansenula,[65] in the shell of the reactor can reduce the extent of inhibition. As soon as cellobiose is produced, it flows towards the shell being converted to glucose by β-glucosidase. In this way, the inhibitor concentration in the reacting stream can be kept low without affecting the overall sugar concentration.[44]

Reactors in this configuration are also employed in therapeutic applications. Bundles of hollow fibers[59,66] or a single large hollow fiber[57,63] in a cylindrical module are used to separate blood flowing within the lumen and mammalian pancreatic islets as assistance to diabetic patients. They have also been suggested[60] for use as extracorporeal blood detoxifiers, where mammalian liver mi-

crosomes are compartmentalized in the shell of the module. In such systems, if the membrane molecular cut-off is carefully chosen, membranes will protect transplanted cells from the immunodefensive action of leukocytes in the blood. The main drawback of membrane reactors in this configuration is the relatively slow response to metabolic stimulation due to large shell volumes required to accommodate a number of large-sized biocatalytic units needed to perform the assistance action.

Diffusion and ultrafiltration fluxes due to pressure drop along the length of fibers play the most important role in substrate and product mass transfer when systems are operated as previously described. However, an ultrafiltration flux can be promoted from the lumen of the fibers outwards and/or from the shell inwards.[44] Better reactor performances should result from such operating conditions.

Perspectives

Most of the membrane segregated enzyme systems previously examined suffer some constitutive drawbacks which limit their yield and area of application. When enzymes are entrapped within the sponge of asymmetric membranes, product and substrate mass transfer occur mainly by a diffusive mechanism; reactor performance is then controlled only by means of the amount and kind of charged enzyme, and the fluid dynamics of the solution in the core of the fibers. UF or RO fluxes, moreover, result in enzyme losses. Enzyme crosslinking in the membrane pores can reduce these losses, but it can lead to an initial activity loss, as compared to that of the native enzyme. Of course, once the enzyme is deactivated, it makes the reactor useless for further operation. Such immobilization techniques are seldom useful for microbial cells due to their large size.

In recent years, membranes have been cast with microbial cells incorporated in the casting solution. To date, the casting of UF and RO membranes charged with enzymes or whole cells on an industrial scale has been limited by the drastic conditions under which the synthetic membranes are usually formed. The presence of nonaqueous solvents in casting solutions, and the high temperatures required by membrane annealing, generally denature enzymatic proteins, with a loss in their catalytic activity. Recently, a number of microorganisms, e.g., *Sulfolobus solfataricus*, have been discovered which can withstand both high temperatures and organic solvents. Microbial enzymes maintain their activity in conditions otherwise denaturating, presumably because of cellular membrane protection.[61] Polysulfone[61,67] and cellulose acetate membranes[68] have been cast with microbial cells in the casting solution using the phase inversion technique, as well as in polyurethane foams.[69] Cell loaded membranes appear to be kinetically active and stable over a long period of time;[67] the resistance to flow is fairly low and is strongly dependent on the forming procedure. It is noteworthy that cell entrapment can enhance microbial activity as compared to cell behavior in homogenous solution,[61] an effect probably due to cellular membrane permeabilization as a consequence of the entrapment procedure.

Entrapped whole cells are the source of a number of microbial enzymes useful for industrial purposes. In addition, the possibility of long term operation make this immobilization procedure extremely attractive. Stable immobilized cells permit the carrying out of an enzyme reaction in one stage alone, an op-

eration which normally requires two different stages, namely enzymatic conversion and membrane separation.

MEMBRANE BOUND ENZYMES IN CONTINUOUS-FLOW SYSTEMS

In recent years a large number of techniques have been suggested in the literature for immobilizing enzymes on insoluble carriers; in particular, immobilization on polymeric solid supports or glass beads. A stable attachment can result from ionic binding, cross-linking and covalent linking to a water-insoluble matrix. A full description of chemical and/or physical procedures required to make enzymes insoluble is beyond the scope of this chapter and is extensively dealt with elsewhere.[112,113]

We will be concerned mainly with enzymes bound to synthetic polymeric membranes via covalent binding. Since 1954, when protease was covalently bound to diazotized polystyrene,[114] enzyme immobilization via covalent bonds has been an established immobilization technique, usually carried out by means of extremely active bridge molecules, such as CNBr, or bi/multi-functional reagents, such as glutaraldehyde.[113] However, the mechanisms involved in enzyme immobilization are not well understood in most cases. When glutaraldehyde is used as a coupling agent, it has been suggested that immobilization results from reaction between the enzyme free amino groups and the glutaraldehyde aldehyde functions with the formation of an intermediate Schiff base. The resultant bonds are generally extremely stable, due to the high binding energy of the covalent bonds. On the other hand, coupling agent molecules, usually quite small, can penetrate deep into the active sites of enzyme protein coils where reaction takes place. Once these sites are involved in linking to the matrix, they are no longer available to substrate molecules, resulting in a irreversible loss of activity as compared to the initial activity of the native enzymes. When the extent of initial denaturation is acceptable in the economics of the process, enzymes bound to membranes can be used in continuous flow reactors. Asparaginase, arginase, ligandine and glutathione-S-transferase,[70] catalase, uricase, allantoinase and allantoicase,[71] have all been immobilized onto Cuprophan hollow fiber membranes; asparaginase and alcohol dehydrogenase onto nylon tubes;[72,73] and urease, dextranase[74] and papain[75] have been attached to cellulosic and polysulfone flat membranes. Apparently the immobilization procedure affects the immobilized enzyme activity more than the membrane configuration.

Enzymes are covalently immobilized primarily onto the surface of the membrane exposed to the feed solution, known as the "active side" of the asymmetric membrane. In general, it is not clear whether reaction between enzymes and polymeric membranes via coupling agents simply results in enzyme attachment to the membrane, or if it leads to an enzyme-carrier network inside the polymer matrix. For the sake of simplicity let us assume that asymmetric membranes are used, that suitable active groups are available on the polymeric surface and that the membrane molecular weight cut-off is such that the active layer is enzyme-impermeable. In this way, even though their activity is often drastically reduced, surface bound enzymes are in close proximity to the substrate solution–thus reducing the mass transfer resistance to that associated with the boundary layer. When enzymes are covalently immobilized in the

sponge of the membranes, the mass transfer through the membrane wall must also be taken into account.

Applications of covalently immobilized systems are essentially:

(1) Membrane electrodes for analytical purposes;

(2) Reactions of substrates whose molecular weight is low as compared to membrane molecular weight cut-off;

(3) Enzymatic conversion of macromolecules to lower molecular weight species able to permeate the supporting membrane.

As far as membrane electrodes are concerned, readers are referred to the literature.[3,112,115-116]

When the substrate has a molecular weight lower than the membrane cut-off, enzymes can be covalently bound either to the "active side" of the membrane or within the sponge-like substructure of the membrane.

If the enzyme kinetic behavior is not affected by compounds in the solution to be processed, enzymes are preferentially bound onto the "active side" of the supporting membrane, thus minimizing the overall substrate mass transfer resistance. When such systems are used for analytical purposes, the diffusional resistance in the bulk phase must be taken into account. Obviously, the kinetic parameters for native enzymes are no longer applicable for the immobilzed-system.[1-3]

Comprehensive descriptions of mass transfer and kinetic effects on the performance of such reactors under different operating conditions are not yet available. A theoretical analysis of a tubular reactor with impermeable inner walls coated with enzymes was carried out by Kobayashi and Laidler[76,77] and experimentally confirmed by Bunting and Laidler.[73] In this analysis, the reacting solution is fed to the core of the fibers. Assuming laminar flow, the steady state mass transport equation for the substrate is:

$$D\left(\frac{\partial^2 S}{\partial r^2} + \frac{1}{r}\frac{\partial S}{\partial r}\right) - v_{max}\left(1 - \frac{r^2}{a^2}\right)\frac{\partial S}{\partial x} = 0 \qquad (65)$$

with the following boundary conditions:

$$\text{B.C. 1} \qquad x = 0 \qquad S = S_f$$

$$\text{B.C. 2} \qquad r = a \qquad D\frac{\partial S}{\partial r} = R(S_W)$$

$$\text{B.C. 3} \qquad r = 0 \qquad S = S_f$$

where S_W is substrate concentration at the membrane wall.

Analytical solutions have been obtained assuming the enzymatic reaction as the controlling step which implies flat substrate concentration profiles all along the tube. Numerical solutions are also available both for diffusion controlled mass transport, when the substrate concentration at the wall can be assumed to

be nil; and in the so-called transition region, when the reaction rate is neither kinetically nor diffusion controlled. They describe the dependence of the overall reaction rate on substrate concentration, the Michaelis constant, and the Damkholer number (the ratio of the reaction rate in the absence of diffusional resistance to the diffusion controlled rate).

This model does not apply to a porous wall tubular reactor. In this case, we must account for solution losses along the tube length, and a radial convective term must be included. Again, the enzymatic reaction at the catalytic wall enters into the model as a boundary condition.

In addition to applications in industrial processes, enzymes bound to the active side of hollow fibers assembled in a "tube-and-shell" configuration[70] have been and are under study as extracorporeal or "in vivo" devices for use in hepatic failure or to assist leukemic patients. For these therapeutic applications, the irreversible binding of the enzyme to the membrane is extremely important. Enzymes are in fact purified from mammalian, non-human sources, and they are continuously in contact with circulating blood; their removal from the solid matrix would result in a series of immunodefensive reactions which would alter liver operating parameters. Enzyme immobilization via covalent binding generally meets this requirement. Hollow fiber membrane reactors with covalently bound enzymes have been proposed as extracorporeal blood detoxifiers or as devices to reduce arginine and asparagine content in the blood of leukemic patients. A group of enzymes from pig liver cytosol, known as glutathione-S-transferase, have been immobilized onto the active side of commercial hemodialyzers in order to reduce the toxin content in blood. These enzymes change the polarity of the toxins through conjugation to glutathione. The resulting shift from hydrophobic to hydrophilic facilitates release through the membrane wall. Arginine and asparagine content in the blood of leukemic patients has been recently related to neoplastic cells growth; therefore their removal should hinder further cell development.[78] Asparaginase and arginase[79] have been immobilized in commercial Spiraflow hemofilters in order to support anti-leukemia therapies. *Ex vivo* and *in vivo* experiments circulating blood through these devices generally confirm an effective decrease in blood arginine and asparagine content after a relatively short time of extracorporeal circulation treatment.[70,79,80]

When symmetric membranes are used or when enzymes are fed to the spongy part of asymmetric membranes, enzyme immobilization results in either a uniform fixation of enzymes throughout the membrane wall, or in the formation of a carrier-enzyme insoluble network in the sponge of the membrane. Mass transfer through this solid phase must therefore be taken into account. A theoretical model neglecting radial convective transport and the dense layer in asymmetric membranes is available in the literature.[81] The reacting solution is still assumed to be fed to the core of the hollow fibers. Steady state, laminar flow, and isothermal conditions are assumed. Moreover, the enzymes are assumed to be uniformly distributed and the membrane wall curvature is neglected. Differential dimensionless mass balance equations can be written as follows:

$$\frac{1}{2}(1 - r'^2)\frac{\partial S^L}{\partial z'} = \frac{1}{r'}\frac{\partial}{\partial r'}\left(r'\frac{\partial S^L}{\partial r'}\right) \qquad (66)$$

in the bulk liquid phase,

$$\frac{\partial^2 S^S}{\partial r''^2} - \frac{1}{\gamma^*} \frac{S^S}{1 + \beta^* S^S} = 0 \qquad 0 < r'' < 1 \qquad (67)$$

in the annular catalyst layer, with the following boundary conditions:

$$\frac{\partial S^L}{\partial r'} = 0 \qquad r' = 0$$

$$S^L = S^S \qquad r' = 1;\ r'' = 0$$

$$\omega \frac{\partial S^L}{\partial r'} = \frac{\partial S^S}{\partial r''} \qquad r' = 1;\ r'' = 0$$

$$\frac{\partial S^S}{\partial r''} = 0 \qquad r'' = 1$$

$$S^L = 1 \qquad z' = 0$$

The concentration history appears to be a function of three dimensionless parameters, a modified Thiele modulus, γ^*, the mass Biot number, ω, and the dimensionless feed concentration, β^*. The set of non-linear equations is uncoupled by introducing an effectiveness factor, η, and numerically solved. In order to reduce computer time, the effectiveness factor has been conveniently expressed as a weighted sum of its value for the zero and first order reaction rate. Different regime conditions are depicted in terms of a dimensionless parameter,

$$(\gamma^* \omega)^{-1} = \frac{V_{max}\ (d-a)}{K'_M} \Big/ \frac{D^L}{a}$$

analogous to the Damkholer number. This is called the reactor modulus and is obtained by collecting the mass Biot number and the Thiele modulus together. The progress of the reaction is described in terms of the reactor modulus, $(\gamma^* \omega)^{-1}$, and the dimensionless reactor length, now $Z' = D^L \times /2\ v_{max}\ a^2$, the latter being equivalent to the inverse Graetz number and proportional to the reactor residence time (see Figure 7.33). Results resemble those obtained by Waterland et al in their model of hollow fiber reactors with the enzyme compartmentalized in the sponge of the polymer matrix.[47] At a low dimensionless reactor length, and a high reactor modulus, the reaction is diffusion-controlled; at low reactor moduli, the reaction is kinetically controlled. As in the model proposed by Waterland et al, the transition region becomes narrower as the feed substrate concentration increases. Dimensionless reactor lengths, Z_{kin} and Z_{diff}, define conditions to achieve a given conversion under diffusion and kinetic control.

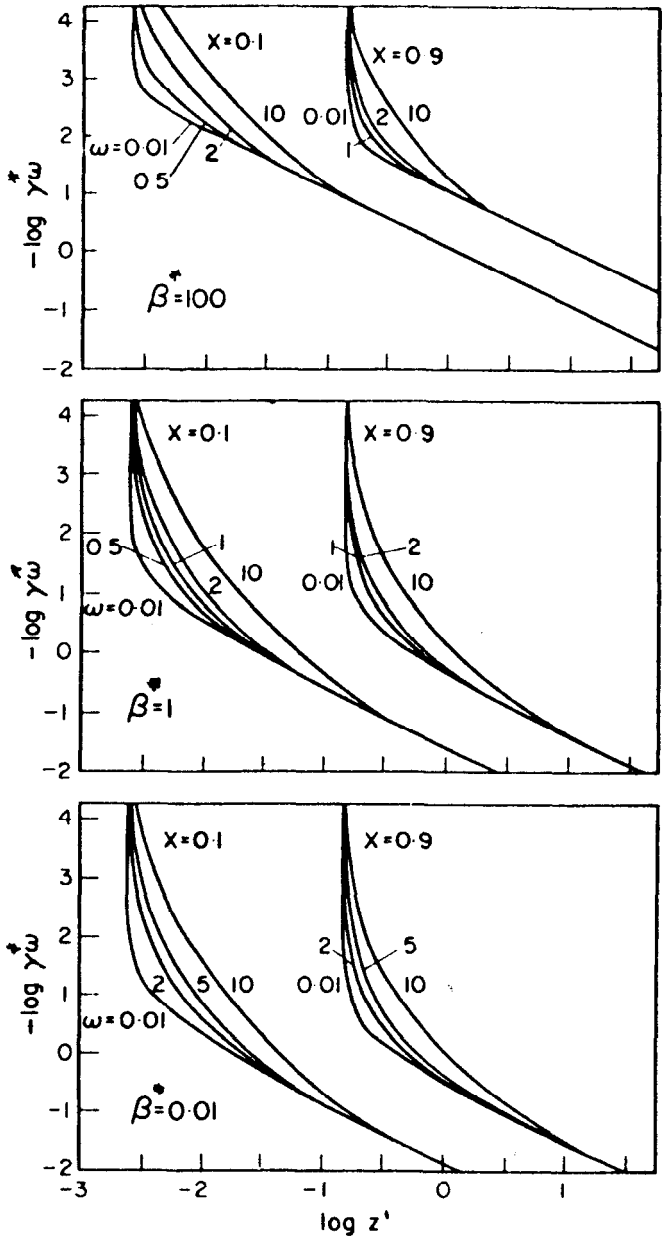


Figure 7.33: Reactor modulus as a function of reactor dimensionless length at various values of the reciprocal of the dimensionless Michaelis constant. The parameter X is substrate conversion.[81]

Generally the dimensionless reactor length required to achieve a given conversion can be expressed by the approximate relation:

$$Z = Z_{diff} + Z_{kin}/\langle\eta\rangle$$

where $\langle\eta\rangle$ is an average catalyst effectiveness factor. This expression simplifies the treatment of data and reactor design considerably.

Horvath et al[81] also give suggestions for the estimate of a reactor effectiveness factor using dimensionless reactor lengths under limiting kinetic and diffusion controlled regimes. The reactor effectiveness factor can be expressed as the ratio of the actual reaction rate to a maximum rate characteristic of the reacting system, at a given conversion. The average reaction rate is inversely proportional to the dimensionless length; the dimensionless reactor length at limiting conditions can therefore be used to define an overall reactor effectiveness factor as the ratio of a minimum length characteristic for the reactor to the actual. Reactor efficiency can thus be related to a kinetic efficiency, $E_{kin} = Z_{kin}/Z'$, and a diffusive efficiency, $E_{diff} = Z_{diff}/Z'$. E_{kin} compares the actual heterogenous catalytic rate to that achievable with the same amount of enzyme in a homogenous plug flow reactor under the same conditions; it is therefore a measure of the degree of utilization of the enzyme. E_{diff} is the ratio of the actual rate to the rate that would produce zero substrate concentration at the catalytic surface. Plots of E_{kin} vs the reactor modulus (see Figure 7.34) show how the functional dependence of E_{kin} on the reactor modulus is similar to that of the catalyst efficiency on the Thiele modulus.

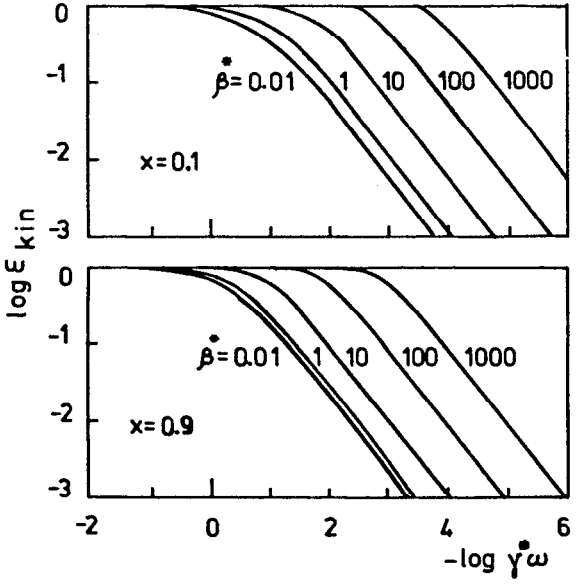


Figure 7.34: Kinetic efficiency as a function of reactor modulus at two values of substrate conversion. The parameter is the reciprocal of the dimensionless Michaelis constant.[81]

When such reactors are used for analytical purposes, the usual Eadie or Hofstee plots should not be used.[81] However, at low reactor moduli (kinetic control), straight lines are obtained and these plots are reliable for evaluating enzyme kinetic parameters. In the diffusion controlled regime, due to axial changes in the boundary layer resistance, no initial rate can be determined in the conventional sense even when the catalyst effectiveness factor is unity. The highest reaction rates are, in any case, obtained when the reaction is rate-limited by substrate transport in the bulk liquid phase. Design equations can then be obtained by the definition of limiting reactor length under bulk diffusion control. When maximum utilization of the available catalyst is the main goal, relatively inactive enzymes are needed. The reactor dimensionless length required to achieve a given conversion is then given by the expression for Z under kinetic control:

$$Z_{kin} = \frac{\gamma^* \omega}{8} (\beta^* X - \ln(1-X))$$

When radial convective fluxes due to transmembrane pressure occur, this model is no longer accurate.

Enzyme immobilization in the sponge of polymeric asymmetric and symmetric membranes has the advantage of a stable immobilized enzyme system along with the improved isolation of enzymatic proteins from immunodefensive system actions, high molecular weight inhibitors and proteolytic enzymes. A suitable choice of membranes based on their separation properties allows substrate molecules to permeate through the membrane while, at the same time, separating undesirable compounds from the enzymatic proteins.

The mass transfer mechanisms operative in substrate conversion are essentially those described by Waterland et al[47] in their model of the compartmentalized enzyme membrane reactor. Since kinetic parameters cannot be assumed equal to those of native enzymes, a kinetic analysis has to be performed in order to characterize enzyme behavior after the immobilization procedure.

Sometimes even membrane transport and mechanical properties are affected by the harsh chemical treatments required in the immobilization procedure. Figure 7.35 shows how immobilization of urease by diazotization on heterogeneous polysulfone flat membranes reduces the membrane hydraulic permeability by 50%.[74] It also shows how the higher permeability membranes are more affected by the immobilization procedure. After the enzyme is immobilized, it is wise to check the integrity of the membrane (e.g., the permeability to the species of interest and the strength).[71,74]

In extracorporeal devices, commercial Cuprophan hollow fiber membranes[71] are often used. In order to reduce the side effects of free enzymes in intravenous injection therapies, asparaginase, catalase, uricase, allantoicase and allantoinase have been immobilized by means of glutaraldehyde or CNBr onto these membranes. In vivo fluid dynamic conditions strongly limit the range of conditions at which such reactors can be operated. Reactors are often forced to operate in the diffusion-controlled regime. Under these operating conditions, the overall reaction rate depends on the substrate supply rate; the apparent enzyme activity can thus increase by increasing the recirculation flow rate. Mazzola et al[71] showed that a value of the axial flow rate exists at which the maximum reaction rate is attained; higher flow rates result in a decrease in apparent enzyme activity. In in

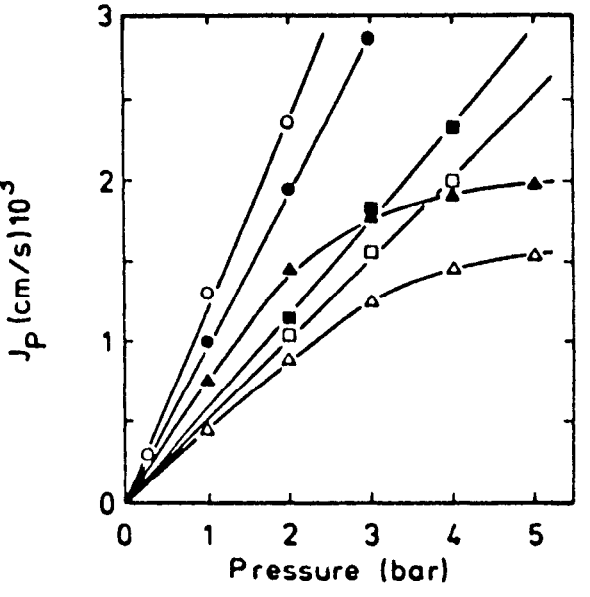


Figure 7.35: Volume flow as a function of pressure using two different types of membranes, type 2 being more permeable than type 3. Blank symbols: membrane type 2. Filled symbols: membrane type 3. Test conditions: uncoupled state, pure water (○); uncoupled state, dextran T4 (4000-6000 daltons) 1 wt% (△); coupled with urease, using a 0.015 M urea solution (□).[74]

vivo experiments, long reactors may not attain maximum reaction rates, due to high pressure drops arising from blood viscosity. Higher apparent reaction rates result when operating with shorter reactors at higher flow rates but under the same pressure drop. In vivo extracorporeal circulation experiments on rats with asparaginase bound to the outer surface of Cuprophan hollow membranes assembled in a "tube-and-shell" reactor configuration confirm that even this kind of reactor can eliminate asparagine after a short period of time, i.e., 3 to 4 hours (Figure 7.36).[71] While asparagine depletion in plasma is accomplished quickly, in blood cells it proceeds more slowly. Unfortunately, after the treatment, the asparagine content in blood cells suddenly rises, and when it levels off at its initial value, asparagine again appears in the plasma. This behavior has been confirmed by experiments on leukemic patients.[83] Even though the use of such reactors as extracorporeal units can result in an effective decrease of asparagine or arginine content in blood, its effect is limited to a few hours after the treatment. This evidence suggests that more than one metabolite has to be removed from blood at the same time to make the extracorporeal treatment effective.

Up to four enzymes involved in the metabolic pathways of purine bases–allantoinase, allantoicase, uricase and catalase–have been immobilized together by means of glutaraldehyde on the outer surface of cellulosic hollow fibers. Reactor performances are depicted in Figure 7.37, when uric acid is fed to the multi-enzyme reactor.[71]

Enzyme stability and activity can be enhanced by performing enzyme immobilization in the presence of inert proteins, such as albumin, or polyamines in order to shift the maximum enzyme activity towards blood pH.

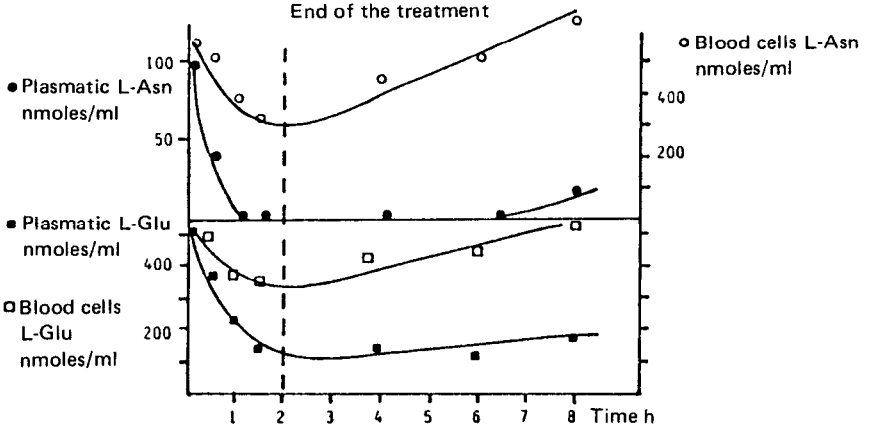


Figure 7.36: L-Asparagine concentration vs. time in in vivo experiments performed on rats. The extracorporeal device is a "tube-and-shell" membrane reactor where asparaginase is bound to the outer surface of Cuprophan membranes.[71]

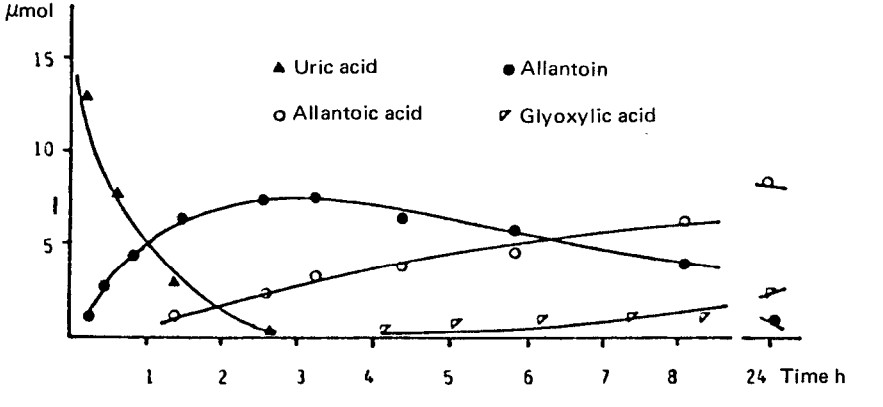


Figure 7.37: Performance of a multi-enzyme membrane reactor when uric acid is fed as a substrate. Allantoicase, allantoinase, uricase and catalase are covalently bound to the outer surface of a cellulosic membrane.[71]

Self-Cleaning Enzymatic Ultrafiltration Membranes

Thus far we have examined some of the possible applications of enzyme membrane reactors, focusing attention on situations in which enzymatic conversion is essential and the membranes act only as porous supports. However, immobilized enzymes can also be used to improve the performance and effectiveness of traditional ultrafiltration processes. Ultrafiltration of macromolecular solutions, especially proteins, is strongly hindered by the so-called concentration polarization and fouling phenomena (see Chapter 3 on ultrafiltration). The irreversible deposition[75] of a macromolecular gel layer on an active membrane surface usually results in a sharp decay in permeate flux. Immobilization of proteolytic enzymes onto the active side of the ultrafiltration membrane can provide a self-cleaning function. The hydrolytic cleavage of large proteins by proteolytic enzyme is controlled by the amount of immobilized enzyme, the fluid dynamic conditions under which the system is operated and by membrane rejection properties. As soon as macromolecules come in contact with the active enzymatic layer, they are converted to low-molecular-weight products which permeate the membrane.

Figure 7.38[74] shows how transmembrane pressure can affect molecular weight distribution in the permeate for the system dextran-dextranase when enzymes are bound to polysulfone flat membranes by means of glutaraldehyde.

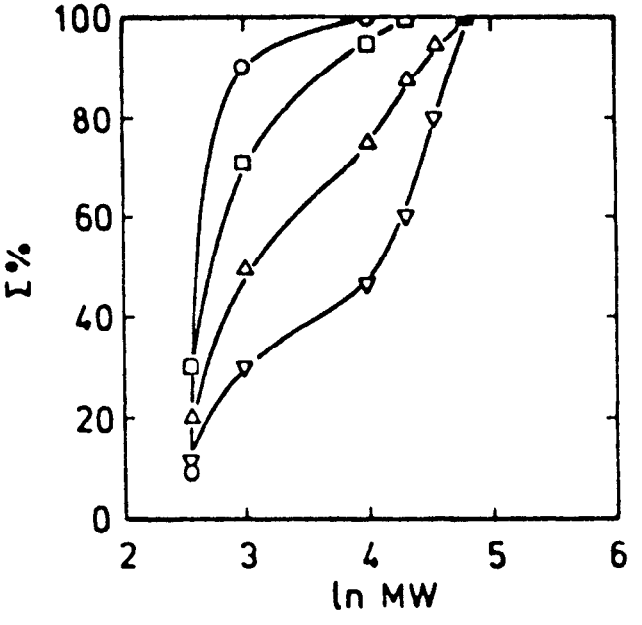


Figure 7.38: Sum curves of molecular weight distribution for different pressures. Polysulfone membrane type 1. T = 40°C, pH = 6.0, dextran T70 1 wt%: (○) 0.5 bar; (□) 1 bar; (△) 3 bar; (▽) 4 bar.[74]

At low transmembrane pressure, macromolecules are nearly 100% converted to products. As the pressure increases, macromolecular concentration in the permeate increases (see Chapter 3). By carefully choosing operating conditions, it is possible to gain a net shift in molecular weight distribution curves (Figure 7.39)[74]

Even though enzymatic conversion is not too effective, it is possible to prepare semipermeable membranes whose ultrafiltration yields are higher than those of passive membranes.[74,75] Ultrafiltration experiments of cheese whey through cellulosic membranes to which papain was covalently bound, show that flux decay curves of enzymatic membranes are even less sensitive to pH changes.[74]

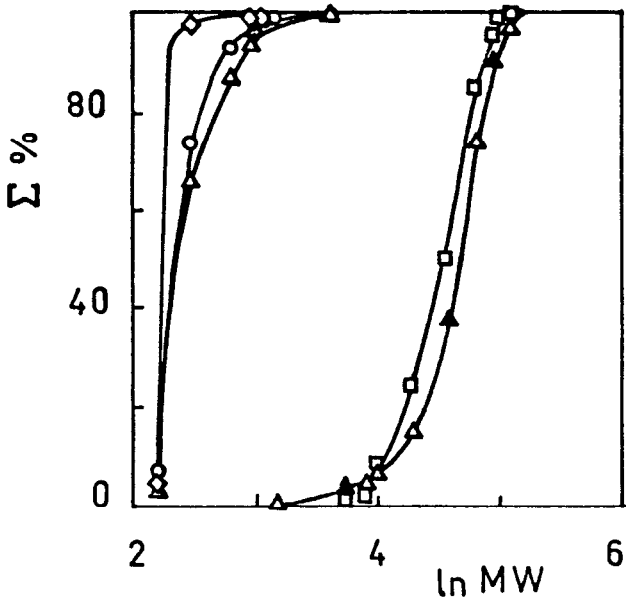


Figure 7.39: Sum curve of molecular weight distribution (Σ, %) in permeate and reactor after 25 hr. Polysulfone membrane type 2, dextran T70 1.19 wt%, pH = 6.0. Blank symbols permeate; filled symbols reactor. (◇) standardization solution, saccharose; (□) standardization solution, dextran T70; (○) 3 bar, (△) 5 bar.[74]

MEMBRANE FERMENTORS

Increasing interest is developing in continuous fermentation processes where microporous membranes are used to separate the fermentation broth from the product stream, thus retaining viable cells in the fermentor.

In 1970, Porter and Michaels[84] first suggested the use of membranes to enhance fermentor productivity; traditional fermentors could in fact be coupled to a membrane separation unit in a configuration called a "membrane fermentor" where flux through the membrane was pressure driven. Since then a number

of different membrane configurations have been proposed. A typical apparatus is shown in Figure 7.40 in which there is a vessel for the growing biomass, where the pH and temperature are strictly controlled and nutrients are added, and a UF unit, with membranes in hollow fiber or flat slab configuration, to withdraw products from the flowing cell slurry.

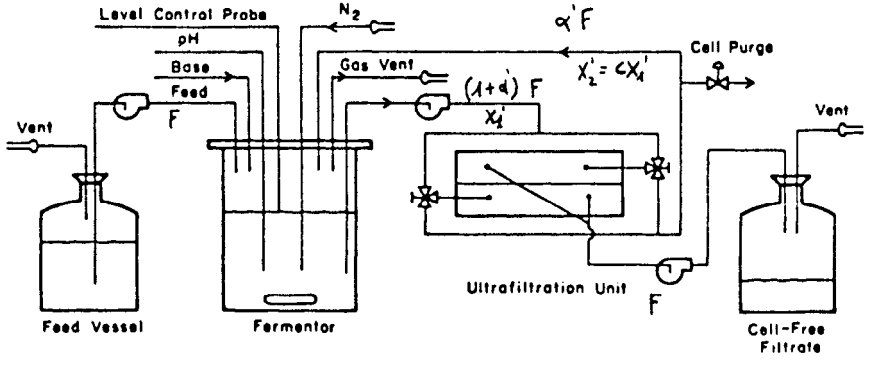


Figure 7.40: Cell recycle fermentation apparatus.[94]

Viable cells can also be confined within the shell of a hollow fiber membrane module[85] (Figure 7.41) or in a cell circuit separated with a dialysis membrane from a dialysate circuit, where water or substrate solution is kept flowing[86] (Figure 7.42). When kinetic models for the growth and fermentation of a specific kind of cell or microbe on the corresponding substrate medium are avail-

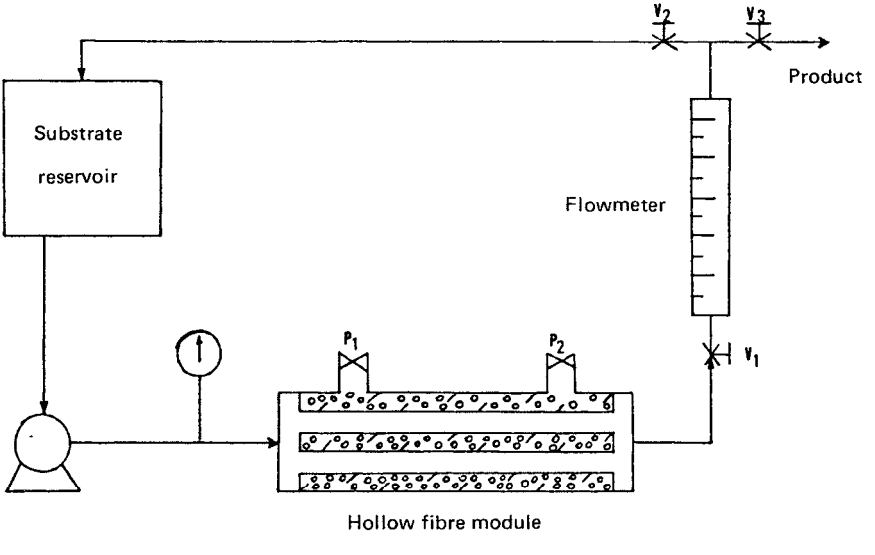


Figure 7.41: Schematic of a hollow fiber fermentor (HFF).[85]

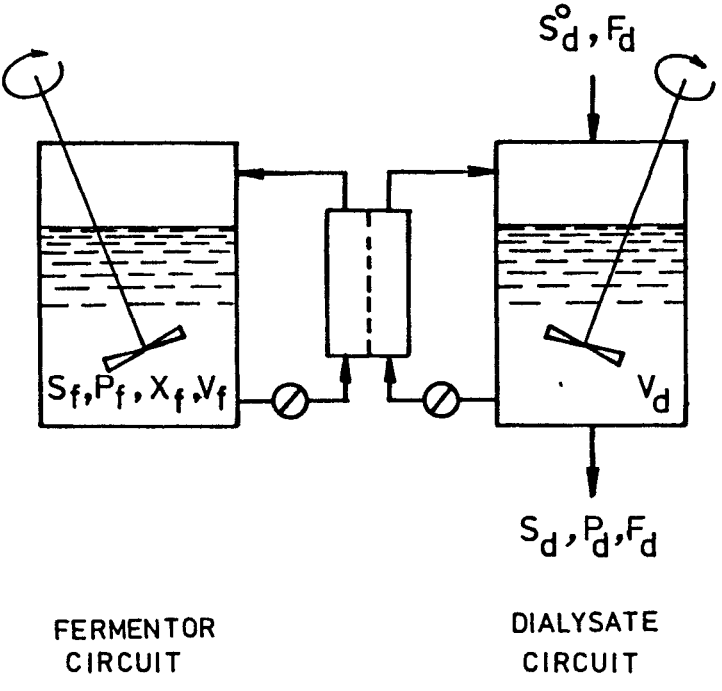


Figure 7.42: Schematic of dialysate-feed, immobilized cell system for dialysis continuous fermentation.[86]

able, as is the case for *Zymononas mobilis*,[87] mathematical modeling of membrane fermentors can be accomplished according to mass balances and the equations reported for the corresponding enzyme reactor configurations examined in the previous sections. In Tables 7.1, 7.2 and 7.3, a summary of the performance of different fermentor configurations is reported for three fermentation processes, carried out by different microorganisms.

Cell Recycle Fermentors

Cell recycle fermentors consist of two main units: a vessel where the biomass is allowed to grow, and a membrane separation unit (as in Figure 7.40). Vessels are usually designed to insure a uniform concentration of nutrients and pH throughout the whole volume. Due to complete mixing, process control and stability of the microbial slurry are not difficult to achieve.[88] After anaerobic stabilization, when the biomass is well developed, the reactor biomass is pumped to the UF unit where solid-liquid separation occurs. The sludge is flushed back to the reactor. In most cases, the flow rate of nutrient feed is kept equal to the permeate flow rate thus keeping a constant liquid level in the anaerobic reactor.

Table 7.1: Comparison of Performances of Different Fermentor Configurations for Lactose to Ethanol Conversion by *Kluyveromyces fragilis*

HF means hollow fiber separation unit

Substrate	Reactor	Sf g/l	Pr g/lh	P g/l	Cell concentration g/l	Ref.
Lactose	batch	50	3	22	3.8	89
Lactose	CSTR+HF	50	25	15	3.8	89
Lactose	CSTR+HF	50	65	10	41	89
Lactose	CSTR+HF	150	240	40	90	89
Lactose	HFF	50	63	15-25	82	85
Whey Lactose	HFF	45	35	5-10	117	85

Table 7.2: Comparison of Performances of Different Fermentors for Glucose to Lactic Acid Transformation by *Lactobacillus delbreuckii*

HF means hollow fiber separation unit

Substrate	Reactor	Sf g/l	Pr g/l	P g/l	cell concentration g/l	Ref.
Glucose	batch		1-2	45	7-8	94
Glucose	batch w/dialysis		2-3	35	11	94
Glucose	CSTR		7	38	7-8	94
Glucose	CSTR+HF	30	76	35	54	94
Glucose	HF reactor		100	2	350	94
Glucose	Ca. Alg. gel beads		3	46	67	94

Table 7.3: Comparison of Performances of Different Fermentors for Glucose Conversion to Ethanol by *S. Cerevisiae*

Substrate	Reactor	Pr g/l	Ref.
Glucose	dialysis	2.1-5.8	86
Glucose	batch multiple	1.8-25	86
Glucose	vacuum continuous	44	86
Glucose	continuum with cell recycle	53	86

Higher cell concentrations are usually achieved in cell recycle fermentors than in the usual fermentor. Steady state mass balances on viable cells and on the limiting growth substrates for a continuous fermentor (Figure 7.43) can be written as:[117]

$$F\ X' = \mu^*\ X'\ V \qquad (68)$$

and $$X' = D'\ Y\ (S_f - S)/\ \mu^* \qquad \text{respectively.}$$

Combining the two equations, the cell concentration within the vessel is:[117]

$$X' = Y(S_f - S) \qquad (69)$$

A steady state mass balance on a continuous cell recycle fermentor, over the vessel alone is as follows (see Figure 7.40):

$$\alpha'\ F\ X_2' - (1 + \alpha')\ F\ X_1' + V\ \mu^*\ X_1' = 0 \qquad (70)$$

on cells, and $X' = Y\ D'\ (S_f - S)/\ \mu^*$ on limiting growth substrate to give a cell concentration value in the vessel equal to:[117]

$$X_1' = Y\ (S_f - S)/(1 + \alpha' - C\ \alpha') \qquad (71)$$

The cell concentration within the vessel of a cell recycle fermentor is then greater by a factor of $1/(1 + \alpha' - C\alpha')$.

The performance and capacity of an anaerobic reactor can be expressed in terms of two parameters: the solid retention time (SRT), and the reactor volume loading (VL).

The SRT is the average retention time of organisms in the reaction vessel. For a suspended growth system, SRT is usually defined as the ratio of volatile suspended solids (VSS) in the reactor to the VSS lost in the effluent or intentionally wasted per day.[88]

The specific growth rate (SGR) is equal to the reciprocal of the SRT; it can be expressed as a linear function of the specific substrate utilization rate, KS, to give:[88]

$$SGR = Y \cdot KS - D$$

where Y = the organism yield coefficient: the mass of cells formed/mass nutrients

KS = the specific substrate utilization rate, mass/mass time

D = the organism decay coefficient, 1/time.

The kinetics of substrate removal in the anaerobic reactor actually determines the SRT required for a given fermentation efficiency. In turn, the presence of the UF unit allows a fine control of SRT, making process control easier. When high biomass concentrations are achieved, longer SRTs can be maintained at lower reactor volumes.

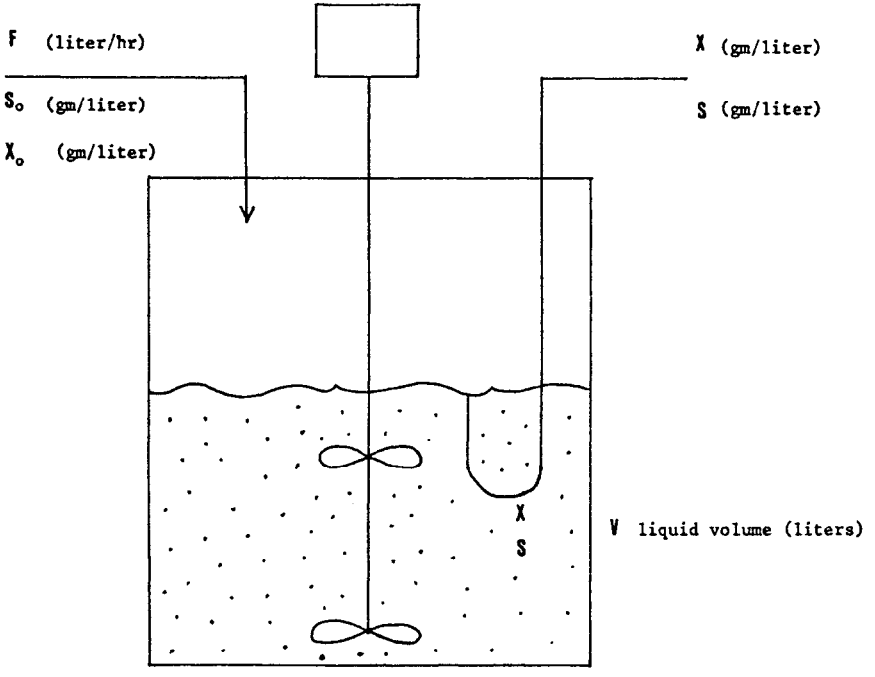


Figure 7.43: Schematic of a single stage chemostat.[118]

The volumetric loading to a reactor, VL, is defined as:[59]

$$VL = Q\,S_f/V = S_f/\tau$$

High biomass concentrations permit operation at higher volumetric loading rates. Reactor design can be carried out by estimating the value of volumetric loading necessary to achieve a given effluent quality. This design criterion is commonly used for biological systems where the evaluation of biomass concentration within the reactor is difficult. This is not the case with cell recycle fermentors, so the VL or the SRT approach can also be used as design criterion.

Figure 7.44 shows the typical dependence at steady state of substrate and product concentrations, and of productivity on permeate flow rate, i.e., dilution rate, for lactose fermentation to ethanol by *Kluyveromices fragilis* in a cell recycle membrane fermentor.[89] As dilution rate increases fermentor productivity increases, attains a maximum value and then decreases. Product and substrate concentrations in the permeate, instead, steadily decrease and increase, respectively, as dilution rate increases. A compromise generally has to be made between production rate and product concentration in the effluent. When the absence of substrate in the permeate is required, it obviously limits fermentor productivity, as in the case of wastewater treatment in the dairy industry. On the other hand, low substrate concentrations in the permeate keep recovery

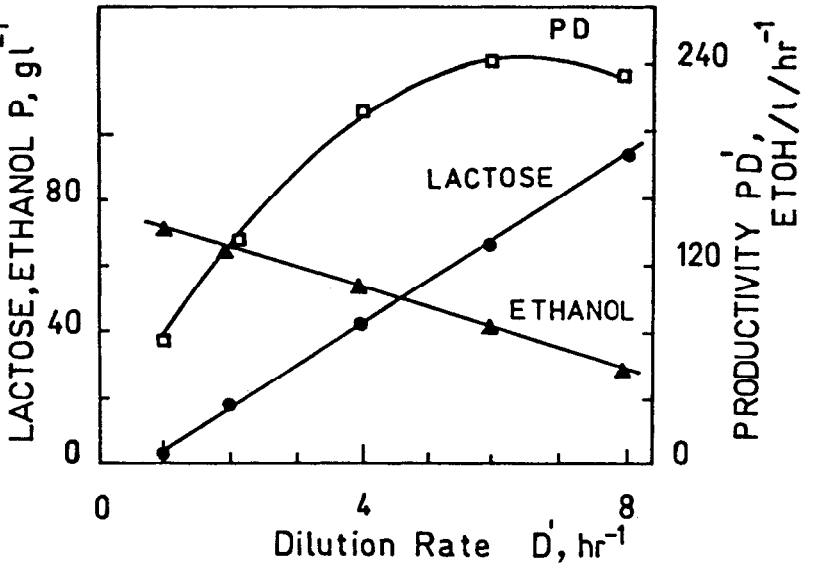


Figure 7.44: Fermentation kinetics of a membrane recycle fermentor. Feed concentration = 150 g/ℓ lactose. Cell concentration = 90 g/ℓ.[89]

costs of products from the effluent stream low. Therefore, the optimum operating conditions will be determined by the economics of the overall process.

Data in Table 7.1 show how the substrate concentration in the feed can affect fermentor performance.

These data outline a dominant feature of the cell recycle membrane fermentor: productivity is a monotonic function of viable cell concentration within the fermentor. Cell recycle makes it possible to operate at higher microbial cell concentrations than in conventional batch fermentors, thus reducing the volume required for a given productivity and hence the capital costs.[90] Invariably, the viscosity of the cell slurry increases with cell concentration, so that concentration polarization phenomena are usually significant. Complex systems such as rotating membrane fermentors have been proposed to overcome fouling and expected concentration polarization problems.[91] In high rate fermentors, concentration polarization is usually controlled by operating the reaction system at high recirculation rates though pumps have to be carefully chosen to avoid cell damage.[86]

When concentration polarization occurs, permeate fluxes become invariant with the transmembrane pressure, and increases in the permeation rate can be achieved only by enlarging the membrane surface area or by improved fluid management. The design of the UF membrane unit in the polarized regime must relate the flux to the optimal level of reactor VSS or total suspended solids (TSS) according to Michaels' gel theory, to give

$$J = K_S \log (C_g/\overline{X})$$

where K_s = the overall mass transfer coefficient,
C_g = apparent solid concentration in the gel, and
$\overline{X}$ = anaerobic reactor VSS or TSS.

High recirculation and dilution rates help in maintaining low levels of inhibitory products. In ethanol fermentation processes, for instance, the removal of these inhibitory products through the UF membrane can lead to significant improvements in reactor performance. Both primary and secondary metabolites freely pass through the membrane thus relieving both primary and secondary inhibition.[86] The use of a membrane able to remove ethanol selectively[92] has been proposed. In this way, primary inhibitors are released through the membrane, but secondary products are allowed to accumulate; their concentration level soon becomes toxic reducing cell viability and alcohol productivity.[93]

Membrane Segregated Fermentors

Continuous fermentation processes can also be carried out in a hollow fiber fermentor (HFF).[85] Cells are packed into the shell side of a hollow fiber module, while substrate solution is fed to the core of the fibers (Figure 7.41). Since the cell slurry is separated from the substrate solution by the membrane, HFFs can be used for fermentation of liquid streams containing low molecular weight fermentable substances. A careful choice of membrane molecular weight cut-off can also assure that the cell environment is fully sterilized. Figure 7.45 shows typical performance of an HFF for whey permeate fermentation to ethanol by

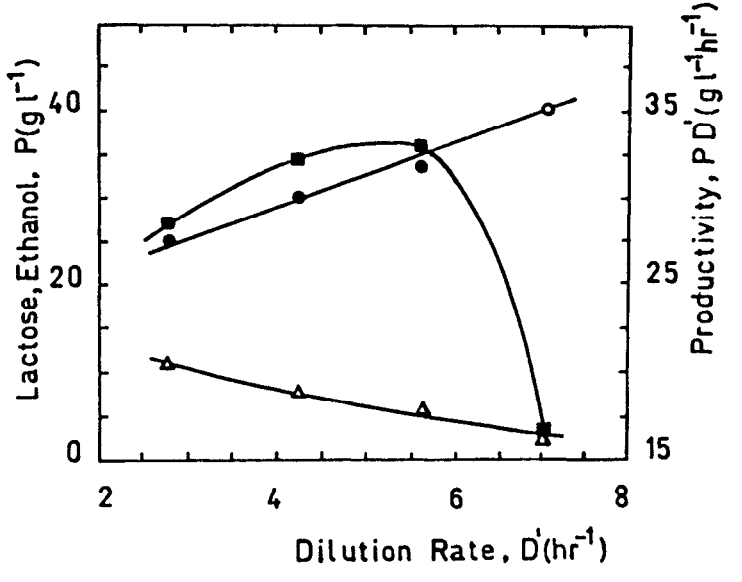


Figure 7.45: Fermentation kinetics of a hollow fiber fermentor in single pass mode processing whey permeate (45 g/ℓ lactose concentration). Initial cell concentration = 117 g/ℓ. (●) lactose, (△) ethanol, (□) productivity.[85]

Kluyveromices fragilis. The behavior of the fermentor is similar to that of a cell recycle reactor with the same fermentation system. Higher productivity and yields than with a batch fermentation are obtained (Tables 7.1, 7.2). The long term cell stability in an HFF (Figure 7.46) is also better than in a batch fermentor. However, even with HFF, reactor productivity is increased at the expense of low substrate conversions, at least at low dilution rates.

In another membrane fermentor configuration, the cell slurry is separated from substrate solution by a dialysis membrane[86] (Figure 7.42). Two different operational modes for this configuration have been proposed. In the first, substrate is fed into a continuous fermentor circuit that is dialyzed against a continuous dialysate circuit where water is kept flowing. In the second, substrate is fed into the dialysate circuit and diffuses towards the batch fermentor circuit through a dialysis membrane. Dialysis membrane fermentors provide a novel approach to the immobilization of microbial cells and the relief of both primary and secondary inhibition, where it occurs. Substrate entering the fermentor is sterilized by passage through the membrane and its consumption for cell growth is reduced to metabolism maintenance. Moreover, cells are effectively immobilized. There are some problems related to attaining steady state in terms of cell growth.[86] In addition, the solute exchange capacity of dialysis membranes limits both productivity and conversion (Table 7.2). Even though improvements can be obtained by operating the fermentor according to the first suggested procedure, performances are not yet comparable to those of other membrane fermentors.

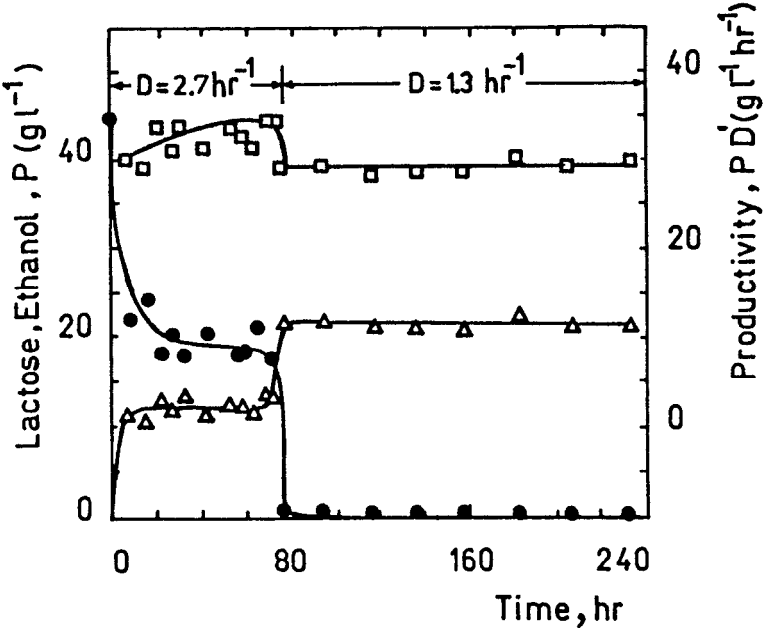


Figure 7.46: Long term stability of a hollow fiber fermenter in single pass mode processing whey permeate. Initial cell concentration is 100 g/ℓ. Dilution rate (D') is changed from 2.7 to 1.3 ℓ/h after 80 hours of operation. (●) lactose, (△) ethanol, (■) productivity.[85]

Complex Fermentation Systems

In some cases, the substrate must be chemically or biochemically hydrolyzed to low-molecular-weight fermentable compounds prior to fermentation. Two steps are then needed to carry out the overall transformation, namely hydrolysis and fermentation. Sometimes, raw substrate hydrolysis is conveniently performed via an enzymatic route, as in the case of ethanol production from cellulose or starch. This two-step transformation can be coupled into a single step in which raw materials are continuously converted to valuable product.

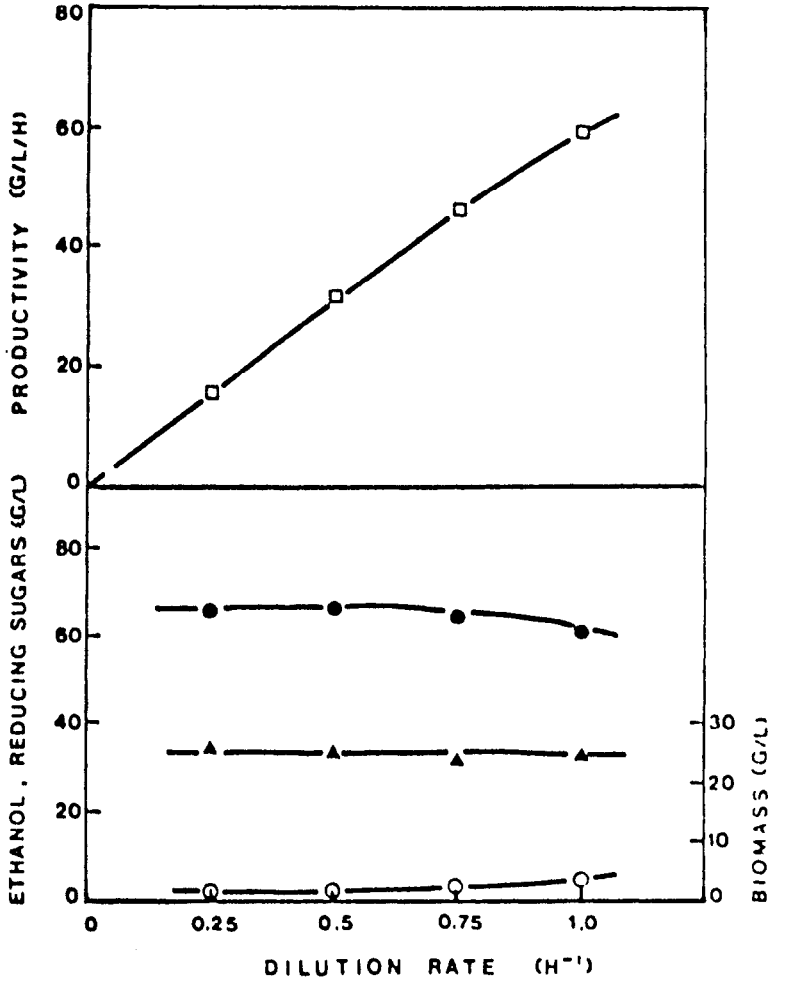


Figure 7.47: Continuous SSF fermentation using starch to produce liquified starch stream of 130 g/ℓ total sugars with *Z. mobilis* ZM4 at pH 5.0 and 35°C. (●) ethanol, (▲) biomass, (○) reducing sugars.[98]

Since the optimum temperature for the hydrolysis step is usually different than that for fermentation, a "one-step transformation" may not be as efficient as two steps.

Enzymes exhibit their highest activity at temperatures appreciably higher than those required for microbial fermentations. When such differences are negligible, enzymatic hydrolysis and fermentation can simultaneously occur. Provided that enzyme concentration is high enough to prevent enzymatic conversion from being rate limiting, fermentation time and capital costs can be reduced.

What has been previously said about the advantages of continuous membrane fermentors also applies to such complex systems. UF membranes can in fact be used to recycle both enzymes and microbial cells thus increasing overall system productivity.[98]

Interesting applications of these systems can be found in ethanol production from cellulose or starch. The overall process is called simultaneous saccharification and fermentation (SSF).[98] In this process, two fermentors are connected in series. The first one provides for the liquefaction of the slurry, which is then pumped into the second fermentor, where simultaneous saccharification and fermentation occur due to the presence of amyloglucosidase and *Z. mobilis* cells.

Typical steady state performance of a continuous SSF membrane process is reported in Figure 7.47. A comparison of continuous SSF to batch SSF shows how performance can be improved with the use of membranes. Enzyme consumption is strongly reduced when the reactor is operated in this way.

The continuous SSF membrane process also offers appreciable increases in productivity, (though at the expense of reduced product concentration in the effluent stream) as well as decreased energy requirements when compared to a conventional two-step process.

REFERENCES

1. Lehninger, A.L., *Biochimica*, Bologna; Zanichelli (1976).
2. Laidler, K.J. and Bunting, P.S., *The Chemical Kinetics of Enzyme Action*, Oxford; Clarendon Press (1973).
3. Trevan, Michael D., *Immobilized Enzymes*, New York; J. Wiley and Sons (1981).
4. Chibata, I., *Immobilized Enzymes*: Halsted Press (1978).
5. Drioli, E. and Catapano, G., *Chimica Oggi* 7/8: 11-16 (1984).
6. Mosbach, K., Immobilized Enzymes. *TIBS* January 1-3 (1980).
7. Wandrey, C., Enzyme Membrane Reactor Systems. *Proceedings of the International Conference on the Commercial Applications and Implications of Biotechnology*, pp. 577-588, Online Publications Ltd., Northwood, UK (1983).
8. Wisniewski, J., Winnicki, T. and Majewska, K., *Biotechnol. Bioeng.* 25: 1441-1452 (1983).
9. Hong, J., Tsao, G.T. and Wankat, P.C., *Biotechnol. Bioeng.* 23: 1501-1516 (1981).

10. Wichmann, R., Wandrey, C., Buckmann, A.F. and Kula, M.R., *Biotechnol. Bioeng.* 23: 2789-2802 (1981).
11. Hagerdal, B., Lopez-Leiva, M. and Matthiason, B., *Desalination* 35: 365-373 (1980).
12. Ohlson, I., Tragardh, G. and Hahn-Hagerdal, B., *Biotechnol. Bioeng.* 26: 647-653 (1984).
13. Azhar, A. and Hamdy, M.K., *Biotechnol. Bioeng.* 23: 1297-1307 (1981).
14. Alfani, F., Cantarella, M. and Scardi, V., *J. Membr. Sci.* 16: 407-416 (1983).
15. Alfani, F., Cantarella, M., Erto, L. and Scardi, V., in: *Energy from Biomass* (A. Strub, P. Chartier and G. Schleser, eds.), pp. 1000-1005, Applied Science Publishers, London (1983).
16. Closset, G.P., Cobb, J.T. and Shah, Y.T., *Biotechnol. Bioeng.* 16: 345-360 (1974).
17. Tachauer, E., Cobb, J.T. and Shah, Y.T., *Biotechnol. Bioeng.* 16: 545-550 (1974).
18. Deeslie, W.D. and Cheryan, M., *Biotechnol. Bioeng.* 23: 2257-2270 (1981).
19. Cheryan, M. and Deeslie, W.D., *JAOCS* 60: 1112-1115 (1983).
20. Leuchtenberger, W., Karrenbauer, M. and Plocker, U., Scale up of an Enzyme Membrane Reactor Process for the Manufacture of L-Enantiomeric Compoungs, presented at the *Europe-Japan Congress on Membranes and Membrane Technology*, Stresa, Italy (1984).
21. Wandrey, C., Wichmann, R. and Jandel, A.S., in: *Enzyme Engineering* (I. Chibata, S. Fukui and L.B. Wingard, Jr., eds.), Vol. 6, pp 61-68, Plenum Press, New York and London (1982).
22. Wandrey, C., Wichmann, R., Leuchtenberger, W., Kula, M.R. and Buckmann, A., U.S. Patent 4,304,858 (1982).
23. Kim, I.H. and Chang, H.N., *AIChE J.* 29: 910-914 (1983).
24. Kim, I.H. and Chang, H.N., *AIChE J.* 29: 645-651 (1983).
25. Urabe, I., Katayama, M. and Okada, H., in: *Enzyme Engineering* (I. Chibata, S. Fukui and L.B. Wingard, Jr., eds.), Vol. 6, pp. 239-240, Plenum Press, New York and London (1982).
26. Deeslie, W.D. and Cheryan, M., *Biotechnol. Bioeng.* 24: 69-82 (1982).
27. Drioli, E., Gianfreda, L., Palescandolo, R. and Scardi, V., *Biotechnol. Bioeng.* 17: 1365 (1975).
28. Drioli, E. and Scardi, V., *J. Membr. Sci.* 1: 237 (1976).
29. Capobianco, G., Drioli, E. and Ragosta, G., *J. of Solid-Phase Biochem.* 2: 315-328 (1977).
30. Greco, Guido, Jr., Alfani, F., Iorio, G., Cantarella, M., Formisano, A., Gianfreda, L., Palescandolo, R. and Scardi, V., *Biotechnol. Bioeng.* 21: 1421-1438 (1979).
31. Rossi, M., Nucci, R., Raia, C.A., Molinari, R. and Drioli, E., *J. Mol. Catal.* 4: 233-236 (1978).
32. Cantarella, M., Gianfreda, L., Palescandolo, R., Scardi, V., Iorio, G., Alfani, F. and Greco, Guido, Jr., *Quaderni dell'Ingegnere Chimico Italiano* 61: 115-123 (1979).
33. Cantarella, M., Gianfreda, L., Palescandolo, R., Scardi, V., Greco, Guido, Jr., Alfani, F. and Iorio, G., *J. of Solid-Phase Biochem.* 2: 163-174 (1977).

34. Iorio, G., Catapano, G., Drioli, E., Rossi, M. and Rella, R., *J. Membr. Sci.* 22: 317-324 (1985).
35. Alfani, F., Iorio, G., Greco, Guido, Jr., Cantarella, M., Remy, M.H. and Scardi, V., *Chem. Eng. Sci.* 34: 1213-1219 (1979).
36. Iorio, G., Catapano, G., Drioli, E., Rossi, M. and Rella, R., *Ann. N.Y. Acad. Sci.* 434: 123-126 (1984).
37. Alfani, F., Albanesi, D., Cantarella, M. and Scardi, V., *Enzyme Microb. Technol.* 4: 181-184 (1982).
38. Virkar, P.D., Narendranathan, T.J., Hoare, H. and Dunnill, P., *Biotechnol. Bioeng.* 23: 425-429 (1981).
39. Alfani, F., Albanesi, D., Cantarella, M. and Scardi, V., *Biotechnol. Lett.* 3: 309-314 (1981).
40. Mansi, F. and Curcio, F., Processi di Denaturazione e Stabilizzazione in Reattori Enzimatici a Membrana Ultrafiltrante. Laurea Degree Thesis, Dept. of Chem. Eng., Fac. of Engineering, Univ. of Naples, Italy (1980).
41. Greco, Guido, Jr., Albanesi, D., Cantarella, M. and Scardi, V., *Biotechnol. Bioeng.* 22: 215-219 (1980).
42. Engasser, J.M., Caaron, J. and Marc, A., *Chem. Eng. Sci.* 35: 99-105 (1980).
43. Engasser, J.M., *Biochim. Biophys. Acta* 526: 301-310 (1978).
44. Klei, H.E., Sundstrom, D.W., Coughlin, R.W. and Ziolkowski, K., *Biotechnol. and Bioeng. Symp.* 11: 593-601 (1981).
45. Glomon, C., Germain, P., Miclo, A. and Engasser, J.M., in: *Enzyme Engineering* (I. Chibata, S. Fukui and L. B. Wingard, Jr., eds.), Vol. 6, pp. 125-126, Plenum Press, New York and London (1982).
46. Rony, P.R., *Biotechnol. Bioeng.* 13: 431-447 (1971).
47. Waterland, L.R., Michaels, A.S. and Robertson, C.R., *AIChE J.* 20: 50-59 (1974).
48. Kitano, H., Yoshijima, S. and Ise, N., *Biotechnol. Bioeng.* 22: 2643-2653 (1980).
49. Kitano, H., Yoshijima, S., Hotogi, S. and Ise, N., *Biotechnol. Bioeng.* 22: 2633-2642 (1980).
50. Fink, D.I. and Rodwell, V.W., *Biotechnol. Bioeng.* 17: 1029-1050 (1975).
51. Davis, J.C., *Biotechnol. Bioeng.* 16: 1113-1122 (1974).
52. Rony, P.R., *J. Am. Chem. Soc.* 94: 8247-8248 (1972).
53. Lewis, W. and Middleman, S., *AIChE J.* 20: 1012-1014 (1974).
54. Korus, R.A. and Olson, A.C., *Biotechnol. Bioeng.* 19: 1-8 (1977).
55. Korus, R.A. and Olson, A.C., *J. Food Sci.* 42: 258-260 (1977).
56. Miyawaki, O., Nakamura, K. and Yano, T., *J. Chem. Eng. Jpn.* 15: 142-147 (1982).
57. Sparks, R.E., Mason, N.S., Finley, T.C. and Scharp, D.W., *Trans. Am. Soc. Artif. Intern. Organs* 28: 229-231 (1982).
58. Reach, G., Jaffrin, M.Y. and Deajeux, U.F., A U-Shaped Flat Membrane Bio-Artificial Pancreas. Application of the Ultrafiltration-Based Model to Its Design. *Proceedings of the European Soc. of Artif. Intern. Organs*, pp. 49-52 (1983).
59. Reach, G., Jaffrin, M.Y. and Assan, R., *Life Support Systems,* 1, Supp.: 73-75 (1982).
60. Kastl, P.R., Baricos, W.H., Chambers, R.P. and Cohen, W., private communication (1978).

61. Drioli, E., Iorio, G., De Rosa, M., Gambacorta, A. and Nicolaus, B., *J. Membr. Sci.* 11: 365-370 (1982).
62. Breslau, B.R. and Kelcullen, B.M., Hollow Fiber Enzymatic Reactors. An Engineering Approach presented at the *Third International Conference on Enzyme Engineering*, Portland, Oregon (1975).
63. Colton, C.K., Solomon, B.A., Galletti, P.M., Richardson, P.D., Takahashi, C., Naber, S.P. and Chick, W.L., in: *Ultrafiltration Membrane and Applications* (A.R. Cooper, ed.), 541-555, Plenum, New York, London (1980).
64. Chambers, R.P., Cohen, W. and Baricos, W.H., *Methods in Enzymology* 44: 291-317 (1976).
65. Craveri, R., Fabiani, C., Leonardi, M. and Pizzichini, M., Performance of Whole Cells possessing Cellobiase Activity Immobilized into Hollow Fiber Membrane Reactors presented at the *Europe-Japan Congress on Membranes and Membrane Processes*, Stresa, Italy (1984).
66. Orsetti, A., Bouhaddioui, N., Finley, T.C., Crespy, S. and Perez, R., *C.R. Soc. Biol.* 175: 189-201 (1981).
67. Drioli, E., Iorio, G., Catapano, G., De Rosa, M. and Gambacorta, A., *J. Membr. Sci.* 27: 253-261 (1986).
68. Drioli, E., Iorio, G., Molinari, R., De Rosa, M., Gambacorta, A., Nicolaus, B. and Esposito, E., *Biotechnol. Bioeng.* 23: 221-223 (1981).
69 Drioli, E., Iorio, G., Santoro, R., De Rosa, M., Gambacorta, A. and Nicolaus, B., *J. Mol. Catal.* 14: 247-251 (1982).
70. Callegaro, L. and Rossi, V., in: *Hollow Fibers and Capillary Membranes in New Separation Processes* (C.N.R. of Italy ed.), pp. 44-51 (1981).
71. Mazzola, G. and Vecchio, G., in: *Hollow Fibers and Caoillary Membranes in New Separation Processes* (C.N.R. of Italy ed.), pp. 52-58 (1981).
72. Mazid, M.A. and Laidler, K.J., *Biotechnol. Bioeng.* 24: 2087-2097 (1982).
73. Bunting, P.S. and Laidler, K.J., *Biotechnol. Bioeng.* 16: 119-134 (1974).
74. Staude, E., Jorisch, W. and Ansorge, W., *J. Membr. Sci.* 11: 289-296 (1982).
75. Howell, J.A., Knapp, J.S. and Velicangil, O., in: *Enzyme Engineering* (G.B. Broun, G. Manecke and L.B. Wingard, Jr., eds.), Vol. 4, pp. 267-271, Plenum Press, New York and London (1978).
76. Kobayashi, T. and Laidler, K.J., *Biotechnol. Bioeng.* 16: 77-97 (1974).
77. Vieth, W.R., Venkatasubramanian, K., Constantinides, A. and Davidson, B., in: *Applied Biochemistry and Bioengineering* (L.B. Wingard, E. Katchalsky-Katzir and L. Goldstein, eds.), Vol. 1, Academic Press, New York (1976).
78. Chang, T.M.S., in: *Biomedical Applications of Immobilized Enzymes and Proteins* (T.M.S. Chang, ed.), p. 105, Plenum Press, New York (1977).
79. Rossi, V., *Int. J. Art. Organs* 4: 102-107 (1981).
80. Rossi, V., *ISAO Congress*, Paris, France (1981).
81. Horvath, C., Shendalman, L.H. and Light, R.T., *Chem. Eng. Sci.* 28: 375-388 (1973).
82. Adu-Amankwa, B. and Constantinides, A., *Biotechnol. Bioeng.* 26: 156-166 (1984).
83. Giordano, C., Esposito, R., Mazzola, G., Vecchio, G., Pluvio, G., Cirillo, D., Capasso, G.B. and Buonanno, G., *Int. J. Artif. Organs* 4: 62-67 (1981).

84. Porter, M.C. and Michaels, A.S., *Chem. Tech.* 2: 56-61 (1970).
85. Mehaia, M.A. and Cheryan, M., *Enzyme Microb. Technol.* 6: 117-120 (1984).
86. Kyung, K.H. and Gerhardt, P., *Biotechnol. Bioeng.* 26: 252-256 (1984).
87. Slotnicki, M.L., Warr, R.G., Goodman, A.E., Lee, K.J. and Rogers, P.L., in: *Biotechnology* (C.F. Phelps and P.H. Clarke, eds.), Vol. 48, pp. 53-86, Biochem. Soc. Symp., Great Britain (1983).
88. Li, A. and Sutton, P.M., Dorr-Oliver's Membrane Anaerobic Reactor System. Internal Report, Dorr-Oliver (1982).
89. Cheryan, M. and Mehaia, M.A., *Biotechnol. Lett.* 5: 519-524 (1983).
90. Maiorella, B., Wilke, Ch.R. and Blanch, H.W., *Adv. Biochem. Eng.* 20: 43-92 (1981).
91. Margaritis, A. and Wilke, Ch.R., *Biotechnol. Bioeng.* 20: 727-753 (1978).
92. Gregor, H. and Jeffries, T., *Ann. N.Y. Acad. Sci.* 326: 273 (1979).
93. Maiorella, B., Blanch, H.W. and Wilke, C.R., *Biotechnol. Bioeng.* 25: 103-121 (1983).
94. Vick Roy, T.B., Mandel, D.K., Dea, D.K., Blanch, H.W. and Wilke, C.R., *Biotechnol. Lett.* 5: 665-670 (1983).
95. Janssens, J.H., Bernard, A. and Bailey, R.B., *Biotechnol. Bioeng.* 26: 1-5 (1984).
96. Dostalek, M. and Haggstrom, M., *Biotechnol. Bioeng.* 24: 2077-2086 (1982).
97. Charley, R.C., Fein, J.E., Lavers, B.H., Lawford, H.G. and Lawford, G.R., *Biotechnol. Lett.* 5: 169-174 (1983).
98. Lee, J.H., Pagan, R.J. and Rogers, P.L., *Biotechnol. Bioeng.* 25: 659-669 (1983).
99. Levenspiel, O., *Chemical Reaction Engineering*, New York, London: J. Wiley & Sons (1972).
100. Michaels, A.S., *Chem. Eng. Progr.* 64: 31-43 (1968).
101. Blatt, W.F., Dravid, A., Michaels, A.S. and Nelsen, L., in: *Membrane Science and Technology* (J.E. Flinn, ed.), pp. 40-97, Plenum Press, New York (1970).
102. Mathiason, E. and Sivik, B., *Desalination* 35: 59-103 (1980).
103. Lowe, C.R. and Mosbach, K., *Eur. J. Biochem.* 49: 511-520 (1974).
104. Zappelli, P., Rossodivita, A. and Re, L., *Eur. J. Biochem.* 54: 475-482 (1975).
105. Adamski-Medda, D., Nguyen, Q.T. and Declacherie, E., *J. Membr. Sci.* 9: 337-342 (1981).
106. Greco, Guido, Jr., Marrucci, G. and Gianfreda, L., in: *Enzyme Engineering* (I. Chibata, S. Fukui and L. B. Wingard, Jr., eds.), Vol. 6, pp. 229-232, Plenum Press, New York and London (1982).
107. Porter, M.C., *Ind. Eng. Chem. Prod. Res. Dev.* 11: 234-248 (1972).
108. Iorio, G., Drioli, E., Memoli, B., Andreucci, V.E., Salvatore, M. and Alfano, B., *J. Membr. Sci.* 18: 297-311 (1984).
109. Pitcher, W.H., Jr., and Havewala, N.B., in: *Enzymology* (H.H. Weetcell, ed.), pp. 1-93 (1974).
110. Davis, E.J., Cooney, D.O. and Chang, R., *Chem. Eng. J.* 7: 213-225 (1974).

111. Wykes, J.R., Dunnill, P., Lilly, M.D., *Biochim. Biophys. Acta* 286: 260-268 (1972).
112. Messing, R.A., in: *Immobilized Enzymes for Industrial Reactors* (R.A. Messing, ed.), pp. 79-99, Academic Press, New York (1975).
113. Weethall, H.H., in: *Immobilized Enzymes for Industrial Reactors* (R.A. Messing, ed.), pp. 99-123, Academic Press, New York (1975).
114. Grubhofer, S. and Schleith, L., *Hoppe-Seyler's Z. Physiol. Chem.* 297: 108 (1954).
115. Mascini, M., Iannello, M. and Palleschi, G., *Anal. Chim. Acta* 146: 135-148 (1983).
116. Karube, I. and Suzuki, S., in: *Enzyme Engineering* (I. Chibata, S. Fukui and L.B. Wingard, Jr., eds.), Vol. 6, pp. 417-418, Plenum Press, New York and London (1982).
117. Wang, I.C.D., Cooney, C.L., Demain, A.L., Dunnill, P., Humphrey, A.E. and Lilly, M.D., *Fermentation and Enzyme Technology*, New York: J. Wiley & Sons (1979).

8

Electrodialysis

Thomas A. Davis

INTRODUCTION

Electrodialysis (ED) is an electromembrane process in which ions are transported through ion-exchange membranes from one solution to another under the influence of an electrical potential. The nature of the membranes and the driving force distinguish ED from the pressure driven membrane processes such as gas permeation, reverse osmosis, and filtration. The electrical charges of ions allow them to be driven through solutions and water-swollen membranes when a voltage is applied across these media. Since pressures are usually balanced across the membranes, the requirements for strength and support of the membranes and containment vessels are less demanding in electromembrane processes than in pressure driven membrane processes. Instead, design emphasis is directed toward maintaining uniform distribution of solution flow and minimizing electrical resistance and current leakage.

Some important concepts of electromembrane processes are presented in Figure 8.1. Ionic transport is illustrated in Figure 8.1a with no membranes present. When NaCl is dissolved in water, it dissociates into Na^+ cations and Cl^- anions. Application of an electric potential to the electrodes causes the ions to move through the solution at velocities proportional to the strength of the electric field. Average ionic velocities in the bulk solution are surprisingly slow, usually less than 1 cm/min, but the ions do not have to travel very far to reach the membranes in the thin solution compartments of ED stacks. The combined motion of Na^+ to the right and Cl^- to the left carries the total electric current flow through the bulk solution (unless other ions are present). Electrode reactions, which will be discussed in detail, transfer the current from the solution to the anode and cathode. Cl_2 gas is generated at the anode while H_2 gas and OH^- ions are generated at the cathode.

One could produce Cl_2, H_2 and NaOH from the electrolytic cell in Figure 8.1a, but the products would be impure. In conventional electrolytic cells, a porous diaphragm between the electrodes prevents bulk mixing of the products

of the electrode reactions. Modern chloralkali cells utilize a cation-exchange membrane between the electrodes as illustrated in Figure 8.1b. This innovation has substantially improved the purity of the caustic produced. The cation-exchange membrane is permeable to Na^+ ion but relatively impermeable to Cl^- and OH^- ions. Therefore, nearly all of the current is utilized to produce Cl_2 and NaOH. This membrane electrolysis cell is expected to dominate chloralkali plants in the future.

When a pair of anion- and cation-exchange membranes is placed between the electrodes as shown in Figure 8.1c, the solution between the membranes becomes depleted of NaCl. This depletion occurs because the membranes are selectively permeable to ions of a specific charge. The anion-exchange membrane allows Cl^- ions to be carried out of the center compartment by the electric potential, but it does not allow Na^+ ions to enter. Similarly the cation-exchange membrane offers a low resistance to Na^+ ions and a high resistance to Cl^- ions.

If the polarity (charge) of the electrodes were reversed or if the positions of the two membranes in Figure 8.1c were switched, the NaCl content of the center compartment would increase. This effect is accomplished in an ED stack by an array of alternating anion- and cation-exchange membranes as shown in Figure 8.1d. The solutions between the membranes are alternately enriched in or depleted of NaCl when the electrodes are energized. The enriched and depleted solutions are withdrawn from their respective compartments to achieve useful changes in the electrolyte content of solutions without substantially affecting the content of nonelectrolytes. It is this selectivity for electrolytes that often makes ED the process of choice for certain separations, e.g., desalting of protein solutions or whey.

Ion-Exchange Membranes

The ion-exchange membranes used in electrodialysis are essentially sheets of ion-exchange resins. Figure 8.2 illustrates the structure of a cation-exchange membrane which has negatively charged groups (e.g., $-SO_3^-$) chemically attached to the polymer chains (e.g., polystyrene). Ions with a charge opposite to the fixed charge (counter ions) are freely exchanged at these sites. The concentration of counter ions (e.g., Na^+) is relatively high; therefore, counter ions carry most of the electric current through the membrane. The fixed charges attached to the polymer chains repel ions of the same charge (co-ions), in this case the anions. Since their concentration is very low, anions carry only a small fraction of the electric current through a cation-exchange membrane. Attachment of positive fixed charges (e.g., $-NR_3^+$) to the polymer chains forms anion-exchange membranes, which are selectively permeable to negative ions, because the fixed $-NR_3^+$ groups repel positive ions. This exclusion, as a result of electrostatic repulsion, is called Donnan exclusion.

Since ion-exchange polymers (e.g., styrenesulfonic acid) are water soluble, crosslinking is needed to prevent dissolution of ion-exchange membranes. Divinylbenzene is used to crosslink styrene. The degree of crosslinking and the fixed-charge density affect the membrane's properties in opposite ways. Higher crosslinking improves selectivity and membrane stability by reducing swelling, but it increases electrical resistance. High charge density reduces resistance and increases selectivity, but it promotes swelling and thus necessitates higher

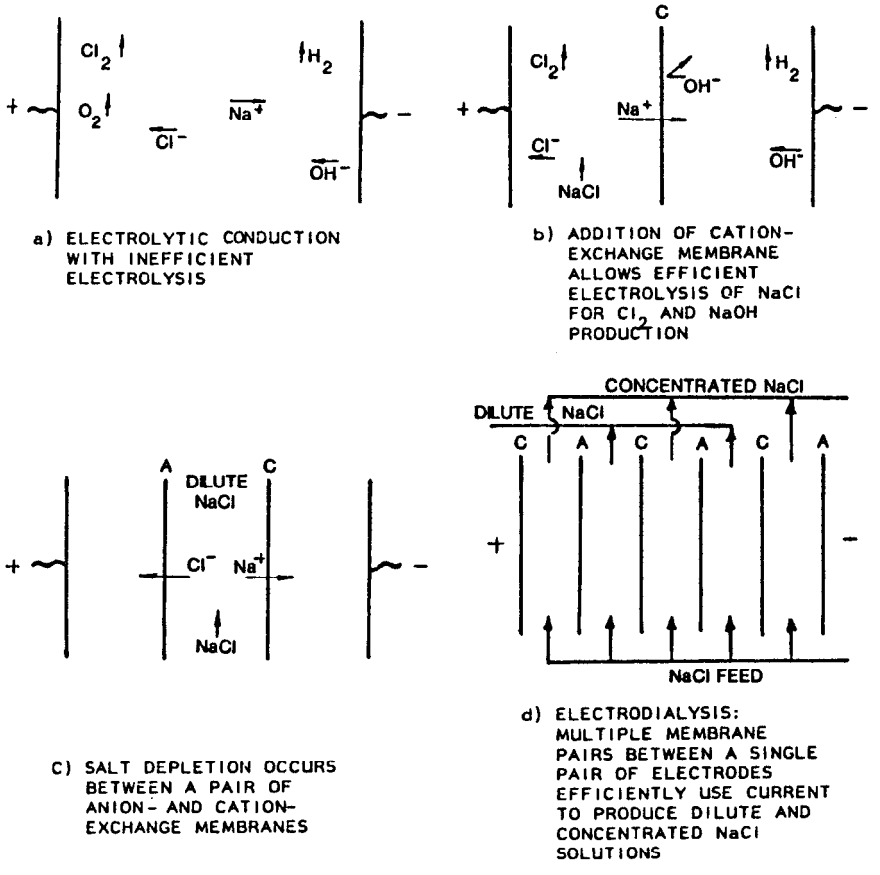


Figure 8.1: Membranes affect ionic transport. (a) Electrolytic conduction with inefficient electrolysis. (b) Addition of cation-exchange membrane allows efficient electrolysis of NaCl for Cl_2 and NaOH production. (c) Salt depletion occurs between a pair of anion- and cation-exchange membranes. (d) Electrodialysis: multiple membrane pairs between a single pair of electrodes efficiently use current to produce dilute and concentrated NaCl solutions.

crosslinking. A compromise among selectivity, electrical resistance, and dimensional stability is achieved by proper adjustment of crosslinking and fixed-charge densities.

Membrane Types

There are two general types of commercially available ion-exchange membranes: heterogeneous and homogeneous. Both types usually contain a reinforcing fabric to increase tensile strength and improve dimensional stability. Heterogeneous membranes have two distinct polymer phases. They are rather

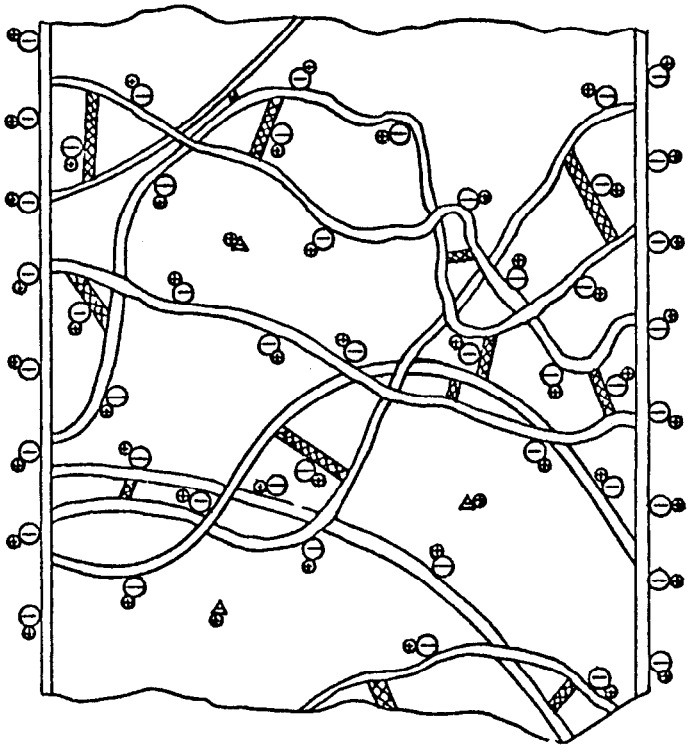


Figure 8.2: Diagram of cation-exchange membrane.

easily made by grinding up ion-exchange resins and dispersing the particles in a film-forming polymer. Most commercially available membranes are of the homogeneous type with a continuous polymer phase containing ionic groups attached to the polymer chains. The most common methods of membrane preparation are listed below.

Heterogeneous. Ion-exchange resin particles dispersed in polymer film.

- Calender or press mixture of resin and polymer.
- Cast film from dispersion of resin in polymer solution.
- Disperse resin in prepolymer, cast film, and polymerize.

Homogeneous. Ionic groups attached to polymer.

- Polymerize ionic monomers.
- Crosslink polyelectrolyte.
- Graft onto preformed films.
- Cast solution of polyelectrolyte in film-forming polymer.
- Imbibe graftable monomers into film, polymerize, and graft.

Membrane Properties

The physical properties of some commercially available ion-exchange membranes are listed in Table 8.1. The information on membrane properties was that supplied by manufacturers unless otherwise indicated. The diversity of membrane thickness is noteworthy. The membranes made by Ionics, Inc. are thick and rigid, because they must span rather wide spaces between supports in the solution compartments without deflection. The thick Ionics membranes have relatively high resistance, but these values are still low compared to the resistance of the brackish water they are designed to treat. RAI developed very thin membranes for battery separators and used the same radiation grafting techniques to make thin ED membranes with low resistance.

Table 8.1: Commercial Ion-Exchange Membranes

DESIGNATION	TYPE	THICKNESS um	RESISTANCE[a] ohm cm^2	COUNTERION[b] TRANSPORT, %
ASAHI CHEMICAL TOKYO, JAPAN				
K101	C	240	2.1	95
A111	A	210	2.5	73
ASAHI GLASS TOKYO, JAPAN				
CMV	C	135	2.7	91
AMV	A	135	2.7	93
IONAC CHEMICAL BIRMINGHAM,N.J., USA				
MC-3470	C	343	9.6	83[c]
MA-3475R	A	368	10.5	85[c]
IONICS, INC. WATERTOWN, MA., USA				
CR-61 CZL-386	C	508	10	90.3
AR 103 QZL-386	A	508	12.5	86.8
AR 204 UZL-386	A	508	9	95.0
RAI RESEARCH CORP. HAUPPAGE, N.Y.,USA				
R-4010	C	114	1	86
R-4035	A	89	1	86
TOKUYAMA SODA TOKYO, JAPAN				
C66-5T	C	155	1.4	94[c]
AF-4T	A	175	2.0	96[c]

a. RESISTANCE MEASURED IN 1.0 N KCl
b. TRANSPORT NUMBER MEASURED BETWEEN 0.5 AND 1.0N KCl
c. DATA FROM REFERENCE 2. ALL OTHER DATA SUPPLIED BY MANUFACTURERS.

The transport number of the counter ion provides an indication of the permselectivity of the membrane. However, the conditions of measurement must be specified, because the counter-ion transport number drops as the concentration of the external solution increases. Techniques for measuring the transport number are described by Helfferich.[1]

The membrane properties reported in Table 8.1 are for new membranes. A long-term study by Kneifel and Hattenbach[2] revealed deterioration in some of these properties after prolonged exposure to 0.1 N solutions of NaCl, NaOH, and HNO_3. NaOH tended to be most destructive.

Water Transport

The permeability of ion exchange membranes to water is seldom tabulated as a membrane property, because it varies so much with types and concentrations of ions. Water transport is not often a significant factor in ED of dilute solutions. However, water transport determines the upper concentration limit of the enriching stream when ED is used to concentrate solutions. Ions that are transported through the membranes by an electric potential drag along about five water molecules on the average.[3] When solutions are dilute and membranes are loosely crosslinked, substantially more water transport occurs. Membranes that are sufficiently crosslinked to restrict water transport in dilute solutions are referred to as "tight" membranes.

ED STACKS

Design Considerations

An ED stack consists of alternating anion- and cation-exchange membranes with solution compartments between them. The solution compartments are bounded by perimeter gaskets that are pressed tightly between the membranes to confine the solutions within the compartments. The compartments usually contain spacers that keep the membranes separated by a constant distance. The spacers also aid in distributing the solution velocity evenly throughout each compartment. (Poor flow distribution within and among the compartments severely limits the performance of an ED stack.) Each solution compartment has a means for introduction and removal of solutions. All of these features are combined into a plastic device called a gasket-spacer. Most ED stacks are designed to use identical gasket-spacers for enriching and depleting compartments.

An exploded view showing the components of an electrodialysis stack is presented in Figure 8.3. The end plate is typically made of rigid plastic. It contains an electrode and the connections for the solution that rinses the electrode. It also contains connections for solution streams into and out of the enriching and depleting compartments. Holes in the inside face of the end plate are aligned with holes in the membranes and gasket-spacers that form manifolds for solution flow through the ED stack. Large stacks have multiple manifold holes on both ends of the gasket-spacers to provide uniform flow over the width of the compartment. The two membranes and two gasket-spacers illustrated in Figure 8.3 constitutes one cell pair. Commercial ED stacks typically contain more than 100 cell pairs between a single pair of electrodes.

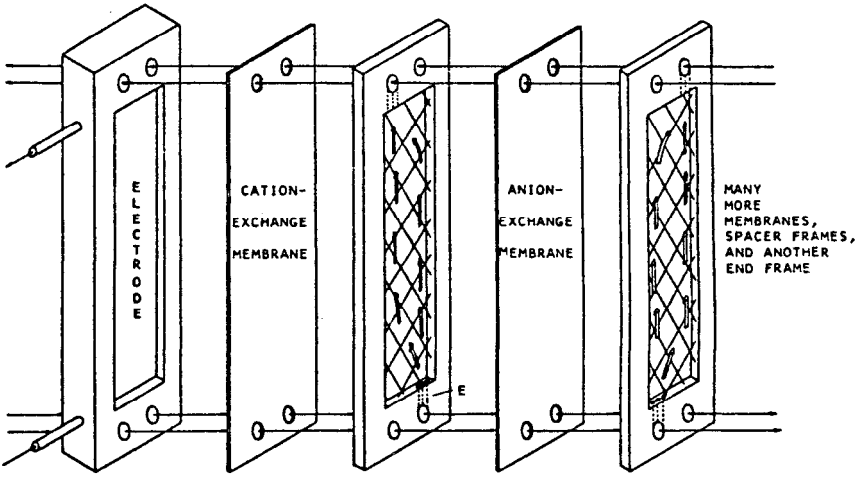


Figure 8.3: Main components of an electrodialysis stack.

The ED stack in Figure 8.3 represents the sheet-flow type. The sheet-flow design is used by most ED manufacturers (Ionics, Inc. is the major exception). The spacing between membranes of sheet-flow stacks is made as thin as practical to reduce electrical resistance and minimize the thickness of hydraulic boundary layers at the membrane surfaces. The thinness is ultimately limited by hydraulic resistance and by problems associated with getting solutions into and out of the solution compartments between the membranes. To maintain constant spacing between the membranes it is necessary to support the membranes at close intervals, but the support material must not cover a large fraction of the membrane surface or cause stagnation in the solutions near the membrane surface. The Vexar® non-woven polyolefin netting developed by DuPont has gained wide acceptance as a spacer that meets these criteria. The flow of solution in the plane of Vexar netting is illustrated in Figure 8.4.

The stack design developed by Ionics, Inc. is quite different from the sheet-flow stacks previously described. The Ionics design utilizes the tortuous-path spacer illustrated in Figure 8.5 to direct solutions over a relatively long, open channel in the solution compartment. Superimposed on this channel is a spacer that supports the membrane and promotes turbulence in the solution compartment. These supports are more widely spaced than those of a sheet-flow design, so a more rigid membrane is required to bridge the space without severe deflection. Therefore, the membranes made by Ionics are substantially thicker than those produced by most other manufacturers. The thick membranes and spacers result in higher electrical resistances than those found in sheet-flow stacks, but the openness of the solution channels should make them less prone to fouling by suspended solids.

Yet another stack design utilizes unit cells. Unit-cell stacks were specifically developed for concentrating solutions. Each concentrating cell consists of one cation-exchange membrane and one anion-exchange membrane sealed at the edges to form an envelope with a spacer screen inside. The envelopes also have

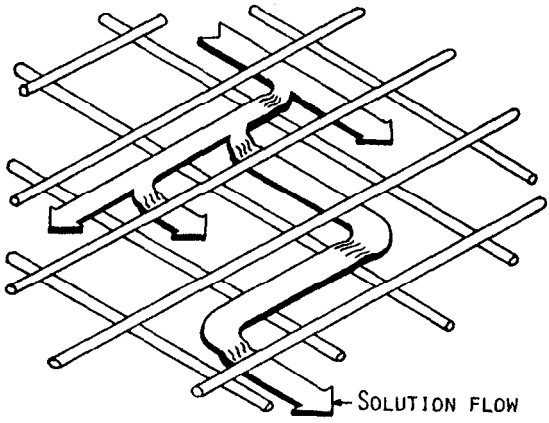


Figure 8.4: Representation of solution flow through Vexar spacers.

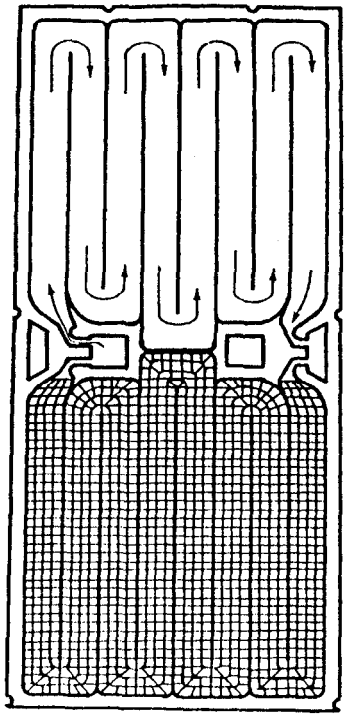


Figure 8.5: Diagram of a tortuous-path spacer for an electrodialysis stack.

spacer screens between them to insure uniform solution flow across the membranes. The entire assembly of alternating membrane envelopes and spacer screens is held between a set of electrodes. The electric current carries ions from the external solutions through the membranes to the inside of the envelopes where they are trapped. Only osmotically and electro-osmotically transferred water flows through the membranes. Thus, unit cells achieve the maximum degree of concentration that is possible with ED. The concentrated solutions inside of the concentrate cells flow through small tubes that lead from inside the concentrate cells to a plenum chamber arranged outside the stack.

STAGING OF ED STACKS

ED differs from other desalting processes in the degree of desalting achieved in a single stage. In evaporation, reverse osmosis, and ion exchange the necessary degree of desalting can often be achieved with one pass through the device. In ED, the degree of desalting is usually limited to about 50% per pass, and some type of staging is needed for further desalting. In large installations such as municipal water supplies this staging is achieved by passing the water through a series of stacks. For example, water with 2,000 ppm TDS (total dissolved solids) could be reduced to 500 ppm TDS by two stacks that each achieve 50% desalting.

For small installations where the throughput does not justify multiple stacks, there are other alternatives including internal staging, feed and bleed, and batch recirculation. Internal staging allows one to utilize one pair of electrodes to achieve multi-stage desalting. For the example cited above, one might use a stack with 150 cell pairs to treat water with 2,000 ppm TDS. The first stage would utilize 100 cell pairs to reduce the salinity to 1,000 ppm. Then a second stage with 50 cell pairs would reduce the salinity to 500 ppm. Each cell pair in the second stage would remove the same quantity of salt as a cell pair in the first stage, but with half the TDS reduction because the water throughput per cell would be doubled.

With feed and bleed or batch recycle systems some or all of the water that has already been processed by the stack is mixed with feed and returned via a recirculation pump. Recycle is inherently less efficient than once-through flow in both stack utilization and in energy consumptions since the same solution must be pumped and desalted repeatedly and then remixed with a more concentrated solution. However, the increased flexibility in process control makes recycle systems attractive for small-scale operations where stacks are over-sized to handle varying loads. Feed and bleed is useful for operations where the enriching stream needs to be as concentrated as possible. Ten-fold enrichment or 90% recovery of some feed waters as diluate can be achieved by concentrate recirculation if solubility limits of the dissolved substances are not exceeded in the concentrate stream.

APPLICATIONS OF ED

Outside of Japan, the largest application of ED has been in the desalination

of brackish water. Most of the early research and development effort had the objective of improving marginal waters to make them potable. During the 1950's, the Netherlands National Research Organization, TNO, the South African Council for Scientific and Industrial Research, and the Office of Saline Water in the U.S.A. funded programs to improve membranes, equipment and processes to produce potable water more economically. Since ED treatment of brackish water is well known, that subject will not be stressed in this chapter.

A potential growth area for ED is in the rough desalting of water that will be subjected to subsequent purification for use as boiler feed or rinse water in the electronics industry. Ion exchange has traditionally been used for preparing waters with low salinity, but the cost of regenerants and the magnitude of the waste disposal problem are proportional to the salinity of the feedwater. The bulk of the dissolved solids can be removed more economically by ED or RO. These two processes are competitive in cost, and both offer the advantage that they do not contribute additional water pollutants.

ED might appear to be at a competitive disadvantage with RO for this application, because RO removes particulates and substantial amounts of organic solutes from the water. Accumulation of these contaminants on membrane surfaces can cause premature failure of RO modules. Therefore, it is common practice to remove organics and particulates before the rough desalting. With such pretreatment, ED stacks operate trouble-free for years with little maintenance. The system shown schematically in Figure 8.6 has been in service at Bell Laboratories since 1975 removing salts, principally $CaSO_4$, from water for use in rinsing integrated circuits.[4]

ED desalting of seawater has also been demonstrated on a commercial scale. The power consumption has been held to tolerable levels (28 watt-hours/gal) by the use of ion-exchange membranes with low resistance.[5] Still the greatest use of ED treatment of seawater has been for the recovery of NaCl. Japan has no natural deposits of NaCl and had formerly obtained the salt by evaporation of seawater. The use of ED to produce a concentrated brine up to 20% TDS has substantially reduced energy costs (less than 200 kwh per ton of salt). Moreover, the use of membranes that are selective for univalent ions has improved salt purity to 97% and reduced precipitation problems. The approach has been so successful that essentially all the table salt in Japan is prepared from ED enriched brines.[6]

Food processing provides many potential applications for ED because of its ability to separate electrolytes from non-electrolytes. Its greatest use has been in whey deashing. Whey is the waste product from cheese making, and it contains useful quantities of proteins, lactose, and lactic acid. However, the high mineral content makes it unacceptable for human consumption and of marginal value as animal feed. Deashing by ED upgrades the whey so that subsequent processing can produce edible whey solids.

Whey processing required several modifications to ED systems. To retard spoilage, the liquid streams had to be cooled. The inevitable accumulation of solids on the membranes and spacers required routine cleaning in place and periodic disassembly of the stacks for mechanical cleaning. These operations are now well established and can be applied to the treatment of other food products.

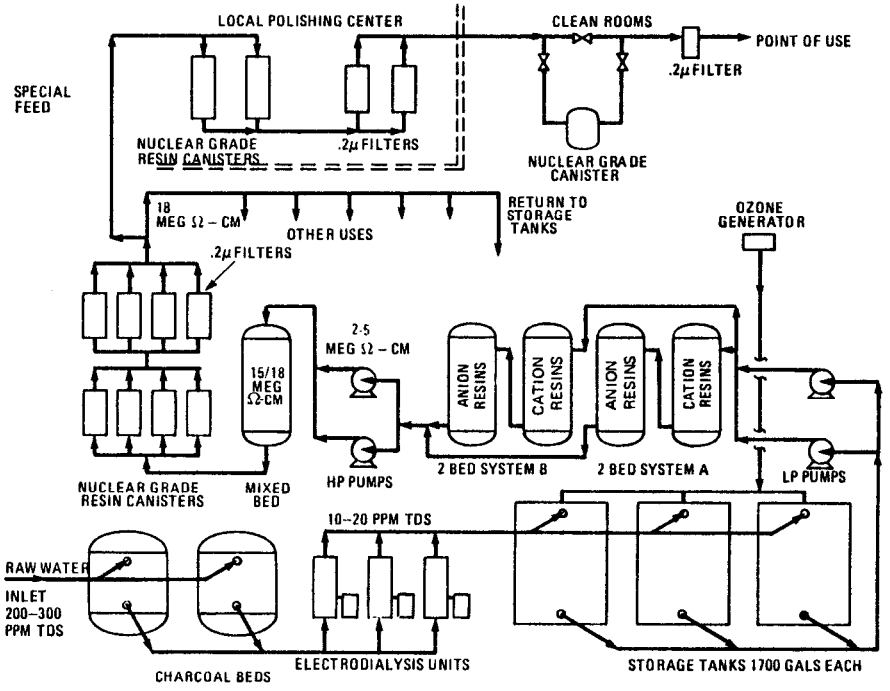


Figure 8.6: Integrated circuit process water system. (Bell Laboratories, Murray Hill, NJ)

Cows' milk is more salty than milk from human mothers, and this limits its use in the preparation of infant formula. Desalting of cows' milk by ED allows larger quantities of cows' milk solids to be used for these purposes. Research has shown that desalting by ED to remove calcium improved the protein stability of frozen skim milk and its concentrates.[7] The lumpy texture of thawed frozen milk has been attributed to clumping of micellar casein, and calcium removal led to the dissociation of micellar to serum casein.

The opposite effect was observed in blood ultrafiltrate. With the apparatus shown in Figure 8.7, Jain[8] used ED to desalt the blood plasma. Chilling aided in the precipitation of proteins which were removed by ultrafiltration. The salt content of the plasma was restored by passing it through the concentrate compartments of the ED stack before returning it to the host. Such a process could be used to treat certain diseases where excessive amounts of undesirable proteins are present in a patient's blood or to obtain needed proteins from a donor.

Other separations of proteins and amino acids have been achieved by pH adjustment of the solution being treated. As in electrophoresis, a molecule that is at its isoelectric point will not migrate in an electric field. However, a molecule migrates as an anion at a pH above its isoelectric point, and as a cation below its isoelectric point. Therefore, a solution of such a material at its isoelectric point can be desalted by ED with minimal loss of the material.

Metal finishing processes offer numerous applications for ED in pollution control and material recovery. The rinse streams from such processes pose particularly troublesome pollution problems. They are usually too dilute for direct metal recovery and too concentrated for disposal. ED processing of a rinse stream from a nickel electroplating system[9] is illustrated in Figure 8.8. The used rinse water flows through the depleting compartments of the ED stack where the metal ions are transferred into the concentrate stream. The treated rinse water can then be reused in the process. The concentrate stream can be recirculated to build up its metal content to a level that is useful for further recovery or direct return to the plating bath.

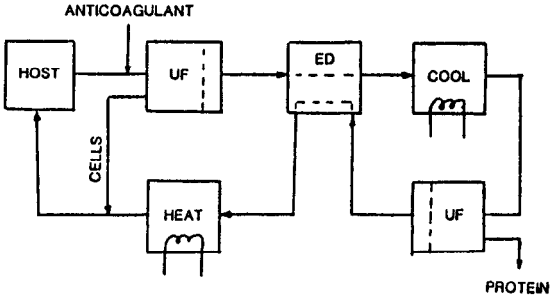


Figure 8.7: Membrane system for recovering proteins from blood.

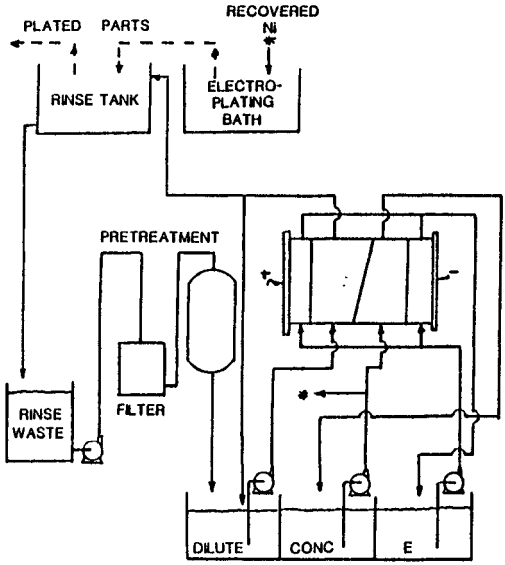


Figure 8.8: ED for recovery of nickel from electroplating waste water.

ED has also been used to improve or maintain the quality of a plating bath and thus eliminate the need for periodic replenishment. An instructive example is shown in Figure 8.9 for the electroless plating of copper onto nonmetallic substrates such as printed circuit boards.[10] The process illustrated utilizes an uncharged EDTA-Cu complex where the reduction of copper is driven by the oxidation of formaldehyde to formic acid. The formate ions and the sulfate ions introduced with the make-up copper are undesirable reaction by-products that are removed by ED. NaOH is added to adjust pH sufficiently to ionize the formic acid. The uncharged EDTA-Cu complex remains in the diluate stream, which is returned to the plating tank.

A similar approach was used to recover silver from spent photographic bleach-fixer solutions.[11] As shown in Figure 8.10, the iron, which was used to oxidize the silver, remains in the bleach-fixer solution, because it forms a complex with EDTA. The silver permeates the cation-exchange membranes to the iron-free concentrate stream from whence it is reclaimed by electrodeposition in a separate cell.

BIPOLAR MEMBRANES

Bipolar membranes consist of an anion-exchange membrane and a cation-exchange membrane laminated together. Application of an electric potential of about one volt to the bipolar membrane exposed to an electrolyte solution will cause current flow, but the amount of current flow will be determined by the orientation of the membrane. If the cation-exchange membrane faces the anode, the current will be relatively high. If the anion-exchange membrane faces the anode, the current will quickly drop to a low value as the anions and cations are depleted from the membranes. Subsequent elevation of the potential in the latter case will increase the current which is carried by the only available ions, H^+ and OH^- ions generated at the junction by water splitting. This results in the production of acidic and basic solutions at the surfaces of the bipolar membranes, as illustrated in Figure 8.11. Multiple bipolar membranes can be placed between a single pair of electrodes in an ED stack along with other ion-exchange membranes for the production of acid and base from a neutral salt.

The current efficiency of acid/base generation and the purity of the acid and base made with bipolar membranes drops off as concentrations increase, because Donnan exclusion diminishes with increasing solution concentrations. Further, the production rate is limited by the rate of diffusion of water into the bipolar membrane. Nevertheless, there are substantial advantages to the process. Since there are no gases evolved at the bipolar membranes, the energy associated with gas evolution is saved, and the power consumption is about half that of electrolytic cells. Compared to the electrodes used in conventional electrolytic cells, the bipolar membranes are inexpensive. Where dilute (e.g., 1 N) acids or bases are needed, bipolar membranes offer the prospect of low cost and minimum unwanted by-products.

A commercially available ED stack with bipolar, anion and cation membranes was used by the author to generate 1 N HCl and NaOH from NaCl. A current density of 100 mA/cm^2 was maintained with an applied potential of 2V/cell.

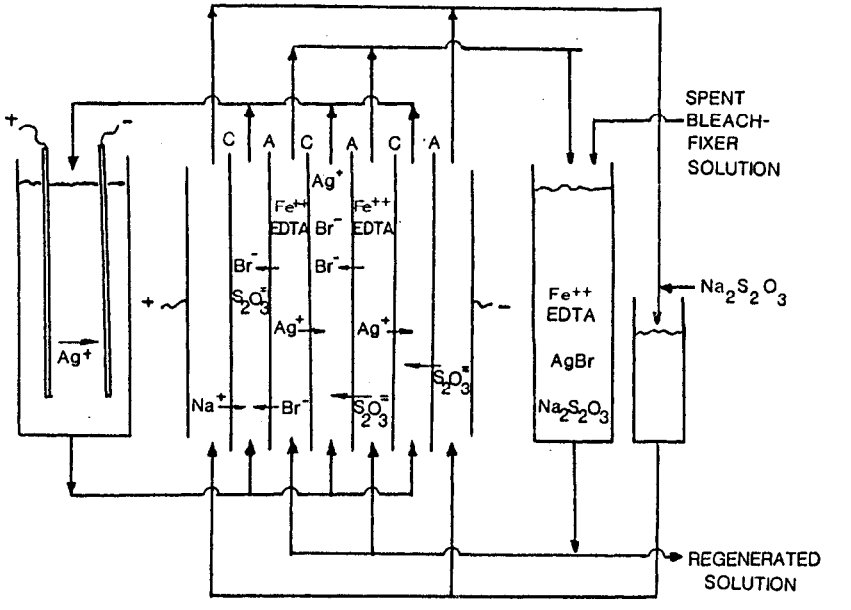


Figure 8.9: Regeneration of chemical copper plating bath by electrodialysis.

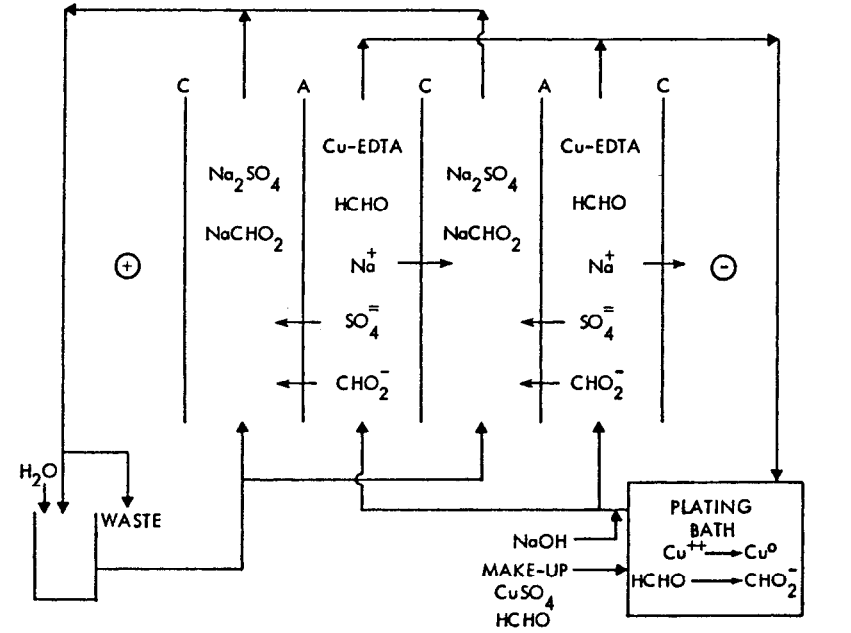


Figure 8.10: Use of ED for regenerating spent photographic bleach-fixer solution.

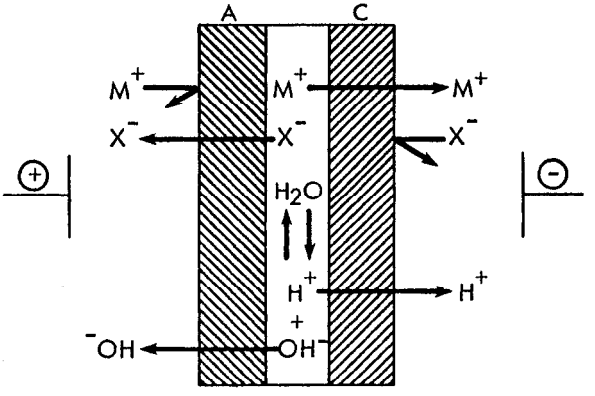


Figure 8.11: Bipolar membrane construction and operation.

The current efficiency was about 80%, and the purity of the acid and base exceeded 98%.

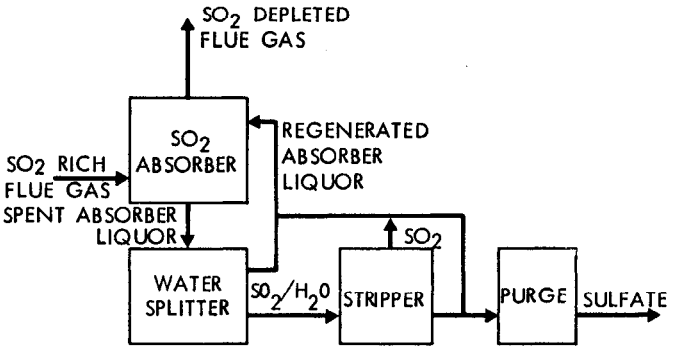
Several applications for bipolar membranes have been reported. Figure 8.12 shows a process for absorbing SO_2 from flue gas with a solution of Na_2SO_3 and regenerating the solution with a water splitter containing bipolar membranes.[12] The regeneration process is shown in Figure 8.13. H^+ ions generated in the bipolar membrane lower the pH of the solution and allow SO_2 to be stripped out. Na^+ ions pass through the cation-exchange membrane into the basic solution. The stripped acidic solution is combined with the basic solution and returned to the absorber.

An ED stack with alternating bipolar and cation-exchange membranes (the arrangement shown in Figure 8.13) was used to convert Na_2CO_3 and/or $NaHCO_3$ to more valuable NaOH with gaseous CO_2 as the by-product.[13] A stack with bipolar, anion-exchange, and cation-exchange membranes was used to convert ethylenediamine dihydrochloride into ethylenediamine and HCl in separate streams.[14] As more bipolar membranes become available in commercial quantities, more applications of bipolar membranes are sure to follow.

ELECTRODES AND STACK POWER

Electrode Reactions and Materials

An electric potential is the driving force for transport of ions in ED. This potential is applied from an external power supply through electrodes situated on either end of the stack of membranes and spacers. Current flow in the circuit external to the stack is electronic, i.e., electrons flowing through metallic conductors. However, current flow within the stack is electrolytic, i.e., ions flowing through solutions. The transfer of electrical charge from electronic to electrolytic conduction is accomplished via electrode reactions.



Block diagram of SO_2 recovery process.
(Allied Chemical Corp.)

Figure 8.12: Block diagram of SO_2 recovery process. (Allied)

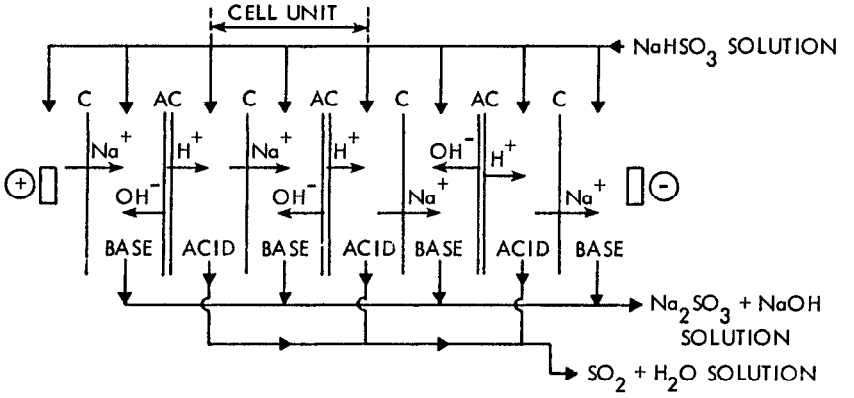


Figure 8.13: Two compartment water splitting process for converting bisulfite solutions to SO_2 and base.

Cathode Reactions

$M^{+x} + xe^- \rightarrow M^o$	metal deposition	
$2H^+ + 2e^- \rightarrow H_2$	(acidic solution)	evolution of
$2H_2O + 2e^- \rightarrow H_2 + 2OH^-$	(basic solution)	gaseous hydrogen

The first cathode reaction is common in electroplating but is undesirable in ED. Evolution of H_2 with the consumption of H^+ or production of OH^- ions is common to all ED cathodes. These reactions are relatively mild compared to the anode reactions, so electrodes that tolerate H_2 and OH^- are employed. Stainless steel is the most common cathode material.

Anode Reactions

$M^o \rightarrow M^{+x} + xe^-$	metal dissolution
$2H_2O \rightarrow O_2 + 4H^+ + 4e^-$	(acidic solution) } evolution of
$4OH^- \rightarrow O_2 + 2H_2O + 4e^-$	(basic solution) } gaseous oxygen
$2Cl^- \rightarrow Cl_2 + 2e^-$	evolution of gaseous chlorine
$M^o + xOH^- \rightarrow M(OH)_x + xe^-$	} oxidation of electrode
$2M^o + 2xOH^- \rightarrow M_2O_x + xH_2O + 2xe^-$	

Anode reactions that produce dissolution or oxidation of the electrode metal are avoided by selection of resistant metals such as platinum. The use of a thin layer of platinum on a substrate of less expensive metal (e.g., titanium) moderates the expenditures for anodes. However, titanium is not suitable for reversible electrodes, because it is attacked by the H_2 generated at the cathode.[15] When the polarity of the electrodes must be reversed periodically, as in the EDR process, platinized niobium has been used.

Some metals, e.g., lead and iron, will form stable conductive oxide coatings under properly controlled anodic conditions.[16–18] Metal electrodes with oxide coatings are economical compared to those with platinum coatings, but they are not reversible. Indeed, reversibility of ED electrodes is exceptional. Care must be exercised to ensure that the polarity of ED electrodes is not inadvertently reversed, because severe electrode deterioration can result.

Electrode Isolation

The reactions that occur at the electrodes are normally incidental and occasionally detrimental to the desired separations that take place in the repeating cell pairs of an ED stack. The H^+ and OH^- ions generated at the electrodes can cause undesired reaction with the components of the feedwater and lead to membrane fouling. Moreover, migration of some feed components into the electrode rinse streams can cause precipitation on the electrodes or the spacers and membranes close by. Therefore, it is prudent to carefully consider such possibilities and isolate the electrodes to minimize undesired reactions.

Although the reactions at the cathode are not severe in terms of electrode deterioration, fouling problems can be severe at the cathode. The presence of pH-sensitive salts, e.g., $Ca(HCO_3)_2$ in the feedwater is a matter of concern, because the OH^- ions generated at the cathode can lead to precipitation.

$$Ca(HCO_3)_2 + 2OH^- \rightarrow CaCO_3 + CO_3^{=} + 2H_2O$$

The problem of pH control in the cathode rinse stream (catholyte) is usually handled by acidification. Faraday's constant, 96,500 A-sec/eq, is used to calculate the amount of acid required to neutralize the OH^- ions generated at the cathode. While acid addition contributes significantly to operating costs of commercial ED plants, the fact that there are hundreds of cell pairs between each pair of electrodes keeps the catholyte acid costs at tolerable levels. In contrast, acidification of the feed stream to prevent precipitation can increase operating costs substantially.

Selection of the type of membrane to be used at the cathode end of the stack is important. If a cation-exchange membrane is used, the catholyte is an enriching stream. This means that cations from the feed solution can enter the catholyte. The use of a univalent-cation-selective membrane next to the cathode can alleviate some of the problems of multivalent cations in the catholyte. An enriching catholyte stream is almost invariably a waste stream, which presents disposal problems. Moreover, makeup water of good quality is required. The overriding advantage of the cation-exchange membrane is that it blocks the entry of cathode-generated OH^- ions into adjacent compartments.

The catholyte is a depleting stream if an anion-exchange membrane is placed next to the cathode. The major advantage to this arrangement is that cations from the feed solution can be almost completely excluded from the catholyte. The price to be paid is that acid must be added to the catholyte in sufficient quantity to supply all of the anions needed to carry current through the membrane.

The major considerations about isolation of the anode pertain to the acidic, oxidizing conditions there. An anion exchange membrane is often used to block the passage of H^+ ions into the rest of the stack. However, anion exchange membranes are only moderately effective at blocking H^+ ions, so neutralization of the anolyte may be needed if acid-sensitive components, e.g., proteins, are present in the feed. The undesirable formation of hypochlorite occurs at the anode whenever chloride ions are present in the anolyte. The use of a cation-exchange membrane at the anode prevents chloride entry from the feed solution to the anolyte, but this arrangement makes the anolyte a depleting stream and requires a supply of electolyte (e.g., NaOH, Na_2SO_4) for the anolyte.

In some circumstances, a common rinse solution can be circulated through the anode and cathode compartments. The simplicity and economy of a single electrode stream must be weighed against the problems of current leakage through the solution lines, buildup of undesirable materials such as hypochlorite, and the mixing of H_2 and O_2 generated at the electrodes. These problems may be conveniently ignored in laboratory experiments, but they are critical issues in large ED stacks.

Kedem et al demonstrated that gas evolution could be avoided by the use of powdered activated carbon in a common electrode rinse stream.[19] The large surface of a carbon particle became charged when it came in contact with the anode or with another positively charged carbon particle. This charge was neutralized by sorption of anions from the rinse solution. When the suspension reached the cathode, the charge on the particle was reversed and the sorbed anions were exchanged for cations. With a 2.5% suspension of carbon in 0.02 to 0.2 normal solution, a current of 10–20 mA/cm^2 could be sustained for weeks with no gas evolution.

The benefits of a common electrode rinse stream were demonstrated in a photographic developer regeneration process illustrated in Figure 8.14. The use of cation-exchange membranes at both electrodes made the anolyte a depleting stream and the catholyte an enriching stream. This kept the Br^- out of the electrode rinse solution and conserved the Na_2CO_3 that maintained the conductivity in the electrode compartments.[20] A similar arrangement with NaOH solution for the electrode rinse allowed the use of an inexpensive ferrous anode in an ED stack.[18]

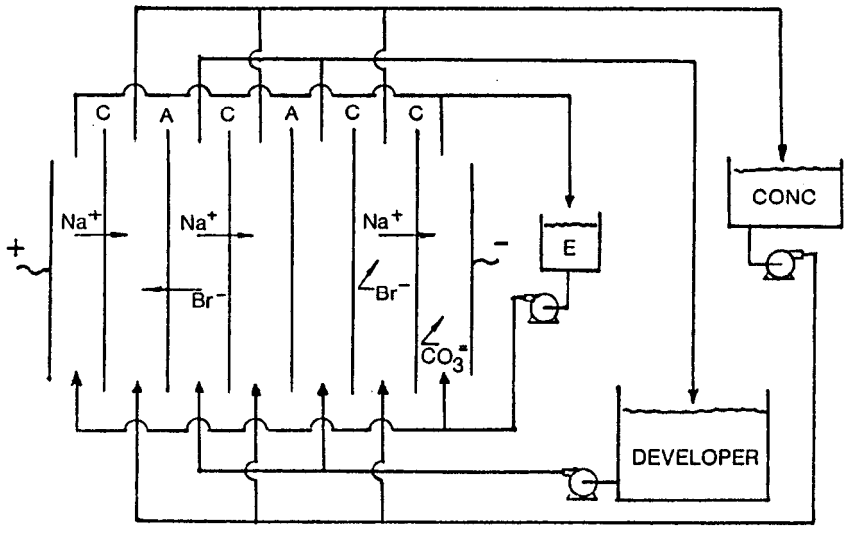


Figure 8.14: The use of cation-exchange membranes at both electrodes conserved the Na_2CO_3 in the common electrode rinse stream of a photographic developer regeneration process.

Power Supplies

Ionic transport through the solutions and membrane of an ED stack is driven by a direct electric potential. The components required to safely deliver current (DC) at the proper voltage are illustrated in Figure 8.15. An isolation transformer contributes measurably to the safety of operating an ED stack, especially an experimental one from which samples are being taken. The output from the isolation transformer has a floating ground if the load is not intentionally grounded. If the circuit is accidentally grounded by an operator's hand, this contact point becomes the zero potential point, but no shock is experienced.

The power level of the ED stack is regulated by adjustments of the stack voltage. In laboratory ED units an autotransformer or a solid state voltage regulator is preferred, because the user will likely want to experiment with the effects of applied voltage on stack performance. In large installations a transformer may be used, or the number of cell pairs in the stack may be varied to match the desired cell-pair voltage drop to the available DC voltage. Since transformers operate on AC, voltage adjustment must occur before conversion to DC.

A full-wave rectifier is commonly used to convert AC to DC. The current from such a rectifier has a 120 Hz ripple which is of no consequence. The rates of build-up and collapse of concentration boundary layers are so slow compared to the ripple frequency that stack performance is unaffected by the ripple.

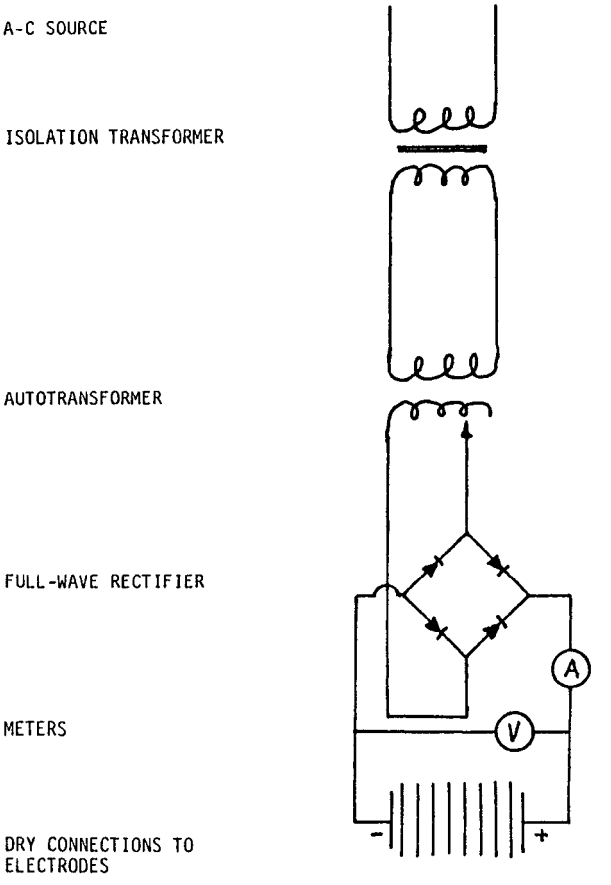


Figure 8.15: Power Supply for ED.

Connections between the power supply and the electrodes are usually made outside the stack so that they can be kept clean and dry. It is advisable that the conductor between this connection and the electrode be of the same material as the electrode and that the connection with the electrode be welded. Otherwise, severe corrosion problems can result.

The observation that the cell-pair resistance is reasonably constant (see Figure 8.16) over the range of safe operation of ED allows one to develop a simplified equation concerning power consumption in an ED stack. With constant R_{cp} the cell voltage is proportional to cell current, i.e., $E_{cp} = IR_{cp}$.

The typical voltage drop across a cell pair is in the range of 1 to 2 volts. E_{cp} does not change greatly as feed concentrations change, because I is proportional to concentration, and R_{cp} varies inversely with concentration.

Assuming constant current efficiency, the current is proportional to the amount of salt removed by the passage of current, i.e., $I \propto C$. Since power consumption is the product of current and voltage, one reaches the not-too-surpris-

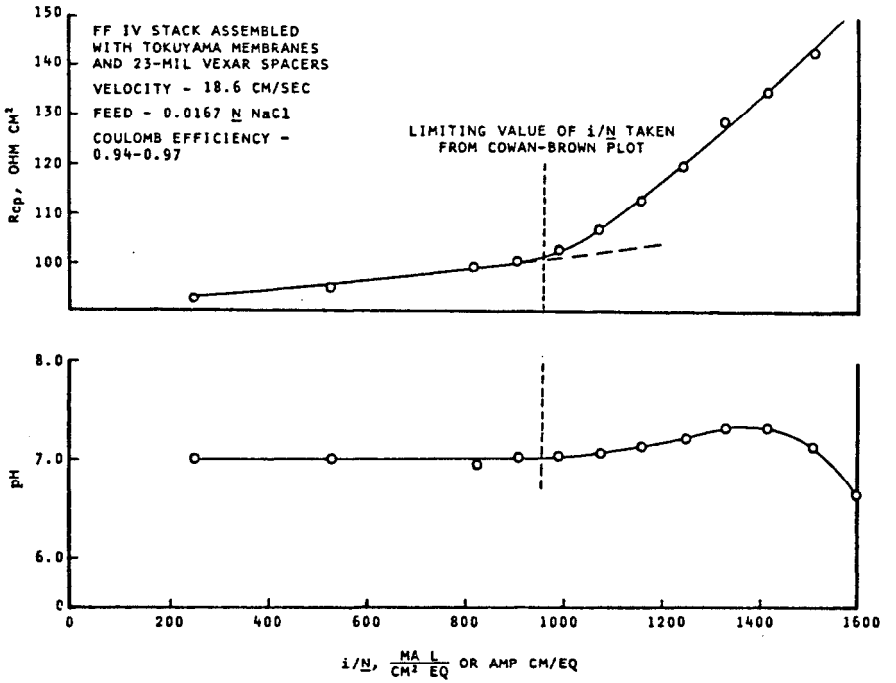


Figure 8.16: Effects of i/N on cell-pair resistance (R_{cp}) and pH of the depleted effluent.

ing conclusion that the power consumption in the ED stack is proportional to the amount of salt removed, i.e., $P \propto \Delta C$. Reductions in power consumption can be achieved for any ED stack by reducing the applied voltage, but a consequent reduction in electrolyte removal would occur.

CONCENTRATION POLARIZATION

The phenomenon of concentration polarization is important in electrodialysis, because it ultimately limits the rate at which ion transport can occur. Concentration polarization will be discussed first in a descriptive manner. Then, a simplified mathematical model will be used to show the quantitative aspects of concentrations polarization and explain the important concept of "limiting current density".

In Figure 8.1, it was shown that the interposition of pairs of anion- and cation-exchange membranes between electrodes resulted in the depletion or enrichment of electrolyte in the alternating solution compartments when an electric potential was applied. Close examination of the system would reveal nonuniformity of electrolyte concentration within a solution compartment. In the enriching compartments, the concentration is higher at the membrane surfaces

than in the bulk solution, and in the depleting compartments, the concentration is lower at the membrane surfaces. The resistance to the flow of electric current increases as this interfacial concentration decreases. The reason for the nonuniformity of concentrations in the solution compartments is that cations carry virtually all of the electric current in the cation exchange membranes but only about half of the current in the solution.

The fraction of the total current carried by a particular ionic species in an electrolyte solution is called the transport number t. For a solution containing a univalent electrolyte like NaCl or KNO_3 the transport number of the cations is:

$$t^+ = \lambda^+/(\lambda^+ + \lambda^-)$$

where λ is the equivalent ionic conductance. Values of λ extrapolated to infinite dilution are shown in Table 8.2. Solutions with more than one salt or with multivalent ions require a more generalized equation to describe transport numbers:

$$t_i = \lambda_i Z_i^2 C_i / \Sigma \lambda_i Z_i^2 C_i$$

where C_i is the molar concentration and Z_i is the ionic charge of each species present in the solution.

Transport numbers within the membranes are not as easily determined as those in solutions because of interactions between the mobile ions and the fixed ionic groups. Although the generalized equation above is applicable to the membrane as well as to the solution phase, the values of λ and C are different in the membrane. Because of Donnan exclusion, the concentration of counter ions (those of opposite charge to the fixed ions) is always much higher than the concentration of co-ions (several orders of magnitude higher when external solutions are dilute). Since most of the ions available to carry current within the membrane are counter ions, the transport numbers of counter ions are high, typically above 0.9 when external solutions are dilute (<1 molar).

What happens with increasing ED current can be presented mathematically with the aid of a simplified model called the Nernst idealization. This model, which is illustrated in Figure 8.17, is based on the simplifying assumptions of stagnant boundary layers of constant thickness and a well-mixed region in the center of the solution compartment. These idealized boundary-layer conditions are obviously unrealistic, especially in the presence of the spacer screens used in an ED stack, but they allow a simplified approach to an otherwise complex problem.

Now, consider the region of the system designated by the square in Figure 8.17 for a single uni-univalent electrolyte such as NaCl. The flow of electrical charge in this region is designated by the symbol i with the units mA/cm^2. With the additional assumption that diffusion is negligible within the membrane, flux of cations through the cation exchange membrane is proportional to the electric current.

$$\bar{J}_e^+ = i\bar{t}^+/F$$

Here the overbar designates the membrane phase, and $\bar{t}^+$ is the transport number for cations in cation exchange membrane. The F is Faraday's constant,

Table 8.2: Equivalent Conductance in Aqueous Solution

	0°C	18°C[a]	25°C[b]
H^+		316.55	349.8
Li^+		33.28	38.69
Na^+		43.39	50.11
K^+	40.4	64.44	73.52
Rb^+		67.5	
Ca^+	44.4	67.65	78.1
Ag^+	32.9	53.77	61.92
Tl^+		65.7	74.7
NH_4^+			73.4
$(C_2H_5)_4N^+$		28.1	
$\frac{1}{2}Mg^{++}$			53.06
$\frac{1}{2}Ca^{++}$			59.50
$\frac{1}{2}Sr^{++}$			59.46
$\frac{1}{2}Ba^{++}$			63.64
$\frac{1}{2}Cu^{++}$		46.3	
$\frac{1}{2}Zn^{++}$		46	
OH^-		176.6	197.6
F^-		46.65	
Cl^-	41.3	65.41	76.34
Br^-	43.1	67.4	78.3
I^-	43.4	67.4	76.8
ClO_3^-		54.99	
BrO_3^-		47.9	
IO_3^-		34.02	
NO_3^-	40.4	61.74	71.44
ClO_4^-		58.4	68.0
MnO_4^-	31.0		61.7
$HCOO^-$		47.0	
CH_3COO^-	20.3	33.5	40.8
Picrate		25.4	
$\frac{1}{2}SO_4^{=}$	41	68	79
$\frac{1}{2}Cr_2O_4^{=}$	39	63	73

[a] C. W. Davies, "Conductivity of Solutions," Chapman and Hall, 1930.

[b] H. S. Harned and B. B. Owen, "Electrochemistry of Solutions," Reinhold, 1950.

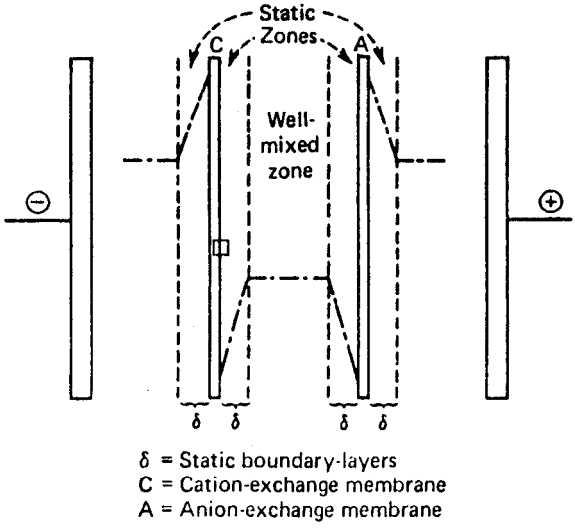


Figure 8.17: Concentration gradients in electrodialysis.

96,500 A-sec/eq. Since $\bar{t}^+ = 1$ in the ideal case, one equivalent of cations is removed through the membrane for every faraday of current flowing through the region of interest. Now in the aqueous phase near the membrane, the flux of cations transported electrically is:

$$J_e^+ = it^+/F$$

If the electrolyte were NaCl where $\bar{t}^+ = 0.4$, the electric current would deliver only 0.4 of an equivalent of cations for each equivalent of cations transported through the cation exchange membrane. The remaining 0.6 faraday of current would be transported by anions that are moving in the opposite direction. The net result would be a depletion of anions and cations from the solution at the membrane surface. This depletion would result in a concentration gradient that would allow diffusive transport of the balance of ions needed for electroneutrality. In this case, the balance would be 0.6 of an equivalent per faraday of current flow. The diffusive flux of ion pairs down this linear concentration gradient is:

$$J_d = D(C_b - C_i)/\delta$$

The subscripts b and i refer to the bulk and interfacial concentrations. Now, one can write the steady-state flux equation for cations in the vicinity of the membrane solution interface.

$$\bar{J}_e^+ = J_e^+ + J_d$$

$$i\bar{t}^+/F = it^+/F + D(C_b - C_i)/\delta$$

Rearrangement yields:

$$i/(C_b - C_i) = DF/\delta(\bar{t}^+ - t^+)$$

F is a constant and D, δ, $\bar{t}^+$ and t^+ are essentially nonvariant for a given set of operating conditions (temperature, flow rate, membrane and salt type). Now, i is an independent variable that can be adjusted by changing the voltage applied to the electrode. When i changes, the value of $C_b - C_i$ changes proportionately. However, there is a limitation on the extent to which the value of i in this equation can be increased. That limit is approached as C_i approaches zero. The limiting current density can thus be expressed:

$$i_{lim}/C_b = DF/\delta(\bar{t}^+ - t^+)$$

For a solution like KCl where the ionic conductances of both ions are the same, $t^+ = \bar{t}$ and i_{lim} is the same value for both interfaces. However, this is not the case for NaCl where $t^+ = 0.4$ and $\bar{t} = 0.6$. The equations above indicate that the value of i_{lim} at the anion exchange membrane would be 1.5 times higher than that at the cation exchange membrane.

The data in Figure 8.16 show the results of an experiment to determine the values of i_{lim}. Those data were obtained from electrodialysis of a solution of NaCl in a stack containing ten cell pairs.[21] The applied voltage, current, and pH of the depleted product water were monitored. A control experiment with one cell pair in the stack was used to determine the voltage drop attributable to the electrodes and rinse streams. The cell-pair resistance, $R_{cp} = (V_{appl} - V_{elec}) \times A_{cp}/I$, was observed to increase slightly for moderate increases in the polarization parameter, i/N. [The polarization parameter is defined as the current density, $i = I/A_{cp}$, divided by the log-mean concentration of the depleting stream, $N = (C_{in} - C_{out})/\ln(C_{in}/C_{out})$.]

However, the value of R_{cp} increased more rapidly when the value of i/N exceeded 950 A-cm/eq, indicating i_{lim} at the cation exchange membrane. Moreover, a slight increase in the pH of the depleted effluent was detected. When the value of i/N reached about 1,400 A-cm/eq, the pH of the depleted effluent dropped precipitously, indicating i_{lim} at the anion exchange membrane. The ratio of the i_{lim} values was 1.5 as expected.

Upon close examination of the data in Figure 8.16, one might question whether the inflection points in the curves truly represent the limiting values of the polarization parameter, i/N, i.e., whether the concentration approaches zero in the solution at the interface of the cation exchange membrane. If the concentration were to reach zero over the entire surface at the same value of i/N, the inflection would likely be more abrupt and the curve would become steeper, because splitting water to form H^+ ions would be the only source of ions to carry the additional current. In fact, the slight increase in pH of the depleting solution suggests that water splitting was not significant. A more reasonable explanation is that localized depletion occurred at the inflection point and expanded as current increased.

The maximum point in the pH curve was attributed to attainment of the limiting value of i/N at the anion exchange membrane. Again this was probably localized depletion that expanded as current increased, but the pH decrease was much more dramatic than the pH increase observed when polarization occurred

at the cation exchange membrane. This observation indicated that water splitting occurred at the anion exchange membrane but not at the cation exchange membrane. The prevailing theory explains that the kinetics of water splitting in solution are too slow to cause appreciable pH changes to occur.[22] Instead substantial water splitting occurs *in* the anion exchange membrane, and it is catalyzed by tertiary amines that withdraw protons from water molecules.

The current density at which R_{cp} begins to rise rapidly is generally referred to as the limiting current density. This terminology obviously does not refer to a physical limitation to the current flow but rather to a practical limitation for trouble-free operation of electrodialysis. Moreover, the precise value of i_{lim} is not as easily established as Figure 8.16 would indicate. Uneven flow distribution within or between solution compartments could lead to localized thick boundary layers that result in lower values of i_{lim}. Also, the presence of non-conductive spacers in the solution compartments causes local current densities to be higher than the calculated average value. Therefore, for a margin of safety, one would operate an electrodialysis stack at a current density substantially below the measured limiting value.

MEMBRANE FOULING

When the feed solutions to ED stacks are clean and are relatively free of sparingly soluble materials, ED stacks can be operated for years with little concern about membrane fouling. However, most feedwaters have constituents that can cause problems for ED stacks. Such problems are usually handled by reducing current densities, periodic current reversal (the EDR process), or pretreatment of the feedwater.

Figure 8.18 illustrates some of the fouling problems. Large organic molecules with ionizable groups (e.g., humic acids from decomposing vegetation) are troublesome foulants for ED membranes. Their negative charges allow them to migrate in the electric field but their large size prevents their passage through the membrane. Consequently, these charged molecules tend to accumulate on the dilute side of anion exchange membranes and result in a buildup of membrane resistance. Colloidal particles, which are also usually negatively charged, cause similar problems.

Sparingly soluble salts such as $CaSO_4$ and $CaCO_3$ can precipitate on the concentrate side of the membrane, because their concentrations are highest there due to concentration polarization. $CaCO_3$ precipitation occurs when the limiting current density is exceeded. The reaction of HCO_3^- ions with OH^- ions generated by water splitting forms $CO_3^=$ ions that pass through the anion exchange membrane and precipitate in the boundary where the concentration of Ca^{++} ions is the highest.

Problems of membrane fouling are generally less severe when current densities are kept low to minimize concentration polarization. $CaSO_4$ precipitation is countered by limiting the concentration in the enriching stream below the saturation level, and by addition of sodium hexametaphosphate to delay crystal formation. $CaCO_3$ precipitation can be prevented by acidification of the enriching-steam feed. Fouling of membranes by organic anions and colloidal material

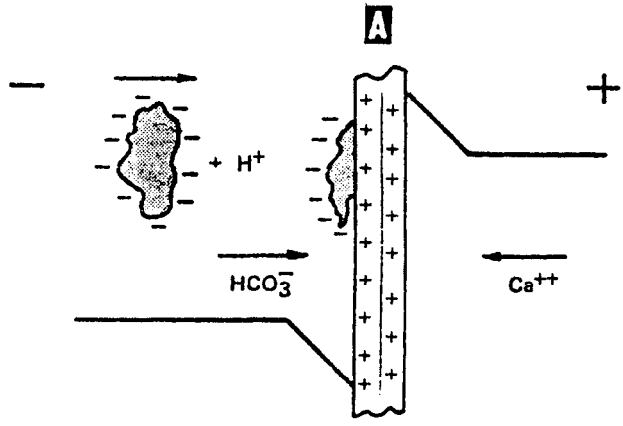


Figure 8.18: Large organic ions and pH-sensitive salts can foul anion-exchange membranes.

is best handled by pretreatment to eliminate the offending material. Alternatively, these membrane-fouling problems can be alleviated to some extent by use of the EDR process.

EDR is the electrodialysis reversal process developed by Ionics, Inc.[23] The EDR process employs reversible electrodes and automatic valves to swap the flows of enriching and depleting product lines. The reversal is programmed to take place about three times per hour. This frequent reversal tends to dislodge the organic and particulate foulants from the membrane surfaces. Moreover, since current reversal causes concentrating boundary layers to become depleting boundary layers, freshly formed precipitates tend to dissolve. Immediately after the current reversal the product water is of poor quality due to the discharge of the aforementioned foulants. Therefore, there is a period of a few minutes when the product water must be diverted to waste. This loss of feedwater along with the high costs associated with the automatic switching valves are the major drawbacks to EDR. The proponents of EDR[23] claim that these disadvantages are more than offset by increased membrane life, reduced chemical costs, higher operating currents, and less maintenance than with conventional ED. Supersaturation of $CaSO_4$ up to 220% in the brine stream was tolerated by EDR. The supersaturation was pushed to 440% with the addition of acid and sodium hexametaphosphate.

Although polarity reversal has been lauded as a major breakthrough by Ionics, Inc., it has not been adopted by other suppliers of ED equipment. This avoidance of polarity reversal does not appear to be due to strong EDR patents, but rather to a general impression that removing foulants by pretreatment is more cost effective than attempts to moderate their damage to the membranes.[15] In fact, the extent of pretreatment in EDR plants would likely make the water acceptable for conventional ED.[24]

COST OF ED

The costs of constructing and operating an ED system are dictated by the quality of the water to be treated and the degree of desalting that must be achieved.[25] There are economies of scale-up in all of the costs except energy and chemicals. The costs are generally divided into capital, fixed operating, and variable operating categories. Capital cost include the site, building, stacks, tanks,, piping, pumps, power supplies, and pretreatment equipment. Capital costs are usually above $1/gpd capacity except for very large plants. These costs can be amortized over the expected life of the system and expressed in terms of product output, e.g., $/kgal. These cost begins at about $1/kgal for large desalting plants for desalting brackish water to drinking water standards, but they can reach several dollars per kgal for small installations. Electrical power consumption varies with the salinity of the feedwater and the applied voltage. Except for seawater where consumption of 28 wh/gal was reported,[5] power costs are usually in the range of $0.50 to $1.00/kgal.

The costs of desalination by ED and RO are very close. ED is generally the less expensive process[26] where the salinity is low, because the current is proportional to the amount of salinity reduction. RO is considered to be less expensive for seawater, but low-resistance membranes and thinner solution compartments could make ED competitive for seawater desalting.

REFERENCES

1. Helfferich, F., *Ion Exchange*, New York: McGraw-Hill (1962).
2. Kneifel, K. and Hattenbach, K., *Desalination* 34: 77-95 (1980).
3. Trivijitkasem, P. and Ostvold, T., Water transport in ion exchange membranes. *Electrochim. Acta* 25: 271 (1980).
4. Zmolek, C.R., *Ind. Water Eng.* Dec: 6-11 (1977).
5. Tani, Y., Energy-saving electrodialyzer for seawater desalination. Tech. Proc. - Annu. Conf. Int. Trade Fair Nat'l. Water Supply Improv. Assoc. 9th. Paper Number 4 (1982).
6. Kawate, H., Seto, T., Komori, R., and Nagasato, Y., *Symp. Salt. Proc.* 5th: 317-24 (1980).
7. Lonergan, D.A., Fennema, O. and Amundson, C.H., *J. Food Sci.* 47: 1429-34 (1982).
8. Jain, S.M., U.S. Patent 4,275,140 (1981).
9. Itoi, S., Nakamura, I. and Kawahara, T., *Desalination* 32: 383-9 (1980).
10. Grenda, D.W., European Patent 0015737 (1980).
11. Ono, T. and Watanabe, M., U.S. Patent 4,204,930 (1980).
12. Liu, K.J., Chlanda, F.P. and Nagasubramanian, K., *J. Membr. Sci.* 3: 57-70 (1978).
13. Gancy, A.B. and Jenczewski, T.J., U.S. Patent 4,238,305 (1980).
14. Chang, V., *J. Appl. Electrochem.* 9: 731-6 (1979).
15. Foster, P.A., Rowe, M.J. and Farrar, J.B. ED: Polarity reversal or not? Paper presented at 46th International Water Conference, Pittsburgh, Pennsylvania (November 1985).

16. Pavlov, D. and Dinev, Z., *J. Electrochem. Soc.* 127 (4): 855-63 (1980).
17. Carr, J.P. and Hampson, N.A., *Chem. Rev.* 72 (6): 679-703 (1972).
18. Tejeda, A.R., U.S. Patent 3,869,364 (1975).
19. Kedem, O., Cohen, J., Warshawsky, A. and Kahana, N., *Desalination* 46: 291-299 (1983).
20. Yamada, M., Matshshita, S., Hirai, H., Tsuyuki, I. and Ogawa, Y., *J. Appl. Photog. Eng.* 7 (2): 53-8 (1981).
21. Davis, T.A. and Lacey, R.E., Forced-flow electrodesalination. OSW R&D Progress Report No. 557 (1970).
22. Rubinstein, I., Warshawski, A., Schechman, W. and Kedem, O., *Desalination* 51: 55-60 (1984).
23. Katz, W.E., *Proc. Int. Water Conf. Eng. So., West Pa.* 44: 51-62 (1983).
24. Mansouri, M., Electrodialysis reversal units used as predemineralizer in boiler feedwater treatment. Paper presented at 45th International Water Conference, Pittsburgh, Pennsylvania (October 1984).
25. Reed, S.A., Desalting seawater and brackish waters: 1981 cost update. ORNL/TM-8191 (1982).
26. Schmoldt, H., Strathmann, H. and Kaschemekat, J., *Desalination* 38: 567-82 (1981).

9

Coupled Transport Membranes

Richard Baker and Ingo Blume

INTRODUCTION

Coupled transport is a membrane process for concentrating ions and separating ions from aqueous solutions. The membrane used in this process consists of a water-insoluble liquid containing an ion-complexing agent that is specific for the ion of interest. The desired ion is complexed at one interface of the membrane, forming a neutral-ion complex. The neutral ion-complex then diffuses across the membrane to the opposite interface, where the reaction is reversed by making appropriate changes in the external solution conditions. The reformed complexing agent then diffuses back across the membrane, where it picks up more of the desired ion. Thus, the complexing agent acts as a shuttle to carry ions across the membrane.

The coupled transport process is illustrated in Figure 9.1 for Cu^{2+} and H^+ ions and a complexing agent denoted by RH. The water-immiscible agent fills the pores of a microporous membrane, thus forming a liquid organic membrane. The equilibrium that exists at the two membrane-solution interfaces is:

$$2RH + Cu^{2+} \rightleftharpoons CuR_2 + 2H^+ \qquad (1)$$

At the feed solution interface (i.e., the left interface in Figure 9.1) , the copper ion reacts with agent, liberating two hydrogen ions. The neutral copper complex CuR_2 is soluble only in the organic phase, and it diffuses across the membrane to the product solution interface, which is maintained at a lower pH. There, the reaction is reversed, liberating the copper ion and consuming two hydrogen ions. This step reforms the neutral complexing agent, which then diffuses back across the membrane. Thus, copper ions move from left to right, and the movement of hydrogen ions in the opposite direction maintains electrical neutrality. It is this coupling between the flow of one species (Cu^{2+}) and the other (H^+) that gives coupled transport its name.

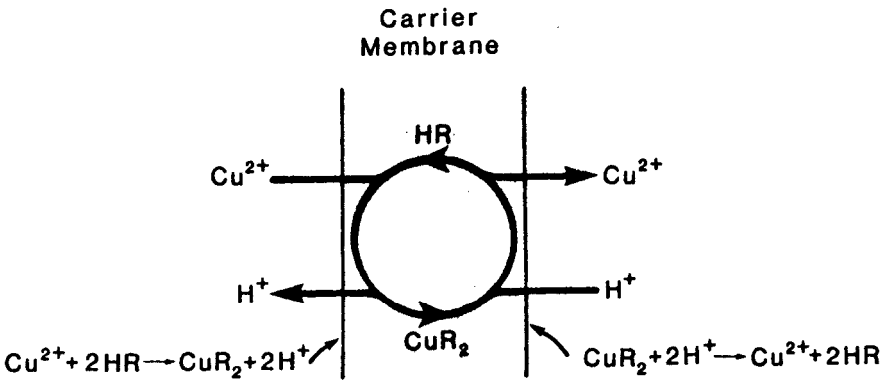


Figure 9.1: Coupled transport scheme for copper.

Proper selection of complexing agent and conditions makes clean separations of metal ions possible. Further, ions of interest can be concentrated against their concentration gradients. Coupled transport membranes can thus be considered as chemical pumps. The energy for the pumping action derives from the flow of one species (hydrogen ion in the example shown here) down its concentration gradient.

Coupled transport is not limited to cations. Anions such as $Cr_2O_7^{2-}$ can be transported by a completely analogous processes using, for example, tertiary amine complexing agents.

HISTORY AND BACKGROUND

The historical development of coupled transport is shown schematically in Figure 9.2.[1] This process originated in early experiments of biologists using natural carriers contained in cell walls. As early as 1890, Pfeffer postulated transport properties in membranes using carriers.[2] Perhaps the first coupled transport experiment was performed by Osterhout, who studied the transport of ammonia across algae cell walls.[3] By the 1950's, the carrier concept was well developed, and workers began to develop synthetic biomembranes analogues of the natural systems. For example, in the mid-1960's, Sollner and Shean[4-6] studied a number of coupled transport systems using inverted U-tubes, shown in Figure 9.3. At the same time, Bloch and Vofsi published the first of several papers in which coupled transport was applied to hydrometallurgical separations, namely the separation of uranium using phosphate esters.[7-10] Because phosphate esters were also plasticizers for polyvinyl chloride (PVC), Bloch and Vofsi prepared immobilized liquid films by dissolving the esters in a PVC matrix. Typically, the PVC/ester film was cast on a paper support. Researchers actively pursued this work until the late 1960's. At that time, interest in this approach lagged, apparently because the fluxes obtained did not make the process competitive with conventional separation processes. Some workers are continuing to apply these membranes to metal separations,[11,12] but most current interest in PVC matrix membranes is in their use in ion selective membrane electrodes.[13]

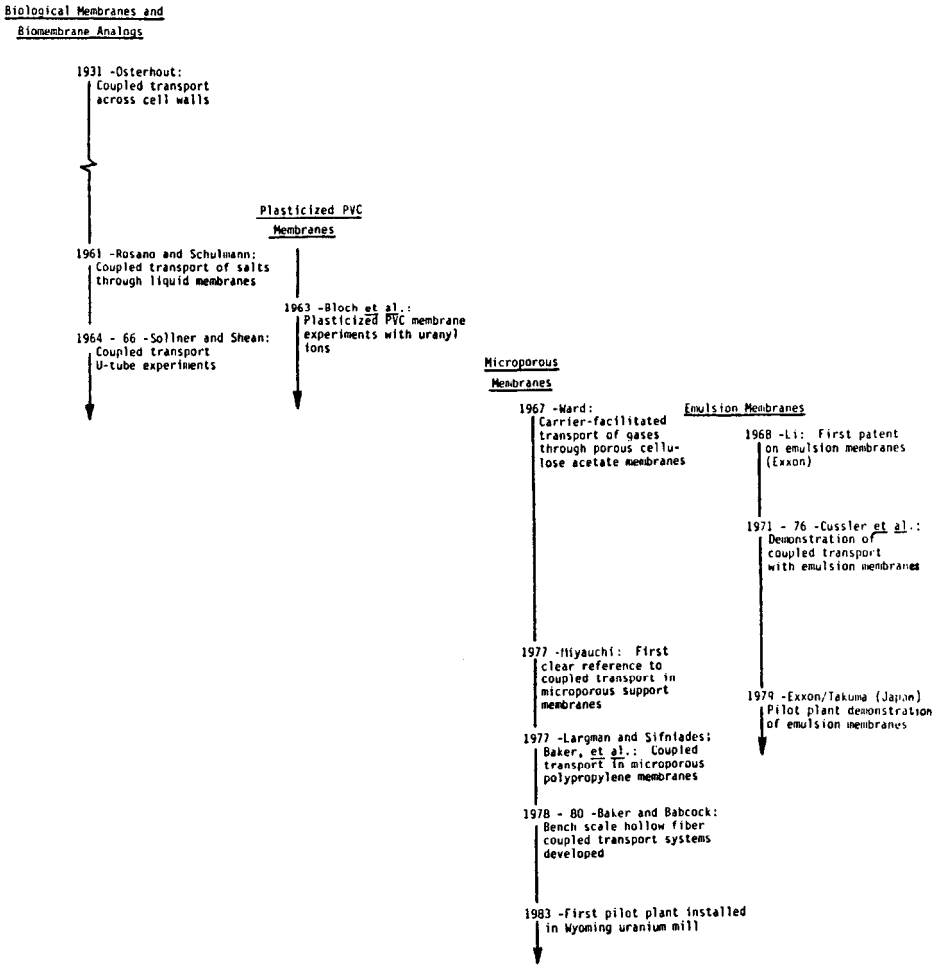


Figure 9.2: Historical development of coupled transport membranes.

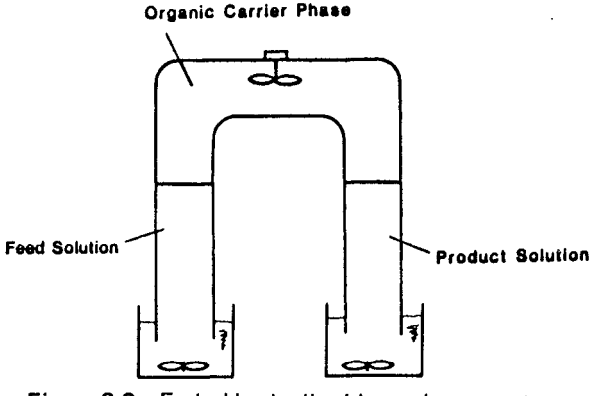


Figure 9.3: Early U-tube liquid membrane system.

Following the work of Bloch and Vofsi, two other methods of producing immobilized liquid films were introduced. Both are still under development. In the first approach, the liquid carrier phase is held by capillarity within the pores of a microporous substrate, as shown in Figure 9.4. This approach was first used by Miyauchi[14] and further developed by Baker et al[15–17] and by Largman and Sifniades.[18] The principal objective of this early work was the recovery of copper and other metals from hydrometallurgical solutions. Despite considerable effort on the laboratory scale, the first pilot plant was not installed until 1980.[19–20] The principal problem is instability of the liquid carrier phase in the microporous membrane support.

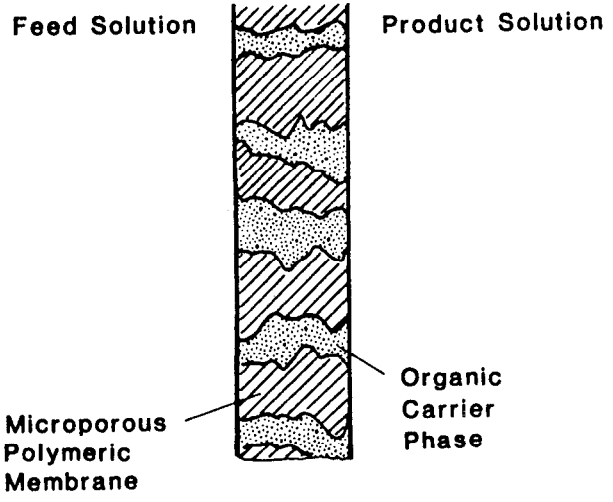


Figure 9.4: Supported liquid membrane.

The second type of immobilized liquid carrier is the emulsion or "bubble" membrane. In this technique, a surfactant-stabilized emulsion is produced as shown in Figure 9.5. The organic carrier phase forms the wall of the emulsion droplet separating the aqueous feed from the aqueous product solutions. Metal ions are concentrated in the interior of the droplets. When sufficient metal has been extracted, emulsion droplets are separated from the feed and the emulsion is broken, liberating a concentrated product solution and an organic carrier phase. The carrier phase is decanted from the product solution and recycled to make more emulsion droplets. The principal technical problem is the stability of the liquid membrane. Ideally, the emulsion membranes must be completely stable during the extraction step, to prevent the two aqueous phases mixing, but must be completely broken and easily separated in the stripping step. Achieving this level of control over emulsion stability has proved difficult.

The technique of emulsion membranes was popularized and fully developed by Li and his coworkers at Exxon.[21–29] Starting in the late 1950's and continuing for more than twenty years, the Exxon group's work led to the installation of the first pilot plant in 1979.[29] Although the process is still not commercial, a number of pilot plants have been installed, principally on hydrometallurgical

feed streams. Another important group working independently on the problem at about the same time was Cussler, Evans and others at Carnegie Mellon.[30–34] More recent workers in the field include Halwachs and Schuger[35–38] in West Germany, Marr and Kapp in Austria,[39,40] Stelmaszek et al in Poland,[41,42] Martin and Davis[43] in the United Kingdom, and Danesi et al,[44,45] Noble et al,[46,47] and Lamb, Christensen and Izatt[48–51] in the United States.

A number of reviews on various aspects of liquid membranes and coupled transport processes have also appeared.[52–55]

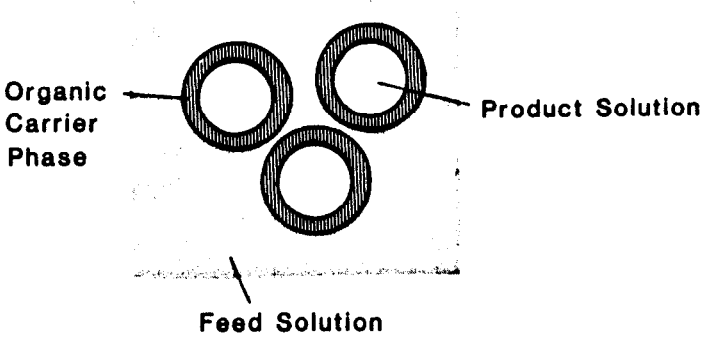


Figure 9.5: Surfactant stabilized emulsion membrane.

COUNTER TRANSPORT AND CO-TRANSPORT

Coupled transport processes can be divided into two categories, depending on the type of reaction occurring between complexing agent and permeant. The first type is called counter transport (shown in Figure 9.6). The key feature of counter transport is that the fluxes of the two permeating ions move counter to each other across the membrane. The reaction in this case is:

$$2RH + Cu^{2+} \rightleftharpoons CuR_2 + 2H^+ \qquad (2)$$

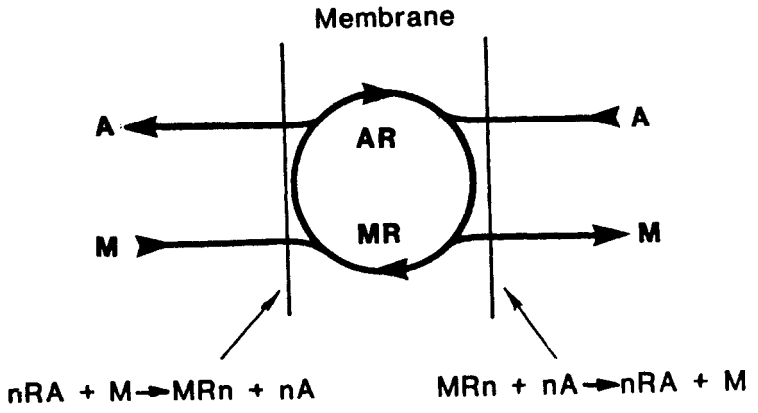
More generally, the reaction can be written

$$nRA + M \rightleftharpoons MRn + nA \qquad (3)$$

In the reaction for the transport of copper, M is Cu^{2+} and A is H^+. Equation 3 does not have to be limited to cation transport. For example, consider the transport of uranyl ions by the tertiary amine salt $(R_3NH)_2SO_4$,

$$(R_3NH)_2SO_4 + UO_2(SO_4)^{2-} \rightleftharpoons (R_3NH)_2UO_2(SO_4)_2 + SO_4^{2-} \qquad (4)$$

In this case, M is $UO_2(SO_4)^{2-}$ and A is SO_4^{2-}.



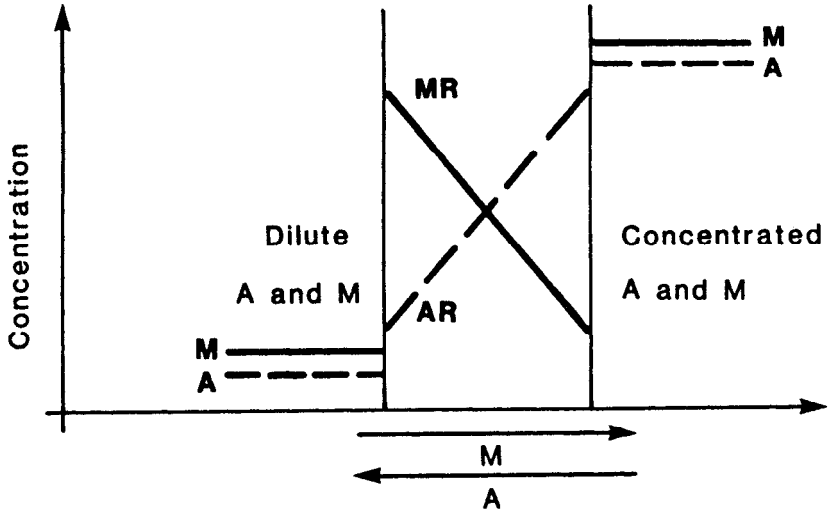


Figure 9.6: Counter-coupled transport.

The second type of coupled transport is co-transport, illustrated in Figure 9.7. The key feature of co-transport is that the fluxes of the two permeating ions move in the same direction across the membrane. The general form of the reaction in this case is:

$$A + M + R \rightleftharpoons RAM \qquad (5)$$

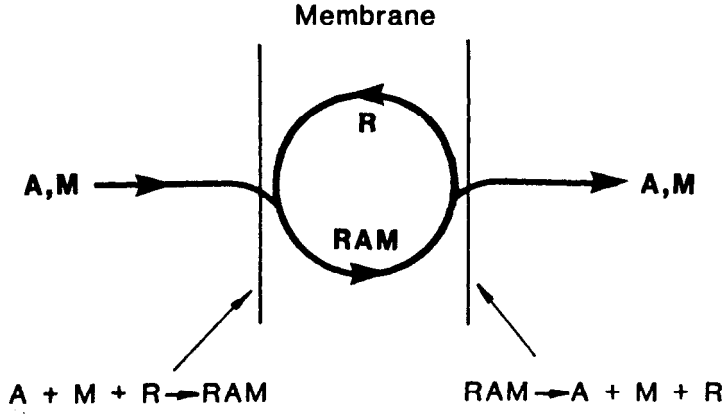
A typical example of this type of process might be the transport of uranyl ions by tertiary amine complexing agents via the reaction:

$$4R_3N + 4H^+ + UO_2(SO_4)_3^{4-} \rightleftharpoons (R_3NH)_4\ UO_2(SO_4)_3 \qquad (6)$$

In this example, M is $UO_2(SO_4)_3^{4-}$ and A is $4H^+$. Another example of co-transport is the transport of alkali metals by crown ethers by reactions of the type:

$$Cl^- + Na^+ + Crown \rightleftharpoons Crown\ (NaCl) \qquad (7)$$

where Crown is a cyclic ether.[50]



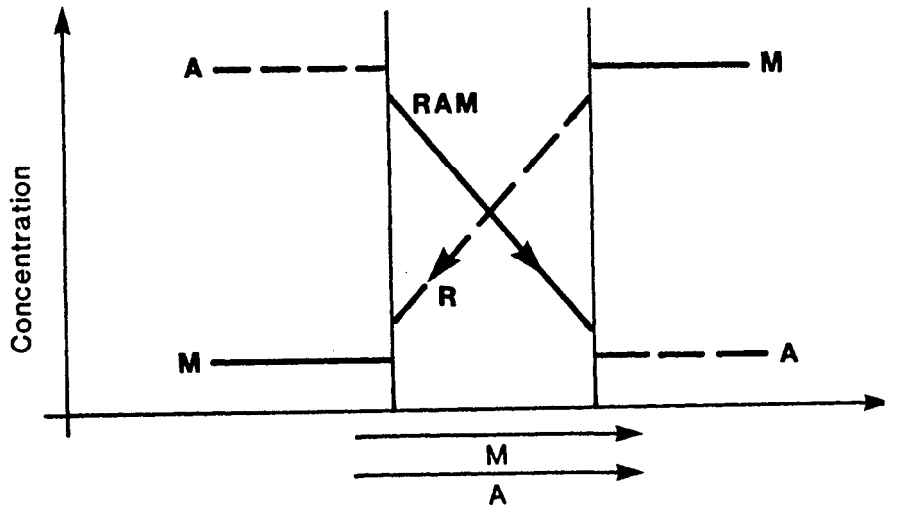


Figure 9.7: Co-coupled transport.

THEORY

Several authors have attempted to provide a general theory of coupled transport and the closely related process of facilitated transport, including Smith

et al,[56] Schultz et al[57-59] Cussler[55] and Danesi.[44,45] The usual approach is to assume an equilibrium between the various reacting species in the membrane phase and link these concentrations by the appropriate equilibrium constants. A diffusion model using Fick's law experiments is then set up for each species and these expressions are integrated between the boundary values defined by the membrane distribution coefficients and the permeant concentrations in the surrounding aqueous solutions. The result is an expression for the permeant flux that includes terms for permeants diffusion coefficients, equilibrium constants, and distribution coefficients. These expressions are complex and of little practical value.

A simpler approach others have followed[15,16,60] is to ignore the effect of minor species in the membrane and aqueous phases. For example, consider the counter transport reaction:

$$2RH + Cu^{2+} \rightleftharpoons CuR_2 + 2H^+ \quad .$$

In principal, all four species are in equilibrium in the aqueous solution and in the organic membrane phase, but in practice CuR_2 and RH are confined to the organic membrane phase and Cu^{2+} and $2H^+$ are confined to the aqueous phase. Equilibrium between the reactants exists only at the membrane interface. We therefore assume that concentrations of the permeants at each interface to be defined by an appropriate equilibrium constant and then substitute these values in a simple Fick's law expression.

Consider the general case of a permeant M of valence n reacting with carrier RA to form the complex MR_n inside the liquid membrane:

$$nRA + M \rightleftharpoons MR_n + nA \quad . \tag{8}$$

This reaction is characterized by an equilibrium constant:

$$K = \frac{[MR_n]\,[A]^n}{[RA]^n\,[M]} \tag{9}$$

This equilibrium constant could be written for either the organic phase or the aqueous phase. However, only $[MR_n]$ and [RA] are measurable in the organic phase, where [A] and [M] are negligibly small. Similarly, only [A] and [M] are measurable in the aqueous phase, where $[MR_n]$ and [RA] are negligibly small. We can, therefore, write Equation 9 as:

$$K' = \frac{[MR_n]'\,[A]''^n}{[RA]'^n\,[M]''} = \frac{k_m}{k_a} \cdot K, \tag{10}$$

where the superscript ' refers to the organic phase, superscript '' refers to the aqueous phase, and k_m and k_a are the partition coefficients of M and A between the aqueous and organic phases. We prefer this formulation of Equation 10 because all the quantities are easily accessible experimentally. For example, $[MR_n]'/[M]''$ is easily recognizable as the distribution coefficient of metal between the organic and aqueous phases.

The same equilibrium constant must apply at both membrane-solution interfaces, and we can recast Equation 10 into the following form:

$$K' = \frac{[MR_n]'_o\,[A]''^n_o}{[RA]'^n_o\,[M]''_o} = \frac{[MR_n]'_\ell\,[A]''^n_\ell}{[RA]'^n_\ell\,[M]''_\ell} \qquad (11)$$

where o and ℓ refer to the two sides of the membrane.

Consider now the situation where a counter ion concentration gradient is established that exactly balances the metal ion concentration gradient, so there is no flux of either ion across the membrane. Under this condition, $[MR_n]'_o = [MR_n]'_\ell$ and $[RA]'^n_o = [RA]'^n_\ell$, and we obtain the expression:

$$\frac{[M]''_o}{[M]''_\ell} = \left(\frac{[A]''_o}{[A]''_\ell}\right)^n \qquad (12)$$

Thus, the maximum concentration factor of metal ion that can be established across the membrane varies with the counter ion concentration ratio (in the same direction) raised to the nth power.

This development, of course, demonstrates nothing about the metal ion flux across the membrane under non-equilibrium situations. For this, we turn to Fick's law. At steady state, the flux J_{MR_n}, in mol/cm^2-sec, of metal complex MR_n across the liquid membrane is given by:

$$J_{MR_n} = \frac{\bar{D}_{MR_n}\,([MR_n]'_o - [MR_n]'_\ell)}{\ell} \qquad (13)$$

where $\bar{D}_{MR_n}$ is the mean diffusion coefficient of the complex in the membrane of thickness ℓ. In principal, J_{MR_n} can be measured experimentally in a permeation experiment, and the values of $[MR_n]$ can be determined in equilibrium distribution coefficient measurements. Thus, $\bar{D}_{MR_n}$ can be measured as a function of concentration, pH, and other conditions. However, this approach demonstrates nothing about coupling.

To illustrate coupling effects, we begin with Equation 13 and eliminate the terms in $[MR_n]$ by introducing Equation 10. This results in a complex expression involving the desired quantities [M] and [A], but also involving [RA]. However, from mass balance considerations, we have the following relationship:

$$n[MR_n] + [RA] = \gamma \,, \qquad (14)$$

where γ is the molar density of pure RA. We have made the reasonable assumption here that there is no volume change in the interconversion of n mols of RA to n mols of MR_n.

We can now substitute Equations 10 and 11 into 13 to arrive at an expression for the metal ion flux in terms only of constants and the concentrations of metal and counter ion in the aqueous solutions on the two sides of the membrane. The solution is simple only when n = 1, in which case:

$$J_{MR_n} = \frac{\bar{D}_{MR_n}\gamma}{\ell}\left[\left(\frac{1}{[A]''/[M]''K'+1}\right)_o - \left(\frac{1}{[A]''/[M]''K'+1}\right)_\ell\right] \qquad (15)$$

This shows the coupling effect. Thus, there will be a positive "uphill" flux of

metal ion from the downstream to the upstream solution (i.e., in the direction from ℓ to o) as long as:

$$\left(\frac{[M]''}{[A]''}\right)_o > \left(\frac{[M]''}{[A]''}\right)_\ell \tag{16}$$

When the inequality is of the opposite sense, the metal ion flux is in the conventional or "downhill" direction. It is also possible to determine the maximum concentration factor, i.e., the point at which metal ion flux ceases, in terms of the hydrogen ion concentration in the two aqueous phases:

$$\frac{[M]''_o}{[M]''_\ell} = \frac{[A]''_o}{[A]''_\ell} \tag{17}$$

This is, of course, identical to Equation 12 for the case of a monovalent metal ion.

It can be easily shown that for co-transport governed by the general equation:

$$A + M + R \rightleftharpoons RAM$$

The equivalent expressions to Equations 15 and 16 are:

$$J_{RAM} = \frac{\bar{D}_{RAM\gamma}}{\ell}\left[\left(\frac{1}{1/K'[A]''[M] + 1}\right)_o - \left(\frac{1}{1/K'[A]''[M]'' + 1}\right)_\ell\right] \tag{18}$$

and

$$\frac{[M]''_o}{[M]''_\ell} = \frac{[A]''_\ell}{[A]''_o} \tag{19}$$

where K' is the equilibrium constant defined as:

$$K' = \frac{[RAM]'}{[R]'[A]''[M]''} \tag{20}$$

Thus, in co-transport the gradient in A and M are in the same direction.

CHARACTERISTICS OF COUPLED TRANSPORT MEMBRANES

In this section, we will discuss the major characteristics of coupled transport systems. The discussion will be illustrated with results obtained with supported liquid membranes. However, the same principles apply to emulsion membranes. We use supported liquid membrane results because the geometry of supported membranes is well-defined and it is possible to maintain the conditions of the feed and product solutions constant. This allows parametric studies to be per-

formed and interpreted easily. The thickness and area of emulsion membranes are much more difficult to define, and the composition of the feed and product solutions changes continuously. This makes the theoretical interpretation of results obtained with emulsion membranes difficult to rationalize.

Experiments described in this section generally utilize LIX 64N® (Henkel Corp.), LIX 54® (Henkel Corp.), and Kelex 100® (Sherex Chemical Co.) oximes, used in the counter transport of copper and other metal cations by the mechanism shown in Figure 9.6, or Alamine 336® (Henkel Corp.), a tertiary amine used in the co-transport of anions by the mechanism shown in Figure 9.7. These reagents are described in more detail in a later section of this chapter.

Concentration Effects

Equations 8 through 20 provide a basis for rationalizing the principal features of coupled transport membranes. Thus, it follows from Equations 15 and 18 that coupled transport membranes are able to move metal ions from a dilute to a concentrated solution against the metal ion concentration gradient provided there is a sufficient gradient in the second coupled ion. A typical experimental result demonstrating this unique feature of coupled transport is shown in Figure 9.8. The reaction is counter transport of copper driven by hydrogen ion, as described in Equation 1. In this particular experiment, a pH difference of 1.5 units is maintained across the membrane. The initial product solution copper concentration is higher than the feed solution concentration. Nonetheless, copper diffuses against its concentration gradient from the feed to the product side of the membrane. The ratio of the counter hydrogen ions between the solutions on either side of the membrane is about 32 to 1 which, according to the appropriate form of Equation 12, should give a copper concentration ratio:

$$\frac{[Cu^{2+}]''_\ell}{[Cu^{2+}]''_o} = \left(\frac{[H^+]''_\ell}{[H^+]''_o}\right)^2 = (32)^2 \simeq 1000 \qquad (21)$$

In the experiment shown in Figure 9.8, this means the feed solution copper concentration should drop to just a few ppm, and this is the case.

A more convenient method of measuring the copper concentration factor is to maintain the product solution at some high copper concentration factor and allow the feed solution copper concentration to reach a steady state value. Figure 9.9 shows the feed copper concentration in this type of experiment. In this example, the product solution was maintained at 9.3% and 3.0% copper and the feed solution was allowed to approach the steady state from both directions, i.e., with an initial copper concentration higher and lower than the predicted value for the given pH gradient. As Figure 9.9 shows, regardless of the starting conditions, the final steady state feed copper concentration was the same. In fact, the copper concentration factors measured this way are in reasonable agreement with the predictions of Equation 21 which can be restated in another form as:

$$\log\left(\frac{[Cu^{2+}]''_o}{[Cu^{2+}]''_\ell}\right) = \log\left(\frac{[H^+]''_o}{[H^+]''_\ell}\right)^2 = 2(pH''_\ell - pH''_o) = 2\Delta pH \qquad (22)$$

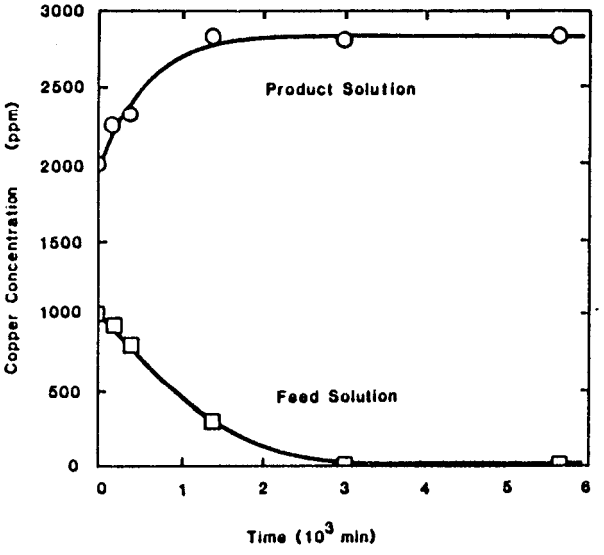


Figure 9.8: Demonstration of coupled transport. In a two-compartment cell, copper flows from the dilute (feed) solution into the concentrated (product) solution, driven by a gradient in hydrogen ion concentration.[20] (Membrane: Microporous Celgard 2400/LIX 64N. Feed: pH 2.5. Product: pH 1.0).

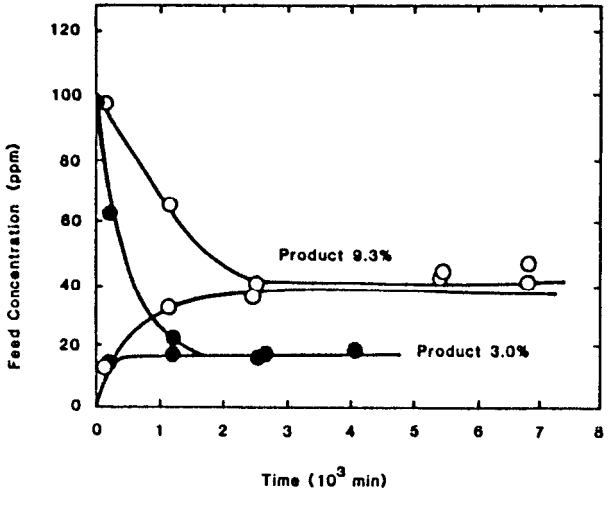


Figure 9.9: Experiments to demonstrate the maximum achievable concentration factor.[61] (Membrane: Microporous Celgard 2400/LIX 64N. Feed: pH 2.5, 0 or 100 ppm copper. Product: pH 1.0, 3.0% or 9.3% copper).

Concentration factors were measured as a function of the pH difference. In one set of experiments, the downstream pH was maintained at 1.0 throughout, while the feed pH was varied from 1.5 to 3.0. In a second set of experiments, the feed pH was maintained at 2.5 while the downstream pH was varied from 0.5 to 2.0. The experimental results are plotted in Figure 9.10 along with the theoretical line obtained from Equation 22. While there is some scatter, the agreement between theory and experiment is generally good.

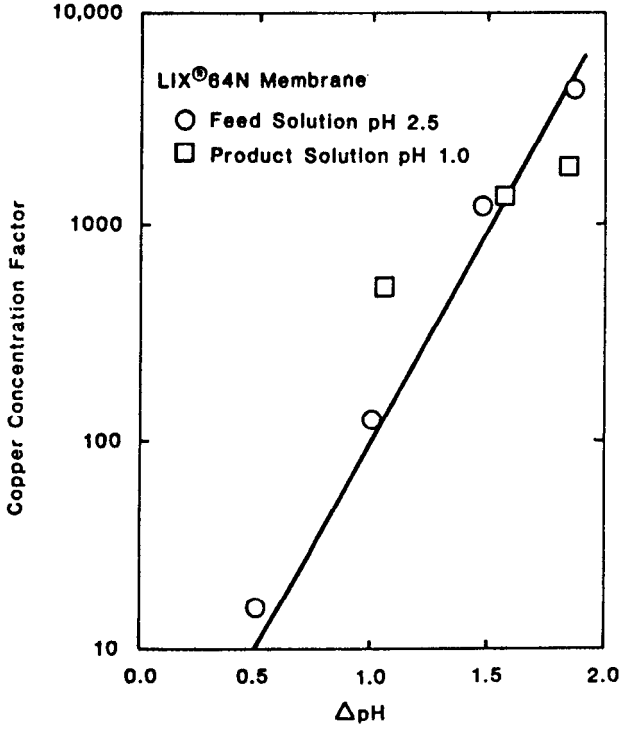


Figure 9.10: Maximum concentration factor vs pH difference across the membrane. The line is calculated from Eq. 27.[15] (Membrane: Microporous Celgard 2400/LIX 64N. Feed: 100 ppm copper. Product: 0.5 to 9 wt % copper).

Feed and Product Metal Ion Concentration Effects

A second characteristic of coupled transport membranes is that the membrane flux usually increases with increasing metal concentration in the feed solution but is usually independent of the metal concentration in the product solution. This behavior follows from the flux Equations 13 and 15. In typical coupled transport experiments, the concentration of the driving ion A in the product solution is very high. For example, in coupled transport of copper, the driving ions are hydrogen ions and 100 g/ℓ sulfuric acid is used as the product solution. As a result, the term $[MR_n]\frac{l}{\ell}$ is very small compared to $[MR_n]_o$ and Equation 15 reduces to:

$$J_{MR_n} = \frac{\bar{D}_{MR_n\gamma}}{\ell} \quad \frac{1}{[A]''_o/[M]''_o K' + 1} \qquad (23)$$

The key feature of Equation 23 is that the term $[M]''_\ell$ does not appear in the flux equation. Thus, the flux is independent of the concentration of metal on the product side of the membrane. However, the flux does depend on the concentration of metal on the feed solution side of the membrane $[M]''_o$. At low values of $[M]''_o$, the flux will increase linearly with $[M]''_o$, but at higher concentrations the flux reaches a plateau value as the term $[A]''_o/[M]''_o K'$ becomes small compared to 1. The form of this dependence is illustrated for the feed and product solution metal ion concentration in Figure 9.11.

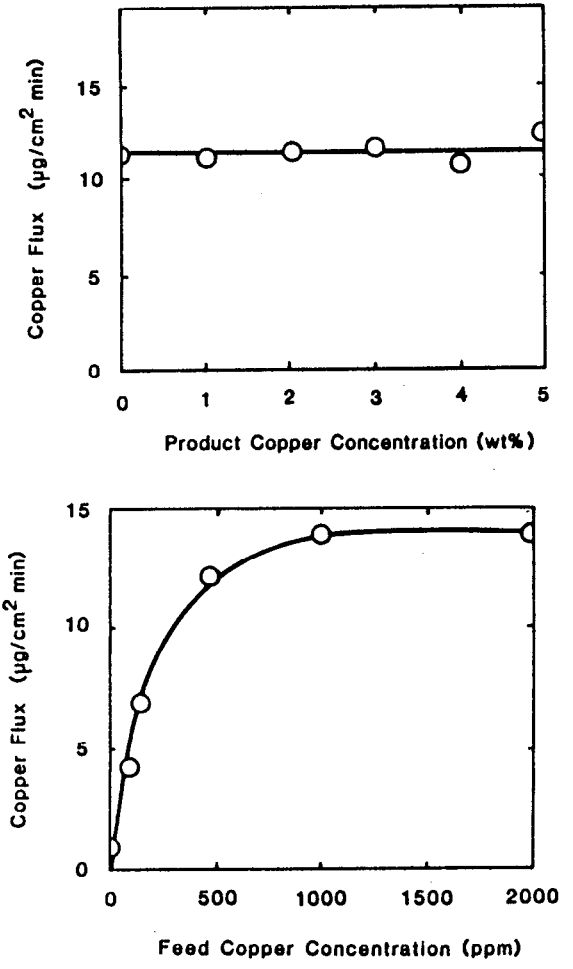


Figure 9.11: Effect of metal concentration in the feed and product solution on flux.[20] (Membrane: Microporous Celgard 2400/30% Kelex 100 in Kermac 470B. Feed: pH 2.5. Product: 100 g/ℓ H_2SO_4).

pH and Metal Ion Effects

It follows from flux Equation 23 that the concentration of the counter hydrogen ion and the equilibrium coefficient K' for a particular metal ion will affect the metal ion flux. The effect of these factors can best be understood by looking at the metal ion extraction curves vs counter ion concentration. These are shown in Figures 9.12 and 9.13 for copper and other metals with a number of liquid ion exchange reagents. The counter ion is hydrogen, and these reagents extract metal ions via reactions of the type shown in Equation 1.

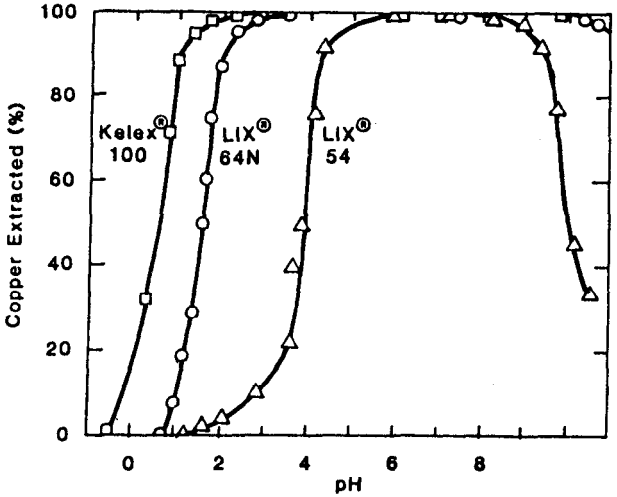


Figure 9.12: Copper extraction vs pH by various complexing agents.

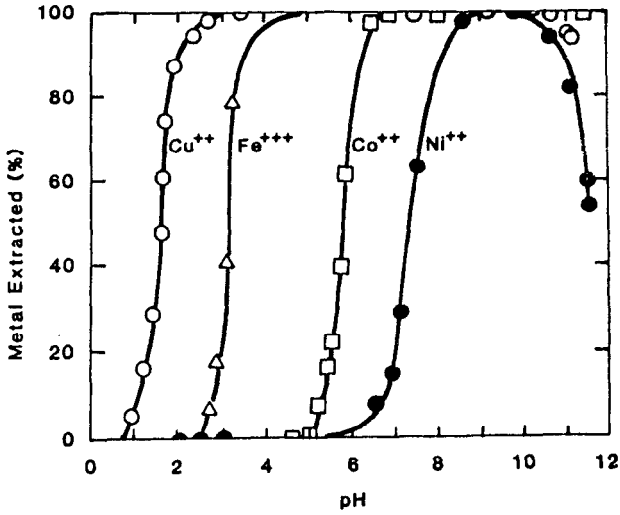


Figure 9.13: Metal extraction curves for four metal ions by LIX 64N. The aqueous phase initially contained 1,000 ppm metal as the sulfate salt.

Consider the copper extraction curves shown in Figure 9.12. These results were obtained by extracting 0.2% copper solutions buffered to the appropriate pH with an equal volume of organic complexing reagent. The percentage of the copper concentrated into the organic phase was then measured. The extraction curves for different reagents have the same form, but the pH extraction isotherms shift depending on the distribution coefficient for the particular agent. At low pH, copper is not extracted because the term $[H^+]^{n/2}/[Cu^{2+}]^n$ in Equation 10 is large and thus the term $[CuR_2]^l/[RH]^{l/2}$ is small. As the pH increases, the term $[H^+]^{n/2}/[Cu^{2+}]^n$ decreases and thus $[CuR_2]^l/[RH]^{l/2}$ increases, producing an increase in copper metal extracted. At very high pH levels, a decrease in copper extraction occurs because copper ions in the aqueous solution begin to form non-extracting basic complexes with other anions in the solution.

The pH at which metal ions are extracted also depends on the distribution coefficient for the particular metal and complexing agent. As a result, the pH at which the metal ions are extracted varies, as shown by the results in Figure 9.13. This behavior allows one metal to be separated from another.

The metal extraction curves described above mirror the behavior of these complexing agents when incorporated into coupled transport membranes. Thus, when the product solution pH is maintained at a very low level, the term $[MR_n]_\ell^l$ in Equation 13 is reduced to zero and the flux is determined by the concentration of complexed metal in equilibrium with the feed solution $[MR_n]_o^l$. As a result, the flux vs pH behavior follows the metal extraction curves. This is shown in Figure 9.14, which shows the flux pH (curves) for copper with each of the three complexing agents whose extraction curves are shown in Figure 9.12. The magnitude of the coupled transport flux depends on the liquid viscosity and complexed metal diffusion coefficient, but the pH dependence of the flux is very similar to the metal ion extraction curves.

The ability of the complexing agents used in coupled transport to complex metals at different pH levels also allows good separation to be obtained. For example, consider the separation of copper and iron with LIX 64N. As Figure 9.13 shows, LIX 64N extracts copper at pH 1.5 to 2.0, while iron is not extracted until above pH 2.5. The separations obtained when 0.2% solutions of copper and iron are tested with a LIX 64N membrane at various pH's are shown in Figure 9.15. The copper flux exceeds the iron flux by approximately 100-fold at a feed pH of 2.5. The copper and iron fluxes through the membrane are not completely independent, as the results in Figure 9.16 show. Thus, a 1.0% iron feed solution in the absence of copper has a flux of 0.15 $\mu g/cm^2$ min, but this flux drops to 0.02 $\mu g/cm^2$ min when 0.2% copper is added and is restored to the original value when the copper is removed. The phenomenon is known as "crowding", a term taken from the solvent extraction literature. Copper reacts preferentially with the complexing agent, reducing the amount of reagent free to extract iron and hence the iron flux. The phenomenon is fairly common and is important in the separation of uranium from vanadium.

Complexing Agent Effects

Complexing agents used in coupled transport membranes are usually diluted with a carrier solvent, typically a mixed aliphatic-aromatic hydrocarbon. We would generally expect the amount of metal extracted by the complexing agent solution to increase with increasing agent concentration, and this is usually the

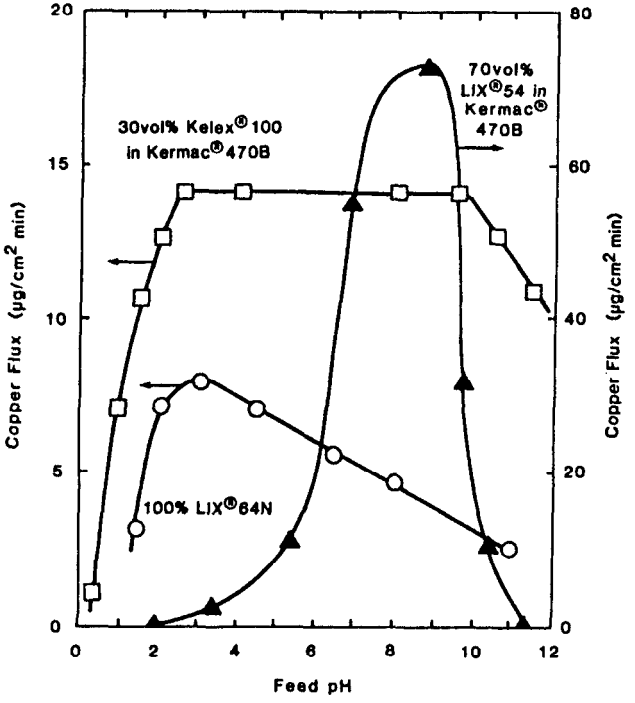


Figure 9.14: Effect of pH on copper coupled transport flux for three different complexing agents.[20] (Membrane: Celgard 2400. Feed: 0.2% copper. Product: 100 g/ℓ H_2SO_4).

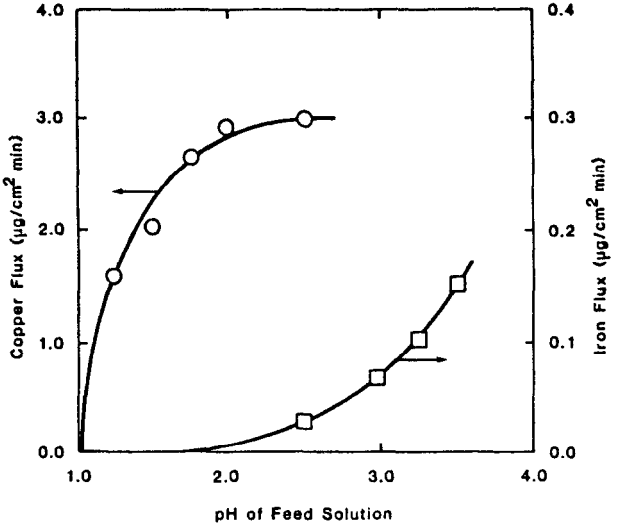


Figure 9.15: Copper and iron fluxes vs feed pH.[15] (Membrane: Celgard 2400/LIX 64N. Feed: 0.2% metal. Product: pH 1.0).

case. For example, the results in Figure 9.17 show the extraction of uranium by a tertiary amine following the reaction shown in Equation 4. It follows that the coupled transport flux would also increase with increasing carrier concentration.

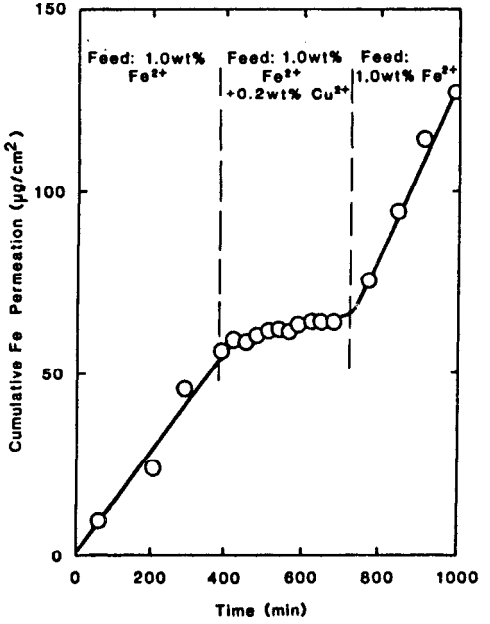


Figure 9.16: The effect of small concentrations of copper in the feed on iron permeation through a coupled transport membrane.[19] (Membrane: Celgard 2400/ LIX 64N. Feed: pH 2.5. Product: pH 1.0).

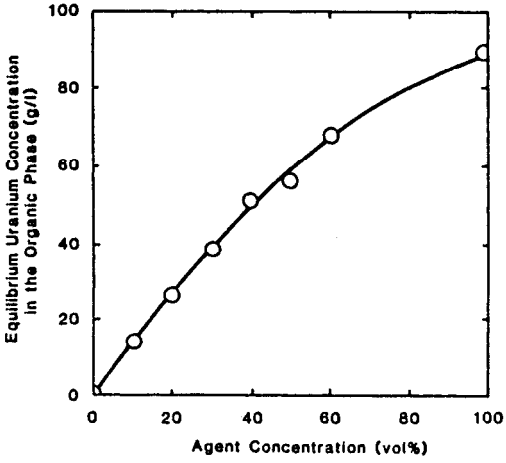


Figure 9.17: The effect of complexing agent concentration in the organic extraction phase on the amount of uranium extracted from an aqueous solution.[17] (Organic Phase: Alamine 336 dissolved in Aromatic 150. Aqueous Phase: 0.2% uranium, pH 1.0).

However, in coupled transport a more complex behavior is observed. Figure 9.18 shows a plot of the uranium flux vs the same amine in a membrane. The flux reaches a maximum value at about 30% amine in the diluent and decreases with increasing concentration thereafter. This appears to be a general phenomenon as, for example, Figure 9.19 illustrates with the flux of copper through various reagent-diluent solutions. The pattern of the results is similar to Figure 9.18.

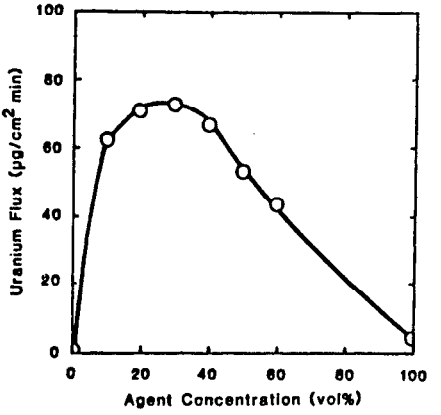


Figure 9.18: The effect of complexing agent concentration on the coupled transport flux of uranium.[17] (Membrane: Celgard 2400/Alamine 336 dissolved in Aromatic 150. Feed: 0.2% uranium, pH 1.0. Product: pH 4.5).

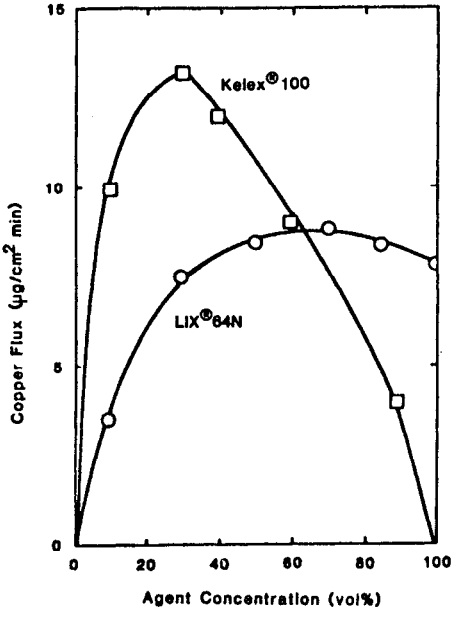


Figure 9.19: The effect of complexing agent concentration on the coupled transport flux of copper.[19,20] (Membrane: Celgard 2400/various agents dissolved in Kermac 470B. Feed: 0.2% copper, pH 2.5. Product: 100 g/ℓ H_2SO_4).

Two competing factors apparently caused this phenomenon: the concentration gradient of the metal complex and the viscosity of the organic phase in the membrane. As the concentration of complexing agents in the membrane is increased, the concentration gradient of the metal complex increases as well. At low agent concentration, this results in an increase in flux. However, the viscosity of the solution also increases with increasing agent concentration, causing the diffusion coefficient of the metal complex to decrease. At some point, the flux increase due to the increasing concentration gradient is no longer sufficient to overcome the flux decrease due to the increasing viscosity. At this agent concentration, the flux reaches its maximum value and subsequently decreases with further increase in agent concentration.

The effect of viscosity on the metal complex diffusion coefficient can be estimated by measuring the viscosity of the organic phase and substituting this value into the appropriate form of the Stokes-Einstein equation:

$$D = kT/6\pi r\eta \qquad (24)$$

where k is the Boltzmann constant, T is the absolute temperature, r is the molecular radius of the metal complex, and π is the viscosity of the organic phase. This calculation has been performed for uranyl ions and the amines used to obtain the results shown in Figure 9.17 and 9.18. To model the organic phase at the feed interface, the viscosity of solutions that had been equilibrated with the feed solution were measured. To model the organic phase at the product solution interface, the viscosity of the uncomplexed amine ions were measured. The results are shown in Figure 9.20. There is a large increase in viscosity with increasing agent concentration, especially when the agent is complexed with uranium.

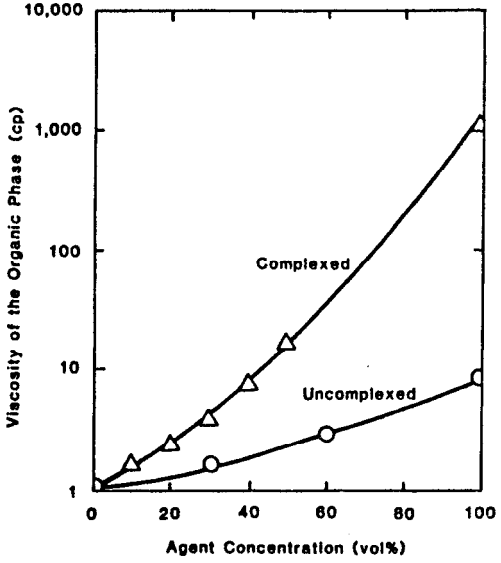


Figure 9.20: The effect of agent concentration in the organic phase on viscosity for solutions containing no uranium (uncomplexed agent) and solutions previously equilibrated with aqueous uranium solution (complexed agent).[17] (Organic phase: Alamine 336 dissolved in Aromatic 150).

Substituting the molecular radius and the viscosity into Equation 24 gives the diffusion coefficient for the uranium complex. Because of the wide range of viscosities, there is a wide range of calculated diffusion coefficients. On the feed side of the membrane, the diffusion coefficient varies from about 4×10^{-6} cm^2/sec for dilute solutions to 6×10^{-9} cm^2/sec for concentrated solutions. For each agent concentration, then, the mean diffusion coefficient is calculated by simply taking the arithmetic mean at the two interfaces. (Use of the arithmetic mean diffusion coefficient is actually justified only when the concentration gradient of a permeant across the membrane is linear. In coupled transport membranes, the concentration gradient would vary as a result of variations in viscosity across the membrane. Calculation of the true mean diffusion coefficient would require knowledge of the concentration profile within the membrane, which is difficult to determine.)

These calculated mean diffusion coefficients are then substituted into Equation 13, together with the measured values of the concentration of uranium complex and the membrane porosity. The calculated flux vs agent concentration is plotted in Figure 9.21. The measured flux is also shown for comparison. It is clear from this figure that the calculated dependence of flux on agent concentration agrees qualitatively with the measured flux dependence. However, the calculated fluxes are as much as five times larger than the experimental values. Various reasons have been suggested for this discrepancy, which is even larger with some other metal complexing agents. Hindered diffusion of the metal complex in the rather small pores of the support membrane is a possibility.

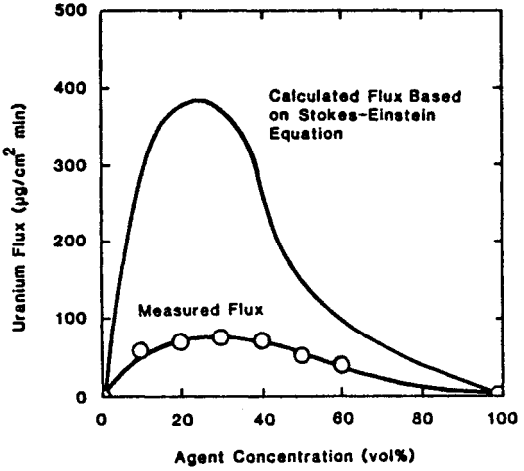


Figure 9.21: The effect of agent concentration on the uranium flux through a coupled transport membrane calculated from Equations 13 and 24. The measured flux data are shown for comparison.[17] (Membrane: Celgard 2400/Alamine 336 dissolved in Aromatic 150. Feed: 0.2% Uranium, pH 1.0. Product: pH 4.5).

Interfacial Reaction Rate Effects

The model for describing coupled transport developed in Equations 8 to 20 contains an implicit assumption that diffusion of the metal agent complex

is the rate-limiting step in metal transport through the liquid membrane. This is not always the case. First, the reactions at the feed and product interfaces of the membrane may be comparable in rate of diffusion through the membrane, resulting in partially reaction-rate-controlled transport. In addition, the rate of diffusion of aqueous reactants to and from the interface through the aqueous boundary layers at the feed and product sides of the membrane may be comparable to the rate of diffusion through the membrane. In this case, the process is partially boundary-layer- or concentration-polarization-controlled.

Figure 9.22A illustrates the purely diffusion-controlled process, in which the effects of boundary layers and interfacial reaction rates are negligible. In this case, the concentrations of the complex at the interfaces are the equilibrium concentrations. Figure 9.22B illustrates the partially boundary-layer-controlled case. Here, prior to steady state, the permeant diffuses across the membrane faster in the feed-side boundary layer and accumulation of permeant in the product-side boundary layer. The consequence of this concentration polarization is a reduction in the net concentration gradient across the membrane, and a reduced flux compared with the diffusion-controlled case. The last case is that of partially reaction-rate-controlled flux, illustrated by the concentration profile in Figure 9.22C. Here, either the permeant initially diffuses away from the feed interface faster than it can be replenished by the interfacial reaction, or the dissociation reaction is not fast enough to prevent accumulation of the complex at the product interface. Again, the net result is a decrease in the concentration gradient compared with that in the purely diffusion-controlled case. In all three cases, the flux is proportional to the slope of the concentration profile across the liquid membrane.

The presence of interfacial reaction effects can be determined by measuring the flux through nominally identical membranes differing only in thickness. With diffusion control, the flux is inversely proportional to the membrane thickness, and thus a plot of flux vs $1/\ell$ is a straight line passing through the origin. This type of plot is shown in Figure 9.23 for coupled transport of copper with three different reagents. The plot is completely linear for LIX 64N, showing complete diffusion rate control. However, the Kelex 100 and LIX 54 curves show some deviations, with thin membranes (high values of $1/\ell$) showing some interfacial effects with these reagents. An extreme example of interfacial reaction rate control is coupled transport of nickel in which the flux is essentially independent of membrane thickness unless the membrane is very thick. A plot of nickel flux vs $1/\ell$ has the form shown in Figure 9.24.

Concentration Polarization Effects

As Figure 9.22 shows, concentration polarization due to inadequate stirring of the aqueous solution on either side of the coupled transport membrane could also cause concentration gradients to build up in the membrane boundary layer, decreasing the membrane flux. In coupled transport, two permeating species are involved and the flux of one permeant is intimately connected to the flux of the other. Hence, concentration polarization of either species will affect the flux of the other. For example, in coupled transport of copper with hydrogen ions, following Equation 1, the copper flux may be limited by concentration polarization of either copper or hydrogen ions, depending on their relative concentrations in the bulk solutions. At low copper concentrations, concentration-polar-

ization of copper may be rate controlling, while at high copper but low hydrogen ion concentration, concentration polarization of hydrogen ion may be rate controlling.[20]

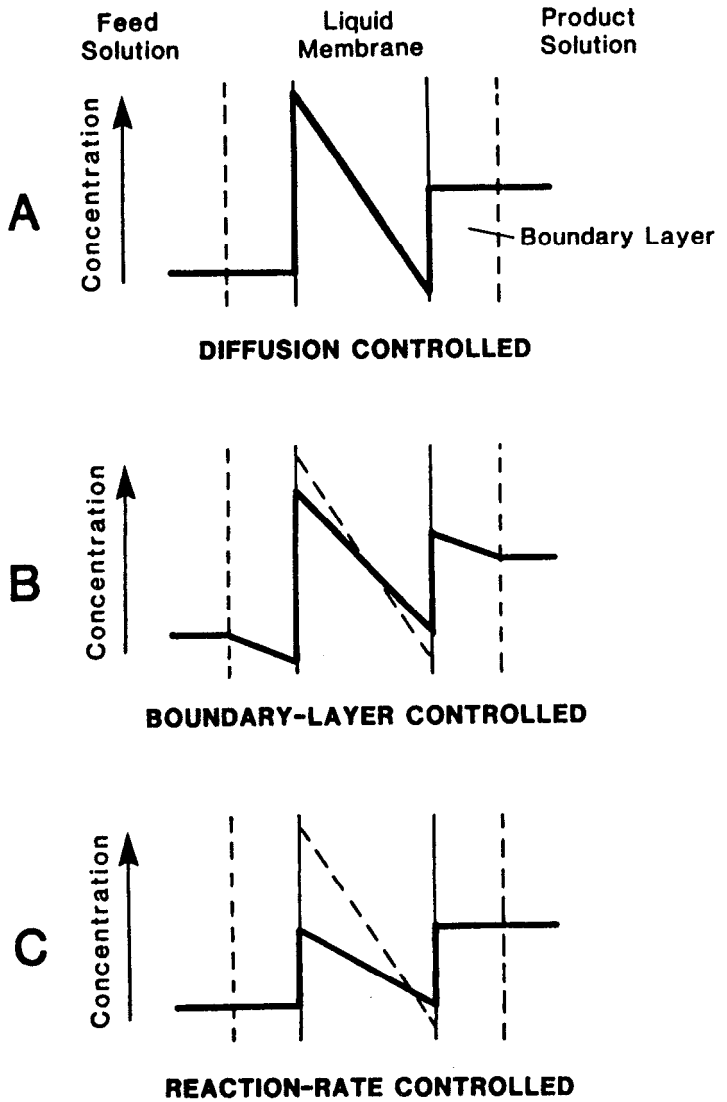


Figure 9.22: A schematic diagram showing the concentration profile of permeant in a liquid membrane when the process is (A) diffusion-controlled, (B) boundary-layer-controlled, and (C) reaction-rate controlled. The concentration profile in the membrane in absence of boundary-layer and reaction-rate effects is shown for comparison.[17]

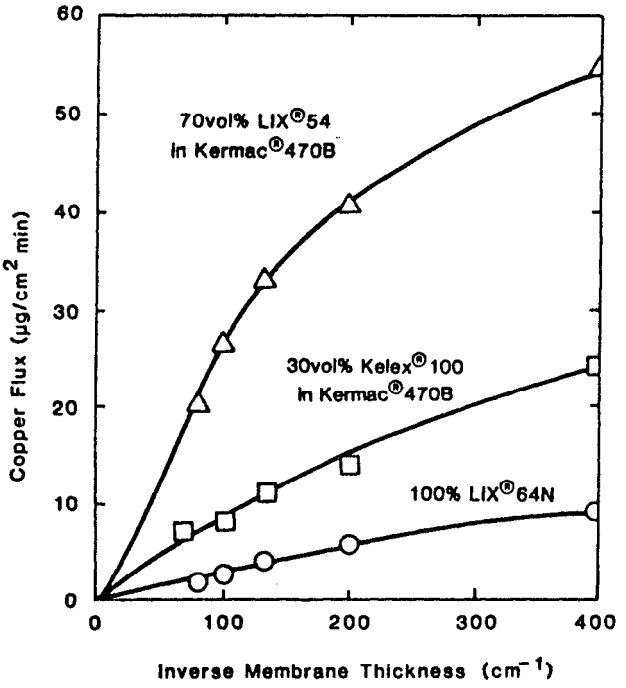


Figure 9.23: The effect of membrane thickness on flux through a coupled transport membrane.[20] (Membrane: Laminated Celgard 2400/various reagents. Feed: 0.2% copper, pH 2.5. Product: 100 g/ℓ H_2SO_4).

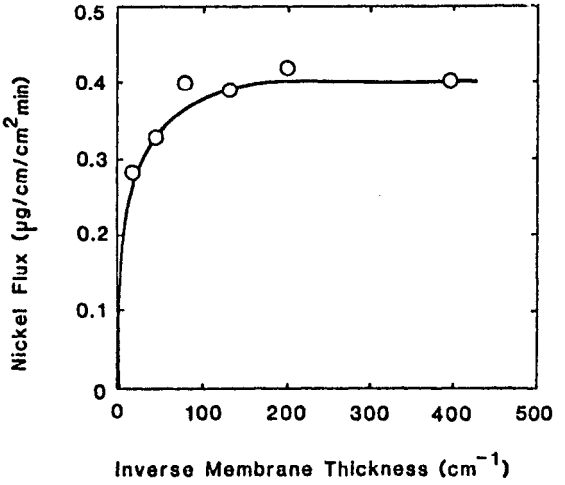


Figure 9.24: The effect of membrane thickness on the coupled transport flux of nickel through reaction rate limited membrane.[73] (Membrane: Laminated Celgard 2400/30% Kelex 100 dissolved in Kermac 470B. Feed: 0.2% nickel, pH 6.0. Product: 100 g/ℓ H_2SO_4).

In general, concentration-polarization effects are much more noticeable on the feed side of the membrane than on the product side. As discussed earlier, the trans-membrane flux is relatively insensitive to the metal ion concentration in the product solution but varies substantially with feed solution metal ion concentration, particularly with low concentration feed solutions. Concentration polarization effects can be a serious problem when treating these solutions with practical membrane systems. Figure 9.25 shows the effect of concentration polarization with a hollow fiber supported membrane system described in the following section. In this system, a feed solution velocity of greater than 20 cm/sec is required to overcome polarization.

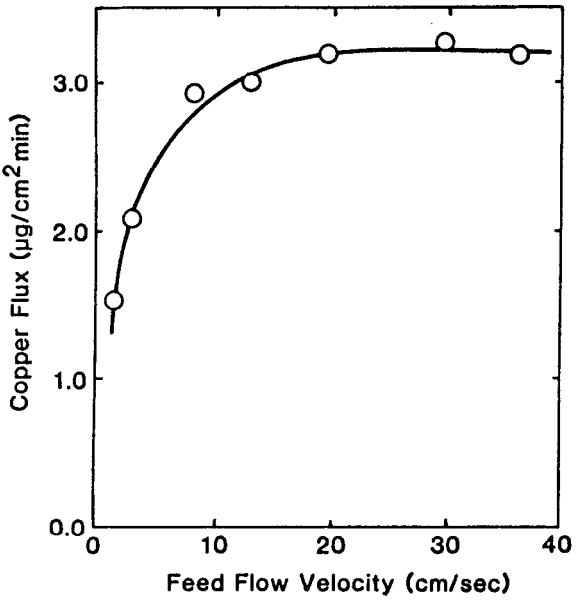


Figure 9.25: The effect of feed solution flow velocity on coupled transport metal flux. The product solution flow was held constant at 0.06 cm/sec.[20] (Membrane: Polysulfone hollow fiber/Kelex 100. Feed: 0.2% copper, pH 2.5. Product: 2% copper, 100 g/ℓ H_2SO_4).

In cases when the H^+ or OH^- is the diffusing counter ion to metal transport, buffer ions in the surrounding aqueous solution can effect the extent of concentration polarization. The mechanism by which a buffer can reduce the concentration of hydrogen ions in the boundary layer is shown in Figure 9.26. In the bulk solution, the pH is high and the acid of the buffer is in its ionized form, denoted B^-. Near the membrane surface, the pH is lower, due to concentration polarization of hydrogen ion, and the acid is in its protonated form, BH. Thus, B^- diffuses toward the membrane surface down its concentration gradient and BH diffuses away from the membrane surface down its concentration gradient. In this way, B^- acts as a shuttle, picking up hydrogen ions near the membrane surface, transporting them out of the boundary layer, and depositing them in the bulk solution.

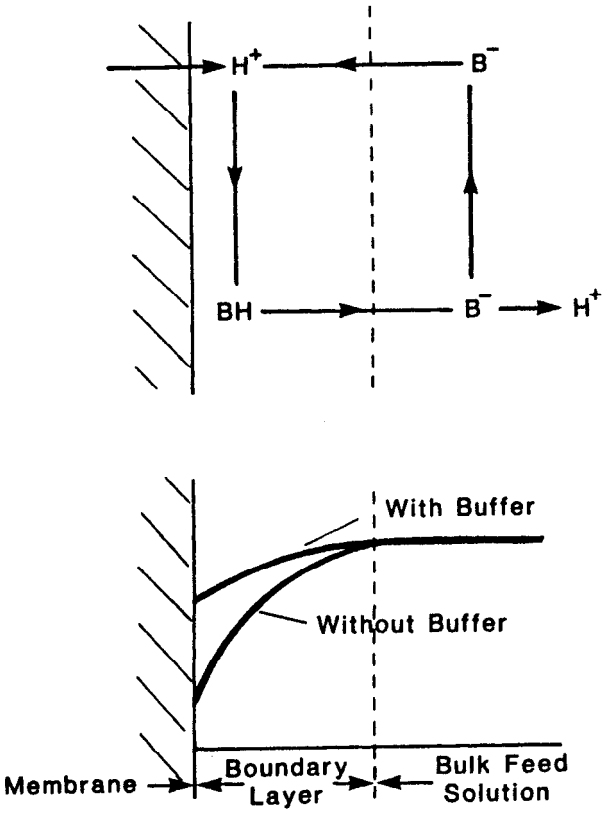


Figure 9.26: Schematic representation of the buffer cycle and pH gradient within the boundary layer of a coupled transport membrane.[20]

For this mechanism to be effective, the pH at the membrane surface must be maintained above a certain value. Below this pH, copper extraction by the ion exchange agent will be reduced and the copper flux will decrease. This pH is about 1.5 for Kelex 100, as determined from flux vs pH data shown in Figure 9.12. Thus, in experiments where the bulk feed solution has a pH of 2.5, the most effective buffer would be one in which the acid is ionized at a pH of 2.5 and protonated at a pH of 1.5, i.e., it should have a pk_a of about 2. This pk_a will maximize both the BH concentration gradient from the membrane surface to the bulk solution and the B^- concentration gradient from the bulk solution to the membrane surface. A weak acid with a pk_a of 4, for example, would be essentially fully protonated both in the bulk solution at pH 2.5 and at the membrane surface at pH 1.5. Thus, there would be no concentration gradient of either B^- or BH. A strong acid, with a pk_a of 0, for example, would be ionized in both the bulk solution and at the membrane surface. Again, there would be no concentration gradient of either B^- or BH.

The results of experiments to test this mechanism by determing the ability of buffers with different pk_a values to reduce concentration polarization effects are shown in Figure 9.27. Low stirring rates (20 rpm) were employed to maximize the concentration polarization effect. The feed solutions contained 2,000 ppm copper and were buffered at pH 2.5, and the product solutions were 100 g/ℓ sulfuric acid. (The buffer concentration refers to the initial amount of acid added to the solution. For example, a 1 molar acetate buffer would be a 1 molar solution of acetic acid to which sufficient NaOH was added to raise the pH to 2.5.)

As expected, the copper flux is most affected by buffer acids with a pk_a near 2.0. Thus, when a feed solution containing 0.05 molar formate buffer (pk_a 3.75) is used, the copper flux is the same as when no buffer is present. When a feed solution containing 0.05 molar dichloroacetic acid buffer (pk_a 1.48) is used, the flux is more than 4 $\mu g/cm^2$-min higher than that for unbuffered solutions.

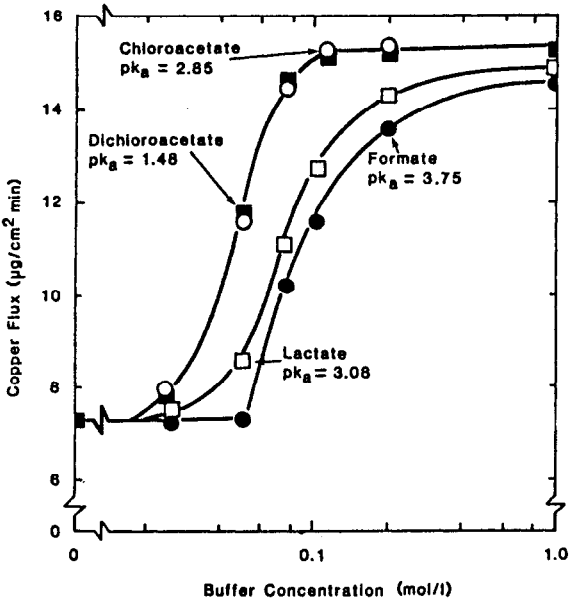


Figure 9.27: The effect of different buffers on coupled transport metal flux.[20] (Membrane: Celgard 2400/Kelex 100. Feed: 0.2% copper, pH 2.5, 0.05 molar buffer. Product: 100 g/ℓ H_2SO_4).

COUPLED TRANSPORT COMPLEXING AGENTS

In the examples given above to illustrate coupled transport, various oxime carriers for copper and other cations and tertiary amines as carriers for uranyl anions were used. However, a large number of complexing agents have been described in the literature; some of them are listed in Table 9.1.

Table 9.1: Coupled Transport Complexing Agents.

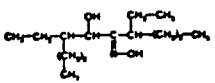
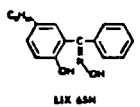
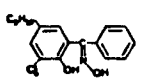
Trade Name and Manufacturers	Chemical Formula	Complexed Ion	References	
			Supported Membranes	Emulsion Membranes
LIX 63® Henkel Corp. Minneapolis, MN		Cu^{2+}, Ni^{2+}, Co^{2+}		
LIX 64N® a mixture of a few percent of LIX 63® in LIX 65N® Henkel Corp.	 LIX 65N	Cu^{2+}, Ni^{2+}	15, 18-20, 34, 43 61, 62, 63	27, 34, 37
LIX 70® a mixture of LIX 63® and this oxime: Henkel Corp.		Cu^{2+}		64

Table 9.1: (continued)

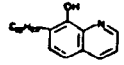
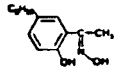
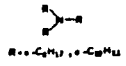
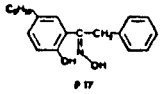
Trade Name and Manufacturers	Chemical Formula	Complexed Ion	References	
			Supported Membranes	Emulsion Membranes
Kelex 100® Sherex Chemical Company Dublin, OH		Cu^{2+}, Co^{2+}, Ni^{2+}	60-62	64
SME 529® Shell Chemical Company Houston, TX		Cu^{2+}		43
Alamine 336® Henkel Corp.		$UO_2(SO_4)_3^{4-}$ $Cr_2O_7^{2-}$	16, 17, 61, 62, 65, 66	70
Acorga P17, P50, P5100, P5300® Acorga, Ltd. London, UK		Cu^{2+}		27

Table 9.1: (continued)

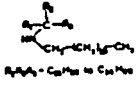
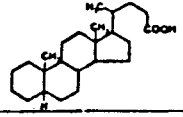
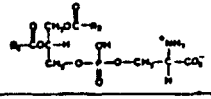
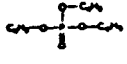
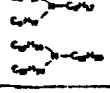
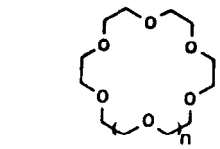
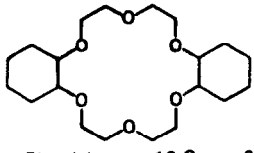
Trade Name and Manufacturers	Chemical Formula	Complexed Ion	References	
			Supported Membranes	Emulsion Membranes
Amberlite LA-2® Rohm & Haas Philadelphia, PA		Cl^-		4-6
Monesin-cholanic acid Various		Li^+, K^+, Cs^+, Na^+		30-32
Cephalin Various		Na^+, K^+		71, 72
Tributyl-phosphate Various		NO_3^-		7-12
Triocytylmine Various		$Cr_2O_7^{2-}$		67
Crown ethers Various	See Table 9.2	Alkali metal cations		30, 33, 48-51

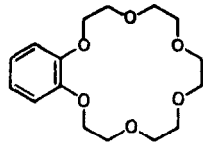
Table 9.2: Some Typical Macrocyclic Crown Ethers Used in Coupled Transport.[50]



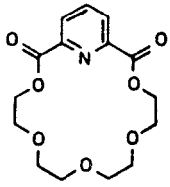
n=1: 18-Crown-6 (18C6)
n=2: 21-Crown-7 (21C7)



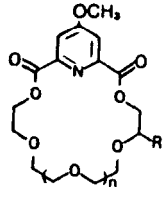
Dicyclohexano-18-Crown-6 (DC18C6)



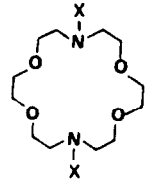
Benzo-18-Crown-6 (B18C6)



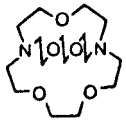
Diketopyridino-18-Crown-6 (DKP18C6)



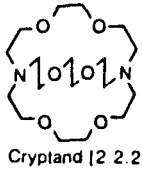
n=1: 4-Methoxydiketo-pyridino-18-Crown-6 (4-MoDKP18C6)
n=2: 4-Methoxydiketo-pyridino-21-Crown-7 (4-MoDKP21C7)



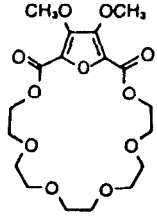
x=H: 1,10-Diaza-18-Crown-6 [2.2]
x=$C_{10}H_{21}$: N,N-Didecyl-1,10-Diaza-18-Crown-6 [2.2DD]



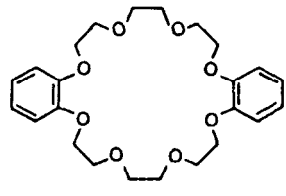
Cryptand [2.2.1]



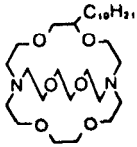
Cryptand [2.2.2]



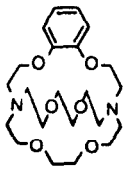
Dimethoxydiketo-furano-21-Crown-7 (DMoDKF21C7)



Dibenzo-24-Crown-8 (DB24C8)



Cryptand [2.2.2D]



Cryptand [2.2.2B]

MEMBRANE SYSTEM APPLICATIONS AND DESIGN

Applications

The principal applications of coupled transport have been the separation and concentration of metals from hydrometallurgical feeds or industrial effluent streams. These streams and the membranes used are briefly described below. In general, the application of a coupled transport process to mining operations involves the installation of a very large plant, and mine operators are reluctant to risk this type of investment in as yet unproven processes. Thus, the first commercial applications of coupled transport are likely to be smaller plants installed in pollution control applications.

Copper Recovery. One of the most extensively studied applications of coupled transport is in the recovery of copper from in situ dump and heap leach

streams. These streams are produced by the extractions of low grade copper ores with dilute sulfuric acid. Typically, the leach stream contains 1,000 to 5,000 ppm copper and various amounts of other metal ions, principally iron, Currently, copper is removed from these streams by cementation or solvent extraction. A scheme for recovering the copper by coupled transport is shown in Figure 9.28. The 1,000 to 5,000 ppm copper solution from the dump forms the feed solution, while concentrated H_2SO_4 from the electrowinning operation forms the product solution. Copper from the feed solution permeates the membrane, producing a raffinate solution containing 100 to 200 ppm copper. This solution is returned to the dump. The product solution, which contains 3 to 5% copper, is sent to the electrowinning tankhouse.

A number of papers have been published describing the application of coupled transport to this application with supported[15,18,63] and emulsion[27,37,41] membranes. The economics of the process appear to be promising, but the copper mining industry is currently very depressed, making installation of a coupled transport plant in the near future unlikely.

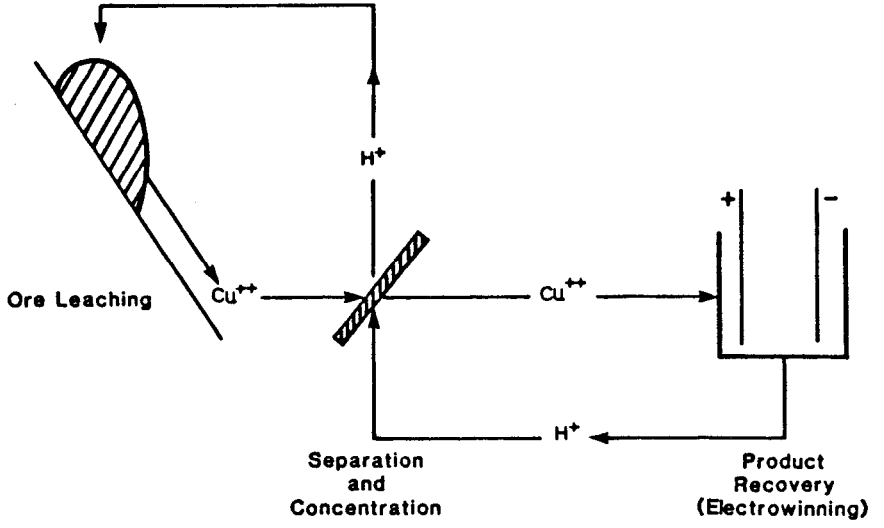


Figure 9.28: Schematic of copper recovery by coupled transport from dump leach streams.

Cobalt and Nickel Recovery. Cobalt and nickel are relatively valuable metals often found in complex ores such as laterites or deep sea nodules. The metals can only be extracted from these ores by hydrometallurgy. A proposed recovery scheme based on coupled transport is shown in Figure 9.29. The first membrane contains LIX 54, which produces a nickel and copper concentrate and a cobalt raffinate stream. The concentrate stream is then passed to a second Kelex 100 membrane, which produces a copper and nickel stream. The cobalt III raffinate stream is neutralized and reduced to cobalt II, which can then be concentrated by a LIX 51 membrane.

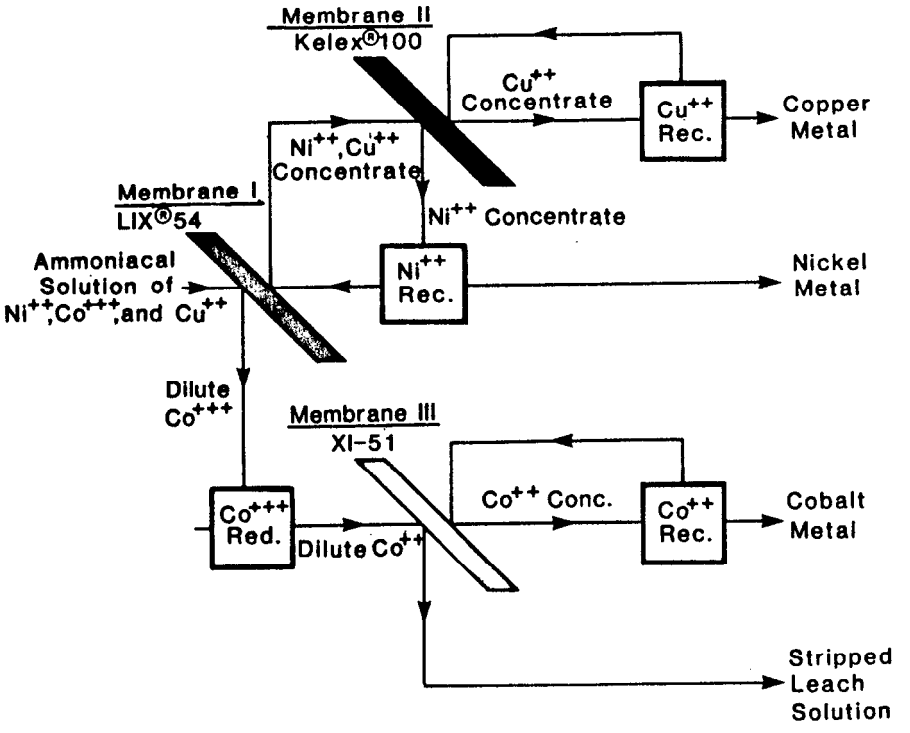


Figure 9.29: An integrated coupled transport processing scheme using membranes containing LIX 54, Kelex 100 and XI-51.[62]

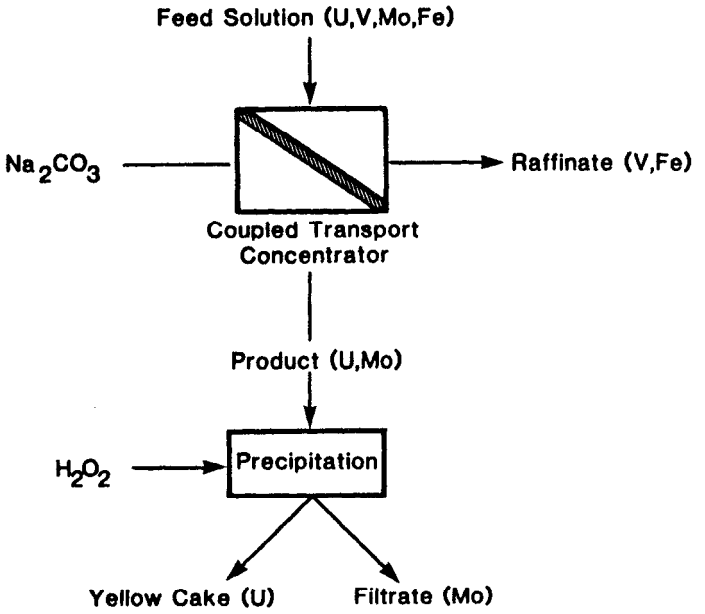
Uranium Recovery. The application of coupled transport to uranium recovery is illustrated in Figure 9.30. Typically, a tertiary amine such as Alamine 336 is used as the complexing agent and transports uranyl sulfate ions to the concentrate stream by co-transport.[65] These uranium feed streams are obtained by acid leaching of uranium ores or as by-product streams from the extraction of other metals, for example, copper. The major impurities are vanadium, molybdenum and iron. Vanadium and iron are present as cations in acid feed solutions and are not transported by amine complexing agents. Molybdenum and uranium are both present as anions and are both concentrated as shown in Figure 9.30. Separation of uranium from molybdenum is achieved by selectively precipitating the uranium with hydrogen peroxide to form yellow cake UO_4. The economics of this scheme have been tested in a 300 ft^2 supported membrane pilot plant installed at a Wyoming uranium mill, but the results are not yet available.

Electroplating Rinse Waters. The general way in which coupled transport might be applied to electroplating rinse waters is shown in Figure 9.31 for a chrome-plating operation.[66] A typical chrome-plating bath contains 25 wt % chromium. The plated parts constantly drag out this solution into the rinse baths. Normally the rinse water flow rate is set at 50 times this drag-out rate, producing a CrO_3 concentration of 5,000 ppm in the first rinse bath. It is this

solution that is fed to the coupled transport concentrator. An amine-containing membrane can be used, and, if the product side of the membrane is maintained at an alkaline pH with NaOH, then chromate anions are transported across the membrane by co-transport via the reaction:

$$2R_3N + 2H^+ + CrO_4 \rightleftharpoons (R_3NH)_2\ CrO_4 \qquad (25)$$

The raffinate from the process is thus a chromate-depleted solution, which can be recycled to the rinse baths, and a concentrated sodium chromate solution, from which the chromate can be recovered. Similar schemes have been proposed for copper, zinc, mercury and nickel rinse waters.[25,26,66–70]



	Concentration (ppm)			
	U	V	Mo	Fe
Feed Solution	2000	100	100	1140
Raffinate	13	100	3	1140
Product	30,000	0.1	1500	0.1

Figure 9.30: A processing scheme and results for the coupled transport separation of a synthetic uranium mine leach stream. Metals were added to the feed solution as UO_2SO_4, $NaVO_3$, Na_2MoO_4, $FeSO_4$, and $Fe_2(SO_4)_3$.[66]

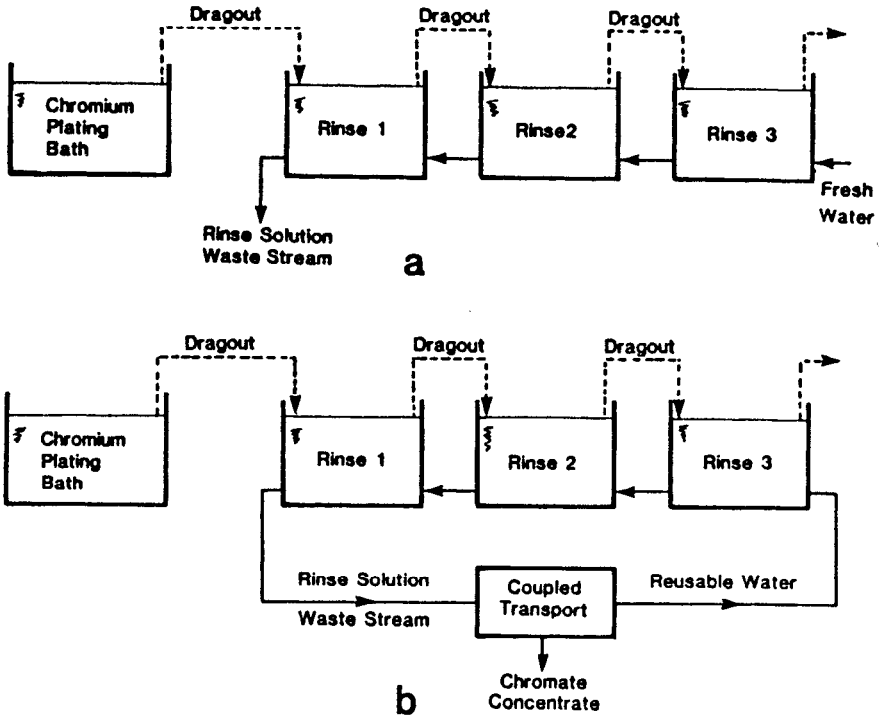


Figure 9.31: Schematic of a typical chromium plating operation (a) without and (b) with coupled transport treatment.[67]

Copper Etchant Baths. One of the most promising applications of coupled transport is the renovation of circuit board etchant solutions that contain copper.[61] The printed circuit board industry produces more than ten million gallons/year of spent etchant solutions in which copper, other salts and etchant chemicals are concentrated. Coupled transport permits continuous on-site removal of copper from the etchant solutions and simultaneous regeneration of the etchant solution. This represents a considerable savings in the costs of manufacturing circuit boards.

The use of coupled transport to continuously renovate the etchant and recover copper is shown schematically in Figure 9.32. The relevant chemical reactions are shown. Copper on the circuit board is dissolved by oxidation with atmospheric oxygen and complexation with ammonia. The etchant, containing the copper complex, is pumped to the coupled transport processor, where copper is extracted into the membrane while ammonia remains in the aqueous phase. (The ammonia is not extracted into the membrane because bidentate complexing agents are used. Two of these complexing agents occupy all four coordination sites on the copper, thereby displacing ammonia from the copper-ammonia complex.) For each mol of copper removed, two mols of water are generated. Half the excess water is consumed in the etching reaction. Thus, except for a slight dilution, the etching solution is restored to its original condition. This dilution

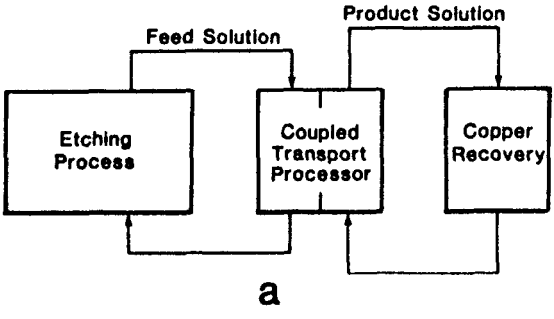
would not present any problems in the etching process because elevated temperatures are used, and water must be continuously added to compensate for evaporation.

On the product side of the membrane, concentrated sulfuric acid (100 g/ℓ) is employed. Thus, copper sulfate is formed. Copper could be recovered by precipitating the copper sulfate or by electrodepositing the copper. In the latter case, the overall oxidation-reduction reaction,

$$2H_2O + 2Cu^{2+} \rightleftharpoons 2Cu + 4H^+ + O_2, \quad (26)$$

would regenerate the hydrogen ions lost in the coupled transport process. If copper sulfate precipitation were used, acid would be continuously metered into the product solution to replace hydrogen ions lost in the coupled transport process.

Copper recovery from etchant baths is a particularly promising application of coupled transport because the high copper concentrations in the etchant solutions result in high fluxes. A relatively small unit is, therefore, able to process a large volume of solution.



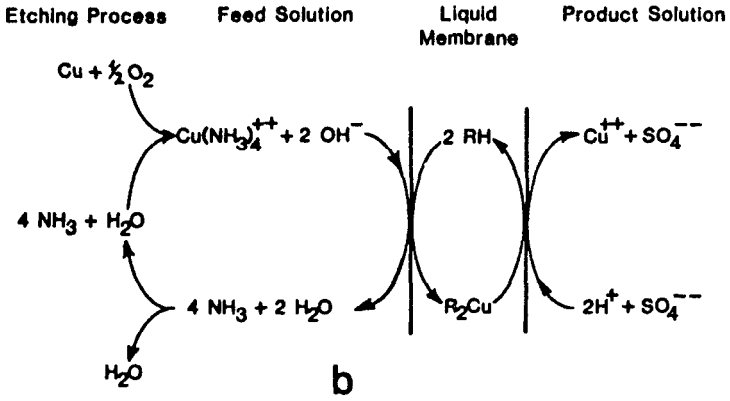


Figure 9.32: Schematic diagram of (a) coupled transport renovation of circuit etchants and (b) relevant chemical reactions.[62]

Phenol and Ammonia Recovery. Finally, the closely related passive and facilitated-transport processes for phenol and ammonia recovery should be mentioned. In these processes, dilute phenol or ammonia feed solutions are contacted with a liquid membrane in which they are freely soluble. They dissolve in the membrane, diffusing to the product side where they are removed by neutralizing with a base (in the case of phenol) or an acid (in the case of ammonia). Although the transport mechanism does not involve a carrier and these are, therefore, passive transport processes, the actual process is quite similar, and Li et al[25] published the details of these separations using emulsion membrane technique.

Supported Liquid Membranes Process Design

In supported liquid membranes, a microporous support is impregnated with the liquid complexing agent phase and used to separate the feed and product solutions. In any large process, this support membrane must be mounted in some form of high surface area module, and the way in which the membrane is modulized strongly influences both the operation and economics of the process. One requirement of this process, in contrast to other membrane processes such as reverse osmosis and ultrafiltration, is that the fluid on both sides of the membrane must be circulated to avoid concentration polarization effects. However, as described earlier, concentration polarization is much more significant on the feed side of the membrane. One possible design would be a simple plate-and-frame module. However, this is unlikely to be the optimum membrane configuration for large-scale plants because of the relatively high cost per unit area. A potentially more economical configuration uses hollow fiber membranes in a tube-and-shell configuration and almost all of the available process data has involved this type of module.

The hollow fibers used in these module configurations are usually made from polysulfone by a solution spinning process.[19,20] Polysulfone is used because of its excellent chemical resistance to acids, bases, and a wide variety of organic compounds. However, other materials have been used, such as polyvinylidene fluoride. A scanning electron micrograph of a cross-section of a representative fiber is shown in Figure 9.33. Permeation occurs not only through the finger-like voids visible in the scanning electron micrograph, but also through much smaller pores, which are not visible at this magnification. Fibers such as these are incorporated into modules of the type illustrated in Figure 9.34. In operation, the organic complexing agent is incorporated into the walls of the fiber, the product solution flows on the outside of the fiber, and the feed solution flows down the fiber lumen.

Large-scale processes require a number of modules to remove most of the metal from a continuous feed stream. In general, a multi-stage system operating in a feed and bleed mode is the most efficient design. A schematic representation of a three-stage system is presented in Figure 9.35. A fixed feed volume is recirculated through each module, as indicated by the bold lines in the figure. Feed solution is continuously introduced into the recirculating volume of the first stage and is bled off at the same rate. This "bleed" from the first stage constitutes the feed for the second. The bleed from the second stage constitutes the feed for the third. In operation, the concentration of metal in the feed solution decreases as it flows from stage 1 to stage 3, with the final raffinate concentration depending on the feed-and-bleed flow rate. The product solution flows

in series through the stages. The advantage of this multi-stage design over a single stage system is that only the final stage operates on feed solution depleted of metal.

Liquid membranes supported by hollow fibers are relatively easy to make and operate and the membrane fluxes can be quite high. However, membrane stability is a problem. The variation in coupled transport flux during long-term tests is shown in Figure 9.36. As these results show, actual behavior varies quite widely, depending on the membrane and the complexing agent. However, each curve is quite reproducible.

The detailed mechanism for this flux instability is unknown but it appears to be related to loss of the organic complexing agent phase from the support membrane. Thus, it is possible to restore membrane fluxes to their original values by reloading the membrane with fresh complexing agent. Figure 9.37 shows this result with polysulfone hollow fiber membranes loaded with Lelex 100, an oxime complexing agent for copper-coupled transport.

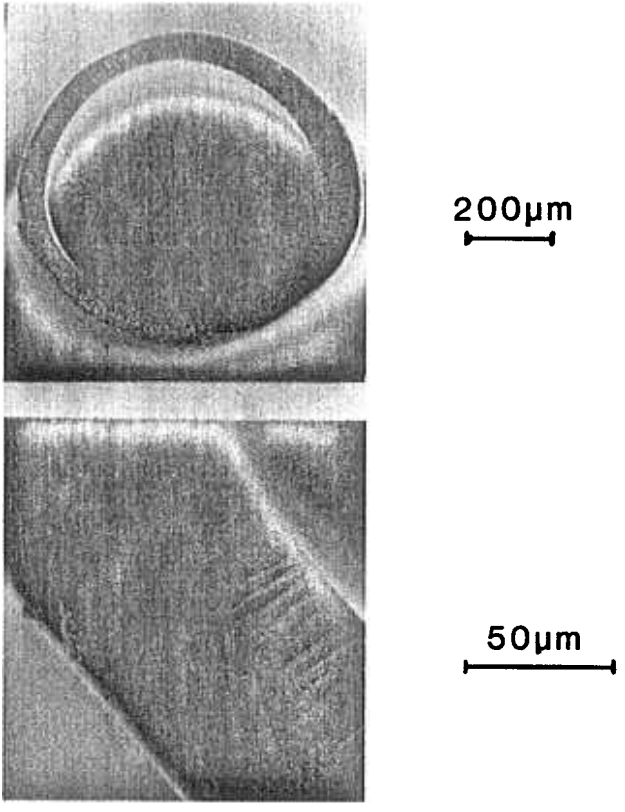


Figure 9.33: Scanning electron micrographs of a polysulfone hollow fiber as a coupled transport support membrane.[19]

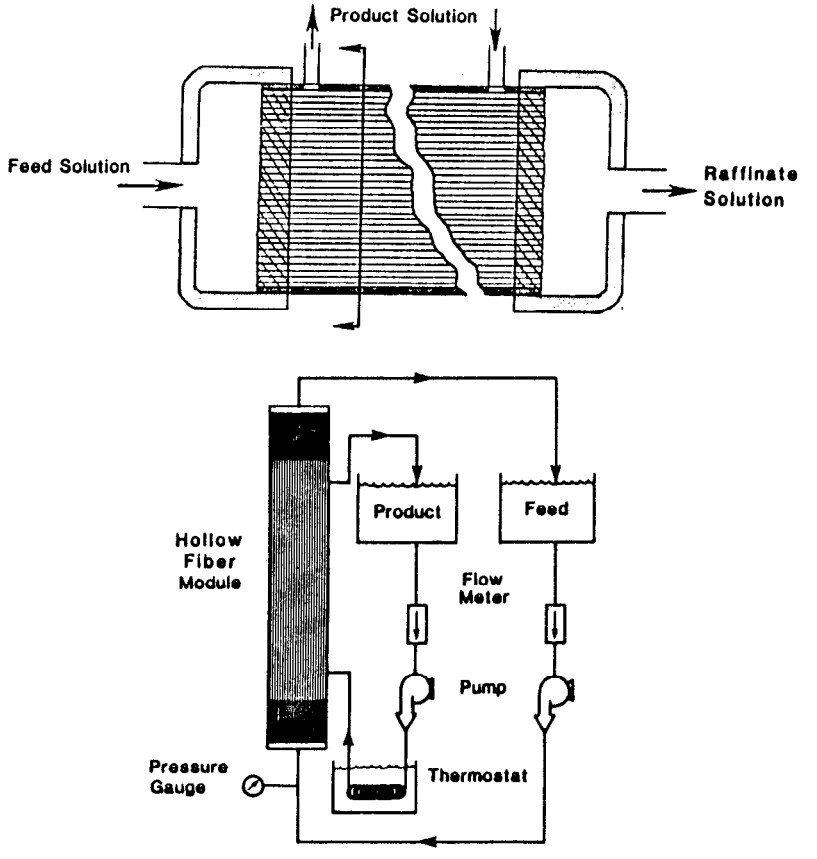


Figure 9.34: Schematic of a hollow fiber module and test unit.[20,62]

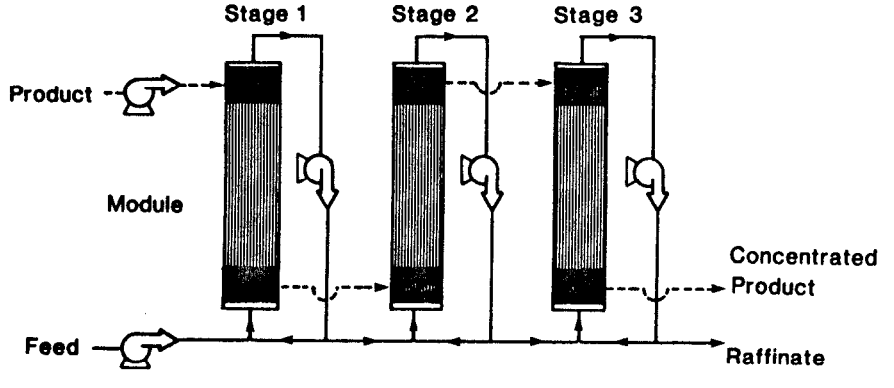


Figure 9.35: Schematic of a three-staged feed and bleed hollow fiber coupled transport concentrator.[20]

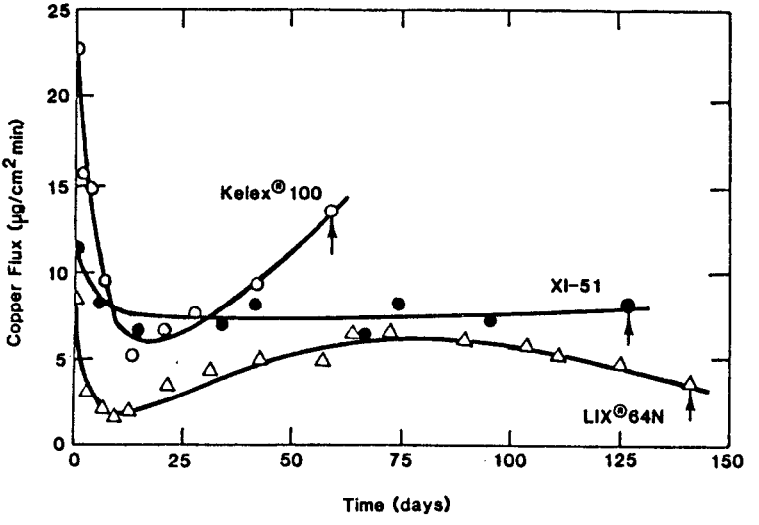


Figure 9.36: Copper flux as a function of time for coupled transport membranes containing different complexing agents. The arrow indicates the time of failure of the membrane.[73] (Membrane: Celgard 2400/various complexing agents. Feed: 0.2% copper, pH 2.5. Product: 100 g/ℓ H_2SO_4).

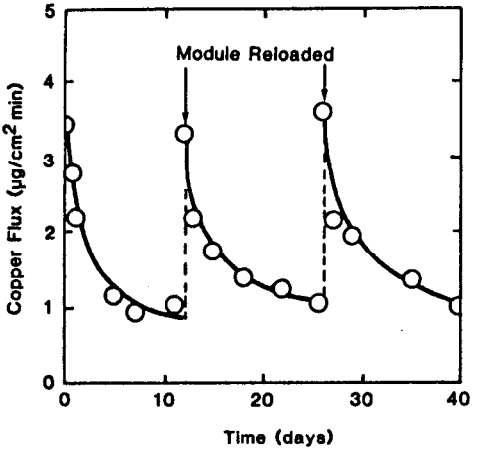


Figure 9.37: The effect of replenishing a hollow fiber coupled transport module with fresh complexing agent.[63] (Membrane: Polysulfone, hollow fiber/Kelex 100. Feed: 0.2% copper, pH 2.5. Product: 2% copper, 100 g/ℓ H_2SO_4).

A model that is consistent with the observed results is spontaneous emulsification of the liquid organic phase, as shown in Figure 9.38. Initially, the emulsion phase formed at the surface of the liquid membrane hinders the diffusion of metal ions through the aqueous phase to the membrane surface. This would be particularly apparent on the feed side of the membrane and would explain the initial drop in flux often observed. As the emulsification process proceeds, some

of the droplets escape to the aqueous solutions and the emulsion layer and the remaining liquid membrane layer gradually becomes thinner. This results in a gradual inverse in the membrane flux until at some point the liquid phase disappears completely and the aqueous feed and product solutions can mix. The process is illustrated in Figure 9.39. The actual form of any particular flux-time curve depends a great deal on the membrane material, its pore size and geometry, and the viscosity and surface tension of the organic liquid phase.

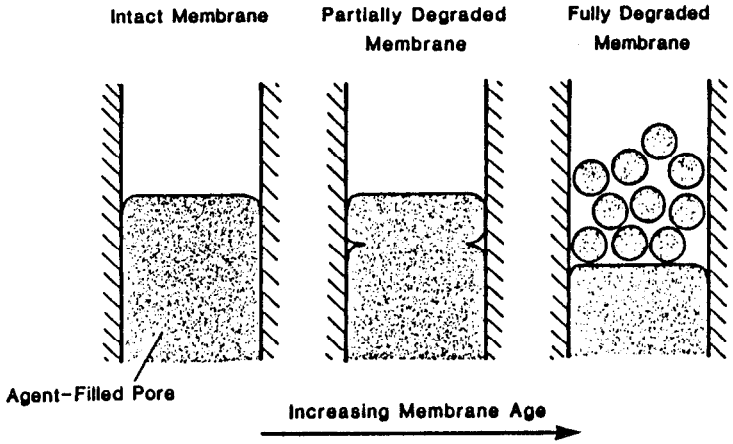


Figure 9.38: A schematic of membrane degradation by formation of an interfacial emulsion.[63]

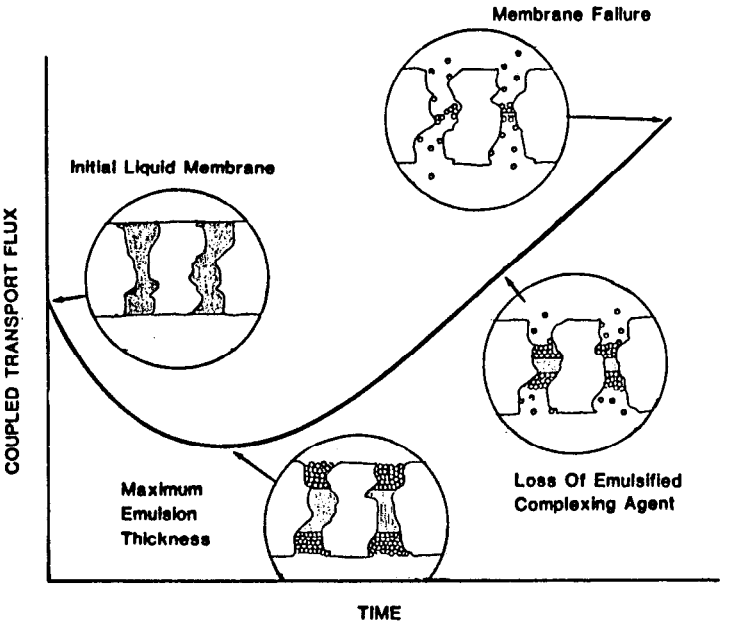


Figure 9.39: Diagram illustrating spontaneous emulsification processes in a liquid membrane and the effect of the process on coupled transport flux.

Emulsion Liquid Membranes Process Design

Figure 9.40 is a schematic illustration of an emulsion liquid membrane process. There are four main operations in this process. First, fresh product solution is emulsified in the liquid organic membrane phase. This water/oil (w/o) emulsion then feeds to a large mixer vessel, where it is again emulsified forming a water/oil/water emulsion (w/o/w). Metal ions contained in the feed solution permeate by coupled transport through the walls of the emulsion to the product solution. A single mixer, as shown in Figure 9.40, or a series of mixers may be used to extract the feed metal completely. The mixture then passes to a settler tank where the oil droplets separate the metal-depleted raffinate solution. The emulsion concentrate then passes to a deemulsifier where the organic and concentrated product solutions are separated. The regenerated organic solution is then recycled to the first emulsifier stage.[25,69]

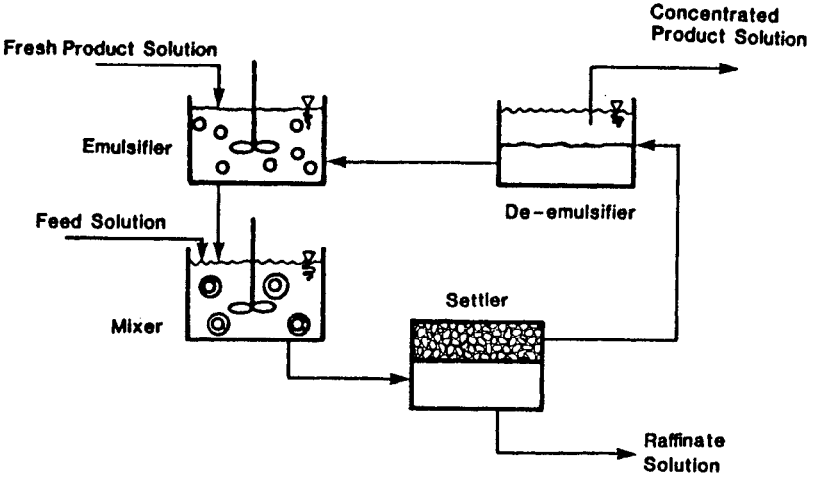


Figure 9.40: Schematic flow scheme of a liquid emulsion membrane process.

The optimum operating conditions for this type of process vary a great deal. The first w/o emulsion typically consists of an approximately 50/50 mixture, which is then mixed with the aqueous feed solution phase at a ratio of 1 part emulsion phase to 5 to 20 parts feed solution phase. A typical extraction curve is shown in Figure 9.41 for copper using SME 529, an oxime complexing agent from Shell.[43] The extraction rate generally follows a first order expression, which can be expressed as:

$$\frac{dC}{dt} = kC \tag{27}$$

where k is the first order rate constant. This expression rearranges to:

$$\ln\left(\frac{C}{C_o}\right) = kt \tag{28}$$

where C is the concentration of copper in the feed solution at time t and C_o is the initial copper concentration. A plot of the results following Equation 28 is shown in Figure 9.42.

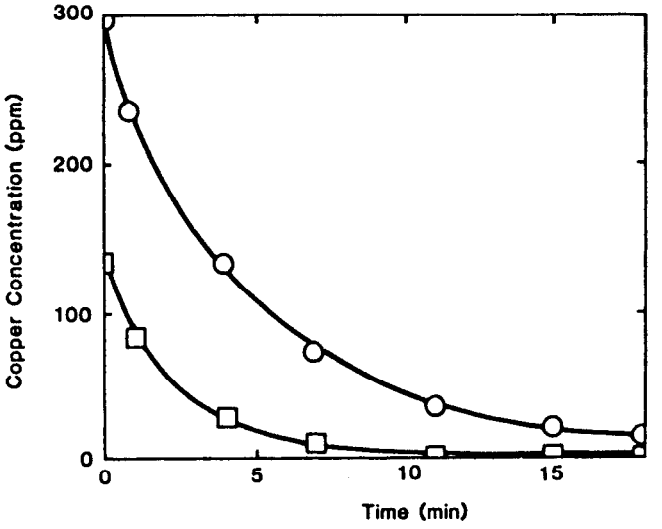


Figure 9.41: Variation of copper concentration in the raffinate during extraction with a liquid emulsion-membrane complexing agent system.[43]

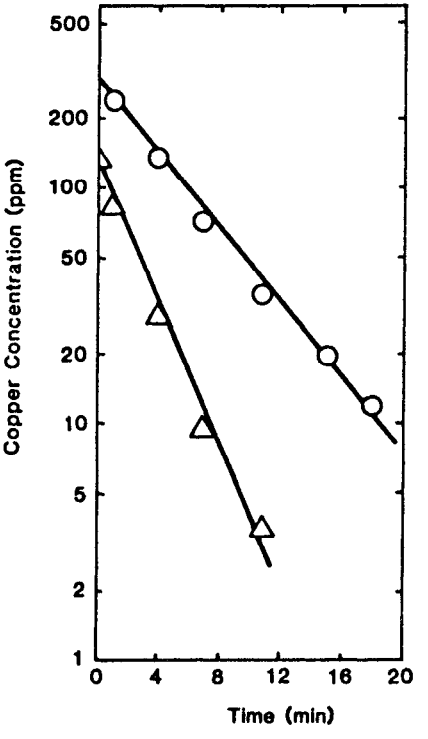


Figure 9.42: Variation of copper concentration with time showing a pseudo first order rate process for the results shown in Figure 9.41.[43]

The slope of the curve in Figure 9.42 is proportional to the loading of complexing agent in the organic phase and the rate of agitation of the mixer vessel. Typical results illustrating this behavior for copper with LIX 64N as the complexing agent are shown in Figures 9.43 and 9.44.

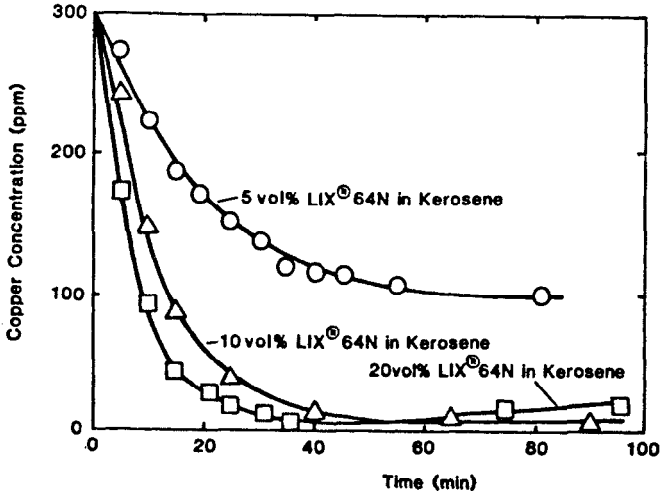


Figure 9.43: Copper extraction by means of a liquid emulsion membrane process.[37] Experimental conditions are as follows. Feed: 200 ml, pH 2.0, 300 ppm Cu^{2+}. Membrane: 15 ml 10% LIX 64N in Kerosene, 3% Span 80. Stripping solution: 15 ml H_2SO_4 solution. Stirrer speed: 500 rpm.

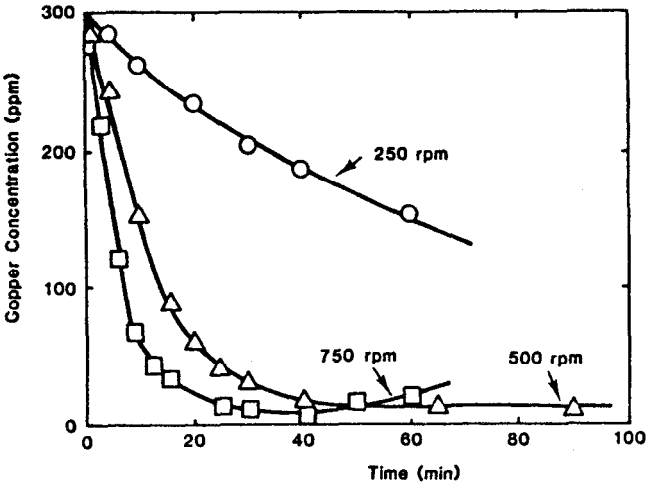


Figure 9.44: Copper removal at different agitation speeds for a liquid emulsion process.[37] Experimental conditions are as follows. Feed: 200 ml, pH 2.0, 300 ppm copper. Membrane: 15 ml 10% LIX 64N in Kerosene, 3% Span 80. Stripping solution: 15 ml H_2HO_4 solution.

Figures 9.43 and 9.44 also illustrate one of the major problems of emulsion membrane systems, i.e., degradation of the emulsion on prolonged contact with the feed solution and high-speed mixing of the product and feed solutions. Prolonged stirring of the emulsion with the feed solution causes the copper concentration in the feed solution to rise as some of the emulsion droplets break. Careful tailoring of the stirring rate and surfactant composition is required in order to minimize premature breaking of the emulsion.

Although emulsion degradation must be avoided in the mixer and settler tanks, complete and rapid breaking is required in the deemulsifer where the product solution is separated from the organic complexing agent. Currently, electrostatic coalescers appear to be the best method of breaking these emulsions. Nonetheless, some loss of the organic phase occurs with the feed solution raffinate.

THE FUTURE

Although coupled transport has been known for many years, it has only been under active development since the mid-1960's. In the laboratory, the process can perform a number of useful separations, but the process has yet to prove itself industrially. The principal problems are related to the stability of the liquid membranes, leading to poor economics either because of loss of reagents or replacement of the support membranes. If these problems can be solved, the process may find industrially important applications.

REFERENCES

1. Babcock, W.C., Kelly, D.J., LaChapelle, E.D., Smith, K.L. and Baker, R.W., "Coupled Transport Membranes in Hydrometallurgy," *The Proceedings of Hydrometallurgy.* Society of Chemical Industry, Manchester, England (1981).
2. Pfeffer, W., *Ges. Wiss.*, 16, 185 (1890).
3. Osterhout, W.J.V., *Proc. Nat. Acad. Sci.*, 21, 125 (1935).
4. Sollner, K. and Shean, G.M., *J. Am. Chem. Soc.*, 86, 1901 (1964).
5. Shean, G.M. and Sollner, K., "Carrier Mechanisms in the Movement of Ions Across Porous and Liquid Ion Exchanger Membranes," *Ann. N.Y. Acad. Sci.*, 137, 759 (1966).
6. Sollner, K. and Shean, G., *Protoplasma*, 63:1-3 (1967).
7. Bloch, R., Kedem, O. and Vofsi, D., *Nature*, 199, 802 (1963).
8. Bloch, R., Finkelstein, A., Kedem, O. and Vofsi, D., *Ind. Eng. Chem. Proc. Des. Dev.*, 6:2 231 (1967).
9. Bloch, R., "Hydrometallurgical Separations by Solvent Membranes" in *Proceedings of Membrane Science and Technology*, Columbus Laboratories of Battelle Memorial Institute, Columbus, Ohio, 1969, Plenum Press (1970).
10. Vofsi, D., Kedem, O., Bloch, R. and Marian, S., *J. Inorg. Nucl. Chem.*, 31, 2631 (1969).
11. Jagur-Grodzinski, J., Marian, S. and Vofsi, D., *Sep. Sci.*, 8, 33 (1973).
12. Vofsi, D. and Jagur-Grodzinski, J., *Naturwissenschaften*, 60, 1 (1973).

13. Moody, G.J. and Thomas, J.D.R., "Poly(vinylchloride) Matrix Membrane Ion-Selective Electrodes" in *Ion-Selective Electrode Methodology*, A.K. Covington (Ed.), CRC Press, Boca Raton, Florida (1979).
14. Miyauchi, T., U.S. Patent 4,051,230 (1977).
15. Baker, R.W., Tuttle, M.E., Kelly, D.J. and Lonsdale, H.K., *J. Membr. Sci.*, 2, 213 (1977).
16. Babcock, W.C., Baker, R.W., LaChapell, E.D. and Smith, K.L., *J. Membr. Sci.*, 7, 71 (1980).
17. Babcock, W.C., Baker, R.W., LaChapell, E.D. and Smith, K.L., *J. Membr. Sci.*, 7, 89 (1980).
18. Largman, T. and Sifniades, S., *Hydrometall.*, 3:2, 153 (1978).
19. Babcock, W.C., Baker, R.W., Kelly, D.J., Lonsdale, H.K., Ray, R.J. and Tuttle, M.E., *Coupled Transport Membranes for Metal Separations, Final Report, Phases I and II.* U.S. Bureau of Mines Technical Report. NTIS No. PB80 11 430 (May), Springfield, Virginia (1977).
20. Babcock, W.C., Baker, R.W., Kelly, D.J. and Lonsdale, H.K., *Coupled Transport Membranes for Metal Separation, Final Report, Phase III.* U.S. Bureau of Mines Technical Report. NTIS No. PB293029 (May), Springfield, Virginia (1978).
21. Li, N.N., U.S. Patent.3,4,0,794 (1968).
22. Li, N.N., *Ind. Eng. Chem. Proc. Des. Dev.*, 10:2 (1971).
23. Li, N.N., *J. Membr. Sci.*, 3, 265 (1978).
24. Li, N.N., *AIChE J.*, 17:2 (1971).
25. Li, N.N. and Shrier, A.L., "Liquid Membrane Water Treating" in *Recent Advances in Separation Science*, Vol. I, N.N. Li (Ed.), CRC Press, Boca Raton, Florida (1972).
26. Frankenfeld, J.W. and Li, N.N., "Waste Water Treatment by Liquid Ion Exchange in Liquid Membrane Systems" in *Recent Developments in Separation Science, Vol. III-Part B*, N.N. Li (Ed.), CRC Press, Boca Raton, Florida (1977).
27. Li, N.N., Cahn, R.P., Naden, D. and Lai, R.W.M., *Hydrometall.*, 9, 277 (1983).
28. Matulevicius, E.S. and Li, N.N., *Sep. and Pur. Methods*, 4:1, 73 (1975).
29. Hayworth, H.C., *Chemtech* 11:6, 342 (1981).
30. Cussler, E.L., *AIChE J.*, 17:6, 1300 (1971).
31. Reusch, C.F. and Cussler, E.L., *AIChE J.*, 19:4, 736 (1973).
32. Schiffer, D.K., Choy, E.M., Evans, D.F. and Cussler, E.L., *Chem. Eng. Prog. Sym.*, 70:144, 150 (1974).
33. Caracciolo, F., Cussler, E.L., and Evans, D.F., *AIChE J.*, 21:1, 160 (1975).
34. Lee, Kyung-Hee, Evans, D.F. and Cussler, E.L., *AIChE J.*, 24:5, 860 (1978).
35. Volkel, W., Wandrey, C. and Schurgerl, K., *Sep. Sci.*, 12:4, 425 (1977).
36. Halwachs, W. and Schurgerl, K., *Intl. Chem. Eng.*, 20:4, 519 (1980).
37. Volkel, W., Halwachs, W. and Schurgerl, K., *J. Membr. Sci.*, 6, 19 (1980).
38. Volkel, W., Poppe, W., Halwachs, W. and Schurgerl, K., *J. Membr. Sci.*, 11, 333 (1982).
39. Marr, R. and Kopp, A., *Chem. Ing. Tech.*, 52:5, 399 (1980).
40. Bouvier, A., Gaubinger, W. and Marr, R., *CAV*, 11:6 (1982).
41. Stelmaszek, J., *J. Membr. Sci.*, 2, 197 (1977).
42. Gladek, L., Stelmaszek, J. and Szust, J., *J. Membr. Sci.*, 12, 153 (1982).
43. Martin, T.P. and Davies, G.A., *Hydrometall.*, 2, 315 (1976/1977).

44. Chiarizia, R., Castagnola, A., Danesi, P.R. and Horwitz, E.P., *J. Membr. Sci.*, 14, 1 (1983).
45. Danesi, P.R., *J. Membr. Sci.*, 20, 231 (1984).
46. Folkner, C.A. and Noble, R.D., *J. Membr. Sci.*, 12, 289 (1983).
47. Bunge, A.L. and Noble, R.D., *J. Membr. Sci.*, 21, 55 (1984).
48. Lamb, J.D., Christensen, J.J., Izatt, S.R., Bedke, K., Astin, M.S. and Izatt, R.M., *J. Am. Chem. Soc.*, 102:10, 3399 (1980).
49. Lamb, J.D., Izatt, R.M., Garrick, D.G., Bradshaw, J.S. and Christensen, J.J., *J. Membr. Sci.*, 9, 83 (1981).
50. Lamb, J.D., Brown, P.R., Christensen, J.J., Bradshaw, J.S., Garrick, D.G. and Izatt, R.M., *J. Membr. Sci.*, 13, 89 (1983).
51. Izatt, R.M., Haws, R.M., Lamb, J.D., Dearden, D.V., Brown, P.R., McBride, D.W., Jr. and Christensen, J.J., *J. Membr. Sci.*, 20, 273 (1984).
52. Way, J.D., Noble, R.D., Flynn, T.M. and Sloan, E.D., *J. Membr. Sci.*, 12, 239 (1982).
53. Pearson, D., "Supported Liquid Membranes for Metal Extraction from Dilute Solutions" in *Ion Exchange Membranes*, D.S. Flett (Ed..), Ellis Horwood Limited, Chichester, England (1983).
54. Chan, C.C. and Lee, C.J., *J. Membr. Sci.*, 20, 1 (1984).
55. Cussler, E.L., *Multicomponent Diffusion*, Elsevier Publishing Co., Amsterdam (1976).
56. Smith, K.A., Meldon, J.H. and Colton, C.K., *AIChE J.*, 19:1, 102 (1973).
57. Schultz, J.S., Goddard, J.D., Suchdeo, S.R., *AIChE J.*, 20:3, 417 (1974).
58. Goddard, J.D., Schultz, J.S. and Suchdeo, S.R., *AIChE J.*, 20:4 (1974).
59. Jain, R. and Schultz, J.S., *J. Membr. Sci.*, 11, 79 (1982).
60. Babcock, W.C., Baker, R.W., Kelly, D.J., Kleiber, J.C. and Lonsdale, H.K., *Coupled Transport Systems for Control of Heavy Metal Pollutants*, U.S. Environmental Protection Agency Technical Report. NTIS No. PB80-103542, Springfield, Virginia (1979).
61. Babcock, W.C., Baker, R.W., Brooke, J.W., Kelly, D.J., LaChapelle, E.D. and Lonsdale, H.K., *Coupled Transport Membranes for Metal Recovery, Final Report, Phase II.* Technical Report, National Science Foundation Report. NTIS No. PB81-179947, Springfield, Virginia (1980).
62. Babcock, W.C., Baker, R.W., Kelly, D.J., Kleiber, J.C. and Lonsdale, H.K., *Coupled Transport Membranes for Metal Separations, Final Report, Phase IV.* U.S. Bureau of Mines Technical Report. NTIS No. PB81-214843, Springfield, Virginia (1979).
63. Komasawa, I., Otake, T. and Yamashita, T., *Ind. Eng. Chem. Fundam.*, 22, 127 (1983).
64. Strzelbicki, J. and Charewicz, W., *Hydrometall.*, 5, 243 (1980).
65. Babcock, W.C., Baker, R.W., Kelly, D.J. and LaChapelle, E.D., "Coupled Transport Membranes for Uranium Recovery" in *Proceedings of ISEC'80*, Liege, Belgium (September 1980).
66. Babcock, W.C., Baker, R.W., Conrod, M.G. and Smith, K.L., "Coupled Transport Membranes for Removal of Chromium from Electroplating Rinse Solutions" in *Chemistry in Water Reuse*, Ann Arbor Science: Ann Arbor, MI (1981).
67. Hochhauser, A.M. and Cussler, E.L., "Concentrating Chromium with Liquid Surfactant Membranes" in *Adsorption and Ion Exchange, AIDhE Symp. Series*, 71:152, 136 (1976).

68. Fuller, E.J. and Li, N.N., *J. Membr. Sci.*, 18, 251 (1984).
69. Halton, T.A., Lightfoot, E.N., Cahn, R.P. and Li, N.N., *Ind. Eng. Chem. Fundam.*, 22, 27 (1983).
70. Boyadzhiev, L. and Bezenshek, E., *J. Membr. Sci.*, 14, 13 (1983).
71. Rosano, H.L., Schulmann, J.H. and Weisbuch, J.B., *Ann. N.Y. Acad. Sci.*, 92, 457 (1961).
72. Rosano, H.L., Duby, P. and Schulmann, J.H., *J. Phys. Chem.*, 65, 1704 (1961).
73. Babcock, W.C., Baker, R.W., Conrod, M.G., Lonsdale, H.K. and Smith, K.L., "Industrial Water Reuse with Coupled Transport Membranes," Office of Water Research and Technology Technical Report. PB No. 80-206014 (1979).

10

The Separation of Gases by Membranes

A. Keith Fritzsche and James E. Kurz

INTRODUCTION

The study of gas transport in membranes has been actively pursued for over 100 years. This extensive research resulted in the development of good theories on single gas transport in polymers and other membranes. The practical use of membranes to separate gas mixtures is, however, much more recent. One well-known application has been the separation of uranium isotopes for nuclear weapon production. With few exceptions, no new, large scale applications were introduced until the late 1970's when polymer membranes were developed of sufficient permeability and selectivity to enable their economical industrial use. Since this development is so recent, gas separations by membranes are still less well-known and their use less widespread than other membrane applications such as reverse osmosis, ultrafiltration and microfiltration. In excellent reviews on gas transport in polymers as recent as 1983, no mention was made of the important developments of the last few years. For this reason, this chapter will concentrate on the more recent aspects of gas separation by membranes. Naturally, many of the examples cited will be from our own experience, but the general underlying principles are applicable to many membrane based gas separating systems.

A Short History

Membranes for the separation of gas mixtures are of two very different kinds: one a microporous membrane, the other nonporous. Microporous membranes were the first to be studied and the basic law governing their selectivity was discovered by Graham.[1] When pore size of a microporous membrane is small compared to the mean-free-path of the gas molecules, permeate will be enriched in the gas of the lower molecular weight. Since molecular weight ratios of most gases are not very large and since the selectivity is proportional to the square

root of this ratio, not only practical but theoretical enrichments achievable by this method necessarily will be small. In order to have an efficient separation of a gas mixture, many separation stages are required. On the other hand, since this method of separation is based strictly on mass ratios and not chemical differences, it is the only membrane based method capable of separating isotopes of a given compound. This is the reason it was chosen as a method to enrich uranium in the fissionable isotope of mass 235 in the development of the atomic bomb in World War II. This separation method inherently is very expensive–it requires a large amount of hardware for a given amount of processed gas, the membrane specifications are stringent (high porosity, small pore size), and the energy requirements are high. The large scale utilization of such a process has been feasible only because economic considerations are not of prime importance in this application.

The other membrane-based gas separation method utilizes non-porous membranes. In permeating through the membrane, the gases are separated due to differences in their diffusivity and solubility in the membrane matrix (normally an organic polymer). Molecular size will play a role in such separations but so will the chemical nature of the gas. Thus, conceptually very efficient separations should be possible this way. As polymer science developed, many polymers were tested for gas permeabilities and indeed some with very good selectivities were found. For example, many polymers are much more permeable to polar gases (H_2O, CO_2, H_2S, SO_2) than to nonpolar gases (O_2, N_2, CH_4). The gases of smallest molecular size (He, H_2) permeate more readily through polymers than larger molecules (CH_4, C_2H_6).[2] Still it took many years to bring this basic knowledge to practical utilization. The major problem was to make membranes that would be both highly selective and allow high transmembrane gas fluxes, otherwise membrane areas required would be so large as to make the technique uneconomical. The same problem had faced desalination membranes. In the latter case, the solution appeared in the form of the Loeb-Sourirajan membrane,[3] a membrane with an asymmetric cross-section, the top thin part being the selective layer and the remainder a porous, nonselective mechanical support. Still, utilization of this technology in gas separations was not a trivial matter. Asymmetric cellulose acetate reverse osmosis membranes have to be kept wet at all times. Since most gas streams are essentially dry, ways had to be found to make good dry membranes. When cellulose acetate membranes are allowed to dry, they lose their separating power due to morphological changes caused by the large interfacial forces involved. Various interesting approaches were suggested to make dry membranes: for example, casting very thin films on a liquid surface, and then supporting them on a porous substrate.[4] Such techniques proved to be too cumbersome to be easily scalable to industrial production. The significant start toward practical, economical gas separating membranes was the development of methods of drying cellulose acetate membranes in a controlled manner. It was found that dry asymmetric membranes are obtained with good permeabilities and good selectivities in many gas separations (e.g., H_2/CH_4, CO_2/CH_4, H_2O/CH_4) when the wet membranes are either freeze dried[5] or solvent exchanged.[6] Some inherent limitations of cellulose acetate membranes are their sensitivity to liquid water and plasticizing gases and their limited temperature and pressure resistance. A second breakthrough came in the form of composite membranes introduced by Monsanto Company.[7] These membranes are highly

unusual in that unlike classical composites, it is not the top layer but the one below in combination with the top layer that is responsible for the membrane's selectivity. The membrane consists of a polysulfone hollow fiber having a small number of surface imperfections which make it quite non-selective. By coating with a highly permeable, non-selective polymer such as silicone, the flux through the imperfections is diminished sufficiently to make the remainder of the membrane matrix dominant in gas transport. Thus, selectivities approaching those inherent to polysulfone are achieved. Also, permeabilities of the membrane are high due to their small effective thickness which can be controlled in the membrane formation process. This new technology makes it possible to fabricate thin membranes which initially are not perfect as the effect of imperfections essentially is eliminated by the coating. With the exception of some short lived projects,[8,9] Monsanto now operating as a separate subsidiary, Permea Inc., was the first to commercialize gas separation membranes on a relatively large scale. This apparently was an incentive to move dry cellulose acetate membranes to the marketplace and these are being marketed today by a number of companies including Dow, Separex, Envirogenics, W.R. Grace and others. The cellulose acetate membranes are made as hollow fibers or as flat sheets which are used in spiral wound modules. Other membranes, including immobilized liquid membranes and facilitated transport, were reviewed by Matson, et al[10] in 1983.

Since 1983, newer systems for hydrogen separations have appeared. Ube Industries, Ltd. announced the development of a polyimide resin in hollow fiber membrane form for H_2/C_1 separations.[11,12] Commercial production of this membrane and the engineering of skid mounted units were to begin in the fall of 1985.[13]

Systems for air separations appeared in this same time period. Asahi Glass Company, Ltd. started the production of a membrane system which is reported to upgrade the oxygen content in air to 40%.[14] The flat sheet membrane is a fluoropolymer based composite mounted in a plate and frame unit. Air is supplied at atmospheric pressure and the permeate enriched in O_2 is recovered under vacuum. Signal's UOP Fluid Systems Division offers a similar system. Their Spiragas® (trademark of Signal Company) membrane for oxygen enrichment, is an ultrathin silicone on a porous polysulfone backing in a spiral wound permeator.[15,16] Dow Chemical Company more recently announced the sale of the Generon® (trademark of The Dow Chemical Company) air separation system to provide 95% N_2 for blanketing applications.[17] The hollow fiber membrane used in this system is made from a polyolefin. Finally, Monsanto announced the development of a new membrane based on crosslinked polyphenylene oxide[18] which is expected to find initial application in air as well as hydrogen and carbon dioxide separations. More details of these systems will be given later in this chapter.

THEORY OF GAS TRANSPORT IN MEMBRANES

Porous Membranes

The separation of gases by microporous membranes depends on the ratio of pore size to the mean free path which is given by:

$$\lambda = \frac{3\mu}{2P}\left[\frac{\pi RT}{2M}\right]^{\frac{1}{2}} \quad (1)$$

where M = molecular weight
P = pressure
μ = viscosity
R = the universal gas constant
T = temperature

Gases at 20°C and 1 atmosphere have a mean-free-path of 1000 to 2000 Å. If pore size is large relative to the mean-free-path, flow (mols per unit time and area) will be given by Poiseuille's Law.[19]

$$Q = \frac{d^2(p_1^2 - p_2^2)}{64\ \ell\ \mu RT} \quad (2)$$

where p_1 & p_2 = the pressures on the high and low pressure sides of the membrane
d = pore diameter
ℓ = pore length

In such flow, energy exchange among molecules will occur within the pore, and no separation is obtained. If, however, pores are substantially smaller than the mean-free-path, Knudsen flow prevails:

$$Q = \frac{4d\ (p_1 - p_2)}{3\ell\ (2\pi MRT)^{\frac{1}{2}}} \quad (3)$$

As this flow is molecular weight dependent, separation is expected. Ideal separation occurs when downstream pressure is negligibly small. Thus, for a gas mixture:

$$Q_1 = \frac{kp_1x}{M_1^{\frac{1}{2}}} \quad (4)$$

$$Q_2 = \frac{kp_1(1-x)}{M_2^{\frac{1}{2}}} \quad (5)$$

where k is a combination of all constants in Equation 3 excluding M, and x is the mol fraction of gas 1 in the feed, separation factor is defined as:

$$\alpha = \frac{Q_1/Q_2}{x/(1-x)} \quad \text{and equals} \left[\frac{M_2}{M_1}\right]^{\frac{1}{2}}$$

The ideal separation factor for $U^{235}F_6/U^{238}F_6$ is 1.0043. In real separations, the ideal separation factor will not be attained because of various adverse factors including back-diffusion, non-ideal membranes, concentration polarization at the feed surface and surface flow phenomena. Since the actual selectivities obtainable are so small, it is clear that a very large number of stages will be required for efficient separations. For a membrane cascade with undiffused gas recycled to a previous stage, a minimum number of stages will be obtained at total reflux (no product taken out). It can be shown[20] that this number is given by:

$$N = \frac{\ell n\left[\frac{y_D/(1-y_D)}{x_B/(1-x_B)}\right]}{\ell n\ a} \qquad (6)$$

where y & x = the mol fractions of gas 1 in the permeated and non-permeated streams respectively

B = bottom stage

D = top stage

a = stage separation factor given as:

$$a = \frac{y/(1-y)}{x/(1-x)}$$

In actual use, the number of stages obviously will be greater since reflux is not total. Available information indicates that U.S. gas diffusion plants for U^{235} production utilize 10,276 stages. Total membrane area for a given separation is given by[21]:

$$S = \frac{3.914\ \Delta U \ell\ (MRT)^{\frac{1}{2}}}{(\alpha-1)^2\ \sigma\ d} \cdot \frac{1}{p_2\ (1-p_r)^3} \qquad (7)$$

where σ = membrane porosity

p_r = p_2/p_1

ΔU = separative capacity given by:

$$\Delta U = \tfrac{1}{4} L\ (a-1)^2 = 0.48L\ (1-p_r)^2\ (\alpha-1)^2 \qquad (8)$$

where L = total molar flow rate through the membrane.

Non-Porous Membranes

As mentioned earlier, the mechanism of gas separation by non-porous membranes basically is different from the one in microporous membranes. Gas molecules actually dissolve and diffuse in the dense membrane matrix. Differences in permeability, therefore, will result not only from diffusivity (mobility) differences of the various gas species but also from differences in physico-chemical interactions of these species within the polymer, determining the amount of gas that can be accommodated per unit volume of the matrix.

Rubbery Polymers. For polymers above their glass transition temperatures, Tg, the permeation behavior is relatively simple phenomenologically. Solubility of the gas in the polymer, as in liquids, follows Henry's law,

$$C = S.p \tag{9}$$

where C is the equilibrium sorption at partial pressure p, and S is Henry's solubility constant for the particular polymer-gas pair. Gas concentration in the polymer thus is related linearly to the external partial pressure. Both positive and negative deviations from this simple relationship have been observed at high gas pressures. Gas flux through the membrane normally is found to follow Fick's first law.

$$Q = -D \frac{dC}{dx} \tag{10}$$

where D is the diffusivity, defined by this equation, and C is the local concentration of gas in the membrane. The diffusivity normally is concentration independent with some deviations in the case of very soluble gases. Integration over the membranes thickness, ℓ, yields:

$$Q = D \frac{C_1 - C_2}{\ell} \tag{11}$$

where C_1 and C_2 are gas concentrations at the high and low pressure faces of the membrane, respectively, and ℓ is the thickness. Substituting Equation 9 into 11 yields:

$$Q = DS \frac{p_1 - p_2}{\ell} = P \frac{p_1 - p_2}{\ell} \tag{12}$$

where p_1 and p_2 are the external partial pressures of the gas on the high and low pressure side of the membrane and P is the permeability defined by this equation. It is, therefore, given by:

$$P = DS \tag{13}$$

Both P and D (and thus S) can be determined in a single experiment, measuring the "time lag" for pressure increase on the low pressure side of the membrane after high pressure had been applied the other side of the membrane. This time lag, obtained by extrapolating the linear portion of the pressure vs time function back to the time axis (Figure 10.1),[22] is given by:

$$\theta = \frac{\ell^2}{6D} \tag{14}$$

The permeability is given by the slope of the function, and solubility can be calculated by dividing the permeability by diffusivity. For most permanent gases, the permeability coefficient P will be pressure independent for all practical purposes. However, for some gases with high boiling points at temperatures lower than the critical temperature, permeability increases with pressure, reflect-

ing an increase in the solubility constant. The effects of temperature on diffusivity and solubility of gas normally are of opposite signs, i.e., diffusivity increasing and solubility decreasing with increasing temperature. The effect of temperature on permeability is, therefore, a composite of these effects. Under most normally encountered conditions, the effect on diffusivity predominates, and permeability increases with temperature. However, below some temperature solubility can become so high as to reverse the effect. These effects are summarized in Figure 10.2.[23] The effect of temperature on gas selectivity of membranes has not been studied very thoroughly. As a rule of thumb, temperature will have a greater effect on the permeability of the gas with the higher diffusion activation energy, i.e., the less permeable gas. Therefore, it is the usual observation that selectivity decreases with increasing temperature.

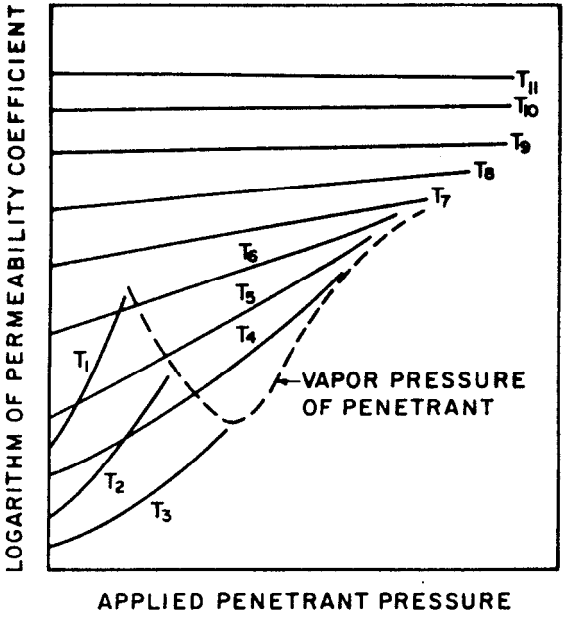


Figure 10.1: Typical result of transient permeation experiment.[23]

Glassy Polymers

Some rubbery polymers are among the most permeable polymers known. Contrary to popular belief, however, it is not true that rubbery polymers as a family are more permeable than glassy polymers. In fact, the most permeable polymers reported to date have quite high glass transition temperatures.[24] An important deficiency of rubbery polymers is their low modulus. Therefore, they will not form thin, self-supporting, pressure resistant membranes. For this reason, most recent interest has been in using glassy polymers to make gas separating membranes. It was found that the solubility of gases in (and hence permeability of) crystalline polymers is extremely low. Therefore, the most practically

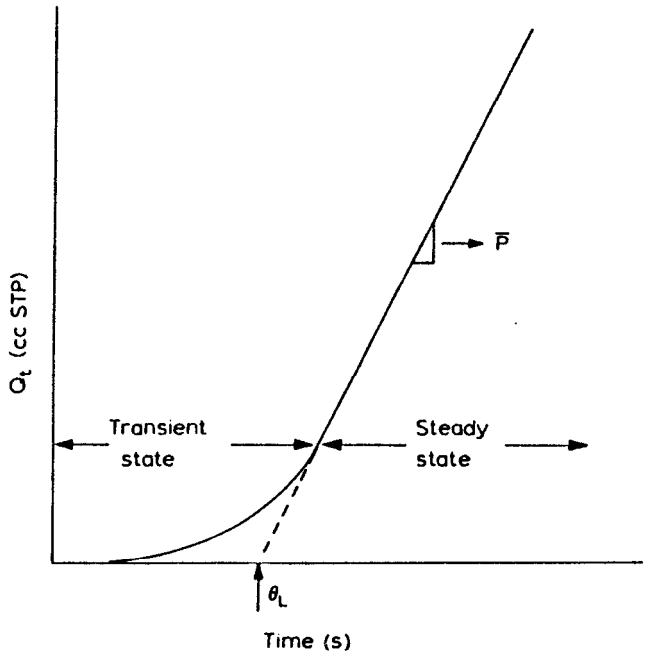


Figure 10.2: Pressure and temperature dependence of permeability.[24]

interesting polymers are amorphous with high glass transition temperatures. Unlike rubbery polymers, sorption of gases in glassy polymers does not follow Henry's law, and a typical sorption isotherm is convex to the pressure axis, as shown in Figure 10.3.[22] This was shown to be the case with a large number of polymers and many gases. One theory that has gained wide popularity in explaining this behavior and a broad range of other experimental data is the dual sorption theory.[22,25,26] It postulates the existence of two types of sorption sites in the glassy polymer. One accommodates mobile gas molecules following Henry's law. The other consists of Langmuir type sites with much less mobile sorbed species. The Langmuir sites have been associated with fixed voids or excess free volume in the glassy state and correlated with the abrupt change in slope of the specific volume vs temperature curve as one passes the glass transition temperature, Figure 10.4.[25] The two sorbed gas populations are in rapid equilibrium throughout the membranes. This behavior is described by the following equation:

$$C = C_D + C_H = Sp + \frac{C'_H \cdot bp}{1 + bp} \qquad (15)$$

where C_D = solubility in the Henry type sites
C_H = solubility in the Langmuir type sites
C'_H = hole saturation constant
b = hole affinity constant

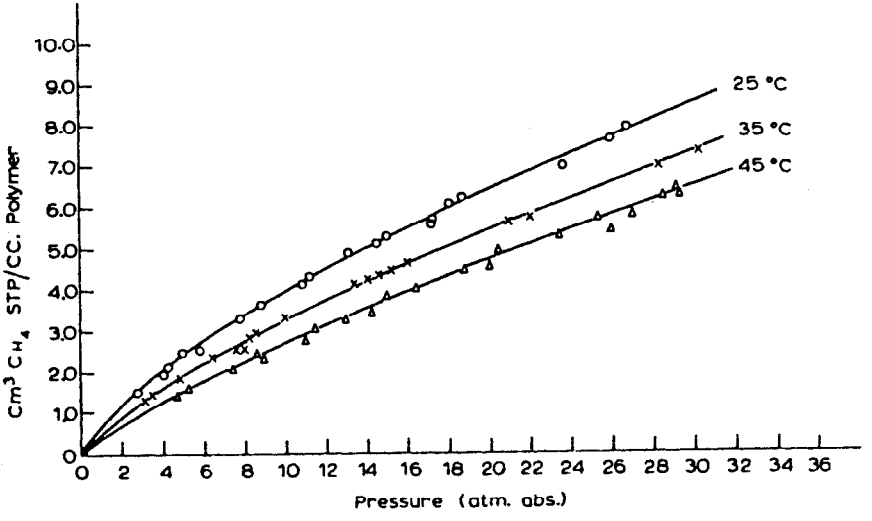


Figure 10.3: Solubility of methane in polystyrene.[23]

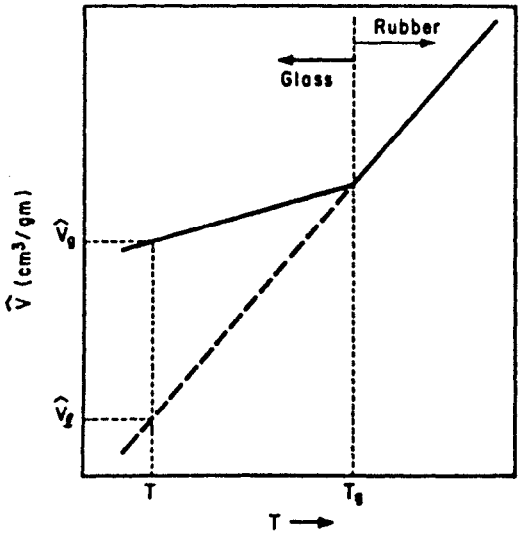


Figure 10.4: Specific volume dependence on temperature in the region of the glass transition.[26]

Sorption behavior at low and high pressure is consistent with the model: At low pressures ($bp < 1$), Equation 15 reduces to:

$$C = (S + C'_H\, b)\, p \tag{16}$$

a modified Henry-like behavior. At high pressure ($bp \gg 1$), Equation 15 becomes:

$$C = Sp + C'_H \tag{17}$$

indicating saturation of the Langmuir sites. Thus, C is a linear function of p at both low and high pressure with a nonlinear region in between. This corresponds well with the results as shown in Figure 10.3. These mathematical relations allow the determination of the various dual sorption parameters. Thus, from the pressure dependence of C at high pressures (Equation 17), S and C'_H can be determined from the slope and intercept, respectively. Writing the Langmuir part of the sorption equation:

$$C_H = \frac{C'_H\, bp}{1 + bp} \tag{18}$$

rearranging to

$$p/C_H = 1/C'_H\, b + p/C'_H \tag{19}$$

and plotting p/C_H vs p, one can determine C'_H and b (C'_H is obtained as the difference between total sorption and Sp).

Total solubility of gases in glassy polymers is higher than in rubbers, which is consistent with the apparent existence of an additional sorption site in such polymers. The temperature dependence of Henry's law constant

$$S = S_o e^{-\Delta H_D/RT} \tag{20}$$

and the dependence of the Langmuir constant:

$$b = b_o e^{\Delta H_H/RT} \tag{21}$$

enable the determination of the sorption enthalpies into the various sites. It was found that the Henry-type sorption enthalpy, ΔH_D, is of the same order as that in rubbers, whereas the enthalpy for sorption in Langmuir sites, ΔH_H is appreciably higher. This accounts for the empirical finding that gas sorption in glassy polymers is substantially more exothermic than in rubbers, and it is explained in dual sorption theory by the sorption of gas into preexisting sites rather than sites that need to be formed by polymer molecular reorientations (as in rubbers).

While the permeability of most rubbery polymers to most gases is pressure independent, the permeability of glassy polymers usually is observed to decline with increasing pressure. This is accounted for by the dual sorption theory if one assumes that both the Henry and Langmuir type sites contribute to per-

meability.[25] Thus, a modified one dimensional Fick's law is:

$$Q = -D_D \frac{dC}{dx} - D_H \frac{dC}{dx} \tag{22}$$

where D_D and D_H are the diffusivities of gas molecules associated with the Henry and Langmuir environments respectively. Solution of this equation yields

$$P = SD_D \left[1 + \frac{FK}{1+bp}\right] \tag{23}$$

where $F = D_H/D_D$ and $K = C'_H\, b/S$.

The time lag also takes on a more complicated form:

$$\theta = \frac{\ell^2}{6D} \quad [1 + f\ (K,F,bp)] \tag{24}$$

where the function f is too complex to reproduce here.

For very high values of bp, such as at high pressures, when Langmuir sites are saturated and thus do not participate in transport, Equation 23 reduces to the simple Henry form.[13]

At low pressure, the following limiting forms are obtained:

$$P = SD_D + b\ C'_H\ D_H \tag{25}$$

$$\theta = \frac{\ell^2\ (1+K)}{6D\ (1+FK)} \tag{26}$$

These relationships were demonstrated for many gases in various polymers. In spite of its wide acceptance and success in representing a large amount of experimental data, the dual sorption theory has come under attack recently. One reason is that it has never been demonstrated conclusively that two sorbed gas molecule populations actually exist in polymers. An alternate model was suggested–the matrix model.[27] In this model, it is assumed that only a single population of sorbed gas molecules exists and that the gas changes the properties of the polymer matrix over the entire pressure–concentration range in a continuous manner. Mathematical expressions were developed to describe the dependence of solubility, apparent diffusivity, permeability and time lag on gas concentration. These are at least as successful as dual sorption expressions in describing experimental data. Thus, the concentration dependent solubility constant is given by:

$$S = \frac{S_o}{1 - \alpha C} \tag{27}$$

where C is the equilibrium concentration of gas in the matrix and α is a constant. The concentration dependent diffusivity is given by:

$$D = D_o\ (1 + \beta C) \tag{28}$$

β, the "interaction parameter" is positive for a plasticizing gas and negative if the gas has antiplasticizing effect. By solving Fick's first law with the appropriate expression for the diffusivity, one obtains the concentration dependent permeability as:

$$P = D_o S_o \frac{(1 + \beta C)}{(1 + \alpha C)} \tag{29}$$

The expression for the concentration dependent time lag is:

$$\theta = \frac{\ell^2}{6D} \frac{10 + 15\beta C + 16\beta^2 C^2}{10\ (1 + \beta C)^3} \tag{30}$$

The fit of these expressions to experimental results is very good. At low pressure regimes, the fit was shown to be even better than that of dual sorption expressions. Except for these regimes, the two models seem to do equally well in describing sorption and permeability data. Concentration dependent diffusivity and permeability have been considered before mainly for vapors. The new aspect of the matrix model is that it broadens these effects to fixed gases. The important difference between the matrix and dual sorption models is in the physical picture they convey of gas transport and interaction with the polymer. Additional experimental evidence will be needed to determine the preference of these different physical representations.

The theories described above, though successful at correlating many experimental data, are phenomenological in nature. Attempts have been made also to explain gas diffusion in polymers on a molecular basis. One of the more recent theories is that by Pace and Datyner[28] which elaborates on earlier theories of Brandt[29] and DiBenedetto.[30] Gas molecules are viewed as being trapped in channels formed from polymer chains over short distances. Longitudinal diffusion along these channels is very rapid with low activation energy. The true activation energy for diffusion is that associated with transverse diffusion out of the molecular cage which depends on polymer chain reorientation. The theory provides an expression for the activation energy for diffusion based on first principles. The expression predicts an apparent activation energy (that obtained from an Arrhenius plot) which is independent of temperature above and below Tg, with the value above Tg higher than below. This general behavior is indeed observed experimentally. The theory also derived an expression for the diffusion constant; however, it contains a parameter, the mean-square-jump displacement of the diffusant, which cannot be determined as yet.

ENGINEERING ASPECTS

The efficiency of a gas separation process can be described by essentially two parameters: the purity of the product gas and the fraction of that gas in the feed recovered as product (the recovery). These parameters in turn will be determined by the membrane's intrinsic properties–its permeability and selectivity and by operating factors such as total and partial pressures on the feed and

permeate sides, feed flow rate and pressure drop on either side of the membrane. These factors will determine the membrane area and compression energy necessary for a given separation, and only with all these parameters can an economic evaluation of the process be made.

The basic engineering analysis of gas separations by membranes was made by Weller and Steiner[31,32] long before good, practical membranes were developed, but it is still useful as a good approximation. Assuming a binary gas feed and laminar flow on both high and low pressure sides of the membrane, permeate composition at any point will be determined by the transport rate of the two gases at that point:

$$-dn_A = P_A\, dA\left[p_1 \frac{n_A}{n_A + n_B} - p_2 \frac{dn_A}{dn_A + dn_B}\right] \tag{31}$$

$$-dn_B = P_B\, dA\left[p_1 \frac{n_B}{n_A + n_B} - p_2 \frac{dn_B}{dn_A + dn_B}\right] \tag{32}$$

where P_A & P_B = the membrane's permeability to gases A and B respectively,

p_1 & p_2 = total pressures on the high and low pressure side respectively,

n_A & n_B = the numbers of mols of gases A and B flowing per unit time on the high pressure side, and

dn_A & dn_B = permeation rates.

An analytical solution to these equations giving the molar ratio of component B leaving and entering the membrane stage is:[29]

$$\ell n \frac{n_B^f}{n_B^o} = R\ell n \frac{t^o - B/A}{t^f - B/A} + U\ell n \frac{t^o - \alpha + C}{t^f - \alpha + C} + T\ell n \frac{t^o - C}{t^f - C} \tag{33}$$

where $\alpha = P_A/P_B$

$A = [(1 - \alpha)p_2/p_1 + \alpha]/2$

$B = -AC + \alpha/2$

$C = -[(1 - \alpha)p_2/p_1 - 1]/2$

$R = 1/(2A - 1)$

$U = [\alpha(A - 1) + C]/(2A - 1)(\alpha/2 - C)$

$T = 1/(1 - A - B/C)$

$t = -Ai + [A^2i^2 + 2Bi + C^2]^{1/2}$

$i = n_A/n_B$

Once n_B^f (rate of gas B leaving the high pressure side) has been determined, bore composition can be calculated by mass balance:

$$y = \frac{n_A^o - n_A^f}{n_A^o - n_A^f + n_B^o - n_B^f} \tag{34}$$

where y is the mol fraction of gas A in the permeate, o and f denote entering and leaving, respectively. The recovery of gas A will be given by:

$$\frac{n_A^o - n_A^f}{n_A^o}$$

Obviously, the higher the recovery the lower the purity of the permeated gas. In the special case of zero recovery or complete mixing (and therefore, constant shell and bore compositions along the membranes), an especially simple expression is obtained by dividing Equation 31 and 32:

$$\frac{y}{1-y} = \alpha \frac{p_1 x - p_2 y}{p_1(1-x) - p_2(1-y)} \tag{35}$$

where y = the mol fraction of gas A in the permeate

x = the mol fraction of gas A on the high pressure side

α = the separation factor P_A/P_B

If, in addition, bore pressure is zero, $p_2 = 0$, the selectivity and the mol fractions show the simple relation:

$$\frac{y/(1-x)}{x/(1-y)} = \alpha \tag{36}$$

Equation 35 clearly shows that product purity is directly related to membrane selectivity. Solving the quadratic Equation 35 for y yields:

$$Y = \frac{-B + [B^2 + 4(1-\alpha)\ \alpha(p_1/p_2)x]^{\frac{1}{2}}}{2(1-\alpha)} \tag{37}$$

where $B = (\alpha - 1)(p_1/p_2)x + p_1/p_2 + \alpha - 1$

Thus, an increase in total pressure ratio p_1/p_2 will improve purity for a given α. The various effects of pressure ratio and membrane selectivity are shown in Figure 10.5.[33] It will be observed that under certain conditions the pressure ratio is of even greater importance than intrinsic selectivity. Thus, with a feed gas relatively poor in the more permeable component, and an α of about 40, further increase in selectivity has little effect on product purity, whereas an increase in

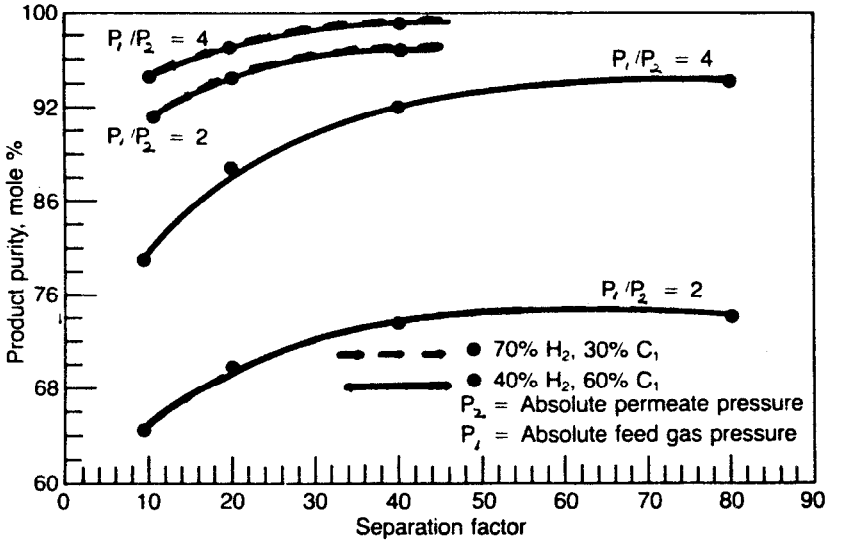


Figure 10.5: Product purity as a function of feed composition and membrane selectivity.[33]

pressure ratio has a substantial effect over the whole selectivity range. The effect of pressure ratio is much smaller if the feed gas is already rich in the more permeable component. It is seen that with any feed composition the effect of membrane selectivity on product purity reaches a plateau above some α value. Therefore, research effort to develop super-selective membranes always should be considered with this trend in mind.

One of the main determinants of process economics is the membrane area required for a given separation. The exact solution, obtainable by numerical methods, is:

$$S = \frac{n_B^o}{p_B} \int_{i^f}^{i^o} \frac{\text{antiln}\,[n_B(i)/n_B^o]\,di}{[f(i)-1][p_1(1/(i+1)) - p_2(1/(f(i)+1))]} \tag{38}$$

where $i = n_A/n_B$

$f(i) = Ai - C + [A^2i^2 + 2Bi + C^2]^{1/2}$ (see Equation 33)

A good approximation for the area can be obtained by averaging the solutions of Equation 35 for inlet and outlet compositions. Thus, a permeate mol fraction at the inlet, y^o, can be determined from:

$$\frac{y^o}{1-y^o} = \alpha \frac{p_1 x^o - p_2 y^o}{p_1 (1-x^o) - p_2 (1-y^o)} \tag{39}$$

(x^o is the mol fraction of gas A at the feed inlet). If it is desired to obtain Δn_A mols of gas A per unit time, a corresponding area will be:

$$S^o = \frac{\Delta n_A}{p_A(p_1 x^o - p_2 y^o)} \tag{40}$$

A similar expression can be written for the stage outlet, and the average of the two areas is taken as the approximate required area. The area is thus seen to be inversely proportional to fast gas permeability and partial pressure differential.

It should be realized that the membrane contributes only a part (sometimes a small part) of total capital cost of the separation system. Compressors, pretreatment facilities and mounting may amount to more than membrane cost. Pretreatment to remove contaminants harmful to the specific membrane can be especially costly. It is, therefore, desirable to have membranes that are highly environmentally resistant or that can be operated under conditions (e.g., high temperature) in which the solubility of the contaminants in the membrane is low. Compression may be a major factor in system operating cost. Therefore, membranes with high permeabilities are desired to minimize the need for high driving force and to minimize membrane area. If membrane selectivity is too low, multistaging will be necessary. As a rule, this will increase both capital and operating cost due to the additional membrane area required and the recompression between the stages.

Gas separation by membranes will always have to compete with other separation processes such as cryogenics, absorption and adsorption systems. Membranes usually are less competitive in very large scale operations where the fast gas is less than about 20% of the feed gas, unless the slow gas is the desired product. Membranes also are not usually the method of choice when extremely pure product gas is required. Membranes do, however, have distinct advantages in small to medium scale operations, in situations where gas is available at pressure, in situations where high recovery is paramount, and in applications where simplicity and minimal maintenance are of prime importance (such as in remote locations). Membranes are very well suited for applications in which the nonpermeate is the product of interest, since it is obtained at pressure. Examples are acid gas removal from natural gas and gas dehydration.

PREPARATION OF MEMBRANES FOR GAS SEPARATION

Permea's (Monsanto) Composite Membrane

Membranes to be used in practical gas separations have to satisfy many requirements; they have to exhibit high fluxes so as not to demand excessive membrane areas for large volume gas processing. They must have good selectivities in order to offer product gas streams of high purity. They must be able to withstand the high gas pressures often encountered in natural and industrial streams. They must withstand reasonable concentrations of contaminants often accompanying the gases of interest (e.g., H_2O, H_2S, hydrocarbons).

It was the combination of these stringent requirements which impeded the development of useful gas separating membranes for so many years. Obviously,

one of the most difficult requirements is the achievement of high permeability and high selectivity simulataneously. A similar problem had hampered the development of reverse osmosis membranes. It was solved brilliantly in the asymmetric Loeb-Sourirajan membrane, having a thin selective layer supported by a much thicker porous, non-selective matrix. In this membrane, the fact was exploited that whereas permeability is thickness dependent, selectivity–being a ratio of permeabilities–is not. The problem with gas separation membranes is even more severe. Reverse osmosis membranes can show good salt rejection even if slightly porous, by virtue of electrostatic interactions (non-availability of free water to solvate ions inside small pores). Most common gases are of very small effective diameters (2 to 5 Å) and mechanisms such as the above to increase selectivity are not available. Also, permeabilities of gases in polymer matrices are usually very low,

$$10^{-12} - 10^{-8} \frac{\text{Scc - cm}}{\text{cm}^2\text{-sec-cmHg}}$$

Therefore, membranes for gas separation are extremely sensitive to the existence of even a relatively few small imperfections, due to the very high permeability of such holes relative to the imperfection-free areas. The solution developed by Monsanto is unique in that it circumvented the need to make a perfect membrane by devising a special coating procedure.[34] On coating the membrane with a thin layer of a highly permeable, non-selective polymer, the permeability through the holes is reduced sufficiently to make the permeation through the matrix predominant (Figure 10.6). Performance close to that expected from intrinsic (dense film) properties is thus achieved. The materials presently used in Permea's (a Monsanto Company) commercial membranes are a polysulfone as the matrix and a silicone rubber as a coating. However, the method is general and any matrix-coating combination with the appropriate permeability ratio can be used. A numerical example will illustrate the utility of such membranes in the separations of CO_2 from CH_4.

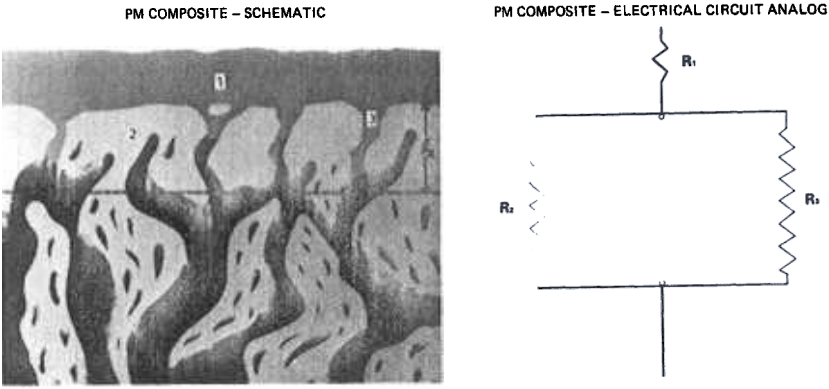


Figure 10.6: Schematic representation of Monsanto's composite membrane. Cross-sectional view on left, electrical circuit analog on right.[34]

Assume a polysulfone fiber with an effective thickness of 1000 Å and a surface porosity of 10^{-6} (ratio of pore area to total area). The fiber is coated with a silicone at a thickness of 1 μm. The intrinsic permeabilities of polysulfone and silicone are:

$$PCO_2 \text{ (polysulfone)} = 6 \times 10^{-10} \quad \frac{Scc - cm}{cm^2\text{-sec-cmHg}}$$

$$PCH_4 \text{ (polysulfone)} = 0.2 \times 10^{-10} \quad \frac{Scc - cm}{cm^2\text{-sec-cmHg}}$$

$$PCO_2 \text{ (silicone)} = 3500 \times 10^{-10} \quad \frac{Scc - cm}{cm^2\text{-sec-cmHg}}$$

$$PCH_4 \text{ (silicone)} = 800 \times 10^{-10} \quad \frac{Scc - cm}{cm^2\text{-sec-cmHg}}$$

Remembering that the permeability term P/ℓ (where ℓ is the effective membrane thickness) is reciprocal resistance, the total CO_2 resistance of the membrane will be:

$$\left(\frac{P}{\ell}\right)_{CO_2} = \left[\left(\frac{P_{CO_2}}{\ell}\right)_{Si}^{-1} + \left[\frac{(PCO_2)\,Si \times porosity + (PCO_2)PS}{\ell_{PS}}\right]^{-1}\right]^{-1}$$

thus

$$(P/\ell)\ CO_2 = \left[\left(\frac{3500 \cdot 10^{-10}}{10^{-4}}\right)^{-1} + \left(\frac{3500 \cdot 10^{-10} \cdot 10^{-6} + 6 \cdot 10^{-10}}{10^{-5}}\right)^{-1}\right]^{-1}$$

$$= 61 \cdot 10^{-6}\ \frac{Scc}{cm^2\text{-sec-cmHg}}$$

Similarly for methane

$$(P/\ell)\ CH_4 = \left[\left(\frac{800 \cdot 10^{-10}}{10^{-4}}\right)^{-1} + \left(\frac{800 \cdot 10^{-10} \cdot 10^{-6} + 0.2\ 10^{-10}}{10^{-5}}\right)^{-1}\right]^{-1}$$

$$= 1.99 \cdot 10^{-6}\ \frac{Scc}{cm^2\text{-sec-cmHg}}$$

the separation factor,

$$\alpha = \frac{(P/\ell)CO_2}{(P/\ell)CH_4} = 30.6$$

is essentially identical to the intrinsic (dense film) separation factor of ~30.

The uncoated membrane has a much lower selectivity: assuming cylindrical pores, the molar Knudsen flow through the pores will be given by:

$$Q = \frac{4d}{3\ell}\ \frac{p_1 - p_2}{(2\pi MRT)^{1/2}}$$

where d = Pore diameter

ℓ = Pore length

M = Molecular weight

R = Gas constant

T = Absolute temperature

If the pressure differential is 1 atmosphere, CO_2 flow through the pores in our example will be:

$$112 \times 10^{-6} \frac{\text{cc STP}}{\text{cm}^2 \text{ membrane area-sec-atm}}$$

methane flux will be

$$186 \times 10^{-6} \frac{\text{cc}}{\text{cm}^2 - \text{sec} - \text{atm}}$$

The corresponding fluxes through the polysulfone matrix will be

$$\text{for } CO_2: \frac{6 \times 10^{-10}}{1000 \times 10^{-8}} \times 76 = 4560 \times 10^{-6} \frac{\text{cc}}{\text{cm}^2 - \text{sec} - \text{atm}}$$

and for methane

$$\frac{0.2 \cdot 10^{-10}}{1000 \cdot 10^{-8}} 76 = 152 \times 10^{-6} \frac{\text{cc}}{\text{cm}^2\text{-sec-atm}}$$

Adding reciprocal permeabilities as resistances, overall selectivity will be

$$\alpha\ CO_2/CH_4 = \frac{4672}{338} = 13.8$$

The coating thus eliminates the detrimental effect of the imperfections without affecting the flux in any major way.

It can be shown that the coating technique will give an almost constant performance over a wide range of surface porosity (Figure 10.7). Only at relatively high porosity (10^{-3} or higher) will flux of the slower gas through the plugged pores become large enough to adversely affect the selectivity. Also, the technique is not very sensitive to coating thickness and only at thicknesses of 1 μm or greater will the coating contribute significantly to the total resistance (thus lowering selectivity). It is this flexibility and the freedom from very stringent and expensive process control which makes this technology so attractive.

A number of advantages of this kind of composite membrane are noteworthy. It is not sensitive to water and, therefore, feed streams do not have to be dry. Its temperature resistance is good and, therefore, operation at elevated temperatures is a simple and inexpensive way to minimize the effect of contaminants and to increase permeability. The pressure rating is excellent, and the

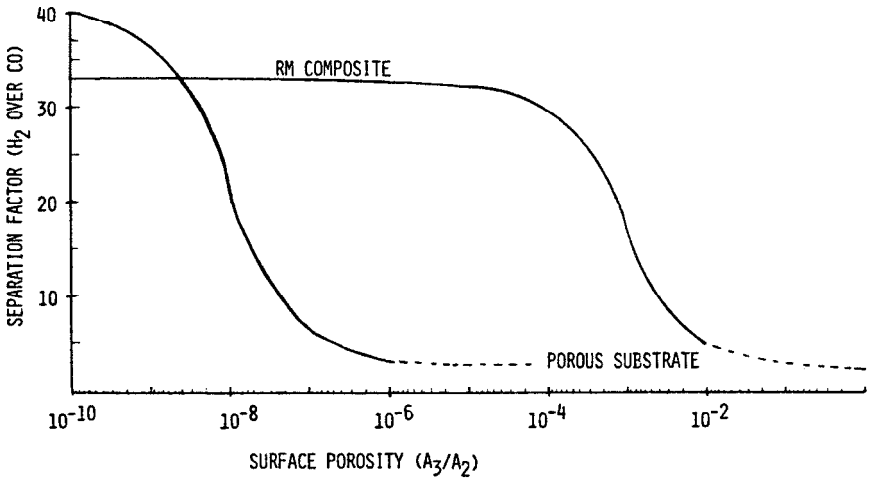


Figure 10.7: Effect of surface porosity on the separation factor (H_2/CO) for a porous substrate and Monsanto's composite membrane.[34]

membranes perform well for extended periods in high pressure feeds such as those encountered in ammonia plants.

The composite membranes were made into successful systems thanks to various additional developments, including appropriate chemical and pressure resistant module seals[35,36] and shell design. These membranes were first used in house and by now have found numerous applications throughout the world.

Dry Cellulose Acetate Membranes

As stated previously, asymmetric cellulose acetate reverse osmosis membranes are kept wet at all times. Uncontrolled drying brings about a loss of selectivity. This results from the large interfacial forces developing during drying of the small pores of this hydrophilic polymer. Such uncontrolled drying can occur on exposing a wet membrane to a gas stream. Therefore, techniques had to be found to dry cellulose acetate in a controlled manner before the membranes could be used to separate gases. In 1968, it was suggested that drying by solvent exchange could lead to a good gas separating membrane.[6,37] The procedure called for soaking the wet membrane in isopropanol for half an hour followed by toluene for several hours. Water is thus removed by dissolution in the alcohol and all polar solvent is removed before exposure to air. It was soon learned that surfactant treatment or freeze drying would achieve a similar result.[38,39]

Thus, a freeze dried membrane showed a He permeability of

$$3 - 10 \times 10^{-5} \frac{cc}{cm^2 - sec - cmHg}$$

and α He/N_2 selectivity of 34–46 vs 97 for the dense film. Apparently, a small number of defects were present in the membrane. Improvements in the drying procedure were then developed such as carrying out the solvent exchange at low temperature.[40] For example, a membrane treated at 0°C with n-butanol followed by n-heptane showed (P/ℓ) He of

$$280 \times 10^{-6} \frac{cc}{cm^2 \quad sec - cmHg}$$

and a He/CH_4 of 62. Heat treatment at 95°C following the drying was found to be beneficial, increasing He/CH_4 selectivity to 75.

Cellulose acetate membranes have been suggested for hydrogen recovery, CO_2/CH_4 separations, gas dehydration and for nitrogen enrichment.[41–43]

Composite Polyimide Membranes

Ube Industry, Ltd. introduced a polyimide membrane which is reported to be made from a condensation polymer of biphenyltetracarboxylic anhydride and an aromatic diamine such as 4,4'-diaminodiphenyl ether or a mixture of two diamines.[44–46] The comparison in Table 10.1 indicates the intrinsic permeabilities for H_2 in these polyimides are similar to polysulfone, and the H_2/CO selectivities are two times greater. Likewise the O_2/N_2 selectivities are twice those of polysulfone, but the O_2 permeabilities are only one-half the polysulfone values. These polyimide materials are good candidates for gas separation membranes owing to their high selectivities, high insolubilities, and high strengths and glass transition temperatures.[45,46]

Asymmetric membranes are made from solution in the form of a hollow fiber, but the process used to form a thin, pore free dense layer on these hollow fibers is not disclosed.[45,46] However, US patent 4,440,643[12] describes a unique process for producing pore-free polyimide composite membranes. An asymmetric polyimide porous substrate is prepared from solution. When fully imidized, the substrate is insoluble. The substrate can now be coated with a polyamic acid from dilute solution (~1%). When fully imidized, the resultant polyimide coating becomes the separating layer. This process allows use of the same or different polyimides for the substrate and the separating membrane. While the examples in the reference describe preparation of flat sheet membranes, this process could be used to prepare hollow fiber membranes.

A recent report[49] indicates the permeabilities of the composite hollow fiber membranes made by Ube may be considerably lower than those of polysulfone when compared at the same temperature. The Japanese literature suggests higher permeabilities than given by Reference 49. It is not known which is the case for the membranes actually used in the separators. The polyimides are reported to be capable of sustained, higher temperature operation to give permeabilities comparable to those of polysulfone while still retaining adequate selectivity.[45,46]

The cited references indicate the hollow fibers are assembled and installed in a module of a design very similar to that employed by Permea. The success of sustained, high temperature operation, which may be needed for permeability, will depend on the development of heat resistant end seal materials. The materials must not only withstand high temperatures, but also survive the effects of

Table 10.1: Intrinsic Permeabilities and Ideal Separation Factors for Selected Polymers

Polymer (Reference)				H_2/CO	H_2/CH_4	H_2/N_2	CO_2/CH_4 [b]	O_2/N_2
Polysulfone[c] (7, 47)	13	6	1	40	60	72	25-30	6
Polyimide (44, 46)	9	-	0.5	76	~200	~200	-	11
Poly(4-methyl pentene-1) (48)	136	93	32	-	-	17	-	4
Crosslinked PPO (18)	22	9	2.3	37	55	56	22	6
Silicone Rubber (51)	550	271	501	-	0.7	2	0.3	2
Cellulose Acetate (64)	12	6	1	40	60	70	30	5.5

(a) Units are cm^3 (STP)-cm/cm^2 sec cmHg at temperatures of 25°-35°C.
(b) Low pressure (<20 atm). The separation factor of this pair varies with pressure.
(c) Product of Union Carbide Corp.

temperature cycling and stream contaminants to prevent failure by cracking.

Polyolefin Membranes for Air Separation

The membrane is made from a polyolefin. Based on work Dow did for the Federal Aviation Agency and reported performance capabilities, it is believed that poly(4-methylpentene-1) is used.[17] A comparison of the intrinsic permeabilities of this polymer with polysulfone and polyimide is given in Table 10.1. Poly(4-methylpentene-1) is highly permeable, but it has low selectivities as indicated by the O_2/N_2 pair data and the α of 17 for H_2/N_2. While the melting point of this crystalline polymer is high, 235°C, the glass transition temperature[50] is much lower than polysulfone or polyimide necessitating operation of a membrane system at temperatures close to ambient to maintain the best selectivities.

The membrane is made in hollow fiber form. It is melt spun to nominal dimensions of 40 μm outside diameter and 30 μm inside diameter to give a wall thickness of about 5 μm. The wall thickness of a melt spun membrane is much thicker than the effective separating layer of an asymmetric membrane which is on the order of 0.1 μm. However, the permeability of the polyolefin is high and the small dimensions allow use of a very large membrane area in a compact unit which together compensate for the large membrane thickness. A disadvantage of small dimension fiber is the large pressure drop in the bore side due to capillary flow which limits the length of the fiber in the separating unit and therefore the area. This effect is accommodated by appropriate module design. This membrane is well suited for air separations, but the low selectivities will prevent its application to hydrogen in carbon dioxide separations.

Other Membranes

Signal's UOP Fluid Systems Division Spiragas (a trademark of Signal Co.) membrane is prepared from an ultrathin silicone material on a porous polysulfone flat sheet. A spiral wound module is prepared from this membrane. Silicones, typically, have very high permeabilities and low selectivities.[2,51] For this reason, Spiragas is sold for oxygen enrichment applications rather than a system to produce nitrogen of greater than 95% purity.

The Asahi Glass membrane also is reported to be a composite based on a fluoropolymer. Flat sheets are assembled into a plate and frame module design rather than spiral wound.

Monsanto announced the development of a crosslinked polyphenylene oxide membrane early in 1985.[18] While the intrinsic permeabilities of this material are lower than polyphenylene oxide, they are higher than those of polysulfone, Table 10.1. The membrane is made by brominating PPO followed by base crosslinking. The transport properties of this material can be manipulated by altering the bromine content and degree of substitution in the ring or methyl groups. The bromine on the methyl group reacts readily with bases affording the opportunity for crosslinking and further transport property modification. This material is spun into hollow fiber membranes using Monsanto technology. Typically, the fiber is treated with aqueous ammonia followed by coating with a silicone rubber.[7,18] The membrane is reported to be more resistant to stream contaminants and due to the higher permeabilities is more productive than polysulfone.

Membrane Testing and Evaluation

Since gas separation by membranes is a relatively recent development, it is still quite common to base selectivity determinations on pure gas tests. This will sometimes give a reasonable estimate of membrane performance but can often lead to erroneous results. The reason is that in many cases one gas in a mixture will influence the transport of the other gases. Usually selectivity measured with mixtures will be lower than that obtained from pure gas measurements.

Also from the discussion in Chapter 1, it is clear that membrane performance will be strongly influenced by testing conditions, i.e., pressure and temperature. Therefore, it is most advisable in evaluating membranes to test them under conditions as close as possible to actual operating conditions.

Future

Present day membranes are capable of separating mainly inherently "fast" gases (e.g., H_2, CO_2) from inherently "slow" gases (e.g., N_2, CH_4). Current technology is not sufficiently refined to efficiently separate different traditionally slow gases (such as N_2 from CH_4, hydrocarbons from each other). Such separations can, in principle, be achieved by facilitated transport. In this process, imitating the function of biological membranes, the membrane contains a compound interacting specifically with only one of the feed constituents. With appropriate binding constants and binding kinetics, very efficient separations can be obtained. To date most work in this area has been confined to liquid membranes (thin liquid films, liquid in liquid microcapsules or liquid impregnated solid films). Transport facilitation was demonstrated for O_2, N_2, CO_2, H_2S and ethylene (extensive work was done on ion transport in liquids). The most practically advanced facilitated gas transport system has been the ethylene/ethane separation studied at Amoco.[52] This separation, based on aqueous silver ion, was scaled up to pilot plant size. Technical problems that have not yet been solved in these systems are associated mainly with the need for water in the membrane and hence in the feed streams. It is difficult to prevent the membrane from drying at all times, especially at high pressure differentials. Once such problems are solved in an economical way, new, previously impractical gas separations should become possible.

APPLICATIONS OF GAS SEPARATING MEMBRANES

Within a relatively short period after their commercialization, membranes for gas separation have been utilized in a wide variety of applications. Among these applications are recovery of hydrogen from purge streams such as encountered in ammonia plants, retrofit chemical plants and from hydroprocessors in refineries. Membrane systems have been introduced into oil fields for CO_2 recovery from well-head gas in enhanced oil recovery, and they have been used to separate oxygen from nitrogen in air. Also, they have been utilized in combination with other recovery systems, such as cryogenic and adsorption, to both reduce cost and increase efficiency.

These applications will be discussed in detail in the remainder of this chapter. The cross section of a PRISM® (trademark of Monsanto Co.) separator is

shown in Figure 10.8. It is a simple, sturdy structure providing feed inlet and outlet for permeate and non-permeate. Feed and permeate flow is countercurrent and the fibers have one end plugged near the non-permeate outlet.

Hydrogen Recovery

Wasted hydrogen from the inert purge of reactors can be recovered by membrane separator systems. This hydrogen had normally been either flared or burned for fuel, and its chemical value was lost. The ammonia purge gas recovery system was developed at the Monsanto ammonia plants in Luling, Louisiana.[53] Figure 10.9 shows a two-stage pressure operation which maximizes recovery while minimizing recompression costs. Systems can now be designed with hydrogen recoveries as high as 95% at a purity of 88%. Operation at differential pressures up to 1,650 psi has been demonstrated.

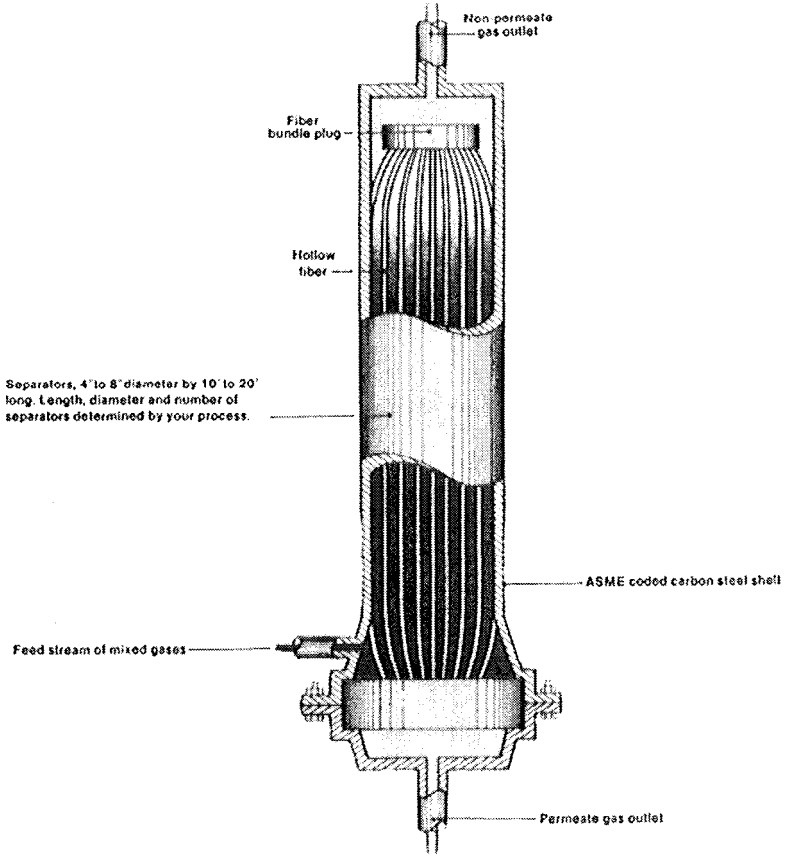


Figure 10.8: PRISM® separator.

Between 1979 and 1985, forty-five PRISM® separator recovery systems have been successfully implemented on ammonia purges around the world. As a result of hydrogen recovery, an incremental ammonia production of 3 to 5% can be achieved. Alternatively, at constant ammonia production energy savings amount to 0.6 to 0.9$\overline{M}$ BTU/ton ammonia. For a typical 1,150 ton/day plant, these improvements translate into \$3$\overline{M}$/year energy savings.

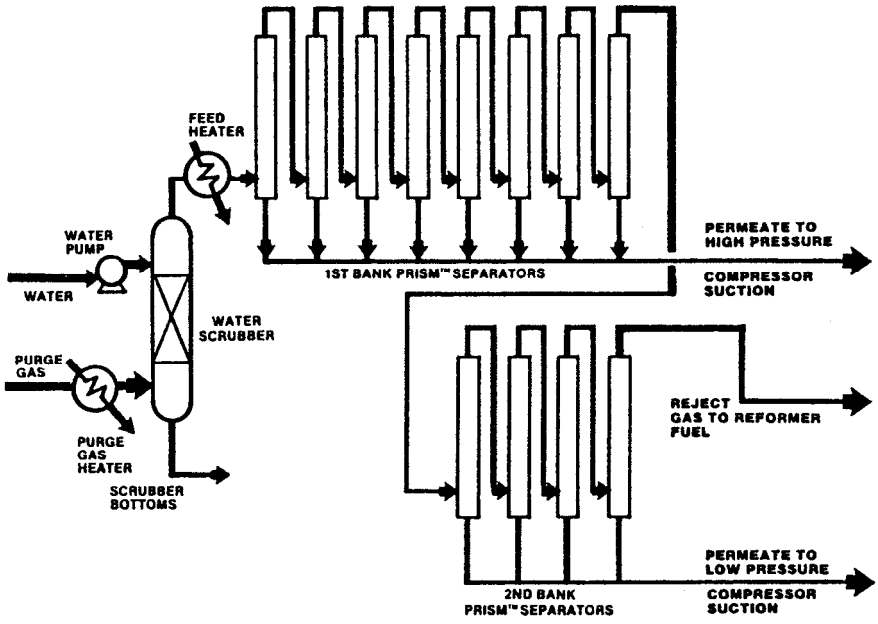


Figure 10.9: Hydrogen recovery from ammonia plant purge.[53]

Prior to entering the hollow fiber PRISM® separators, the feed gas is passed through a water scrubber. This serves a dual purpose of recovering ammonia and extending the fiber life. The ammonia scrubber pretreatment alone contributed about \$200,000/year to the equipment payback in recovered ammonia.[54] Typically, the recovered hydrogen is recycled back to the ammonia synthesis compressor. However, if a source of high purity hydrogen is needed within the complex, some or all of the gas from the first bank of separators can be used for that application. If higher purity hydrogen is desired, the permeate from the first bank can be processed by an additional PRISM® separator to produce, for example, 99% hydrogen.

In methanol synthesis purge recovery, a water scrubber is also used with a similar purpose, and it too pays for itself in recovered methanol. The methanol/water mixture is simply sent to the existing crude methanol distillation column. Hydrogen recovered from this purge can result in energy savings or if additional carbon oxide is available, it can be used to obtain increased methanol production. PRISM® separators have operated on stoichiometric as well as non-

stoichiometric $H_2/(CO)_X$ ratio methanol plants at 75° and differential pressures up to 1,000 psi.

As a major user of expensive and often scarce hydrogen, hydrocrackers are also prime candidates for hydrogen use optimization. This enables not only the conservation of hydrogen by purge recovery, but also high-pressure loop modifications to adjust hydrogen partial pressure in the reactor. A simplified process flow diagram of a typical hydrocracker is shown in Figure 10.10. The oil and hydrogen feed (including recycle hydrogen) are charged to the reactors at the desired space velocity. The effluent liquid and vapor pass through a heat exchanger to a high-pressure separator, where the recycle gas is separated from the liquid. The recycle gas is returned to the reactor inlet by a recycle compressor. The liquid is let down in pressure, and hydrogen and light hydrocarbon gas are released in a low pressure separator. The liquid product from the low pressure flash is sent to fractionation. In the reactor, hydrogen partial pressure is reduced by consumption through chemical reaction, by dissolved hydrogen being carried out in the product, and by the formation of light hydrocarbons which dilute the remaining hydrogen. There are several ways of maintaining reactor hydrogen partial pressure within the desired range. The most common involve the addition to the high pressure loop of either a purge or an oil absorber. Hydrocarbons, which dilute the reactor hydrogen, can be removed by purging a part of the gas stream coming from the high-pressure separator. A purge, however, is not selective; for every mol of hydrocarbon purged, typically four mols of hydrogen are lost. Because of the expense of replacing this lost hydrogen, high-pressure purge rates are usually kept to a minimum.

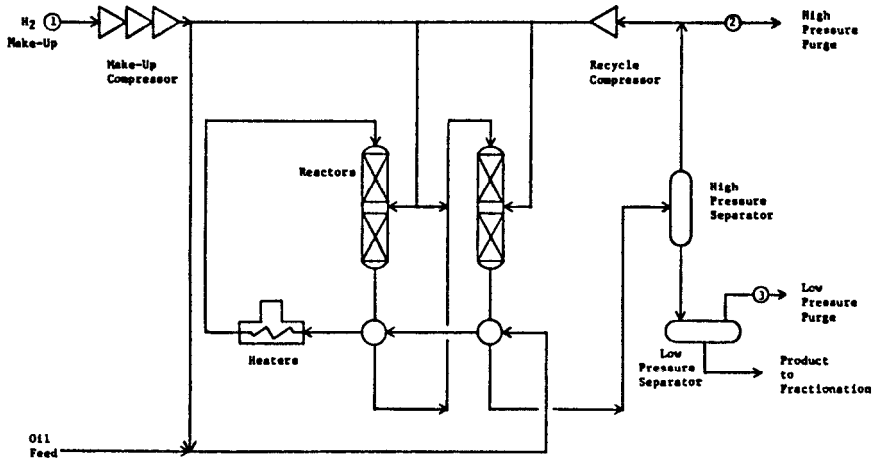


Figure 10.10: Hydrocracker.[55]

The most common alternative to the high pressure purge is oil scrubbing. This involves an absorber vessel in the high-pressure loop, a low-pressure flash drum, and a high pressure pump to return the lean oil to the absorber. The

principal advantage this system has over purging is hydrogen conservation. The oil scrubber flash-drum offgas typically contains one mol of hydrogen per mol of hydrocarbon; thus absorbers lose only about 25% as much hydrocarbon as high-pressure purges. The main disadvantage of the absorber systems is their cost. High operating pressures makes the mechanical components expensive, and pump power requirements often exceed 1000 kW.

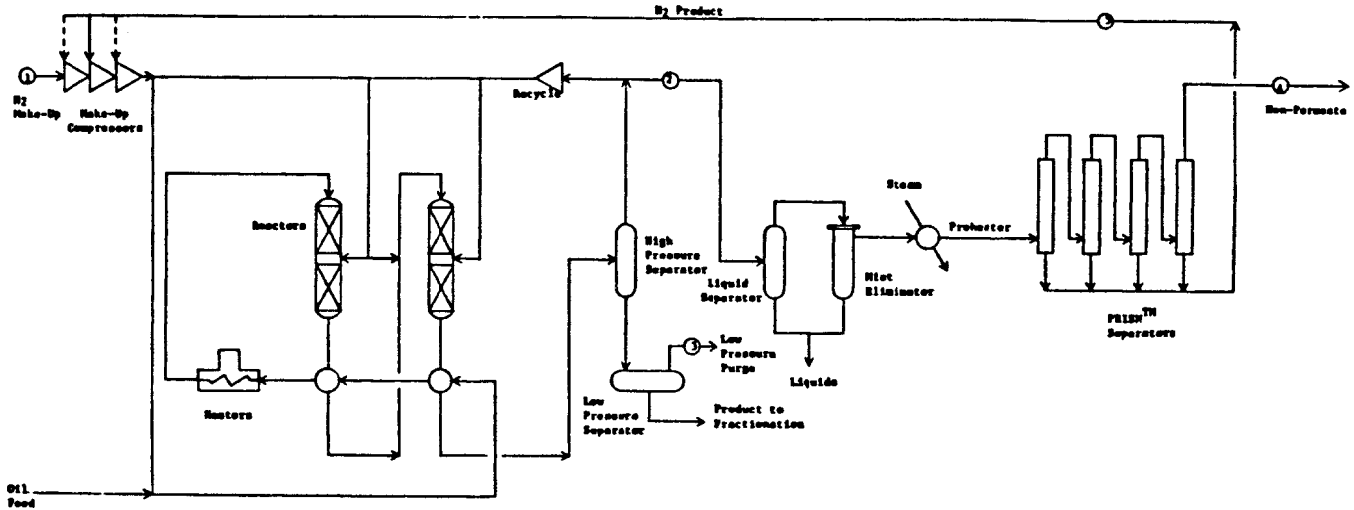
The addition of a PRISM® separator to the recycle loop will effectively remove gases such as methane from the process. A simple flow diagram of a hydrocracker with the addition of the PRISM® separators is shown in Figure 10.11. A recycle gas slip stream is fed to a liquid separator, where any entrained liquids and mist are removed. The gas is then heated to 150° to 180°F (339° to 355°K) prior to entering the PRISM® separators. Hydrogen which permeates the fibers is recovered and returned to the make-up compressor. With about 90% of the hydrogen removed, the non-permeate is primarily hydrocarbons and can be used as fuel gas. Because of the low hydrogen content of the non-permeate, three to four mols of hydrocarbon are rejected for each mol of hydrogen lost. By comparison, simple purges lose 12 to 15 times as much hydrogen.[55]

Other refinery applications in which PRISM® separators have been successfully used are naphtha hydrotreaters, middle distillate hydrotreaters, cat crackers, and toluene hydrodealkylation.[56,57]

The Ube system was designed to be capable of handling the applications described above for PRISM® separators. Compared at the same temperature, it is reported that the permeabilities of the Ube composite polyimide hollow fiber membranes may be substantially lower than those of polysulfone,[49] but with two times the selectivities. The lower permeabilities are overcome in two ways. The Ube module contains 9000 (m^2/m^3) membrane area per unit volume compared with 4000 (m^2/m^3) in a PRISM® separator. Since the separator units are approximately the same size (from Permea, Inc. and Ube product brochures), the Ube membrane must be smaller in diameter than is the PRISM® separator membrane in order to increase the unit membrane area. In transporting large volumes of H_2, small diameter hollow fiber membranes often lead to a large bore pressure drop on the permeate side. The pressure drop is due to flow of gas in a long capillary and is inversely proportional to the inside radius of the hollow fiber to the fourth power, i.e., Poiseuille's law. Pressure buildup on the permeate side of the membrane results in a reduction of the differential partial pressure driving force with attendant reductions in product recovery and purity. Thus, fiber dimensions are important in designing a system for a given separation. In practice, the Ube module most likely will not function as if the unit membrane area is more than twice that of a PRISM® separator due to differences in fiber dimensions. The penalty, however, will depend greatly on operating conditions.

The polyimide membrane is reported to be capable of operating at temperatures up to 150°C compared to upper limits of 100°C for PRISM® separators and 60°C for cellulose acetate.[46] Permeabilities increase with temperature while selectivities normally drop. The second way to overcome the lower permeabilities is to operate the Ube system at higher temperatures than possible with polysulfone or cellulose acetate. Even at the high temperatures, the polyimide selectivity will remain high enough for the abovementioned hydrogen separations. Thus, one expects the Ube system to be competitive with PRISM® separators for many hydrogen applications.

Figure 10.11: Hydrocracker with PRISM® separators.[55]



The cellulose ester systems have some application in hydrogen separations, but are more limited in capability due to temperature limitations. Operation at higher temperature minimizes the need for stream pretreatment to remove components which may attack the membranes. The PRISM® separators and the Ube systems are superior to the cellulose esters in this respect.

Carbon Dioxide Separation

Both hollow fiber and spiral-wound membrane systems have been utilized to recover carbon dioxide in sour gas purification and in enhanced oil recovery.

Removal of hydrogen sulfide (H_2S) and carbon dioxide (CO_2) from natural gas is an ideal application for membranes in that both H_2S and CO_2 permeate through membranes at a much higher rate than methane, enabling a high recovery of the acid gases without significant loss of pressure in the methane pipeline product gases.[41-43, 58-60]

Membrane gas separation by PRISM® separators offers a low cost processing alternative to conventional CO_2 removal processes[61,62] as shown in Table 10.2.

Once the needed partial pressure driving force is achieved by compressing the feed gas, no further expenditure of energy is necessary to separate the CO_2.[63]

Separex's,[41-43] Grace Membrane Systems cellulose ester,[60] Envirogenics GASEP® (trademark of Envirogenics Company)[64] cellulose triacetate spiral-wound membranes, and Dow cellulose acetate hollow fibers are used to produce a salable product from sour gas streams.

Table 10.2: Product Purity and Recovery

SEPARATORS SYSTEM	HOT POTASSIUM CARBONATE	CRYOGENIC SEPARATION	PRISM® SEPARATORS
CO_2 Product Stream			
CO_2 Recovery %	96.9	93.0	96.9
CO_2 Purity %	99.8	95.1	95.5
Overall Hydrocarbon Stream			
Hydrocarbon Recovery %	99.5	81.0[1]	83.5
Hydrocarbon Gas Product			
CO_2 %	2.0	2.0	2.0
C_1 Recovery %			78.2
C_2 Recovery %			90.1
C_3^+ Recovery %			97.0

[1]The recovery is based on CO_2 rejection column being operated for ethane reflection/propane recovery.

For enhanced oil recovery programs utilizing CO_2 injections,[45] membrane separation technology is also finding increasing application. Carbon dioxide is injected into the well as a miscible flood to remove additional oil from depleted fields. It has been found that CO_2 at concentrations above 90% will solubilize oil absorbed in the substrata, allowing secondary and tertiary recovery. In EOR production, CO_2 injected into the formation eventually reemerges mixed with light hydrocarbon gases associated with crude oil. A membrane system can be used to recover CO_2 for reinjection and recover the light hydrocarbons for sale as pipeline gas.

Goddin[63] presented a detailed cost analysis for recovering CO_2 from casinghead gas where bulk removal is effected by membrane separation followed by a conventional gas treating process. His analysis showed that for feed gas containing more than 30% CO_2, the process heat requirements for a membrane separation process are approximately 30 to 40% lower than for a cryogenic process. When compared to an acid gas removal process using DEA as a solvent, the membrane separation process requires only 20 to 25% of the process heat requirement.

There are many wells containing about 40 to 80% CO_2 that could be processed with a membrane system, providing a high purity CO_2 for EOR and a fuel gas by-product.

Membrane gas separators may also be used to separate methane from carbon dioxide formed during the decomposition of organic matter in landfills.[64] Permea's PRISM® gas separators are being used in a Florence, Alabama landfill to upgrade raw to 95% methane purity so that it can be routed to the city gas department.

The Ube system may also be useful for CO_2 separations,[46] but no data have been reported.

Oxygen/Nitrogen Separation

The U.S. produces approximately 15 millions tons of oxygen from air each year.[66] Most of this production is accomplished cryogenically, and in large plants the cost is very low. Uses of oxygen in quantities of less than 10 tons per day, however, constitute a substantial share of this market. It is thought that membrane systems could economically enrich air at this smaller plant size.[67]

In many applications, such as inert blankets for combustible materials or chemicals, nitrogen rather than oxygen is the desired separator product. Permea in conjunction with Maritime Protection S.A. (wholly owned subsidiary of Permea Kristiansand, Norway) commercialized a system to provide >95% pure nitrogen aboard ships using PRISM® separators.[68,69] The system can process up to 100,000 scf/d of air and operates at 120° to 150°F and pressures up to 425 psig. At the optimum operating conditions, the system can produce nitrogen at less than 4¢ per normal cubic meter or less than $1.40 per thousand scfm.[17,69] More recently, membrane systems are planned to provide nitrogen on offshore platforms and in remote landbased applications. Other possible applications include nitrogen blanketing of food to prevent spoilage and to provide nitrogen for manufacturing plant operations.

Permea has under development a new membrane which has approximately 3 times the permeability of the currently used PRISM® separator and the same

selectivity.[18] This membrane system should provide nitrogen at a significantly lower cost thus broadening the applicability of membranes for O_2/N_2 separations.

The Generon Air Separation Membrane System which was introduced by Dow Chemical Company in 1985, also is used to provide 95% nitrogen for blanketing. The cost per unit volume nitrogen produced is similar to that reported by Permea.[17] One major difference is the Generon system uses 75 to 90 psi air with an upper limit of 115 psig whereas Permea prefers to use air at 300 to 600 psi. The Permea system operates over a rather broad temperature range and is quite flexible. The Generon system operates preferably at about 15° to 25°C which requires refrigeration of the feed stream. The choice of system will depend largely on the availability of compressed air and the constraints of a given application. Both systems produce nitrogen with a dew point of about -65°C.

The Asahi Glass system is designed to produce oxygen enriched air of up to 40% for medical applications. The driving force is maintained by a vacuum on the permeate side of the plate and frame system. Air at atmospheric pressure is the feed.

Signal's UOP Fluid Systems Division system also produces oxygen enriched air of 30% O_2 for commercial applications. Japan's Osaka Gas has developed a similar system.[15] Again, air is supplied to the membrane at atmospheric pressure and the driving force is maintained by a vacuum on the permeate side of the membrane. Oxygen enriched air can be supplied at very attractive costs.

Dehydration

A potentially large market for membrane separators exists in dehydration. A hollow fiber membrane separator system is being developed by Permea Inc. to dehydrate water/alcohol mixtures including methanol, ethanol, isopropanol, and/or butanol. The system is not limited to azeotropic mixtures, but it will eventually be used in the dehydration of a wide variety of water/alcohol mixtures.[70] Although the first system investigated was ethanol/water, the work aims at separating water/organic mixtures in general.[71] One such application is the removal of water from natural gas to bring it to pipeline specifications. The cellulose acetate systems also are useful for natural gas dehydration. A major problem is the loss of CH_4 during dehydration, and it appears that currently available membranes are not suitable in this regard.[72] More water permeable and more selective systems are required.

Other Separations

Pervaporation is a special case of gas separations in that it is a concentration driven process. The feed mixture is supplied as a liquid to the membrane and the permeate is recovered as a vapor on the low pressure side of the membrane. Pervaporation finds application in dehydration as well as the separation of a variety of liquid mixtures. A discussion of pervaporation is beyond the scope of this review.

Liquid separations including reverse osmosis, ultra and microfiltration are pressure driven membrane processes. Membranes are broadly applied to effect separations in these areas. They are used in the making of potable water, in filtration and concentration in the food industries, in the electronic industries

and find wide application in medicine and health care. As with pervaporation, these membranes also are beyond the scope of this review. The reader is referred to an outstanding, up to date discussion of the membranes which are used for these processes as well as summary of the processes themselves by R.E. Kesting.[73]

ACKNOWLEDGEMENT

We wish to thank Dr. M.A.E. Kraus, now with Gelman Industries, who contributed the introductory membrane and fundamental sections of the text, and Dr. R.S. Narayan for his support and contributions to the writing of this chapter.

REFERENCES

1. Graham, T., *Phil. Mag.*, 32, 402 (1866).
2. Yasuda, H. and Stannett, V., in *Polymer Handbook*, D. Brandrup and E.N. Immergut, eds., John Wiley and Sons, New York, p. 111-229 (1975).
3. Loeb, S. and Sourirajan, S., Report No. 6060, Dept. of Engineering, University of California, Los Angeles (1960).
4. Ward, W.J., III, Browall, W.R. and Salemme, R.N., *J. Membr. Sci.*, 1, 99 (1976).
5. Gantzel, P.K. and Merten, U., *Ind. Eng. Chem. Process Res. Dev.*, 9, 331 (1970).
6. Merten, U. and Gantzel, P.K., U.S. Pat. 3,415,038 (1968).
7. Henis, J.M.S. and Tripodi, M.K., U.S. Pat. 4,230,426 (1980).
8. McBride, R.B. and McKinley, D.L., *Chem. Eng. Prog.*, 61, (3) 81 (1965).
9. DuPont Company, Permasep Technical Bulletins 105, 110 (1972); Gardner, R.J., Crane, R.A. and Hannan, J.F., *Chem. Eng. Prog.*, 73, 76 (1977).
10. Matson, S.L., Lopez, J. and Quinn, J.A., *Chem. Eng. Sci.*, 38, 503 (1983).
11. *Chemical Economy and Engineering Review*, 16, No. 7-8, p. 37 (1984).
12. Makino, H., Kusuki, Y., Harada, T., Shimazaki, S. and Isida, T., U.S. Pat. 4,440,643 (1984).
13. *Chemical Week*, 137, p. 39 (July 10, 1985).
14. *Chemical Week*, 134 (January 19, 1984).
15. *Chemical Week*, 135, p. 38 (July 24, 1984).
16. *Membrane Separation Technology News*, 3, p. 1 (1985).
17. McReynolds, K.B., *Chem. Eng. Prog.*, 81, 27 (1985); *Industrial Chemical News*, 6 (April 1985).
18. Zampini, A. and Malon, R.F., *Proc. ACS Div. Polym. Mat., Sci. & Eng.*, 52 345 (1985).
19. Hwang, S. and Kammermeyer, K., *Membranes in Separations*, John Wiley and Sons, New York, p. 501 (1975).
20. Reference, 19, p. 506.
21. Perry, R.H. and Chilton, C.H., *Chemical Engineers' Handbook*, McGraw-Hill Co., New York, p. 17-45 (1973).
22. Vieth, W.R., Howell, J.M. and Hsieh, J.H., *J. Membr. Sci.*, 1, 122 (1976).

23. Stern, S.A. and Frisch, M.L., *Ann. Rev. Mater. Sci.*, 11, 523 (1981).
24. Masuda, T., Isobe, E. and Migashimuna, T., *J. Am. Chem. Soc.*, 105, 7473 (1983).
25. Paul, D.R., *Ber. Bunsenges. Phys. Chem.*, 83, 294 (1979).
26. Koros, W.J. and Paul, D.R., *J. Polym. Sci., Polym. Phys. Ed.*, 16, 1947 (1978).
27. Raucher, D. and Sefcik, M., in *Industrial Gas Separations*, T.E. Whyte, Jr., C.M. Yon and E.H. Wagener, eds., ACS Symposium series 223, American Chemical Society, Washington, D.C., p. 111 (1983).
28. Pace, R.T. and Datyner, A., *J. Polym. Sci., Polym. Phys. Ed.*, 17, 437 (1979).
29. Brandt, W.W., *J. Phys. Chem.*, 63, 1080 (1959).
30. DiBenedetto, A.T., *J. Polym. Sci.*, A1, 3477 (1963).
31. Weller, S. and Steiner, W.A., *J. Appl. Phys.*, 21, 279 (1950).
32. Weller, S. and Steiner, W.A., *Chem. Eng. Prog.*, 46, 585 (1950).
33. McLean, D.L., Stookey, D.J. and Metzger, T.R., *Hydrocarbon Process.*, 62 (8), 47 (1983).
34. Henis, J.M.S. and Tripodi, M.K., *J. Membr. Sci.*, 8, 233 (1981).
35. Fritzsche, A.K., Holladay, H.P. and Woodcock, M.L., U.S. Pat. 4,323,453 (1982).
36. Zampini, A., U.S. Pat. 4,323,453 (1982).
37. Vos, K.D. and Burris, F.O., Jr., *Ind. Eng. Chem. Prod. Res. Dev.*, 8, 84 (1969).
38. Agrawal, J.P. and Sourirajan, S., *J. Appl. Polym. Sci.*, 14, 1303 (1970).
39. McDonald, W. and Pan, C., U.S. Pat. 3,842,515 (1974).
40. Manos, P., U.S. Pat. 4,080,743 (1978).
41. Schell, W.J. and Houston, C.D., *Hydrocarbon Process.*, p. 249 (September 1982).
42. Schell, W.J., *Hydrocarbon Process.*, p. 43 (August 1983).
43. Schell, W.J., *J. Membr. Sci.*, 22, 217 (1985).
44. Makino, H., Kusuki, Y., Harada, T. and Shimazaki, H., U.S. Pat. 4,378,400 (1983).
45. Nakamura, A., *Energy and Resources*, 6, #3, 67 (1985).
46. Nakamura, A. and Hotta, M., *Kagaku Keizai*, pp. 13-19 (May 1985).
47. Erb, A.J. and Paul, D.R., *J. Membr. Sci.*, 8, 11 (1981).
48. Yasuda, H. and Rosengren, K., *J. Appl. Polym. Sci.*, 14, 2839 (1970).
49. Koros, W.J., Separations Research Program, Fall Meeting (October 28-29, 1985).
50. Dyer, B.S., Day, M.R. and Bergenn, W.R., *Encyclopedia of Polymer Science and Technology*, John Wiley and Sons, NY, Vol. 9, pp. 450-459 (1968).
51. Paul, D.R. and Morel, G., *Kirk-Othmer Encyclopedia of Chemical Technology*, John Wiley and Sons, NY, Third Edition, Vol. 15, p. 118 (1981).
52. Steigelman, E.F., U.S. Pat. 4,014,665 (1977).
53. MacLean, D.L., Prince, C.E. and Chae, Y.C., *Chem. Eng. Prog.*, 76, 98 (1980).
54. Shirley, J. and Coreik, D., *Chemical Processing*, 30 (Jan. 1982).
55. Bollinger, W.A., Long, S.P. and Metzger, T.R., *Chem. Eng. Prog.*, 80, 51 (1984).

56. MacLean, D.L., Bollinger, W.A., King, D.E., Narayan, R.S., Paper presented ACS meeting (Aug. 1981).
57. Bollinger, W.A., MacLean, D.L. and Narayan, R.S., *Chem. Eng. Prog.*, 78, 27 (1982).
58. Schell, W.J., Lawrence, R.W. and King, W.M., *Membrane Applications to Fuel Conversion Processes*, Final Report to the Energy Research and Development Administration, Report No. RE-2000-4 (1976).
59. Cooley, T.E. and Coady, A.B., U.S. Pat. 4,130,403 (1978).
60. Cooley, T.E. and Dethloff, W.L., *Chem. Eng. Prog.*, 81, 45 (1985).
61. Boustany, K., Narayan, R.S., Patton, C.J. and Stookey, D.J., paper presented GAP National meeting (March 1983).
62. Waste Age, pp. 28-30 (November 1983).
63. Goddin, C.S., *Hydrocarbon Process.*, p. 125 (May 1982).
64. Mazur, W.H. and Chan, M.C., *Chem. Eng. Prog.*, 78, 38 (1982).
65. *Enhanced Oil Recovery*, H.K. Van Poolen and Associates, Inc., Pennwell Publishing Company, pp. 132-141 (1980).
66. Follwell, W.F., *Chem. Eng. News*, 7 (July 15, 1974).
67. Schell, W.J. and Hoenschemeyer, D.L., Paper presented AIChE Symposium (June 1982).
68. *Chemical Engineering*, p. 10 (October 17, 1983).
69. Metzger, T.R., Handermann, A.C. and Stookey, D.J., *Plant/Operations Prog.*., 4, 168 (1985).
70. *Membrane and Separation Technology News*, 1, p. 1 (July 1983).
71. *Chem. Eng. News*, p. 22 (June 27, 1983).
72. Fournie, F. and Agostini, J.P., *Proc. of the Offshore Technology Conference*, Houston, TX, pp. 113-121 (1984).
73. Kesting, R.E., *Synthetic Polymeric Membranes*, Second Edition, John Wiley and Sons, Inc., NY, Chapter 2 (1985).

While this information is presented in good faith and believed to be accurate, Monsanto Company does not guarantee satisfactory results from reliance upon such information and disclaims all liability for any loss or damage arising out of its use and makes no express or implied representation or warranty as to the fitness, merchantability or any other matter with respect to the products or processes referred to herein. Nothing contained herein is to be construed as a recommendation to use any product in process in conflict with any patent.

Index

"Absolute" membranes - 78
"Absolute" retention - 81, 219
Absorption - 574
Acid dosing - 374
Activated sludge reactor - 254
Activated transport - 403
Activation energy - 401, 435, 570
Active charcoal filtration - 376
"Active" transport - 3
Adsorption - 402, 574
Adsorption losses - 159-160
Aerosol retention - 86-90
Alamine® - 336, 521, 528-531, 539, 543
Amination - 43
Ammonia plants - 578, 582
Ammonia purge gas - 583-584
Ammonia recovery - 547
Ammonia synthesis - 387-388
Anion-exchange membranes - 40, 43, 499
Anisotropic membranes - 106, 138, 140, 145, 166
Anisotropy - 94-95
Annealing - 35-36
Arrhenius equation - 412
Asymmetric hollow fiber - 149, 151
Asymmetric membranes - 2, 4, 12-14, 30, 32, 35, 45, 54, 138, 351-352, 404, 445, 450-451, 455-456, 458, 462, 579
Augmented cross-flow effects - 192-195
Autoclave - 116
Automotive industry - 382-384

Back diffusion - 413-414
Back-diffusive transport - 173, 186, 195
Backflush reactor - 250
Back-wash fluid - 206
Backwashing - 99-101, 118
Bacteria - 61-62, 71, 78-81, 158
Bacteria retention - 78-81
Batch fermentation - 402, 474
Batch fermentor - 253
Batch operating mode - 216

Batch reactors - 422
Batch recirculation - 490
Beer - 240-241
BET adsorption data - 78
Beta ratio - 71
Biomass - 467-468, 470-471
Biomembrane plants - 255
Bipolar membranes - 490-496
Blood - 458, 462, 492-493
Blood plasma processing - 242-243
Boundary layer conditions - 503
Boundary layer thickness - 415, 417
Brackish water membrane - 267
Bubble-point - 78-81, 158
Bubble-point equation - 72
"Bubble-point" pressure - 116
Bubble-point test - 61, 71-76
Bubble-pointable cartridge - 69, 111
Bubble-pointable tube - 109
Bubble-pointed unit - 106

Capillary membranes - 53-54, 421
Capillary module - 50-53
Capillary-pore membranes - 7-9, 62-64, 66-69, 78, 82-83, 90, 98-99, 106, 108
Carbon dioxide separation - 588-589
Carnell-Cassidy technique - 310
Cartridge filtration - 375
Cartridge-type filters - 50
Cascade without reflux - 364
Cascades - 360-373
Casein - 492
Casing-head gas - 589
$CaSO_4$ precipitation - 507
Cassette plate and frame system - 209, 211
Casting anisotropic ultrafiltration membranes - 140
Casting machine - 54
Casting process - 64
Casting solution - 17, 28, 30-32, 35, 146
Casting tube - 144
Cathode rinse stream (or catholyte) - 498-499
Cation-exchange membranes - 40, 42, 499
Caustic extraction effluent-color rejection - 232
Cell concentrations - 470, 472
Cell harvesting/washing - 128-131, 242
Cell pair - 487
Cell recycle fermentors - 470-472
Cellular structure - 21, 23, 34
Cellulose acetate - 23-25, 36, 46, 309, 578-580
Cellulose acetate membranes - 270-271, 273, 309-311, 455, 560-561, 586, 588
Cellulose ester - 588
Cellulose nitrate membrane - 9
Cellulose triacetate - 310, 588
Centrifugal force - 192
Ceramic membranes - 4, 5, 105, 115, 154-155
Challenge tests - 70-71
"Charged" membranes - 161, 201, 220
Cheese whey protein recovery - 232-236
Chloralkali cells - 483-484
Chlorine dosing - 374
Chlorine resistance - 324
Cleaning by recycling - 206-207
Cleaning in place - 491
Coating - 575, 577
Cobalt recovery - 542-543
Co-coupled transport (or co-transport) - 516-517
Coenzymes - 424-425
Cofactor - 403, 409, 453-454
Co-ions - 40, 483
Collapse of pores - 143

Collodion membranes - 61
Colloidal particles - 189
Colloidal suspensions - 180-186
Compaction - 312
Complexing agents - 526-531, 537-541
Composite membranes - 45-49, 271, 273, 560-561, 574-579
Compression - 574
Concentration - 3, 37
Concentration difference - 3
Concentration effects - 521-523
Concentration gradient - 3
Concentration polarization - 163-164, 166-198, 268-269, 349-351, 403, 410-411, 413-415, 417-419, 421, 426, 428, 465, 472, 502-507, 532-537
Concentration profiles - 29, 31-32, 349, 352, 357, 372-373
Conductance - 504
Confinement - 402
Constant reflux - 364
Contact angle - 72, 77
Continuous cell culture - 131
Continuous fermentor - 253
Continuous flow reactors - 402
Convection - 435, 437
Conversion - 404, 410-411, 417-418, 422, 426, 435, 437-438, 440-441, 444-448, 450-451, 454, 456-457, 459, 461-462, 465-466, 474, 476
Copolymerization - 403
Copper etchant baths - 545-546
Copper recovery - 541-542, 545-546
Corn starch - 241
Counter-coupled transport (or counter transport - 515-516
Counter ions - 40, 483
Coupled transport membranes - 511-558
  characteristics - 520-537
  history - 512-515
  theory - 517-520
Coupling agent - 403, 456
Covalent binding - 403, 456, 458
Critical voltage - 195
Cross-flow electrofiltration - 193-195
Cross-flow filtration - 99, 102-106, 109, 112, 124-134, 382-384
Cross-flow membrane cassette - 108
Cross-flow process - 268
Cross-flow ultrafiltration system - 171
Cross-flow velocity - 199
Crosslinked PPO (polyphenylene oxide) - 580
Crosslinking - 456, 483-484
Crown ethers - 517, 540-541
Cryogenic process - 588-589
Cryogenics - 574

Dairy applications - 232-237
Dead-end units - 410, 421
Dead-ended filtration - see "Through-flow filtration"
Dehydration - 590
Dehydration of sour gases - 389-390
Deionized water - 119-120, 123, 218
Density of pores - see Porosity
Desalination membranes - 560
Desalination of brackish water - 376-382
Desalination of seawater - 299-302, 336, 374-376, 490-491
Desalting of seawater - 491
Detergent cleaning - 199
Diafiltration - 129, 243-247, 418, 422
Dialysis - 1
Dialysis membranes - 410, 445, 467, 474

Diffusion - 435, 437, 444-448, 450-451, 455, 459, 461-462, 570
Diffusional deposition - 88-90
Diffusional flow - 74
Diffusional resistance - 409-410, 446, 450, 457-458
Diffusivity - 3, 37, 564-565, 569
Dip-coating - 46
Direct interception - 88
Dirt-loading capacity - 90, 93
Disperse soluble immobilized enzyme - 251
Donnan exclusion - 161, 483, 494, 503
Donnan ion effect - 322, 339
Driving forces - 2-4
Drum-casting machine - 140-141
Drying - 560, 578-579
Dual sorption theory - 566, 568
Dyestuff recovery and purification - 229
Dynamic membranes - 153-154, 281
Dynamic secondary membrane - 164, 167

EDR process - 498, 507-508
EDTA-Cu complex - 494
Egg white - 237-238
Electric field - 192-195
Electrical potential difference - 3
Electrical resistance - 486, 488
Electrocoat paint - 222-224
Electrode isolation - 498-499
Electrode reaction - 496-498
Electrodes - 496-502
Electrodialysis - 1, 482-510
  applications - 490-494
  costs - 509
Electrodialysis stack - 487-490
Electrokinetic adsorption - 83
Electrolytic cells - 482-483
Electrophoretic deposition - 222
Electrophoretic transport - 195
Electroplating - 493
Electroplating rinse waters - 543-545
Electrostatic attraction - 84
Emulsion liquid membrane process design - 552-555
Emulsion membranes - 514-515, 520
Encapsulation - 402
End seal - 579-581
Enhanced oil recovery - 582, 588-589
Entrapment - 404, 455
Enzyme activity - 409, 411, 417, 422, 424, 444-445, 451, 462, 464
Enzyme concentration and purification - 242
Enzyme deactivation - 415, 417, 419, 440, 445
Enzyme depth of penetration - 427, 434
Enzyme engineering - 401
Enzyme half-life - 411-413, 422
Enzyme membrane reactors - 403-404, 409-426, 428, 465
Enzyme reactors - 247-252
Enzyme stability - 404, 411, 427, 464
Equilibrium curve - 363, 367
Equilibrium state - 19
Evaporation - 14, 16, 382-384
External mass transfer resistances - 435
Extractive distillation - 396-398

"Facilitated" transport - 2-3, 38
"Fast" gases - 582
FDA approval - 330
Feed and bleed - 490

Feed and blend mode - 216
Feed composition - 573
Feed pretreatment - 374
Feedwater analysis - 282
Feedwater pH - 284, 289
Fermentation - 466
Fermentation efficiency - 470
Fermentor productivity - 466, 471-472, 474
Fick's law - 3, 18, 518-519, 564, 569-570
Filtration properties - 25, 27
Finger-type structure - 20-21, 25, 27, 33-34
Flat membranes - 410, 419, 434-435, 437, 465
Flat-plate cartridge - 210
Flat-plate membrane - 210
Flat sheet membranes - 37, 50, 53-54
Float casting - 309
Flow permeability test - 77
Flue gas - 496
Fluid polymer layer - 30
Flux decay - 104, 198-202
Flux variation - 172
Fluxes - 2-4
"Forward-flow" test - 74-75
Fouling resistance - 150
Fractionation capability - 86
Fruit juice - 238-240
FT-30 composite membrane - 327-331
Functional synthetic membranes - 56
Furfuryl alcohol - 334

Galvanic industry - 384-387
Gas permeation - 351-352, 357, 359, 363
Gas-phase deposition - 46-47
Gas separation - 12, 37, 360
Gasket spacer - 487
Gel (cake) resistance - 168
Gel concentration - 426, 428
Gel formation - 426-428, 434, 438-439
Gel layer - 169-170, 186, 383-384, 403-404, 418, 426-428, 434-436, 438, 465
Gel polarization - 164, 167-174, 196
Gel-polarization model - 167
Gelatin - 238
Gelation time - 23, 27
Glassy polymers - 565-570
Glycerin - 28
Grow-through - 78

Heavy metals - 124
Heavy metals removal - 230
Henry's law - 564, 566
Henry-type sites - 566-569
Heterogeneous membranes - 2, 44, 484-485
Hollow fiber fermentor - 473
Hollow fiber module - 50-52, 354-360, 380
Hollow fibers - 37, 53-55, 205-207, 214, 357, 404, 410, 421, 440, 445, 450-451, 454, 458-459, 463, 467, 473, 547-550, 561, 581, 586, 588
Hollow fine fiber packaging - 279-281, 285
Homogeneous membranes - 2, 4, 37-45, 486
Homogeneous metal and glass membranes - 37-38
Homogeneous polymer membranes - 37
Hydrocrackers - 585-587
Hydrogen - 38
Hydrogen recovery - 387-389, 583-588
Hydrogen sulfide - 588

Hydrolysis - 43, 418, 421, 426, 440, 450, 454, 467, 475-476
Hydrophilic polymers - 160
Hydrophobic membrane - 116
Hydrophobic polymers - 160
Hydroprocessors - 582
Hydrostatic pressure - 3
Hydrotreaters - 586

Immobilization techniques - 402-403, 409, 438, 440, 455
Immobilized cells - 254
Immobilized enzyme batch membrane reactor - 428-429, 432
Immobilized enzymes - 249, 251, 402-403, 418, 426, 434, 437-438, 450, 456, 458, 462, 465
Imperfections - 577
Industrial laundry wastewater - 125-126
Industrial reverse osmosis at a refinery - 290-296
Industrial scale membrane production - 49-53
Industrial wastes - 303
Industrial water - 302-303
Inertial impaction - 88
Inhibitors - 410, 418, 440, 454, 473-474
Inorganic coatings - 201
Inorganic materials - 11-12
Inorganic membranes - 153-155
Integrated circuits - 491-492
Interaction parameter - 570
Interfacial membrane formation, mechanism - 332-333
Interfacial polymerization - 46-48
Intrusion pressures - 77
Ion exchange, reverse osmosis and - 296-298
Ion exchange demineralization - 290, 296-298
Ion exchange membranes - 39-45, 483-484, 486-487
Ionic binding - 456
Ionic velocities - 482
Ionics, Inc. - 488, 508
Isoelectric point - 173-174, 492
Isotopes - 560

Kelex® 100 - 521, 524-525, 527, 529, 532, 534-535, 539, 542-543, 550
Kermac® 470B - 524, 527, 529, 534
Knudsen flow - 562, 576

Lactose - 234
Laminar flow - 174-176, 177, 350, 438, 441, 447, 452, 457-458
Landfills - 589
Langmuir constant - 568
Langmuir-type sites - 566-569
Latex concentration/recovery - 229-230
Lime clarification - 290, 292-293
Limiting current density - 502, 506-507
Liquid films - 4
Liquid membranes - 38-39
LIX® 54 - 521, 525, 527, 532, 534, 542-543
LIX® 64N - 521-523, 525-529, 532, 538, 554
Lock, Sidney - 137, 139, 270
Loeb-Sourirajan membrane - 137, 139, 309, 311-312, 560, 575
Long-term flux decay - 199

Macromolecular substrates - 409-410, 418, 426
Manufacturing equipment - 53
Mass transfer coefficient - 174-179, 349, 435

Mass transfer diffusional resistance - 445, 450, 456-457
Media migration - 91
Membrane barrier layers - 272
Membrane column - 360, 368-373
Membrane configuration - 106-114, 202-214
Membrane (definition) - 2
Membrane degradation - 551
Membrane distillation - 6-7, 132-134
Membrane electrodes - 457
Membrane fermentors - 252-254, 404, 466-476
Membrane flux - 166-198, 288, 523
Membrane fouling - 198-202, 224, 285, 327, 418, 465, 472, 507-508
Membrane modules - 50-53
Membrane plugging - 90-106
Membrane preparation - 4-56
Membrane properties - 486-487
Membrane reactor - 249
Membrane rejection - 413
Membrane structure - 20-28, 62-64, 138-155
Membrane surface treatments - 200-202
Membrane testing and evaluation - 582
Meniscus coating - 310
Mercury intrusion test - 77
Mercury porosimetry data - 81
Metal alloys - 11
Metal cleaning - 225
Metal finishing - 493
Metal ion concentration effects - 523-524
Metal ion effects - 525-526
Methanol synthesis purge - 584-585
Michaelis-Menten model - 411, 421, 437
Michaelis-Menten rate equation - 442, 447
Microbial cells - 402, 455, 474, 476
Microelectronics - 120
Microfiltration - 5, 50, 61-135, 383-384, 439
  applications - 114-134
Microorganisms - 11, 70-71, 116, 401-402, 451, 455, 468
Microporous membranes - 4-36, 466, 559-561
Microporous metal membranes - 12
Microporous polysulfone - 311-313, 333, 343
Microporous sintered membrane - 4-5
Microporous support - 48-49
Milk - 492
Milk concentration - 236-237
Miscibility gap - 15-17
Mobile cells - 252-254
Mobile enzyme - 248-249
Molecular weight cut-off - 155-156
Municipal potable water - 302
Municipal wastes - 303

Natural gas - 588
Nernst idealization - 503
NF-40 composite membrane - 323-324
NF-50 composite membrane - 332
Nickel plating - 385-386
Nickel recovery - 542-543
Nitrocellulose - 61
Nodular structure - 20-21, 23, 34
Nonpolar gases - 560
Nonporous membranes - 560-561, 563-565
Nonsolvent addition - 15, 17
NS-100 membrane - 314-316
NS-200 membrane - 333-335
NS-300 membrane - 320-323

NTR-7250 composite membrane - 324-326

Oil fields - 582
Oil-water separation - 224-226
Oily wastewaters - 226, 384
Operating line - 363
Optimum recirculation rate - 216-217
Organic rejection - 317
Osmotic pressure model - 166-167
Oxygen enrichment - 581
Oxygen/nitrogen separation - 589-590

PA-300 membrane - 316-318
Parasite drag - 204-205
"Passive" transport - 2
PEC-1000 membrane - 335-338
Peptides - 402
Permeability - 3, 563-566, 569-571, 574-576, 578, 580-581
Permeate - 351, 353, 356, 362, 391, 410-411, 415, 417-418, 421-422, 425, 428, 434, 438, 465-466, 471-473
Permselectivity - 40, 487
Pervaporation - 37, 390-398, 590-591
Pesticide removal - 316
pH and gel polarization - 173-174
pH effects - 525-526
Phase-inversion membranes - 9-12, 20-28
Phase-inversion process - 12, 64
Phase separation, mathematical description of - 18-20
Phase separation process - 14-15
Phenol - 42
Phenol recovery - 547
Photographic solutions - 494-495
Piperazine - 320-323
Plasma polymerization - 47, 340
Plasmapheresis - 126-128
Plasticizers - 142
Plate and frame configuration - 274-275
Plate and frame module - 50-51, 581
Plate and frame units - 106-109, 208-211, 214
Pleated cartridges - 50-51, 106, 109-110
Point-of-use processing - 221
Poiseuille's law - 452-453, 562, 586
Polar gases - 560
Polarization layer - 410, 417
Pollution control, reverse osmosis and - 298-299
Polyacrylonitrile - 341
Polyamide - 23-27, 271, 314
Polybenzimidazolone membrane - 342-343
Polycondensation - 42
Poly(diallyl amine) - 319
Polyelectrolyte complex ultrafiltration membranes - 161
Polyepiamine - 316
Polyepichlorohydrin - 316, 318
Polyethylene - 10, 41
Polyethylenimine - 48, 314
Polyimide - 579-581, 586
Polyimide composite membrane - 342
Polyimide resin - 561
Polymer concentration - 23-27, 29, 35
Polymer content additives - 146-147
Polymerization - 42
Poly(4-methyl pentene-1) - 580-581

Polyolefin - 561, 581
Polyphenylene oxide (PPO) - 561, 581
Polyphosphate dosing - 375
Polypropylene - 10
Polystyrene - 41, 567
Poly(styrenesulfonic acid) - 343
Polysulfone - 9, 23-25, 41, 43, 47-48, 455-456, 462, 465, 561, 575-576, 579-581, 586
Polytetrafluoroethylene - 4, 44
Polyurea - 314
Polyvinyl alcohol - 326
Polyvinyl alcohol recovery - 227-229
Poly(4-vinylphenol) - 343
"Pore-flow" model - 161-163
"Pore-former" - 64-65
Pore size - 4-9, 12, 61, 73, 155-156, 158
Pore size determination - 70-78, 155-158
Porosity - 6, 23, 25, 49, 64, 69, 75, 77, 145, 148
Porous support - 45
Posttreatment design - 290
Power supplies - 500-502
Pre- and post-precipitation procedures - 35-36
Precipitant - 14, 27, 29, 31-32, 34
Precipitation - 14, 25-28, 30
Preferential sorption-capillary flow mechanism - 264
Prefilters - 90-94, 198
Prefiltration - 131
Pressure effect - 200
Pretreatment - 508
Pretreatment design - 283-285
Product flow as function of temperature - 266
Product-inhibited enzymes - 403, 450
Product water flow - 264
Proteins - 493
Pulp and paper waste treatment - 230-232
Purity - 570, 572-573
Pyrogens - 84, 142, 221

Quaternization - 43

RAD wastes - 124
RC-100 membrane - 316-318
Reactor capacity - 422
Reactor productivity - 421-422, 437
Recarbonation - 293
Recovery - 570, 572
Recovery of reverse osmosis plant - 267
Rectifier - 500
Recycle reactor - 250
Reflux cascades - 364-366, 394
Rejection of sodium chloride - 267
Resistivity of deionized water - 120, 122
Retention - 164-165
Retention by adsorption - 82-83
Retention by "charged" membranes - 83-86
Retention characteristics - 78-90, 159-166
Retention of deformable particles - 82
Retention of spherical and linear molecules - 157-158
Retentivity - 156-158
Reverse osmosis - 1, 20, 37, 119, 136, 233, 260-306, 352, 356, 359, 374-382, 384-387, 403, 424, 450

applications - 260-262, 302-303
costs - 303-304
design - 286-290
future projections - 305
plant design - 281-290
process considerations - 263-270

Salt flow - 265-266, 269
Salt rejection - 35-36
Sanitizing agents - 220
Seawater desalination - 299-302, 336, 374-376, 490-491
Seawater membrane - 267
Secondary flow effects - 177
Seeding technique - 382
Selective barrier - 45
Selectivity - 362, 570, 573-575, 577, 579
Semiconductor industry - 218-221
Semiconductor process fluids - 119-124
Separation factors - 563, 580
Separation of gases - 559-593
Separation unit - 361
Shape-factor - 80
Shear-stresses - 418, 426, 434, 438, 441, 445
Sheet-flow stack - 488
Shrinkage - 30, 33
Sieve mechanism - 264
Silica rejection - 329
Silicone - 575-576, 580-581
Silt density index - 282-284
Silver - 494
Skin - 20-21, 33-34
Skin-type membranes - 14, 32-33
"Slow" gases - 582
Smoke DOP test - 78
Sodium base spent sulfite liquor - 231
Sodium bisulfite dosing - 376
Sodium hexametaphosphate - 507-508
Solid polymer layer - 30
Solrox 0200 membrane - 340-342
Soluble enzyme batch membrane reactor - 428-429, 432
Solubility - 565, 568-569
Solubility parameter - 148
Solubility parameter disparity - 27-28
Solution coating technique - 272
"Solution-diffusion" model - 161-162, 264-265
Sorption enthalpies - 568
Sour gas purification - 588
Sourirajan - 137, 139
Soy whey - 237
Spacers - 487, 489
Spherical cells - 20, 22
Spinneret - 54-55, 151
Spinning hollow fibers - 149-153
Spiral wound configuration - 274-278, 285
Spiral wound modules - 50-51, 212-214, 379, 561, 581
Sponge ball cleaning - 203
Sponge-type structure - 20-22, 25, 33, 35
Stable state - 19
Stack power - 496-502
Stage - 361
Steam sterilization - 116
Sterilization - 114-119
Stokes-Einstein relation - 181, 185, 530-531
Stretched membranes - 6-7
Stretching-process - 64-65
Sulfochlorination - 43
Sulfonated polyphenylene oxide membranes - 339
Sulfonated polysulfone membranes - 338-339
Supported liquid membranes - 38, 514, 520, 547-551

Surface texture - 328
Symmetric membranes - 2, 4, 12-13, 21, 30, 404, 458, 462

"Tapered design" - 376, 378
Temperature - 565
Temperature effect - 195-198
Ternary phase diagram - 16-17, 145, 147
Tetrafluoroethylene - 6
Thermal gelation (thermo-gelation) - 10, 14-16
Thermal-phase-inversion process - 65-66
Thiele modulus - 435-437, 444-445, 448-450, 459-461
Thin film composite reverse osmosis membranes - 307-348
Thin film polymerization - 272
Threshold pressure - 170, 200
Through-flow filtration - 99, 102, 114-124, 131
Throughput - 90, 95-98, 112
Time lag - 564, 569
Tortuosity factor - 78
Tortuous-path spacer - 488-489
"Tortuous-pore" membranes - 62-66, 82-83, 86, 90, 98-99, 103, 106, 109, 111, 113
"Track-etch" process - 7, 66-67
Transport number - 487, 503
Transport rate - 571
Trimellitic anhydride acid chloride - 330
Trimesoyl chloride - 320-321
Tubular configuration - 214, 277-279, 285
Tubular membranes - 53-54, 434, 437-438
Tubular module - 50-52, 354
Tubular pinch effect - 186-192
Turbulent flow - 176-178, 184

Ultrafiltration - 5, 53, 136-259, 382-384, 403, 410, 421, 426, 428, 434, 438-440, 445, 450-453, 455, 465-466, 476, 492
  operating modes - 214-216
Ultrapure water - 8, 121, 218-221
Ultrasonic welding process - 54
Ultraviolet sterilization - 122
Unit-cell stack - 488-490
Univalent-cation-selective membrane - 499
Unstable state - 19
Unsupported liquid membranes - 38-39
UOP Butamer process - 389
Uranium recovery - 543-544
U-tube liquid membrane - 512-513

Vent filters - 116
Vexar® spacer - 488-489
Viable cells - 466-467, 470-473
Virus concentration - 247
Volatile solvent - 16
VTE (vertical tube evaporator) seeding process - 382

Waste lubricating oil - 226-227
Waste treatment - 254-255
Wastewater treatment - 382
Water - 24-26, 28, 31
Water clustering concept - 264
Water transport - 487
Watts-nickel bath - 385, 387
Well-head gas - 582
Wet-spinning process - 54-55
Wetted surface mechanism - 264
Whey - 324, 473, 491
Whey protein concentrate - 235
Whole cells - 401, 404, 455
Wine - 240

Yield - 362

Zr(IV) oxide - 154